Bauhaus-Universität Weimar
Professur Stahl- und Hybridbau

Master Thesis

Comparison of geometrical nonlinear analysis and second-order theory for steel members in torsion

Submitted by

Bonilla Sánchez, David Jahel

Matriculation number 121932

Reg.-Nr.: NHRE/2021/16

This thesis has been submitted in partial fulfilment to obtain the academic degree of Master of Science (M.Sc.) in Natural Hazards and Risks in Structural Engineering

BAUHAUS-UNIVERSITÄT WEIMAR

Faculty of Civil Engineering

Chair of Steel- and Hybrid-Construction

Declaration

Hereby, I declare that I worked on this Master Thesis independently and using only the specified sources and programs which are referred.

Weimar, 07.09.2021 David Jahel Bonilla Sánchez

_____

Abstract

Steel structures are normally comprised of slender elements, for which stability plays an important role. In that context, geometrical nonlinear analysis (GNA) provides accurate results, however, its use translates into higher computational demands. Consequently, simplifying GNA would be convenient in practice. A common approach called second-order theory (SOT) arises where numerical efforts are reduced while preserving accuracy. This study is then referred to evaluating up until which stage of deformation displacements and internal forces can be accurately described following SOT instead of GNA, specifically for torsion and bending loads that can cause lateral torsional buckling.

Several numerical analyses following SOT and GNA have been performed using the commercial software RFEM. For the simulations, different variables have been considered: 4 structural systems, 2 types of FE, 43 profiles (38 open and 5 closed), and 3 external loads. Every analysis has been performed 10 times, in each one, the external loads are increased up to 100% of the maximum value. As a result, critical loads, displacements, internal forces, and stresses have been analyzed.

It is found that the discrepancy between SOT and GNA grows when displacements increase. The same behavior is observed for the loads, higher forces result in greater displacements and consequently, the variation increases between the two approaches.

For closed profiles, low variation of both displacements and internal forces has been found. Their analysis can also be simplified with the use of 1D-beam elements. It is established that for closed profiles the rotation will be limited to the section's capacity. In addition, closed profiles present an excellent behavior for torsion and in this case, SOT can be used safely as an approximation for GNA.

Ultimately, as a result of the study, a stage where SOT provides sufficiently reliable results has been established in the form of fitting curves, which are found for IPE and HEB profiles. The fitting curves present a practical way to estimate which type of analysis should be followed for steel members in bending and torsion. Whether SOT or GNA should be applied strongly depends on the cross-section profile and the load level. Additionally, boundary conditions and load types play an important role as well. The latter, has shown that even for a different load distribution the curves still give a good estimate. Moreover, IPE fitting curves can also be useful for UPE profiles.

Acknowledgments

First, I would like to thank God for blessing me with such a wonderful life, full of opportunities and amazing people.

A special thanks to my beloved wife Grecia Hurtado, you have been with no doubt the supporting pillar in this journey and in all these years you have shown me your utmost love, dedication, and respect. Thank you for always pushing me to be better, to thrive, and to excel. Thank you for believing in me, because of that I know that I can do anything. You are the most wonderful person I have met, I will always love you and always be by your side.

I would like to thank my parents Cruz Sánchez and Fileto Bonilla for your life teachings, for supporting me reach all my goals, for making me the person I am today, for always being there for me, and for your unconditional love. I love you so much and I will be eternally grateful to you.

I want to thank my supervisors Prof. Matthias Kraus and Stalin Ibañez, for your continuous guidance and support given through every phase of this project. For resolving my doubts, and providing the feedback necessary to improve myself.

Last, I would like to acknowledge and thank every person that has contributed in some way so I could reach this point. My siblings Christian, Fileto and Jade. My friends from Ecuador Gabriel, Liz, Raúl, Víctor, Andrés, Pame, Angel, Chris, Marcos, Nina, Rocio, and many more. My classmates and friends from the master Ivan, Dulce, Saqlain, and Diego.

Table of Contents

List of Figures

page

page

List of Tables

Chapter 1: Introduction

1.1 Motivation

Nonlinear analysis is comprised by two parts: material and geometrical. Material nonlinearity covers plastic behavior while geometrical nonlinearity considers the influence of element deformations on stress states forming equilibrium. Geometrical nonlinear analysis (GNA) provides accurate results for stability problems, however, its use translates into higher computational demands as well as higher modelling efforts. Consequently, simplifying GNA would be convenient for practice use in engineering offices. A common approach called second-order theory (SOT) arises as a linearization where numerical efforts are reduced while accuracy is preserved. Nevertheless, some assumptions are considered, such as displacements remaining small [1] and the loading not reaching the lowest critical value [2].

Thin-walled steel elements are in general slender and may show, comparably to compact elements, large displacements due to torsional rotations. The large torsional rotations have to be considered if the position of the elements become notable different to their initial state. In addition, large torsional rotations will influence the numerical solution, and therefore, an accurate geometric stiffness is necessary [3]. By using GNA, the effect of large deformations is accurately described, however, in practice this analysis is not time-efficient. Hence, SOT is utilized as a proper alternative, mainly when displacements are restricted up to a certain value, such as the rotation angle of elements. A rough limit of 0.3 radians (17.2º) has been suggested [4], nonetheless, deeper analyses on valid deformation limits, e.g. up to which stage SOT represents sufficiently well GNA, have not been properly addressed.

Thus, the objective of this study is to identify the validity of SOT for representing GNA, particularly for torsion and bending loads that can cause lateral torsional buckling (LTB). Solving this problem will utterly help in the design of steel structures. Furthermore, establishing a fitting model that can define meaningful deformation limits is of importance. In practice, an ease of use model, which can provide guidance for whether SOT or GNA should be considered, can prove to be convenient.

1.2 Objectives

- Evaluate until which stage of deformation displacements and internal forces can be accurately described following SOT instead of GNA. Special interest in torsion and bending that cause LTB will be considered.
- Find a fitting model that can define significant deformation limits in thin-walled elements subjected to torsional and bending effects.

1.3 Structure

This work is structured in five chapters:

Chapter 2 provides the fundamentals of second-order theory and geometrical nonlinear analysis. Developments in the field of SOT and GNA regarding torsional and bending effects are reviewed. An introduction to steel structural analysis with the finite element method (FEM) for 1D-beam and 2D-shell elements is presented.

Chapter 3 focuses in the methodology of this work. First, the numerical analysis with SOT and GNA is introduced. Second, the parametric study is described with its different variables. The modelling is described and additionally, some benchmark problems are studied. Third, the simulation procedure and the measurement of results are presented. Finally, the procedure for presenting and comparing the results is given.

The analysis and discussion of results is offered in Chapter 4. The main results of the parametric study are described and supported. Furthermore, the stage of deformation where SOT accurately describes GNA is discussed. Ultimately, practical curves for establishing the use of SOT instead of GNA are established, particularly regarding torsion.

In Chapter 5 a summary of the work is presented, along with conclusions and an outlook for further research.

Chapter 2: Literature Review

In this chapter, first, SOT and GNA are introduced. Moreover, the structural stability problems in steel structures and how they are treated in modern codes are presented. Then, torsional and bending effects that may cause instability are described. After that, previous studies that have addressed GNA, SOT, and torsional behavior are given. Finally, the analysis and modelling of steel structures is introduced.

2.1 Second-order theory and geometrical nonlinear analysis

Large deformations are referred to large displacement gradients. Large strains can occur due to large displacements but it does not necessarily occur the other way around [5]. Hence, linear constitutive laws (material linearity) might still be applicable while large deformations are present [3]. In this case, only GNA is of relevance. Furthermore, elements subjected to large deformations have to be analyzed for stability. Flexural buckling (FB), lateral torsional buckling (LTB), and plate buckling, also called local buckling, are of relevance.

Second-order theories are formulated with assumptions that make the theory linear. If displacements of a structure remain small prior to instability, it can be sufficient to analyze it using linear formulations of SOT. However, if the displacements are large, the structure has to be analyzed with GNA [6].

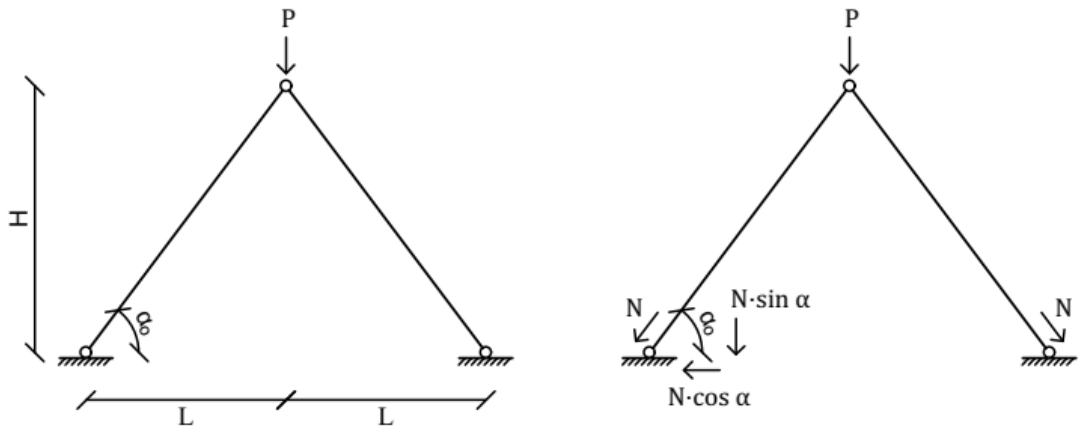

Figure 2.1 Two truss system example

In order to understand SOT and GNA a two truss system is presented in Figure 2.1. The system is symmetric to the middle plane and it is statically determinate. A single nodal force P is applied in vertical direction in the center. The system is solved for displacements and internal forces. Because of the static determinacy, equilibrium equations can be directly applied to obtain internal forces. The equilibrium equation is given as follows:

$$\Sigma F_v = 0 \;\rightarrow\; 2 \cdot N \cdot \sin\alpha + P = 0 \;\rightarrow\; N = \frac{-P}{2 \cdot \sin\alpha} \qquad \textit{Eq. 2.1}$$

From Eq. 2.1 it is observed that as long as the angle α remains equal to α_o it is a linear problem. Two models are developed for comparing the influence of two kinematical assumptions. Model A is the exact one (GNA) considering actual deformation of the truss following a curvilinear path. Model B considers an approximation (SOT) of the truss' deformation and it follows a linear path as observed in Figure 2.2.

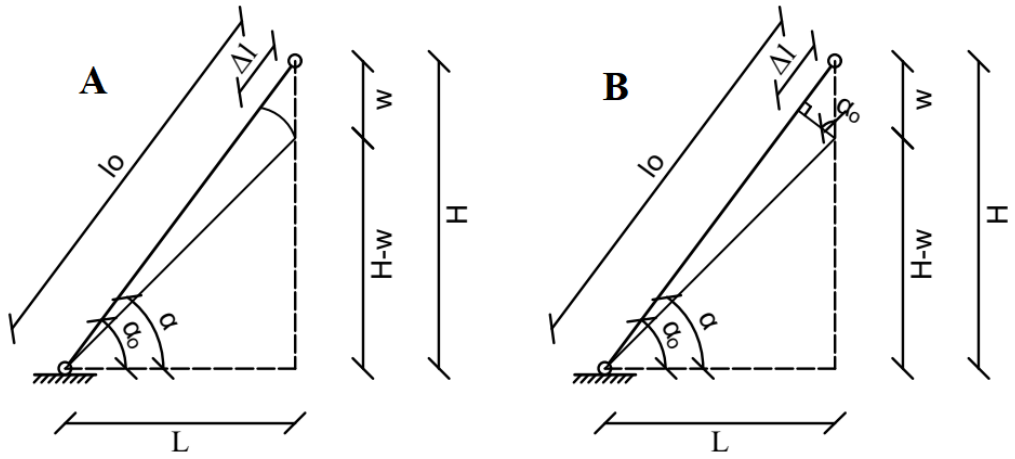

Figure 2.2 (Left) Model A exact (GNA), (Right) Model B approximated (SOT)

The formulation of equilibrium in models A and B is done with respect to the deformed system. Vertical displacement w of the middle node is unknown. Hence, the solution has to be obtained iteratively and certain tolerance has to be defined. The constitutive law is considered elastic for small strain levels, hence, Eq. 2.2 and Eq. 2.3 are planted.

$$\varepsilon = \frac{N}{E \cdot A} \qquad \textit{Eq. 2.2}$$

$$\Delta l = \varepsilon \cdot l_o \qquad \textit{Eq. 2.3}$$

The solution for model A is presented next. Eq. 2.4 describes the length of the deformed truss. Eq. 2.5 is the kinematic relation that solves for the vertical displacement w. Eq. 2.6 shows how the angle α varies due to w. Eq. 2.7 is obtained by replacing Eq. 2.2 into Eq. 2.3 and then into Eq. 2.5.

$$(l_o - \Delta l)^2 = (H - w)^2 + L^2 \qquad \textit{Eq. 2.4}$$

$$w = H - \sqrt{(l_o - \Delta l)^2 - L^2} \qquad \textit{Eq. 2.5}$$

$$\alpha = \tan^{-1}\left(\frac{H - w}{L}\right) \qquad \textit{Eq. 2.6}$$

$$w = H - \sqrt{\left(l_o - \frac{N}{E \cdot A} \cdot l_o\right)^2 - L^2} \qquad \textit{Eq. 2.7}$$

In a similar way, model B is presented as follows. Eq. 2.4 and Eq. 2.6 remain the same. Eq. 2.8 is the kinematic relation that solves for the vertical displacement w. Eq. 2.9 is then obtained by replacing Eq. 2.2 into Eq. 2.3 and then into Eq. 2.5.

$$w = \frac{\Delta \mathrm{l}}{\sin \alpha_o} \qquad \textit{Eq. 2.8}$$

$$w = \frac{\frac{N}{E \cdot A} \cdot l_o}{\sin \alpha_o} \qquad \textit{Eq. 2.9}$$

The iterative procedure for both models consists in solving the initial system for the internal axial force N, calculating the vertical displacement w and calculating the new angle α. Then the process repeats calculating once again for N until the difference of the new N and previous N satisfy the tolerance. It is observed that Model A has higher quality and it is more complex and hence more effort is required for solving the system. On the other hand, model B has a simpler kinematic equation and requires less effort. However, for large deformations only Model A is the correct or usable one [7].

2.1.1 Imperfections and structural stability

In real world structures, imperfections always exist. In steel structures, these imperfections may occur due to residual stresses after rolling or welding, lack of longitudinal linearity, and eccentricity of loads and connections. Due to their presence, imperfections can introduce additional forces that must be considered in the analysis and design of structural members.

Structural stability is addressed in modern codes. For instance, according to EC3 imperfections should be considered in the analysis as equivalent geometrical imperfections. The values of these equivalent imperfections have to represent the effects of all types of possible imperfections, which would reflect the P-Δ and P-δ effects also called second-order effects (SOE). The P-Δ effect refers to the effects of displacements at the ends of members while the P-δ effects correspond to the effects of displacements along the member (see Figure 2.3).

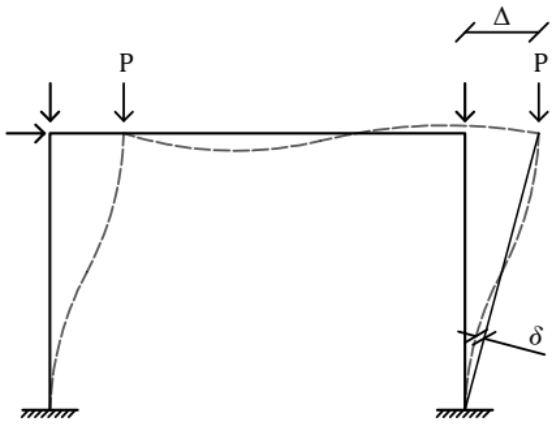

Figure 2.3 Visualization of the P-Δ and P-δ effects

EC3 provides three methods for considering SOE. These effects also provide the basis for determining the critical load according to the buckling mode of the system. The methods are described next:

- Method 1 verifies global stability by directly taking into account all imperfections (material and geometrical) and SOE.
- Method 2, partially considers imperfections (global structural) and global SOE. Intrinsically, member imperfections and local SOE are addressed with individual members' verification.
- Method 3 allows for basic cases individual stability verifications of equivalent members (corresponding buckling lengths related to global buckling mode).

Method 1 is the most accurate and no individual stability check is required, however, it is complex and requires high computational power, and it is not the preferred option. Method 2 and method 3 are the analysis procedure usually performed in practice. In method 2, the P-δ effects are considered in local member imperfections, whereas the P-Δ effects are considered in the global analysis with global imperfections [8].

Imperfections have to be considered in the direction and shape that causes the most disadvantageous effect. For this, the buckling shape is necessary, which is found by obtaining the lowest eigenvector of the system. In the case of lateral torsional buckling of beams, refer to Figure 2.10 for illustration.

In global analysis according to EC3, the P-Δ effects due to imperfections in sway frames can be considered as an equivalent sway imperfection, which is defined by an angle of rotation ϕ as shown in Figure 2.4. The value of ϕ is calculated with the aid of Eq. 2.10.

$$\phi = \phi_0 \cdot \alpha_h \cdot \alpha_m \qquad \textit{Eq. 2.10}$$

Where:

ϕ_0 = basic constant value 1/200
α_h = reduction factor for the total height h in meters (calculated as Eq. 2.11)
α_m = reduction factor for number of columns in a row m (calculated as Eq. 2.11)

$$\frac{2}{3} \leq \alpha_h = \frac{2}{\sqrt{h}} \leq 1\,;\ \alpha_m = \sqrt{0.5 \cdot \left(1 + \frac{1}{m}\right)} \qquad \textit{Eq. 2.11}$$

For members in flexural buckling, imperfections can be considered as equivalent local bow imperfections e_o (see Figure 2.5), which are related to the P-δ effects. The value of e_o corresponds to the maximum lateral displacement of the member. This value is calculated depending on the member's length L, the buckling curve, and the e_o/L ratios as presented in Table 2.1.

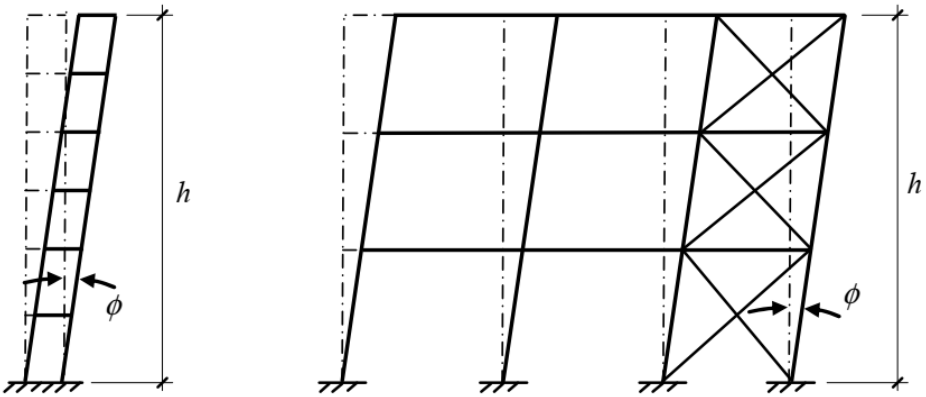

Figure 2.4 Initial sway imperfections [8]

Table 2.1 Values of initial local bow imperfections e_o/L [8]

Buckling curve	**Elastic analysis e_0/L**
a_o	1 / 350
a	1 / 300
b	1 / 250
c	1 / 200
d	1 / 150

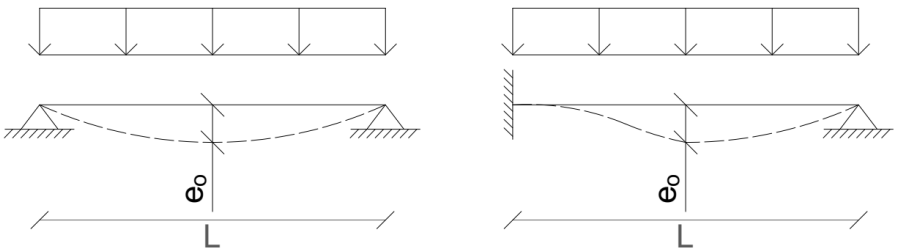

Figure 2.5 Initial bow imperfections

2.2 Torsional and bending stability

2.2.1 Torsion

Torsional rotation occurs when forces do not act on the shear center of the cross-section of a member. In steel structures, torsion may not be the predominant internal force in comparison to bending moments, axial or shear forces, however, instability regarding LTB of beams are related to torsional behavior [2].

Members subjected to torsion develop rotation around their longitudinal axis and warping as well (differential longitudinal displacements), which means that plane sections are not plane anymore and if restricted, additional axial stresses are produced. If the member has a closed or box section, then it can be said that the member undergoes St. Venant torsion or primary torsion M_{xp}. However, if the member has an open profile (e.g. H, I, or U), then it undergoes warping torsion, which includes secondary torsion M_{xs} and the warping bimoment M_{ω} [9].

Thin-walled members with open cross-sections (H or I profile) are not the most appropriate to resist torsion and they develop both primary and secondary torsion whether warping is restrained or not. On the other hand, closed cross-sections (HSS profile) perform better under torsion and normally only primary torsion is predominant even if warping is restrained [2]. For illustration, consider the cantilever beams shown in Figure 2.6.

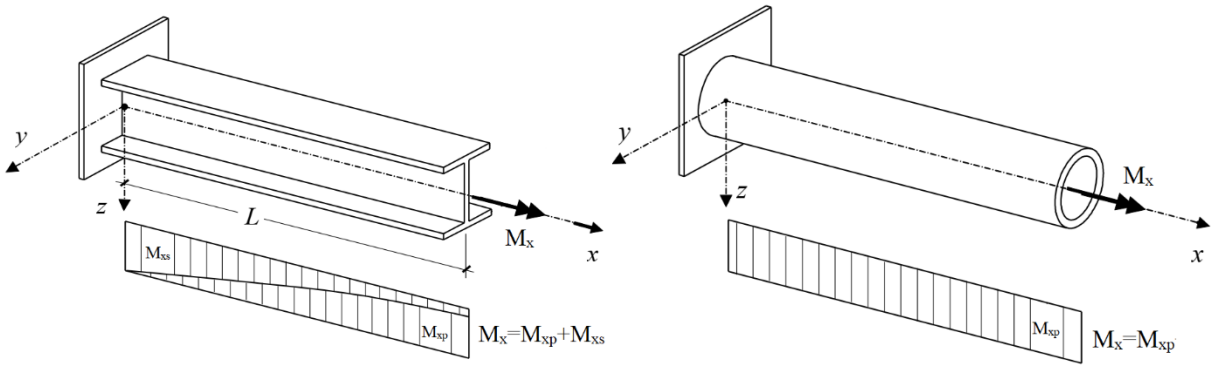

Figure 2.6 (Left) I section under both M_{xp} and M_{xs}, (Right) O section under M_{xp} [2](Modified)

The cantilever I-beam from Figure 2.6 is restrained to warping at the support, thus, it cannot warp. The cross-section then undergoes differential longitudinal deformations, which generate the secondary torsion M_{xs} component in addition to the primary torsion M_{xp} as shown in Figure 2.7.

Regarding serviceability, usually vertical and horizontal deflections are restricted in codes, such as Eurocode, however, a proper mention of rotational limits is not given. A limiting value is necessary both for analysis and practice. In the latter for instance, in the case of facades even a 2º rotation of a steel beam where a 4-meter wall stands translates into an unacceptable 14 cm displacement at the top. In this context, elements which are flexible in torsion are likely to be governed by rotation at serviceability limits. Nevertheless, the specific limit for rotation still remains as a matter of judgement for the designer [10].

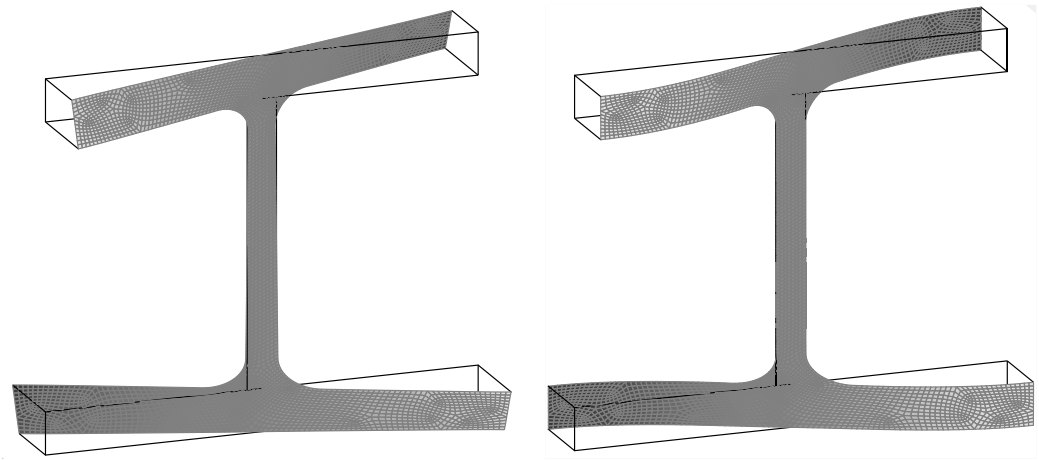

Figure 2.7 Deformed I section: (Left) due to M_{xp}, (Right) due to M_{xs}

2.2.2 Lateral torsional buckling

Continuing with the example of a cantilever I-beam, consider the beam subjected to bending about its strong axis (due to a transverse vertical load F) as shown in Figure 2.8. LTB is distinguished by lateral displacements of the compressed area (top flange). This area behaves like a compressed member, but with the distinction that is continuously restrained by the area that is in tension, which does not have propensity to buckle (initially). However, to find the lowest energy equilibrium state the section tends to rotate, hence, the instability of LTB occurs. Furthermore, the point of application of the load plays a direct role, which can be whether a stabilizing, a neutral, or a destabilizing effect [2] as shown in Figure 2.9.

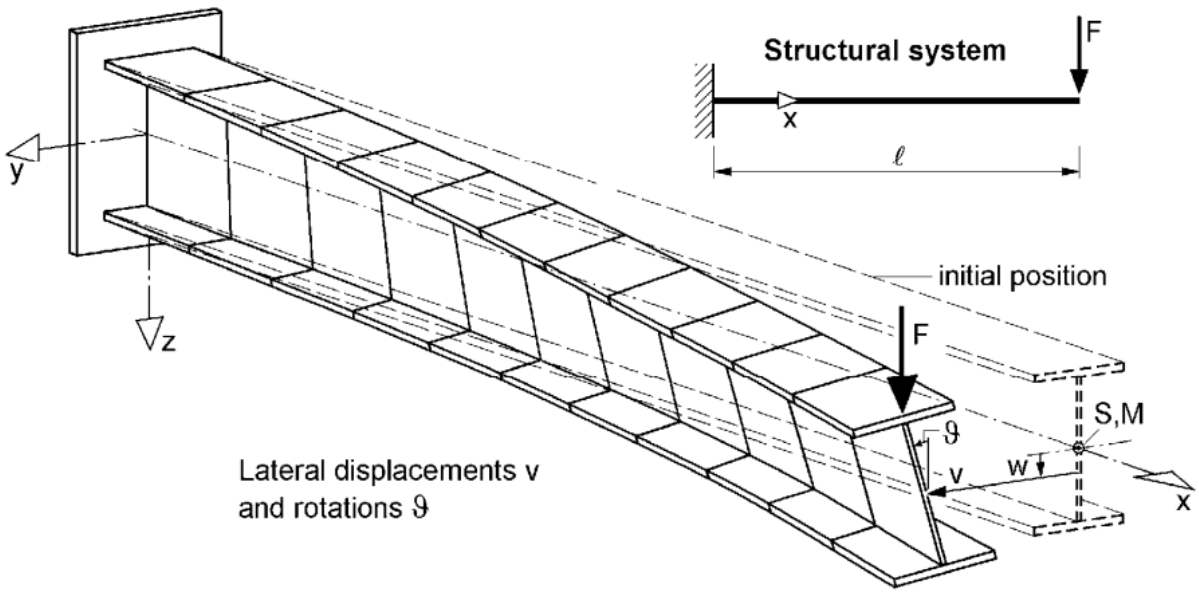

Figure 2.8 Lateral torsional buckling of an I-beam due to bending [4](Modified)

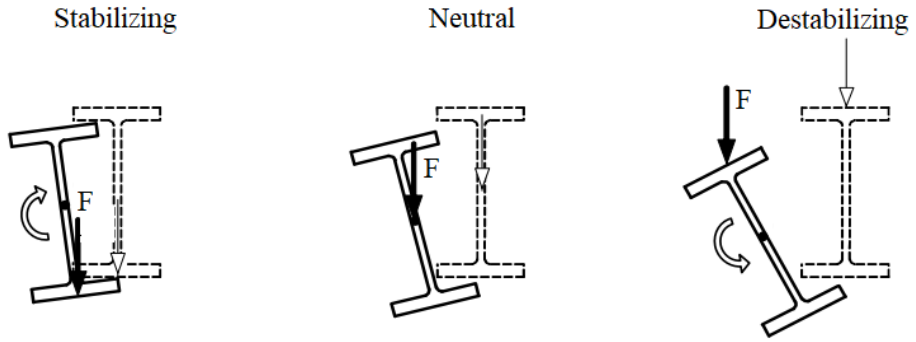

Figure 2.9 Influence of the point of load application in LTB [2] (Modified)

An important parameter that distinguishes instability of a structural system is the critical load, which is related to the called eigenvalue. In finite element analysis (FEA), This value corresponds to either when the determinant of the stiffness matrix becomes zero or when small increases in loads result in high displacements.

For SOT calculations with imperfections, it is important to have previous knowledge of the first buckling mode or buckling shape. The buckling modes are obtained by solving the eigenvalue problem between the stiffness matrix and the geometrical stiffness matrix, the first or lowest mode corresponds to the lowest energy state of the system and shows where it is prone to deform or in what direction shows weaker behavior. For better illustration consider the four I-beams with different support conditions shown in Figure 2.10.

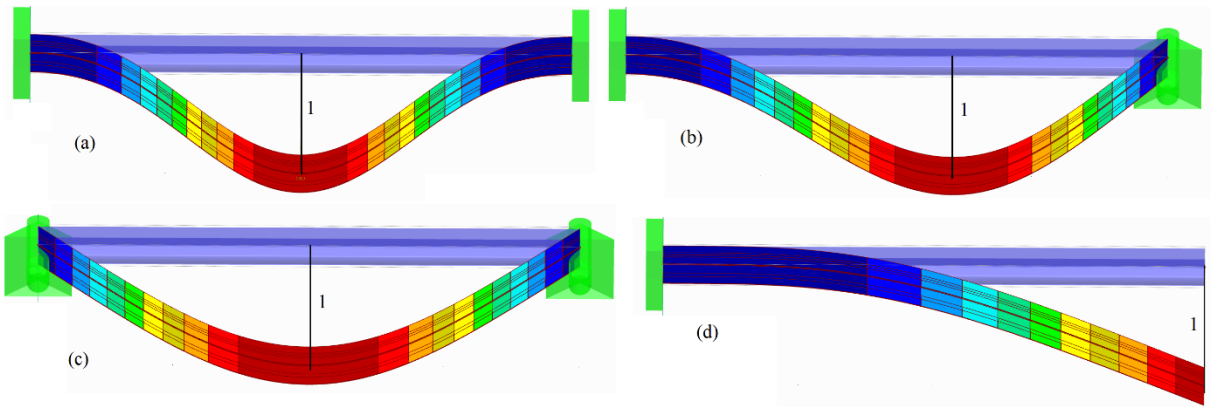

Figure 2.10 First buckling modes of I-beams: (a) fixed-fixed, (b) fixed-fork, (c) fork-fork, and (d) fixed-free

From Figure 2.10 it can be observed that the buckling modes correspond to lateral torsional buckling of the beams (since rotation and lateral displacements occurs simultaneously). Depending on the support conditions the buckling shape changes, meaning that the deformation behavior is unalike and that the maximum normalized nodal displacement (value of 1) occurs at a different location along the beam. In this context, the geometric imperfections have to be defined in such a way that they adjust to this lowest buckling mode and that they are applied in the most unfavorable direction [4].

2.3 Previous studies

2.3.1 Geometrical nonlinear analysis

Many efforts have been made in the direction of simplifying geometrical nonlinear analysis and reducing computational demands. For instance, Makode et al. [11] propose an approach based on pseudodistortions (PD) that performs second-order analysis of 2D-frame structures. It saves computational effort because no reformulation of the global stiffness matrix is required, hence, it proves useful in incremental analyses, such as pushover for seismic assessment. An example of this type of analysis is done for Vogel's six-story frame, the result and its comparison with developed software (DS) is shown in Figure 2.11.

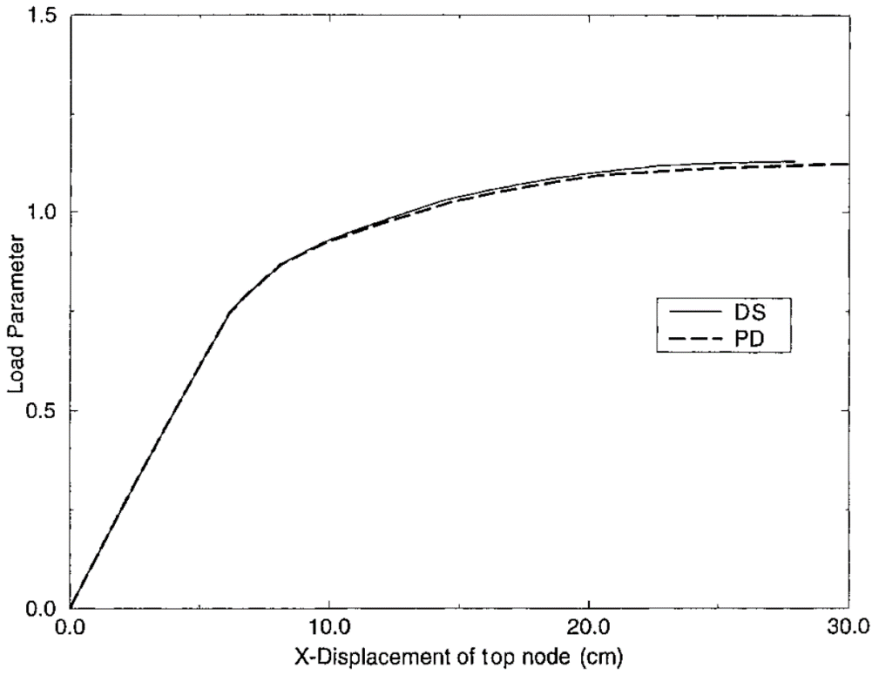

Figure 2.11 Pushover analysis Vogel's six-story frame [11] (Modified)

For 3D-frame structures, Cai et al. [12] developed a simple finite element for beams which can consider large deformations. The approach is based on the Reissner variational principle and von Karman nonlinear theory. While using only 10 elements accurate solutions can be obtained, thus, showing its efficiency. For clarity consider a cantilever beam subjected to transversal load at the free end in Figure 2.12. The proposed method shows good agreement even up to high deformations as much as 40% of the cantilever's length.

In the studies of Maghami et al. [13] and Mohit et al. [14] a comparison of high order methods for solving the nonlinear system of equations in truss systems is presented. The results show that the developed algorithms require a lower number of iterations to converge than the Newton-Raphson method, hence reducing total calculation time. In the example of Schwedler's dome truss, the computation time could be reduced up to 26.83% [13] and 63.38% [14] in comparison to the Newton-Raphson method.

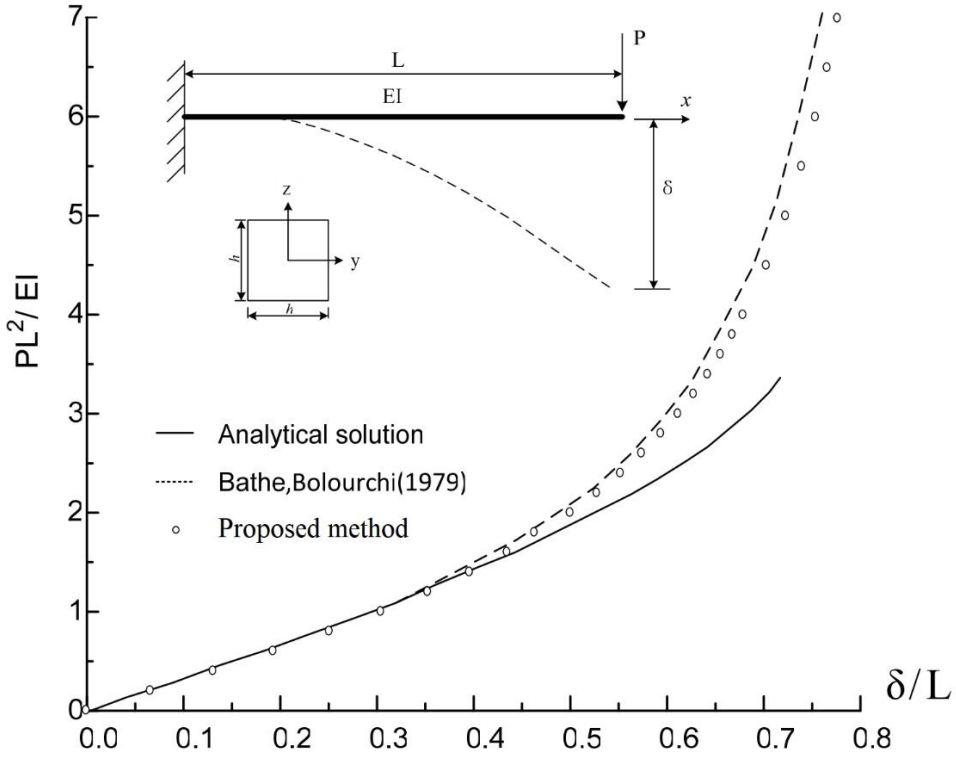

Figure 2.12 Large deflection cantilever beam [12] (Modified)

Iu and Bradford [15] and Andrew Kwok Wai So and Siu Lai Chan [16] present a high order formulation of beam finite elements for predicting post-buckling behavior. This approach can reduce computational effort by reducing the number of finite elements while still obtaining accurate solutions of systems prone to instabilities. By using only one element per member the reticulated shallow shell in Figure 2.13 can be analyzed. Furthermore, it can be observed that a good agreement exists with previous studies.

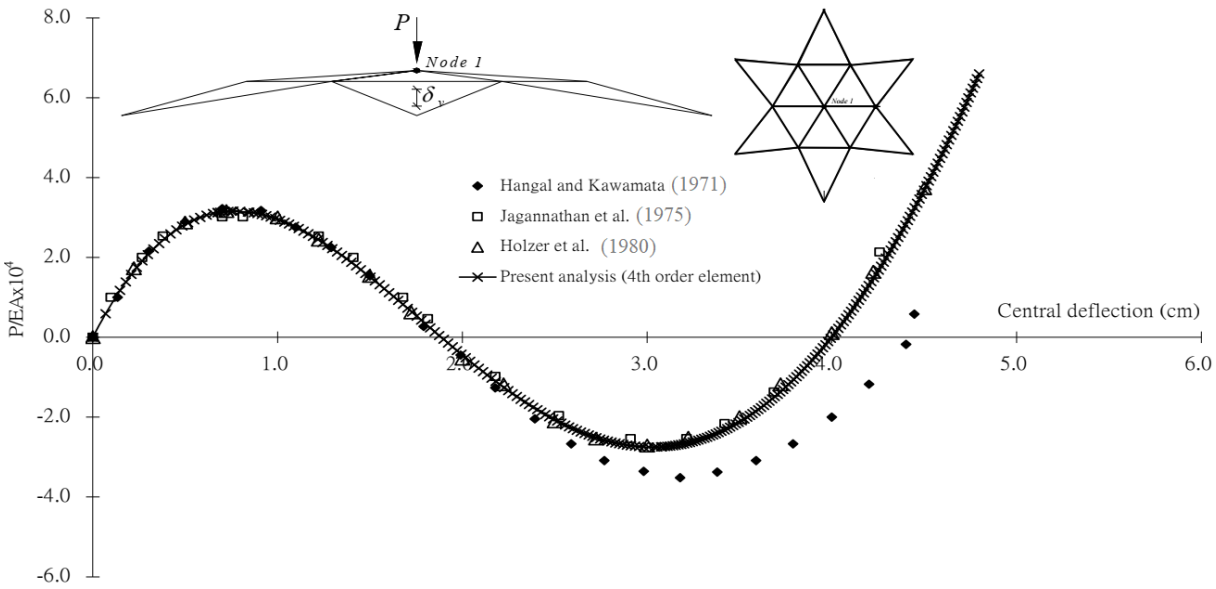

Figure 2.13 Load vs central deflection of reticulated shell structure [15] (Modified)

GNA has been studied in thin-walled composite beams. Mororó et al. [17] evaluated an approach using beam finite elements rather than shell elements in cantilever box beams. The results show that natural frequencies, buckling loads and displacements are in good agreement as shown in Figure 2.14 and Table 2.2. This approach serves as a simplification of the process of mesh generation and lowers the computational cost by using only beam elements instead of shell elements. However, it is only applicable for closed sections since warping effects are neglected. Moreover, Hui et al. [18] has solved this problem in the formulation of the beam elements by accounting for shear deformation and warping effects at cross-section level.

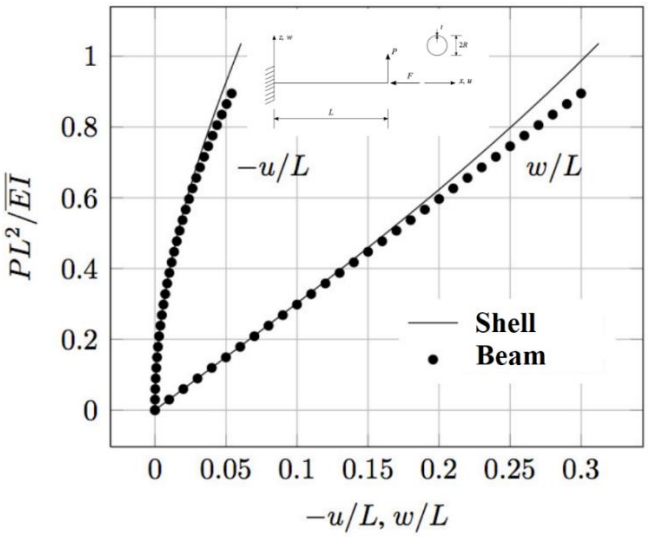

Figure 2.14 Displacements at free end of cantilever box beam [17](Modified)

Table 2.2 Natural frequencies and buckling loads for shell and beam elements [17]

Modes	Frequencies (Hz)			Buckling loads (kN)		
	Shell elements	**Beam elements**	**Difference %**	**Shell elements**	**Beam elements**	**Difference %**
1	3.52	3.54	0.40	16.53	16.54	0.05
2	4.52	4.53	0.29	16.53	16.54	0.05
3	21.94	22.17	1.01	147.28	148.86	1.07

Despite all these advancements, a comparison that presents up until what stage the simplified approaches are accurate enough in contrast with geometrical nonlinear analysis has not been properly investigated yet.

2.3.2 Imperfections and second-order theory

Sato and Ikarashi [19] studied the effects of initial imperfections on the large deformation behavior governed by local buckling of square hollow members. They found that safe values for strength and plastic deformation capacity can be obtained by the use of initial imperfections corresponding only to local buckling modes. Based on that understanding, the width-thickness ratios of standards have to be carefully considered for design and analysis.

Regarding initial bow imperfections, Walport et al. [20], expanded the use of imperfections of EC3 to the inclusion of material nonlinearity. The values of e_o of EC3 are kept, however, its value has to be divided by a factor of 150. This values are found to be suitable in many cases.

For stability analysis of columns, Galishnikova et al. [6] present the use of linear and second-order theory to investigate the influence of imperfections. Findings suggest that columns can be studied either with linear theory or with the use of geometric imperfections (SOT) for obtaining the buckling load. Similarly, Mageirou and Gantes [21] showed that the linearized buckling analysis gives an accurate prediction of the critical load. Nevertheless, structural behavior beyond the critical load has significant variation when accounting for material and geometrical nonlinearities. The latter is considered with initial imperfections (SOT). As reference consider a pinned I-column under axial compression where the lateral displacement in the middle height is studied. In Figure 2.15, the influence of either material or geometrical nonlinearities and their combined effect for post-buckling analysis is shown. This suggests that plastic behavior has to some extent influence in GNA results, which are yet to be fully implemented due to high computational demands, especially for large structures.

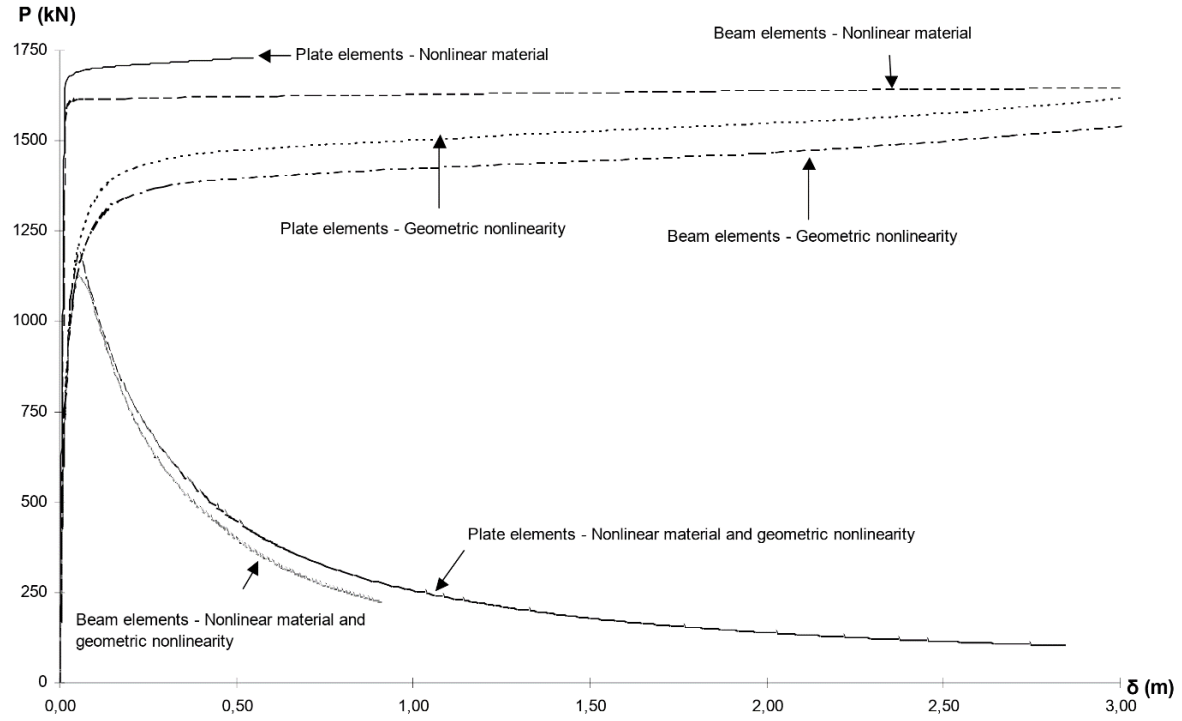

Figure 2.15 Influence of material and geometrical nonlinearities [21](Modified)

2.3.3 Torsion

Aminbaghai et. al [22] formulated a finite beam element to account for primary and secondary torsional deformations with the inclusion of variable axial forces, which are important due to the influence of warping bimoments on the total axial stresses. In the case of a cantilever I-beam subjected to torsion and variable axial force with eccentricity (see Figure 2.16), there is a direct effect in the primary and secondary torsional moments (M_{xp}, M_{xs}), and the angle of twist (θ) due to change in axial stresses for both tension or compression. For better illustration see Figure 2.17. The calculations consider the length L equal to 2.5 m, the variable axial force n_x in a range between -3000 to 3000 kN/m, and the torsional moment M_x equal to 10 kNm.

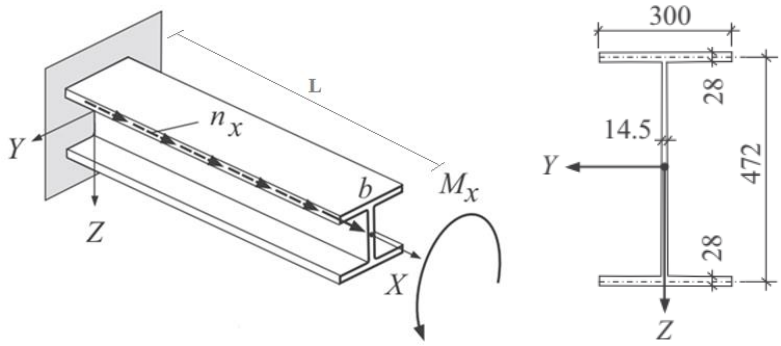

Figure 2.16 (Left) cantilever I-beam and (Right) I cross-section dimensions in mm [22] (Modified)

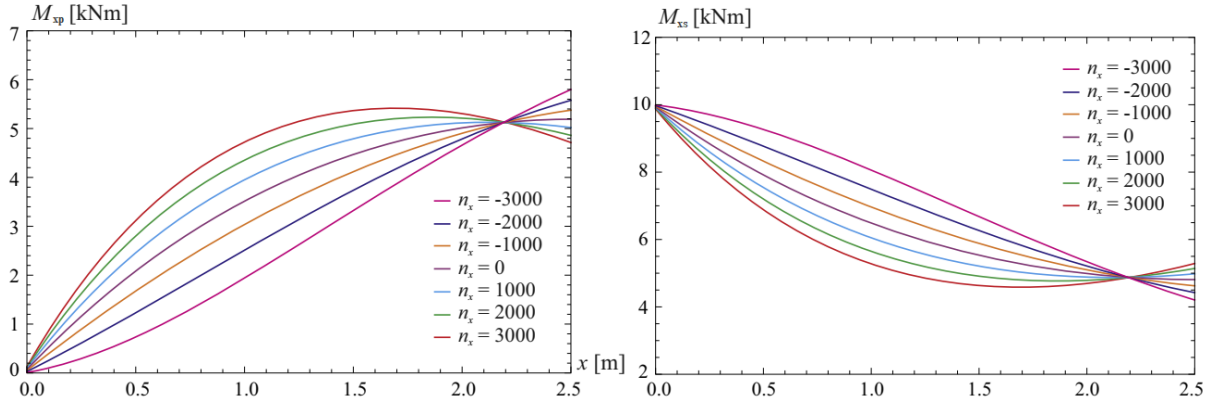

Figure 2.17 (Left) variation M_{xp} and (Right) variation for M_{xs} [22] (Modified)

Murín and Kutiš [23] suggest that the influence of warping torsion is significant not only in open but in closed cross-sections as well. The authors developed a new beam finite element by which they demonstrated the need for including secondary torsion moment deformations on closed cross-sections with constant geometry. In the cantilever example used (see Figure 2.18), the maximum normal and secondary shear stresses are significant in magnitude in comparison with the primary shear stress. For open cross-sections, sufficient agreement in results exists with commercial software, however, for closed cross-sections that is not the case. More information about the authors' findings is presented in Table 2.3 and Table 2.4.

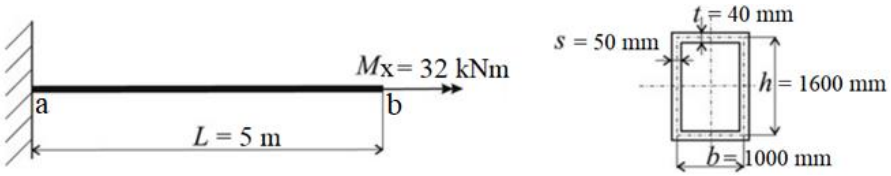

Figure 2.18 Cantilever beam of a closed cross-section example [23] (Modified)

Table 2.3 Warping bimoment and angle of twist closed cross-section [23]

	Murtín and Kutiš	**ANSYS BEAM188 100 elements**	**ANSYS BEAM188 200 elements**	**ANSYS BEAM188 1000 elements**
$M_{\omega a}$ (Nm²)	-263.95	-1618	-1789	-1954
Relative error (%)	-	513	578	640
θ_b (mrad)	0.022	0.021363	0.021363	0.021363
Relative error (%)	-	2.9	2.9	2.9

Table 2.4 Axial stresses, primary and secondary shear stresses of closed cross-section [23]

	Maximum primary shear stress	**Maximum secondary shear stress**	**Maximum axial stress**
Stresses (kPa)	246.96	36.09	67.17
Relative magnitude(%)	-	14.6	27.2

Another study from Addessi and Cimarello [24] proposed three different beam finite element formulations for considering secondary shear deformations in warping torsion. The finer approach considered detailed variation of warping on the cross-section while the two more coarse approaches adopted a previously defined warping profile. The results of 3 cantilever beam examples (I, C, and O shapes) show that a more refined approach is required when analyzing non-symmetric or closed cross-sections. This is important particularly because of local variation of stresses that overall affect the structural behavior. Nonetheless, when the warping mechanism is not complex (symmetric sections) the coarser approaches can provide satisfactory results.

A better understanding of torsion and its influence in displacements and internal forces/stresses is of utter importance in analysis and design. And even though, many studies have tried to address this influence, there still exists a gap concerning the magnitude of torsional rotation allowed in steel members, particularly, for large deformations.

2.4 Steel structural analysis and FEM

Steel structures design generally is comprised by analyses and verifications. First, displacements and internal forces are obtained and evaluated, considering equilibrium and agreement. Second, these results are treated against section-resistance, stiffness, and ductility to guarantee structural safety. This 2-step procedure is now more integrated due to the growing understanding of steel and development of numerical tools.

In general, for structural analysis the finite element method (FEM) is used. In the case of steel structures, usually linear beam elements are accurate enough. The modelling of structures with beam elements needs certain considerations, such as the description of the structural axis, eccentricities, supports, curved members, and joints' stiffness. Furthermore, a combination between area/shell and beam elements can occur, such as a concrete slab in a 3D steel frame. This interaction between finite elements has to be carefully considered [2].

An option for steel modelling is the use of not only beam elements, but also shell and solid elements (see Figure 2.19). In the latter two, transverse shear deformation and warping can be better observed and stresses can be obtained in more directions. However, the computational demands and the process of creating the geometry and the meshing are high, except for small systems. This problem can notably increase when geometrical nonlinearity is considered [17].

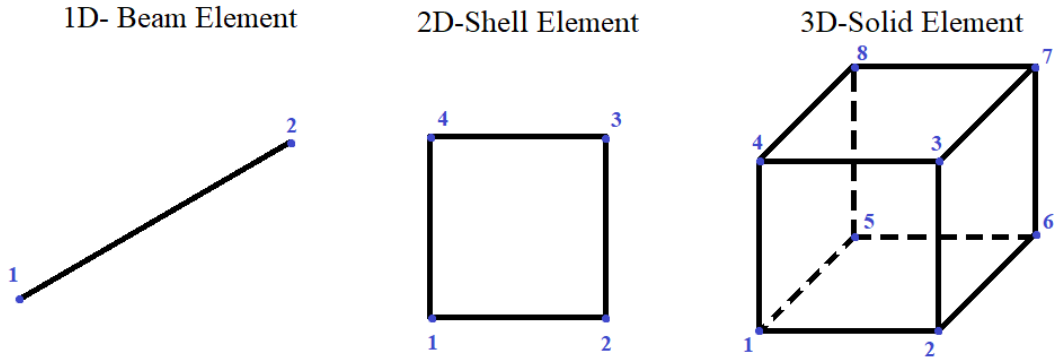

Figure 2.19 1D-beam (2-nodes element), 2D-shell (4-nodes element), and 3D-solid elements (8-nodes element)

Chapter 3: Methodology

This chapter presents the methodology and the considerations taken for the parametric study. The numerical analysis with SOT and GNA in RFEM software is introduced. Then, the different parameters included in the simulations are described. The modelling process is described and additionally, some benchmark problems are reviewed. Afterwards, the simulation procedure and the measurement of results are presented, which include critical loads, displacements, internal forces and stresses. Finally, the procedure for presenting and comparing the results is given.

3.1 Numerical analysis

For the present work the finite element analysis software RFEM 5 64bits version 25.01 is used. Its selection has been based on the scope of nonlinear analysis and the consideration of warping torsion for stability analysis.

3.1.1 Second-order theory

SOT can be considered with geometric imperfections in the case of 1D-beam members with open cross-sections. The imperfections are applied based on the first buckling shape of the system and as precamber according to DIN 18800 Part 2 [25]. The buckling curves are cross-section dependent considering built-up members (see Appendix I). Moreover, no reduction of the precamber is considered in this study therefore the values presented in Table 2.1 are taken. The precamber is selected as with variation in the strain tensor, which follows internal equilibrium based on the deformed shape.

Some other considerations for SOT are:

- Material is considered constant (linear), no plastic deformations occur.
- Shear deformations must be taken into account regarding numerical stability and for calculation of the critical load factor α_{cr}.
- Cross-sections are assumed to be shape constant to avoid local instabilities.
- Cross-sections are thin-walled with constant thickness.
- Displacements and torsional rotations are considered small compared to the dimensions of the system [26].

Second-order analysis for closed cross-sections (1D and 2D) is done considering P-Δ effects in an iterative procedure solved by the method according to Picard [27]. The same procedure applies for 2D-shell elements for open cross-sections. In this context, no initial geometric imperfections are considered.

3.1.2 Geometric nonlinear analysis

In RFEM, GNA is called large deformation analysis. Torsional rotations and displacements are not considered small anymore in contrast to SOT. Furthermore, there are some additional considerations, such as:

- The analysis is done for both 1D-beam and 2D-shell elements.
- Longitudinal and transversal actions are considered for obtaining internal forces.
- The tangential stiffness matrix of the deformed system is calculated after every iteration step.
- The nonlinear equation system is solved using the Newton Raphson method and no results beyond the critical value are obtained [27].

3.1.3 1D-beam and 2D-shell elements

1D-beam elements of open cross sections (2 nodes) can be solved with 7 degrees-of-freedom (DOF) per node considering warping in the RFEM module RF-FE-LTB, which is related to stability analysis of beam elements under SOT with imperfections and under GNA. The 7 DOF are axial displacement u_x, displacement in Y u_y, displacement in Z u_z, torsional rotation φ_x, rotation around Y φ_y, rotation around Z φ_z and variation of the angle of twist Ω. The corresponding internal forces are axial force N, shear force in Y V_y, shear force in Z V_z, torsional moment M_T, bending moment around Y M_y, bending moment around Z M_z, and warping bimoment M_ω (see Figure 3.1). However, in the case of closed cross sections, the warping effect is neglected and they are considered with just 6 DOF per node (no variation of Ω and M_ω).

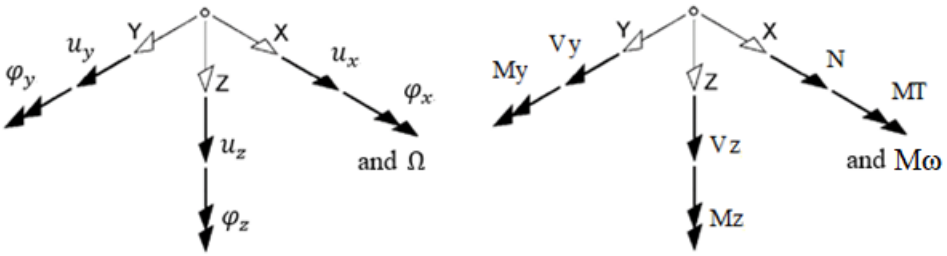

Figure 3.1 Nodal 1D displacements and internal forces in global coordinate system [4](Modified)

2D-shell elements are normally modelled as quadrangle elements (4 nodes) with the property of thickness. These elements are solved with 6 DOF per node u_x, u_y, u_z, φ_x, φ_y, and φ_z (see Figure 3.2). In contrast to 1D-elements, the warping effect is observable due to a better discretization in the transversal direction of the cross section. Moreover, each individual element is solved for stresses, which provides area results instead of individual internal forces.

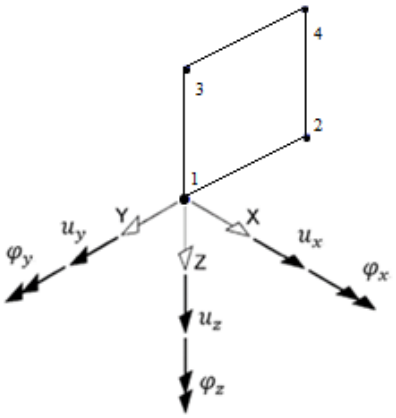

Figure 3.2 Nodal 2D displacements in global coordinate system [4](Modified)

3.2 Structural models

Different variables are considered in this study for assessing and comparing geometrical nonlinear analyses of individual steel members. A summary of these variables is presented in Table 3.1

Table 3.1 Summary of variables

Variables		Description	Quantity	Reference
Profile / Cross-section	Closed	Square and rectangular	5	Table 3.2
	Open	3-plate I section (IPE and HEB)	38	Table 3.3
Structural systems		Beams: fixed-free, fork-fork, fixed-fixed, and fork-fixed	4	Figure 3.3
Type of finite element		1D-beam and 2D-shell	2	Figure 3.4
Analysis		SOT and GNA	2	-
External loads		V_z, M_y, M_T	3	Figure 3.3

As a parameter of selection of the different profiles/cross sections, the torsional bending constant is considered. The parameter describes the relative magnitude of the primary torsion and warping torsion and it can be calculated by following Eq. 3.1:

$$a = \sqrt{\frac{E \cdot I_\omega}{G \cdot I_T}} \qquad \textit{Eq. 3.1}$$

Where:

a = torsional bending constant
E = Young's modulus (for steel 21000 kN/cm²)
G = shear modulus (for steel 8077 kN/cm² with ν = 0.3)
I_ω = warping constant
I_T = torsion moment of inertia

The torsional bending constant is expressed in length units and it can tell us whether the effect of warping torsion or St. Venant's torsion is higher for elements subjected to torsion [10]. For this purpose, a wide variety of profiles with different torsional bending constants is selected. In the case of closed cross-sections a total of 5 profiles are selected (1 SHS and 4 RHS), their geometrical properties are summarized in Table 3.2. For open cross-sections a total of 38 profiles are chosen and are presented in Table 3.3. These profiles are built-up by three plates whose cross-section dimensions are taken as reference from rolled profiles IPE and HEB.

Table 3.2 Closed cross-section properties square and rectangular profiles [28]

Closed profile	I_y (cm⁴)	I_z (cm⁴)	I_T (cm⁴)	I_ω (cm⁶)	a (cm)	I_y/I_T (-)	I_y/I_z (-)
SHS 200x200x6	2833.0	2833.0	4459	39.2	0.15	0.6	1.0
RHS 100x50x6	179.0	58.7	154	74.6	1.12	1.2	3.0
RHS 200x100x8	2091.0	705.0	1811	3593.4	2.27	1.2	3.0
RHS 300x100x6	4777.0	842.0	2403	19800.9	4.63	2.0	5.7
RHS 300x150x6	6074.0	2080.0	4988	23244.9	3.48	1.2	2.9

Table 3.3 Open cross-section properties for 3-plate I profiles referenced to IPE and HEB [29]

Open profile 3-plate I	I_y (cm^4)	I_z (cm^4)	I_T (cm^4)	I_ω (cm^6)	a (cm)	I_y/I_T (-)	I_y/I_z (-)
IPE80	77.7	8.5	0.6	118	23.24	137	9.2
IPE100	163.3	15.9	0.9	351	31.94	182	10.3
IPE120	306.3	27.6	1.4	890	40.80	220	11.1
IPE140	525.3	44.8	2.1	1981	50.02	255	11.7
IPE160	834.6	68.2	2.9	3959	60.09	293	12.2
IPE180	1272	101	4.0	7431	69.85	321	12.6
IPE200	1846	142	5.2	12988	80.47	354	13.0
IPE220	2653	204	7.2	22672	90.78	371	13.0
IPE240	3671	283	9.4	37391	101.92	392	13.0
IPE270	5505	419	12.0	70578	123.45	457	13.1
IPE300	7999	603	15.7	125934	144.41	509	13.3
IPE330	11145	786	20.7	199097	158.13	538	14.2
IPE360	15524	1041	29.1	313580	167.26	533	14.9
IPE400	21876	1314	37.7	490048	183.79	580	16.6
IPE450	32140	1672	51.5	791005	199.88	624	19.2
IPE500	46207	2137	71.7	1249365	212.80	644	21.6
IPE550	63965	2661	95.5	1884098	226.45	670	24.0
IPE600	88326	3380	134.1	2845527	234.92	659	26.1
HEB100	432	167	7.3	3375	34.64	59	2.6
HEB120	838	317	11.6	9410	45.83	72	2.6
HEB140	1471	549	17.6	22479	57.64	84	2.7
HEB160	2414	888	25.9	47943	69.32	93	2.7
HEB180	3729	1362	36.3	93746	81.91	103	2.7
HEB200	5513	2001	49.5	171125	94.81	111	2.8
HEB220	7865	2841	65.9	295418	107.96	119	2.8
HEB240	10893	3919	86.0	486946	121.30	127	2.8
HEB260	14351	5128	101.0	753651	139.30	142	2.8
HEB280	18597	6588	119.0	1130155	157.16	156	2.8
HEB300	24187	8553	149.6	1687791	171.24	162	2.8
HEB400	55871	10807	307.3	3817152	179.71	182	5.2
HEB500	104255	12611	487.0	7017696	193.56	214	8.3
HEB550	133086	13064	546.4	8855763	205.28	244	10.2
HEB600	166679	13517	610.8	10965375	216.06	273	12.3
HEB650	205425	13970	680.3	13362740	225.98	302	14.7
HEB700	250796	14426	764.8	16064064	233.70	328	17.4
HEB800	349052	14883	855.8	21840229	257.60	408	23.5
HEB900	481183	15794	1040.1	29461359	271.38	463	30.5
HEB1000	628590	16253	1153.5	37636488	291.26	545	38.7

From Table 3.3, it can be observed that a wide variety of torsional bending constants are considered as well as bending inertia ratios I_y/I_z and bending-torsional inertia ratios I_y/I_T.

3.2.1 Modelling

The structural systems shown in Figure 3.3 are modelled with a constant length L = 4.0 m. The fixed supports are fully restricted including warping deformation while the fork supports consider only translational and torsional rotation restrictions. Moreover, the nodes indicated with a circle in the figure are the points where the individual external actions of V_z, M_y, and M_T are acting. The point of action is localized at the free end for the cantilever beam (fixed-free) and for the other three structural systems it is located in the mid-span (L/2 = 2.0 m). Within the cross-section the loads act in the centroid, which corresponds to shear center in the case of double-symmetrical profiles. Furthermore, the vertical load is considered acting downwards and the bending and torsional moments are considered anticlockwise. Finally, in this study self-weight is neglected as to consider only the individual effect of each load case.

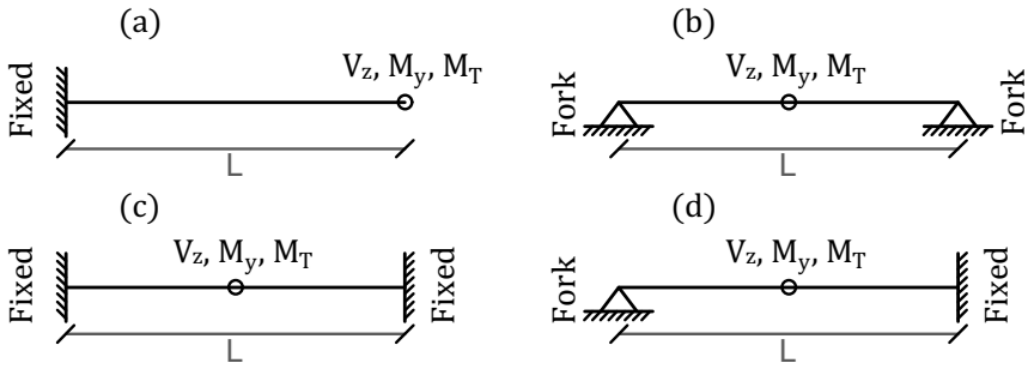

Figure 3.3 Structural systems: (a) fixed-free cantilever beam, (b) fork-fork beam, (c) fixed-fixed beam, and (d) fork-fixed beam

The type of finite element (FE) used for modelling is illustrated in Figure 3.4 and Figure 3.5 for closed and open profiles respectively. The linear 1D-beam elements are simpler and require less number of elements to model. For all 1D-models a FE mesh of 5-centimeter length elements is chosen based on convergence criteria as explained in section 3.2.2. Hence, a total of 80 elements for a 4-meter beam is obtained. However, in the case of 2D-models different discretization is taken. Based on convergence criteria as well, the maximum size for quadrangles and curved surfaces is defined as 2.5 cm and the amount of elements depends on the individual cross-section properties.

Some considerations have been taken for 2D-models in order to have the same behavior as 1D-models. For instance, supports in 1D-models are considered as nodal supports and in 2D-models they are considered as linear supports. These linear supports must represent the same degree of fixity as of nodal supports. In the case of fixed supports, the linear support restricts all displacements (u_x, u_y and u_z) along the whole cross-section. For fork supports, linear supports restrict u_y and u_z only as to permit free bending and warping. For numerical stability, u_x is restricted by a nodal support in the shear center the same as in 1D-models. For illustration of both supports see Figure 3.6.

One last consideration is how the load is applied. In the case of V_z action, direct application of the nodal load in the shear center is done. For nodal moments M_y and M_T convergence in the point application is not satisfied, hence, nodal constraints have to be used for a more adequate

distribution of the nodal load on the whole cross-section. The nodal constraints are φ_y and φ_x for M_y and M_T respectively. Furthermore, the web of I and H sections is stiffed for convergence with the addition of a linear constraint, which does not restrict warping of the flanges. The constraints for M_y and M_T are shown in Figure 3.7.

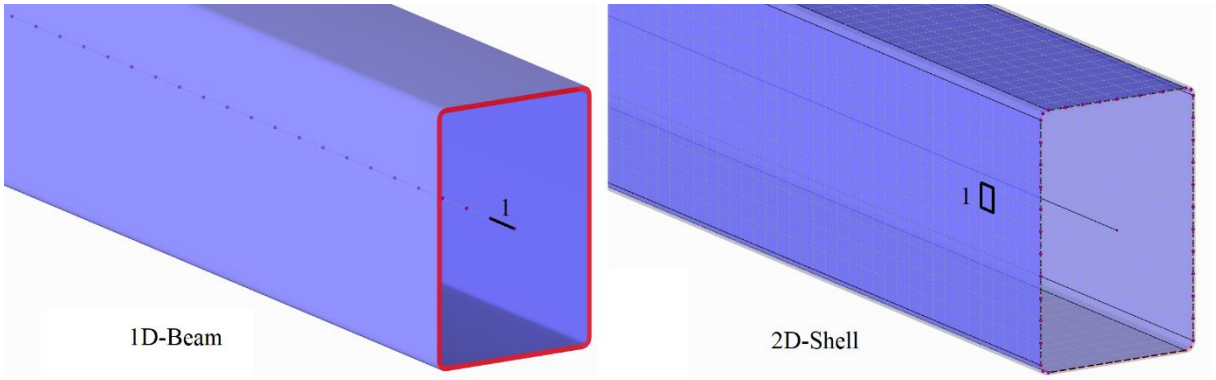

Figure 3.4 Closed profiles: (Left) 1D-beam element and (Right) 2D-shell element

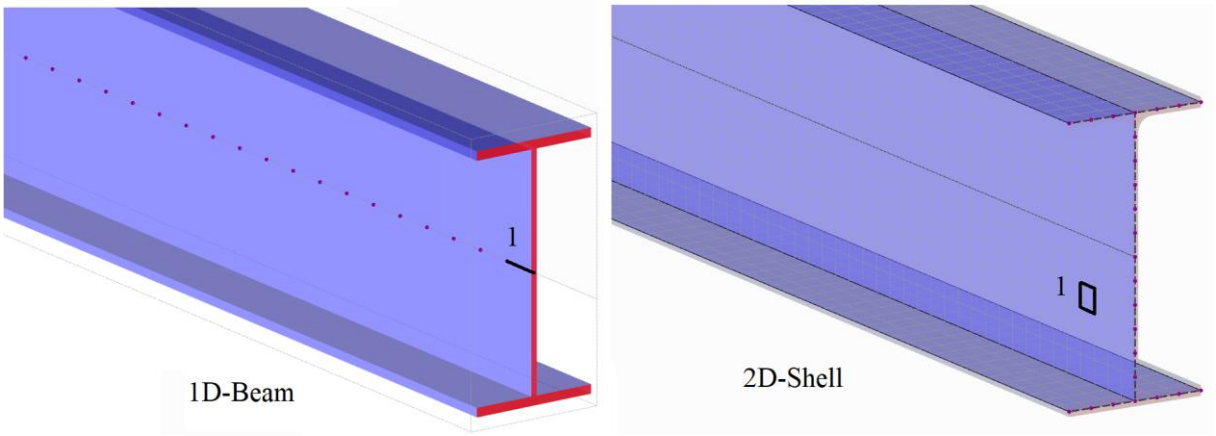

Figure 3.5 Open profiles: (Left) 1D-beam element and (Right) 2D-shell element

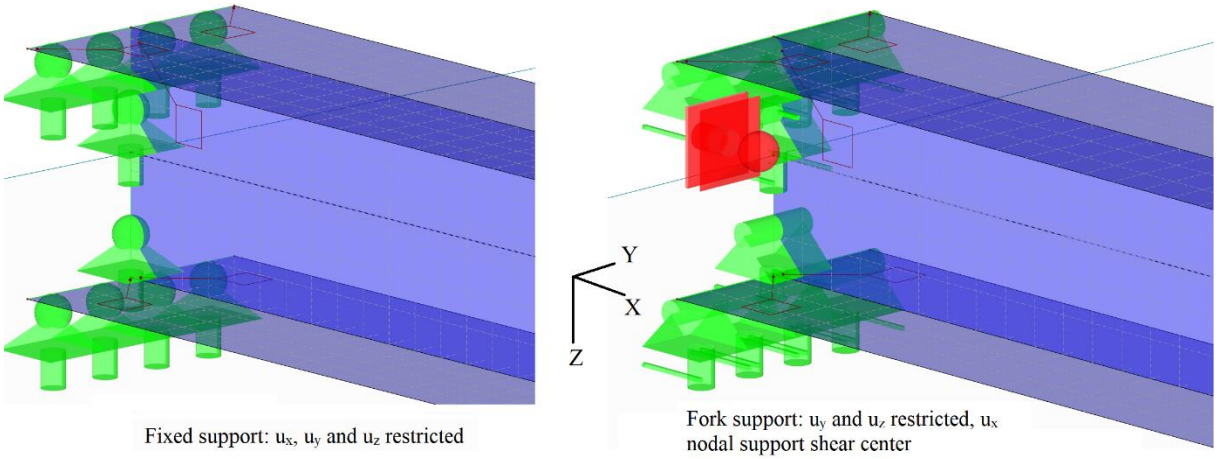

Figure 3.6 2D-model open profile: (left) fixed support and (right) fork support

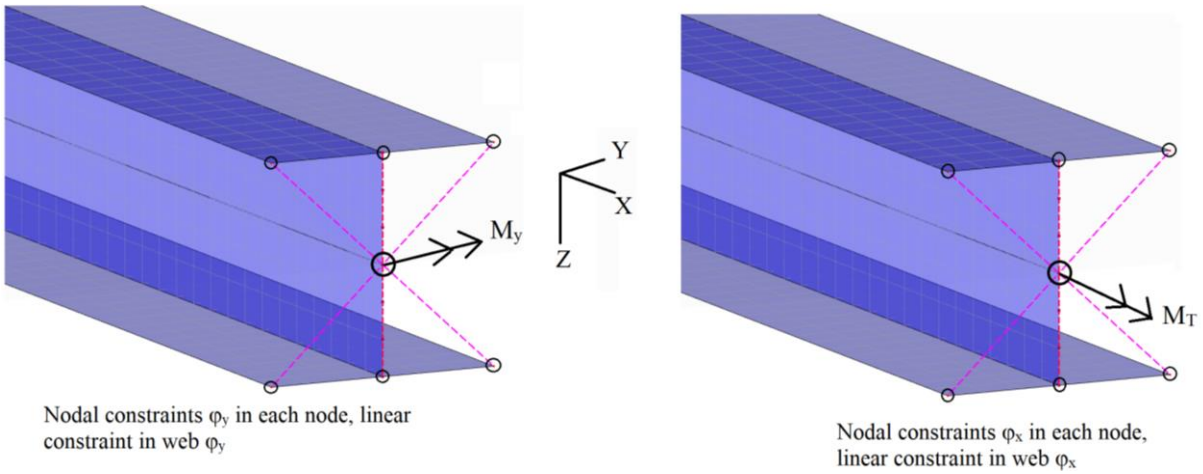

Figure 3.7 2D-model open profile nodal and linear constraints: (left) My and (right) M_T

Finally, for calculation of stresses in the cross-section the material properties of steel S355 shown in Table 3.4 are considered. The material was kept constant for all calculations as only geometrical nonlinear analysis is contemplated in this study. Furthermore, this same material is used for the class verification with each c/t ratio in members subjected to bending.

Table 3.4 Steel material properties considered

Steel	E (kN/cm²)	G (kN/cm²)	ν (-)	γ (kN/m³)	f_y (kN/cm²)	f_u (kN/cm²)
S355	21000	8077	0.3	78.5	35.5	49.9

3.2.2 Benchmark problems

Some test examples are developed to study the efficiency and convergence of the numerical models as well as the selected FE mesh refinement. Both 1D-beam and 2D-shell elements subjected to the three load cases of bending and torsion (V_z, M_y, and M_T) are considered.

Consider the cantilever steel I-beam built-up by 3 plates (IPE300) subjected to V_z, M_y, and M_T at the free end as shown in Figure 3.3 (a). An elastic analysis is performed individually for each external action and results are obtained at the free end of the beam. In the case of V_z and M_y, the vertical displacement u_z is obtained and for M_T the torsional rotation φ_x is extracted. The results from 1D-beam, 2D-shell elements and the analytical solutions are compared.

The results for V_z (1 kN), M_y (1 kNm) and M_T (0.1 kNm) acting at the tip are presented in Figure 3.8, Figure 3.9, and Figure 3.10 respectively. It is observed that the results show good agreement considering the type of finite element and also with the analytical solutions. A reliable convergence of the numerical models is obtained, which shows that an adequate FE mesh refinement has been selected.

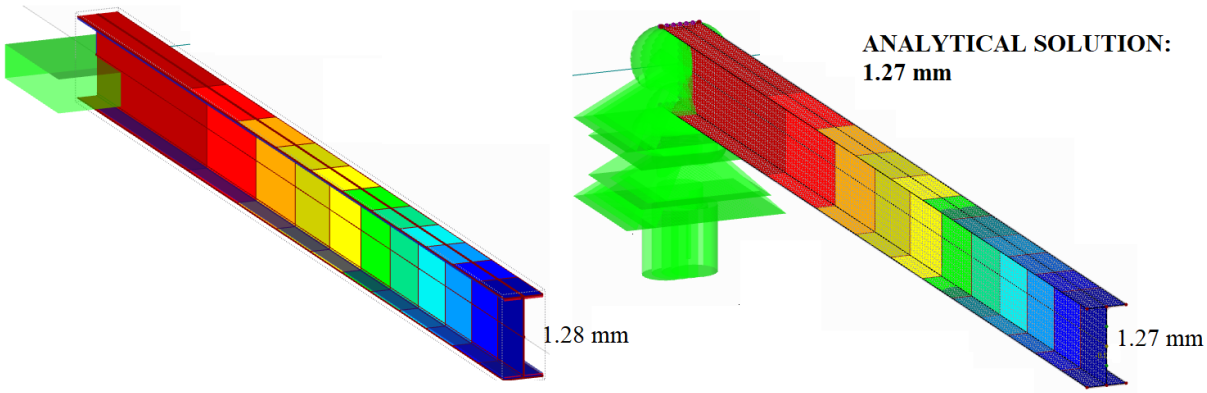

Figure 3.8 Cantilever beam vertical displacement u_z at the tip under vertical load V_z: (Left) 1D-beam elements and (Right) 2D-shell elements

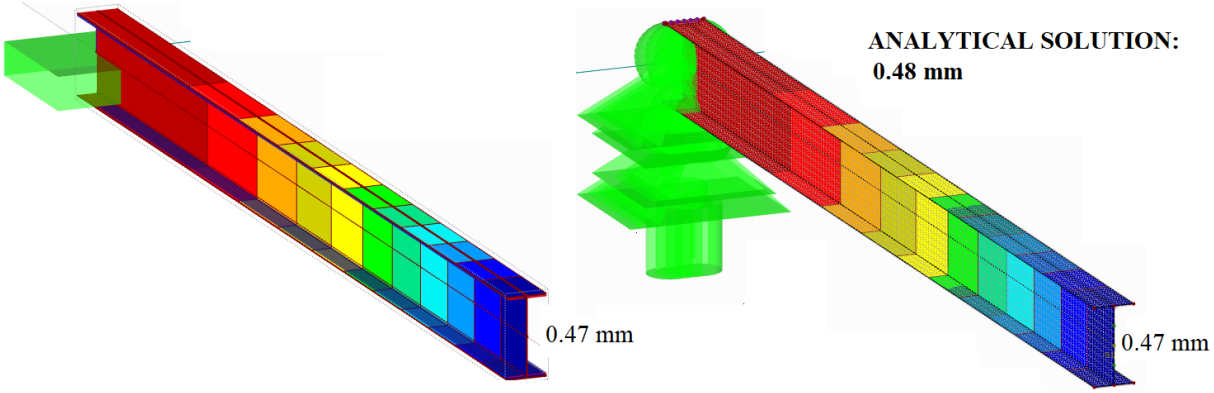

Figure 3.9 Cantilever beam vertical displacement u_z at the tip under bending moment M_y: (Left) 1D-beam elements and (Right) 2D-shell elements

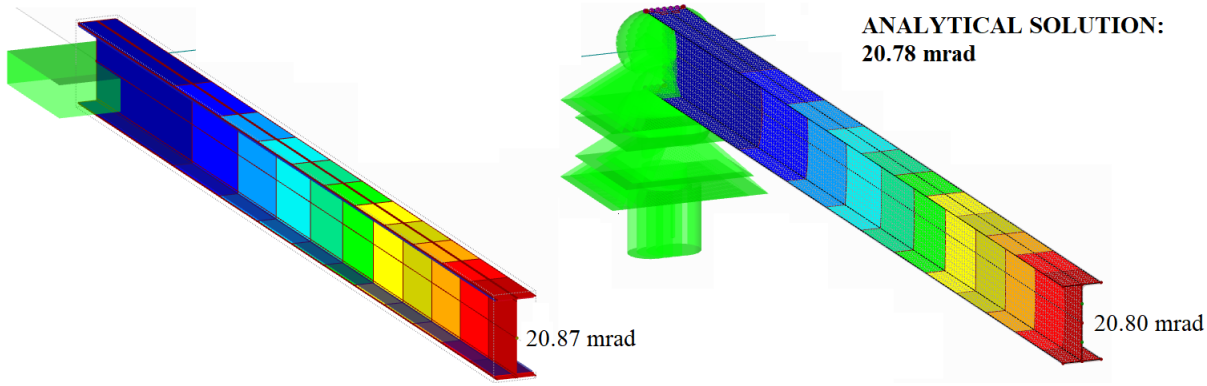

Figure 3.10 Cantilever beam torsional rotation φ_x at the tip under torsional moment M_T: (Left) 1D-beam elements and (Right) 2D-shell elements

3.3 Simulations and measurements

3.3.1 Critical loads

The simulations are performed in an incrementally manner with load factors corresponding to a percentage of the critical loads ($V_{z,cr}$, $M_{y,cr}$, $M_{T,cr}$) as presented in Table 3.5. In RFEM, it is possible to calculate the critical load factors for each individual system and load case. The factors correspond to the first positive value of α_{cr} calculated following Eq. 3.2.

$$det\left(K - \alpha_{cr} \cdot \underline{G}\right) = 0 \qquad \textit{Eq. 3.2}$$

Where:

K = stiffness matrix
α_{cr} = critical load factor
$\underline{G}$ = geometrical stiffness matrix

Table 3.5 Load factors for nonlinear simulations

Load Case	Load factor α_{cr} (%)										
V_z	0	10	20	30	40	50	60	70	80	90	100
M_y	0	10	20	30	40	50	60	70	80	90	100
M_T	0	10	20	30	40	50	60	70	80	90	100

The final critical load that is used in the SOT and GNA corresponds to the lowest value of the three criteria described below:

- The first load corresponds to the critical load calculated from the software RFEM module RF-FE-LTB, which is based on Eq. 3.2.
- The second value is defined as the maximum load that the 1D-beam and 2D-shell structural systems can support without obtaining any local instabilities or lack of convergence.
- The third limiting value is the maximum load that the cross-section can withstand in each structural system. The plastic capacity of the sections $V_{z,pl}$, $M_{y,pl}$ and $M_{T,pl}$ are of importance. Furthermore, a conservative linear approach is assumed in the case of combined effects of V_z and M_y.

Table 3.6 Final critical loads closed profiles

Section Hollow	Cantilever			Fork-fork			Fixed-fixed			Fork-fixed		
	$V_{z,cr}$ (kN)	**$M_{y,cr}$ (kNm)**	**$M_{T,cr}$ (kNm)**	**$V_{z,cr}$ (kN)**	**$M_{y,cr}$ (kNm)**	**$M_{T,cr}$ (kNm)**	**$V_{z,cr}$ (kN)**	**$M_{y,cr}$ (kNm)**	**$M_{T,cr}$ (kNm)**	**$V_{z,cr}$ (kN)**	**$M_{y,cr}$ (kNm)**	**$M_{T,cr}$ (kNm)**
200x200x6	27.56	116.99	92.41	104.21	208.42	184.83	187.90	197.63	184.83	127.36	185.26	184.83
100x50x6	4.09	16.67	10.02	16.09	32.18	20.04	31.10	31.63	20.04	20.85	28.61	20.04
200x100x8	23.10	95.93	57.25	89.14	178.27	114.50	166.49	172.18	114.50	112.23	158.46	114.50
300x100x6	34.76	146.06	67.82	132.67	265.33	135.64	243.04	253.69	135.64	164.33	235.85	135.64
300x150x6	41.77	177.34	103.97	157.97	315.94	207.95	284.83	299.58	207.95	193.05	280.84	207.95

Table 3.7 Final critical loads open profiles

Section 3-Plate	Cantilever			Fork-fork			Fixed-fixed			Fork-fixed		
	$V_{z,cr}$ (kN)	$M_{y,cr}$ (kNm)	$M_{T,cr}$ (kNm)	$V_{z,cr}$ (kN)	$M_{y,cr}$ (kNm)	$M_{T,cr}$ (kNm)	$V_{z,cr}$ (kN)	$M_{y,cr}$ (kNm)	$M_{T,cr}$ (kNm)	$V_{z,cr}$ (kN)	$M_{y,cr}$ (kNm)	$M_{T,cr}$ (kNm)
IPE80	0.28	0.44	0.04	2.85	5.06	0.24	9.00	6.25	0.29	5.82	6.49	0.31
IPE100	0.57	1.14	0.04	4.99	9.59	0.33	16.50	11.77	0.65	10.42	12.32	0.41
IPE120	0.99	1.88	0.12	8.37	17.27	0.43	28.52	21.14	0.87	17.89	22.36	0.91
IPE140	2.03	2.94	0.16	13.31	29.24	1.12	40.73	41.01	1.12	27.54	34.09	1.20
IPE160	3.11	4.30	0.18	19.92	46.25	1.39	55.10	57.77	2.78	37.31	53.97	1.53
IPE180	5.64	6.22	0.50	29.48	61.25	1.73	72.76	76.68	3.47	49.35	72.03	3.93
IPE200	8.11	8.58	0.54	41.73	89.97	2.10	92.67	98.08	4.20	62.94	92.59	4.93
IPE220	11.98	12.21	1.24	60.95	134.28	5.26	118.03	125.63	5.26	80.30	119.36	9.58
IPE240	16.96	12.50	1.37	83.97	167.94	9.63	146.05	156.23	16.05	99.53	149.28	12.10
IPE270	25.67	17.85	1.44	109.47	218.94	11.90	188.40	202.52	19.84	128.59	194.61	15.87
IPE300	38.41	25.33	3.16	140.35	280.70	14.93	239.28	258.34	24.88	163.54	249.51	28.01
IPE330	48.12	26.46	3.66	174.66	349.32	18.52	294.77	319.73	30.87	201.76	310.50	53.79
IPE360	60.92	31.46	4.53	219.34	438.67	23.99	365.59	398.81	39.98	250.69	389.93	67.05
IPE400	76.06	41.46	5.24	272.69	545.38	80.09	451.70	494.14	49.67	310.01	484.78	80.09
IPE450	97.54	46.94	6.36	348.27	696.54	96.85	573.39	628.99	64.23	393.86	619.15	96.85
IPE500	124.32	51.37	7.91	441.21	882.42	117.92	720.06	793.01	117.92	495.23	784.37	117.92
IPE550	154.05	67.91	23.99	544.68	1089.4	140.28	884.10	976.05	140.28	608.51	968.32	140.28
IPE600	192.72	92.13	30.35	676.56	1353.1	170.41	1087.1	1205.6	170.41	749.27	1202.8	170.41
HEB100	3.36	7.88	0.41	27.74	55.48	3.08	48.62	51.82	6.16	33.10	49.31	3.22
HEB120	8.74	13.83	1.48	43.11	86.22	4.15	74.00	79.64	8.30	50.53	76.64	8.82
HEB140	15.12	25.13	1.77	62.65	125.30	5.43	105.45	114.52	10.87	72.21	111.38	11.86
HEB160	24.41	39.31	4.10	87.86	175.72	21.20	146.44	159.75	35.33	100.42	156.20	15.98
HEB180	32.90	58.44	9.19	117.04	234.09	26.72	191.72	210.79	44.53	131.79	208.08	31.47
HEB200	43.00	84.09	10.24	151.26	302.52	33.31	243.74	269.96	55.51	167.93	268.91	54.52
HEB220	54.82	106.00	11.40	190.72	381.43	68.58	302.60	337.48	68.58	208.93	339.05	105.10
HEB240	68.45	145.17	12.71	235.59	471.19	84.07	368.40	413.51	84.07	254.87	418.83	133.54
HEB260	81.54	123.58	32.63	277.14	554.28	96.91	426.21	481.88	96.91	295.52	492.70	160.46
HEB280	96.73	130.76	34.41	326.75	653.49	113.06	498.42	565.52	113.06	345.96	580.88	193.64
HEB300	115.66	137.15	39.01	386.90	773.79	136.65	582.90	664.91	136.65	405.26	687.82	239.13
HEB400	195.10	223.65	61.63	650.17	1300.3	389.09	974.93	1114.4	389.09	678.24	1155.9	389.09
HEB500	281.73	233.57	81.23	928.66	1857.3	455.58	1373.9	1579.4	455.58	957.45	1650.9	455.58
HEB550	322.77	257.49	172.16	1064.0	2128.1	473.10	1574.3	1809.8	473.10	1097.1	1891.6	473.10
HEB600	366.03	282.71	183.12	1206.7	2413.3	490.76	1785.4	2052.4	490.76	1244.2	2145.2	490.76
HEB650	411.52	309.22	195.20	1356.6	2713.2	508.58	2007.1	2307.3	508.58	1398.7	2411.7	508.58
HEB700	462.44	338.18	210.49	1530.4	3060.8	527.51	2275.2	2610.2	527.51	1584.6	2720.7	527.51
HEB800	549.74	381.04	225.76	1819.1	3638.2	547.12	2704.0	3102.3	547.12	1883.3	3234.0	547.12
HEB900	659.51	444.43	258.31	2181.0	4362.0	584.34	3239.5	3717.8	584.34	2256.4	3877.3	584.34
HEB1000	758.69	493.80	279.47	2508.2	5016.4	604.83	3724.1	4274.7	604.83	2594.1	4459.0	604.83

The resulting critical loads are presented in Table 3.6 and Table 3.7 for closed and open profiles respectively. In the case of closed profiles, all final critical loads correspond to the maximum load (see Appendix I). However, that is not the case for open profiles, which present lower values. This means that open profiles have weaker stability behavior in comparison to closed profiles.

3.3.1.1 Cross-section capacity

The cross-section capacity of the profiles is defined as their plastic resistance of the corresponding load case. This consideration is satisfied based on the cross-section class of members subjected to bending, which is 1 for all profiles used in this study (see Appendix I).

The plastic capacity of each cross-section has been calculated following [29] for both open and closed profiles. Regarding the torsional plastic capacity of built-up members (3-plate open sections), as a conservative approach, primary torsion is neglected and only torsional warping is considered. The warping resistance $M_{w,Rd}$ used for verification is considered as approximately half of the plastic bending moment around the weak axis $M_{z,pl}$ [10].

Regarding the structural system, the maximum values for each external load are calculated assuming an elastic global analysis. Internal forces V_z, M_y, and M_T are calculated in the most unfavorable location where the maximum combined effect occurs. Finally, the maximum capacity is obtained by solving the plastic interaction criterion as given in Eq. 3.3:

$$\frac{V_{z,max}}{V_{z,pl}} + \frac{M_{y,max}}{M_{y,pl}} + \frac{M_{T,max}}{M_{T,pl}} = 1 \qquad \textit{Eq. 3.3}$$

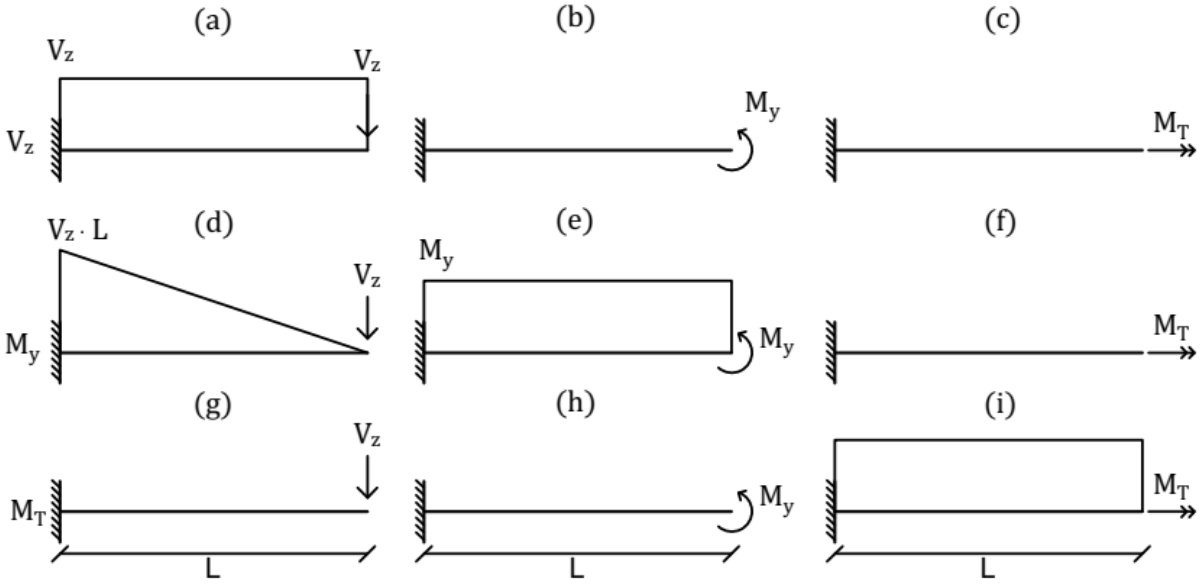

Figure 3.11 Fixed-free cantilever beam, shear diagram due to: (a) V_z, (b) M_y, (c) M_T, bending moment diagram: (d) V_z, (e) M_y, (f) M_T, and torsion diagram: (g) V_z, (h) M_y, (i) M_T

For better understanding, consider the cantilever beam in Figure 3.11. The beam is subjected to 3 types of external actions, V_z, M_y, and M_T and for each one the shear, bending moment, and torsional moment diagrams are obtained. Following Eq. 3.3 the maximum load can be obtained for each external action. Eq. 3.5 comes from solving Eq. 3.4 for $V_{z,max}$, which is the result of replacing the maximum shear and bending moment values that occur at the fixed support. In a similar way, Eq. 3.6 for $M_{y,max}$ and Eq. 3.7 for $M_{T,max}$ are obtained.

$$\frac{V_{z,max}}{V_{z,pl}} + \frac{V_{z,max} \cdot L}{M_{y,pl}} + \frac{0}{M_{T,pl}} = 1 \qquad \textit{Eq. 3.4}$$

$$V_{z,max} = \frac{1}{\frac{1}{V_{z,pl}} + \frac{L}{M_{y,pl}}} \qquad \textit{Eq. 3.5}$$

$$M_{y,max} = M_{y,pl} \qquad \textit{Eq. 3.6}$$

$$M_{T,max} = M_{T,pl} \qquad \textit{Eq. 3.7}$$

For the complete equations and tables of maximum loads for each structural system and cross-section refer to Appendix I.

3.3.2 Displacements

The location where displacements are extracted remained constant for all profiles, type of FE, external load, and type of analysis. The only variation is due to the structural system. This is shown in Figure 3.12, where the circle shows the position of the extracted displacement. This point was chosen in order to obtain the highest values of displacement D. For the cantilever beam the point is located at the free end and for all other systems it is located at midspan. In addition, all displacements are taken from the center of gravity of the cross section, which also corresponds to the point of application of the external loads.

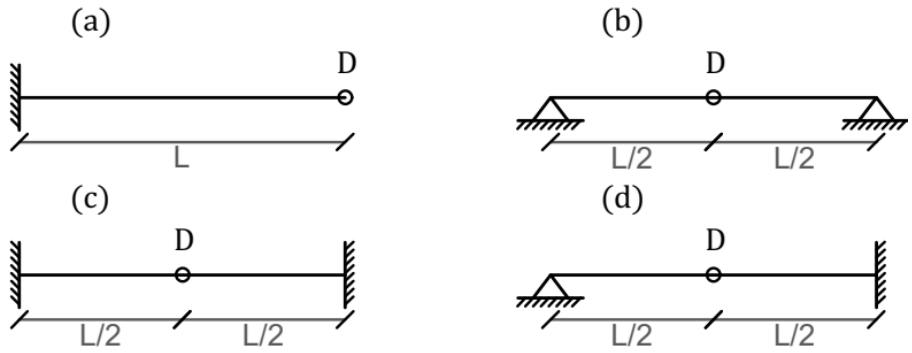

Figure 3.12 Location of extracted displacements for each structural system: (a) fixed-free, (b) fork-fork, (c) fixed-fixed, and (d) fork-fixed

Table 3.8 Main displacements measurements

External load	**V_z**		**M_y**		**M_T**	
Type of finite element	1D	2D	1D	2D	1D	2D
Main displacements Open	u_z, φ_x, φ_y	u_z, φ_y	u_z, φ_x, φ_y	u_z, φ_y	φ_x, Ω	φ_x
Main displacements Closed	u_z, φ_y	u_z, φ_y	u_z, φ_y	u_z, φ_y	φ_x	φ_x

In Table 3.8, the main displacements, considered for analysis of the results, are presented. These displacements are considered relevant for the corresponding external loads. As only torsional and bending effects are considered, axial displacement u_x, lateral displacement u_y, and rotation around the weak axis φ_z are neglected in the analysis of the results. Moreover, 2D-shell elements and closed profiles give almost no torsional rotation when subjected to bending, therefore φ_x is neglected for V_z and M_y.

3.3.3 Internal forces

For the extraction of internal forces, different locations have been selected depending only on the structural system as shown in Figure 3.13. The circle shows the position of the extracted internal forces F_L corresponds to the left support, F_m to the midspan, and F_R to the right support. These point were selected in order to obtain the highest values of forces. For the cantilever beam, the point corresponds only to the fixed support. For the fork-fork and fixed-fixed systems, both midspan and the left support are considered, the right support is neglected due to symmetry. Finally, in the fork-fixed system all three locations have been taken.

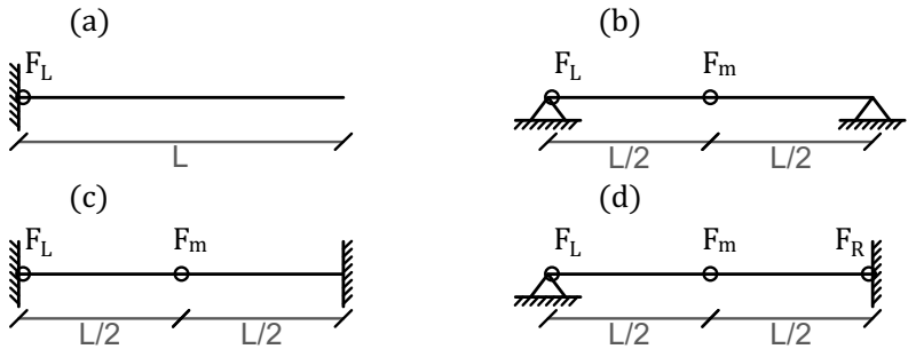

Figure 3.13 Location of extracted internal forces for each structural system: (a) fixed-free, (b) fork-fork, (c) fixed-fixed, and (d) fork-fixed

Only 1D-beam elements are considered in the analysis of internal forces due to the software output. The main internal forces corresponding to each external load are shown in Table 3.9. Only the relevant forces for bending and torsional actions have been selected. Therefore, N, V_y, and M_z are not considered. In the case of closed sections that were modelled with 6 DOF, the internal forces do not account for primary and secondary torsion (M_p, M_s) as well as the warping bimoment M_w.

Table 3.9 Main internal forces measurements

External load	V_z	M_y	M_T
Main internal forces Open	V_z, M_y	V_z, M_y	M_T, M_w
Main internal forces Closed	V_z, M_y	V_z, M_y	M_T

3.3.4 Stresses

The equivalent stresses (von Mises) for 1D open profiles haven been extracted from the GNA simulations in the RF-FE-LTB module. The location of maximum values of stress corresponds to the same as of internal forces from Figure 3.13. Within the cross-section, the highest stressed point corresponds to the corners of the I-beam flanges. The von Mises equivalent stress is determined from the normal and shear stresses as shown in Eq. 3.8.

$$\sigma_{eqvi} = \sqrt{\sigma_x^2 + 3 \cdot \tau^2} \qquad \textit{Eq. 3.8}$$

Where:

σ_{eqvi} = von Mises equivalent stress
σ_x = total normal stress
τ = total shear stress (includes primary and secondary shear)

With the equivalent stress the elastic ratio e_r can be calculated using Eq. 3.9. The yielding strength f_y of steel S355 is kept constant for all simulations and load levels. Hence, it can be observed whether or not the cross-section remains fully elastic (e_r lower than 1).

$$e_r = \frac{\sigma_{eqvi}}{f_y} \qquad \textit{Eq. 3.9}$$

3.3.5 Results and comparison

The displacements and internal forces obtained from the numerical simulations are compared between them. Different schemes have been defined in order to do so. First, the relative error between GNA and SOT for each load level has been calculated. This was done using absolute values and fixing the difference to the results of GNA as shown in Eq. 3.10. This means that if the r_{error} is positive then GNA values are higher, and if negative then SOT values are higher.

$$r_{error}(\%) = \frac{(abs(d, f_{GNA}) - abs(d, f_{SOT}))}{abs(d, f_{GNA})} \cdot 100 \qquad \textit{Eq. 3.10}$$

Where:

r_{error} = relative error in percentage
d,f_{GNA} = results of displacements or internal forces for GNA
d,f_{SOT} = results of displacements or internal forces for SOT

In order to establish a limit for deformation, a relative error threshold has been defined. The threshold where SOT remains accurate enough to GNA is considered as 5% in this study.

In the case of displacements, several comparisons were performed in order to study the influence of each parameter, such as the external load, structural system, type of FE, cross-section (open or closed), and the torsional bending constant a. The comparisons are summarized in Table 3.10.

Table 3.10 Comparison of displacement results GNA and SOT

Comparison	System	Load	Profile	FE
1	Fixed-free	V_z M_y M_T	Open (38)	1D
2				2D
3			Closed (5)	1D
4				2D
5	Fork-fork	V_z M_y M_T	Open (38)	1D
6				2D
7			Closed (5)	1D
8				2D
9	Fixed-fixed	V_z M_y M_T	Open (38)	1D
10				2D
11			Closed (5)	1D
12				2D
13	Fork-fixed	V_z M_y M_T	Open (38)	1D
14				2D
15			Closed (5)	1D
16				2D

Furthermore, according to Eurocode 8 considering seismic actions, a limit reference for large displacements can be taken from 1.25 up to 1.875% of the element's length. The story drift limits the damage to the nonstructural elements and also limits the P-Δ effects on columns [30]. At ultimate limit state the combination of all actions can reach the critical loads of the elements and, therefore, instabilities might occur. Although this large displacement limit is defined for vertical elements (columns), which are more critical for stability, for horizontal ones (beams) it might prove as a reference for comparison.

Considering the length of 4 m used in all structural models and the limit of 1.25% drift, the displacement limit for this study is taken as 5 cm. Regarding the rotation angle of elements, the limit of 0.3 rad (17.2º) as suggested in [4] is considered for comparison.

Another aspect to have in mind is the serviceability limit state, which considers the vertical deflection limits which are presented in different national annexes of Eurocode. For instance the Portugal annex gives values of total deflection (dead plus imposed loads) as shown in Table 3.11.

Table 3.11 Total vertical deflection limits [2]

Member location	Deflection limit	Drift (%)	Deflection limit (cm) L = 4 m
Roofs in general	L/200	0.50	2.00
Floors in general	L/250	0.40	1.60
Floors that bear columns	L/400	0.25	1.00

With regard to internal forces, the comparisons are summarized in Table 3.12. In a similar way as for displacements the influence of the same parameters is studied with the exception of the type of FE, which is only done for 1D-beam elements.

Table 3.12 Comparison of internal forces results GNA and SOT

Comparison	Load	System	Profile
1	V_z, M_y, M_T	Fixed-free	Open (38)
2			Closed (5)
3	V_z, M_y, M_T	Fork-fork	Open (38)
4			Closed (5)
5	V_z, M_y, M_T	Fixed-fixed	Open (38)
6			Closed (5)
7	V_z, M_y, M_T	Fork-fixed	Open (38)
8			Closed (5)

Regarding stresses, the elastic ratio e_r is compared for both SOT and GNA. It is done for visualizing how elastic the cross-section remains. Furthermore, the individual influence of the external load, structural system, and torsional bending constant *a* are reviewed.

3.3.5.1 Fitting curves

Fitting curves are determined by using the displacement results of open profiles with 1D-beam elements. The curves are a practical way to check whether SOT or GNA should be used by limiting the relative error. The information needed for establishing the type of analysis are the load factor LF and the torsional bending constant *a* which has to be divided by the length of the system *a*/L. For ease of use, the fitting curves are prepared as contour figures where the different color levels represent the magnitude of the r_{error}.

Furthermore, the fitting curves are prepared by means of triangle surface linear interpolation of the results between sets of three points in a 3D-scatter [31]. The 3D-scatter includes three parameters: the torsional bending constant divided by the length *a/L*, the load factor LF, and the relative error r_{error}. The surface linear interpolation also results in r^2 value of 1 and sum of estimated errors of zero.

Finally, a deformation limit has not been considered because the variation of results strongly depends on the cross-section and the load level, but not in the displacement values themselves.

Chapter 4: Results and Discussion

The analysis and discussion of results is offered in this chapter. Findings regarding critical loads and the results of displacements, internal forces and stresses are described and supported. Furthermore, the stage of deformation where SOT is valid for describing GNA is discussed. Ultimately, fitting curves for establishing the use of SOT instead of GNA are presented.

4.1 Modelling output

4.1.1 Critical loads

In general, some patterns have been found during the numerical simulations. For instance, 1D elements have a higher critical load in contrast to 2D elements. This can be due to the effect of local buckling which is not considered in 1D elements. An example of it is shown in Figure 4.1, the built-up HEB1000 cross-section shows the start of web buckling when subjected to pure bending around its strong axis.

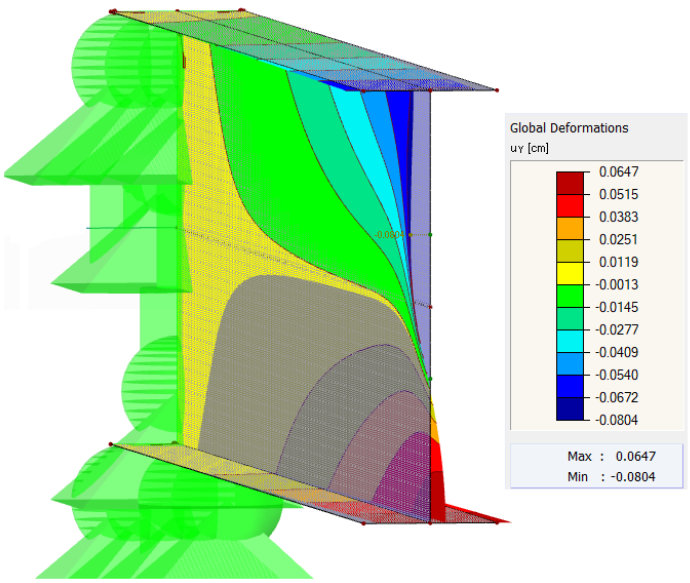

Figure 4.1 Pure bending M_y effect on open 2D-shell elements

Another remark is the influence of the cross-section profile. Normally, closed sections show an adequate behavior for both torsion and bending effects, which is why the critical load corresponds to the plastic capacity of the section (see Appendix I).

Between open profiles (built up IPE and HEB) on the other hand, IPE profiles show weaker behavior (stability) for both torsion and bending around the strong axis. The vice versa effect occurs for HEB profiles. In addition, the smaller the torsional bending constant *a* is the weaker their behavior is for both torsion and bending. This is supported in Table 4.1, where the relative critical loads (ratio of critical load vs plastic capacity) are given.

Table 4.1 Relative critical loads for open profiles

Section 3-Plate	a (cm)	FIXED-FREE			FORK-FORK			FIXED-FIXED			FORK-FIXED		
		$V_{z,cr}$ (kN)	$M_{y,cr}$ (kNm)	$M_{x,cr}$ (kNm)	$V_{z,cr}$ (kN)	$M_{y,cr}$ (kNm)	$M_{x,cr}$ (kNm)	$V_{z,cr}$ (kN)	$M_{y,cr}$ (kNm)	$M_{x,cr}$ (kNm)	$V_{z,cr}$ (kN)	$M_{y,cr}$ (kNm)	$M_{x,cr}$ (kNm)
IPE80	23.2	0.18	0.07	0.04	0.46	0.41	0.12	0.77	0.52	0.14	0.74	0.59	0.15
IPE100	31.9	0.22	0.11	0.02	0.50	0.48	0.10	0.88	0.61	0.20	0.82	0.69	0.13
IPE120	40.8	0.25	0.11	0.05	0.54	0.56	0.09	1.00	0.71	0.18	0.93	0.82	0.19
IPE140	50.0	0.35	0.12	0.05	0.60	0.66	0.17	1.00	0.96	0.17	1.00	0.86	0.18
IPE160	60.1	0.39	0.13	0.04	0.66	0.76	0.15	1.00	1.00	0.30	1.00	1.00	0.17
IPE180	69.9	0.52	0.14	0.08	0.73	0.76	0.14	1.00	1.00	0.28	1.00	1.00	0.32
IPE200	80.5	0.58	0.14	0.07	0.80	0.86	0.13	1.00	1.00	0.27	1.00	1.00	0.32
IPE220	90.8	0.66	0.16	0.12	0.91	1.00	0.26	1.00	1.00	0.26	1.00	1.00	0.47
IPE240	101.9	0.75	0.13	0.11	1.00	1.00	0.37	1.00	1.00	0.62	1.00	1.00	0.47
IPE270	123.5	0.86	0.14	0.08	1.00	1.00	0.35	1.00	1.00	0.58	1.00	1.00	0.47
IPE300	144.4	1.00	0.15	0.14	1.00	1.00	0.34	1.00	1.00	0.57	1.00	1.00	0.64
IPE330	158.1	1.00	0.12	0.14	1.00	1.00	0.34	1.00	1.00	0.57	1.00	1.00	1.00
IPE360	167.3	1.00	0.11	0.14	1.00	1.00	0.36	1.00	1.00	0.60	1.00	1.00	1.00
IPE400	183.8	1.00	0.12	0.13	1.00	1.00	1.00	1.00	1.00	0.62	1.00	1.00	1.00
IPE450	199.9	1.00	0.11	0.13	1.00	1.00	1.00	1.00	1.00	0.66	1.00	1.00	1.00
IPE500	212.8	1.00	0.09	0.13	1.00	1.00	1.00	1.00	1.00	1.00	1.00	1.00	1.00
IPE550	226.5	1.00	0.10	0.34	1.00	1.00	1.00	1.00	1.00	1.00	1.00	1.00	1.00
IPE600	234.9	1.00	0.10	0.36	1.00	1.00	1.00	1.00	1.00	1.00	1.00	1.00	1.00
HEB100	34.6	0.45	0.24	0.05	1.00	1.00	0.17	1.00	1.00	0.34	1.00	1.00	0.18
HEB120	45.8	0.74	0.27	0.10	1.00	1.00	0.15	1.00	1.00	0.29	1.00	1.00	0.31
HEB140	57.6	0.87	0.33	0.08	1.00	1.00	0.13	1.00	1.00	0.26	1.00	1.00	0.28
HEB160	69.3	1.00	0.36	0.14	1.00	1.00	0.35	1.00	1.00	0.59	1.00	1.00	0.27
HEB180	81.9	1.00	0.39	0.23	1.00	1.00	0.33	1.00	1.00	0.55	1.00	1.00	0.39
HEB200	94.8	1.00	0.42	0.19	1.00	1.00	0.31	1.00	1.00	0.52	1.00	1.00	0.51
HEB220	108.0	1.00	0.41	0.16	1.00	1.00	0.49	1.00	1.00	0.49	1.00	1.00	0.76
HEB240	121.3	1.00	0.44	0.14	1.00	1.00	0.48	1.00	1.00	0.48	1.00	1.00	0.76
HEB260	139.3	1.00	0.31	0.31	1.00	1.00	0.46	1.00	1.00	0.46	1.00	1.00	0.76
HEB280	157.2	1.00	0.28	0.27	1.00	1.00	0.45	1.00	1.00	0.45	1.00	1.00	0.77
HEB300	171.2	1.00	0.24	0.25	1.00	1.00	0.45	1.00	1.00	0.45	1.00	1.00	0.78
HEB400	179.7	1.00	0.23	0.32	1.00	1.00	1.00	1.00	1.00	1.00	1.00	1.00	1.00
HEB500	193.6	1.00	0.16	0.36	1.00	1.00	1.00	1.00	1.00	1.00	1.00	1.00	1.00
HEB550	205.3	1.00	0.16	0.73	1.00	1.00	1.00	1.00	1.00	1.00	1.00	1.00	1.00
HEB600	216.1	1.00	0.15	0.75	1.00	1.00	1.00	1.00	1.00	1.00	1.00	1.00	1.00
HEB650	226.0	1.00	0.15	0.77	1.00	1.00	1.00	1.00	1.00	1.00	1.00	1.00	1.00
HEB700	233.7	1.00	0.14	0.80	1.00	1.00	1.00	1.00	1.00	1.00	1.00	1.00	1.00
HEB800	257.6	1.00	0.14	0.83	1.00	1.00	1.00	1.00	1.00	1.00	1.00	1.00	1.00
HEB900	271.4	1.00	0.13	0.88	1.00	1.00	1.00	1.00	1.00	1.00	1.00	1.00	1.00
HEB1000	291.3	1.00	0.13	0.92	1.00	1.00	1.00	1.00	1.00	1.00	1.00	1.00	1.00

4.1.2 Displacements

In this section, displacement results (see Table 3.8) are analyzed and compared as presented in Table 3.10. For this purpose, 2 types of figures have been prepared. The first one presents the relative error r_{error} related to the bending torsional constant *a* for every load level (0 to 100%). Similarly, the second type shows the magnitude of displacement related to *a* for every load level. Moreover, the displacement thresholds for u_z and φ_x are considered as introduced in section 3.3.5. In addition, the figures named "1D" represent the comparison between GNA and SOT for beam elements, while the figures named "2D" represent the comparison between GNA and SOT of shell elements. Only the most relevant figures are presented here. The complete set of figures can be found in Appendix II.

In general, findings show that when the displacement increases, the variation of results (r_{error}) increases too. This variation is consistent with the increment in the load factor as well.

4.1.2.1 Fixed-free system

For the fixed-free system under $\mathbf{V_z}$ action, the following observations have been made:

- **Open:** all displacements u_z, φ_x, and φ_y show almost no variation for both 1D and 2D elements with relative errors under 1%. The higher values of error correspond to the IPE profiles (see Figure 4.2 to Figure 4.4). Displacements are in agreement between 1D and 2D elements (u_z and φ_y). Moreover, u_z surpasses the threshold value of 5 cm for many IPE profiles (see Figure 4.5). For φ_x and φ_y the values remain below 0.3 rad.
- **Closed**: u_z and φ_y also show almost no variation for both 1D and 2D elements with relative errors under 0.35%. A higher peak is observed for the RHS profile with the lowest value of *a* (see Figure 4.6 and Figure 4.7). For closed profiles, it is found that the limit for u_z is surpassed in all profiles (see Figure 4.8).

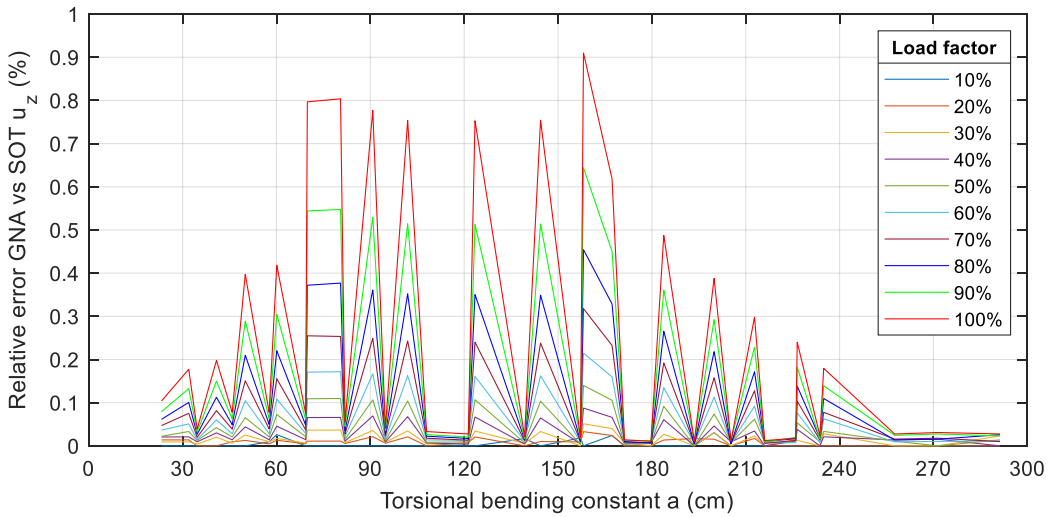

Figure 4.2 Relative error u_z: fixed-free system, V_z load, open profiles, and 1D elements

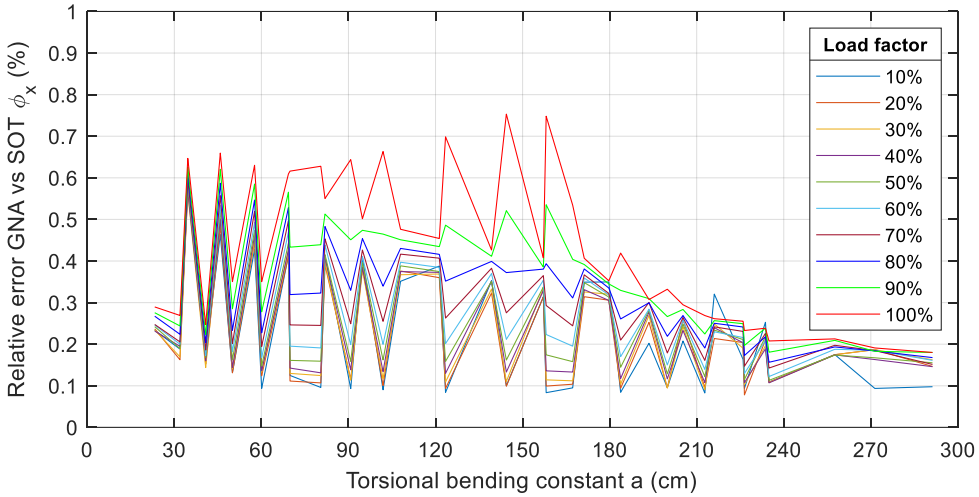

Figure 4.3 Relative error φ_x: fixed-free system, V_z load, open profiles, and 1D elements

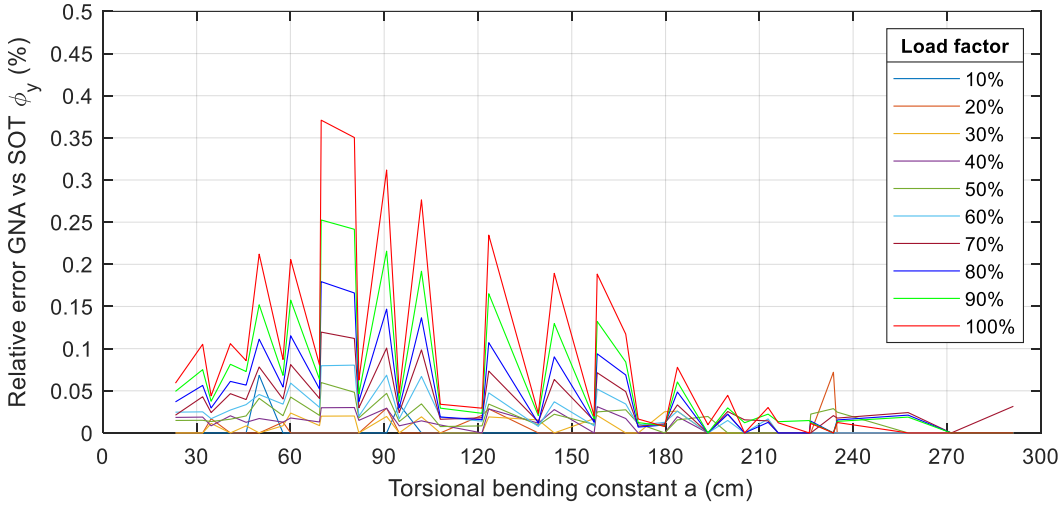

Figure 4.4 Relative error φ_y: fixed-free system, V_z load, open profiles, and 1D elements

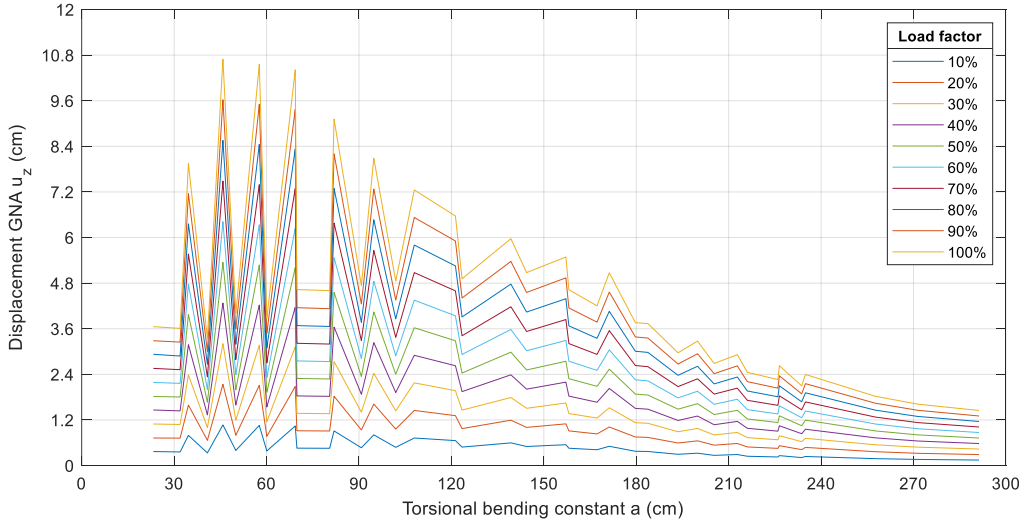

Figure 4.5 Displacement u_z: fixed-free system, V_z load, open profiles, and 1D elements

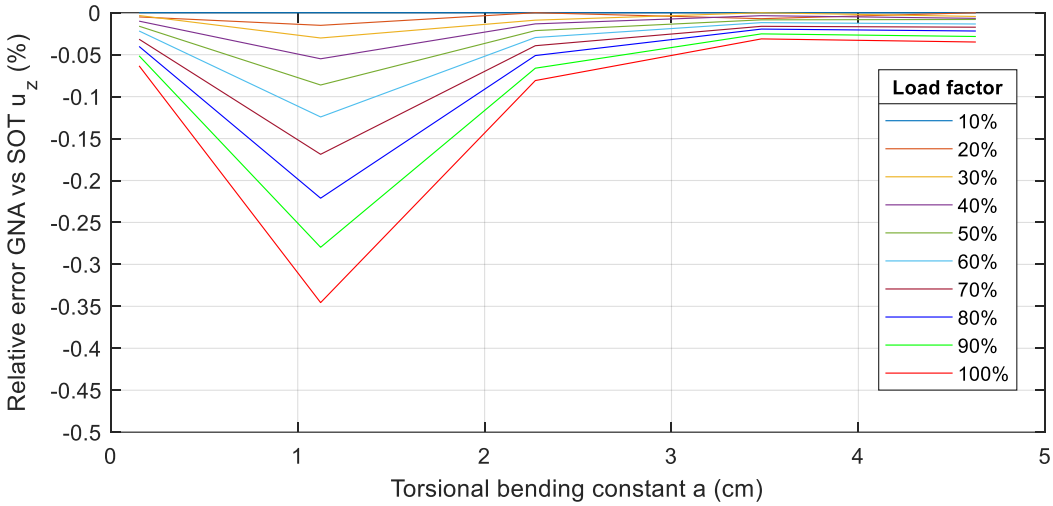

Figure 4.6 Relative error u_z: fixed-free system, V_z load, closed profiles, and 1D elements

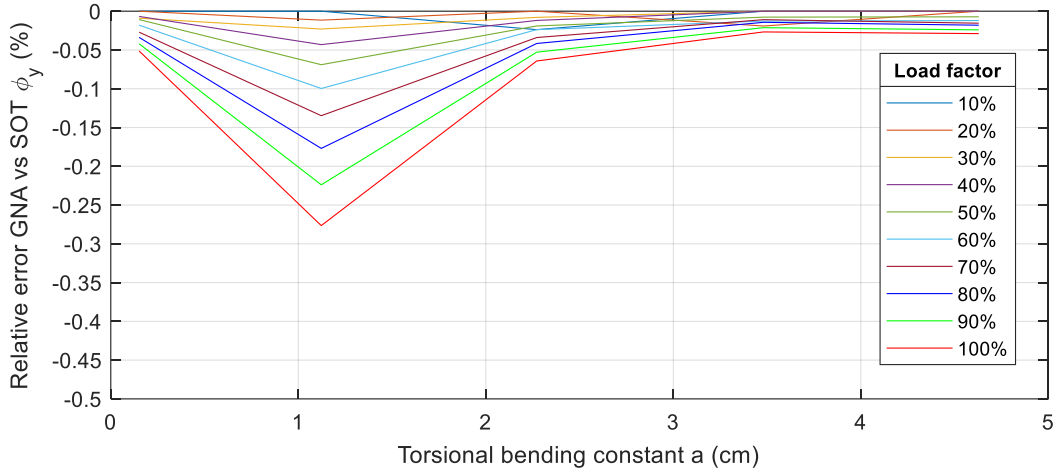

Figure 4.7 Relative error φ_y: fixed-free system, V_z load, closed profiles, and 1D elements

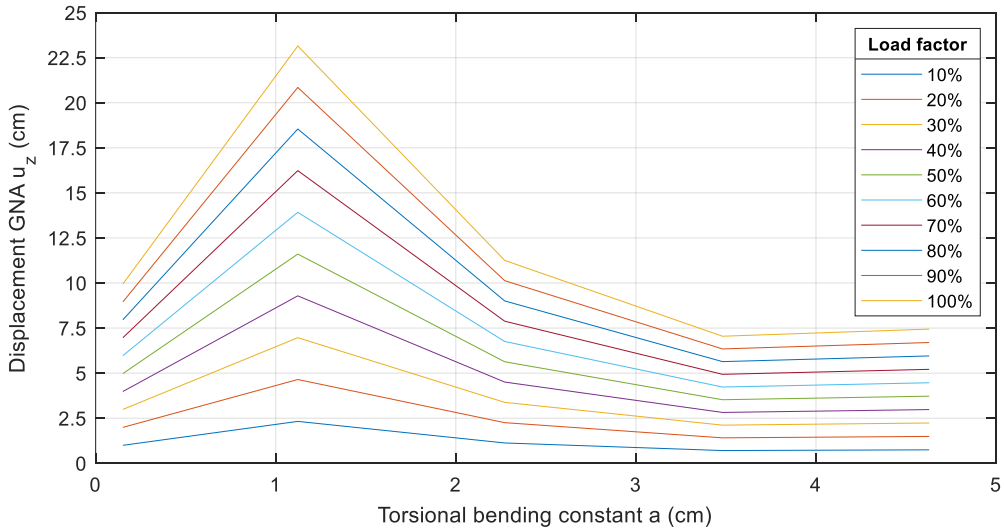

Figure 4.8 Displacement u_z: fixed-free system, V_z load, closed profiles, and 1D elements

In refer to **M_y** action, the following remarks have been found:

- **Open:** for 1D elements u_z and φ_y show low variation with relative errors under 2%. As in V_z case, the same trend is observed, where the peaks are higher for IPE profiles (see Figure 4.9 and Figure 4.10). Moreover, some IPE profiles have also surpassed the threshold as seen in Figure 4.11. The same trend is seen for φ_y, nevertheless, the values remain below 35 mrad (2º).
- **Open:** In the case of φ_x, high variation exists starting from a load factor of 0.4 the threshold is surpassed for many sections including both IPE and HEB profiles. Here SOT gives higher values (see Figure 4.12). Nevertheless, the magnitude of rotation remains below 40 mrad (2.29º) at a load factor of 1 as seen on Figure 4.13. For better visualization of the variation see Figure 4.14 where φ_x is plotted along the length of the beam for GNA and SOT for the 3 profiles with the highest rotation values at a load factor of 1. One possible explanation for this behavior is that imperfections in SOT of members subjected to bending result in an initial deformed shape that is closer to the lateral torsional buckling shape. At this stage of deformation, SOT has a higher influence in rotation φ_x as in comparison to GNA.
- **Open:** for 2D elements u_z and φ_y show high variation (up to almost 150%), in general SOT returns higher values. The variation is observed in all load levels, however, even for lower load levels higher errors are visible for some profiles (120cm>*a*>60cm) (see Figure 4.15 and Figure 4.16). Moreover, considerable variation exists for the magnitude of u_z and φ_y, lower and higher values as in contrast to 1D elements (see Figure 4.17). This suggests that there is not a good agreement of results for GNA and SOT for M_y in 2D elements the way they are modelled.
- **Closed:** u_z and φ_y show almost no variation for both 1D and 2D elements with relative errors under 2%. A high peak is observed again for the RHS profile with the lowest value of *a*. It is found again that the limit for u_z is surpassed in all profiles. The magnitudes of displacement remain close for 1D and 2D elements.

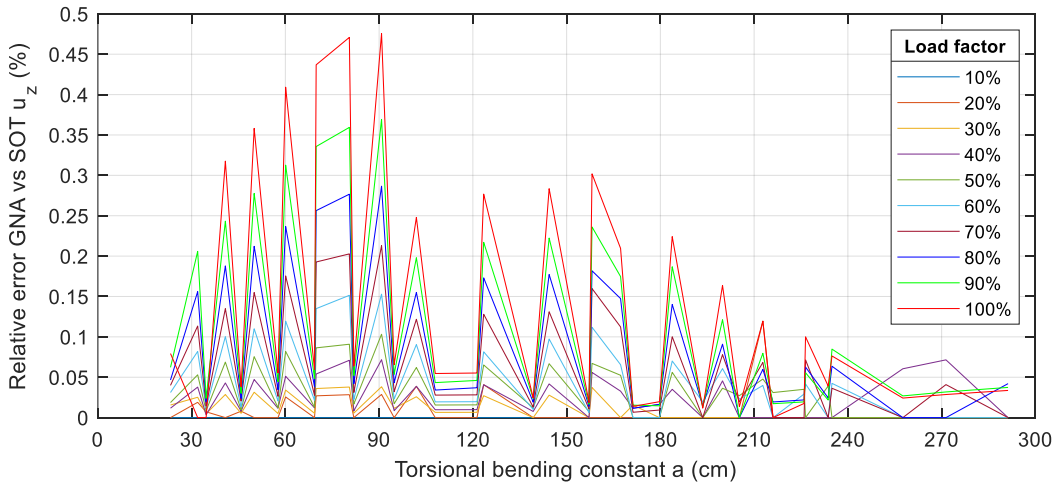

Figure 4.9 Relative error u_z: fixed-free system, M_y load, open profiles, and 1D elements

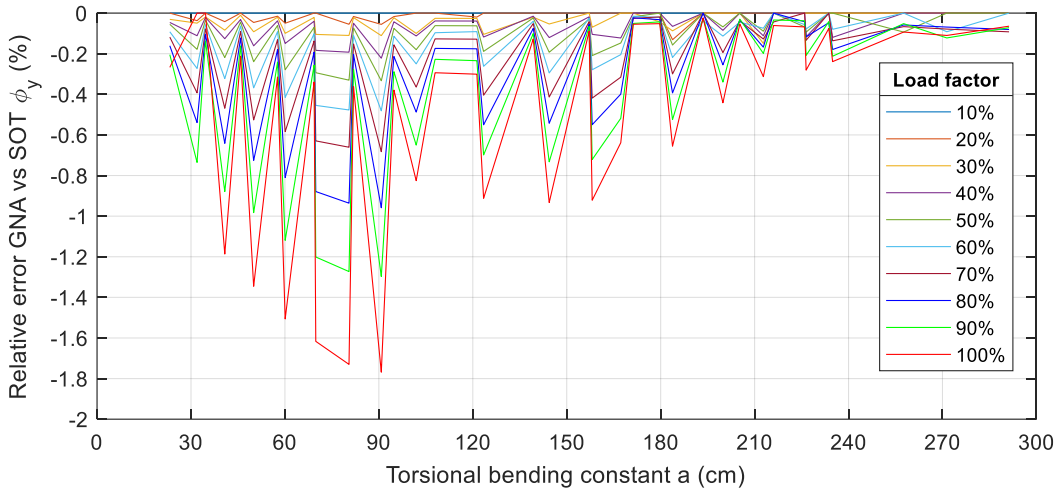

Figure 4.10 Relative error φ_y: fixed-free system, M_y load, open profiles, and 1D elements

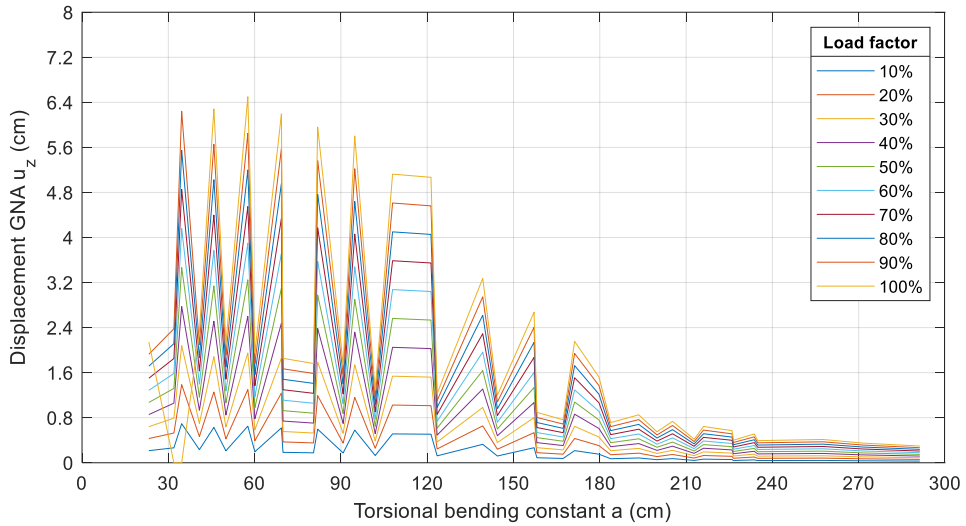

Figure 4.11 Displacement u_z: fixed-free system, M_y load, open profiles, and 1D elements

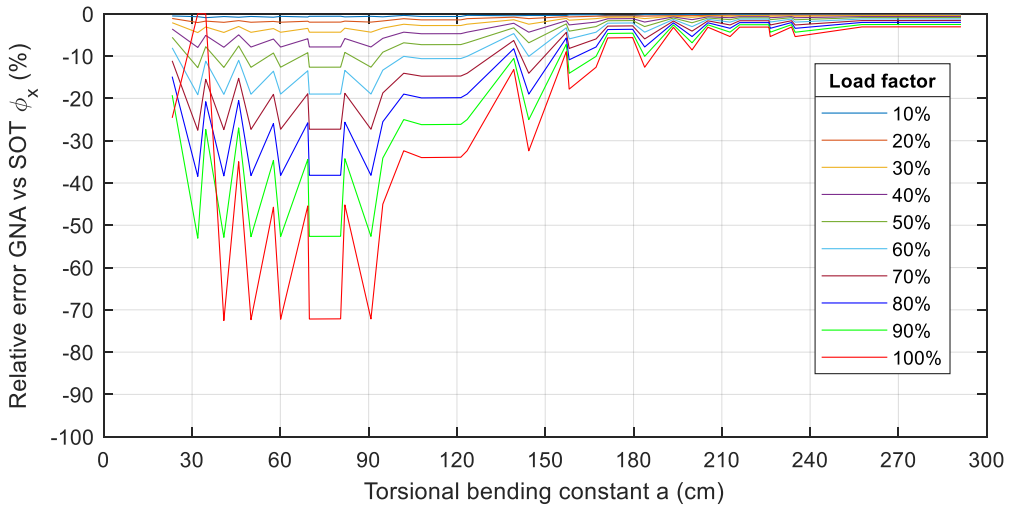

Figure 4.12 Relative error φ_x: fixed-free system, M_y load, open profiles, and 1D elements

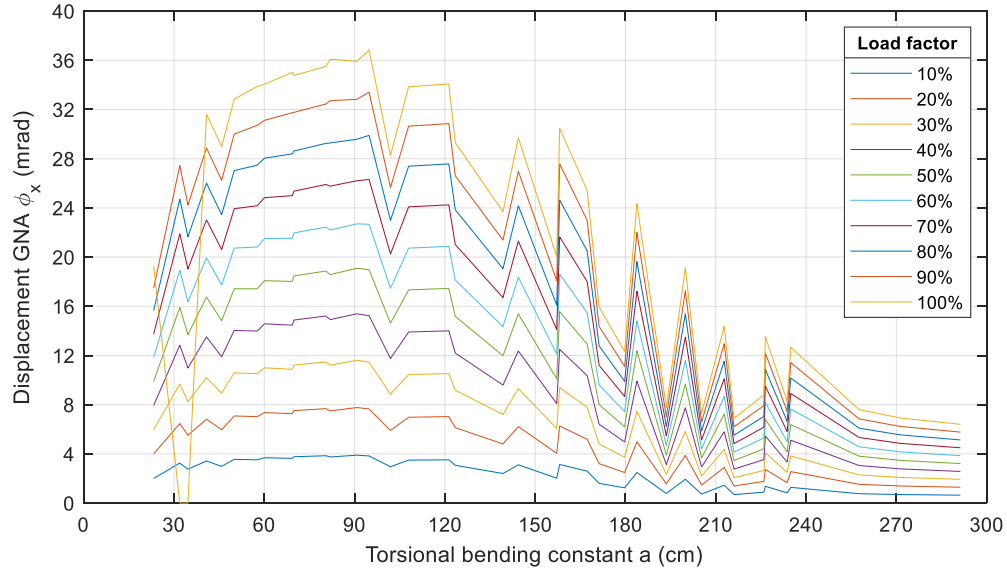

Figure 4.13 Displacement φ_x: fixed-free system, M_y load, open profiles, and 1D elements

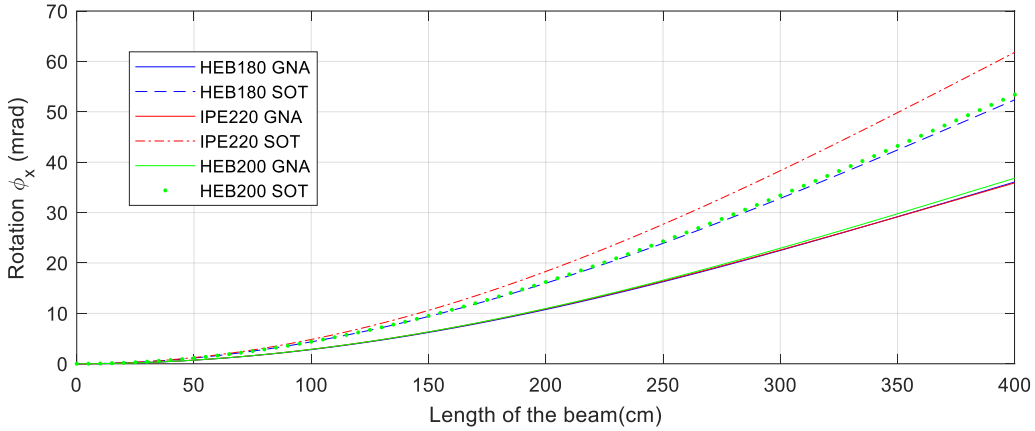

Figure 4.14 Variation of φ_x along the length load factor of 1: fixed-free system, M_y load, open profiles, and 1D elements

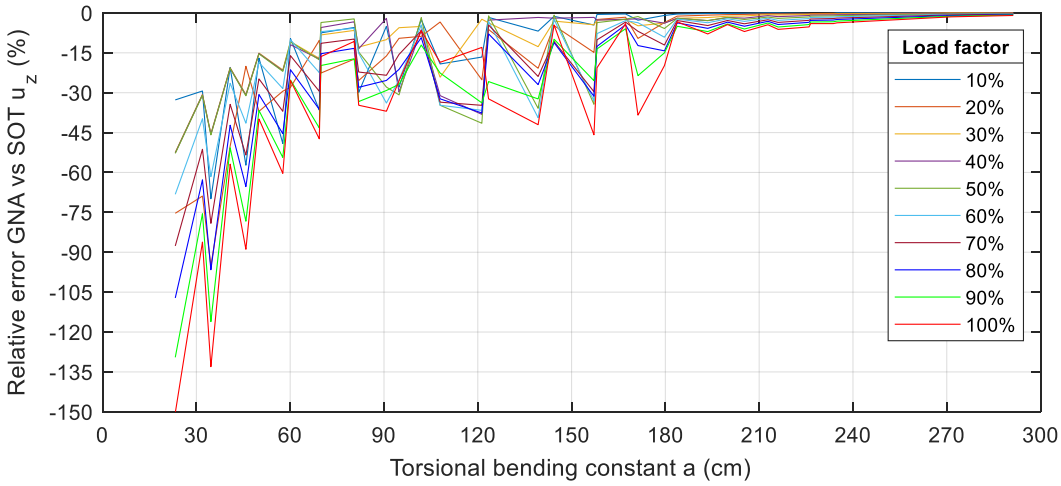

Figure 4.15 Relative error u_z: fixed-free system, M_y load, open profiles, and 2D elements

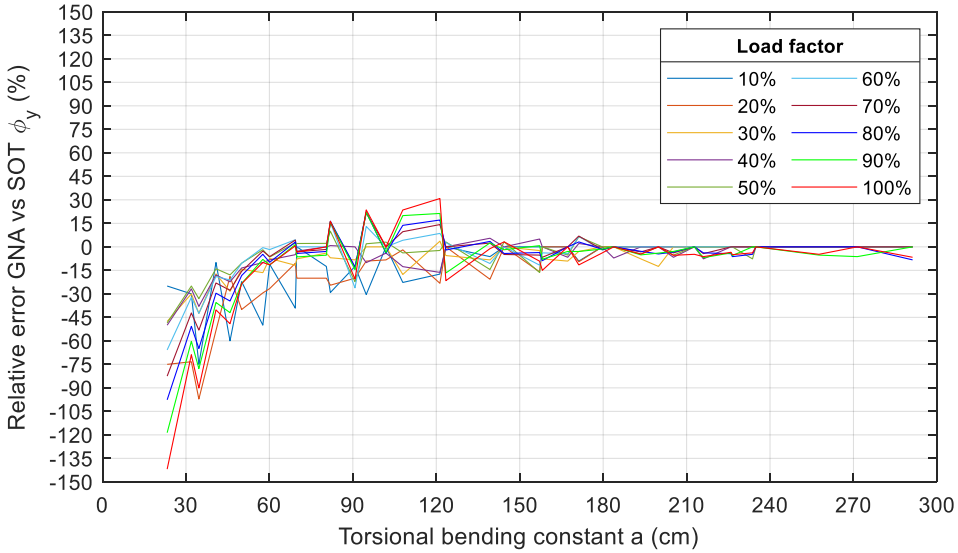

Figure 4.16 Relative error φ_y: fixed-free system, M_y load, open profiles, and 2D elements

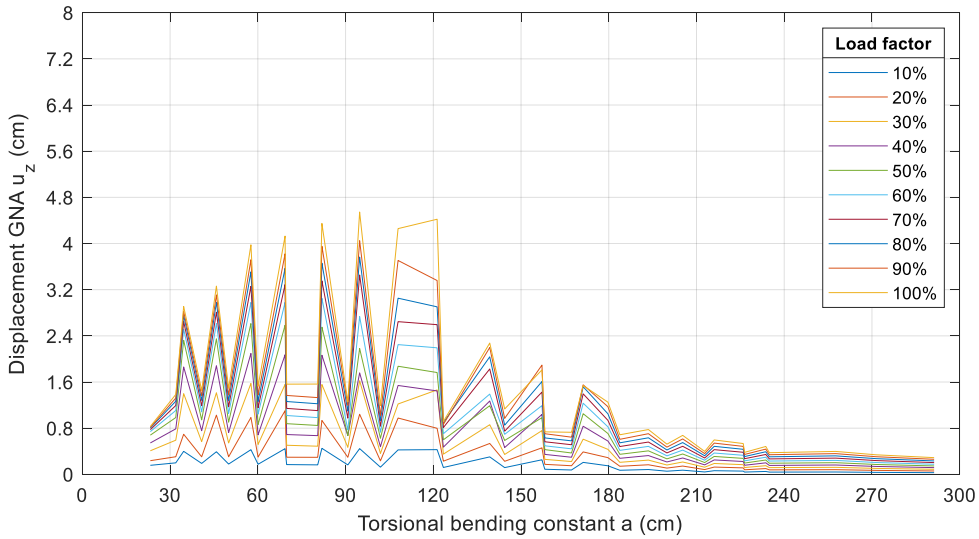

Figure 4.17 Displacement u_z: fixed-free system, M_y load, open profiles, and 2D elements

Regarding **M_T** action, the following assertions have been found:

- **Open:** for 1D elements φ_x and Ω show almost no variation with relative errors under 1.1%, even though, values of rotation reach up to approximately 1.1 rad (63º) at a load factor of 1 (see Figure 4.18). Moreover, almost all sections are over the limit value of 0.3 rad.
- **Open:** for 2D elements the variation for φ_x is higher than the limit (up to about 14%). No clear pattern of variation regarding the profile is seen in Figure 4.19. In some cases, GNA gives higher values and in others SOT. Additionally, profiles with low *a* show no clear behavior as higher errors are seen with lower load levels. Because of it, GNA and SOT are not considered to be in agreement in the case of M_T for 2D elements (considering the modelling approach of this thesis).

- **Closed:** φ_x shows no variation for 1D elements and low variation for 2D elements with r_{error} under 3.6%. For this type of profiles, the warping effect is low, and therefore, more uniform behavior is seen. The highest peak is observed again for the RHS profile with the lowest value of *a* (see Figure 4.20). Moreover, it is found that the magnitude of rotation is smaller in comparison to open profiles ($\varphi_{x,max} \approx 0.32$ rad = 18.3º), as closed profiles have higher torsional stiffness, and only for one profile the limit for φ_x is surpassed as seen in Figure 4.21. Finally, the magnitudes of displacement stay close for both 1D and 2D elements.

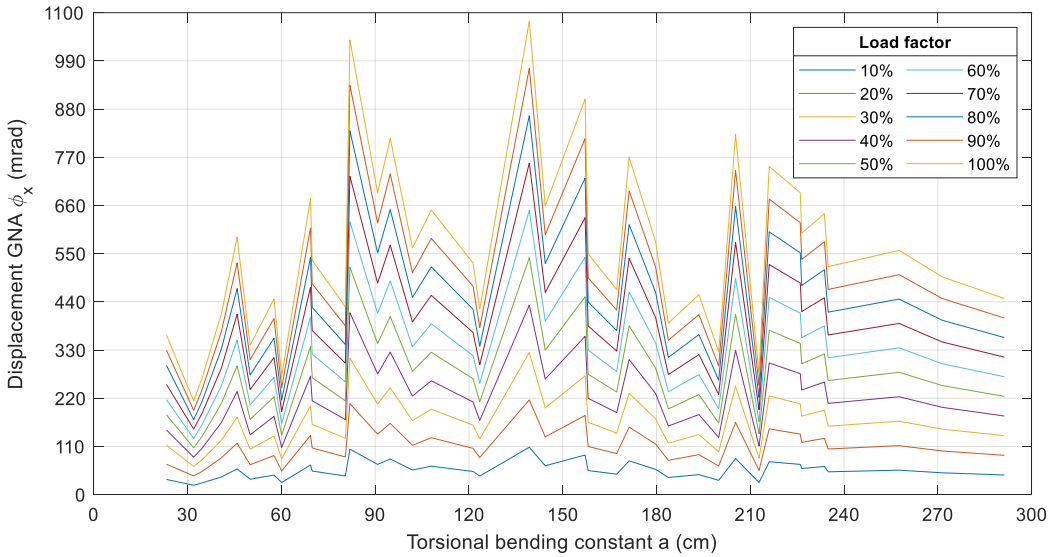

Figure 4.18 Displacement φ_x: fixed-free system, M_T load, open profiles, and 1D elements

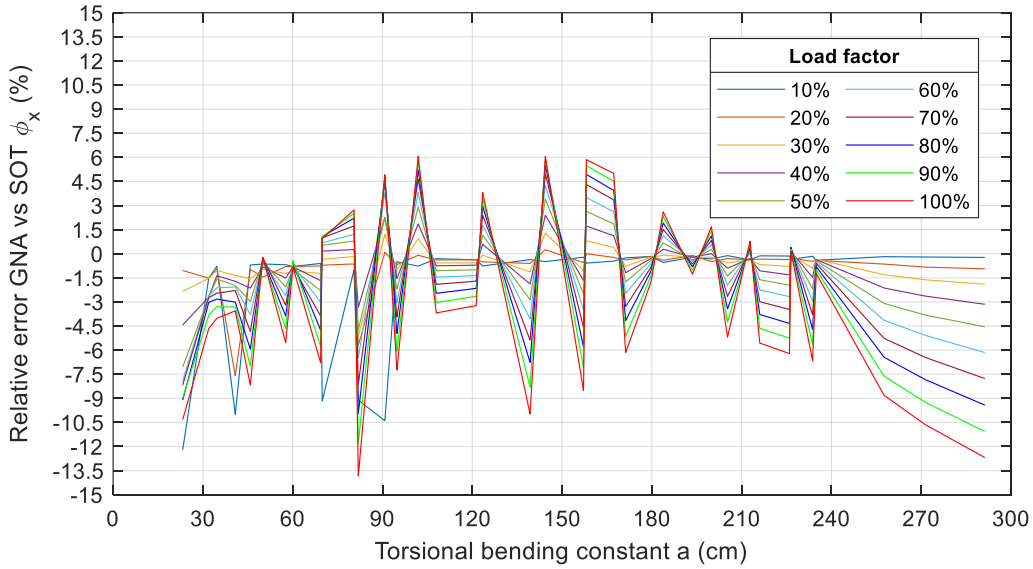

Figure 4.19 Relative errort φ_x: fixed-free system, M_T load, open profiles, and 2D elements

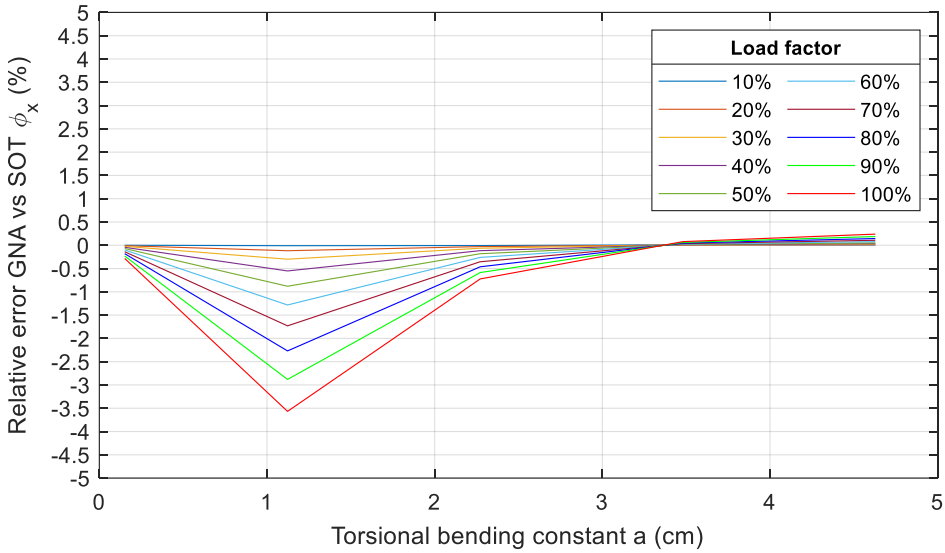

Figure 4.20 Relative errort φ_x: fixed-free system, M_T load, closed profiles, and 1D elements

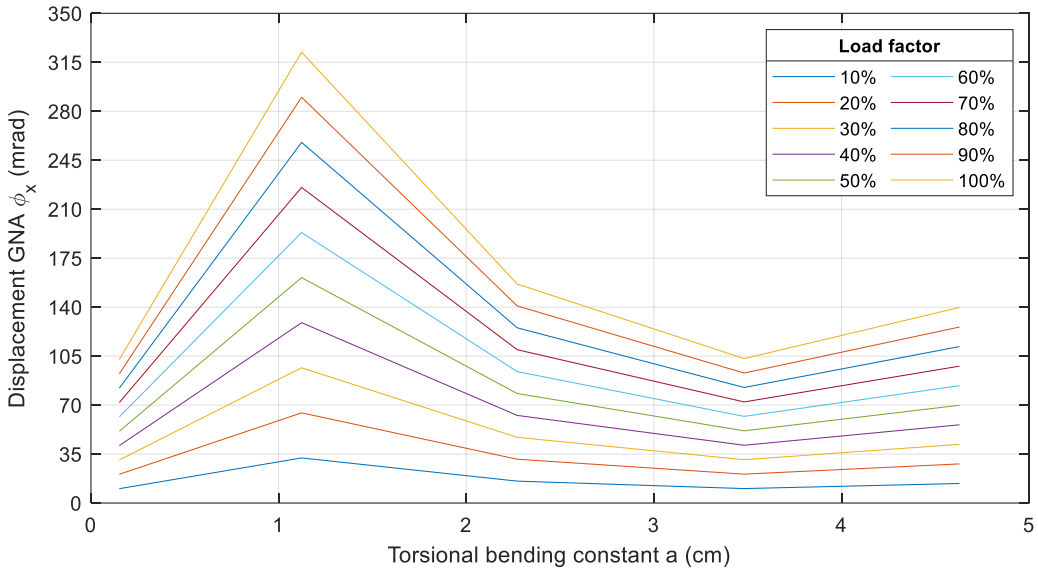

Figure 4.21 Displacement φ_x: fixed-free system, M_T load, closed profiles, and 1D elements

4.1.2.2 Fork-fork system

Under $\mathbf{V_z}$ action, the following observations have been made for the fork-fork system:

- **Open:** for 1D and 2D elements u_z shows higher r_{error} for IPE profiles. In 2D elements, all profiles stay below the threshold but the three with the lower *a*. For 1D elements, some additional IPE profiles surpass the threshold (see Figure 4.22 and Figure 4.23). Moreover, the variation of displacements is similar for both 1D and 2D elements and all profiles stay below the threshold of 5 cm (see Figure 4.24 and Figure 4.25).
- **Open:** for φ_x in 1D elements high variation is observed for many profiles particularly more for IPE profiles. The r_{error} also tends to be higher for profiles with low values of *a* (see Figure 4.26). Moreover, SOT gives higher values. φ_x for GNA doesn't surpass 0.15 rad (8.6º) (see Figure 4.27). This behavior may be explained by the influence of imperfections in SOT. At this stage of deformation, SOT has a higher influence in rotation φ_x as in comparison to GNA.
- **Open/Closed:** for φ_y no variation is found due to the point of extraction (midspan) which is located in the inflection point (zero displacement).
- **Closed**: u_z shows relevant variation just for the RHS profile with the lowest value of *a*. For this profile, the r_{error} reaches 36% for 1D elements and 1% for 2D elements (see Figure 4.28 and Figure 4.29). The error in 1D elements is due to the effect of tension forces that are present in GNA but not in SOT without imperfections. Moreover, for the same profile, a variation of about 1.5 cm for a load factor of 1 is also seen (see Figure 4.30 and Figure 4.31). For this case, when the profile is subjected to a tension force, lower vertical displacements are obtained which is the case of 1D elements, for 2D elements, however, the tension effect does not occur because of how the modelling was addressed. The rest of the profiles remain with close values of displacement and low r_{error}.

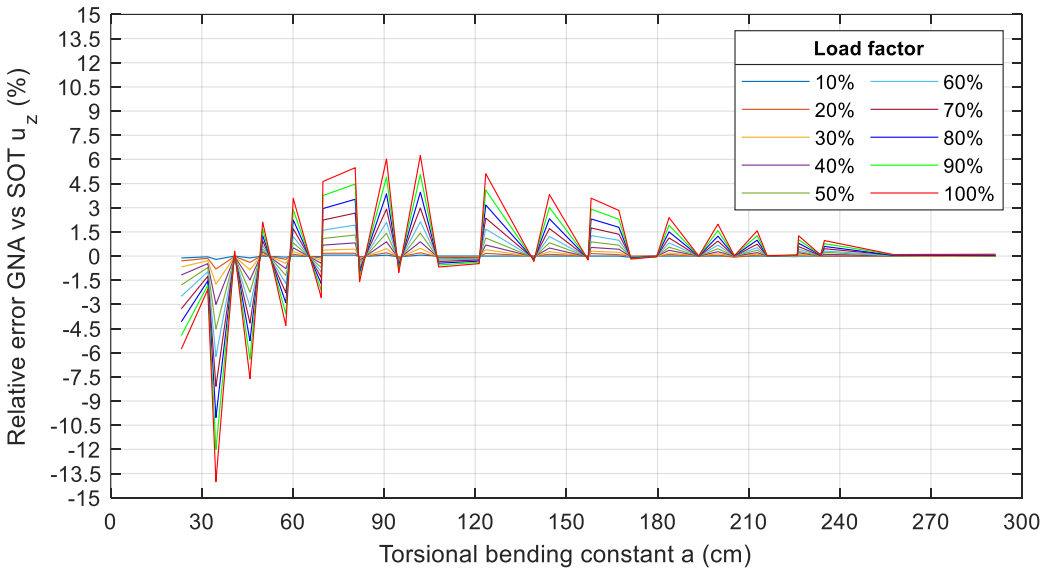

Figure 4.22 Relative error u_z: fork-fork system, V_z load, open profiles, and 1D elements

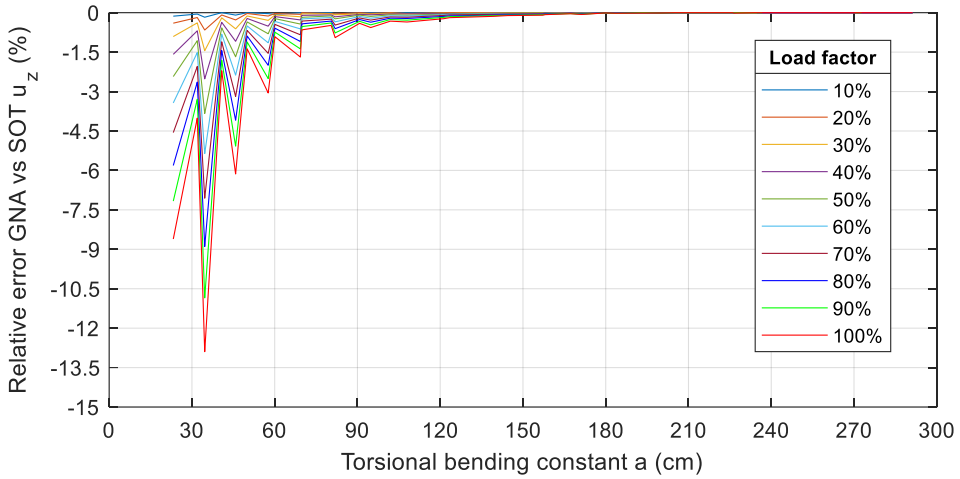

Figure 4.23 Relative error u_z: fork-fork system, V_z load, open profiles, and 2D elements

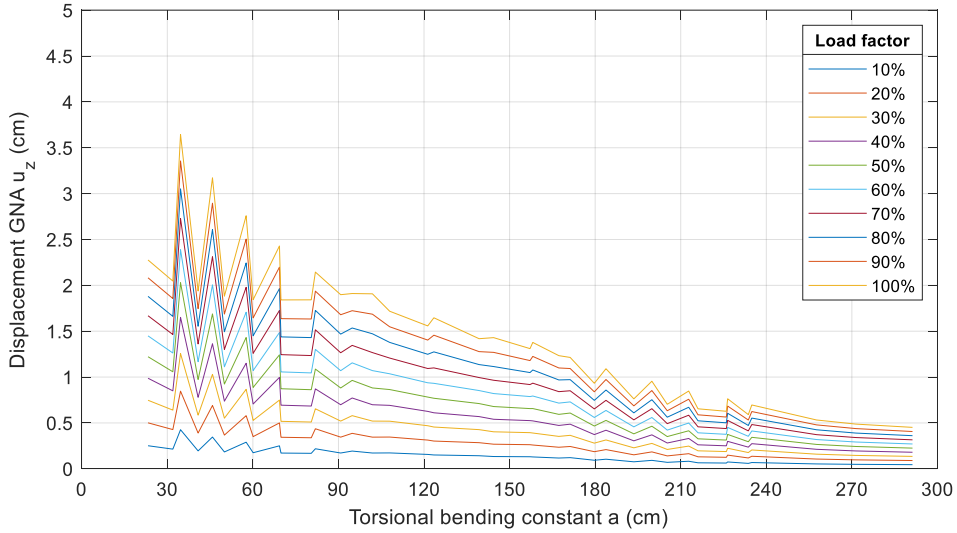

Figure 4.24 Displacement u_z: fork-fork system, V_z load, open profiles, and 1D elements

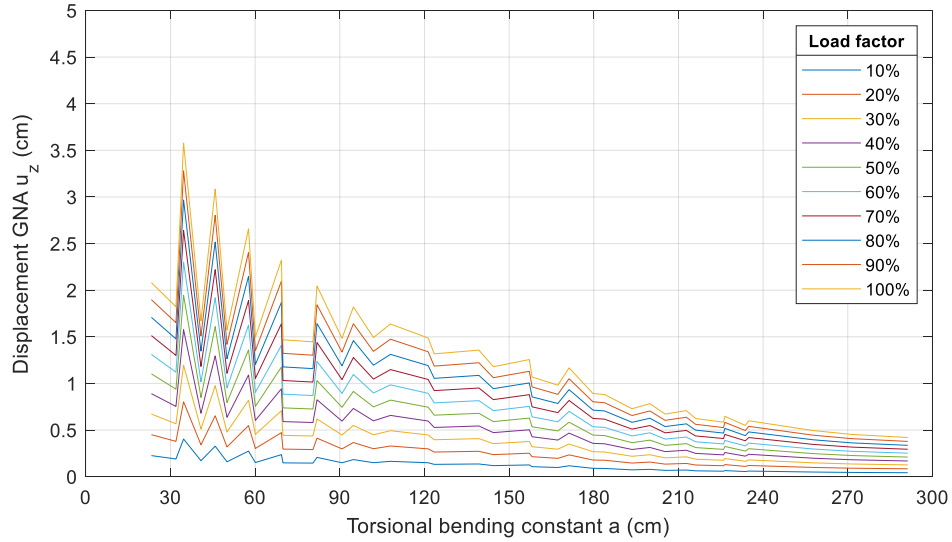

Figure 4.25 Displacement u_z: fork-fork system, V_z load, open profiles, and 2D elements

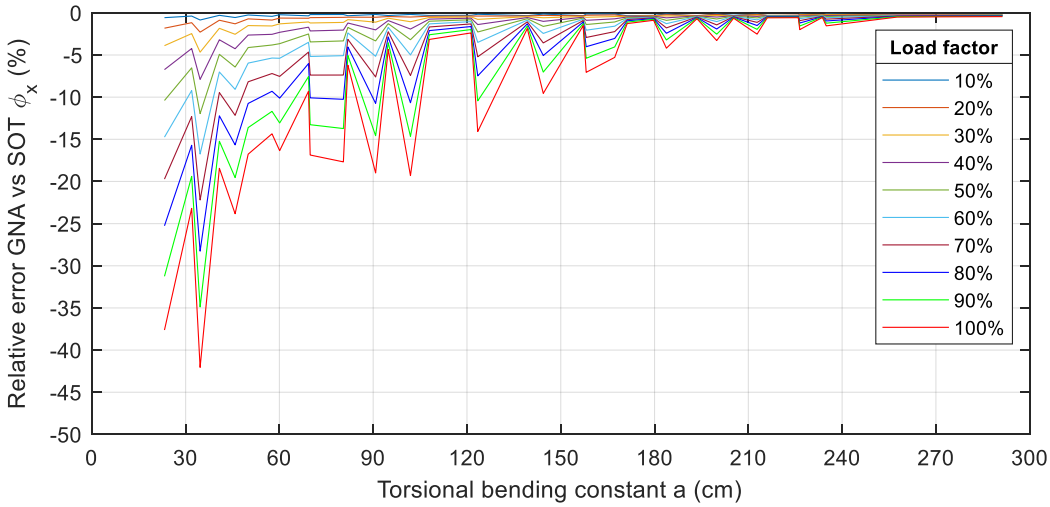

Figure 4.26 Relative error φ_x: fork-fork system, V_z load, open profiles, and 1D elements

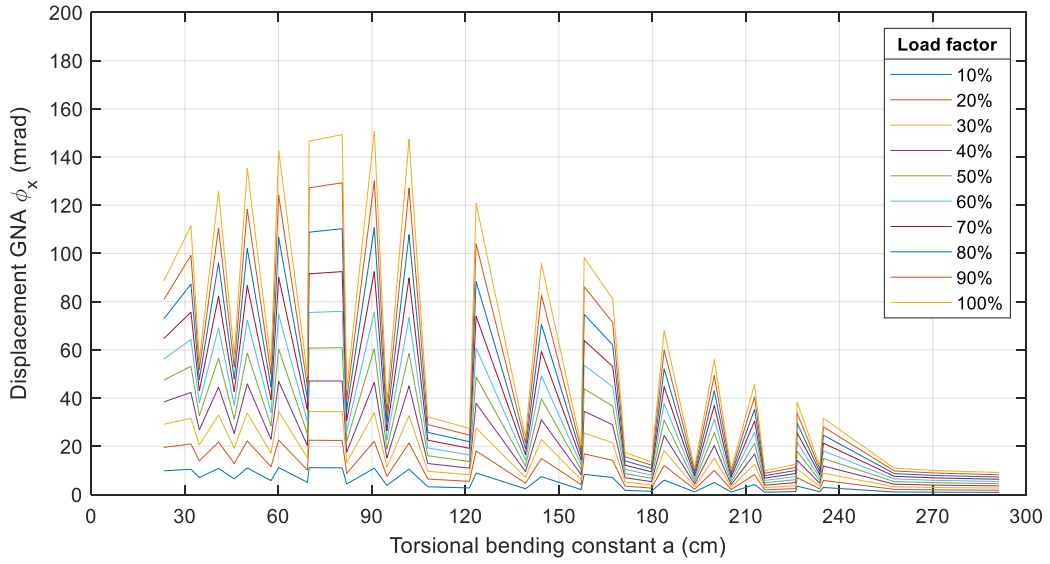

Figure 4.27 Displacement φ_x: fork-fork system, V_z load, open profiles, and 1D elements

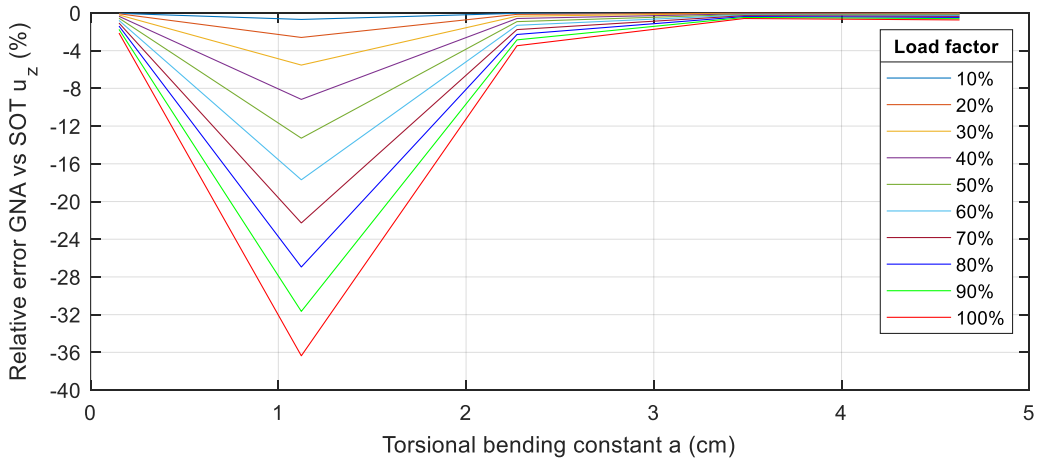

Figure 4.28 Relative error u_z: fork-fork system, V_z load, closed profiles, and 1D elements

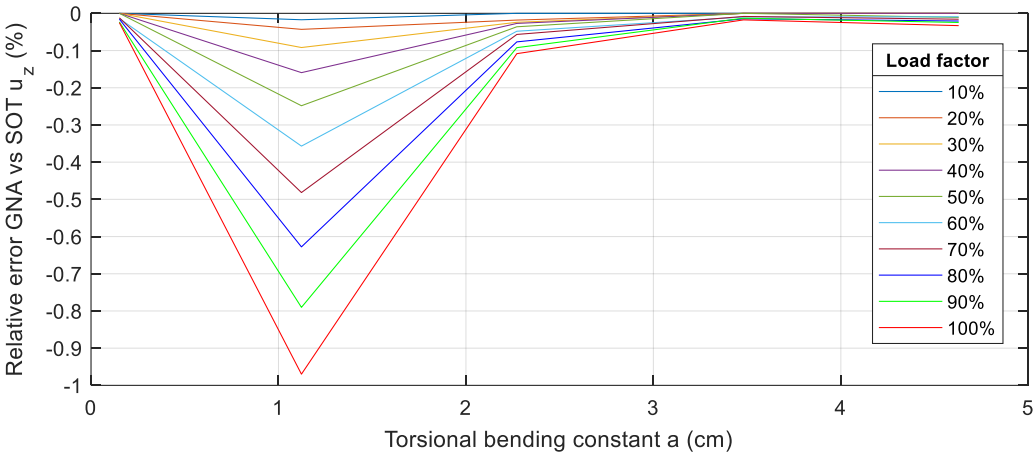

Figure 4.29 Relative error u_z: fork-fork system, V_z load, closed profiles, and 2D elements

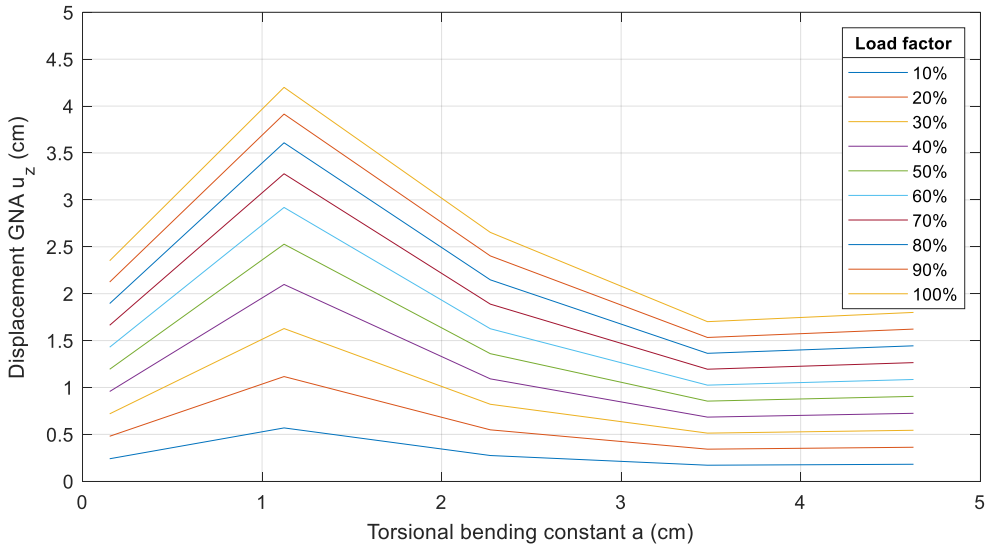

Figure 4.30 Displacement u_z: fork-fork system, V_z load, closed profiles, and 1D elements

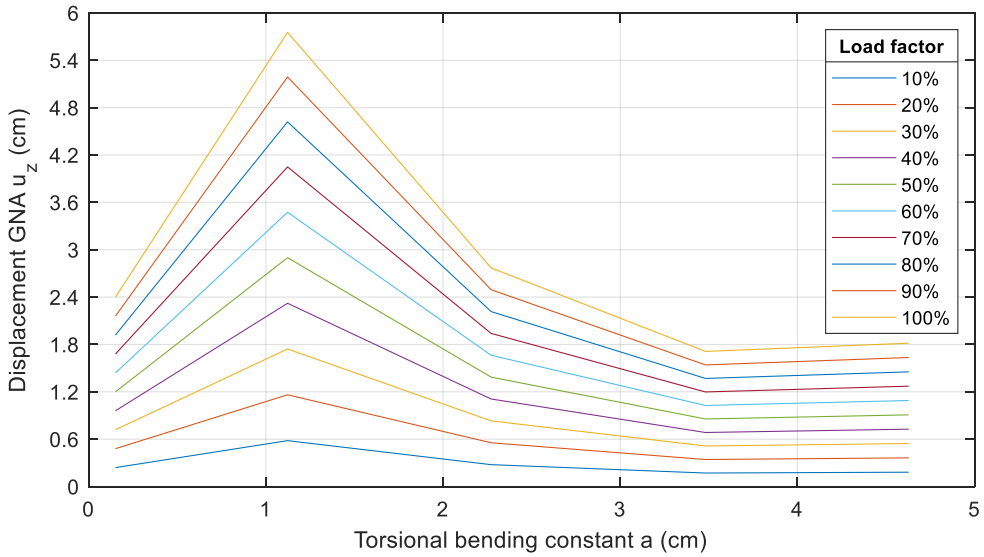

Figure 4.31 Displacement u_z: fork-fork system, V_z load, closed profiles, and 2D elements

In regard to $\mathbf{M_y}$ action, the following remarks have been found:

- **Open/Closed:** no variation exists in 1D and 2D elements for u_z due to the fact that displacements at midspan are zero.
- **Open:** similar as in V_z, φ_x for 1D elements shows higher values for SOT. The r_{error} (5-12% at a load factor of 0.7 as seen on Figure 4.32) is higher for profiles with low *a* especially for IPE sections. Additionally, φ_x doesn't surpass 0.13 rad (7.4º) (see Figure 4.33).
- **Open:** φ_y presents almost no variation for 1D elements (less than 1.4% as shown in Figure 4.34). 2D elements on the other hand show again high r_{error} and variation of magnitude without a clear pattern as in the fixed-free system. Therefore, no good agreement of results exists for M_y in 2D elements.
- **Closed:** φ_y shows almost no variation for both 1D and 2D elements with r_{error} under 1.8%. The magnitudes of displacement also remain close for 1D and 2D elements.

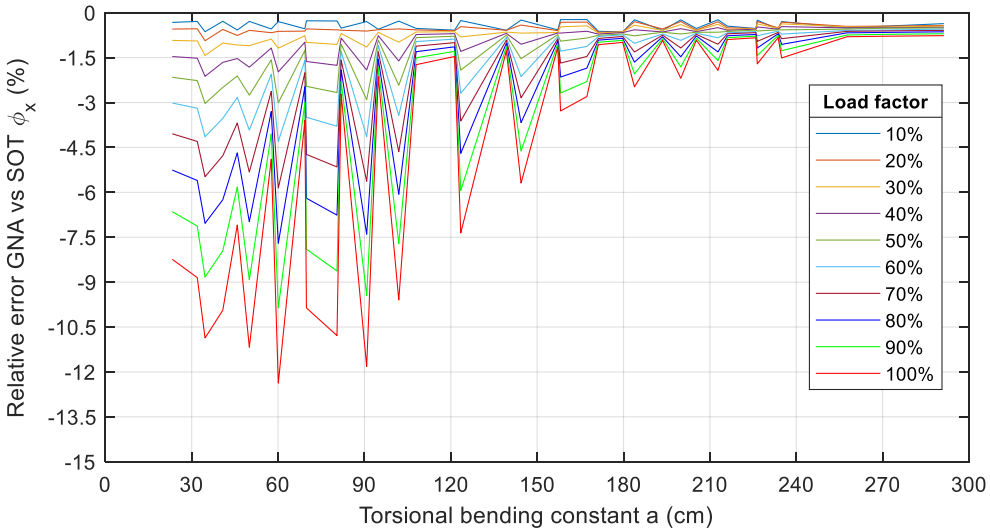

Figure 4.32 Relative error φ_x: fork-fork system, M_y load, open profiles, and 1D elements

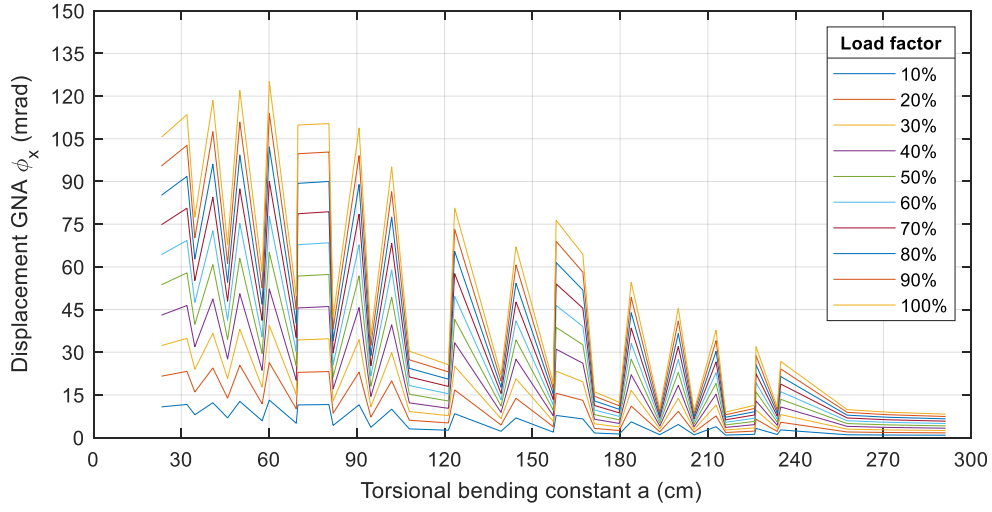

Figure 4.33 Displacement φ_x: fork-fork system, M_y load, open profiles, and 1D elements

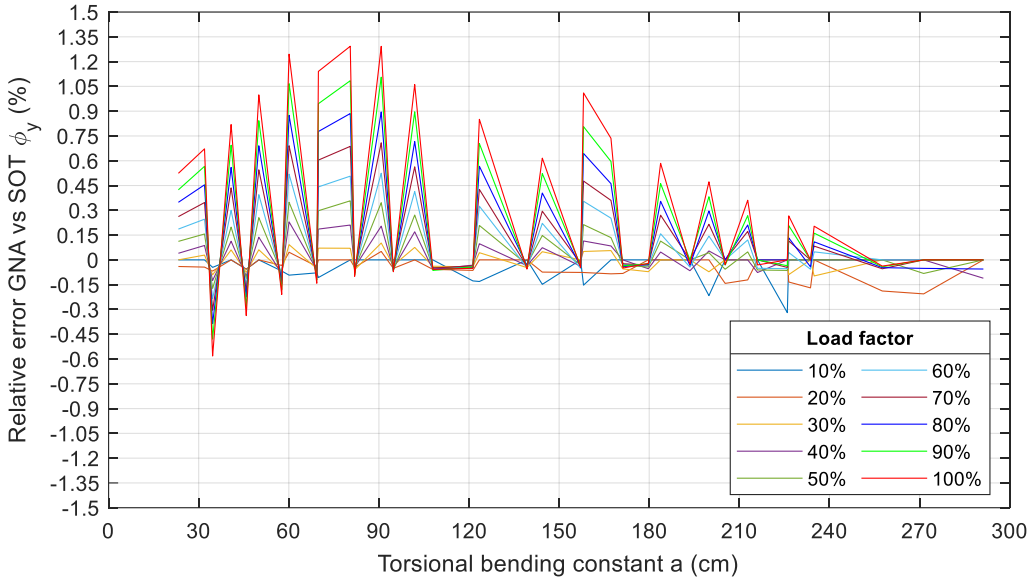

Figure 4.34 Relative error φ_y: fork-fork system, M_y load, open profiles, and 1D elements

Concerning **M_T** action, the following assertions have been found:

- **Open:** starting from a load factor of 0.3 the r_{error} threshold is surpassed for φ_x in both 1D and 2D elements (see Figure 4.35 and Figure 4.36). Higher values for SOT are observed especially for 2D elements, the values of φ_x reach up to 0.64 rad (36.7º) at a load factor of 1 in 1D elements (see Figure 4.37). However, for 2D elements the values are not close and they differ depending on the section as shown in Figure 4.38. One reason for this difference is the effect that the stiffening of the web causes. Again as for the fixed-free system GNA and SOT are not considered to be in agreement in the case of M_T for 2D elements.
- **Open:** no variation is found for Ω because in midspan φ_x inflection point is present.
- **Closed:** φ_x shows almost no variation for 1D and 2D elements with relative errors under 0.9% (see Figure 4.39). The magnitudes of displacement also remain close. The maximum value reaches 0.16 rad (9.2º) for a load factor of 1 as seen in Figure 4.40.

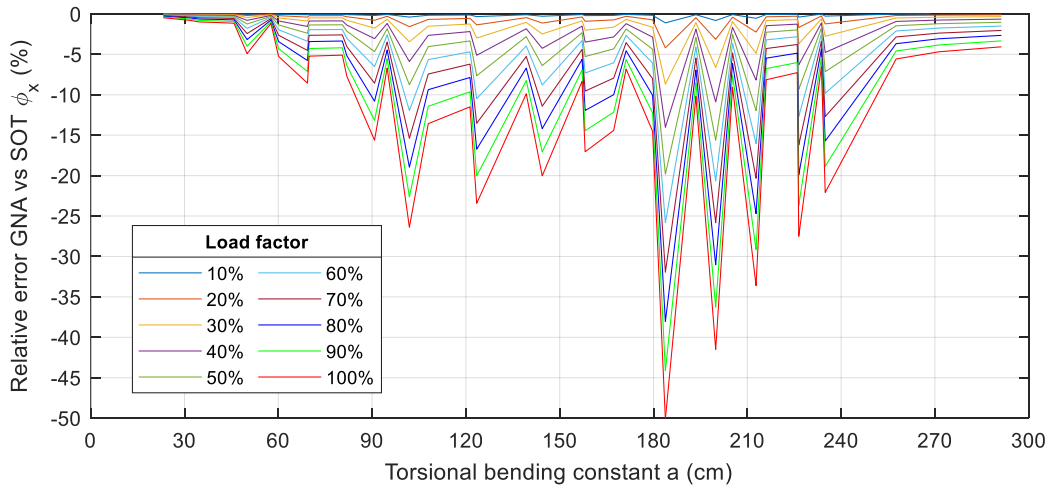

Figure 4.35 Relative error φ_x: fork-fork system, M_T load, open profiles, and 1D elements

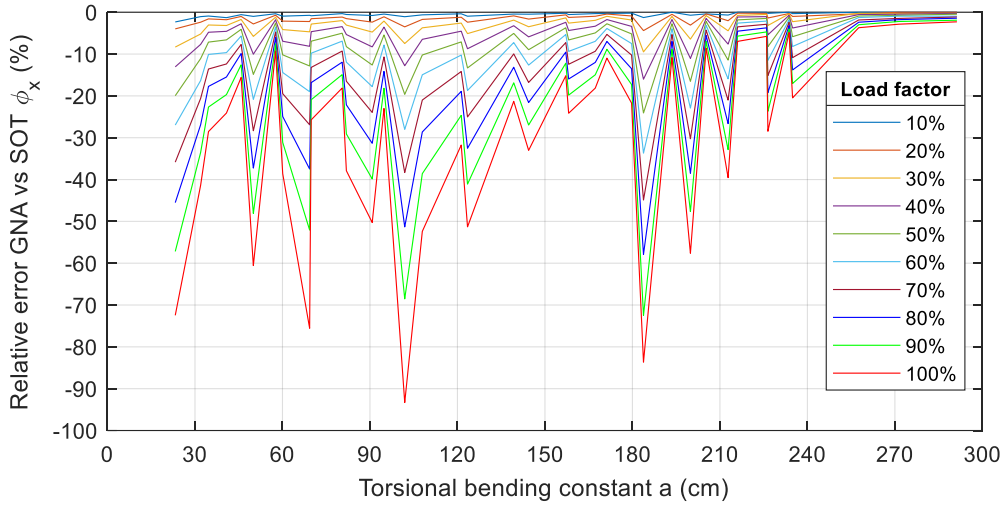

Figure 4.36 Relative error φ_x: fork-fork system, M_T load, open profiles, and 2D elements

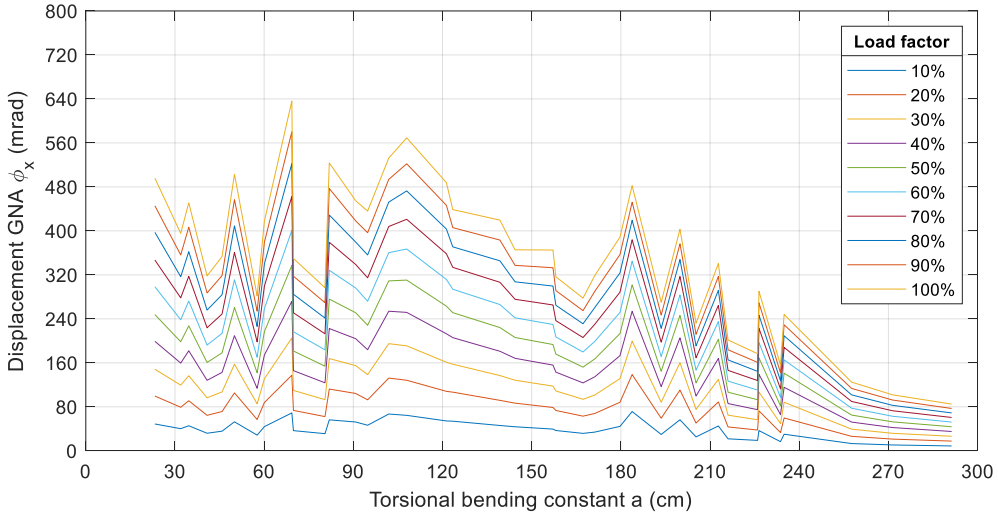

Figure 4.37 Displacement φ_x: fork-fork system, M_T load, open profiles, and 1D elements

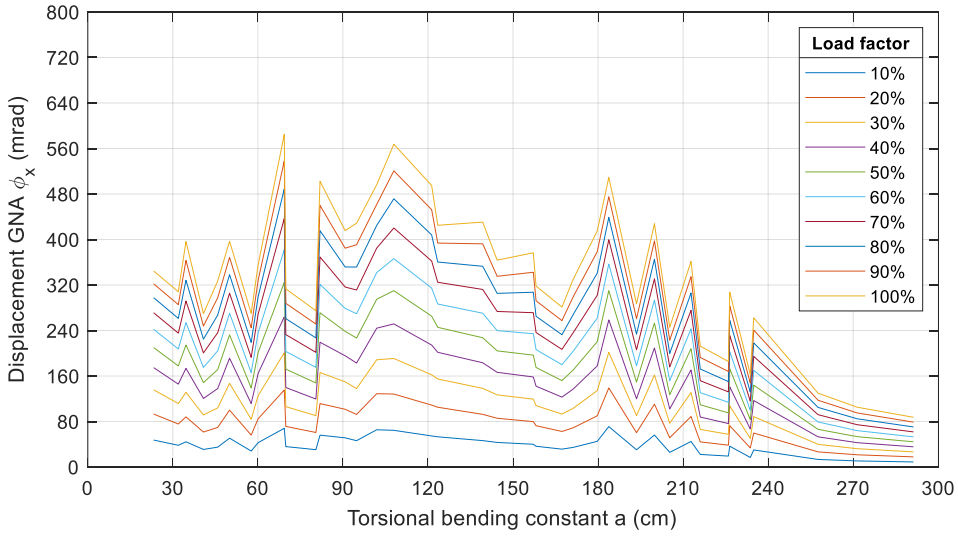

Figure 4.38 Displacement φ_x: fork-fork system, M_T load, open profiles, and 2D elements

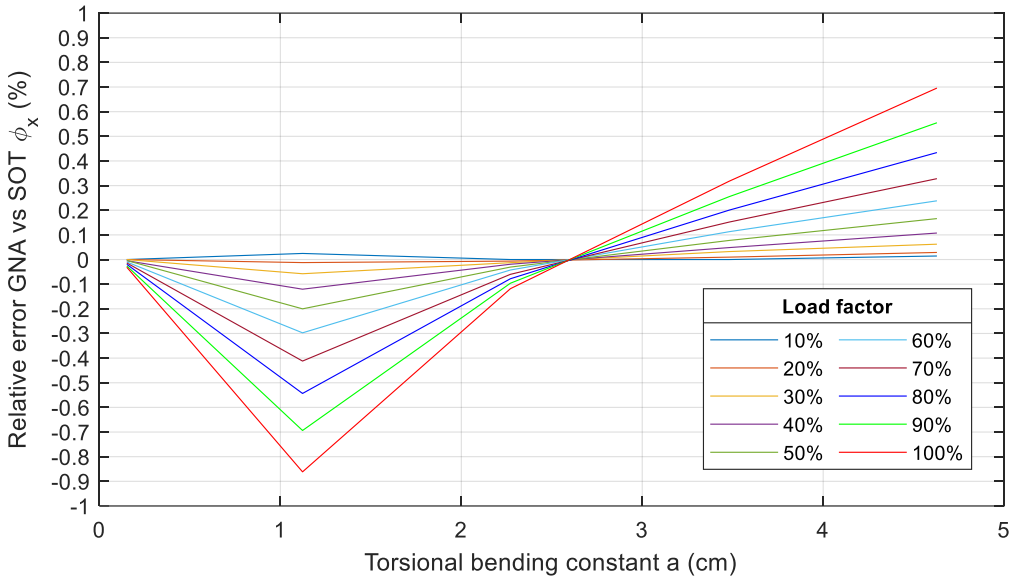

Figure 4.39 Relative error φ_x: fork-fork system, M_T load, closed profiles, and 2D elements

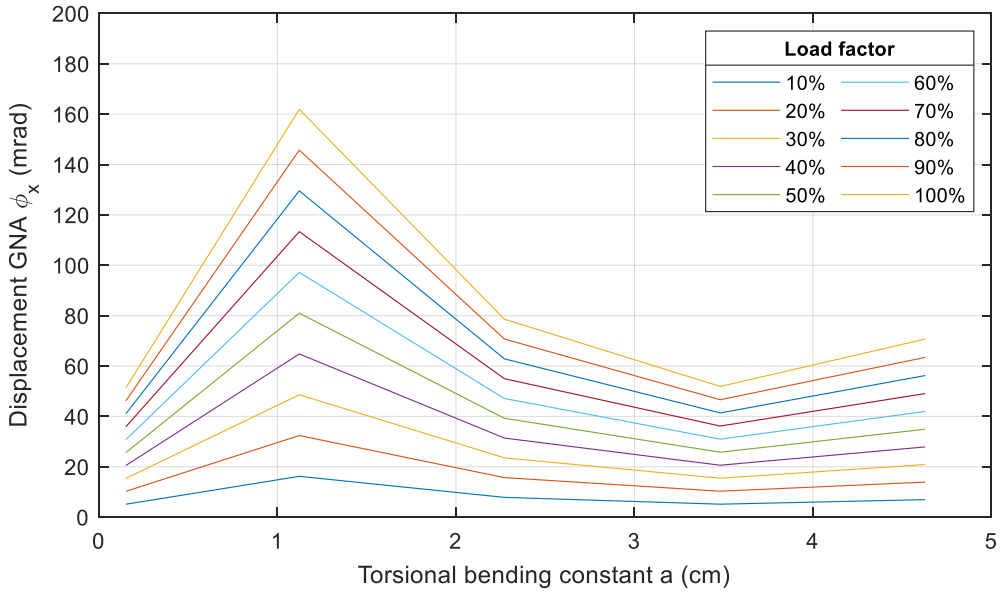

Figure 4.40 Displacement φ_x: fork-fork system, M_T load, closed profiles, and 2D elements

4.1.2.3 Fixed-fixed system

For $\mathbf{V_z}$ action in the fixed-fixed system, the following observations have been made:

- **Open:** for 2D elements u_z shows almost no variation, less than 2% (see Figure 4.41). In the case of 1D elements, normally all elements show low variation as well (lower than 2%) except for the seven IPE profiles with the lowest torsional bending constants which show variation up to 9% as seen in Figure 4.42. Moreover, u_z remains below the limit and shows higher values the smaller *a* is (see Figure 4.43). 2D elements in contrast show stiffer behavior as the maximum u_z differs about 0.45 cm at a load factor of 1 (see Figure 4.44). This difference is attributed to the stiffening of the web at midspan for the application of V_z which was used in this system.
- **Open:** for 1D elements φ_x shows similar variation as to u_z, the seven IPE profiles with the lowest *a* present variation higher than 2% and up to 10% as seen in Figure 4.45. Furthermore, the rotation is high for the same 7 profiles reaching up to 0.27 rad (15.5º) at a load factor of 1 (see Figure 4.46).
- **Open/Closed:** φ_y is zero at midspan (inflection point), thus, no variation is found.
- **Closed:** u_z shows similar behavior for 1D and 2D elements. The relative errors stay below the threshold with a peak for the RHS with smaller *a* (see Figure 4.47). The maximum displacement amounts to 2.7 cm at a load factor of 1 (see Figure 4.48).

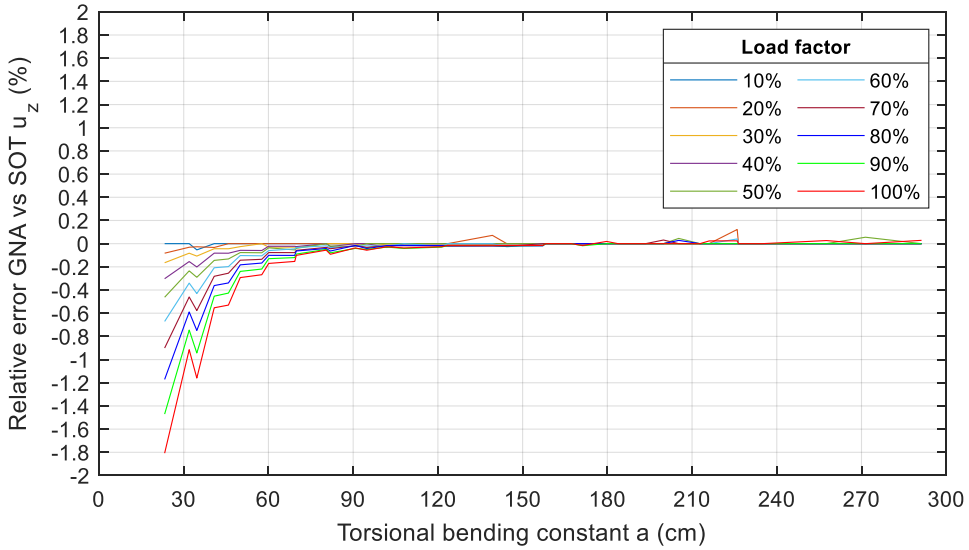

Figure 4.41 Relative error u_z: fixed-fixed system, V_z load, open profiles, and 2D elements

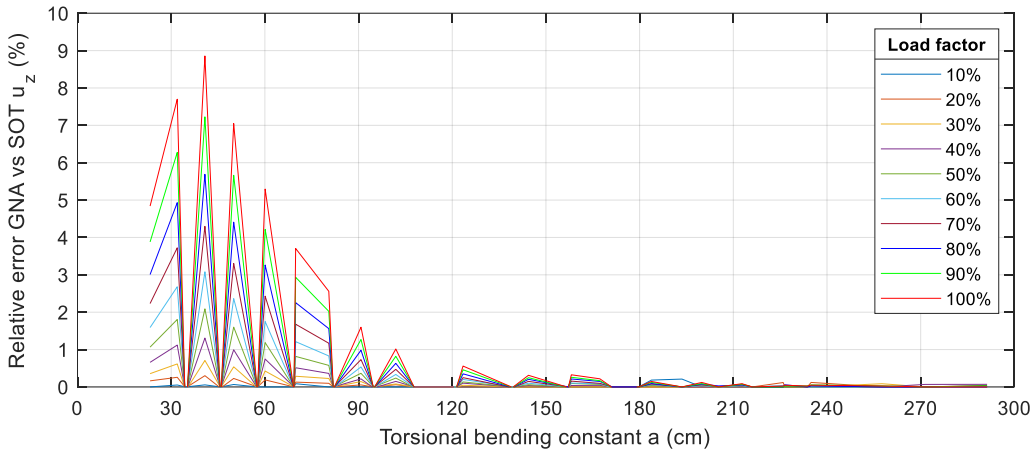

Figure 4.42 Relative error u_z: fixed-fixed system, V_z load, open profiles, and 1D elements

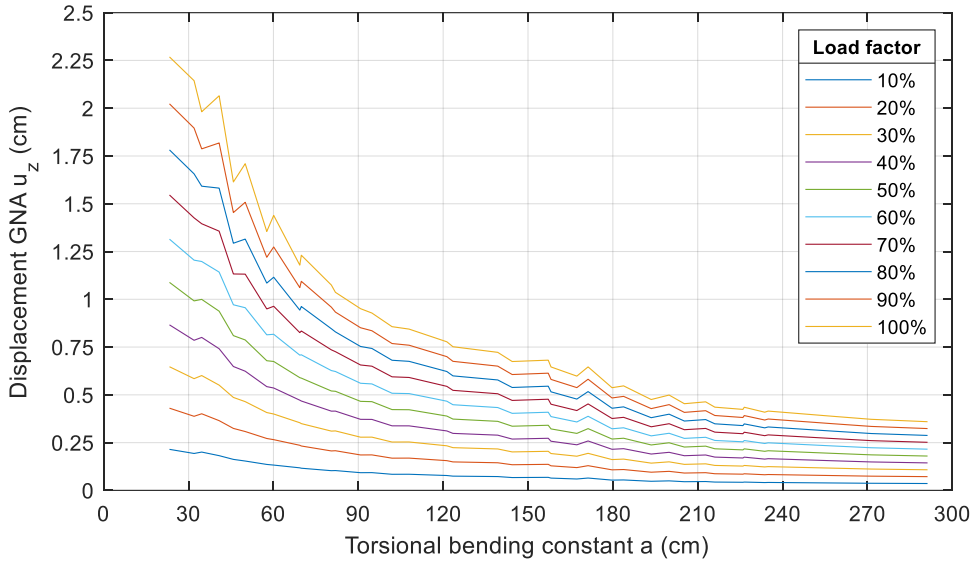

Figure 4.43 Displacement u_z: fixed-fixed system, V_z load, open profiles, and 1D elements

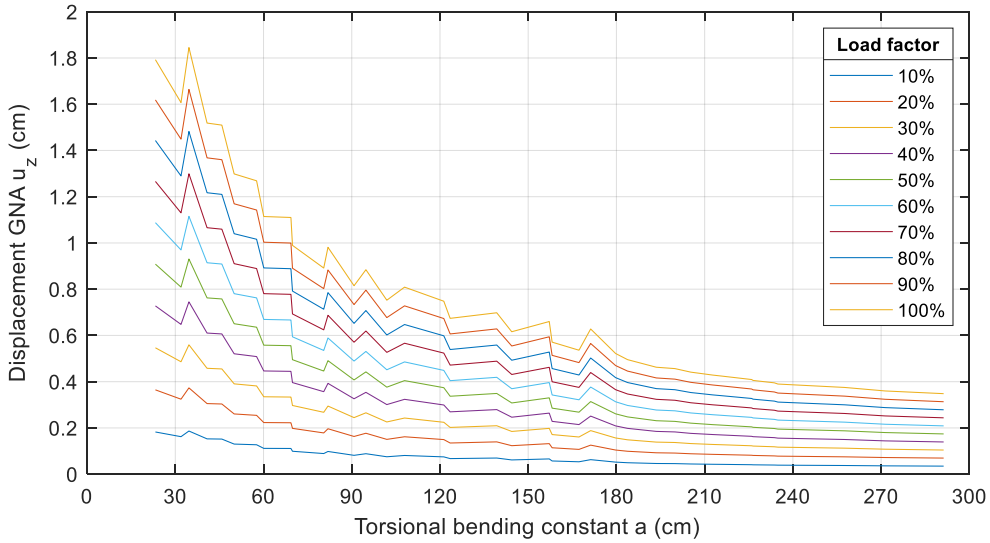

Figure 4.44 Displacement u_z: fixed-fixed system, V_z load, open profiles, and 2D elements

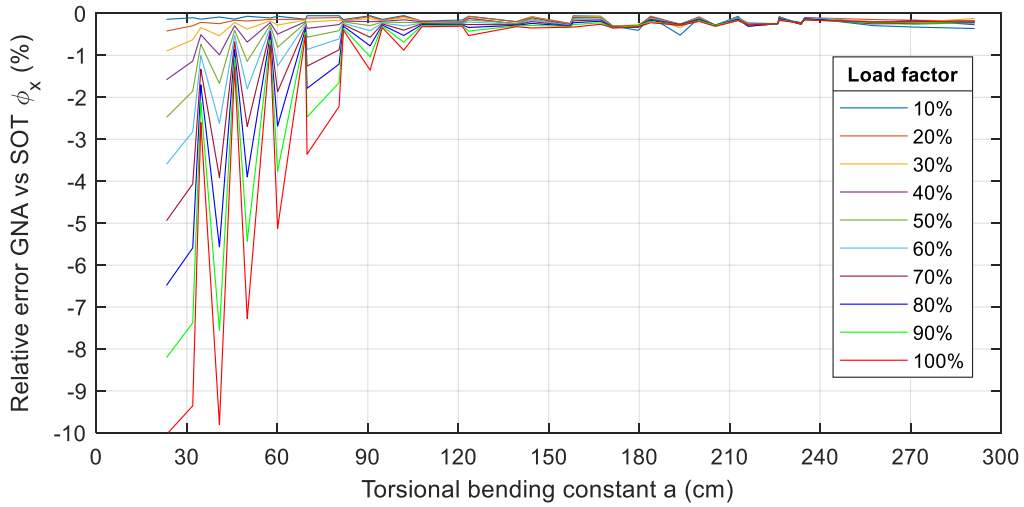

Figure 4.45 Relative error φ_x: fixed-fixed system, V_z load, open profiles, and 1D elements

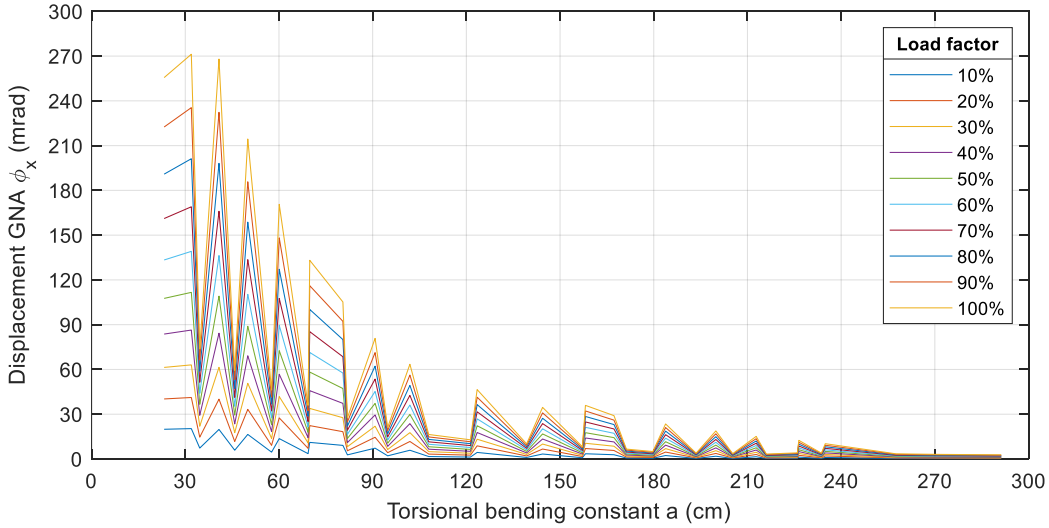

Figure 4.46 Displacement φ_x: fixed-fixed system, V_z load, open profiles, and 1D elements

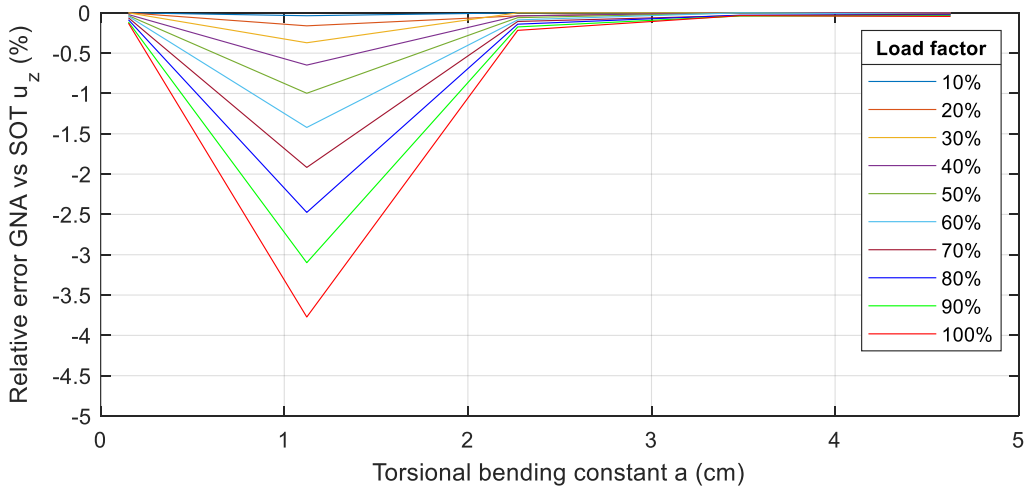

Figure 4.47 Relative error u_z: fixed-fixed system, V_z load, closed profiles, and 1D elements

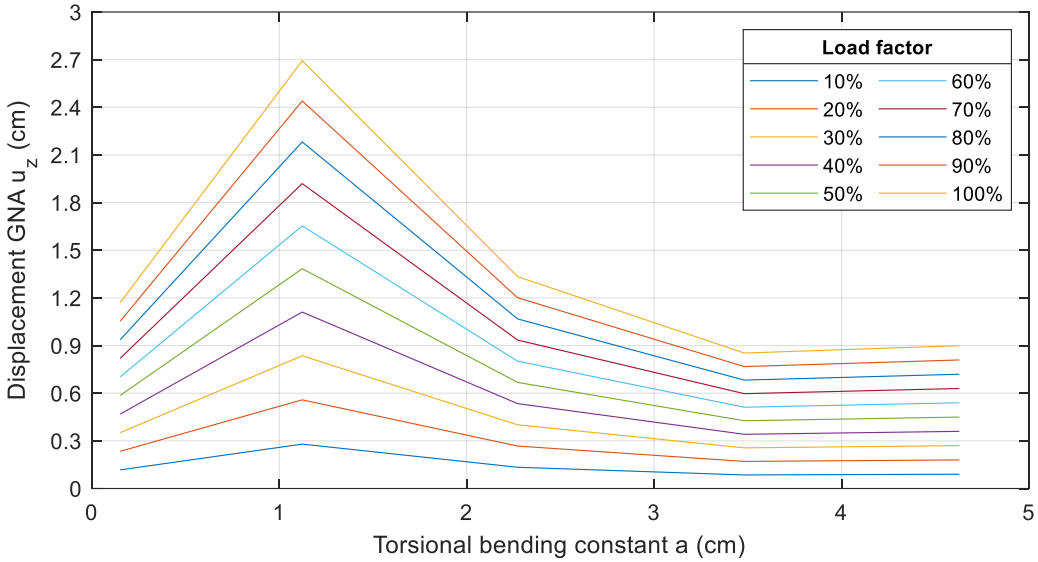

Figure 4.48 Displacement u_z: fixed-fixed system, V_z load, closed profiles, and 1D elements

In regard to $\mathbf{M_y}$ action, the following findings are given:

- **Open/Closed:** no variation exists in 1D and 2D elements for u_z due to zero displacement at midspan.
- **Open:** for 1D elements the seven IPE profiles with the lowest *a* show variation for φ_x higher than 5% and up to 12.4% as observed in Figure 4.49. The same profiles show the highest rotations as well up to 0.18 rad (10º) at a load factor of 1 (see Figure 4.50).
- **Open:** φ_y presents almost no variation for 1D elements (less than 2.1% as seen in Figure 4.51). 2D elements show high r_{error} without any clear trend. Moreover, the magnitude of φ_y differs to 1D elements. Thus, no good agreement of results exists for M_y in 2D elements as they were modelled.
- **Closed:** φ_y shows almost no variation for 1D and 2D elements with r_{error} under 0.35%. The magnitudes of displacement also remain close for 1D and 2D elements.

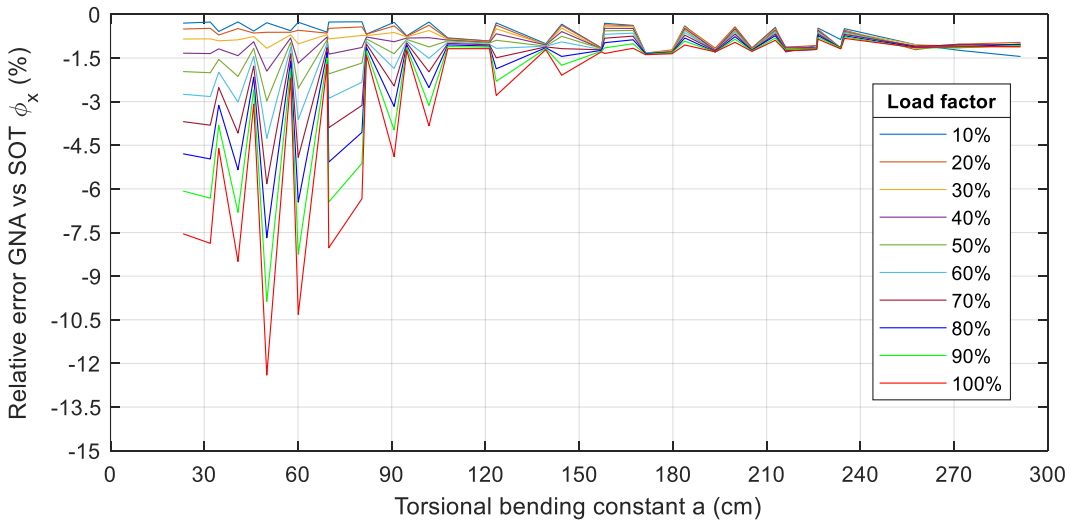

Figure 4.49 Relative error φ_x: fixed-fixed system, M_y load, open profiles, and 1D elements

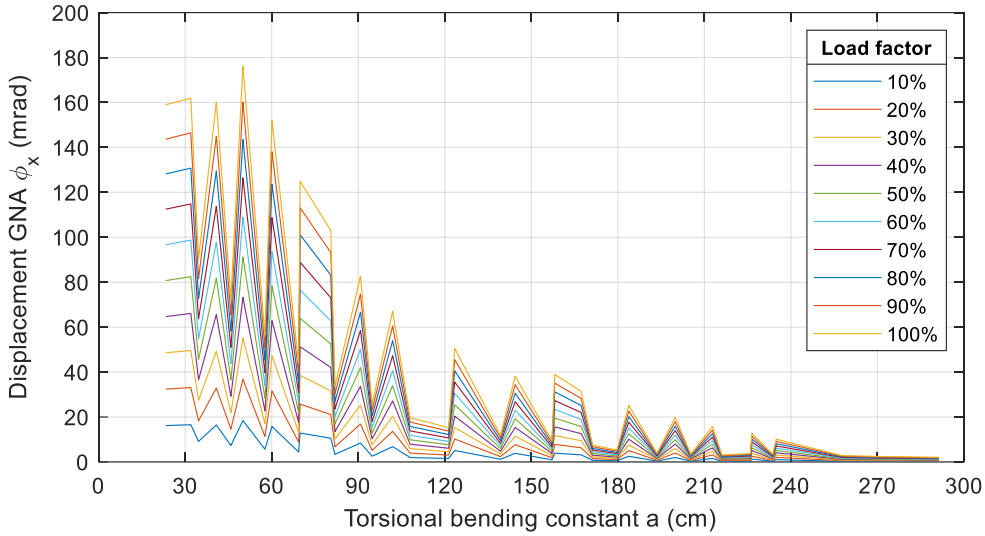

Figure 4.50 Displacement φ_x: fixed-fixed system, M_y load, open profiles, and 1D elements

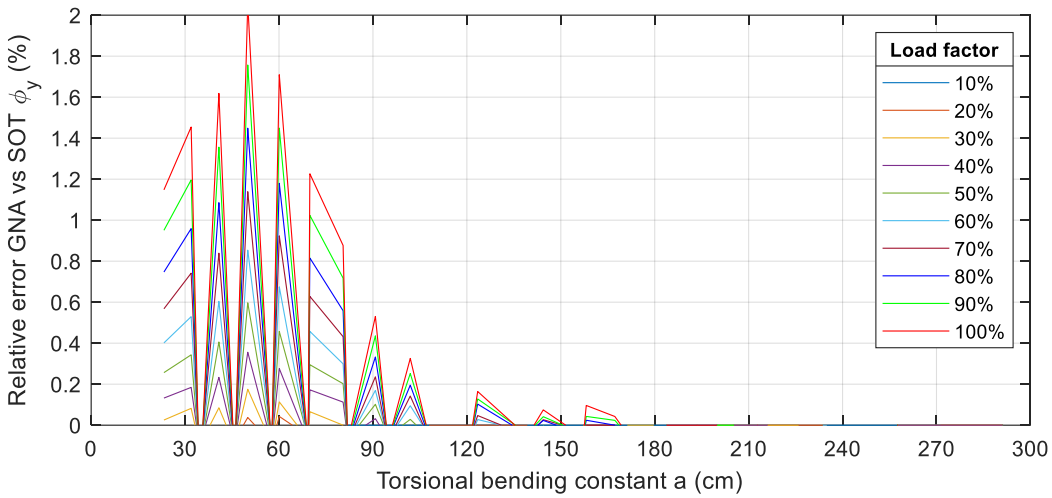

Figure 4.51 Relative error φ_y: fixed-fixed system, M_y load, open profiles, and 1D elements

With regard to $\mathbf{M_T}$ action, the following assertions have been found:

- **Open:** for 1D elements 3 IPE profiles surpass the limit of 5% up to 11.3% for φ_x as seen in Figure 4.52. Higher values for SOT are observed, the rotation reaches up to 0.68 rad (39º) at a load factor of 1 (see Figure 4.53). For illustration see Figure 4.54, where the variation of rotation along the length for the 3 profiles with the highest r_{error} is shown. Furthermore, starting from a load factor of 0.2, the r_{error} threshold is surpassed in 2D elements and high variation of rotation with 1D elements is found. Thus, GNA and SOT are again not considered to be in agreement in the case of M_T for 2D elements.
- **Open:** no variation is found for Ω due to zero displacement at midspan.
- **Closed:** similarly as the fork-fork system, φ_x shows almost no variation for 1D and 2D elements with relative errors under 0.9% (see Figure 4.39). The magnitudes of displacement also remain close. The maximum value reaches up to 0.16 rad (9.2º) for a load factor of 1 as previously shown in Figure 4.40.

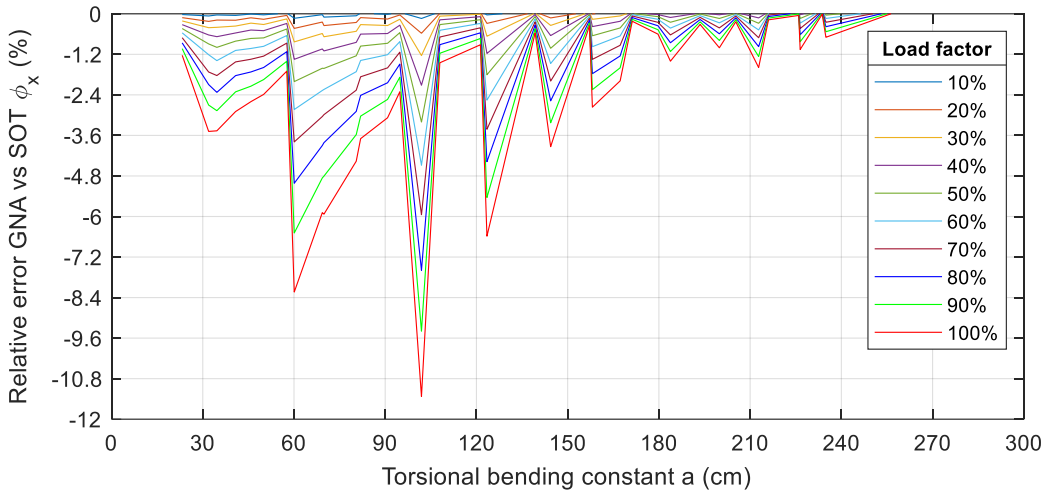

Figure 4.52 Relative error φ_x: fixed-fixed system, M_T load, open profiles, and 1D elements

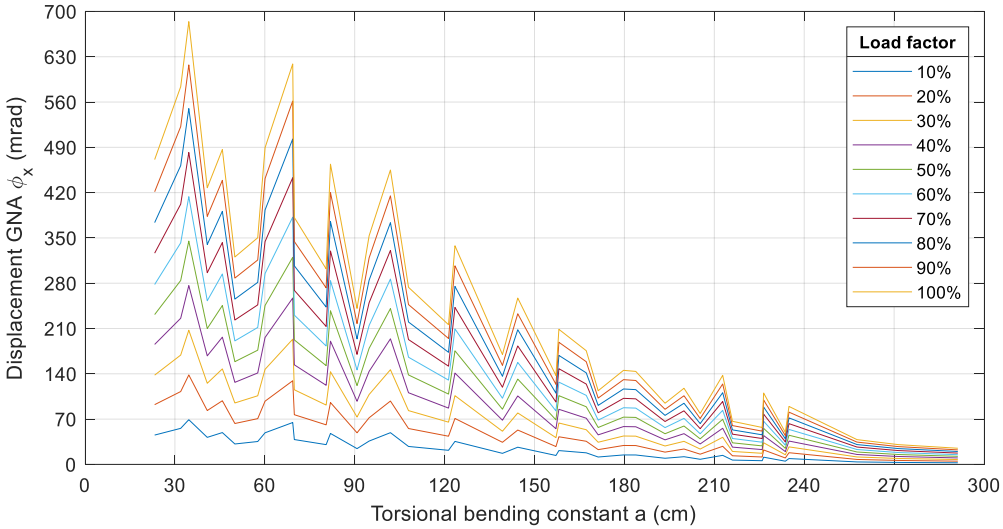

Figure 4.53 Displacement φ_x: fixed-fixed system, M_T load, open profiles, and 1D elements

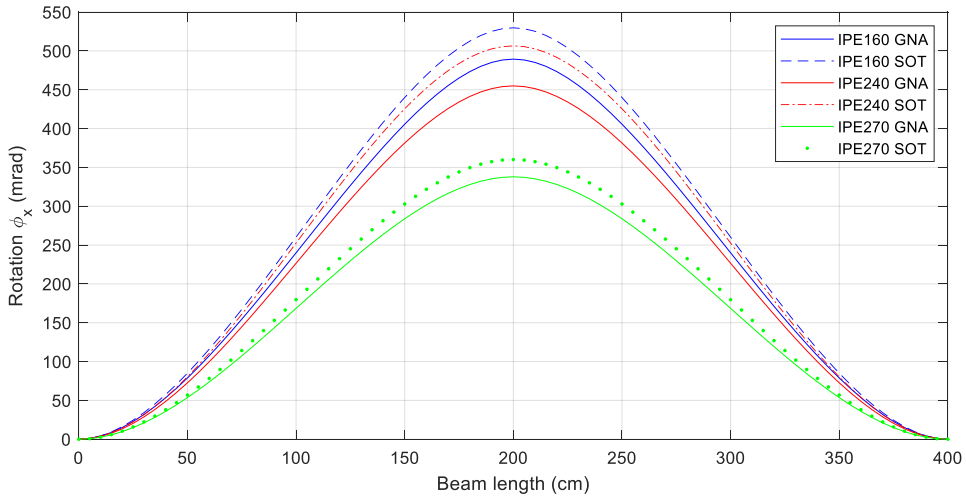

Figure 4.54 Variation of φ_x along the length load factor of 1: fixed-fixed system, M_T load, open profiles, and 1D elements

4.1.2.4 Fork-fixed system

For the fork-fixed system under $\mathbf{V_z}$ action, the following observations have been made:

- **Open:** the variation of u_z for 1D and 2D elements remains below 5% for all profiles except one, IPE140 (5.3%) as seen in Figure 4.55 and Figure 4.56. Moreover, higher peaks are observed for IPE profiles. The maximum displacement amounts to 2.25 cm (see Figure 4.57) and the same behavior between 1D and 2D elements is seen, higher displacements the lower *a* is.
- **Open:** for 1D elements the profiles with low values of *a* (particularly IPE profiles) show variation for φ_x higher than 5% as shown in Figure 4.58. This variation is consistent when values of rotation are high as seen in Figure 4.59. φ_x reaches to about 0.2 rad (11.5º) at a load factor of 1.
- **Open:** φ_y for 1D elements presents higher variation for the IPE profiles with the lowest *a* (similarly as in u_z) up to 9.8%. In the case of 2D elements, the error is high only the IPE profile with the lowest *a*. Nevertheless, φ_y is close to the inflection point and its maximum value amounts only to 4.15 mrad (0.24º) (see Figure 4.60).
- **Closed**: similarly, as in the fork-fork system, u_z and φ_y show relevant variation for the RHS profile with the lowest value of *a*. For u_z, the r_{error} reaches 9.1% for 1D elements and 0.12% for 2D elements (see Figure 4.61 and Figure 4.62). The error in 1D elements happens due to tension forces that are present in GNA but not in SOT without imperfections. Moreover, for the same profile, a variation of about 0.3 cm (10% difference) between 1D and 2D elements at a load factor of 1 is also seen (see Figure 4.63 and Figure 4.64). For this case, when the profile is subjected to a tension force, lower displacements are obtained which is the case of 1D elements, for 2D elements, however, the tension effect does not occur because of how the modelling was addressed. The rest of the profiles remain with close values of displacement and low r_{error}.

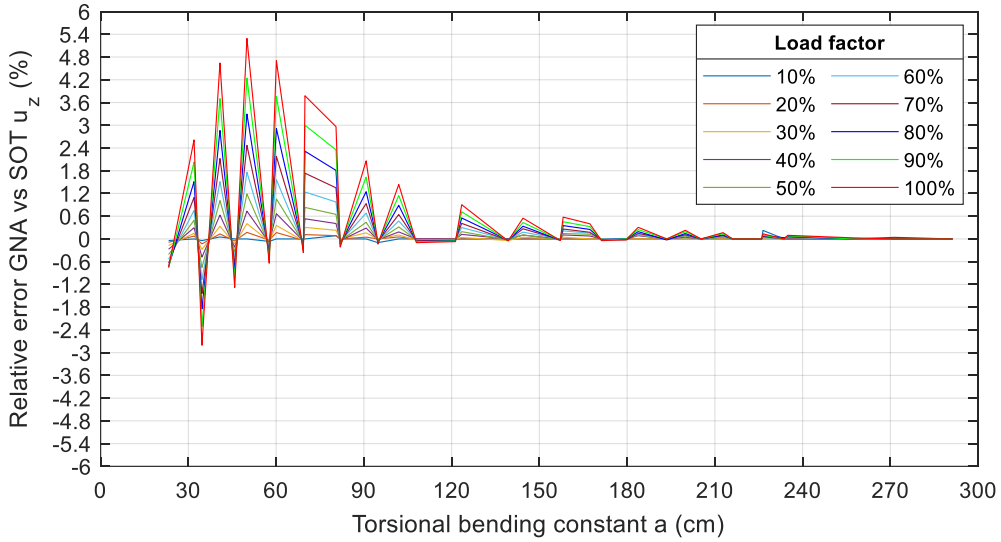

Figure 4.55 Relative error u_z: fork-fixed system, V_z load, open profiles, and 2D elements

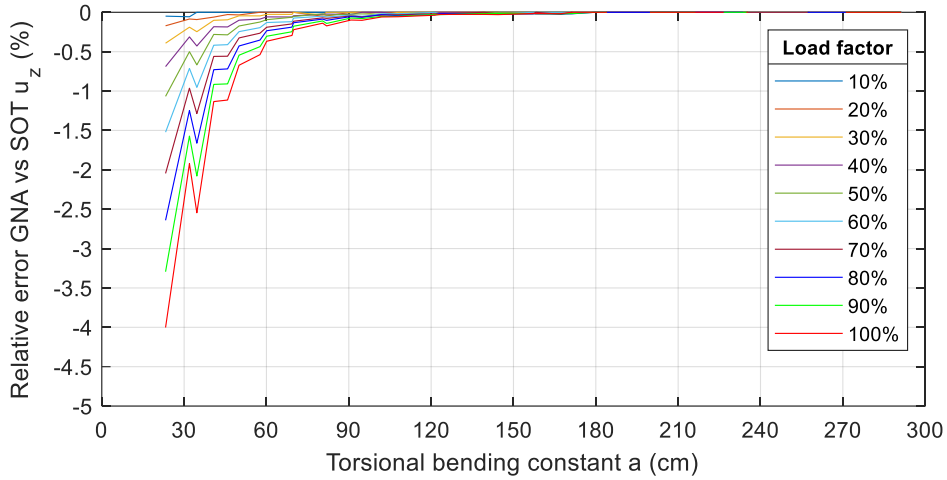

Figure 4.56 Relative error u_z: fork-fixed system, V_z load, open profiles, and 1D elements

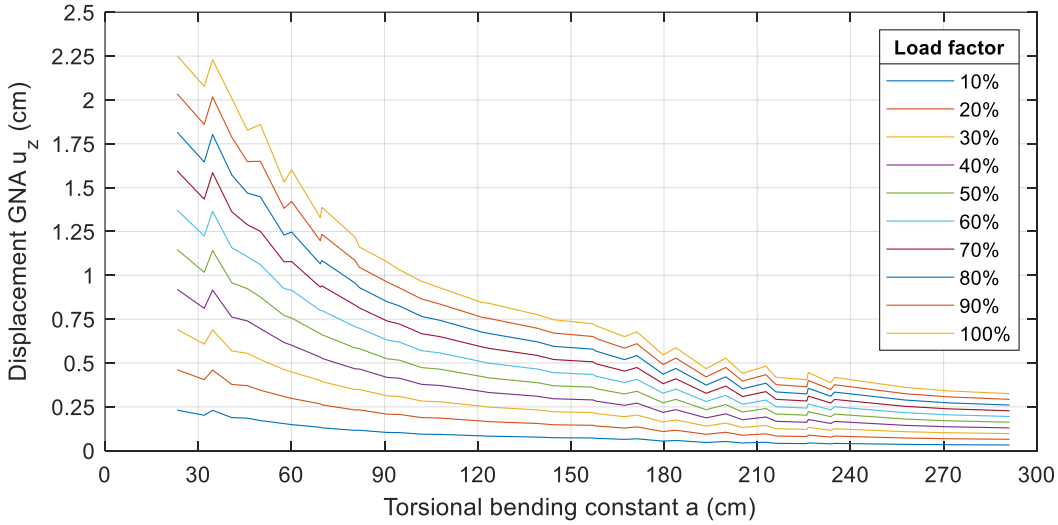

Figure 4.57 Displacement u_z: fork-fixed system, V_z load, open profiles, and 1D elements

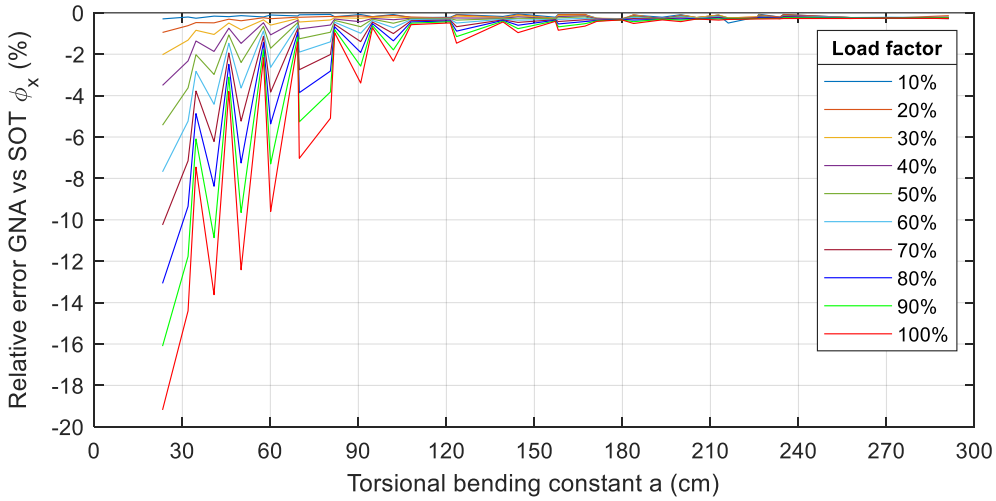

Figure 4.58 Relative error φ_x: fork-fixed system, V_z load, open profiles, and 1D elements

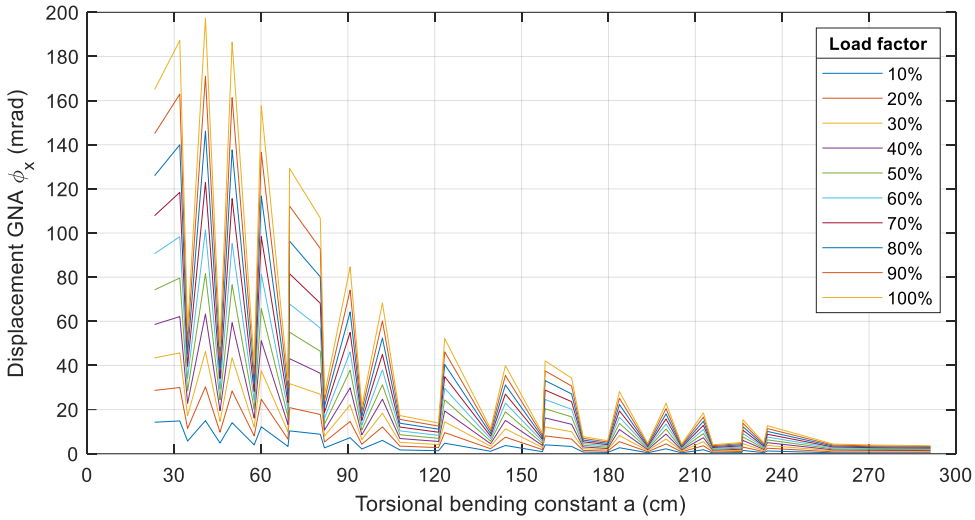

Figure 4.59 Displacement φ_x: fork-fixed system, V_z load, open profiles, and 1D elements

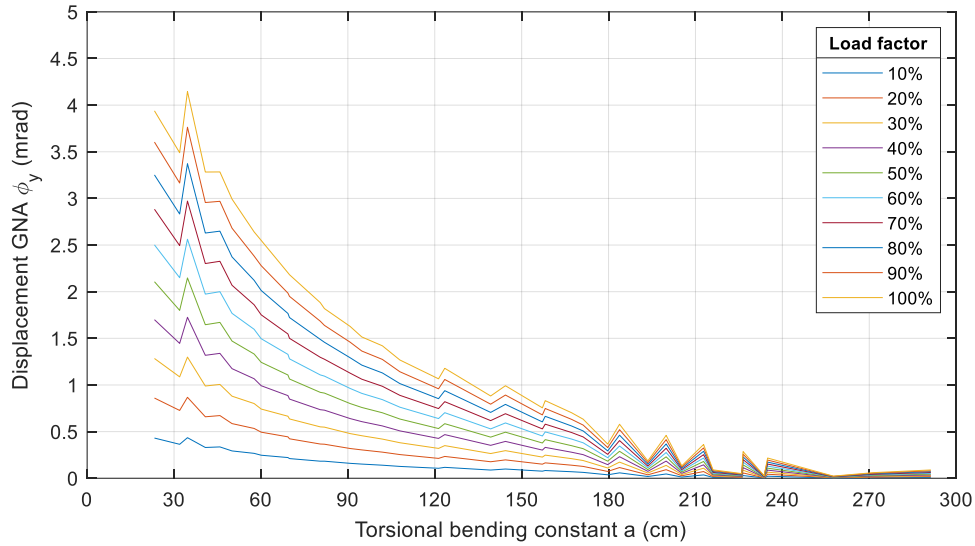

Figure 4.60 Displacement φ_y: fork-fixed system, V_z load, open profiles, and 1D elements

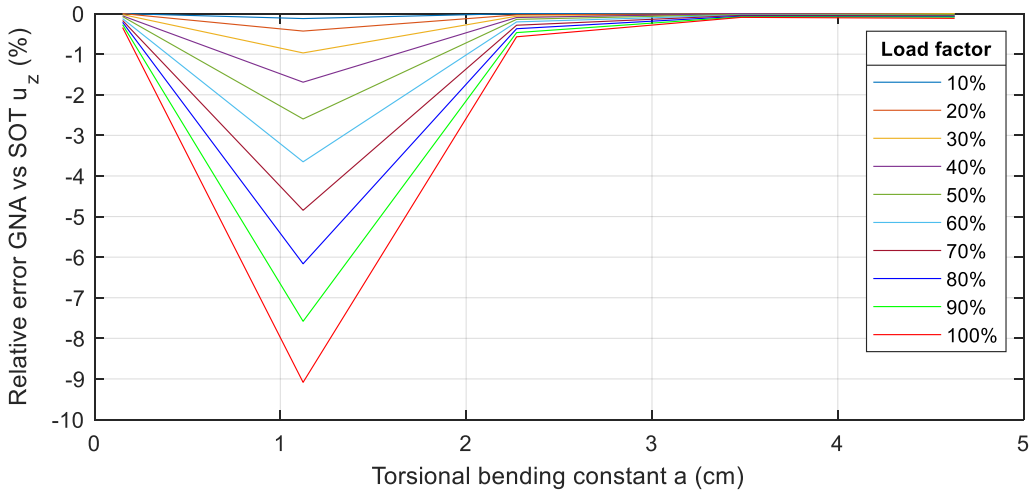

Figure 4.61 Relative error u_z: fork-fixed system, V_z load, closed profiles, and 1D elements

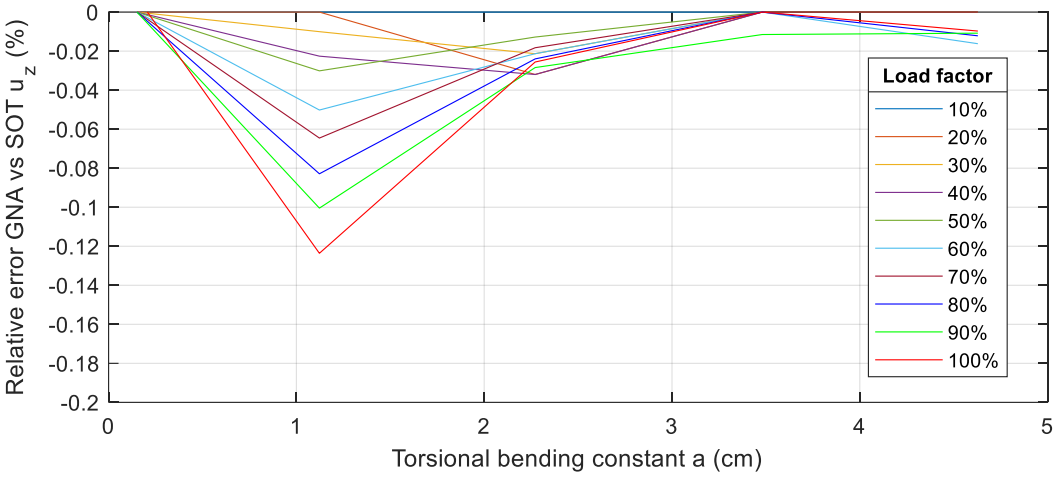

Figure 4.62 Relative error u_z: fork-fixed system, V_z load, closed profiles, and 2D elements

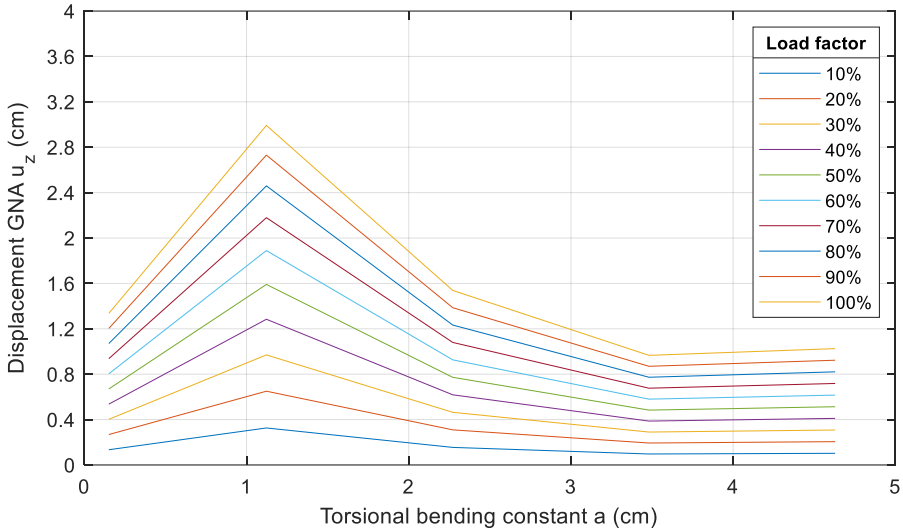

Figure 4.63 Displacement u_z: fork-fixed system, V_z load, closed profiles, and 1D elements

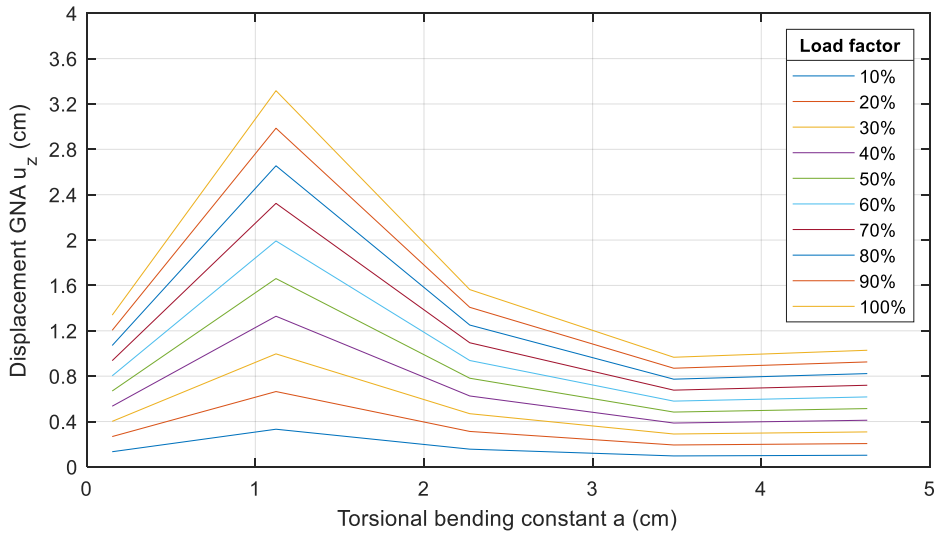

Figure 4.64 Displacement u_z: fork-fixed system, V_z load, closed profiles, and 2D elements

In regard to $\mathbf{M_y}$ action, the following remarks have been found:

- **Open:** low variation exists in 1D elements for u_z (less than 2.5%) and the maximum displacement is 1.26 cm (0.315% drift). 2D elements show high r_{error} without any clear trend. Moreover, the magnitude of u_z differs to 1D elements. Thus, no good agreement of results exists for M_y in 2D elements as they were modelled.
- **Open:** for 1D elements with the lowest *a* (particularly IPE) show r_{error} for φ_x higher than 5% and up to 31% as seen in Figure 4.65. In this case, the maximum rotation is 55 mrad (3.15º) as seen in Figure 4.66.
- **Open:** φ_y shows almost no variation for 1D elements (less than 1%). 2D elements similar to u_z present no good agreement of results.
- **Closed:** similarly, as for V_z, u_z and, φ_y show higher variation for the RHS profile with the lowest value of *a*. For u_z, the r_{error} reaches 6% for 1D elements and 0.1% for 2D elements. Moreover, lower values for u_z and φ_y are found in 1D elements. For, 2D elements it is higher due to the inexistence of tension forces. The rest of the profiles remain with close values of displacement and low r_{error} (see Figure 4.67 and Figure 4.68).

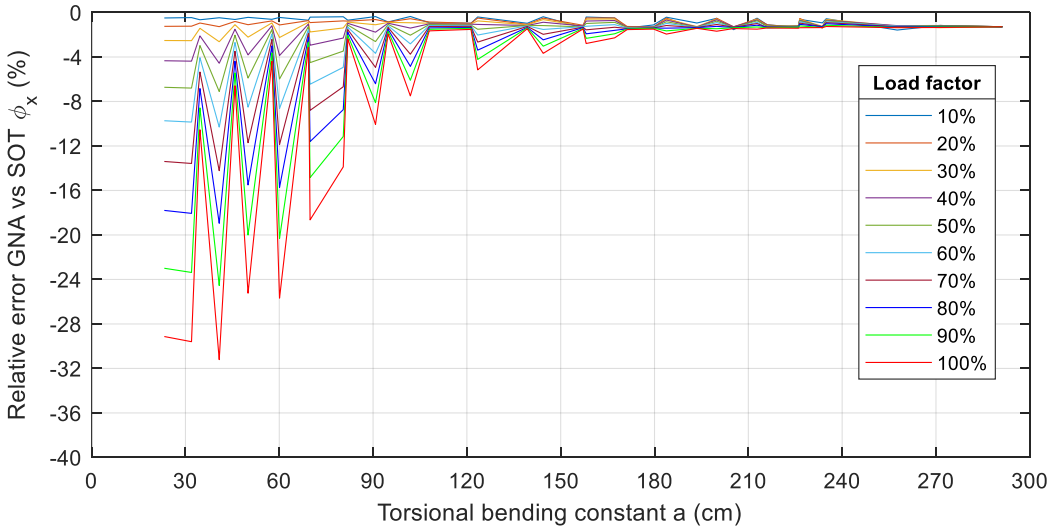

Figure 4.65 Relative error φ_x: fork-fixed system, M_y load, open profiles, and 1D elements

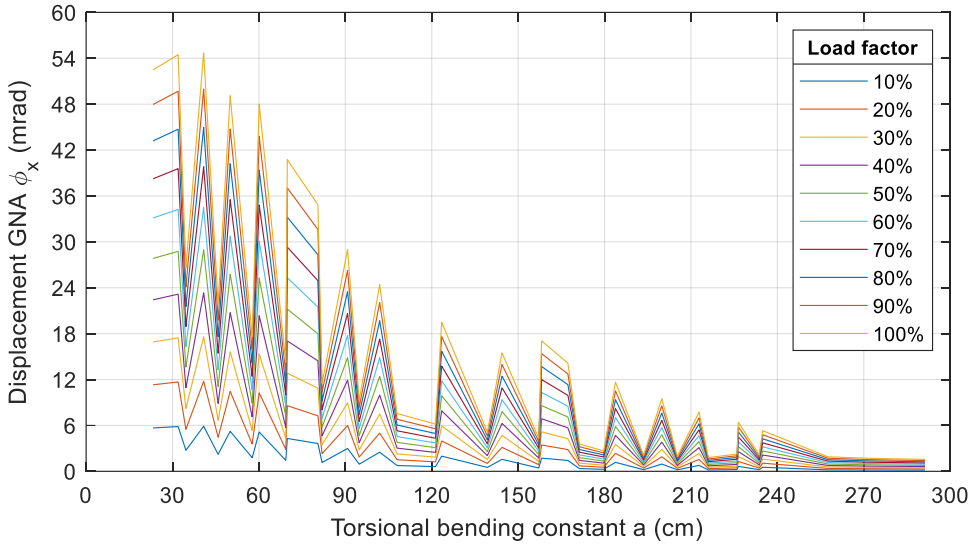

Figure 4.66 Displacement φ_x: fork-fixed system, M_y load, open profiles, and 1D elements

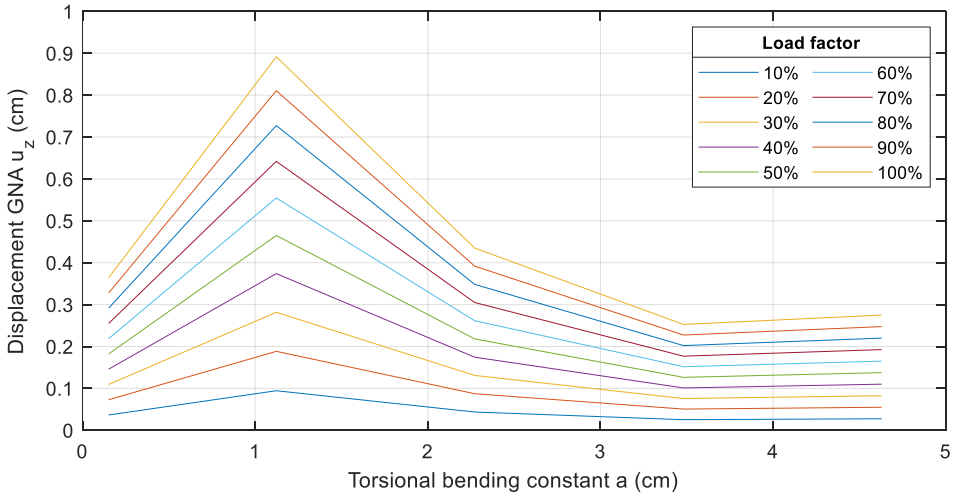

Figure 4.67 Displacement u_z: fork-fixed system, M_y load, closed profiles, and 1D elements

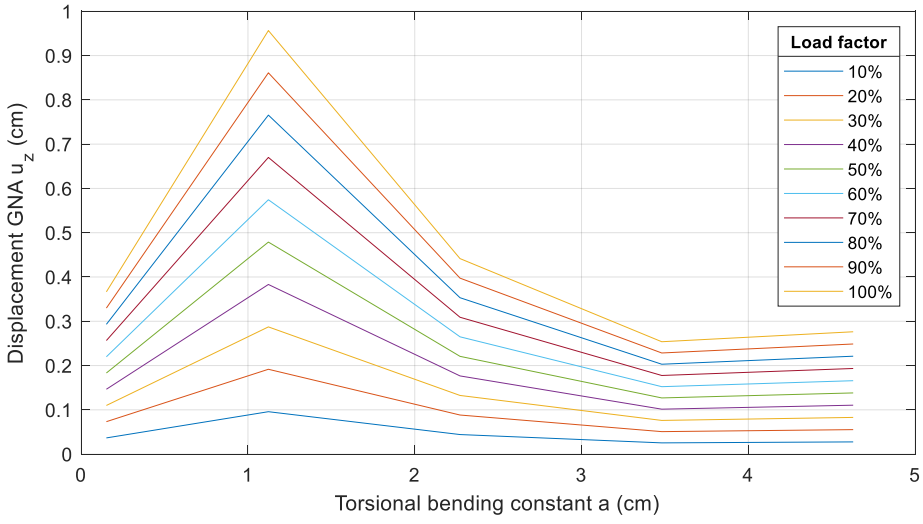

Figure 4.68 Displacement u_z: fork-fixed system, M_y load, closed profiles, and 2D elements

Concerning **M_T** action, the following assertions have been found:

- **Open:** starting from a load factor of 0.4 the r_{error} threshold is surpassed for φ_x in 1D elements as seen in Figure 4.69. φ_x reaches 0.61 rad (35º) as illustrated in Figure 4.70. Furthermore, at a load factor of 0.3, the r_{error} threshold is surpassed in 2D elements and high variation of rotation values with 1D elements is found. Thus, as in the fixed-fixed system, GNA and SOT are not in agreement for M_T with 2D elements.
- **Open:** for 1D elements Ω has a variation up to 34% (see Figure 4.71). The highest values are seen especially for IPE profiles. The maximum Ω reaches 0.091 m^{-1} as shown in Figure 4.72 for GNA.
- **Closed:** similarly, as the fork-fork system, φ_x shows almost no variation for 1D and 2D elements with relative errors under 0.9%. The magnitudes of displacement also remain close. The maximum value reaches up to 0.16 rad (9.2º) for a load factor of 1.

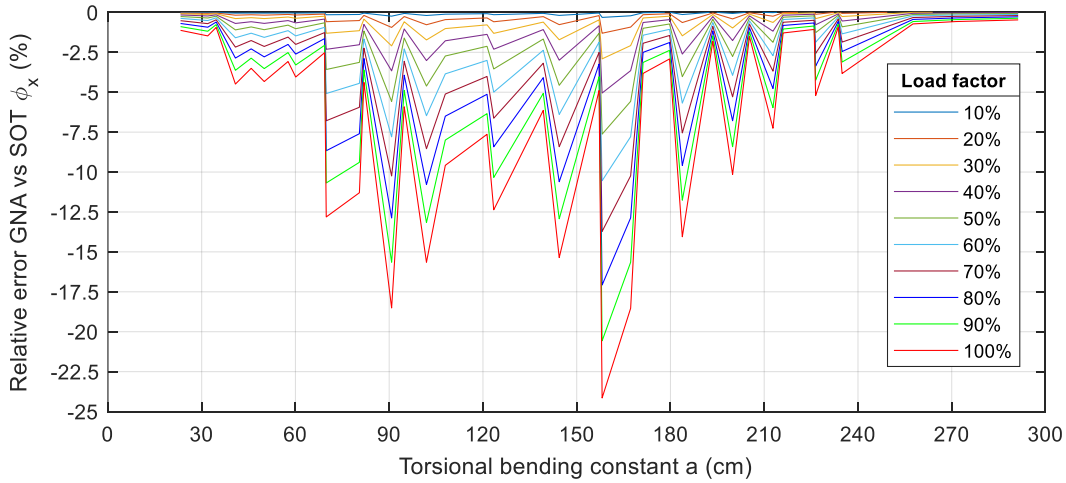

Figure 4.69 Relative error φ_x: fork-fixed system, M_T load, open profiles, and 1D elements

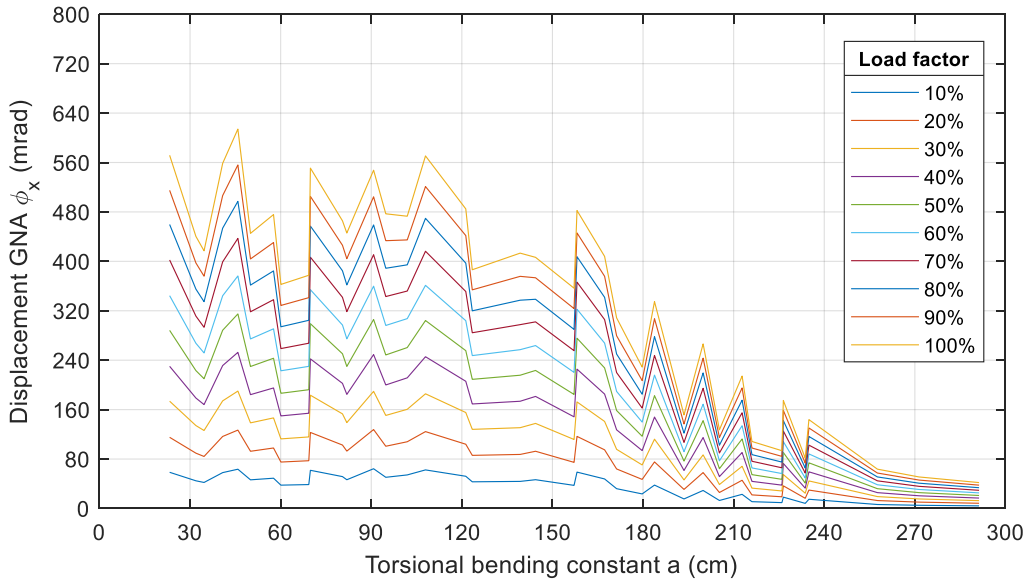

Figure 4.70 Displacement φ_x: fork-fixed system, M_T load, open profiles, and 1D elements

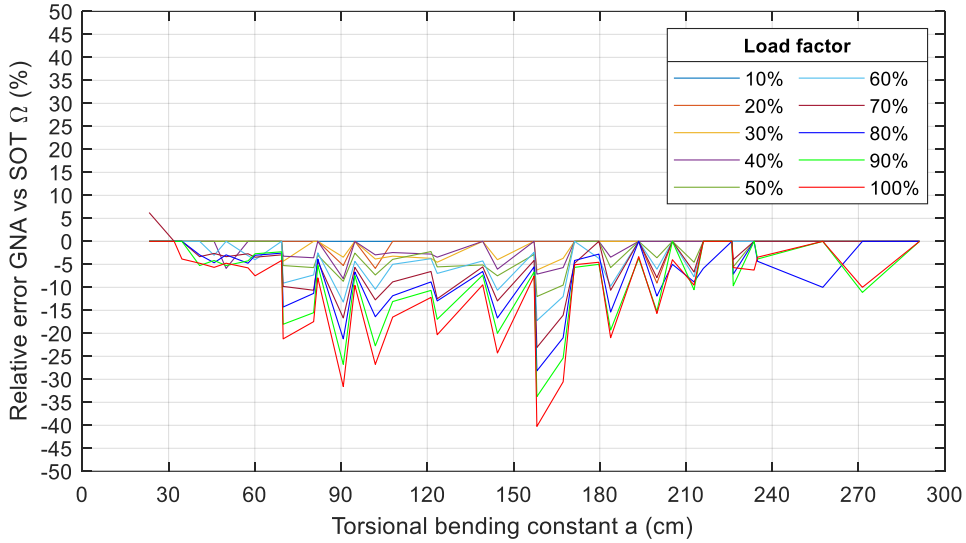

Figure 4.71 Relative error Ω: fork-fixed system, M_T load, open profiles, and 1D elements

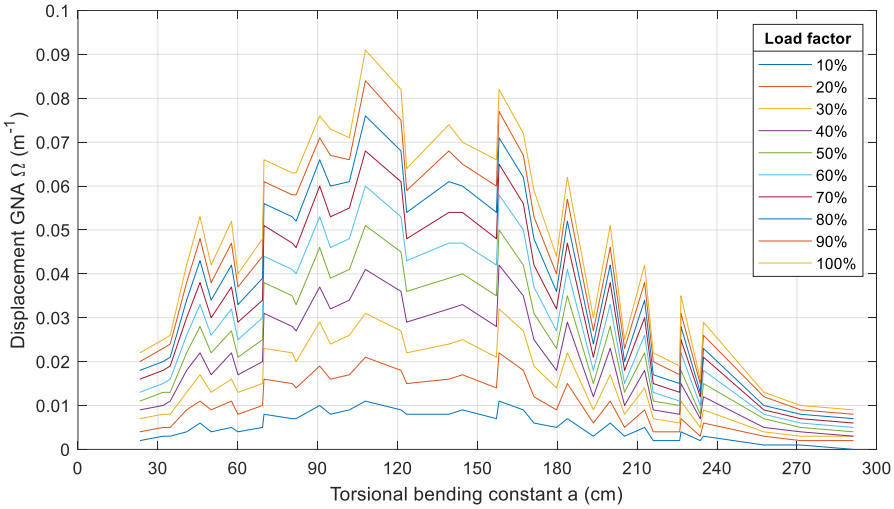

Figure 4.72 Displacement Ω: fork-fixed system, M_T load, open profiles, and 1D elements

It has been found that the modelling of fork supports in the case of 2D models with closed cross-section subjected to bending (V_z and M_y) is not the adequate. It results in variation for the fork-fork and fork-fixed systems. The effect was observed particularly for the RHS 100x50x6 (lowest value of *a*). The supports don't consider axial displacement restriction u_x at both ends (see Figure 4.73), therefore, no introduction of axial force exists, consequently, variation of u_z occurs. The presence of tension forces gives lower values of u_z and φ_y because it reduces compression stresses caused by bending. In Figure 4.74, the magnitude of tension forces for GNA, which are introduced in closed profiles (V_z action at a load factor of 1) with 1D elements but not in 2D elements, are shown.

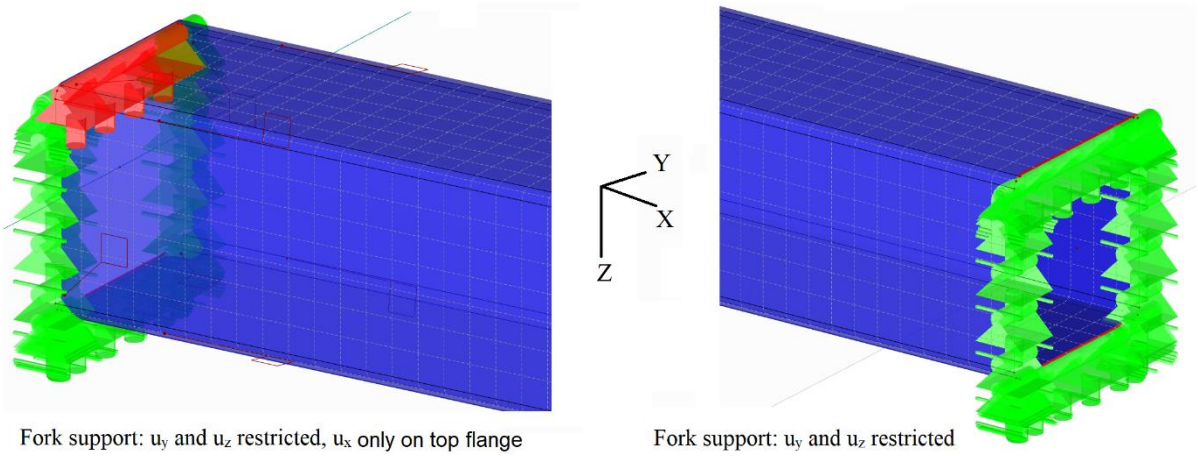

Figure 4.73 Fork-fork supports of closed profiles with 2D elements: (left) left end (right) right end

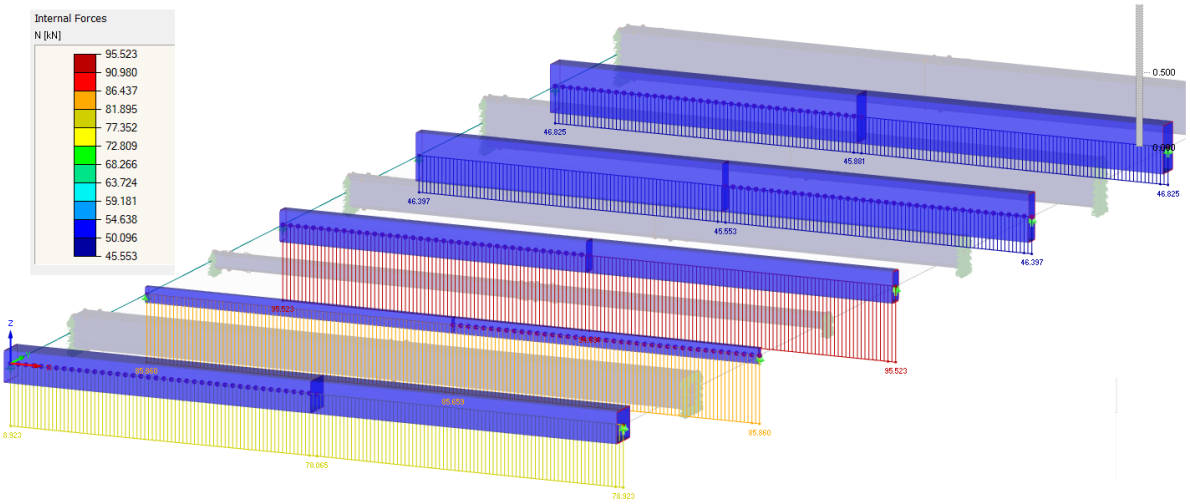

Figure 4.74 Fork-fork system: tension force GNA, V_z load, closed profiles 1D elements

The assumptions for modelling using 2D elements should be carefully considered, particularly regarding the assignment of loads and supports. For instance, the nodal moments (M_y and M_T) applied in 2D elements of open profiles do not give accurate results, and in this project are not considered useful. In the case of elastic analysis (benchmark problems section 3.2.2), the assumptions used in this study, such as the nodal constraints, the stiffening of the web, and the application of nodal moments, produce no relevant difference in the results. However, they prove to be of importance in the analysis with SOT and GNA. This is the case of M_y and M_T for all open cross-section models with 2D-shell elements.

4.1.3 Internal forces

In this section, internal forces results (see Table 3.9) are analyzed and compared as presented in Table 3.12. Two types of figures have been prepared. The first one shows the relative error r_{error} vs the bending torsional constant *a* for every load level (0 to 100%). Similarly, the second type shows the magnitude of internal forces vs *a* for every load level. In this figure, for open profiles, an inset of the values of *a* up until 170 cm is also presented. Only the most relevant figures are presented here. The complete set of figures can be found in Appendix III.

4.1.3.1 Fixed-free system

The following observations have been made for the fixed-free system under $\mathbf{V_z}$ action:

- **Open:** internal forces V_z and M_y show almost no variation with relative errors under 0.1%. The point of extraction corresponds to the support for this system, hence, considering stability, all forces have to be in equilibrium at the support even for high values of V_z and M_y (see Figure 4.75 and Figure 4.76)
- **Closed**: similarly, as in open profiles, V_z and M_y show almost no variation with r_{error} under 0.2%.

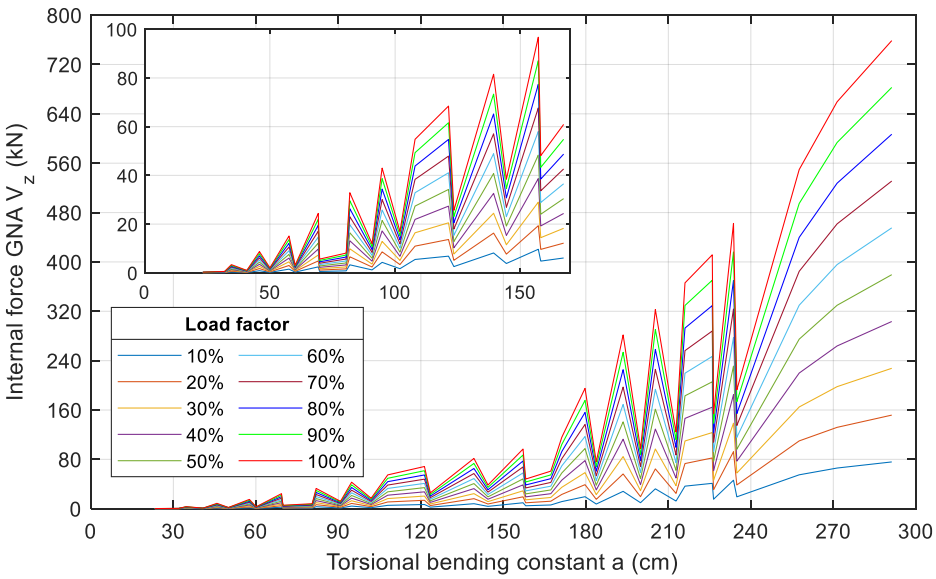

Figure 4.75 Internal force V_z: fixed-free system, V_z load, open profiles / Inset of the graphic corresponds to values of a up to 170cm

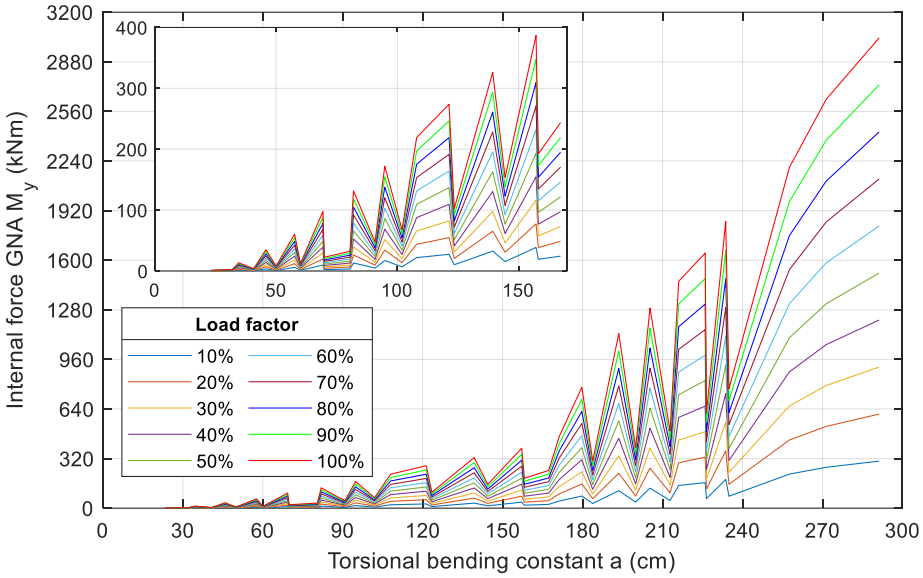

Figure 4.76 Internal force M_y: fixed-free system, V_z load, open profiles / Inset of the graphic corresponds to values of a up to 170cm

In refer to **M_y** action, the following remarks have been found:

- **Open:** no variation is found for M_y for all profiles. For the fixed-free system, M_y values remain the same at support for SOT and GNA.
- **Closed:** same as in open profiles, no difference is found for M_y.

Regarding **M_T** action, the following assertions have been found:

- **Open:** M_T and M_w present almost no variation with relative errors under 0.1%, even though, values of the torsional and warping bimoment reach up to approximately 280 kNm and 735 kNm² respectively at a load factor of 1 (see Figure 4.77 and Figure 4.78). A similar trend is seen for both internal forces. Moreover, the higher M_T is the higher M_w is. In Figure 4.79, the variation of primary torsion M_p and secondary torsion M_s is observed for the 3 profiles with the highest value of *a* at the highest load factor. It shows that for open profiles, in the most critical location (support), secondary torsion presents the highest action, thus, it can be used for design of this type of profiles.
- **Closed:** M_T shows no variation at support. In contrast to open profiles, all torsion M_T in closed profiles may be taken as pure St. Venant's torsion M_p.

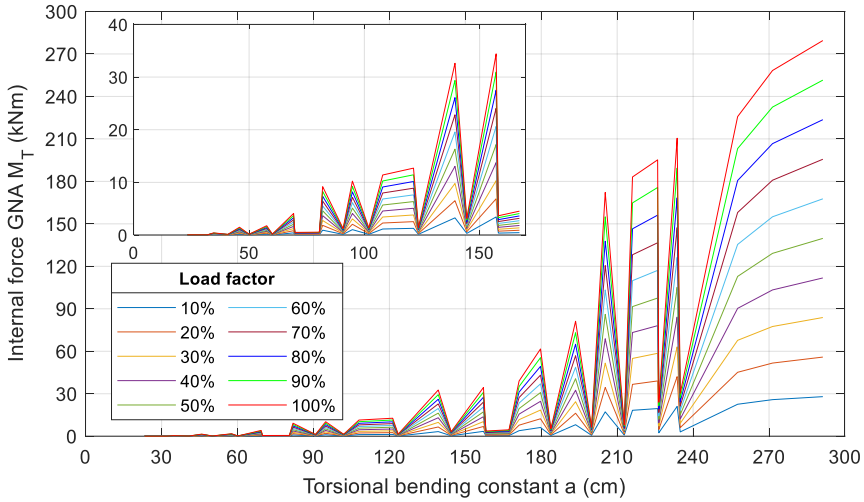

Figure 4.77 Internal force M_T: fixed-free system, M_T load, open profiles / Inset of the graphic corresponds to values of a up to 170cm

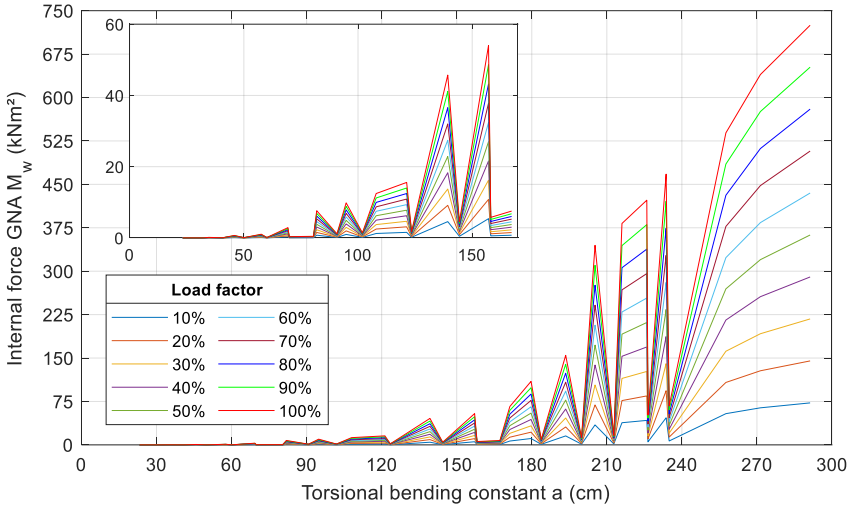

Figure 4.78 Internal force M_w: fixed-free system, M_T load, open profiles / Inset of the graphic corresponds to values of a up to 170cm

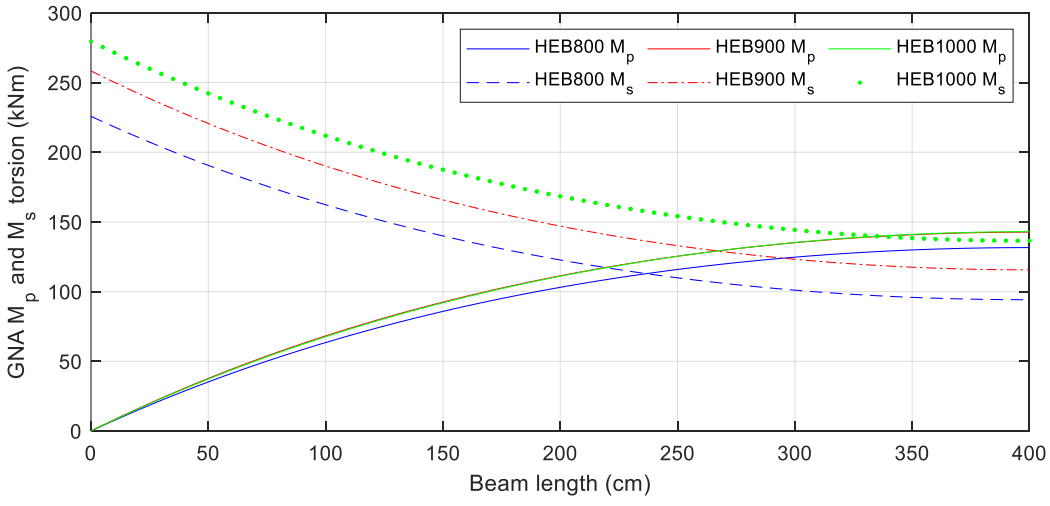

Figure 4.79 Variation of M_p and M_s along the length: fixed-free system, M_T load, open profiles

4.1.3.2 Fork-fork system

Under $\mathbf{V_z}$ action, the following observations have been made for the fork-fork system:

- **Open:** V_z shows almost no variation at midspan (r_{error} lower than 0.5%) but higher variation at supports, where the threshold is surpassed for 3 IPE profiles with low *a* as seen in Figure 4.80. Similarly, for the same profiles M_y shows high variation at midspan as observed in Figure 4.81. The magnitude of the forces are presented in Figure 4.82 and Figure 4.83.
- **Closed**: V_z and M_y show relevant variation just for the RHS profile with the lowest value of *a*. For this profile, the r_{error} reaches 50% for V_z at support and 30% for M_y at midspan (see Figure 4.84 and Figure 4.85). This variation occurs due to the effect of tension forces that are present in GNA but not in SOT without imperfections. When the profile is subjected to a tension force, lower bending moments and shear forces are obtained which is the case of GNA.

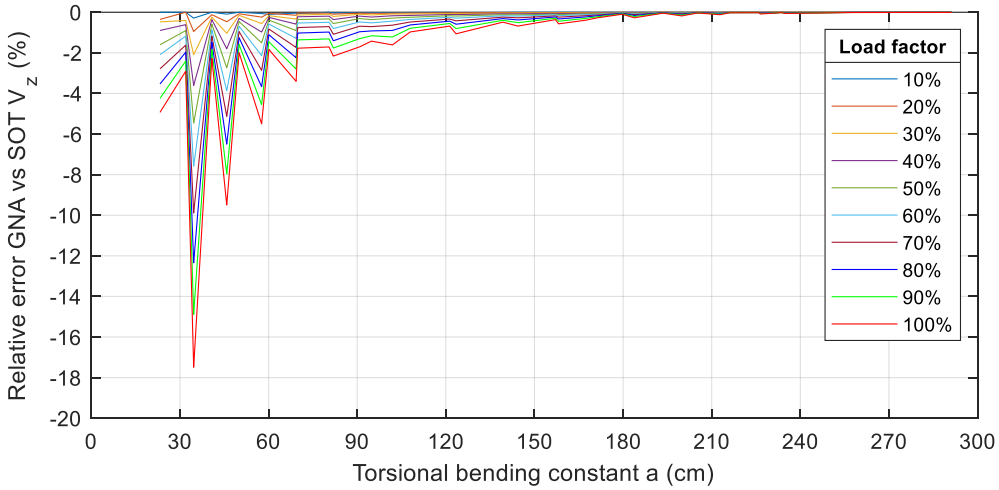

Figure 4.80 Relative error support V_z: fork-fork system, V_z load, open profiles

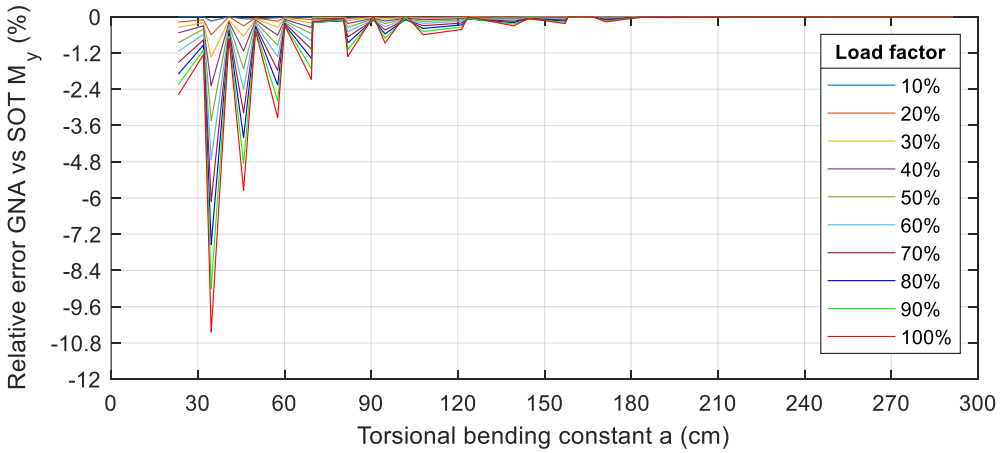

Figure 4.81 Relative error midspan M_y: fork-fork system, V_z load, open profiles

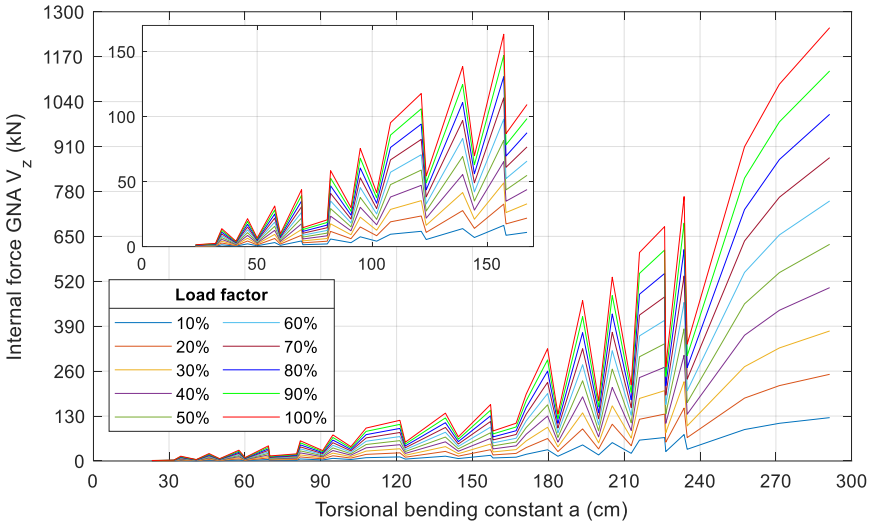

Figure 4.82 Internal force support V_z: fork-fork system, V_z load, open profiles / Inset of the graphic corresponds to values of a up to 170cm

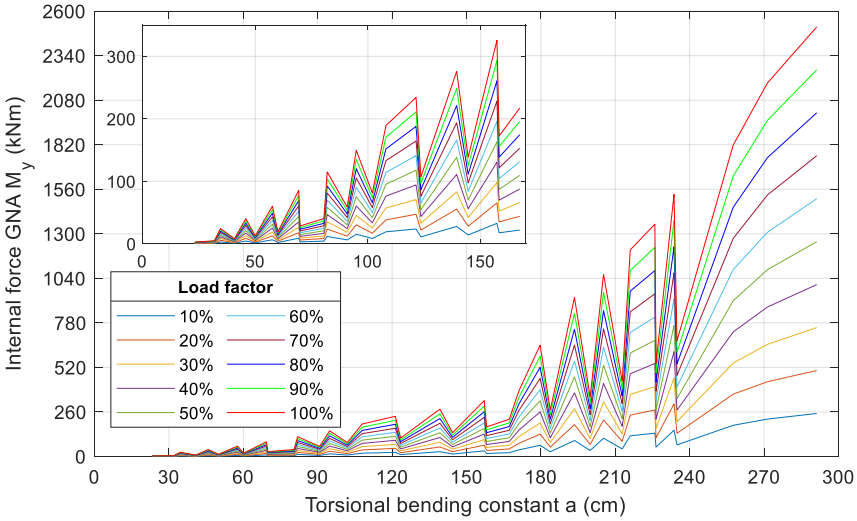

Figure 4.83 Internal force midspan M_y: fork-fork system, V_z load, open profiles / Inset of the graphic corresponds to values of a up to 170cm

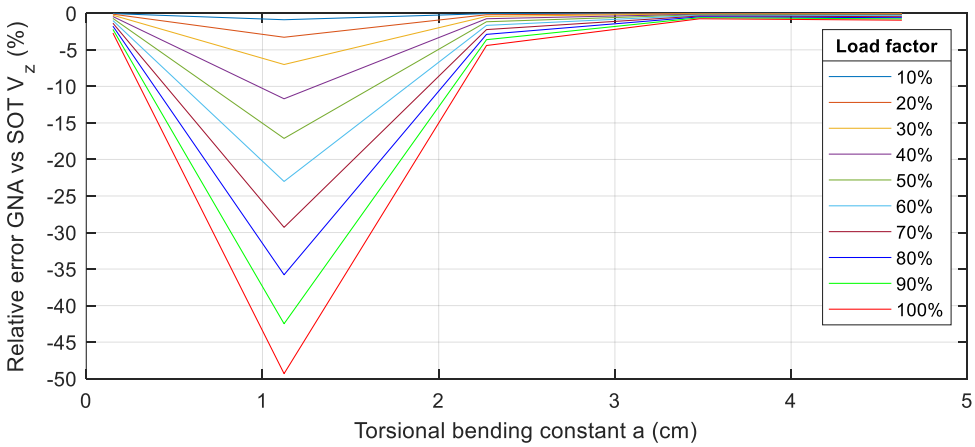

Figure 4.84 Relative error support V_z: fork-fork system, V_z load, closed profiles

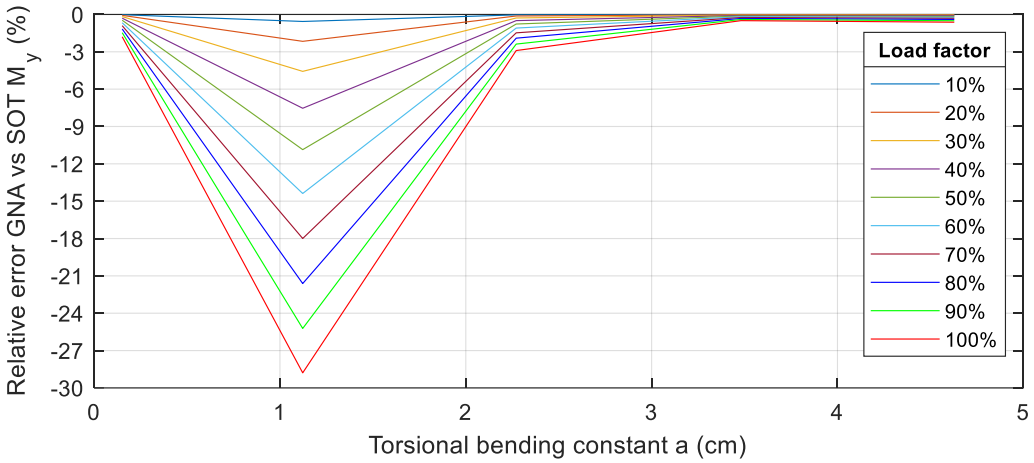

Figure 4.85 Relative error midspan M_y: fork-fork system, V_z load, closed profiles

In regard to $\mathbf{M_y}$ action, the following remarks have been found:

- **Open:** V_z at midspan shows higher r_{error} for profiles with lowest *a* specially for IPE sections as shown in Figure 4.86. Moreover, the magnitude of V_z is presented in Figure 4.87. For V_z at support and M_y at midspan, the variation is low and it remains below 1.7%.
- **Closed:** V_z and My show low variation with relative errors under 0.5%, except for the RHS profile with the lowest *a* (up to 4.6% as shown in Figure 4.88). This occurs due to the effect of tension forces that are not introduced in SOT without imperfections.

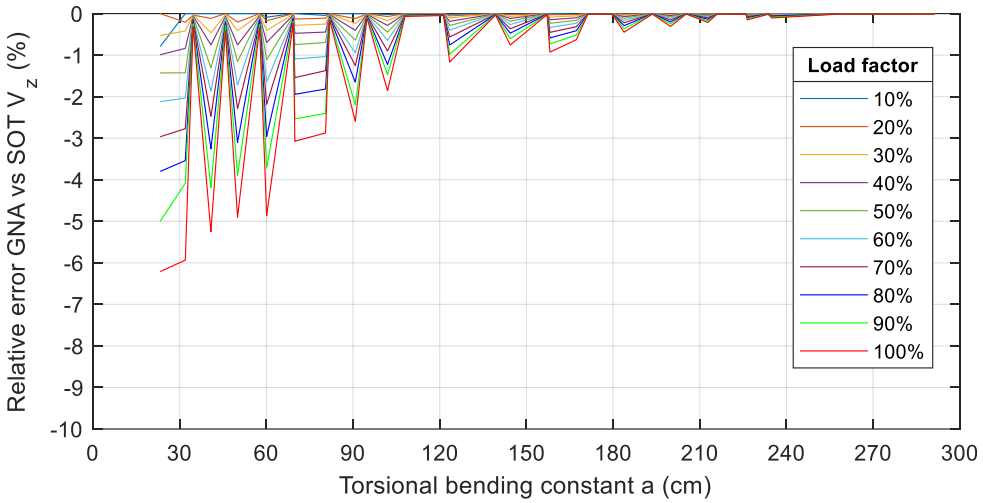

Figure 4.86 Relative error midspan V_z: fork-fork system, M_y load, open profiles

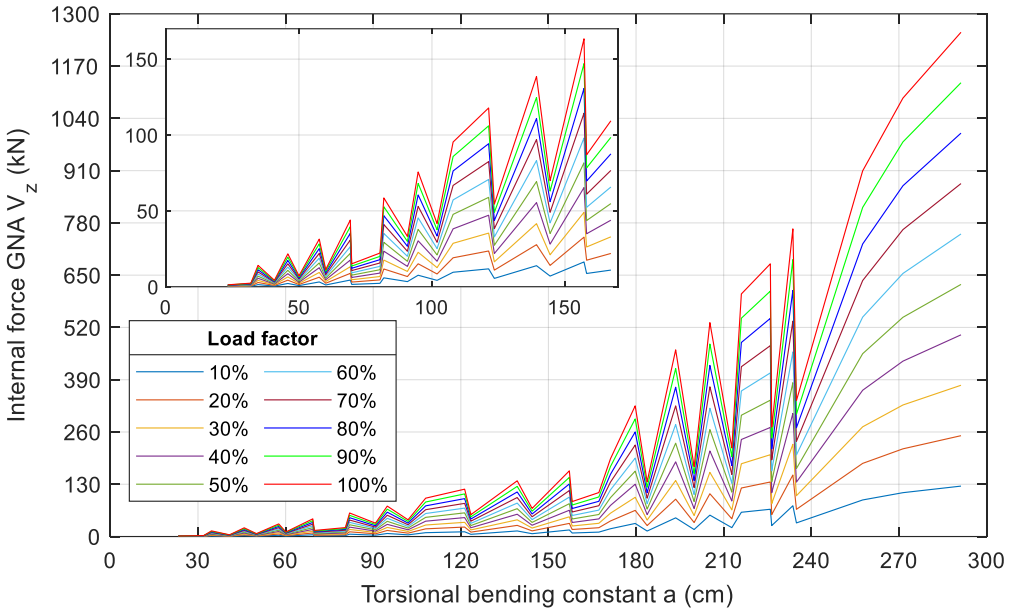

Figure 4.87 Internal force midspan V_z: fork-fork system, M_y load, open profiles / Inset of the graphic corresponds to values of a up to 170cm

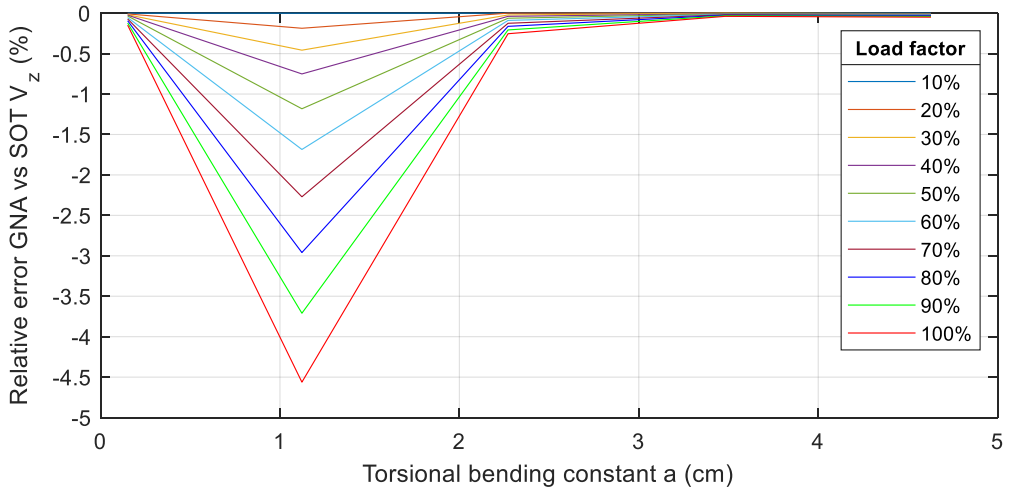

Figure 4.88 Relative error V_z: fork-fork system, M_y load, closed profiles

Concerning **M_T** action, the following assertions have been found:

- **Open:** for M_T at support and midspan almost no variation is found with r_{error} lower than 0.2%. However, for M_w at midspan higher variation is observed up to 36% at a load factor of 1 (see Figure 4.89). The magnitude of M_w at midspan is presented in Figure 4.90. The distribution of M_w along the length of the beam for the 3 profiles with the highest r_{error} and a load factor of 1 is illustrated in Figure 4.91.
- **Closed:** M_T shows no variation both at support and midspan.

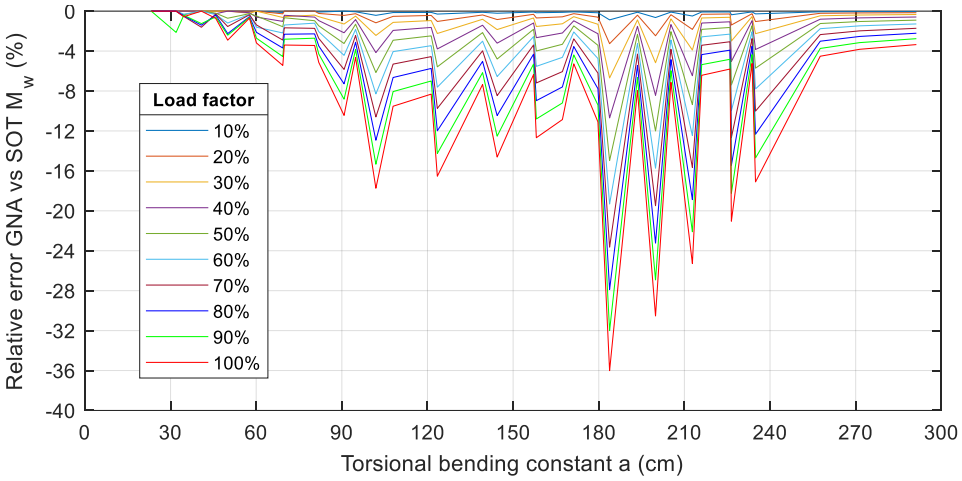

Figure 4.89 Relative error midspan M_w: fork-fork system, M_T load, open profiles

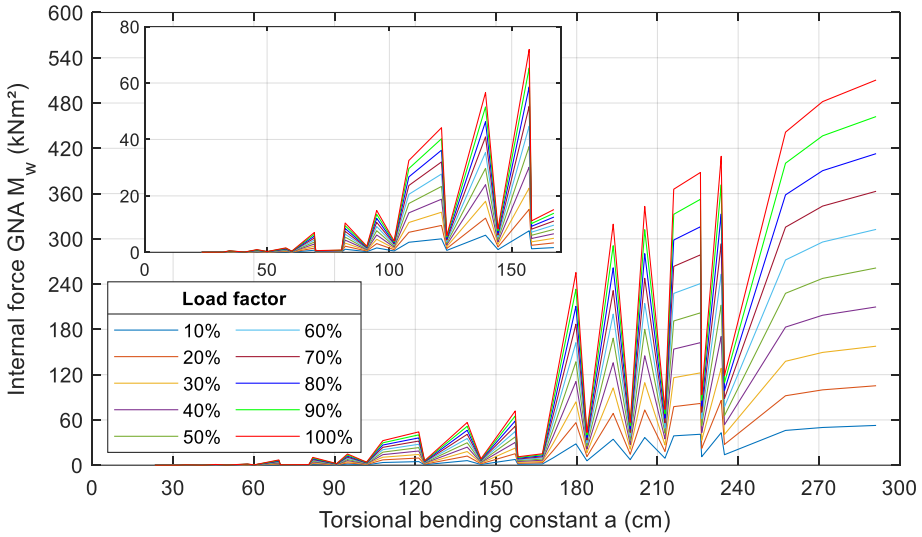

Figure 4.90 Internal force midspan M_w: fork-fork system, M_T load, open profiles / Inset of the graphic corresponds to values of a up to 170cm

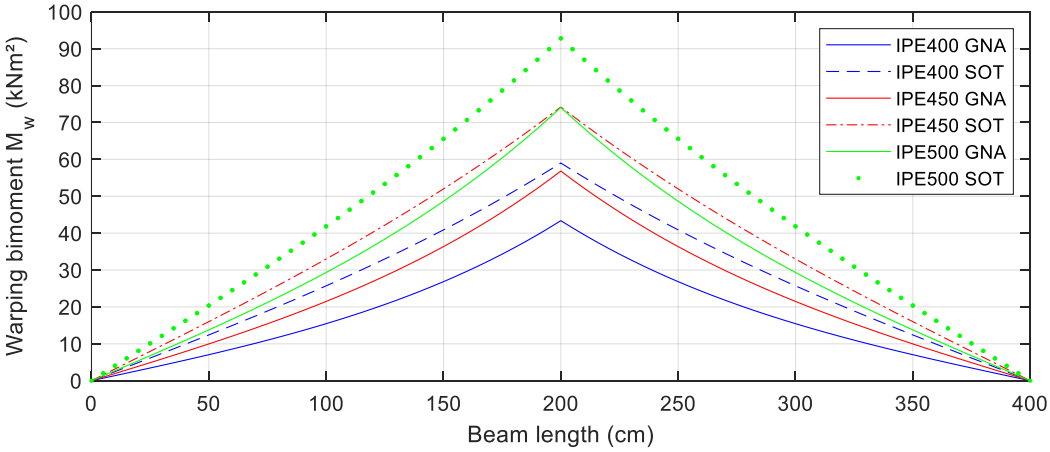

Figure 4.91 Variation of M_w along the length: fork-fork system, M_T load, open profiles

4.1.3.3 Fixed-fixed system

For $\mathbf{V_z}$ action in the fixed-fixed system, the following observations have been made:

- **Open:** V_z shows almost no variation, less than 0.7% at both midspan and supports. In the case of M_y, all members show low variation as well (lower than 3.3%). Particularly for IPE profiles with low values of *a* variation is higher as seen in Figure 4.92.
- **Closed:** V_z shows r_{error} lower than 0.3%. For M_y, the r_{error} amounts up to 3.2% with a peak for the RHS with smaller *a* (see Figure 4.93). This variation is explained again due to inexistence of tension forces in SOT without imperfections.

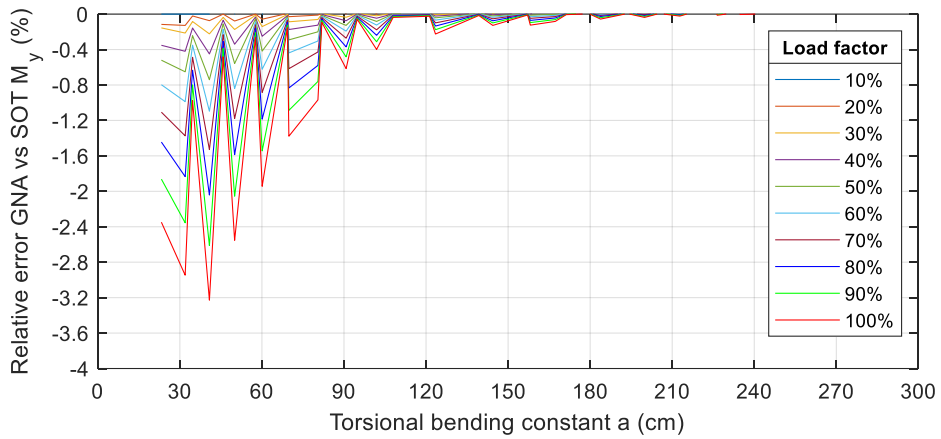

Figure 4.92 Relative error midspan M_y: fixed-fixed system, V_z load, open profiles

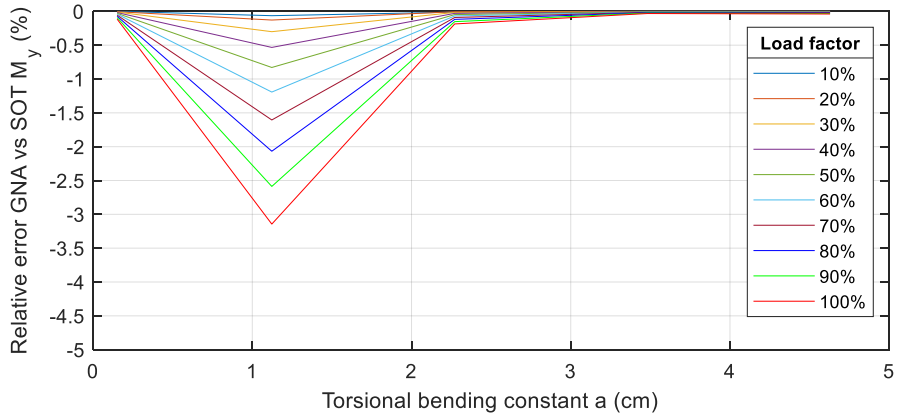

Figure 4.93 Relative error midspan M_y: fixed-fixed system, V_z load, closed profiles

In regard to $\mathbf{M_y}$ action, the following findings are given:

- **Open:** V_z shows low variation at supports (r_{error} lower than 2.7%) but higher variation at midspan, where the threshold is surpassed for the 2 IPE profiles with lowest *a* as seen in Figure 4.94. In the case of M_y, at supports higher variation than the threshold is observed (see Figure 4.95) and r_{error} lower than 2.7% at midspan. The magnitude of the forces are presented in Figure 4.96 and Figure 4.97.
- **Closed:** V_z and M_y show almost no variation at support and at midspan with r_{error} under 1.5%.

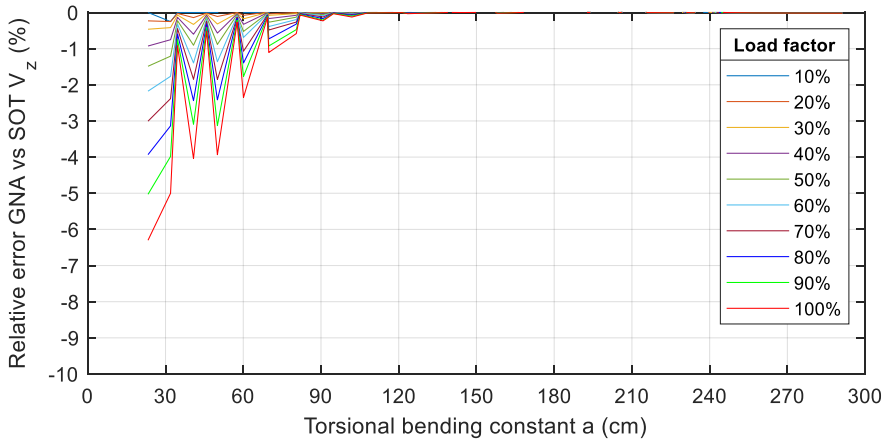

Figure 4.94 Relative error midspan V_z: fixed-fixed system, M_y load, open profiles

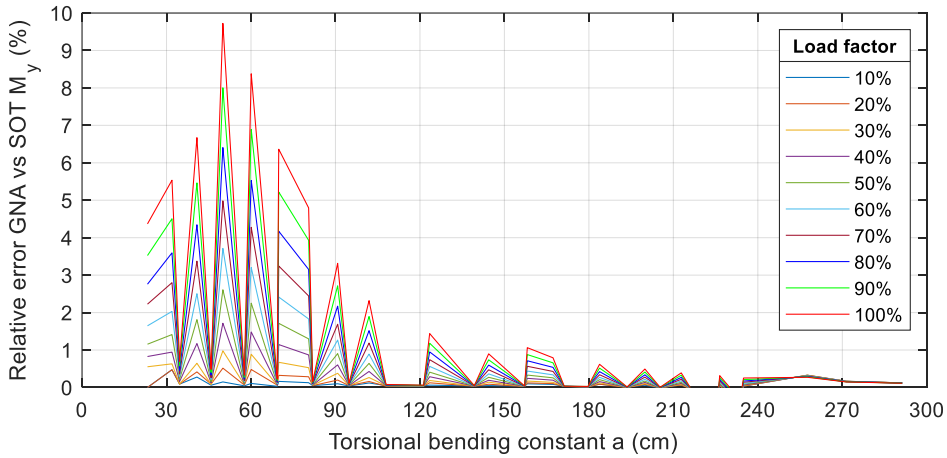

Figure 4.95 Relative error supports M_y: fixed-fixed system, M_y load, open profiles

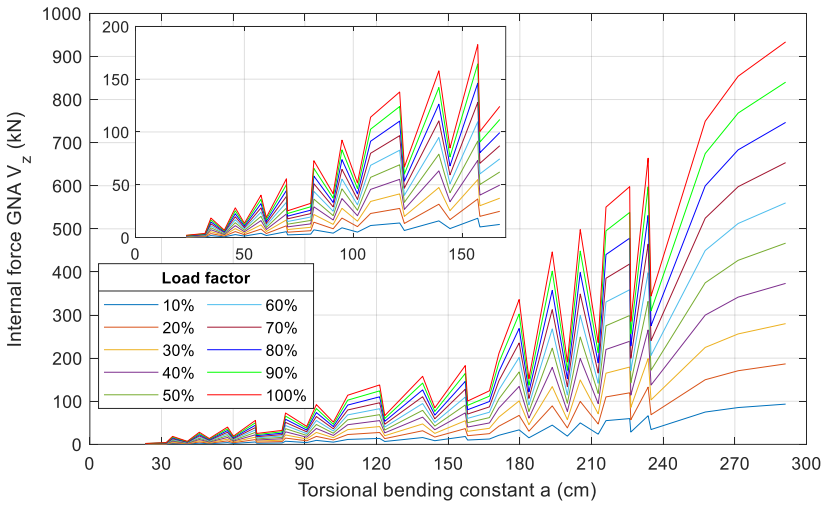

Figure 4.96 Internal force V_z: fixed-fixed system, M_y load, open profiles / Inset of the graphic corresponds to values of a up to 170cm

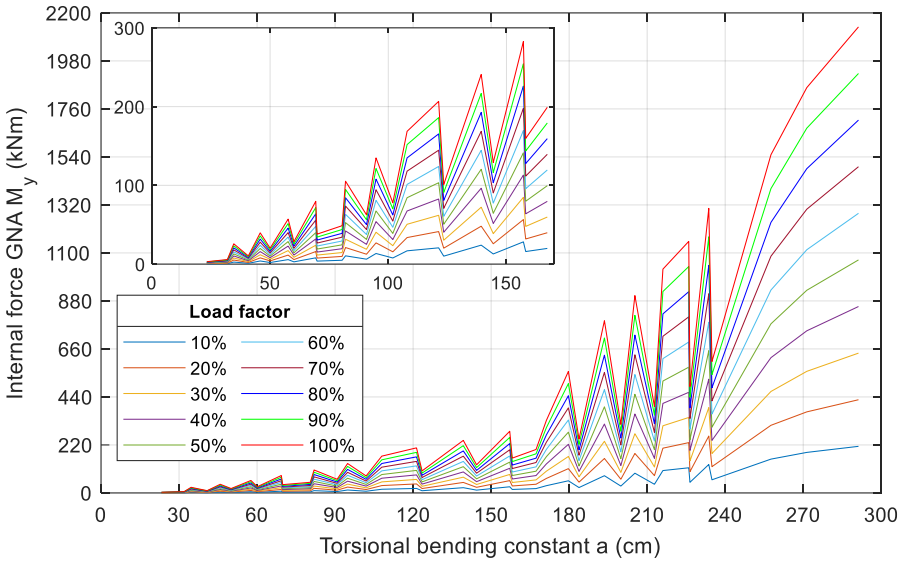

Figure 4.97 Internal force midspan M_y: fixed-fixed system, M_y load, open profiles / Inset of the graphic corresponds to values of a up to 170cm

With regard to $\mathbf{M_T}$ action, the following assertions have been found:

- **Open:** M_T shows r_{error} lower than 0.3% at midspan. At supports, the variation reaches up to 5.2% (see Figure 4.98). M_w presents similar variation at both midspan and supports with r_{error} higher than the threshold up to 9.5% (see Figure 4.99 and Figure 4.100). Furthermore, in Figure 4.101, the variation of primary torsion M_p and secondary torsion M_s is observed for the 3 IPE profiles with the lowest value of *a* at the highest load factor. It shows that for open profiles, in the most critical location (supports and midspan), secondary torsion presents the highest action, therefore, their design can be simplifying by considering only secondary torsion and neglecting St. Venant's torsion.
- **Closed:** M_T shows no variation both at support and midspan.

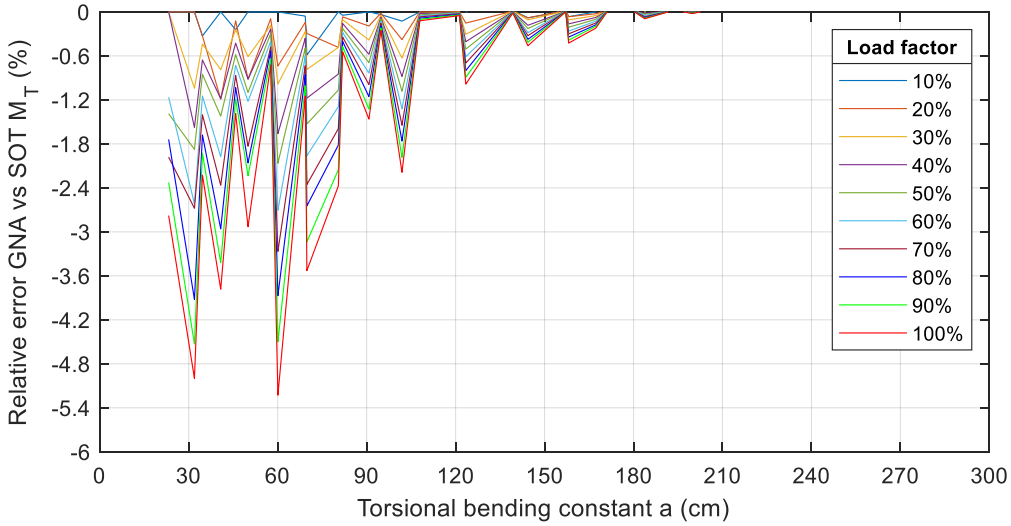

Figure 4.98 Relative error supports M_T: fixed-fixed system, M_T load, open profiles

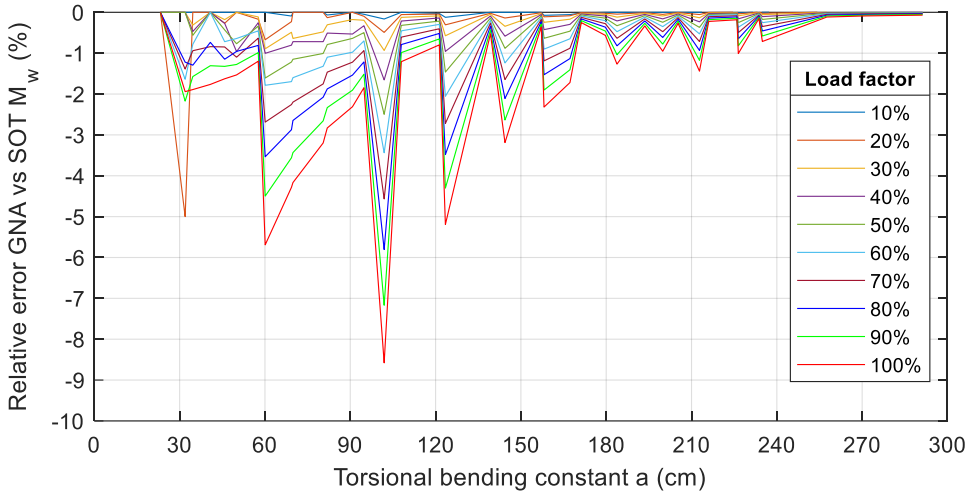

Figure 4.99 Relative error midspan M_w: fixed-fixed system, M_T load, open profiles

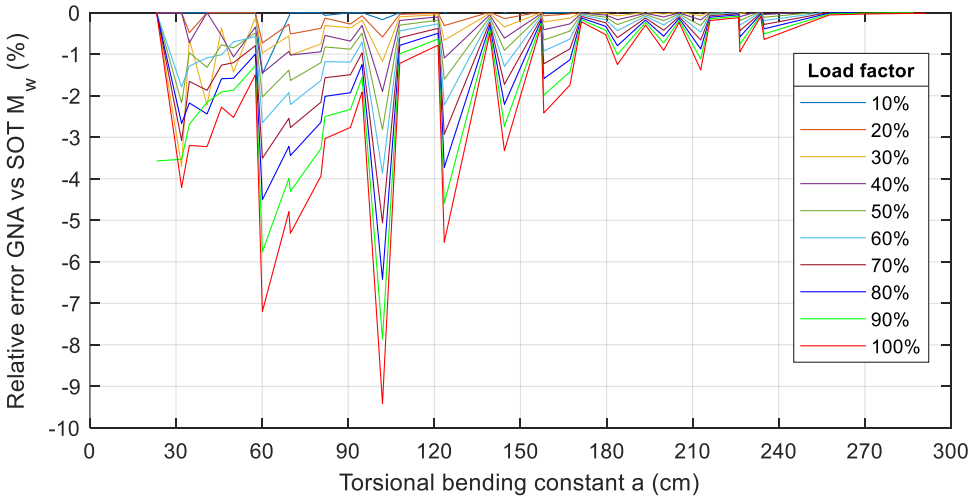

Figure 4.100 Relative error supports M_w: fixed-fixed system, M_T load, open profiles

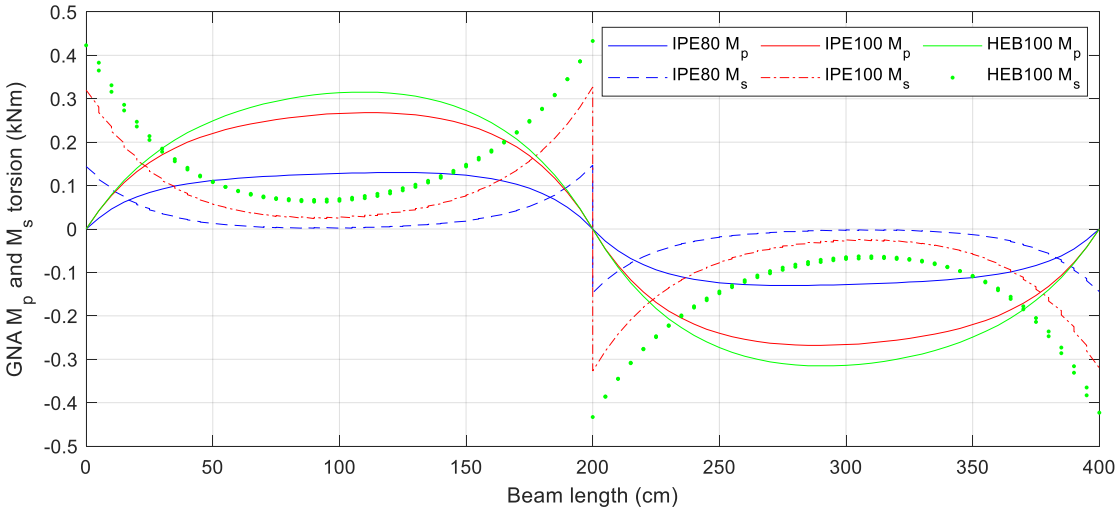

Figure 4.101 Variation of M_p and M_s along the length: fixed-fixed system, M_T load, open profiles

4.1.3.4 Fork-fixed system

For the fork-fixed system under $\mathbf{V_z}$ action, the following observations have been made:

- **Open:** V_z and M_y show low variation at midspan and fixed support (r_{error} lower than 2.5%). Higher variation is seen for V_z at fork support, where the threshold is surpassed for IPE80 profile with the lowest *a* as seen in Figure 4.102. The magnitude of V_z at fork support is presented in Figure 4.103.
- **Closed**: V_z and M_y show relevant variation for the RHS profile with the lowest value of *a*. For this profile, the r_{error} reaches 16% for V_z at fork support and 7.3% for M_y at fixed support (see Figure 4.104 and Figure 4.105). This variation occurs due to the effect of tension forces that are present in GNA but not in SOT without imperfections. When the profile is subjected to tension forces, lower bending moments and shear forces are obtained in GNA.

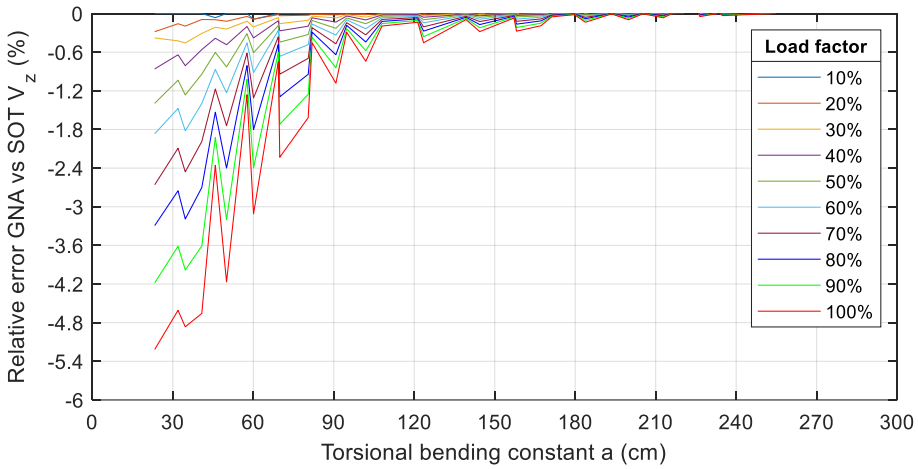

Figure 4.102 Relative error fork support V_z: fork-fixed system, V_z load, open profiles

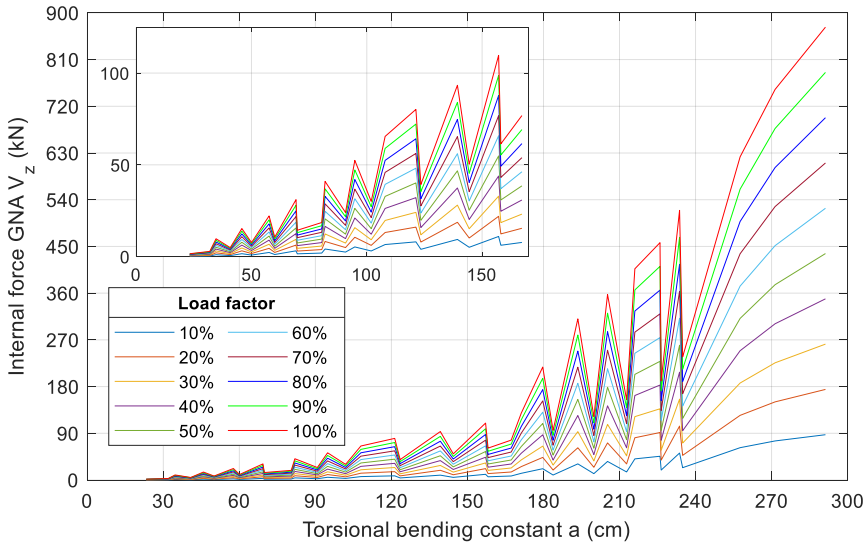

Figure 4.103 Internal force fork support V_z: fork-fixed system, V_z load, open profiles / Inset of the graphic corresponds to values of a up to 170cm

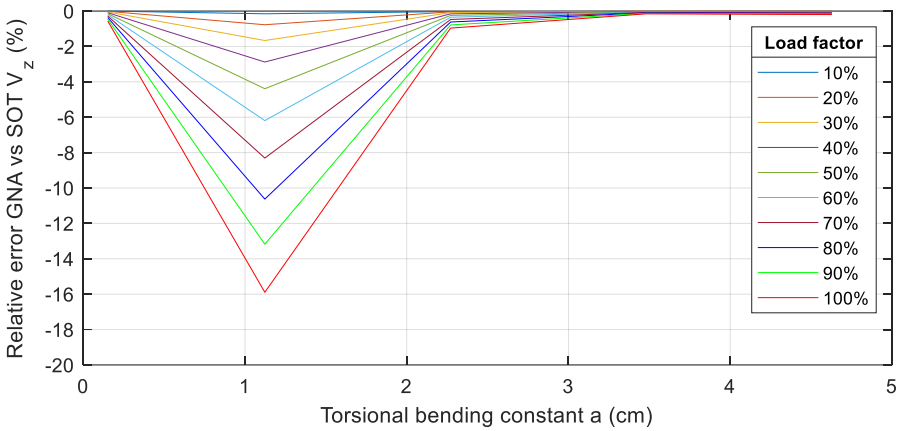

Figure 4.104 Relative error fork support V_z: fork-fixed system, V_z load, closed profiles

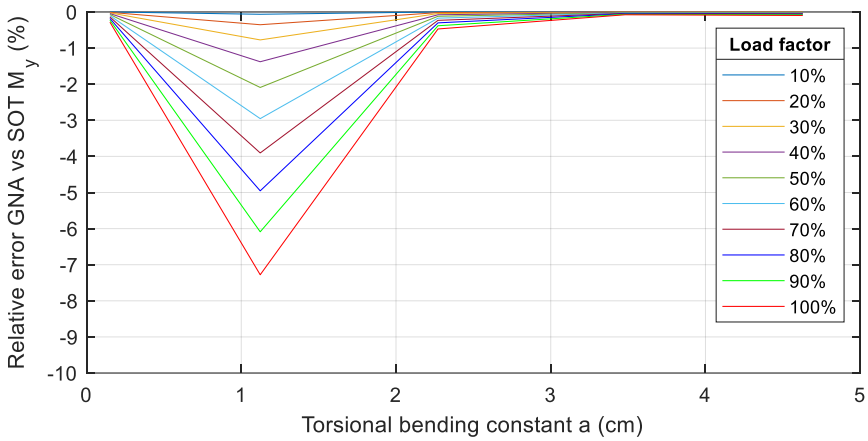

Figure 4.105 Relative error fixed support M_y: fork-fixed system, V_z load, closed profiles

In regard to **M_y** action, the following remarks have been found:

- **Open:** V_z and M_y show almost no variation with r_{error} lower than 1.5% at supports and midspan. Nevertheless, peaks are observed particularly for IPE profiles with low values of *a* variation.
- **Closed:** V_z and M_y show relevant variation just for the RHS profile with the lowest value of *a*. For this profile, the r_{error} reaches 5.7% for V_z at midspan and 3% for M_y at fixed support (see Figure 4.106 and Figure 4.107). This variation occurs again due to the effect of tension forces that are present in GNA but not in SOT without imperfections.

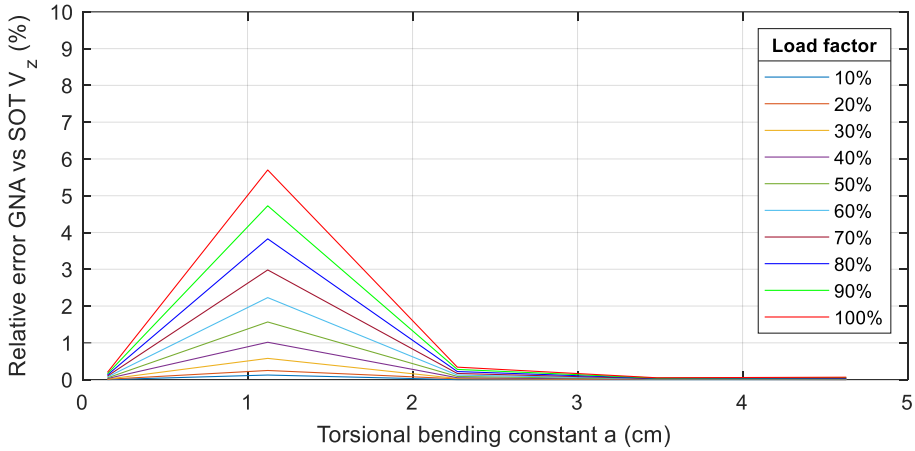

Figure 4.106 Relative error midspan V_z: fork-fixed system, M_y load, closed profiles

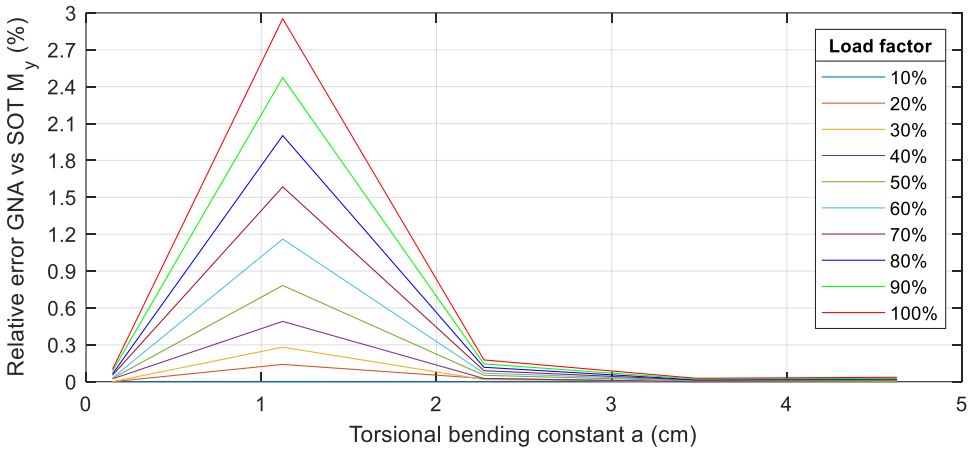

Figure 4.107 Relative error fixed support M_y: fork-fixed system, M_y load, closed profiles

Concerning **M_T** action, the following assertions have been found:

- **Open:** M_T shows r_{error} lower than 4.2% both at supports and midspan. M_w presents similar variation at both midspan and fixed support with r_{error} higher than the threshold up to 18.5% (see Figure 4.108 and Figure 4.109). Furthermore, the magnitude of M_w at fixed support is presented in Figure 4.110.
- **Closed:** M_T shows no variation both at supports and midspan.

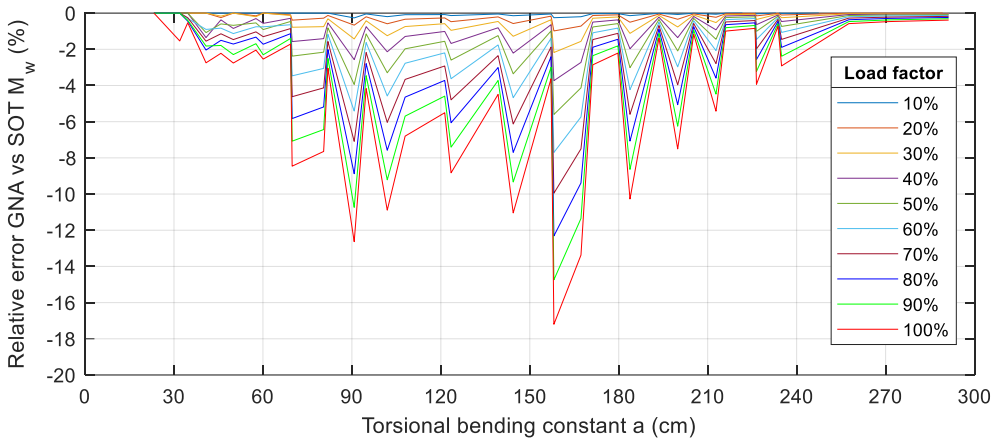

Figure 4.108 Relative error midspan M_w: fork-fixed system, M_T load, open profiles

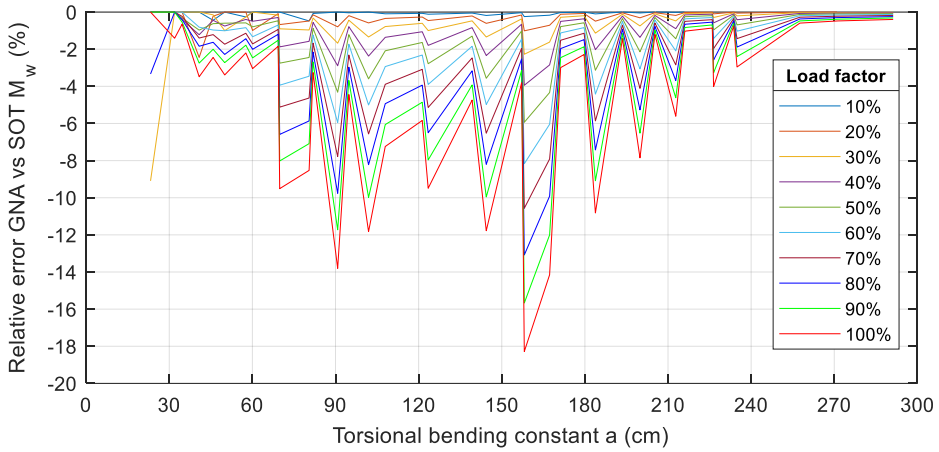

Figure 4.109 Relative error fixed support M_w: fork-fixed system, M_T load, open profiles

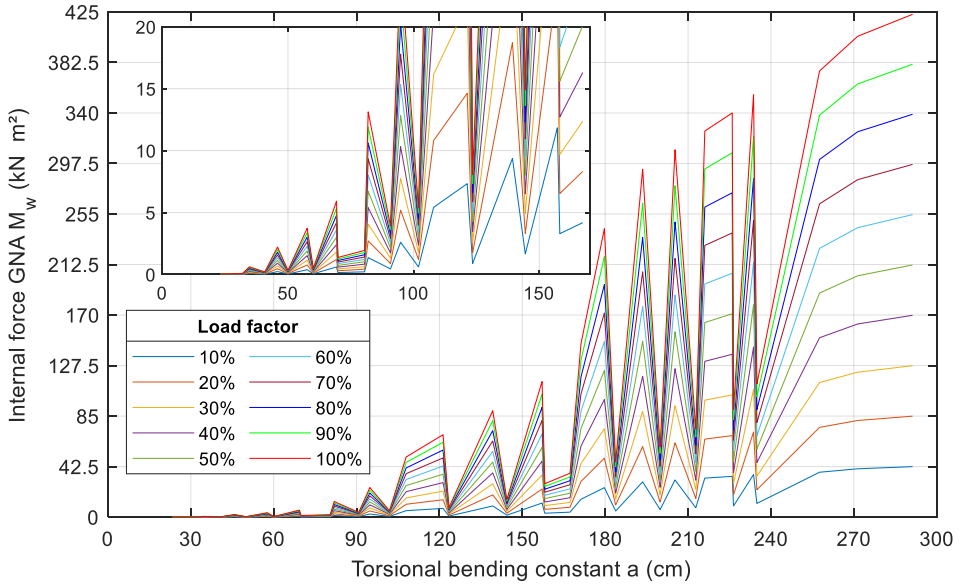

Figure 4.110 Internal force fixed support M_w: fork-fixed system, M_T load, open profiles / Inset of the graphic corresponds to values of a up to 170cm

4.1.4 Stresses

In this section, stress results for open profiles modelled with 1D-beam elements are analyzed and compared. For this purpose, several figures have been prepared regarding the structural system and the external load. The figures show the elastic ratio e_r vs the bending torsional constant *a* for every load level (0 to 100%).

Values higher than 1 for the elastic ratio exist, however, it does not mean that the section has surpassed their plastic capacity. It means how high the stress level is in the critical corner (flanges) within the cross-section. Furthermore, it is observed that stresses are higher for torsion (M_T) than for bending (V_z and M_y) in the most stressed corner. Due to torsion, secondary shear stresses occur, as well as additional normal stresses (warping bimoment).

In Figure 4.111 to Figure 4.114, the stresses due to V_z are presented. Normally, IPE profiles have higher stress values than HEB profiles. Furthermore, the fixed-free system shows that almost all profiles stay below 1. For the other systems, the limit is surpassed. The more stiffness the system provides the higher the stress, as can be seen for the fixed-fixed system.

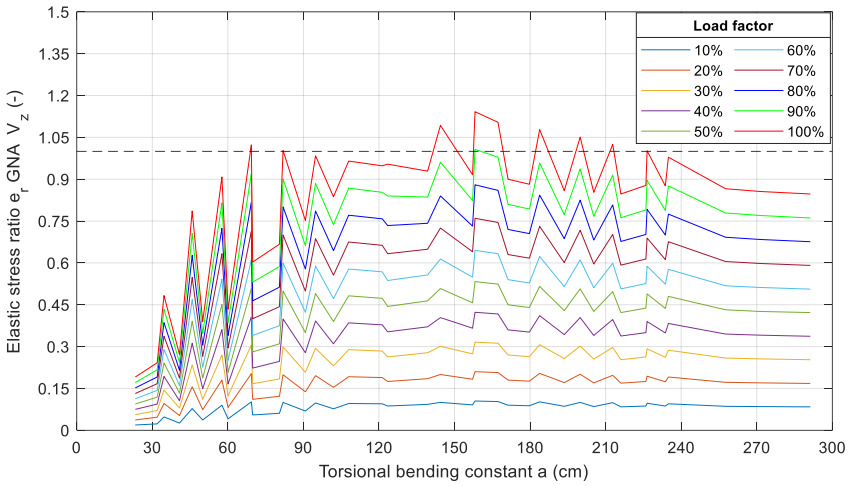

Figure 4.111 Elastic stress ratio: fixed-free system, V_z load

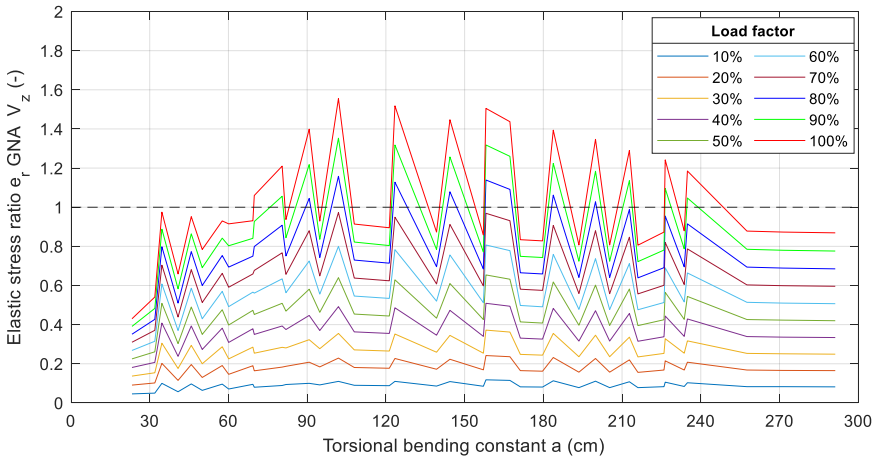

Figure 4.112 Elastic stress ratio: fork-fork system, V_z load

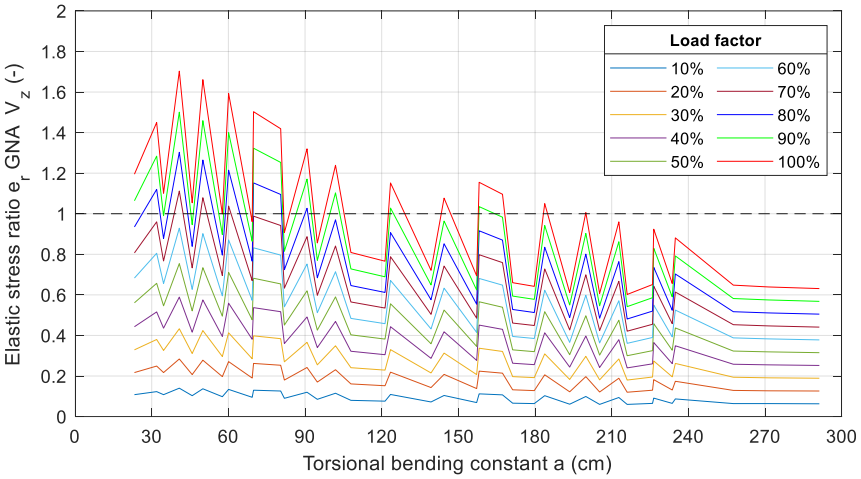

Figure 4.113 Elastic stress ratio: fixed-fixed system, V_z load

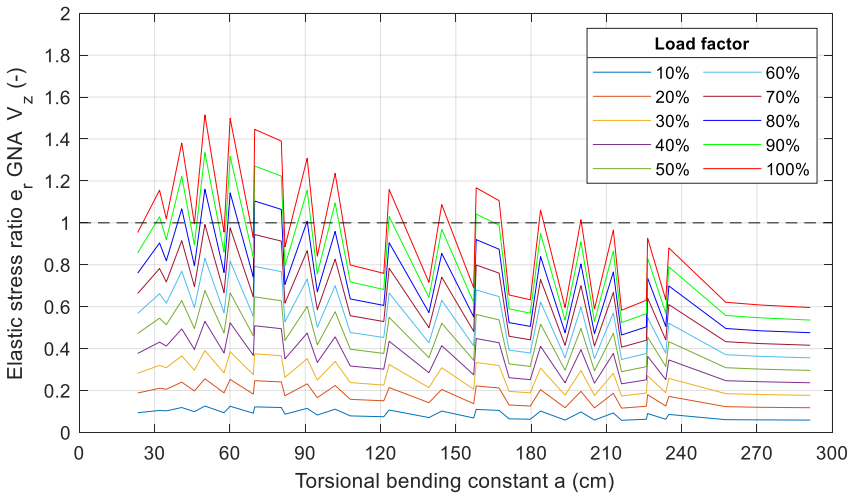

Figure 4.114 Elastic stress ratio: fork-fixed system, V_z load

From Figure 4.115 to Figure 4.118, the stresses due to M_y are presented. Similar to V_z, IPE profiles have higher stresses than HEB profiles. Moreover, the fixed-free system shows that all profiles stay below the limit. This might be due to the stability that the system provides. However, for the other 3 systems, the elastic limit is surpassed, as these systems provide higher stability.

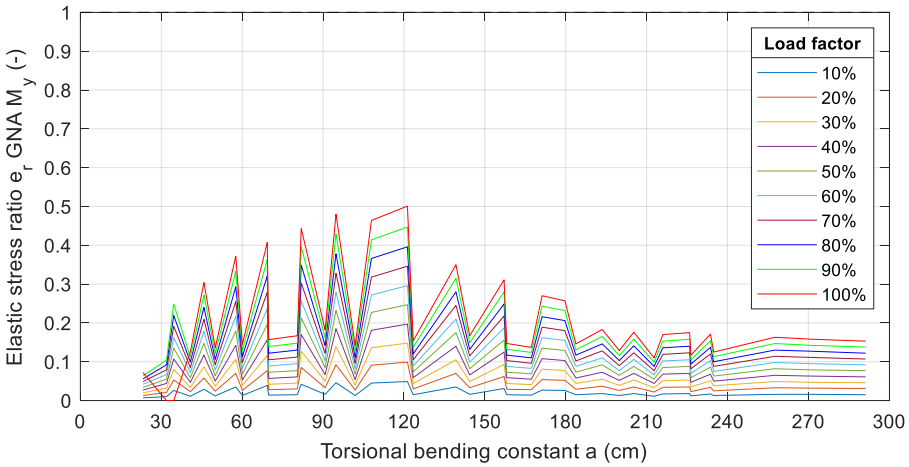

Figure 4.115 Elastic stress ratio: fixed-free system, M_y load

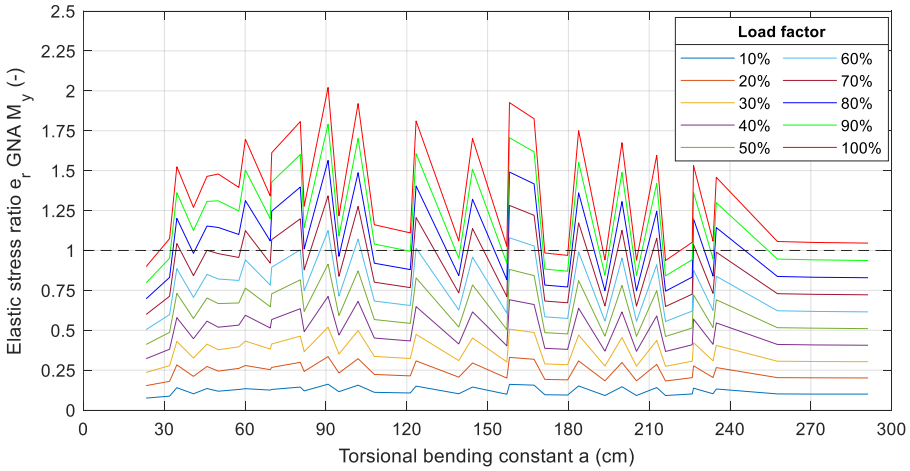

Figure 4.116 Elastic stress ratio: fork-fork system, M_y load

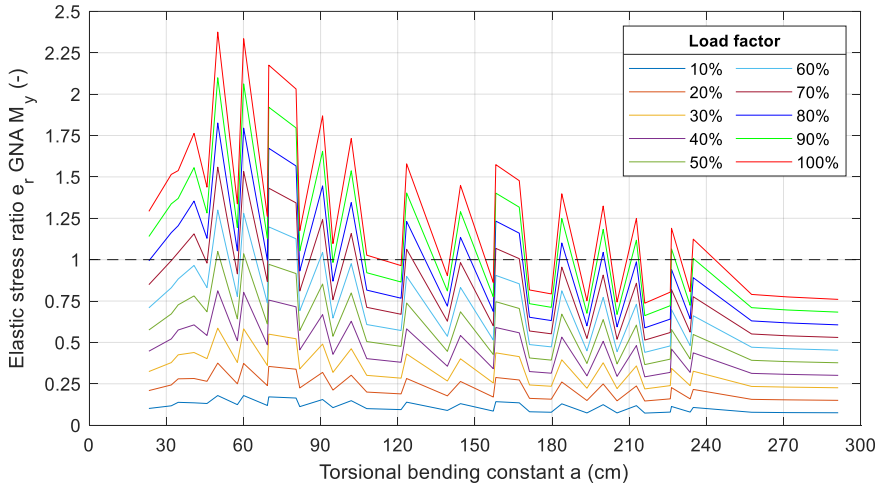

Figure 4.117 Elastic stress ratio: fixed-fixed system, M_y load

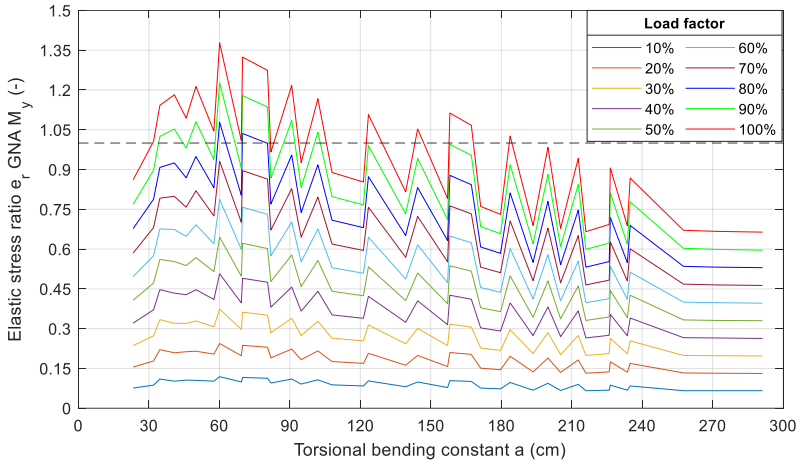

Figure 4.118 Elastic stress ratio: fork-fixed system, M_y load

Finally, for torsion M_T, the stresses are as 2 times higher as in the case of bending loads. From Figure 4.119 to Figure 4.122 the stresses can be seen. In general, the stresses are higher for profiles with intermediate and high values of *a*, which correspond to the cross-sections with larger dimensions.

For open profiles, stresses are as 2 times higher for torsion than for bending in the most stressed points. Considering the type of profile, IPE sections reach lower values than HEB sections. Nevertheless, HEB profiles can reach a higher torsional load compared to their plastic capacity (see Table 4.1).

Considering bending actions, on the other hand, IPE sections give higher values of stress than HEB profiles, which means that HEB sections have a more adequate distribution of bending stresses due their geometric properties.

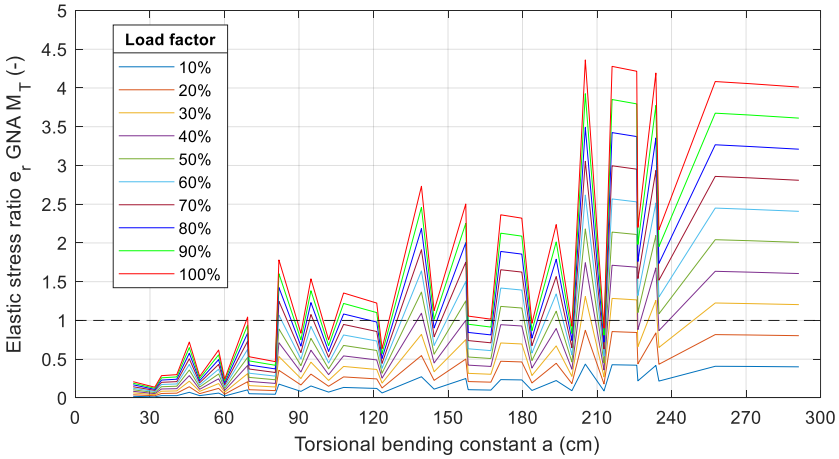

Figure 4.119 Elastic stress ratio: fixed-free system, M_T load

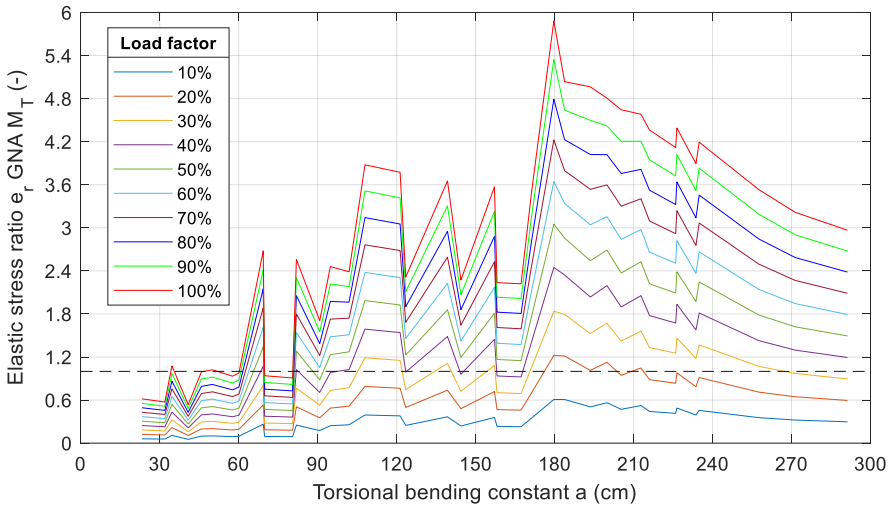

Figure 4.120 Elastic stress ratio: fork-fork system, M_T load

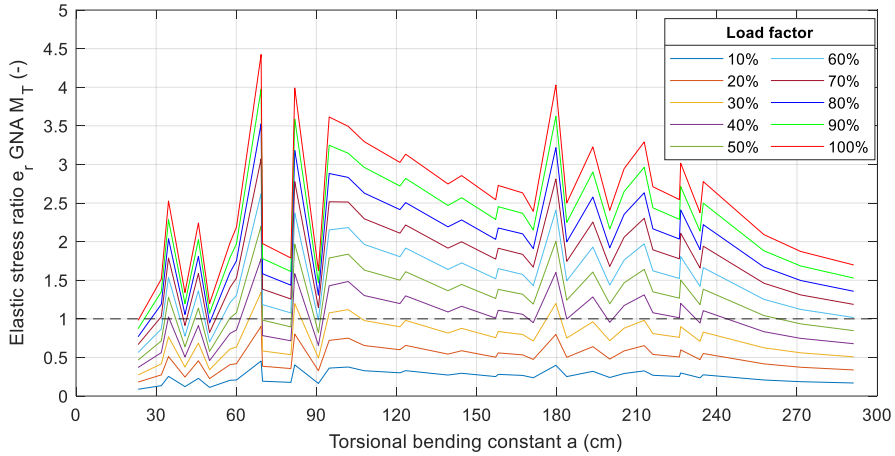

Figure 4.121 Elastic stress ratio: fixed-fixed system, M_T load

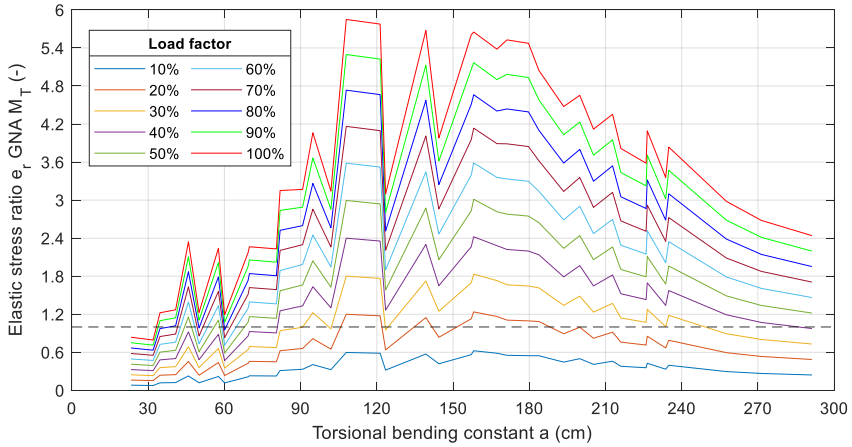

Figure 4.122 Elastic stress ratio: fork-fixed system, M_T load

4.2 Validity of second-order theory

It has been observed that the higher the displacement is, the higher the variation of results between GNA and SOT is. The same is true for the load factor increase (higher forces), which means higher displacements, and hence, higher variation.

Studying bending under GNA, axial forces can be introduced depending on the support conditions, which will affect the results when the values are significant. For instance, an introduced tension force will reduce compression stresses, and in that case, it will have a favorable effect reducing vertical displacements u_z and providing a stabilizing effect for LTB. This is not properly considered in SOT without geometrical imperfections, which is the case of 2D open sections and 1D and 2D closed cross sections, here no axial loads have been introduced. The tension force produces lower bending moments M_y and shear forces V_z. In the case of closed sections, this effect is clear for the RHS 100x50x6 profile.

The structural system with the lowest variation of results (both for displacement and internal forces), for all load cases, is the fixed-free system. Due to its boundary conditions, equilibrium has to be satisfied at support only, thus, keeping the r_{error} low. In this context, in most cases the system can be analyzed with either SOT or GNA for both open and closed sections. The exception exists for nodal bending moments M_y in open profiles, where the angle of rotation φ_x presents considerable difference. This effect is addressed in section 4.2.1.

In general, φ_x shows difference between GNA and SOT for open sections subjected to bending (V_z and M_y). SOT gives higher results, which leads to conservative rotation values specially for profiles with low *a* and more specifically for IPE profiles. However, for economy, SOT may not be the most adequate approach of analysis as serviceability limits will be surpassed at a lower load value. Similarly, for the torsion case (M_T), SOT gives higher results, nevertheless, higher variation is seen not only for profiles with low values of *a*.

SOT gives higher values of internal forces as well, which shows that this theory is conservative in some cases. For instance, in the case of bending, higher shear V_z and bending moment M_y are obtained. And for torsion, higher warping bimoment M_w results.

4.2.1 Open profiles

All 1D models for open profiles subjected to bending (V_z and M_y) result in high variation of rotation φ_x. One possible explanation for this behavior is that imperfections in SOT of members subjected to bending result in an initial deformed shape that is closer to the lateral torsional buckling shape. At this stage of deformation, SOT can reach higher values of rotation φ_x than GNA. Furthermore, this is observed particularly for profiles with low values of *a*.

Additionally, slender systems with low values of *a*/L are more prone to instabilities, thus, they have more variation in displacements between GNA and SOT. In this cases, GNA should be preferably used. Furthermore, IPE profiles are more susceptible to LTB in comparison with HEB profiles, therefore, careful consideration has to be taken when studying geometrical nonlinearity of such profiles.

Finally, open profiles subjected to bending (V_z and M_y), u_z, φ_x, and φ_y present higher variation when the torsional bending constant *a* is lower. Similarly, higher variation for internal forces V_z and M_y is seen particularly for IPE profiles with low *a*.

4.2.2 Closed profiles

Other than the models where tension forces where introduced, there is low variation of both displacements and internal forces for closed profiles.

No limiting value of rotation φ_x has been found for closed profiles. In the analyses, the values are not as high as in comparison with open profiles. Even for the most critical system (less redundant) which corresponds to the fixed-free system, the maximum rotation reached 0.32 radians with low variation of results (less than 4%). For all other systems the maximum rotation reached 0.16 rad (9.2º) and with variation lower than 1%. However, the torsional moment has been limited to the plastic capacity of each profile. Hence, if neglecting serviceability limits, it is established that for closed profiles the rotation will be limited to the section's capacity.

Additionally, for closed profiles subjected to bending, u_z and φ_y results show good agreement between 1D and 2D elements. In this sense, closed profiles analysis can be simplified with the use of 1D-beam elements accurately. Moreover, closed profiles can reach higher displacements of u_z and φ_y than open profiles while still maintaining a r_{error} lower than 5%. For u_z, higher values than the threshold (1.25% drift) will still give accurate results for SOT as observed in the fixed-free system.

Moreover, square hollow sections have the lowest values of bending torsional constant *a* for closed sections, however they can still present slightly higher variation of results in comparison with RHS with higher values of *a*.

4.2.3 Torsion

In GNA and SOT for open cross-sections, it is adequate to assume that the secondary torsional moment M_s accounts for the total torsional moment M_T in the most stressed locations. M_s may be used for design of open profiles with scheduled torsion and M_p (St. Venant's torsion) may be neglected. The other way around is true in the case of closed cross-sections, where only M_p may be considered for design.

Closed cross-sections with scheduled torsion show no relevant difference in the internal force M_T and rotation φ_x between GNA and SOT. Closed profiles have reduced rotation φ_x than for open profiles. Closed profiles present an excellent behavior for torsion. In this case, SOT can be used safely as an approximation for GNA.

4.2.4 2D-shell elements

In general, the variation trend for 2D elements is similar as in 1D elements for both open and closed sections.

Furthermore, 2D-shell elements' results are only useful for the external load V_z in all structural systems with open profiles. In this case, a trend for the relative error exists, where the lower the bending torsional constant *a* is the higher the r_{error}. The same trend is seen for 1D-beam elements of the same profiles. The usability of the results is based on the assignment of loads and supports in 2D models. The nodal moments (M_y and M_T) applied in 2D elements of open profiles do not give accurate results, and therefore, they are not useful in this study. Finally, 2D-shell elements can react sensitively when subjected to point-by-point torsional stresses which is the case of nodal bending M_y or torsional moments M_T.

4.3 Fitting curves

In this section, fitting curves are determined by a surface linear interpolation of the displacement results of open profiles with 1D-beam elements. The curves are presented as contour plots and they are a practical way to check whether SOT or GNA should be used by limiting the relative error. The information needed for establishing the type of analysis are the load factor LF and the torsional bending constant *a* divided by the length of the system *a*/L.

Furthermore, the fitting curves are considered only for displacements where variations higher than the threshold are found. These variations correspond to the specific structural system and external load as summarized in Table 4.2. Additionally, differentiation between IPE and HEB profiles is done. Moreover, closed sections are not considered due their low variation of results for GNA and SOT.

Table 4.2 Displacements with high variation for each system and load case

Structural system	Load case	Displacement	IPE fitting curves	HEB fitting curves
Fixed-free	V_z	-	-	-
	M_y	φ_x	Figure 4.123	Figure 4.138
	M_T	-	-	-
Fork-fork	V_z	u_z, φ_x	Figure 4.124, Figure 4.125	Figure 4.139, Figure 4.140
	M_y	φ_x	Figure 4.126	Figure 4.141
	M_T	φ_x	Figure 4.127	Figure 4.142
Fixed-fixed	V_z	u_z, φ_x	Figure 4.128, Figure 4.129	-
	M_y	φ_x	Figure 4.130	-
	M_T	φ_x	Figure 4.131	Figure 4.143
Fork-fixed	V_z	u_z, φ_x, φ_y	Figure 4.132, Figure 4.133, Figure 4.134	Figure 4.144
	M_y	φ_x	Figure 4.135	Figure 4.145
	M_T	φ_x, Ω	Figure 4.136, Figure 4.137	Figure 4.146, Figure 4.147

The contours of the fitting curves represent the magnitude of relative error in percentage. Furthermore, for clarity, the r_{error} limit established for this thesis project of 5% is included in the figures. The recommendation is to use SOT whenever the intersection of the LF and *a*/L are within the area of 5% r_{error}, and if outside this area, consider the use of GNA. Nevertheless, if one wants to have higher or lower accuracy, it can be done by using the different levels of r_{error} presented. Finally, if a different structural system (different boundary conditions) is needed, the curves can at the least give an idea of which theory to use.

4.3.1 IPE profiles

The fitting curves for IPE profiles are presented in this section. All displacements summarized in Table 4.2 are applicable for IPE profiles. Localized variations for Ω are observed in Figure 4.137, these are in accordance to specific profiles and load factors, which in general do not follow the main trend, hence, careful consideration has to be taken of which theory to use for those areas.

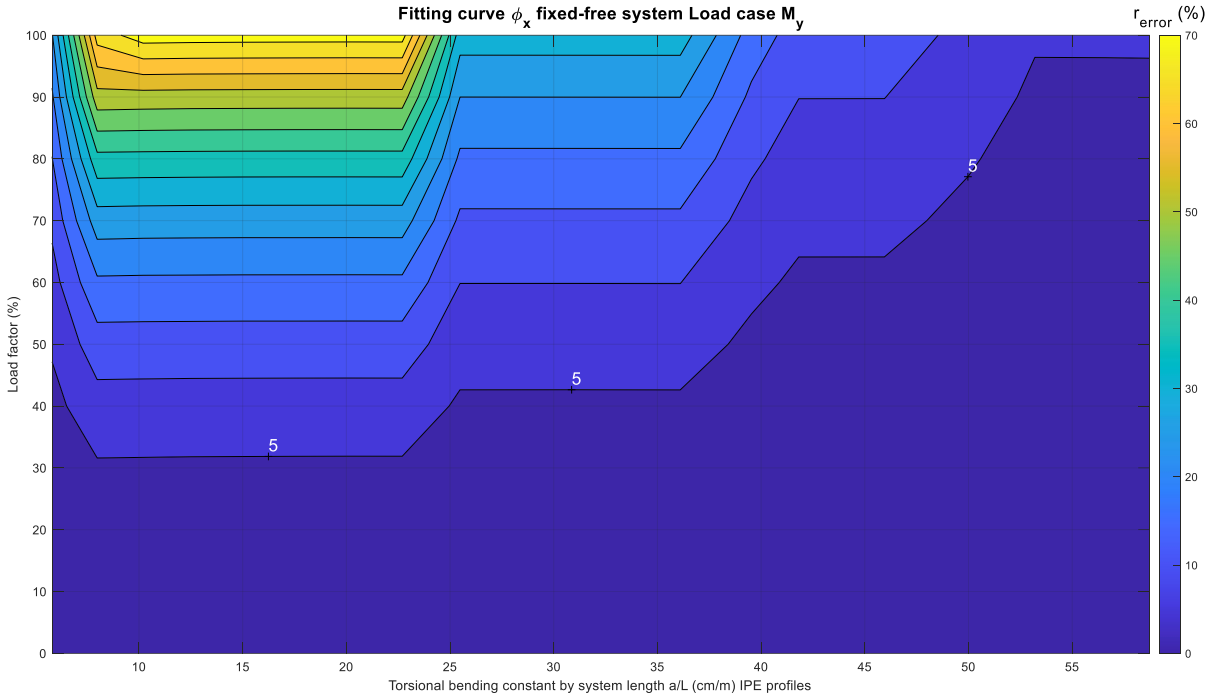

Figure 4.123 Fitting curve φ_x: fixed-free system, M_y load, IPE profiles

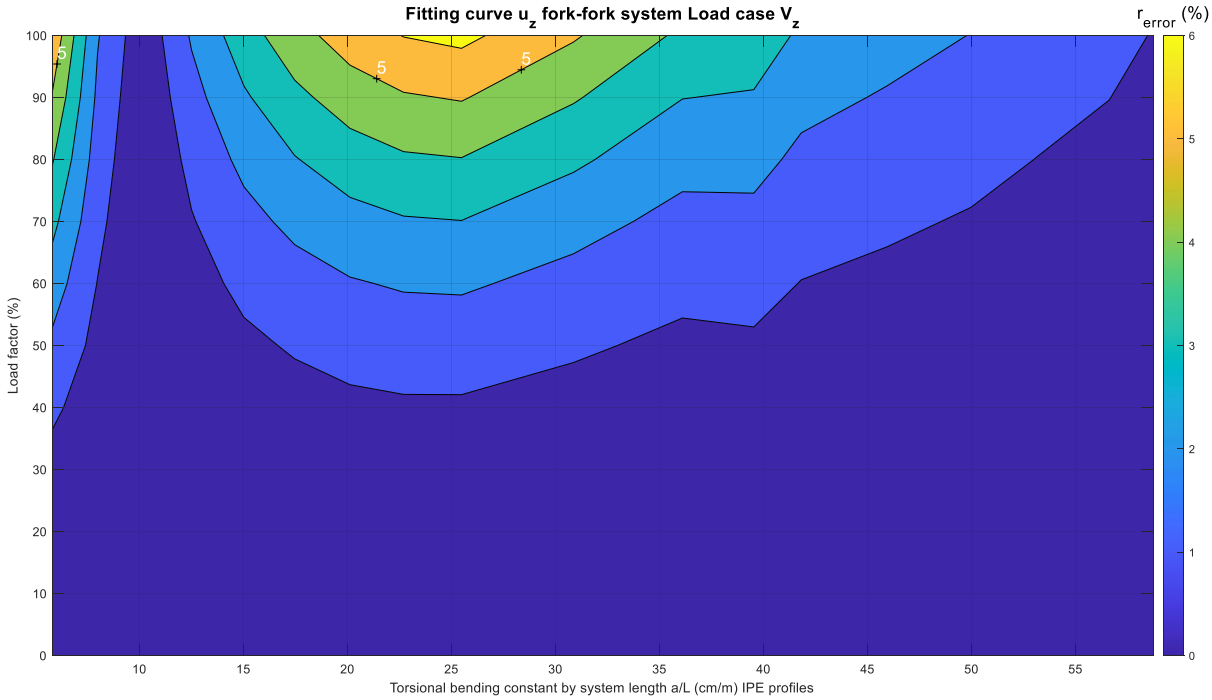

Figure 4.124 Fitting curve u_z: fork-fork system, V_z load, IPE profiles

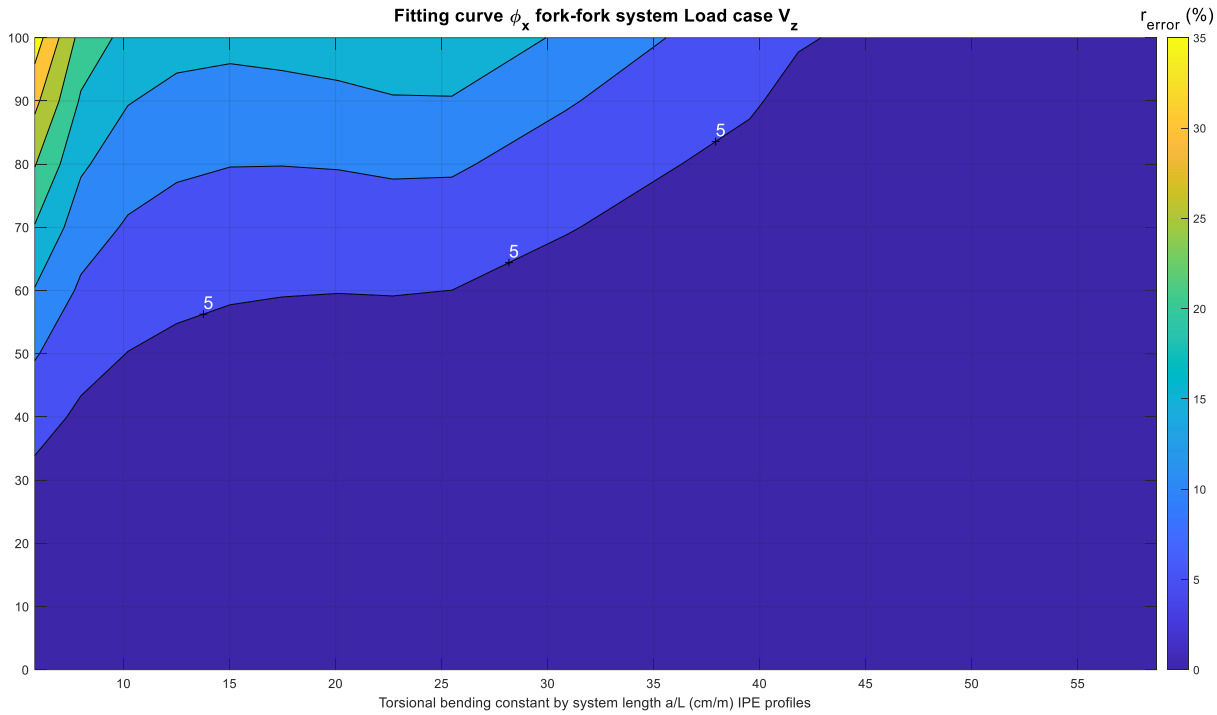

Figure 4.125 Fitting curve φ_x: fork-fork system, V_z load, IPE profiles

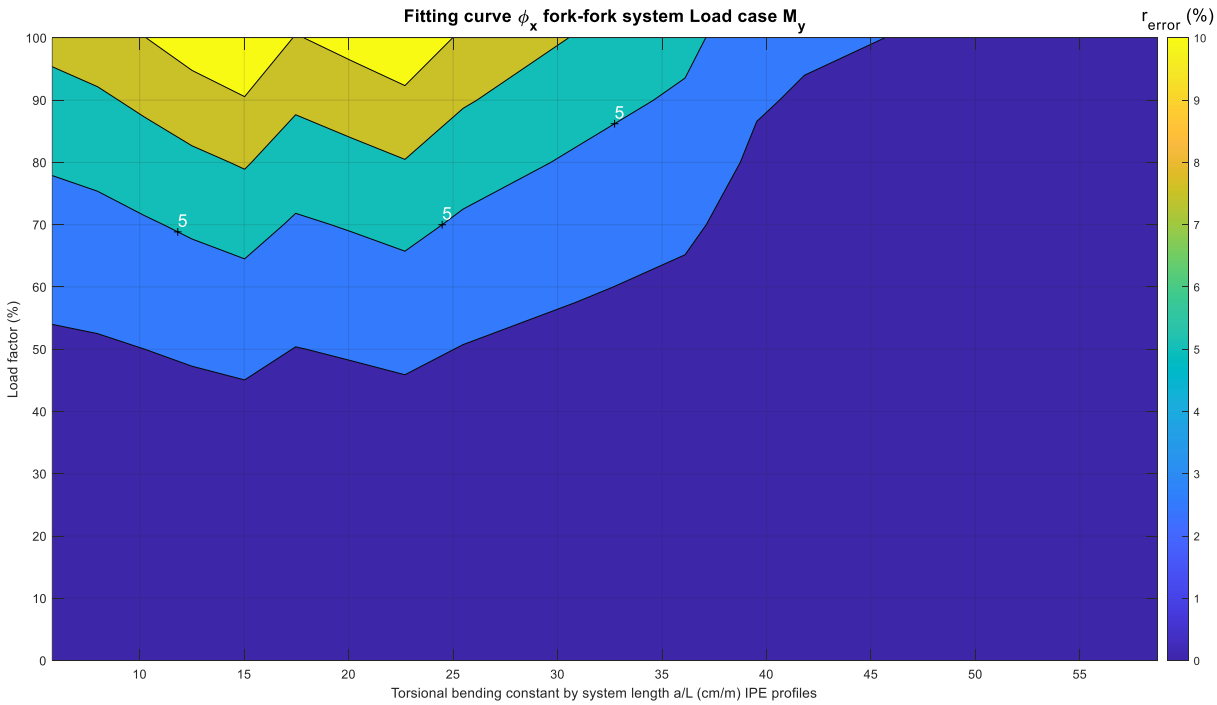

Figure 4.126 Fitting curve φ_x: fork-fork system, M_y load, IPE profiles

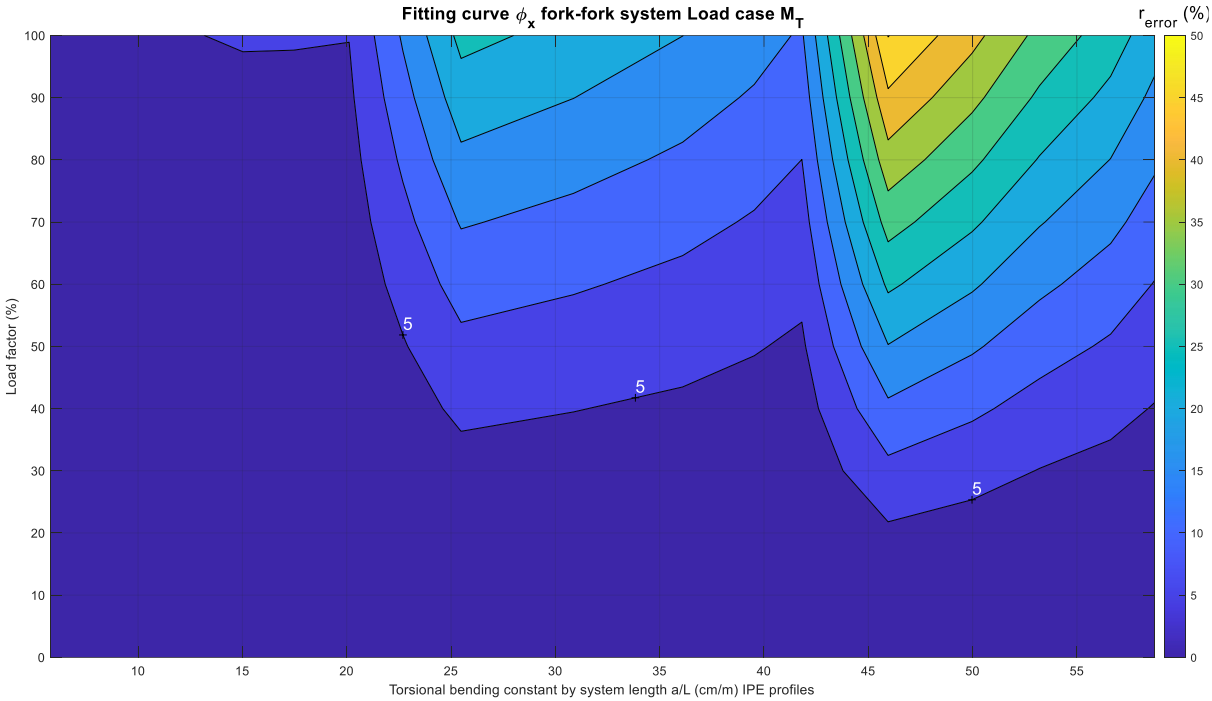

Figure 4.127 Fitting curve φ_x: fork-fork system, M_T load, IPE profiles

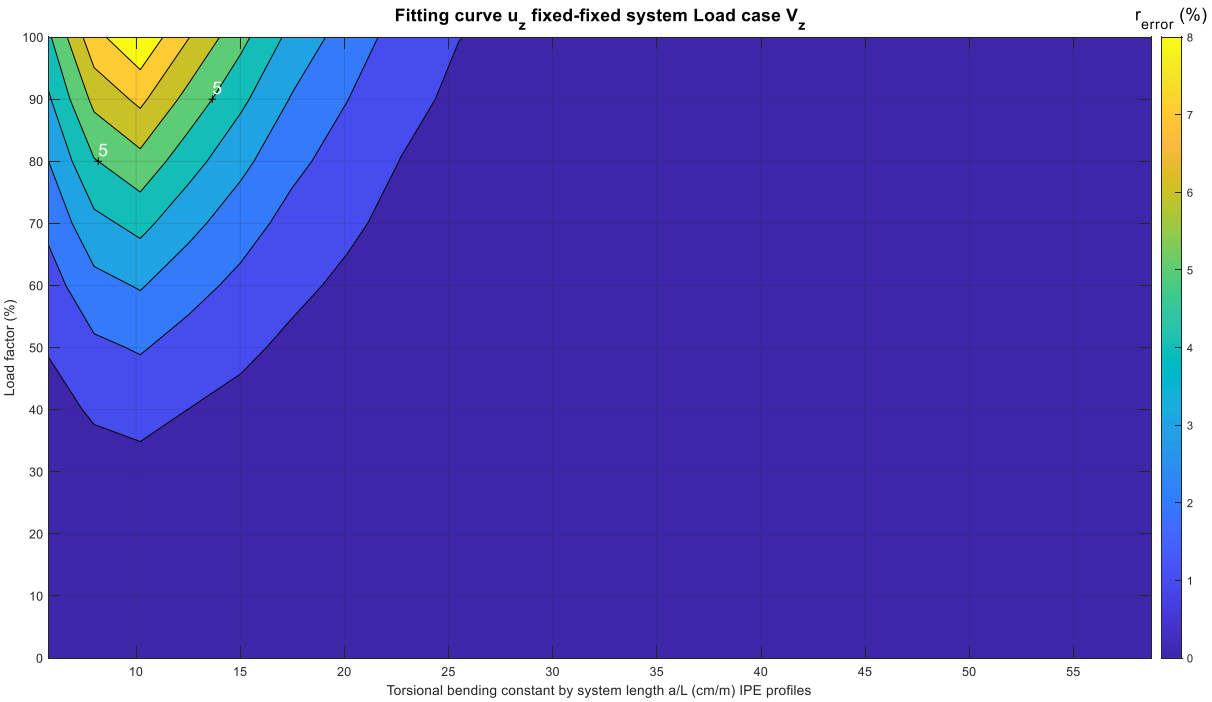

Figure 4.128 Fitting curve u_z: fixed-fixed system, V_z load, IPE profiles

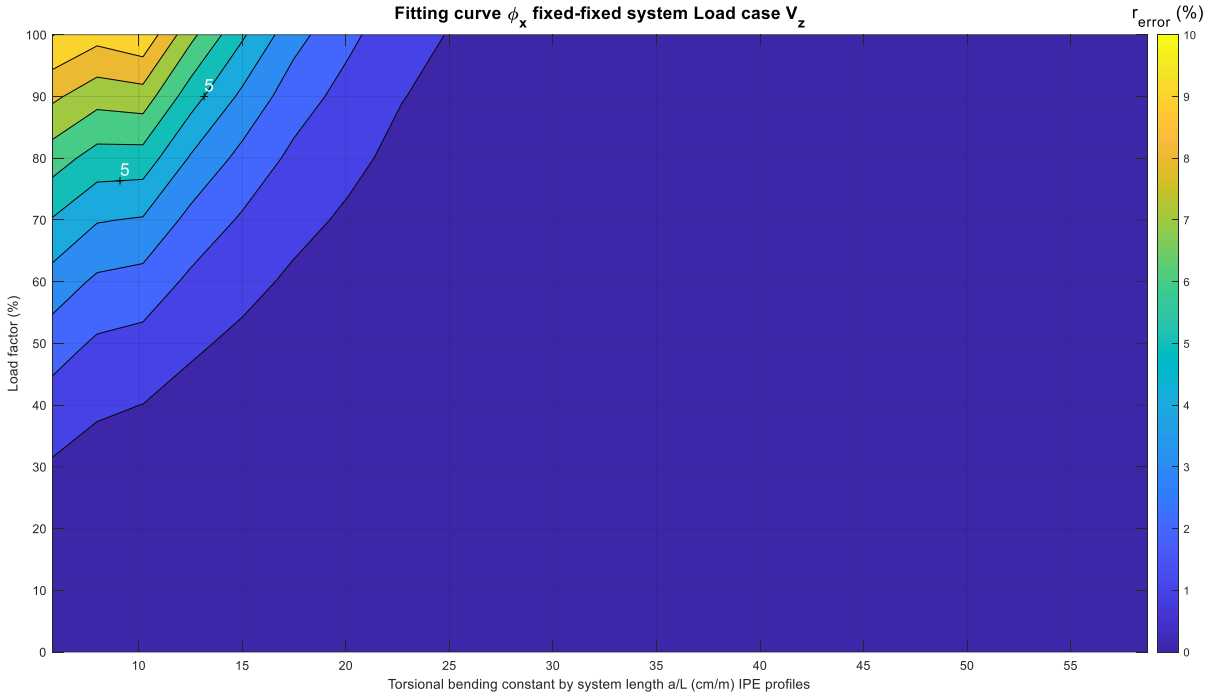

Figure 4.129 Fitting curve φ_x: fixed-fixed system, V_z load, IPE profiles

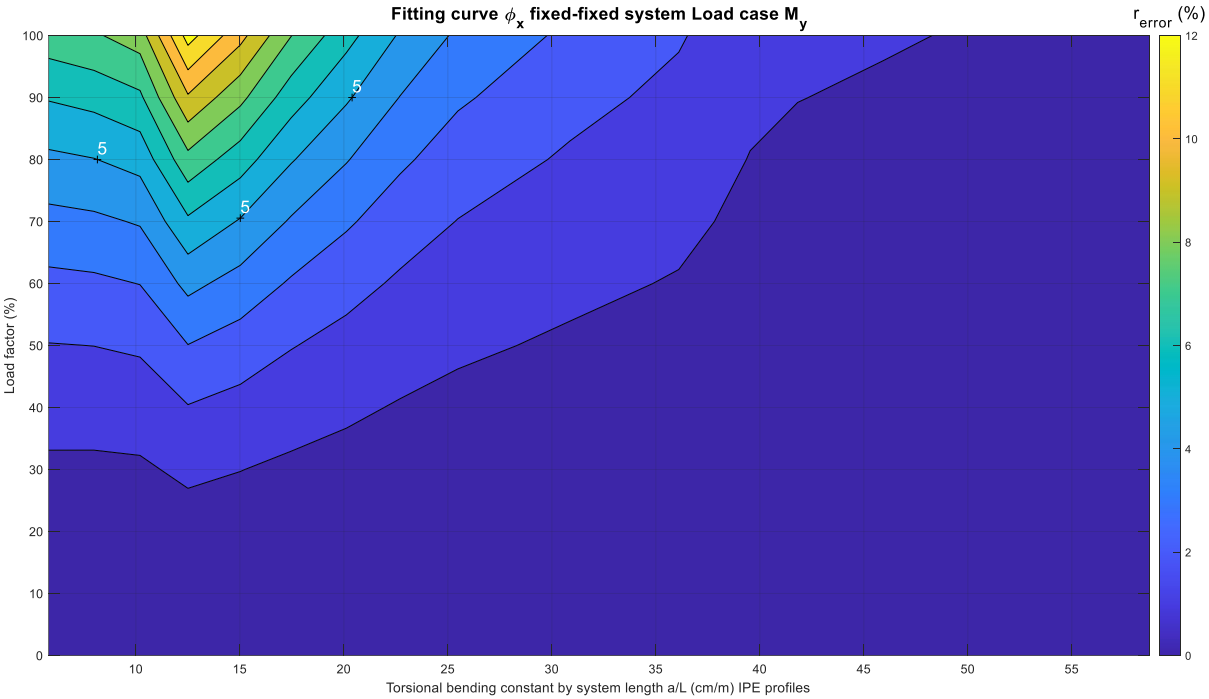

Figure 4.130 Fitting curve φ_x: fixed-fixed system, M_y load, IPE profiles

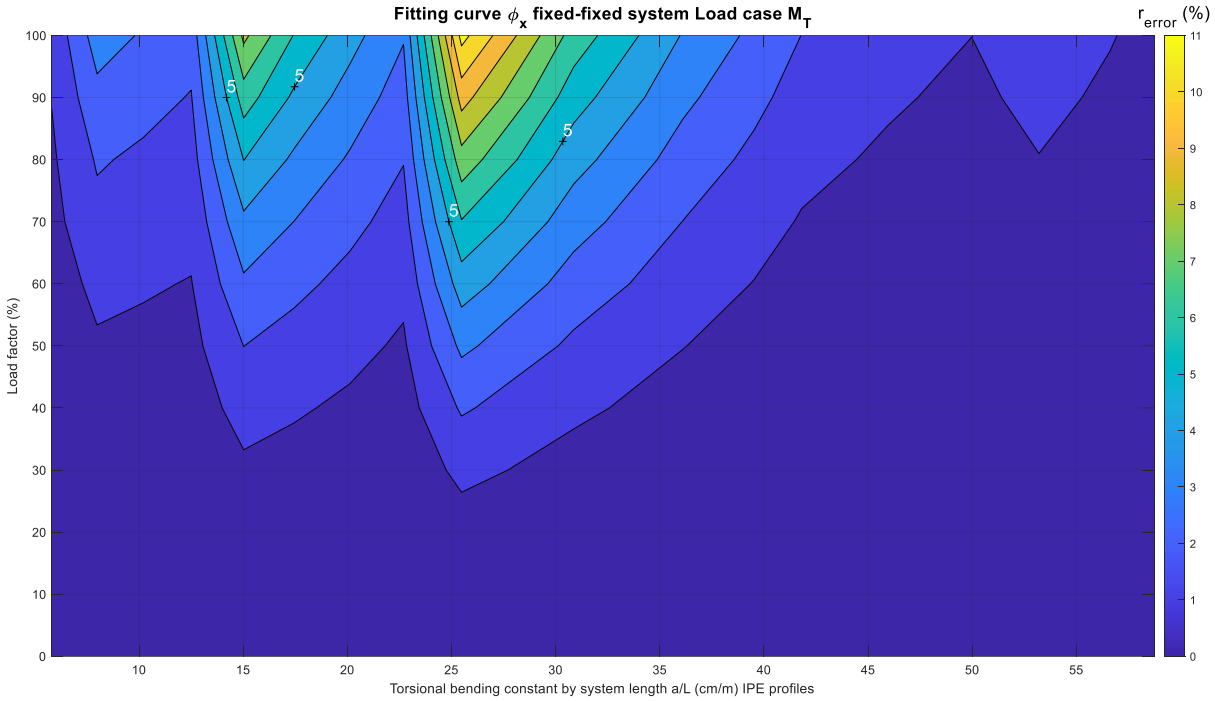

Figure 4.131 Fitting curve φ_x: fixed-fixed system, M_T load, IPE profiles

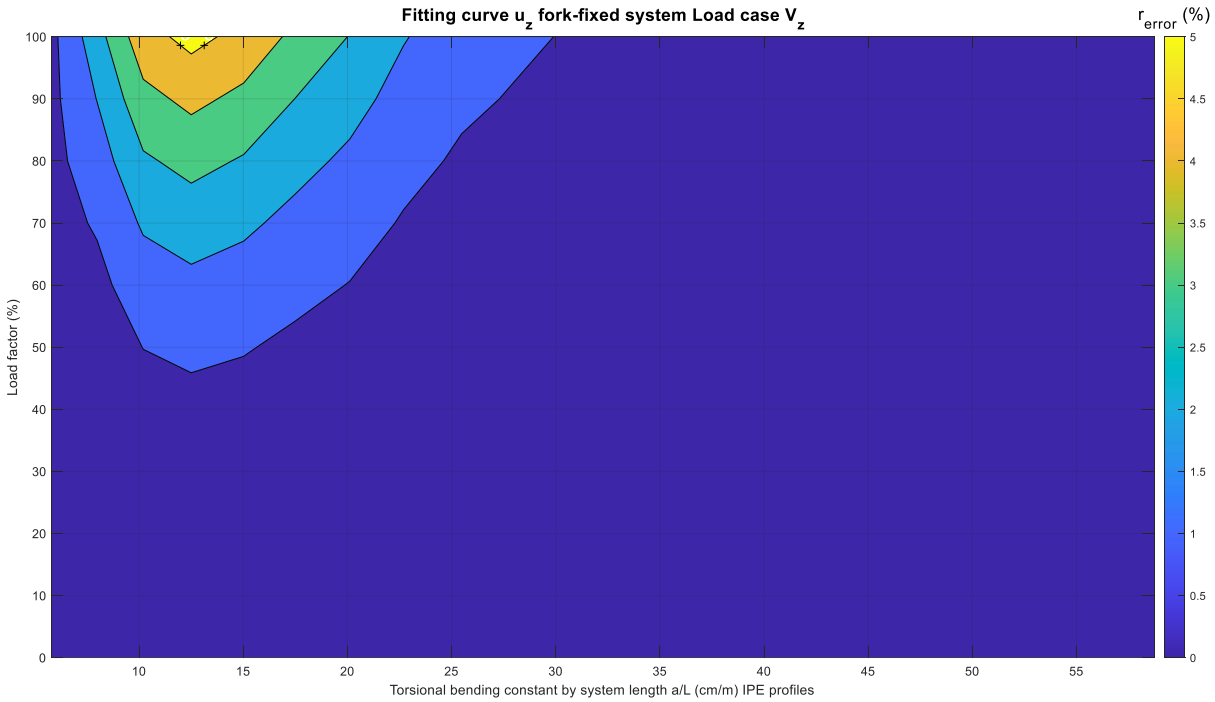

Figure 4.132 Fitting curve u_z: fork-fixed system, V_z load, IPE profiles

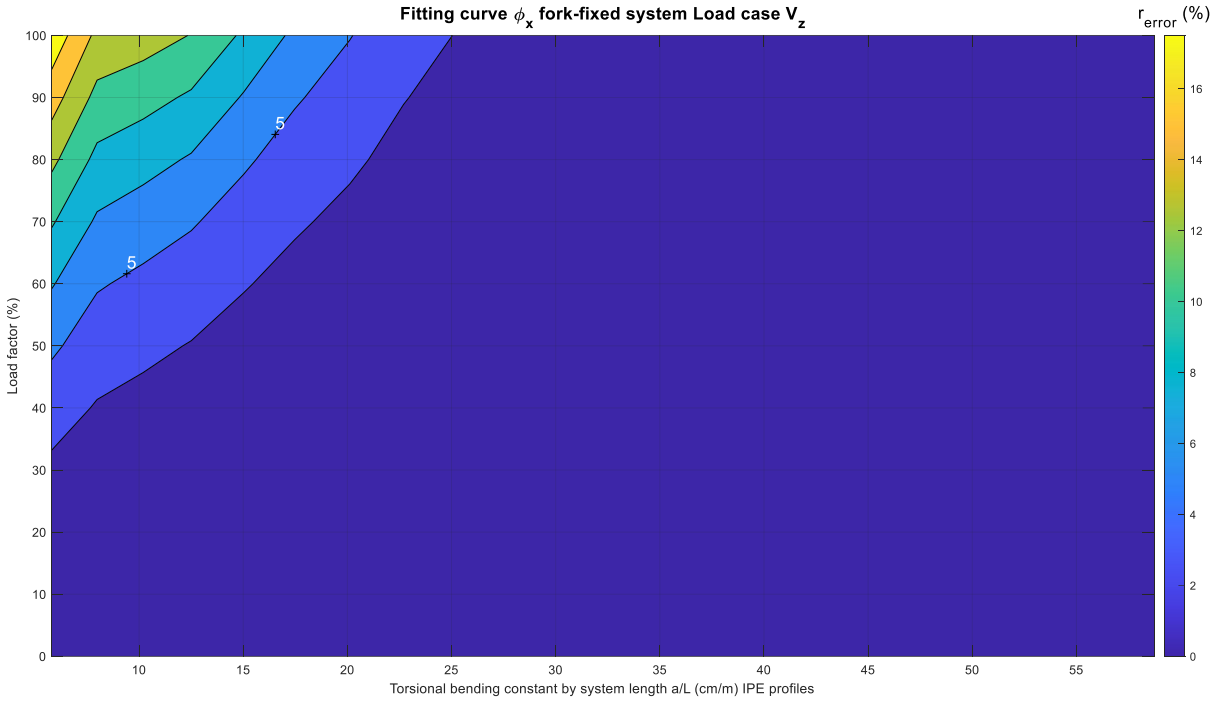

Figure 4.133 Fitting curve φ_x: fork-fixed system, V_z load, IPE profiles

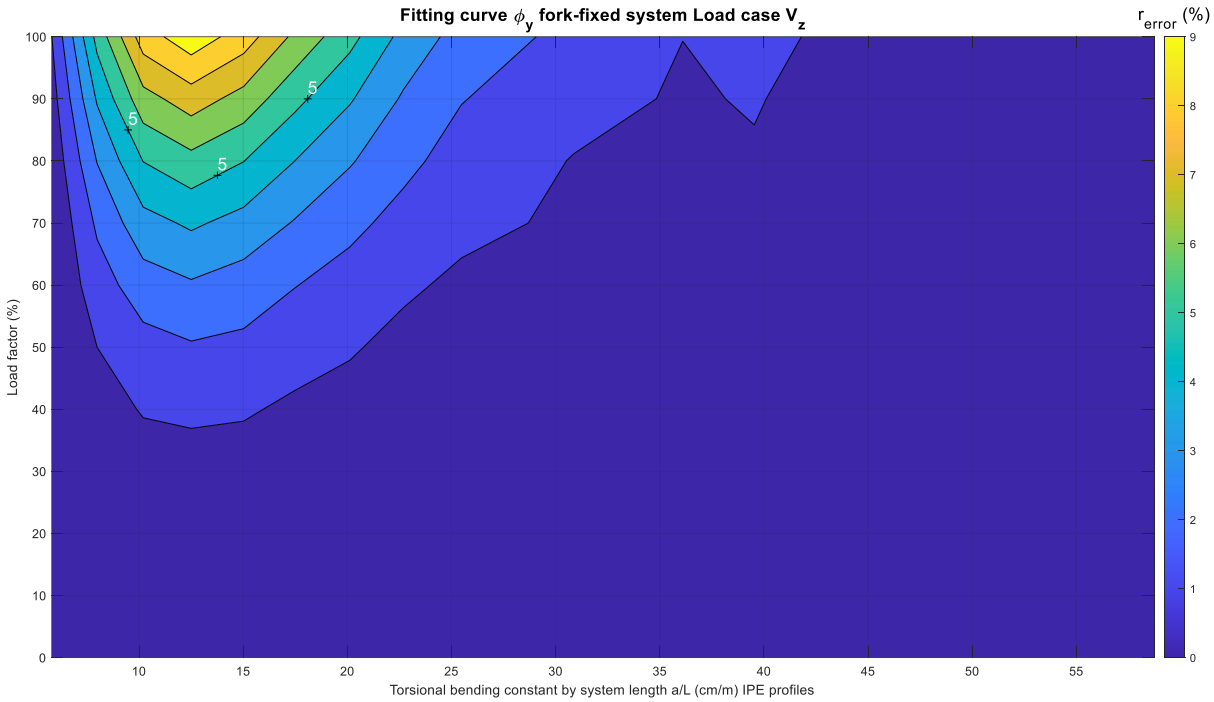

Figure 4.134 Fitting curve φ_y: fork-fixed system, V_z load, IPE profiles

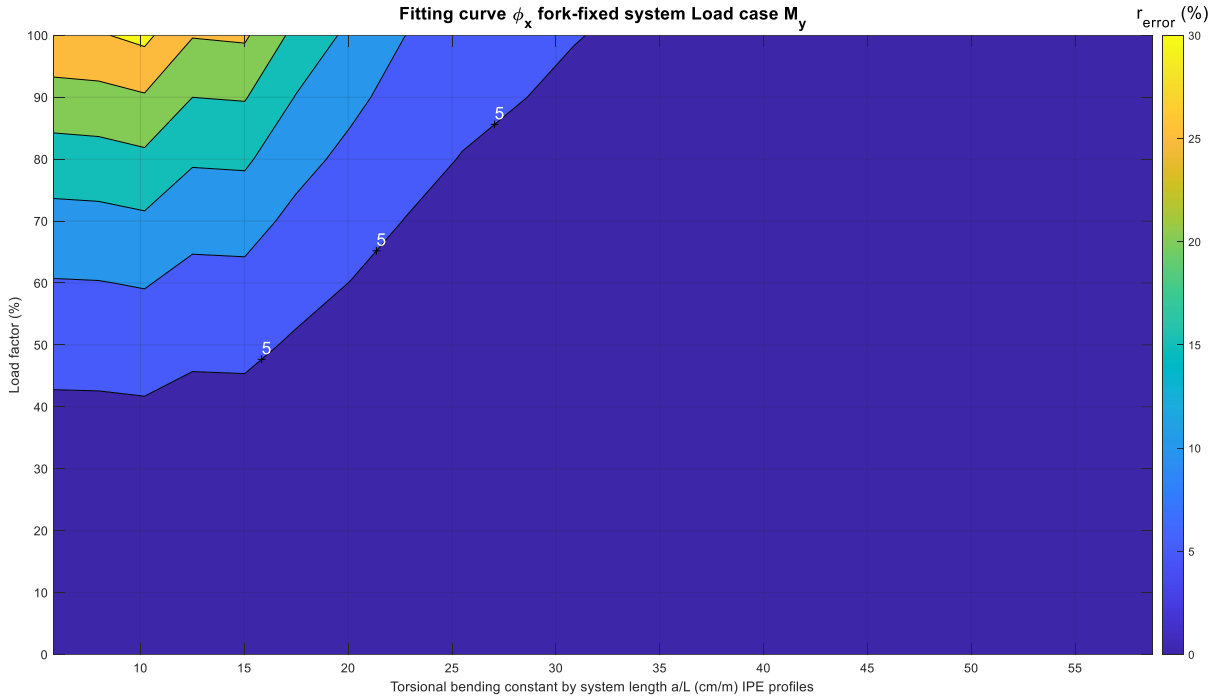

Figure 4.135 Fitting curve φ_x: fork-fixed system, M_y load, IPE profiles

Figure 4.136 Fitting curve φ_x: fork-fixed system, M_T load, IPE profiles

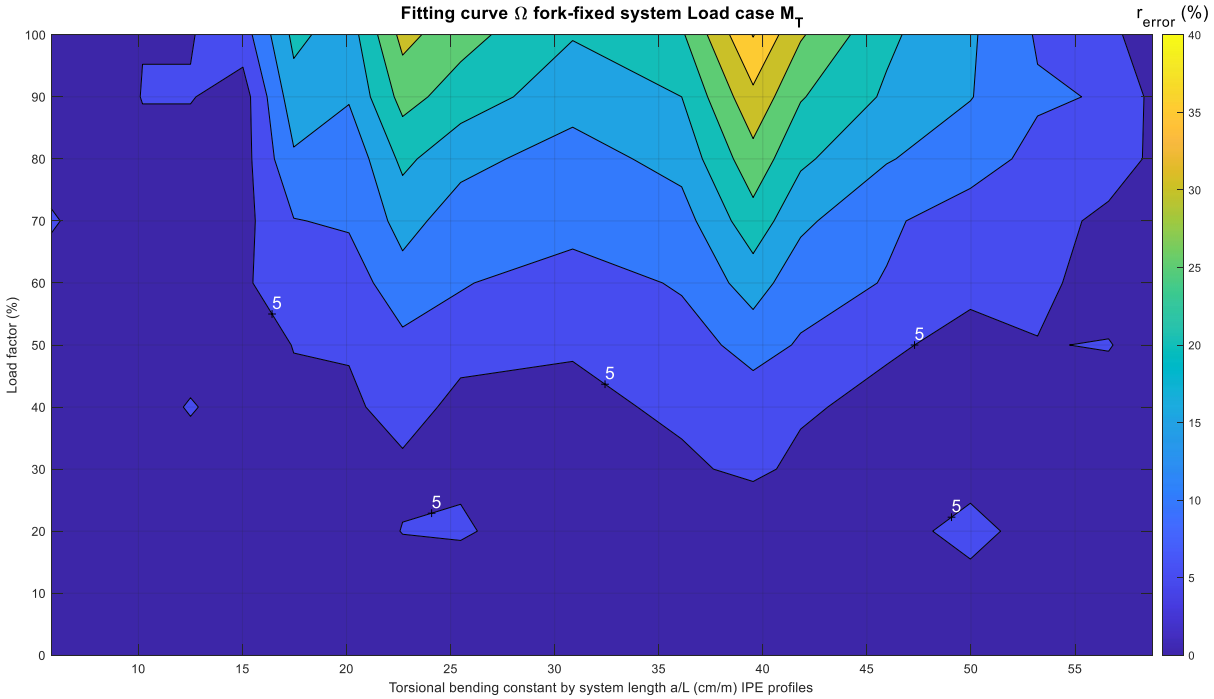

Figure 4.137 Fitting curve Ω: fork-fixed system, M_T load, IPE profiles

4.3.2 HEB profiles

The fitting curves for HEB cross-sections are presented in this section. Not all displacements presented in Table 4.2 are applicable for this profile. As it is mentioned in section 4.1.2.3, no relevant variation for u_z and φ_x is observed for HEB profiles in the case of V_z action in the fixed-fixed system. In the same system, also no relevant variation occurs for φ_x under M_y action. Additional, for the fork-fixed system no relevant variation occurs for u_z and φ_y under V_z action. Finally, some localized variations for Ω are observed in Figure 4.147, these are isolated to a specific profile and load factor, which do not follow the main trend, hence, careful consideration has to be taken of which theory to use for those areas.

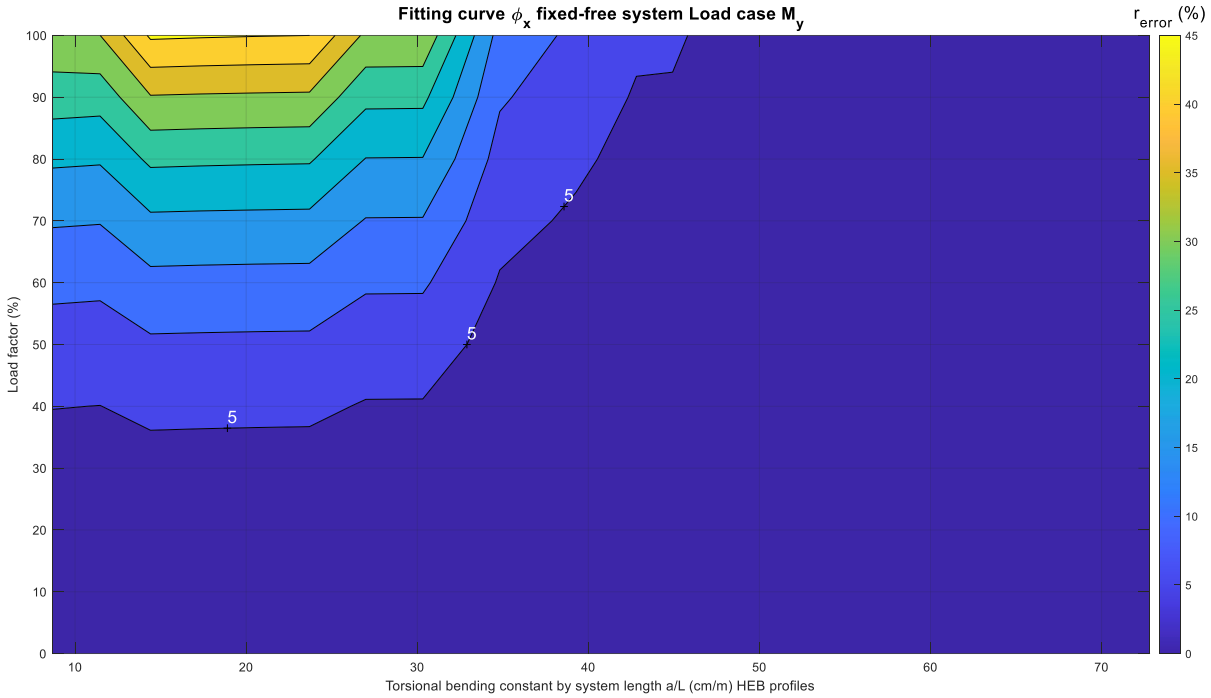

Figure 4.138 Fitting curve φ_x: fixed-free system, M_y load, HEB profiles

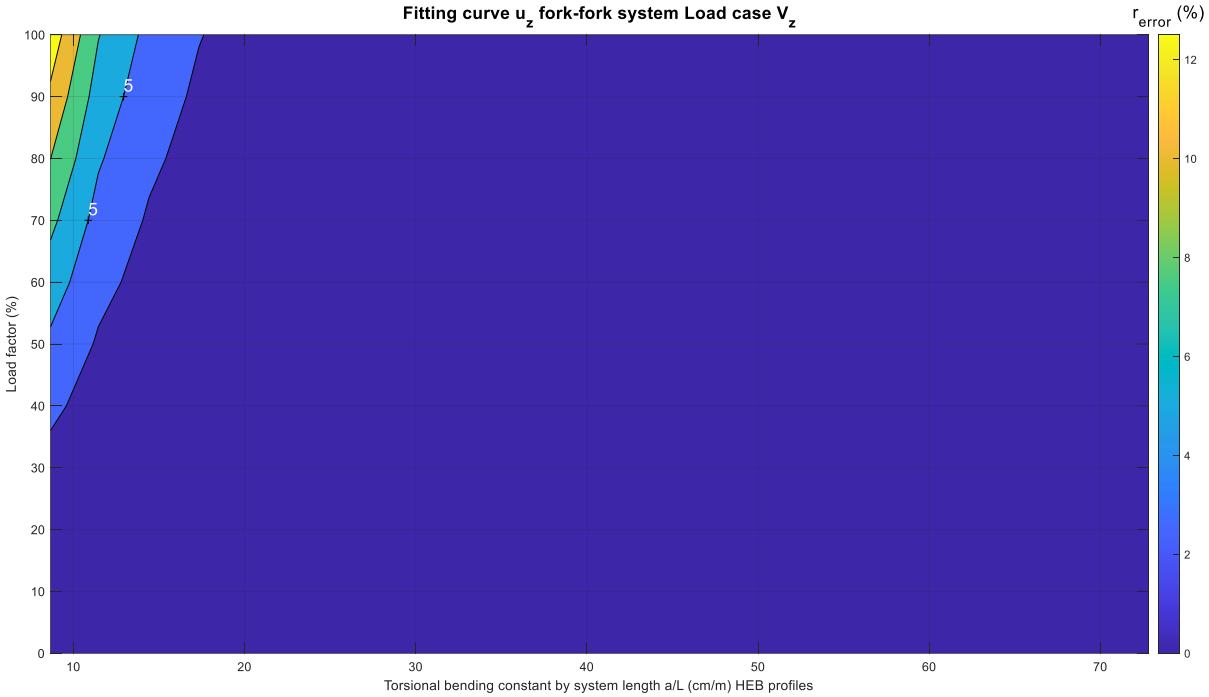

Figure 4.139 Fitting curve u_z: fork-fork system, V_z load, HEB profiles

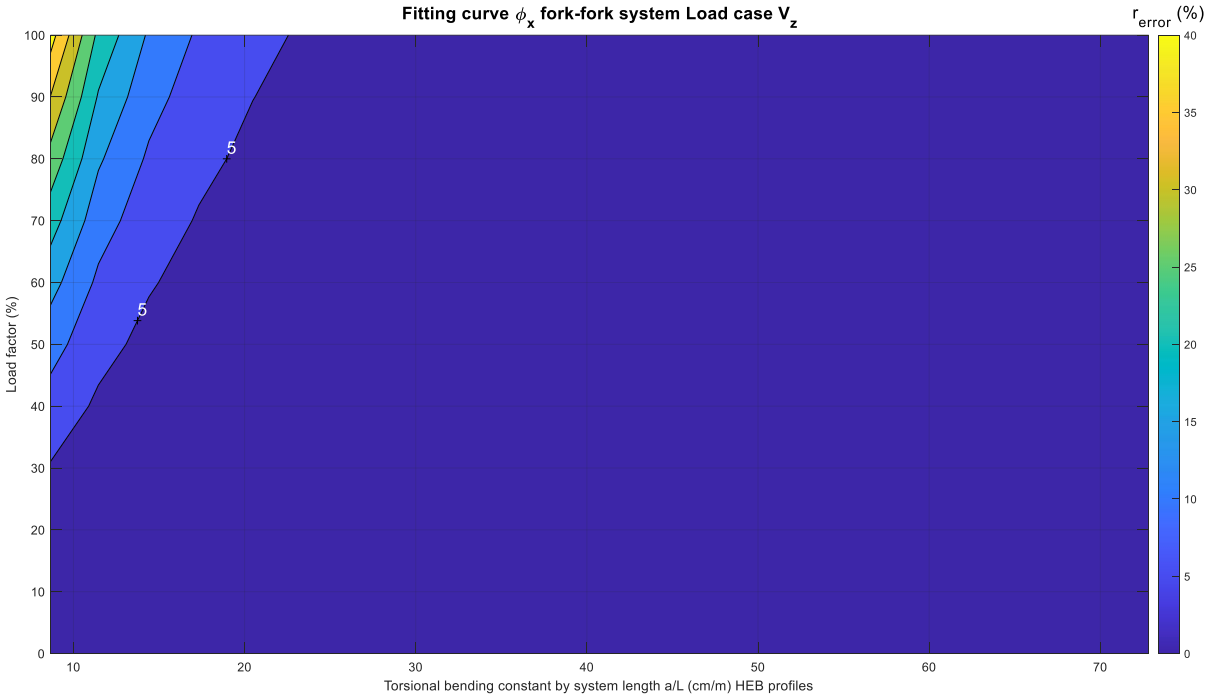

Figure 4.140 Fitting curve φ_x: fork-fork system, V_z load, HEB profiles

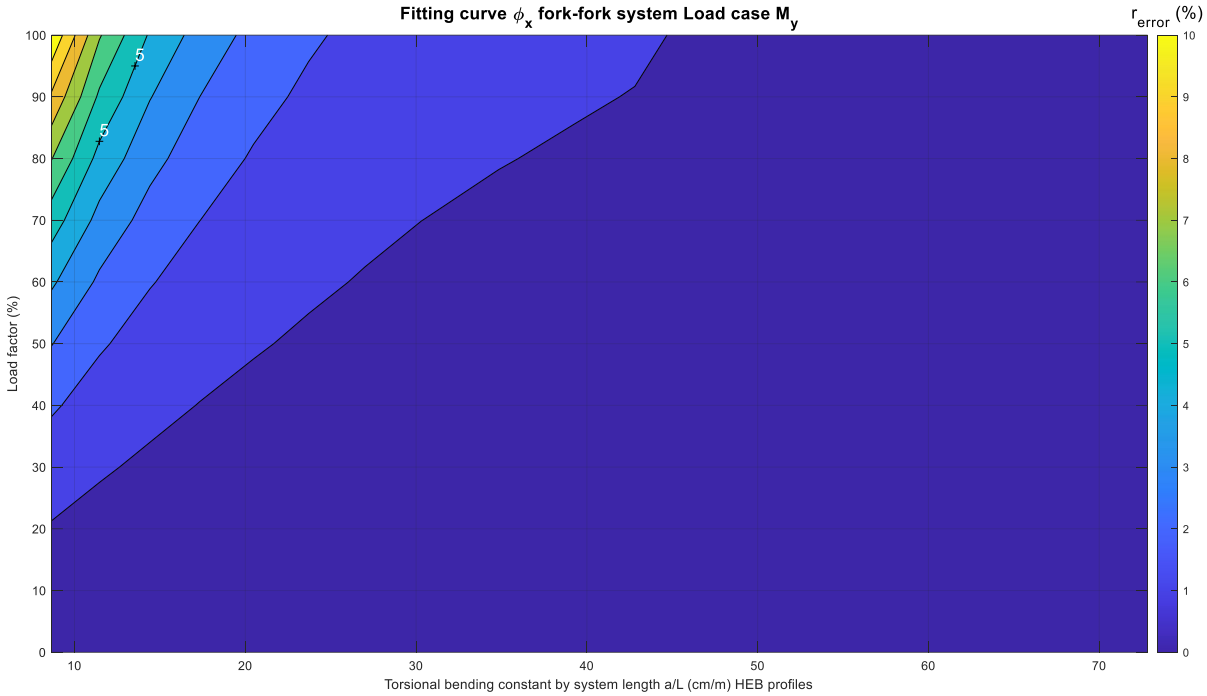

Figure 4.141 Fitting curve φ_x: fork-fork system, M_y load, HEB profiles

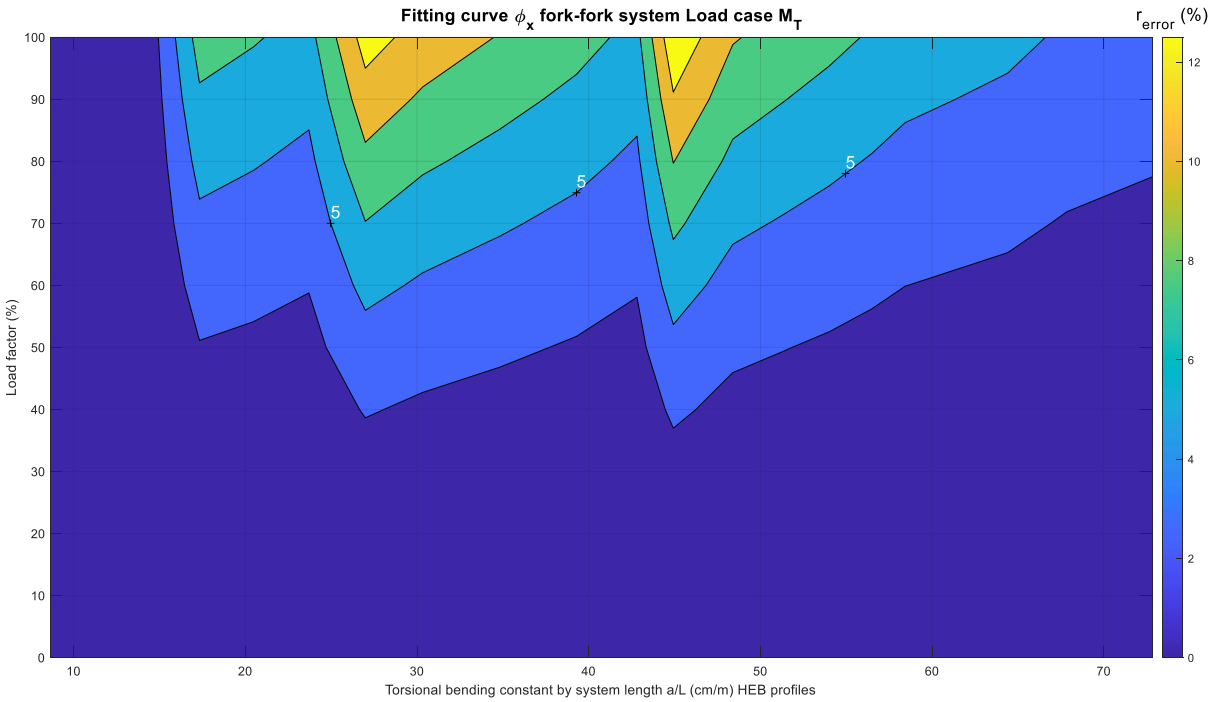

Figure 4.142 Fitting curve φ_x: fork-fork system, M_T load, HEB profiles

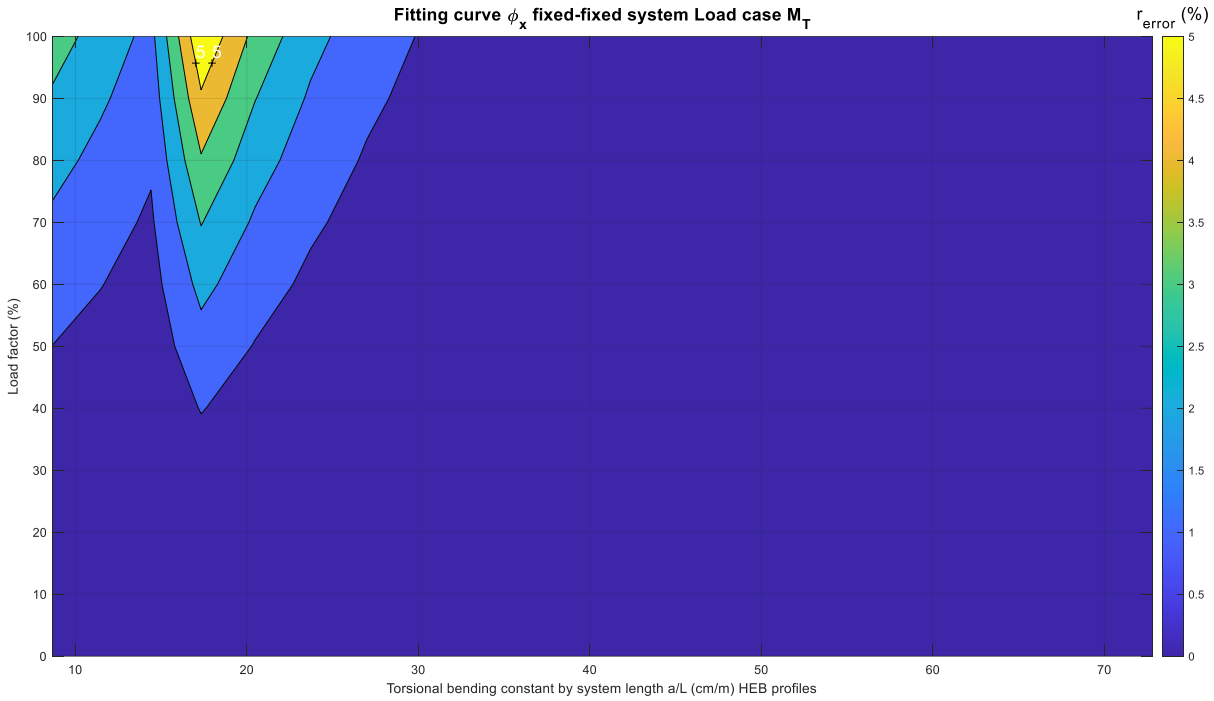

Figure 4.143 Fitting curve φ_x: fixed-fixed system, M_T load, HEB profiles

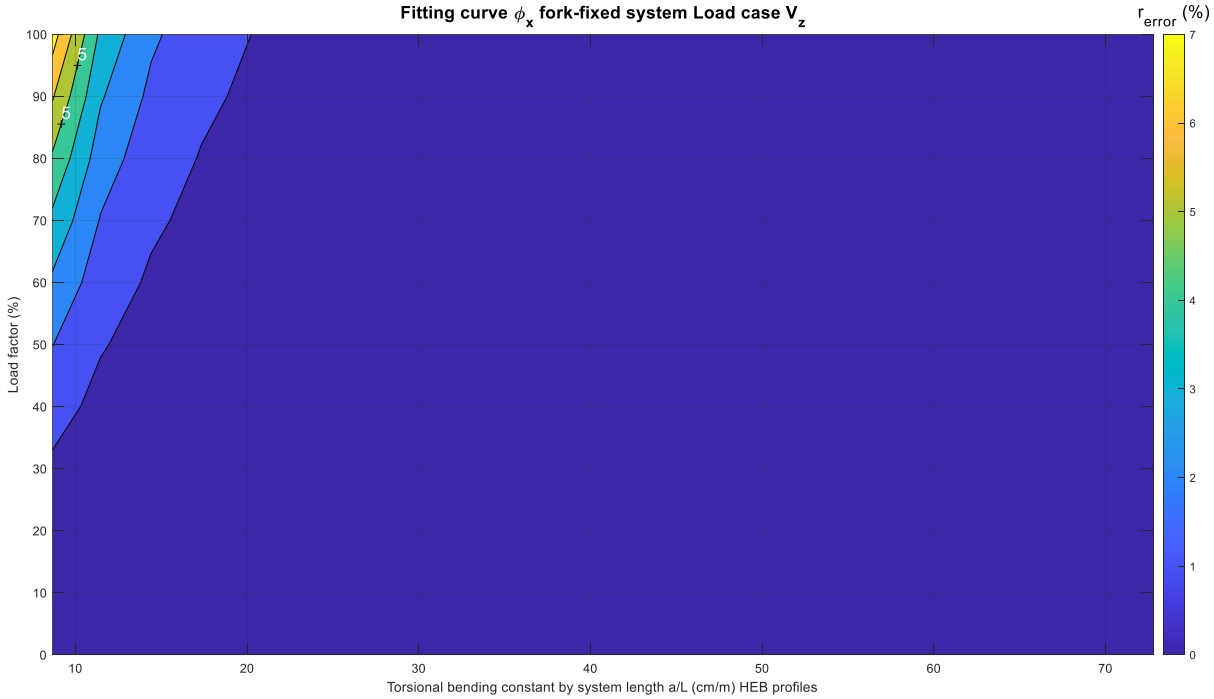

Figure 4.144 Fitting curve φ_x: fork-fixed system, V_z load, HEB profiles

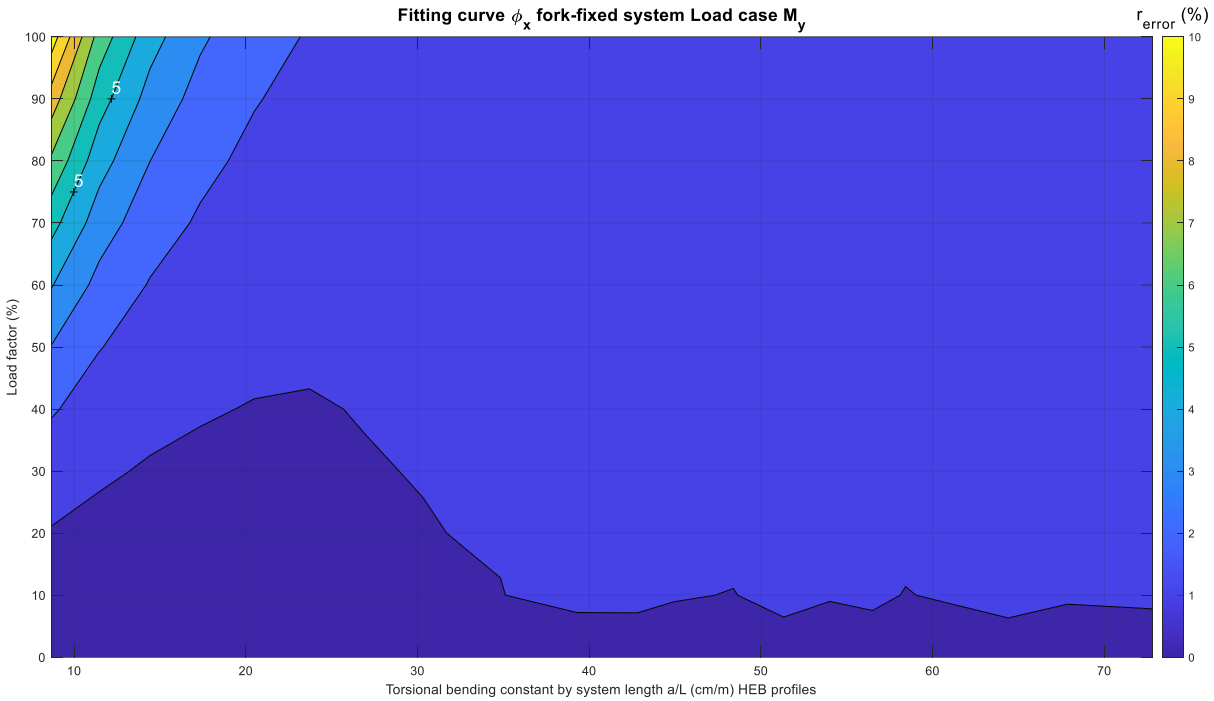

Figure 4.145 Fitting curve φ_x: fork-fixed system, M_y load, HEB profiles

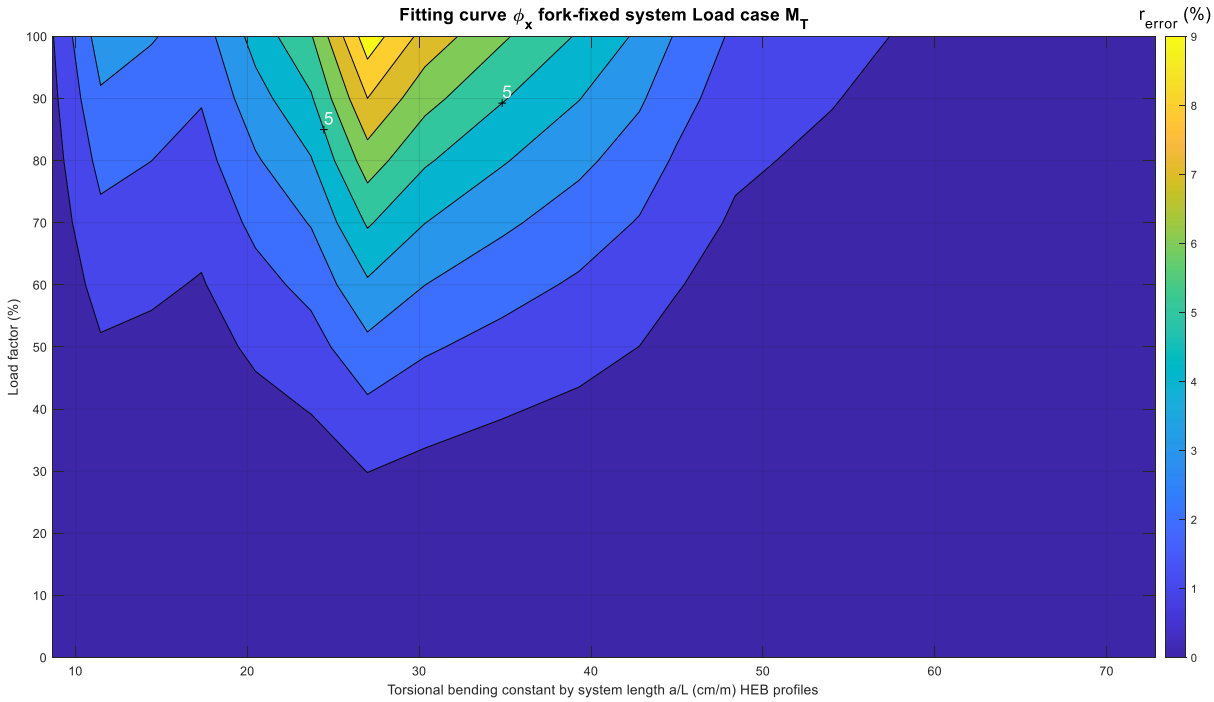

Figure 4.146 Fitting curve φ_x: fork-fixed system, M_T load, HEB profiles

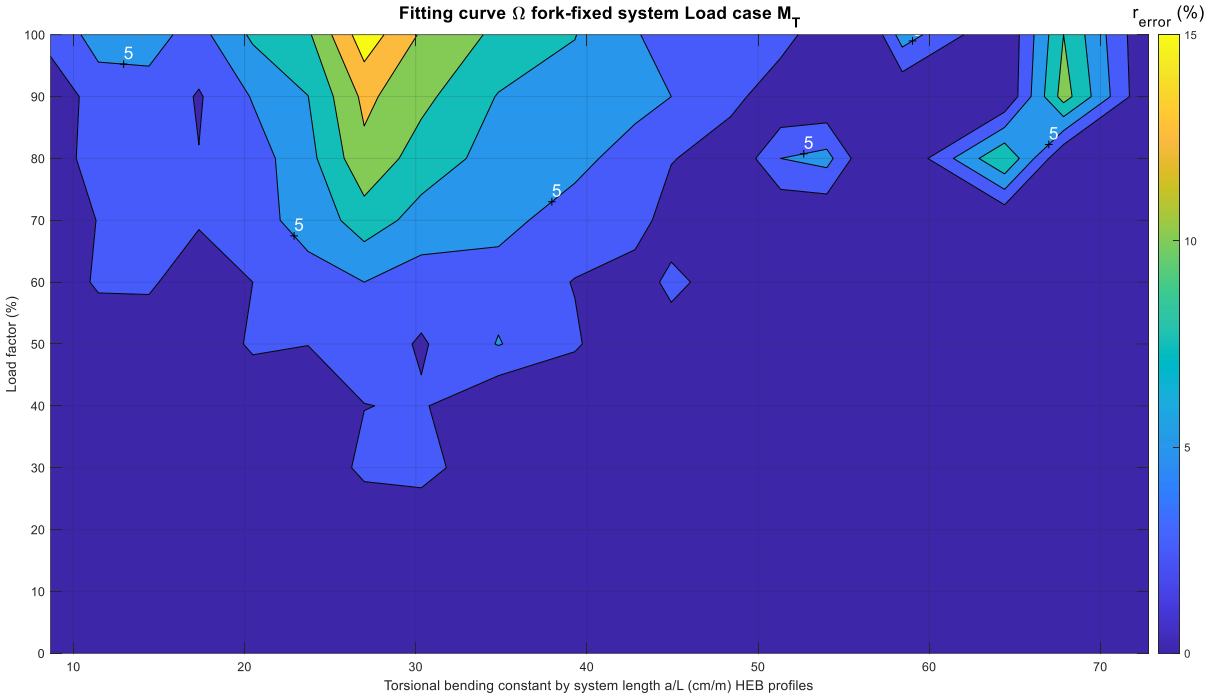

Figure 4.147 Fitting curve Ω: fork-fixed system, M_T load, HEB profiles

4.3.3 Validation of the fitting curves

Six examples are prepared in order to validate the use of the fitting curves, 3 with IPE profiles, 2 with HEB profiles and 1 with a UPE profile. The different systems, types of loads, and cross-sections used are shown in Figure 4.148. The IPE profile under distributed load case is used to observe the influence of different types of load action with bending and shear effects similar as to single V_z or M_y. Furthermore, for the UPE profile, the fitting curves of IPE profiles are considered in order to observe their validity for other types of open profiles. Finally, in each system all displacements with relevant variation are checked.

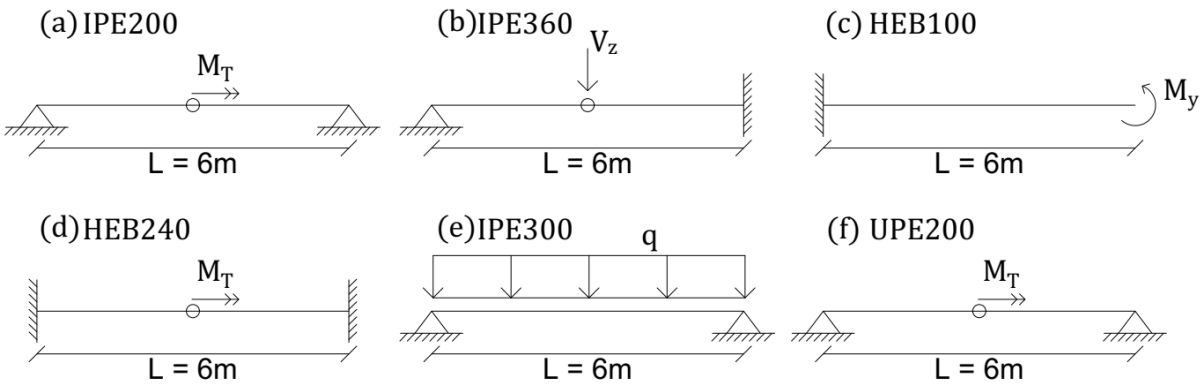

Figure 4.148 Examples validation of fitting curves: (a) fork-fork system under M_T IPE200, (b) fork-fixed system under V_z IPE360, (c) fixed-free system under M_y HEB100, (d) fixed-fixed system under M_T HEB240, (e) fork-fork system under linear distributed load IPE300, (f) fork-fork system under M_T UPE200

Some important geometrical properties are listed in Table 4.3. They include torsional and warping inertia as well as the bending torsional constant *a*, the length of the system L, the buckling curves, and the geometrical imperfections (refer to section 3.1.1).

Material S355 is considered for calculation of maximum capacity. In addition, the critical loads for each example are calculated and they are presented in Table 4.4. Finally, a load level of 80% of the critical load is considered for each profile. The corresponding load is then assigned to each system (see Table 4.4).

Table 4.3 Geometrical properties [29][25]

Example	System	Profile	I_T (cm^4)	I_w (cm^6)	a (cm)	L (m)	a/L (cm/m)	Buckling curve	Imperfection SOT (cm)
1	Fork-fork	IPE200	6.85	12746	69.58	6	11.60	a	2.00
2	Fork-fixed	IPE360	37.08	309370	147.28	6	24.55	b	2.40
3	Fixed-free	HEB100	9.31	3233	30.05	6	5.01	a	2.00
4	Fixed-fixed	HEB240	103.60	476280	109.33	6	18.22	a	2.00
5	Fork-fork	IPE300	19.75	124260	127.90	6	21.32	a	2.00
6	Fork-fork	UPE200	8.88	11880	58.96	6	9.83	d	4.00

Table 4.4 Critical loads, section capacity, and assignment of loads [29]

Example	System	Profile	Acting load	Maximum capacity	Critical load	Final critical load	Assigned load (80%)
1	Fork-fork	IPE200	M_T (kNm)	15.83	3.57	3.57	2.86
2	Fork-fixed	IPE360	V_z (kN)	246.05	374.51	246.05	196.84
3	Fixed-free	HEB100	M_y (kNm)	37.00	5.93	5.93	4.74
4	Fixed-fixed	HEB240	M_T (kNm)	18.25	605.00	18.25	14.60
5	Fork-fork	IPE300	q (kN/m)	49.58	24.20	24.20	19.36
6	Fork-fork	UPE200	M_T (kNm)	22.09	2.36	2.36	1.89

Depending on the load and structural system, different fitting figures are checked for each example. A summary of whether SOT or GNA should be used are presented in Table 4.5. For observing the intersecting location of the values of *a*/L and LF (80%) refer to Appendix IV.

Table 4.5 Type of analysis suggested

Example	System	Profile	Acting load	Displacement	Figure of reference	Type of analysis
1	Fork-fork	IPE200	M_T	φ_x	Figure 4.127	SOT
				u_z	Figure 4.132	SOT
2	Fork-fixed	IPE360	V_z	φ_x	Figure 4.133	SOT
				φ_y	Figure 4.134	SOT
3	Fixed-free	HEB100	M_y	φ_x	Figure 4.138	GNA
4	Fixed-fixed	HEB240	M_T	φ_x	Figure 4.143	SOT
5	Fork-fork	IPE300	q	u_z	Figure 4.124	SOT
				φ_x	Figure 4.125	GNA
6	Fork-fork	UPE200	M_T	φ_x	Figure 4.127	SOT

It is found that for most of the examples SOT is suggested as the preferred type of analysis. Nevertheless, for example 3, it is observed that GNA is needed in order to preserve accuracy. Finally, the fork-fork system with IPE300 and distributed load suggests the use of SOT for u_z but GNA for φ_x.

At this point with all the information obtained, as a next step numerical simulations are performed. In order to validate the curves then, both analysis SOT and GNA are performed and the results (relevant displacements) are compared in the most critical locations following the same procedure as explained in section 3.3.5. The results are then summarized in Table 4.6.

Table 4.6 Numerical simulations results and fitting curves validation

Example	System	Profile	Acting load	Max Displacement	SOT	GNA	r_{error} (%)
1	Fork-fork	IPE200	M_T	φ_x (mrad)	581.83	541.04	-7.54
				u_z (cm)	1.40	1.43	1.77
2	Fork-fixed	IPE360	V_z	φ_x (mrad)	68.53	66.39	-3.22
				φ_y (mrad)	1.40	1.44	2.99
3	Fixed-free	HEB100	M_y	φ_x (mrad)	14.68	12.22	-20.08
4	Fixed-fixed	HEB240	M_T	φ_x (mrad)	92.56	92.44	-0.13
5	Fork-fork	IPE300	q	u_z (cm)	2.08	2.15	3.25
				φ_x (mrad)	115.58	96.97	-19.19
6	Fork-fork	UPE200	M_T	φ_x (mrad)	327.50	320.48	-2.19

The results from Table 4.6 show that the type of analysis defined in Table 4.5 are in accordance with was expected and accuracy has been preserved when performing the analysis. The only exception is example 1. For all red values (r_{error} higher than 5%) GNA should be used, however, in example 1 SOT was suggested following the fitting curves. In this case, the r_{error} reached 7.54% with higher values for SOT. This suggest that the fitting curves for φ_x can still be improved, particularly for low values of *a*, nonetheless, these curves still give a general good idea of what type of analysis to follow.

Furthermore, for the case of linear distributed load *q*, the curves prove to be useful because this type of action still introduces shear and bending moments, hence, in this sense V_z curves could be used for this load case. Moreover, fitting curves of IPE profiles could also be extended to profiles such as UPE as they have similar geometric proportions than with HEB profiles. Ultimately, it is then stablished that the fitting curves can give a good estimation of whether SOT or GNA should be used.

Chapter 5: Conclusions

5.1 Summary

The main aim of this project has been to evaluate until which stage second-order theory gives sufficiently accurate results to geometrical nonlinear analysis. Particularly regarding torsion and bending that can cause LTB. In addition, a model that can define significant deformation limits is deemed to be found. To begin a literature review has been done, afterwards a methodology is defined, then numerical simulations are performed. Finally, results are analyzed and conclusions are reached.

First, the literature review has been done of developments in the field of SOT and GNA regarding torsional and bending effects. Then several numerical analyses following SOT and GNA have been performed using the commercial software RFEM. Here different variables have been considered: 4 structural systems, 2 types of FE, 43 profiles (38 open and 5 closed), and 3 external loads. Every analysis has been performed 10 times, in each one, the load factor is increased up to a value of 100%.

The analysis and discussion of results have been done in chapter 4. The results include critical loads, displacements, internal forces, and stresses. A stage where SOT provides sufficiently reliable results is given in the form of fitting curves, which are found for the open profiles of this study.

5.2 Conclusions

The fitting curves present a practical way to estimate which type of analysis should be followed for steel members in bending and torsion. Whether SOT or GNA should be applied strongly depends on the cross-section profile and the load level. Additionally, boundary conditions and load types play an important role as well. The latter, has shown that even for a different load distribution the curves of V_z still give a good estimate. Moreover, IPE fitting curves can also be useful for UPE profiles.

It is found that when displacements increase so does the variation of results between GNA and SOT. The same is true for the load factor, higher forces translate in higher displacements and then higher variation.

Slender systems with low values of *a*/L are more prone to instabilities, thus, they have more variation in displacements between GNA and SOT. In this cases, GNA should be preferably used. Furthermore, IPE profiles are more susceptible to LTB in comparison with HEB profiles, therefore, careful consideration has to be taken when studying geometrical nonlinearity of such profiles.

Generally, φ_x shows difference between GNA and SOT for **open sections** subjected to bending. SOT gives higher results, which leads to conservative rotation values specially for IPE profiles with low *a*. However, for economy, SOT may not be the most adequate approach of analysis as rotational limits will be surpassed at a lower load value. Similarly, under torsional load, SOT gives higher values of φ_x, nevertheless, higher variation is seen for profiles with intermediate and high values of *a*. SOT gives higher internal forces as well, which shows that this type of analysis can be conservative.

In almost all cases the **fixed-free system** can be analyzed either with SOT or GNA for both open and closed sections. The exception exists only for nodal bending moments M_y in open profiles.

Studying bending under GNA, axial forces can be introduced depending on the support conditions. For instance, tension forces will reduce compressions stresses and in that case it will have a favorable effect reducing vertical displacements u_z and providing a stabilizing effect for LTB. This is not properly considered in SOT without geometrical imperfections, which has been the case for 2D open sections and 1D and 2D closed cross-sections.

There is low variation of both displacements and internal forces for **closed profiles**. Additionally, for closed profiles subjected to bending, displacements show good agreement between 1D and 2D elements. Therefore, for closed profiles, the analysis can be simplified with the use of 1D-beam elements. Moreover, closed profiles can reach higher displacements than open profiles while still maintaining a r_{error} lower than 5%.

No limiting value of rotation φ_x has been found for **closed profiles**. Even for the less redundant system which corresponds to the fixed-free system, the maximum rotation reached 0.32 radians with low variation of results (less than 4%). For all other systems the maximum rotation reached 0.16 rad (9.2º) and with variation lower than 1%. However, the torsional moment has been limited to the plastic capacity of each profile. Hence, if neglecting rotational limits, it is established that for closed profiles the rotation will be limited to the section's capacity. In addition, closed profiles present an excellent behavior for torsion. In this case, SOT can be used safely as an approximation for GNA.

Regarding torsion design, in GNA and SOT for open cross-sections, it is adequate to assume that the secondary torsional moment M_s accounts for the total torsional moment M_T in the most stressed locations. M_s may be used for design of open profiles with scheduled torsion and M_p may be neglected. The other way around is true in the case of closed cross-sections, where only M_p may be considered for design.

5.3 Outlook

The methodology followed in this project leaves room for improvement and further research.

For instance, further work can focus on improving the fitting curves by obtaining more data of models particularly with low *a*/L ratio. In addition, more boundary conditions can be studied, be it at end supports or at intermediate locations of the member. Furthermore, this study could also be extended for more open profiles such as G, L, and T profiles.

Presently, the analyses have been performed under the consideration of fully elastic material. Moreover, plastic capacity of the profiles has been used as limitation. Future studies should consider the change in displacements and internal forces due to plastification of the cross-section. Both geometrical and material nonlinearity for a single analysis should be studied in order to understand the influence material has.

Finally, additional commercial software could be considered in the context of nonlinear analysis, which results could be compared to the ones obtained in this study. However, this software should be able to consider the warping degree of freedom and also SOT with imperfections.

Bibliography

[1] A. Ibrahimbegović, H. Shakourzadeh, J.-L. Batoz, M. AI Mikdad, and Y.-Q. Guo, "On the role of geometrically exact and second-order theories in buckling and post-buckling analysis of three-dimensional beam structures," *Computers & Structures*, vol. 61, no. 6, pp. 1101–1114, Dec. 1996, doi: 10.1016/0045-7949(96)00181-2.

[2] L. S. da Silva, R. Simões, and H. Gervásio, *Design of Steel Structures*, 1st ed. ECCS – European Convention for Constructional Steelwork, 2013.

[3] M. Peksen, *Multiphysics Modelling*. Elsevier, 2018. doi: 10.1016/C2016-0-01710-2.

[4] R. Kindmann and M. Kraus, *Steel Structures: Design using FEM*. Berlin, Germany: John Wiley & Sons, Ltd, 2012.

[5] R. De Borst, M. A. Crisfield, J. J. C. Remmers, and C. V. Verhoosel, *Non-Linear Finite Element Analysis of Solids and Structures*, 1st ed. John Wiley & Sons, Ltd, 2012. doi: 10.1002/9781118375938.

[6] V. Galishnikova, T. Gebre, S. Al-Sabri, and O. Saffia-Doe, "Second order structural theory for the stability analysis of columns," *Structural Mechanics of Engineering Constructions and Buildings*, vol. 14, pp. 192–197, Dec. 2018, doi: 10.22363/1815-5235-2018-14-3-192-197.

[7] C. Könke, "Applied Finite Element Methods Handout," Weimar, 2019.

[8] CEN, "Eurocode 3: Design of steel structures -Part 1-1: General rules and rules for buildings." May 2005.

[9] C. F. Kollbrunner and K. Basler, *Torsion in Structures: An Engineering Approach*. Berlin Heidelberg: Springer-Verlag, 1969. doi: 10.1007/978-3-662-22557-8.

[10] A. F. Hughes, D. C. Iles, and A. S. Malik, *Design of Steel Beams in Torsion: In Accordance with Eurocodes and UK National Annexes*. Beliveau Editeur, 2011.

[11] P. V. Makode, R. B. Corotis, and M. R. Ramirez, "Geometric Nonlinear Analysis of Frame Structures by Pseudodistortions," *Journal of Structural Engineering*, vol. 125, no. 11, pp. 1318–1327, Nov. 1999, doi: 10.1061/(ASCE)0733-9445(1999)125:11(1318).

[12] Y. Cai, J. Paik, and S. Atluri, "Large Deformation Analyses of Space-Frame Structures, Using Explicit Tangent Stiffness Matrices, Based on the Reissner variational principle and a von Karman Type Nonlinear Theory in Rotated Reference Frames," 2009, doi: 10.3970/CMES.2009.054.335.

[13] A. Maghami, F. Shahabian, and S. Mahmoud Hosseini, "Geometrically Nonlinear Analysis of Structures Using Various Higher Order Solution Methods: A Comparative Analysis for Large Deformation," *Computer Modeling in Engineering & Sciences*, vol. 121, no. 3, pp. 877–907, 2019, doi: 10.32604/cmes.2019.08019.

[14] M. Mohit, Y. Sharifi, and A. Tavakoli, "Geometrically nonlinear analysis of space trusses using new iterative techniques," *Asian J Civ Eng*, vol. 21, no. 5, pp. 785–795, Jul. 2020, doi: 10.1007/s42107-020-00239-x.

[15] C. K. Iu and M. A. Bradford, "Higher-order non-linear analysis of steel structures part I: elastic second-order formulation," *Advanced Steel Construction*, vol. 8, no. 2, p. 15, 2012, doi: 10.18057/IJASC.2012.8.2.5.

[16] Andrew Kwok Wai So and Siu Lai Chan, "Buckling and geometrically nonlinear analysis of frames using one element/member," *Journal of Constructional Steel Research*, vol. 20, no. 4, pp. 271–289, Jan. 1991, doi: 10.1016/0143-974X(91)90078-F.

[17] L. A. T. Mororó, A. M. C. de Melo, E. Parente Junior, L. A. T. Mororó, A. M. C. de Melo, and E. Parente Junior, "Geometrically nonlinear analysis of thin-walled laminated composite beams," *Latin American Journal of Solids and Structures*, vol. 12, no. 11, pp. 2094–2117, Nov. 2015, doi: 10.1590/1679-78251782.

[18] Y. Hui *et al.*, “Geometrically Nonlinear Analysis of Beam Structures via Hierarchical One-Dimensional Finite Elements,” *Mathematical Problems in Engineering*, vol. 2018, p. e4821385, Nov. 2018, doi: 10.1155/2018/4821385.
[19] K. Sato and K. Ikarashi, “Effect of initial imperfection on local buckling behavior of square hollow section member,” *Journal of Structural and Construction Engineering (Transactions of AIJ)*, vol. 81, pp. 893–903, May 2016, doi: 10.3130/aijs.81.893.
[20] F. Walport, L. Gardner, and D. A. Nethercot, “Equivalent bow imperfections for use in design by second order inelastic analysis,” *Structures*, vol. 26, pp. 670–685, May 2020, doi: 10.1016/j.istruc.2020.03.065.
[21] G. Mageirou, V.-B. M., M. M., and C. Gantes, “Comparison of linear and nonlinear analysis methods for steel columns,” Patra, Greece, Jun. 2002, vol. I, p. 8.
[22] M. Aminbaghai, J. Murin, G. Balduzzi, J. Hrabovsky, G. Hochreiner, and H. A. Mang, “Second-order torsional warping theory considering the secondary torsion-moment deformation-effect,” *Engineering Structures*, vol. 147, pp. 724–739, Sep. 2017, doi: 10.1016/j.engstruct.2017.06.023.
[23] J. Murin and V. Kutiš, “An effective finite element for torsion of constant cross-sections including warping with secondary torsion moment deformation effect,” *Engineering Structures - ENG STRUCT*, vol. 30, pp. 2716–2723, Oct. 2008, doi: 10.1016/j.engstruct.2008.03.004.
[24] D. Addessi, P. Di Re, and G. Cimarello, “Enriched beam finite element models with torsion and shear warping for the analysis of thin-walled structures,” *Thin-Walled Structures*, vol. 159, p. 107259, Nov. 2020, doi: 10.1016/j.tws.2020.107259.
[25] CEN, “DIN 18800-2 Steel structures - Part 2: Stability - Buckling of bars and skeletal structures,” Nov. 2008.
[26] Dlubal Software, “RF-FE-LTB Program Description.” Aug. 2013. [Online]. Available: https://www.dlubal.com/en/downloads-and-information/documents/manuals
[27] Dlubal Software, “RFEM 5 User Manual.” Mar. 2020. [Online]. Available: https://www.dlubal.com/en/downloads-and-information/documents/online-manuals/rfem-5/01/01
[28] CEN, “DIN EN 10219-2:2006-07, Kaltgefertigte geschweißte Hohlprofile für den Stahlbau aus unlegierten Baustählen und aus Feinkornbaustählen_- Teil_2,” 2006. doi: 10.31030/9666330.
[29] R. Kindmann, M. Kraus, and H. Joachim, *Stahlbau Kompakt*, 4th ed. Dortmund, 2017.
[30] CEN, “Eurocode 8: Design of structures for earthquake resistance.” 2004. Accessed: Jan. 02, 2020. [Online]. Available: https://www.phd.eng.br/wp-content/uploads/2015/02/en.1998.1.2004.pdf
[31] MathWorks, “Matlab Documentation.” https://de.mathworks.com/help/index.html?s_tid=CRUX_lftnav (accessed Aug. 27, 2021).

Appendix

Appendix I Cross-sections

In this appendix, the dimensions, structural class, and c/t ratio of all the different profiles used in this study are given. The plastic capacity for shear V_z, bending moment M_y and torsional moment M_T are also calculated considering steel S355. In addition, the buckling curves for the 3-plate open sections are presented. Furthermore, the maximum loads for each structural system corresponding to the external action (section 3.3.1.1) are given. The resulting equations (by using Eq. 3.3) for the calculation of the maximum loads in each structural system are also presented.

Table A I.1 Geometry, class, and plastic capacity closed profiles

Section	h (mm)	b (mm)	t (mm)	r (mm)	c (mm)	c/t (-)	Class (Bending)	$V_{z,pl}$ (kN)	$M_{y,pl}$ (kNm)	$M_{T,pl}$ (kNm)
200x200x6	200	200	6	12	164	27	1	477.1	117.0	92.4
100x50x6	100	50	6	12	64	11	1	231.2	16.7	10.0
200x100x8	200	100	8	20	144	18	1	629.6	95.9	57.2
300x100x6	300	100	6	12	264	44	1	723.1	146.1	67.8
300x150x6	300	150	6	12	264	44	1	723.1	177.3	104.0

Table A I.2 Maximum load (elastic) closed profiles

Section Hollow	Fixed-free			Fork-fork			Fixed-fixed			Fork-fixed		
	$V_{z,max}$ (kN)	$M_{y,max}$ (kNm)	$M_{T,max}$ (kNm)	$V_{z,max}$ (kN)	$M_{y,max}$ (kNm)	$M_{T,max}$ (kNm)	$V_{z,max}$ (kN)	$M_{y,max}$ (kNm)	$M_{T,max}$ (kNm)	$V_{z,max}$ (kN)	$M_{y,max}$ (kNm)	$M_{T,max}$ (kNm)
200x200x6	27.56	116.99	92.41	104.21	208.42	184.83	187.90	197.63	184.83	127.36	185.26	184.83
100x50x6	4.09	16.67	10.02	16.09	32.18	20.04	31.10	31.63	20.04	20.85	28.61	20.04
200x100x8	23.10	95.93	57.25	89.14	178.27	114.50	166.49	172.18	114.50	112.23	158.46	114.50
300x100x6	34.76	146.06	67.82	132.67	265.33	135.64	243.04	253.69	135.64	164.33	235.85	135.64
300x150x6	41.77	177.34	103.97	157.97	315.94	207.95	284.83	299.58	207.95	193.05	280.84	207.95

Table A I.3 Geometry, class, buckling curve, and plastic capacity open profiles

Section 3-Plate	h (mm)	b (mm)	t_w (mm)	t_f (mm)	c web (mm)	c/t (-)	Class (bending)	Buckling curve	$V_{z,pl}$ (kN)	$M_{y,pl}$ (kNm)	$M_{T,pl}$ (kNm)
IPE80	80	46	3.8	5.2	70	18	1	c	54.2	6.5	2.0
IPE100	100	55	4.1	5.7	89	22	1	c	74.5	10.8	3.2
IPE120	120	64	4.4	6.3	107	24	1	c	96.9	16.7	4.8
IPE140	140	73	4.7	6.9	126	27	1	c	121.6	24.5	6.8
IPE160	160	82	5.0	7.4	145	29	1	c	148.8	33.8	9.2
IPE180	180	91	5.3	8.0	164	31	1	c	178.2	45.7	12.2
IPE200	200	100	5.6	8.5	183	33	1	c	210.0	59.4	15.6
IPE220	220	110	5.9	9.2	202	34	1	c	243.8	77.9	20.4
IPE240	240	120	6.2	9.8	220	36	1	c	280.1	98.8	25.8
IPE270	270	135	6.6	10.2	250	38	1	c	337.6	130.6	34.0
IPE300	300	150	7.1	10.7	279	39	1	c	405.4	169.7	44.0
IPE330	330	160	7.5	11.5	307	41	1	d	471.9	214.3	53.8
IPE360	360	170	8.0	12.7	335	42	1	d	548.6	274.1	67.0
IPE400	400	180	8.6	13.5	373	43	1	d	657.5	344.0	80.1
IPE450	450	190	9.4	14.6	421	45	1	d	810.7	443.5	96.9
IPE500	500	200	10.2	16.0	468	46	1	d	978.4	569.7	117.9
IPE550	550	210	11.1	17.2	516	46	1	d	1173.0	709.4	140.3
IPE600	600	220	12.0	19.0	562	47	1	d	1382.2	895.8	170.4
HEB100	100	100	6.0	10.0	80	13	1	c	98.4	32.3	18.0
HEB120	120	120	6.5	11.0	98	15	1	c	130.6	51.6	28.5
HEB140	140	140	7.0	12.0	116	17	1	c	166.4	77.2	42.3
HEB160	160	160	8.0	13.0	134	17	1	c	219.7	109.8	59.8
HEB180	180	180	8.5	14.0	152	18	1	c	264.8	150.2	81.5
HEB200	200	200	9.0	15.0	170	19	1	c	313.6	199.3	107.7
HEB220	220	220	9.5	16.0	188	20	1	c	366.1	257.9	139.0
HEB240	240	240	10.0	17.0	206	21	1	c	422.2	326.8	175.6
HEB260	260	260	10.0	17.5	225	23	1	c	461.2	396.2	212.0
HEB280	280	280	10.5	18.0	244	23	1	c	525.1	474.3	252.9
HEB300	300	300	11.0	19.0	262	24	1	c	590.7	575.3	306.3
HEB400	400	300	13.5	24.0	352	26	1	c	974.0	975.9	389.1
HEB500	500	300	14.5	28.0	444	31	1	c	1319.5	1432.9	455.6
HEB550	550	300	15.0	29.0	492	33	1	c	1512.6	1641.3	473.1
HEB600	600	300	15.5	30.0	540	35	1	c	1715.5	1861.3	490.8
HEB650	650	300	16.0	31.0	588	37	1	d	1928.3	2092.7	508.6
HEB700	700	300	17.0	32.0	636	37	1	d	2216.0	2337.6	527.5
HEB800	800	300	17.5	33.0	734	42	1	d	2632.7	2779.3	547.1
HEB900	900	300	18.5	35.0	830	45	1	d	3147.2	3337.4	584.3
HEB1000	1000	300	19.0	36.0	928	49	1	d	3613.8	3841.2	604.8

Table A I.4 Maximum load (elastic) open profiles

Section 3-Plate	Fixed-free			Fork-fork			Fixed-fixed			Fork-fixed		
	$V_{z,max}$ (kN)	$M_{y,max}$ (kNm)	$M_{T,max}$ (kNm)	$V_{z,max}$ (kN)	$M_{y,max}$ (kNm)	$M_{T,max}$ (kNm)	$V_{z,max}$ (kN)	$M_{y,max}$ (kNm)	$M_{T,max}$ (kNm)	$V_{z,max}$ (kN)	$M_{y,max}$ (kNm)	$M_{T,max}$ (kNm)
IPE80	1.58	6.52	1.02	6.15	12.29	2.04	11.63	11.95	2.04	7.82	10.93	2.04
IPE100	2.60	10.78	1.60	10.05	20.11	3.19	18.83	19.45	3.19	12.69	17.87	3.19
IPE120	4.01	16.72	2.38	15.40	30.79	4.76	28.52	29.61	4.76	19.25	27.37	4.76
IPE140	5.82	24.46	3.39	22.23	44.46	6.77	40.73	42.51	6.77	27.54	39.52	6.77
IPE160	8.00	33.81	4.58	30.36	60.72	9.15	55.10	57.77	9.15	37.31	53.97	9.15
IPE180	10.74	45.72	6.08	40.52	81.04	12.17	72.76	76.68	12.17	49.35	72.03	12.17
IPE200	13.88	59.45	7.80	52.08	104.16	15.60	92.67	98.08	15.60	62.94	92.59	15.60
IPE220	18.03	77.86	10.19	67.14	134.28	20.38	118.03	125.63	20.38	80.30	119.36	20.38
IPE240	22.69	98.78	12.90	83.97	167.94	25.80	146.05	156.23	25.80	99.53	149.28	25.80
IPE270	29.78	130.65	16.98	109.47	218.94	33.96	188.40	202.52	33.96	128.59	194.61	33.96
IPE300	38.41	169.73	21.99	140.35	280.70	43.98	239.28	258.34	43.98	163.54	249.51	43.98
IPE330	48.12	214.32	26.89	174.66	349.32	53.79	294.77	319.73	53.79	201.76	310.50	53.79
IPE360	60.92	274.14	33.52	219.34	438.67	67.05	365.59	398.81	67.05	250.69	389.93	67.05
IPE400	76.06	344.03	40.04	272.69	545.38	80.09	451.70	494.14	80.09	310.01	484.78	80.09
IPE450	97.54	443.54	48.43	348.27	696.54	96.85	573.39	628.99	96.85	393.86	619.15	96.85
IPE500	124.32	569.65	58.96	441.21	882.42	117.92	720.06	793.01	117.92	495.23	784.37	117.92
IPE550	154.05	709.38	70.14	544.68	1089.4	140.28	884.10	976.05	140.28	608.51	968.32	140.28
IPE600	192.72	895.78	85.21	676.56	1353.1	170.41	1087.1	1205.6	170.41	749.27	1202.8	170.41
HEB100	7.46	32.29	9.00	27.74	55.48	18.01	48.62	51.82	18.01	33.10	49.31	18.01
HEB120	11.75	51.63	14.24	43.11	86.22	28.48	74.00	79.64	28.48	50.53	76.64	28.48
HEB140	17.29	77.18	21.13	62.65	125.30	42.25	105.45	114.52	42.25	72.21	111.38	42.25
HEB160	24.41	109.82	29.92	87.86	175.72	59.83	146.44	159.75	59.83	100.42	156.20	59.83
HEB180	32.90	150.25	40.74	117.04	234.09	81.49	191.72	210.79	81.49	131.79	208.08	81.49
HEB200	43.00	199.33	53.86	151.26	302.52	107.72	243.74	269.96	107.72	167.93	268.91	107.72
HEB220	54.82	257.90	69.48	190.72	381.43	138.96	302.60	337.48	138.96	208.93	339.05	138.96
HEB240	68.45	326.76	87.82	235.59	471.19	175.64	368.40	413.51	175.64	254.87	418.83	175.64
HEB260	81.54	396.19	105.99	277.14	554.28	211.98	426.21	481.88	211.98	295.52	492.70	211.98
HEB280	96.73	474.32	126.44	326.75	653.49	252.88	498.42	565.52	252.88	345.96	580.88	252.88
HEB300	115.66	575.30	153.17	386.90	773.79	306.34	582.90	664.91	306.34	405.26	687.82	306.34
HEB400	195.10	975.90	194.55	650.17	1300.3	389.09	974.93	1114.4	389.09	678.24	1155.9	389.09
HEB500	281.73	1432.9	227.79	928.66	1857.3	455.58	1373.9	1579.4	455.58	957.45	1650.9	455.58
HEB550	322.77	1641.3	236.55	1064.0	2128.1	473.10	1574.3	1809.8	473.10	1097.1	1891.6	473.10
HEB600	366.03	1861.3	245.38	1206.7	2413.3	490.76	1785.4	2052.4	490.76	1244.2	2145.2	490.76
HEB650	411.52	2092.7	254.29	1356.6	2713.2	508.58	2007.1	2307.3	508.58	1398.7	2411.7	508.58
HEB700	462.44	2337.6	263.76	1530.4	3060.8	527.51	2275.2	2610.2	527.51	1584.6	2720.7	527.51
HEB800	549.74	2779.3	273.56	1819.1	3638.2	547.12	2704.0	3102.3	547.12	1883.3	3234.0	547.12
HEB900	659.51	3337.4	292.17	2181.0	4362.0	584.34	3239.5	3717.8	584.34	2256.4	3877.3	584.34
HEB1000	758.69	3841.2	302.42	2508.2	5016.4	604.83	3724.1	4274.7	604.83	2594.1	4459.0	604.83

- Fixed-free beam, critical location at fixed support:

$$V_{z,max} = \frac{1}{\frac{1}{V_{z,pl}} + \frac{L}{M_{y,pl}}} \qquad \textit{Eq. A 1}$$

$$M_{y,max} = M_{y,pl} \qquad \textit{Eq. A 2}$$

$$M_{T,max} = M_{T,pl}\,(closed) = \frac{M_{z,pl}}{2}(open) \qquad \textit{Eq. A 3}$$

- Fork-fork beam, critical location at midspan:

$$V_{z,max} = \frac{1}{\frac{1}{2 \cdot V_{z,pl}} + \frac{L}{4 \cdot M_{y,pl}}} \qquad \textit{Eq. A 4}$$

$$M_{y,max} = \frac{1}{\frac{1}{L \cdot V_{z,pl}} + \frac{1}{2 \cdot M_{y,pl}}} \qquad \textit{Eq. A 5}$$

$$M_{T,max} = 2 \cdot M_{T,pl}\,(closed) = M_{z,pl}(open) \qquad \textit{Eq. A 6}$$

- Fixed-fixed beam, critical location at midspan:

$$V_{z,max} = \frac{1}{\frac{1}{2 \cdot V_{z,pl}} + \frac{L}{8 \cdot M_{y,pl}}} \qquad \textit{Eq. A 7}$$

$$M_{y,max} = \frac{1}{\frac{3}{2 \cdot L \cdot V_{z,pl}} + \frac{1}{2 \cdot M_{y,pl}}} \qquad \textit{Eq. A 8}$$

$$M_{T,max} = 2 \cdot M_{T,pl}\,(closed) = M_{z,pl}(open) \qquad \textit{Eq. A 9}$$

- Fork-fixed beam, critical location at fixed support for V_z and midspan for M_y and M_T:

$$V_{z,max} = \frac{1}{\frac{11}{16 \cdot V_{z,pl}} + \frac{3 \cdot L}{16 \cdot M_{y,pl}}} \qquad \textit{Eq. A 10}$$

$$M_{y,max} = \frac{1}{\frac{9}{8 \cdot L \cdot V_{z,pl}} + \frac{9}{16 \cdot M_{y,pl}}} \qquad \textit{Eq. A 11}$$

$$M_{T,max} = 2 \cdot M_{T,pl}\,(closed) = M_{z,pl}(open) \qquad \textit{Eq. A 12}$$

Appendix II Displacement results

In this appendix, all figures related to the main displacements are presented. Both figures for relative errors and displacement values for all structural systems, external loads, profiles, and finite element types are shown.

Appendix II-1 Fixed-free system

Appendix II-1.1 Open cross-sections

V_z

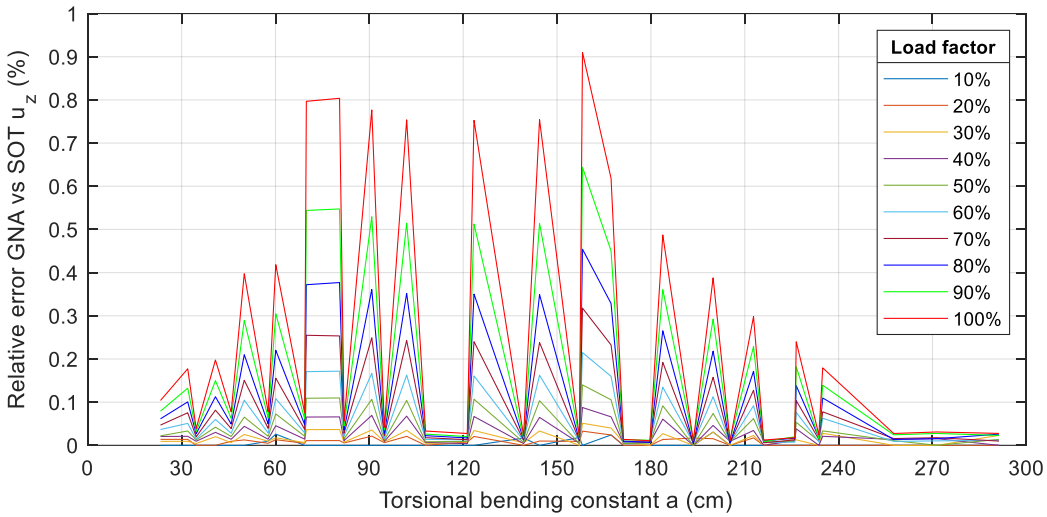

Figure A II.1 Relative error u_z: fixed-free system, V_z load, open profiles, and 1D elements

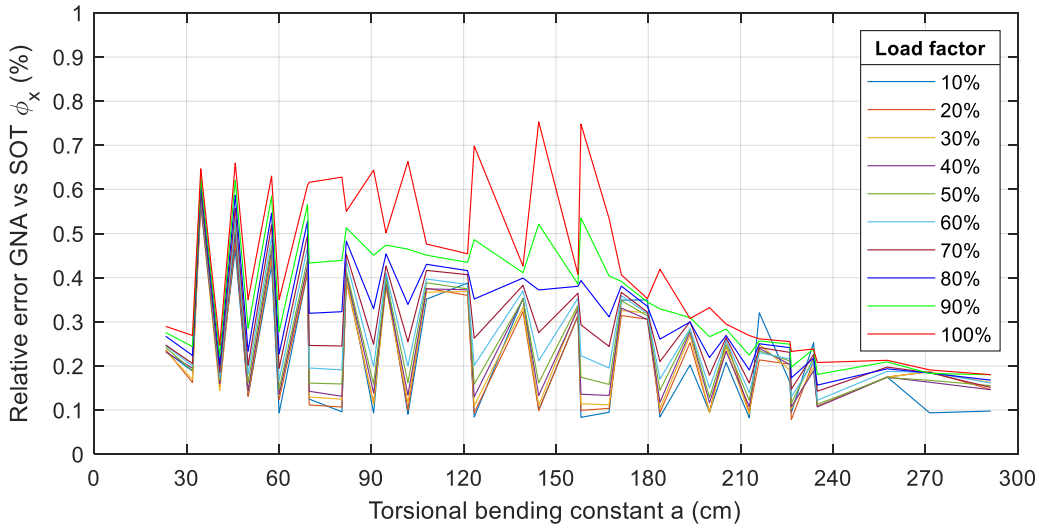

Figure A II.2 Relative error φ_x: fixed-free system, V_z load, open profiles, and 1D elements

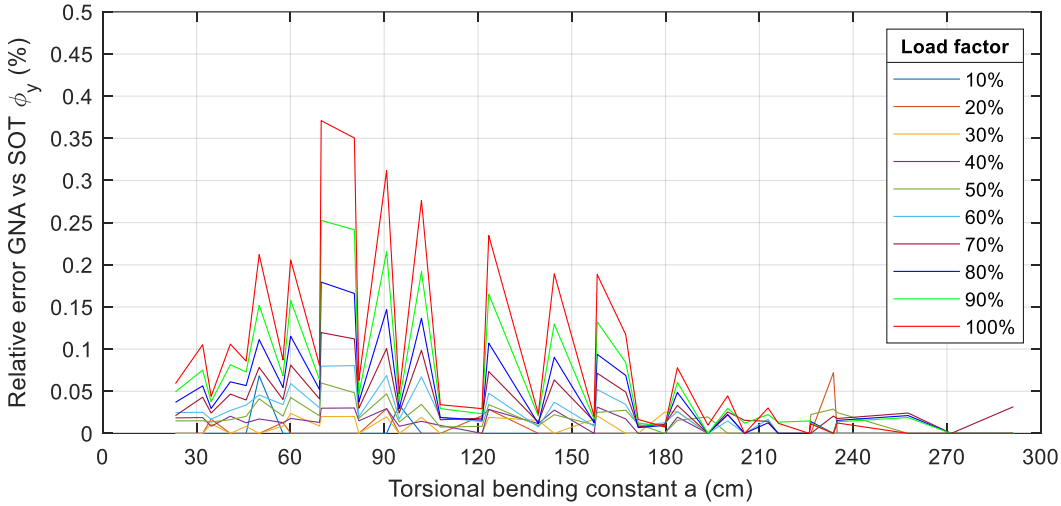

Figure A II.3 Relative error φ_y: fixed-free system, V_z load, open profiles, and 1D elements

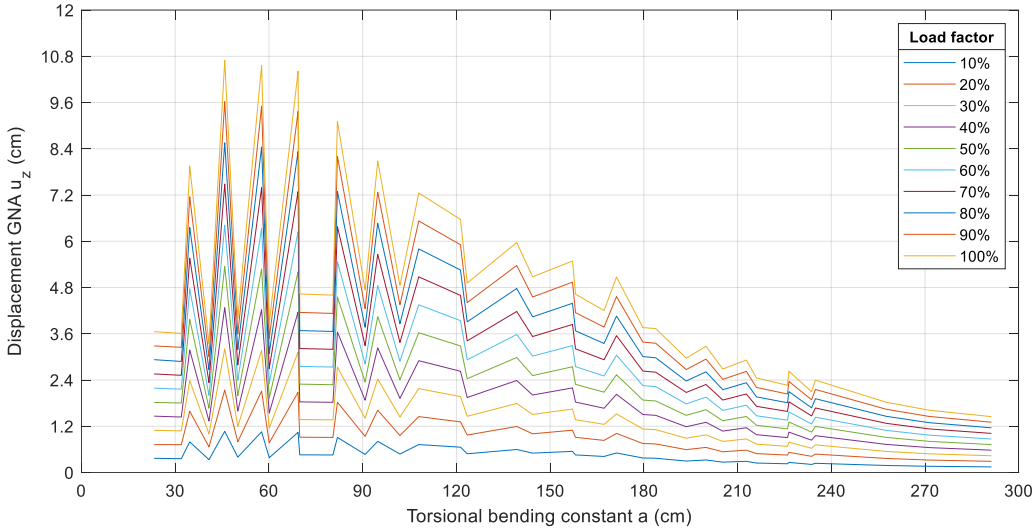

Figure A II.4 Displacement u_z: fixed-free system, V_z load, open profiles, and 1D elements

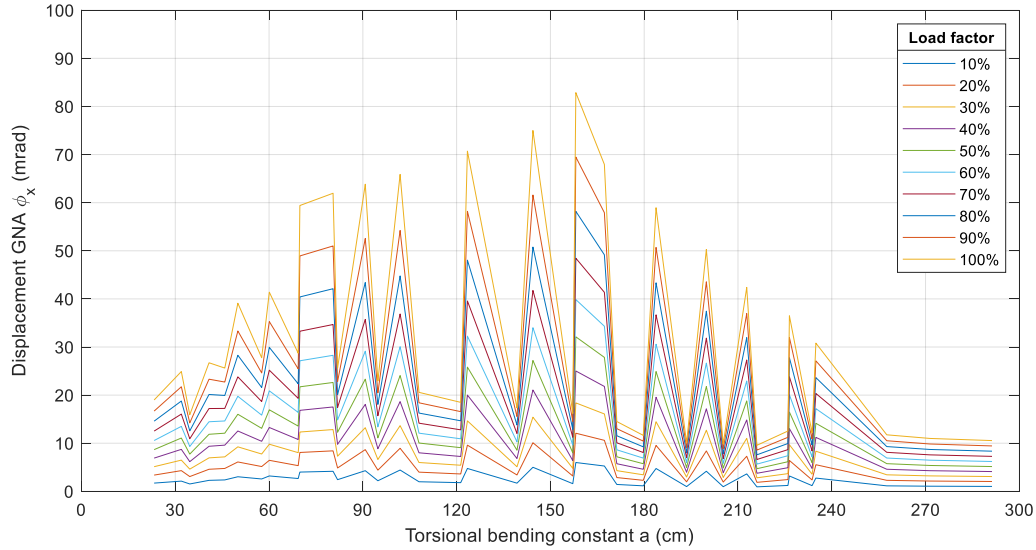

Figure A II.5 Displacement φ_x: fixed-free system, V_z load, open profiles, and 1D elements

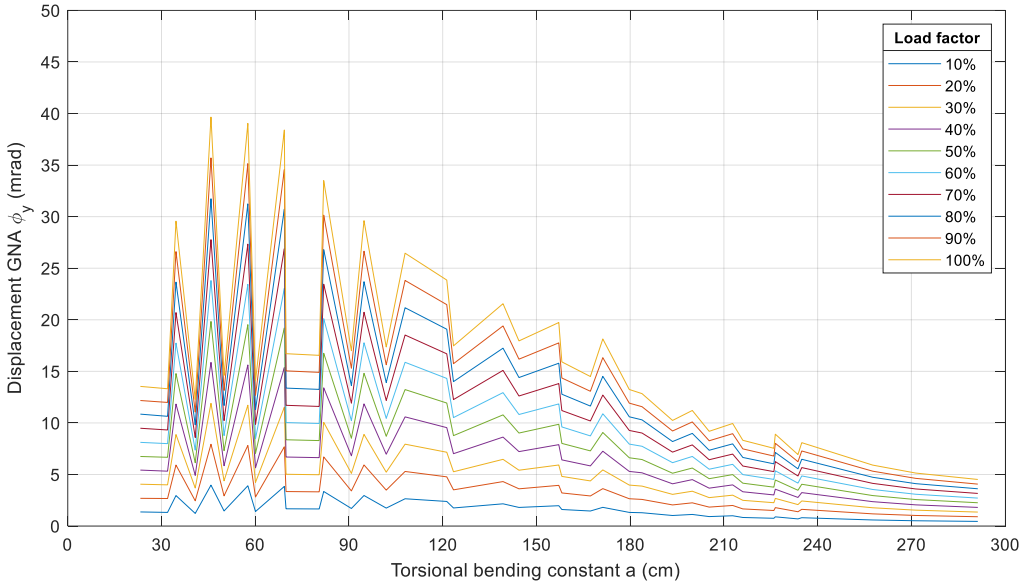

Figure A II.6 Displacement φ_y: fixed-free system, V_z load, open profiles, and 1D elements

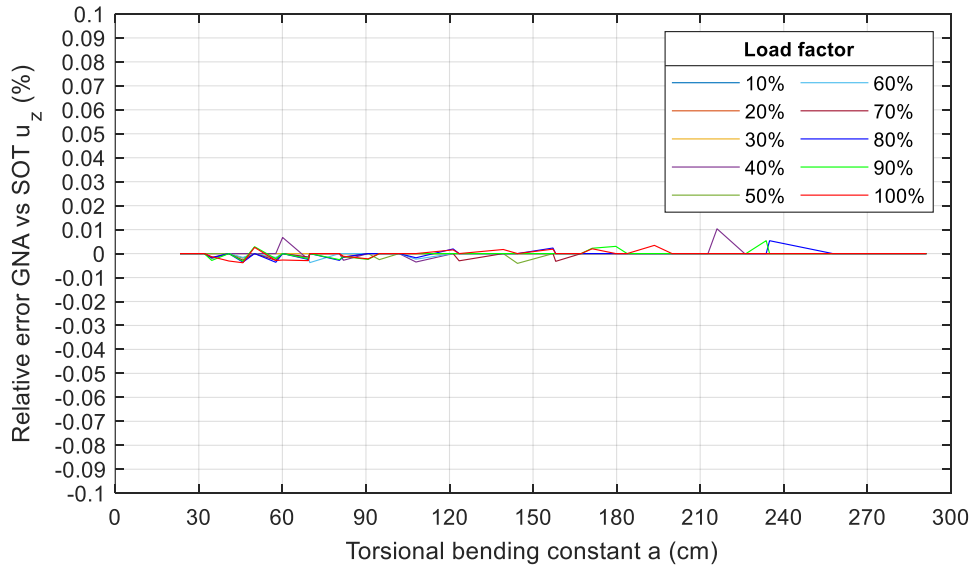

Figure A II.7 Relative error u_z: fixed-free system, V_z load, open profiles, and 2D elements

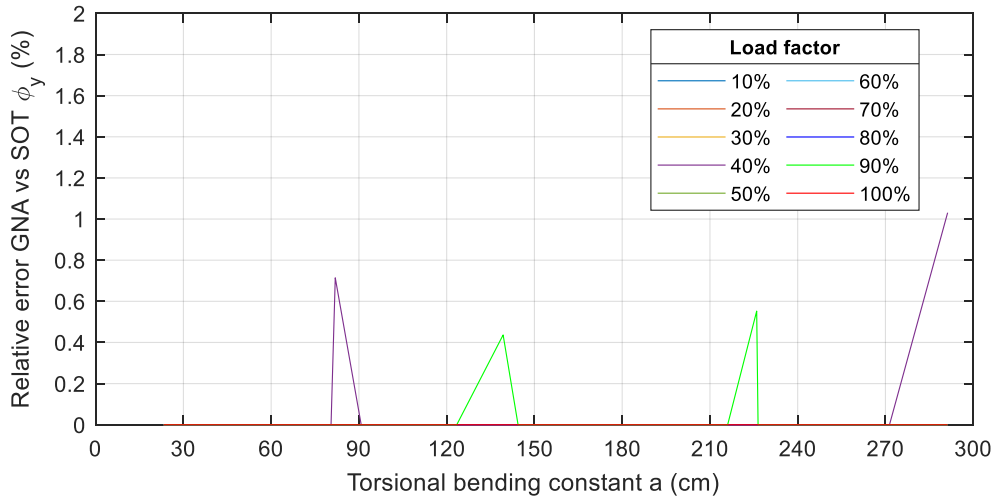

Figure A II.8 Relative error φ_y: fixed-free system, V_z load, open profiles, and 2D elements

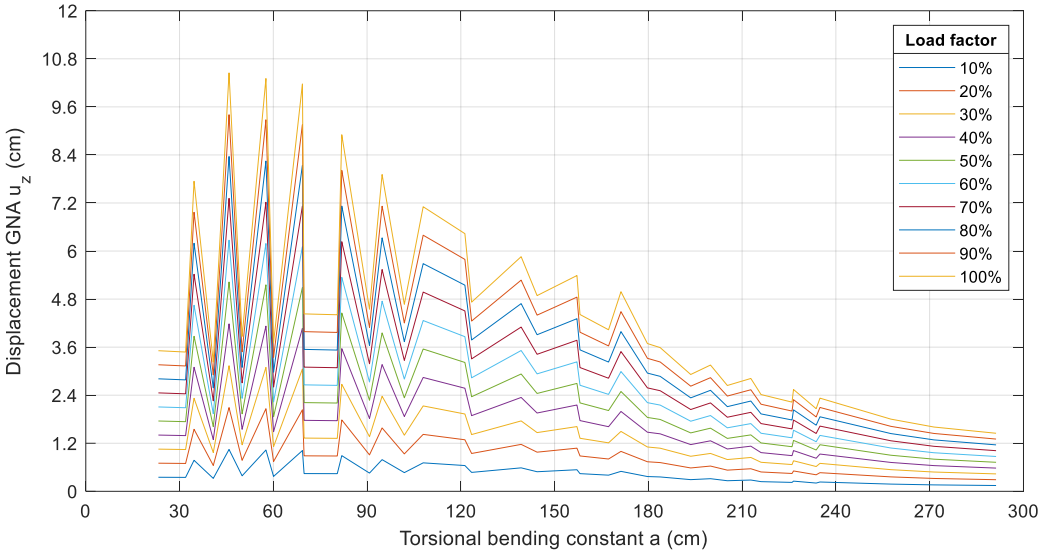

Figure A II.9 Displacement u_z: fixed-free system, V_z load, open profiles, and 2D elements

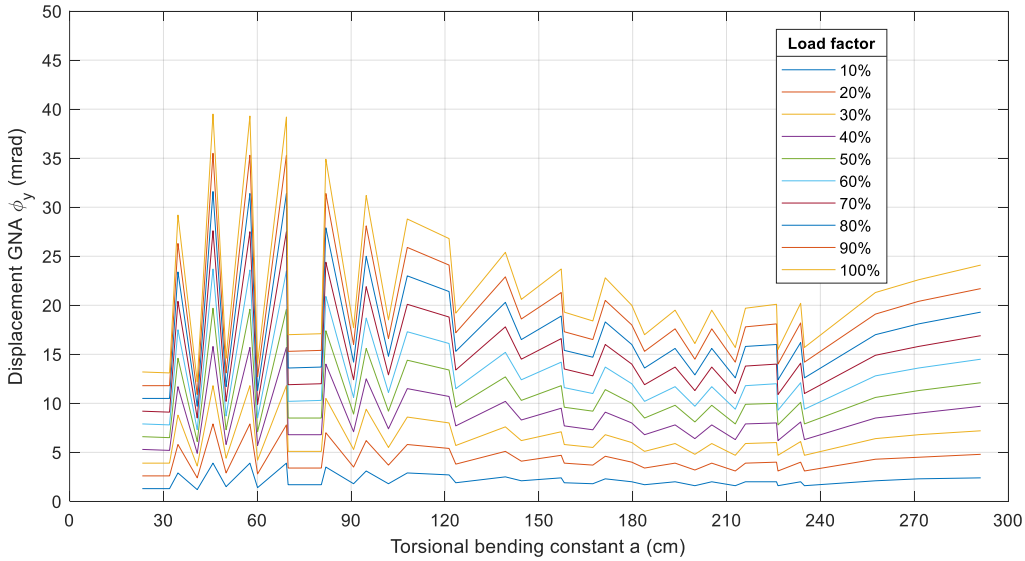

Figure A II.10Displacement φ_y: fixed-free system, V_z load, open profiles, and 2D elements

M_y

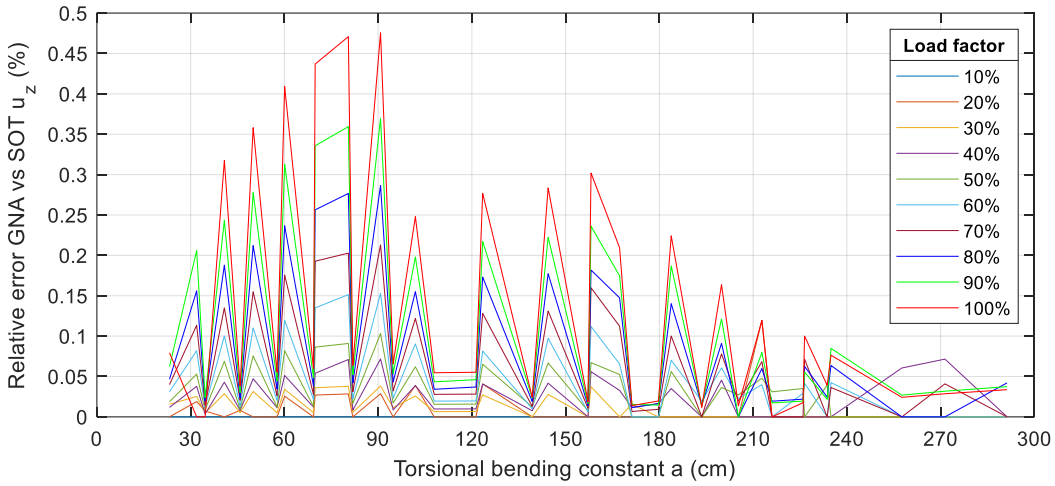

Figure A II.11Relative error u_z: fixed-free system, M_y load, open profiles, and 1D elements

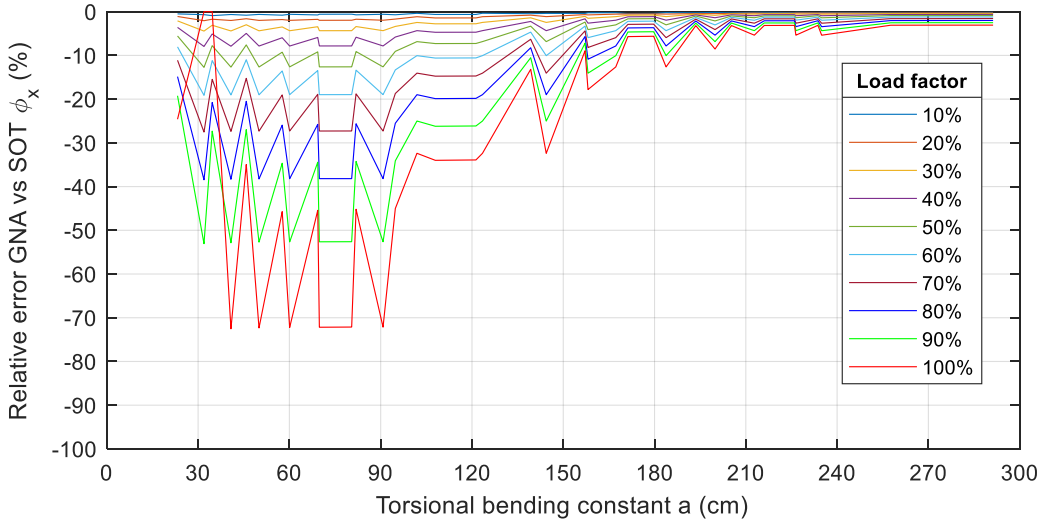

Figure A II.12Relative error φ_x: fixed-free system, M_y load, open profiles, and 1D elements

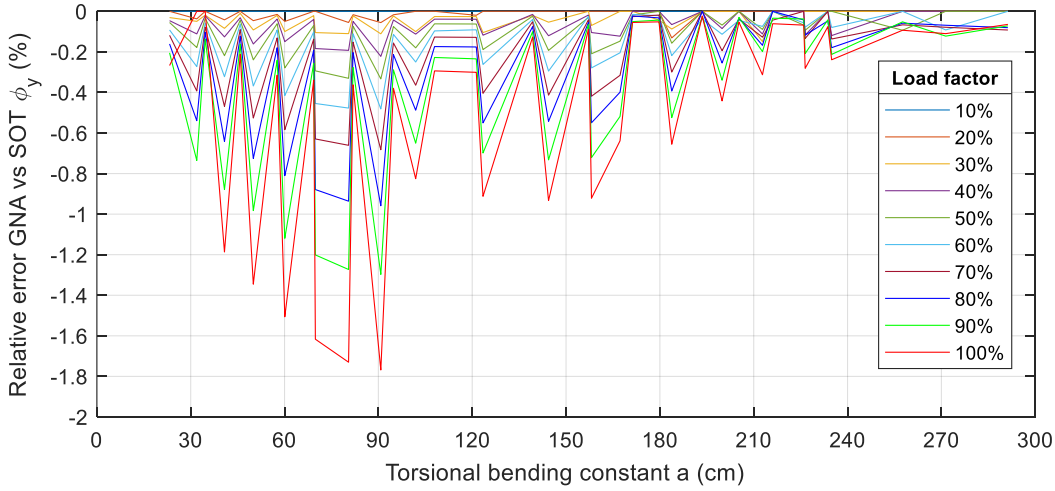

Figure A II.13Relative error φ_y: fixed-free system, M_y load, open profiles, and 1D elements

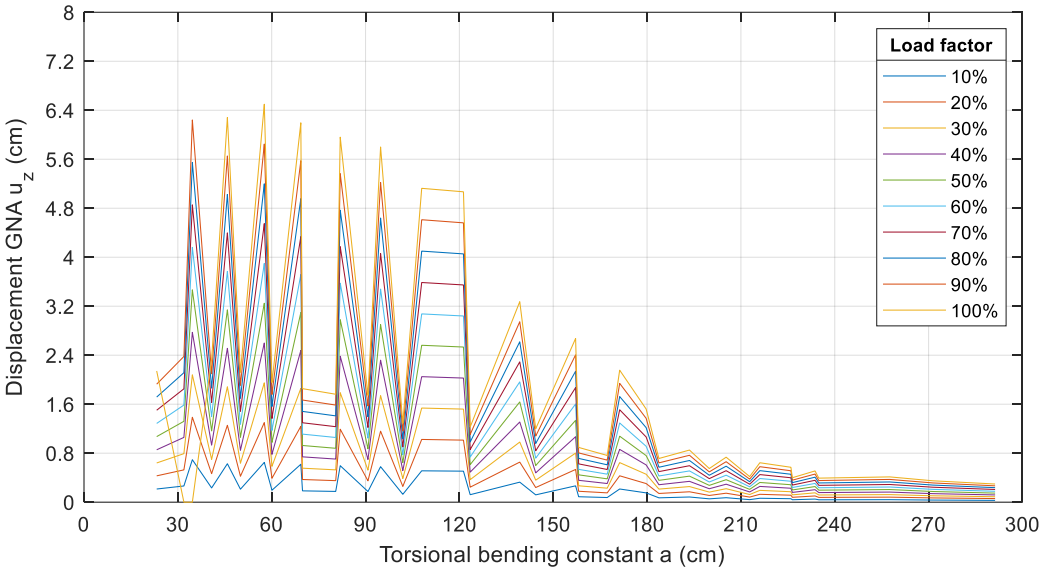

Figure A II.14Displacement u_z: fixed-free system, M_y load, open profiles, and 1D elements

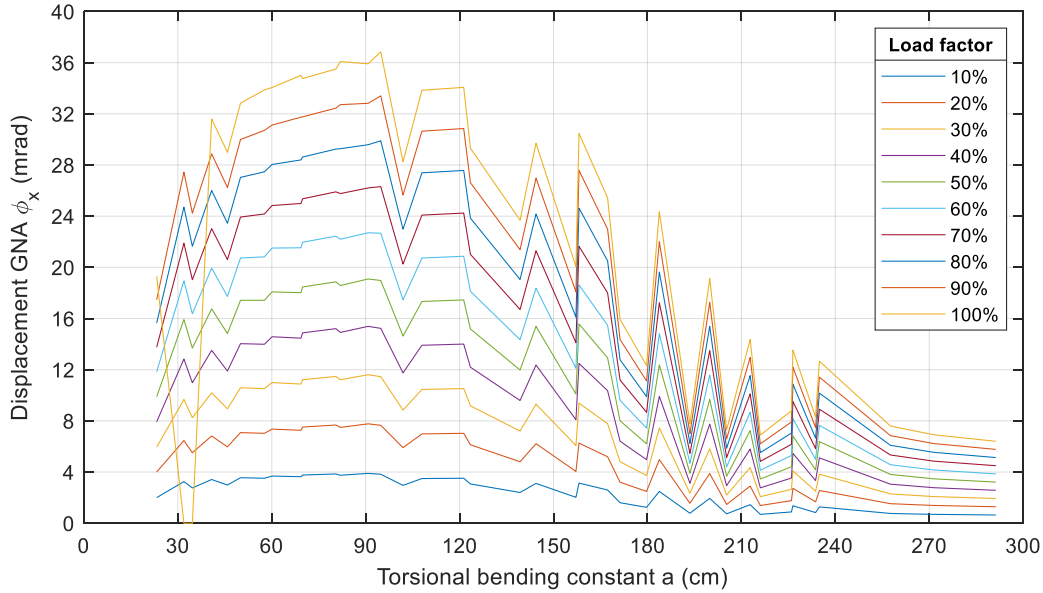

Figure A II.15Displacement φ_x: fixed-free system, M_y load, open profiles, and 1D elements

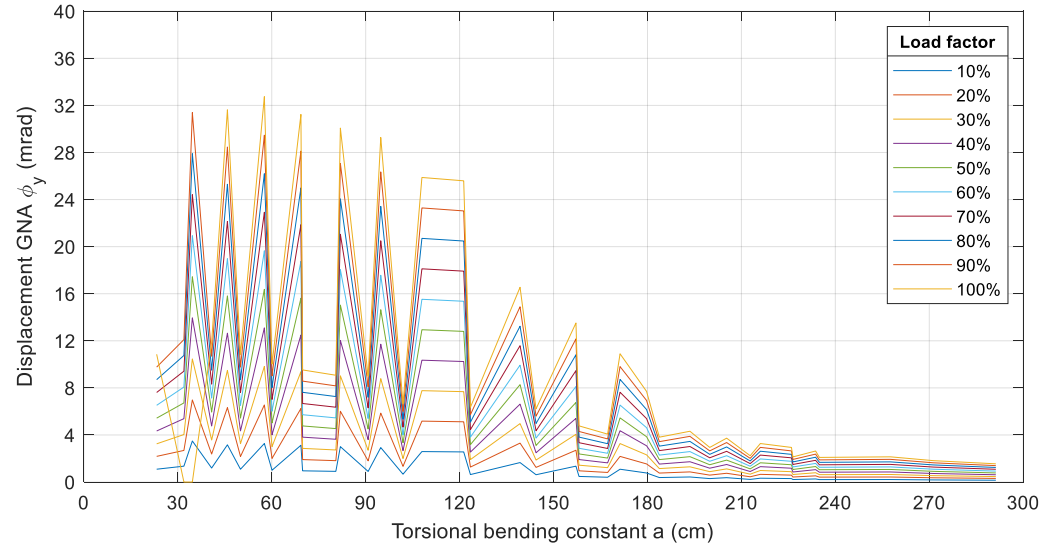

Figure A II.16Displacement φ_y: fixed-free system, M_y load, open profiles, and 1D elements

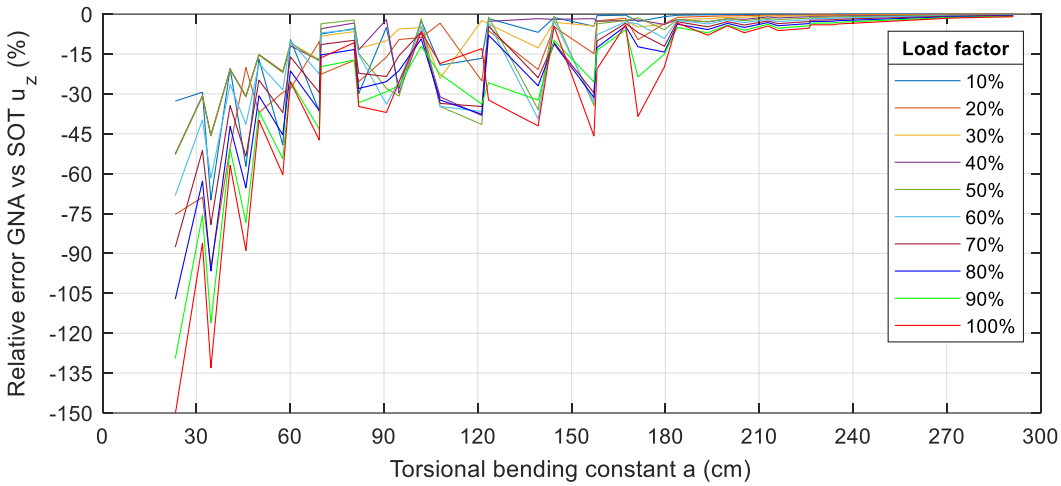

Figure A II.17Relative error u_z: fixed-free system, M_y load, open profiles, and 2D elements

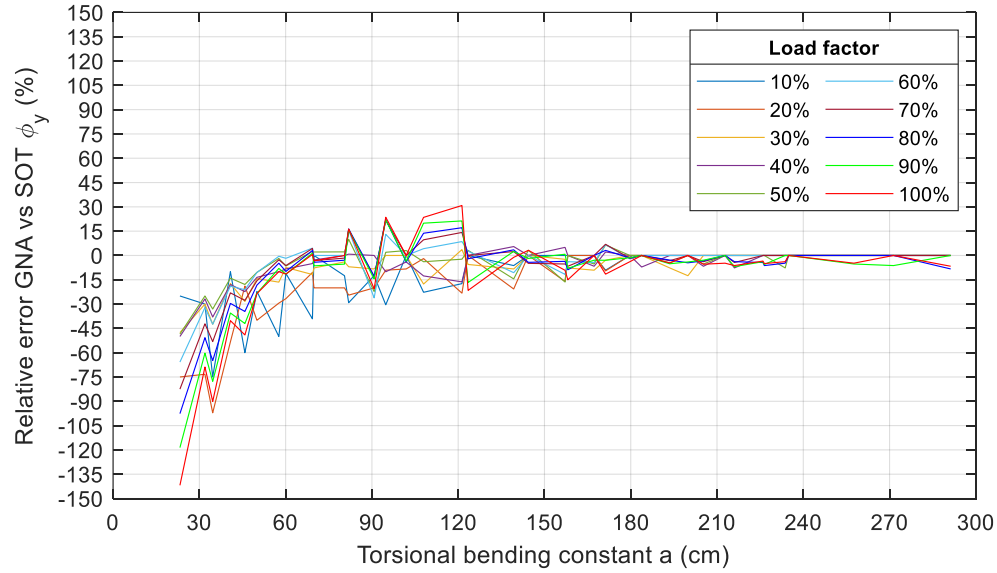

Figure A II.18Relative error φ_y: fixed-free system, M_y load, open profiles, and 2D elements

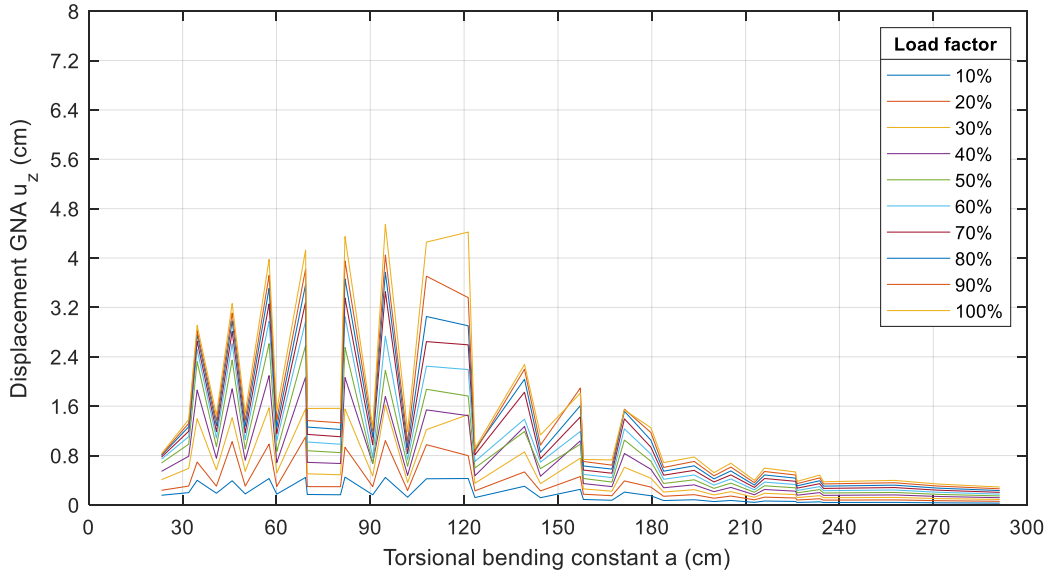

Figure A II.19Displacement u_z: fixed-free system, M_y load, open profiles, and 2D elements

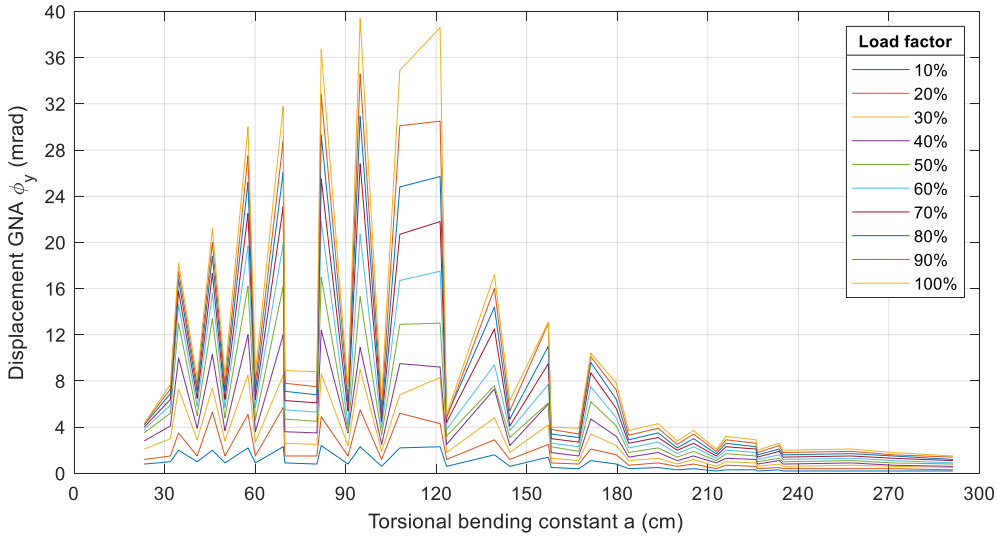

Figure A II.20Displacement φ_y: fixed-free system, M_y load, open profiles, and 2D elements

M_T

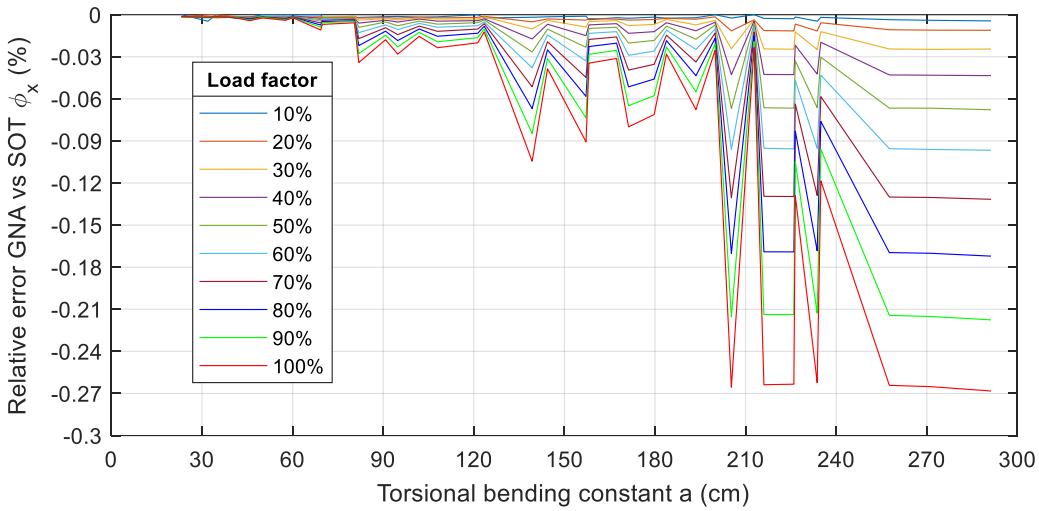

Figure A II.21Relative error φ_x: fixed-free system, M_T load, open profiles, and 1D elements

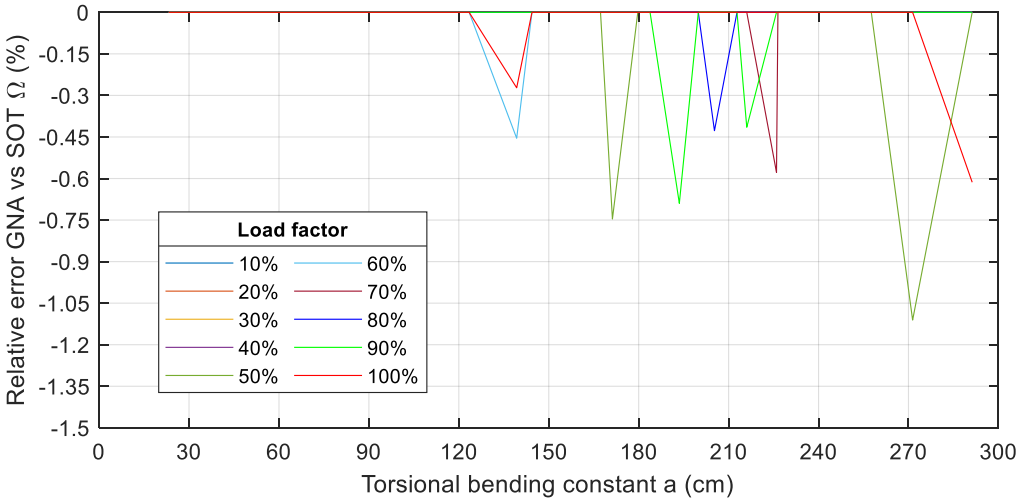

Figure A II.22Relative error Ω: fixed-free system, M_T load, open profiles, and 1D elements

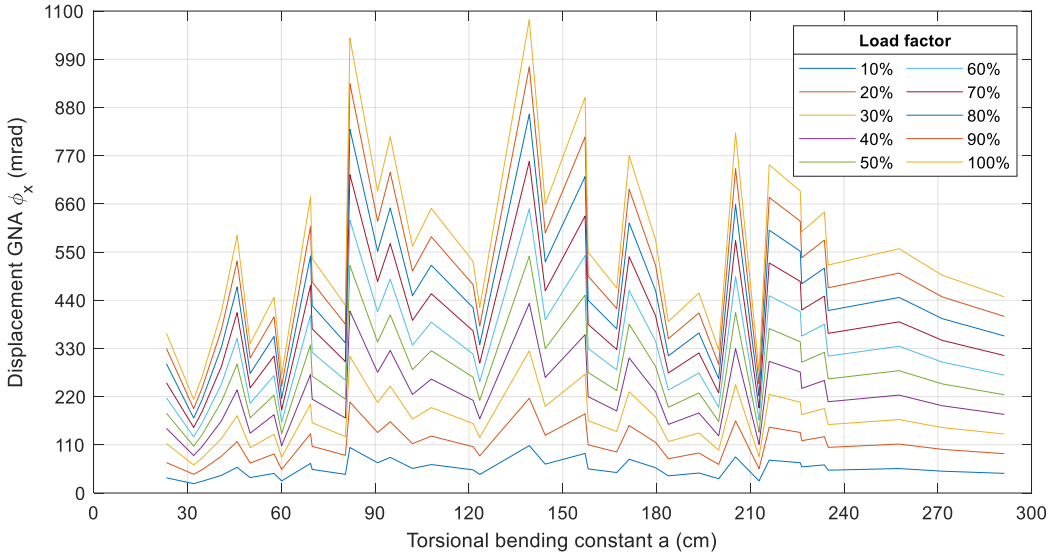

Figure A II.23Displacement φₓ: fixed-free system, M_T load, open profiles, and 1D elements

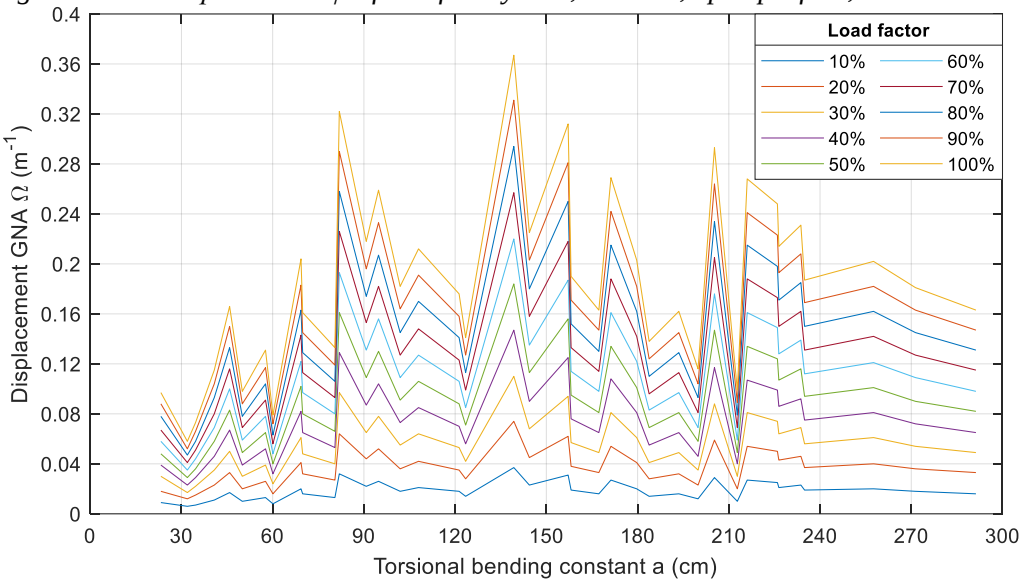

Figure A II.24Displacement Ω: fixed-free system, M_T load, open profiles, and 1D elements

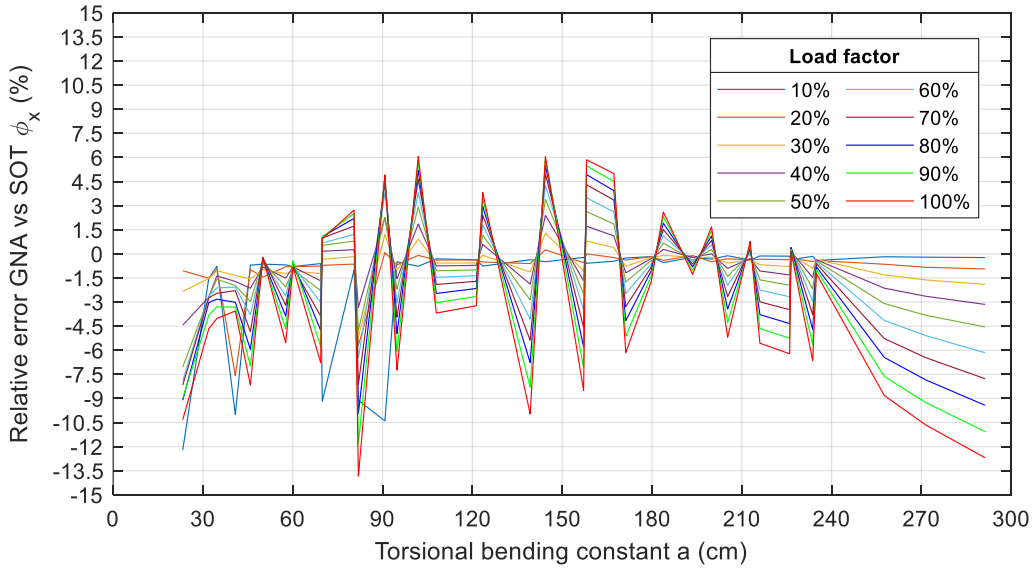

Figure A II.25Relative error φₓ: fixed-free system, M_T load, open profiles, and 2D elements

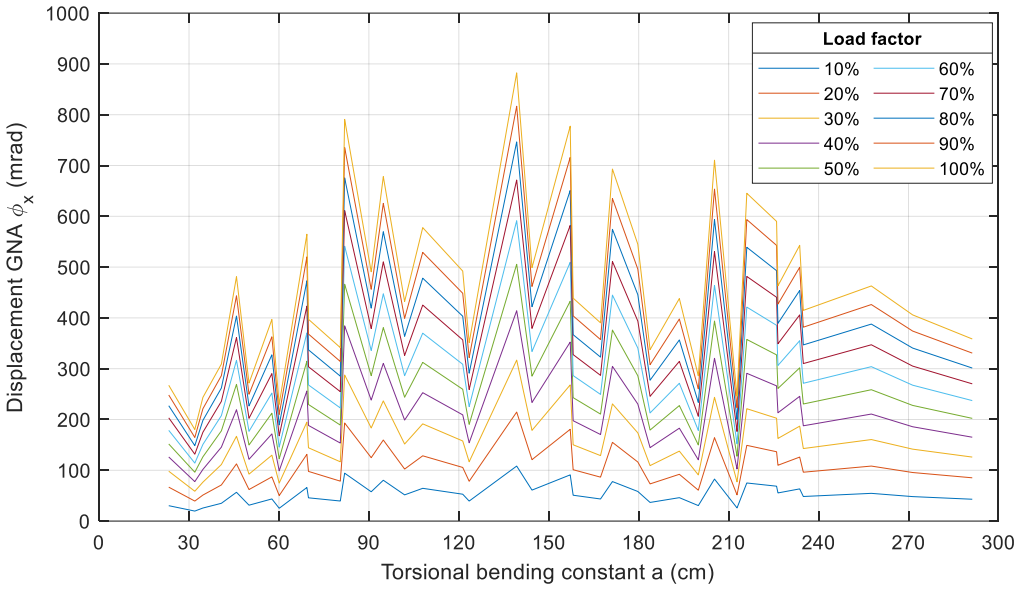

Figure A II.26Displacement φ_x: fixed-free system, M_T load, open profiles, and 2D elements

Appendix II-1.2 Closed cross-sections

V_z

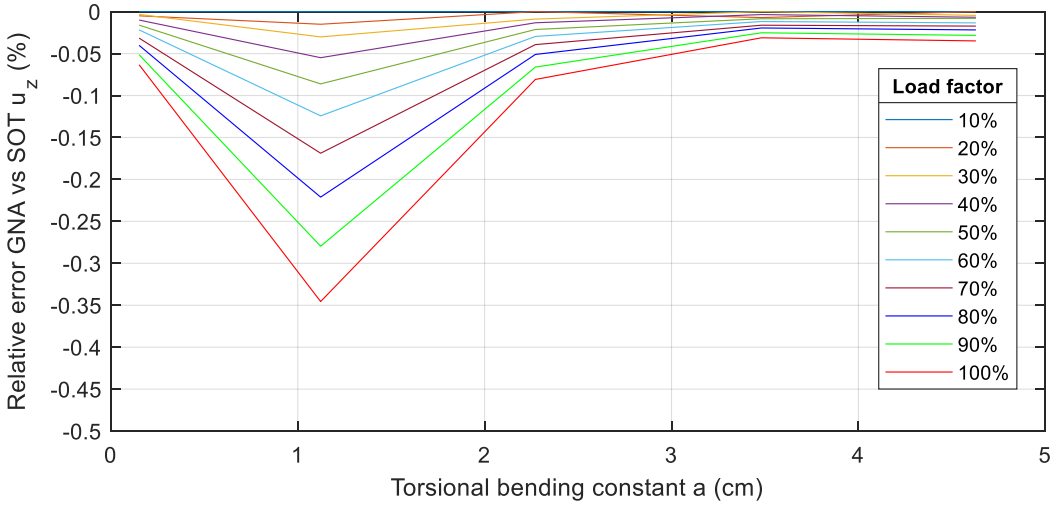

Figure A II.27Relative error u_z: fixed-free system, V_z load, closed profiles, and 1D elements

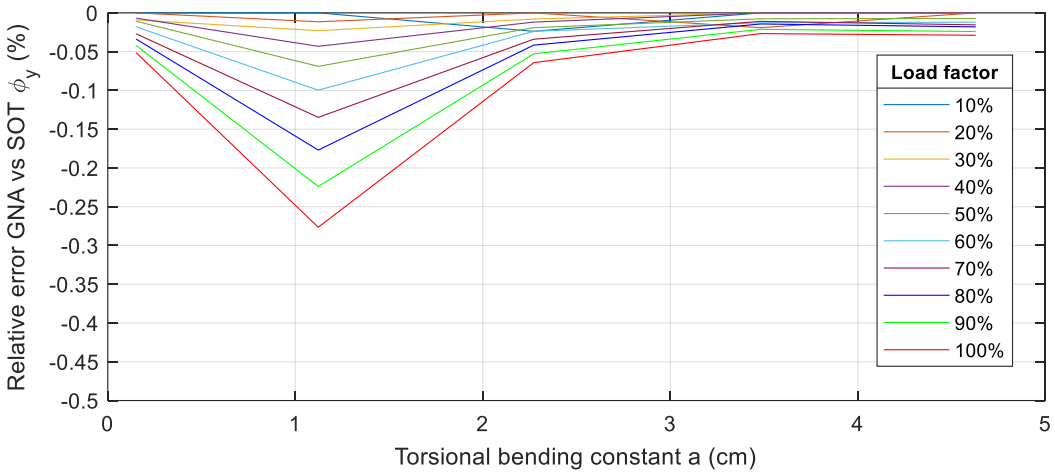

Figure A II.28Relative error φ_y: fixed-free system, V_z load, closed profiles, and 1D elements

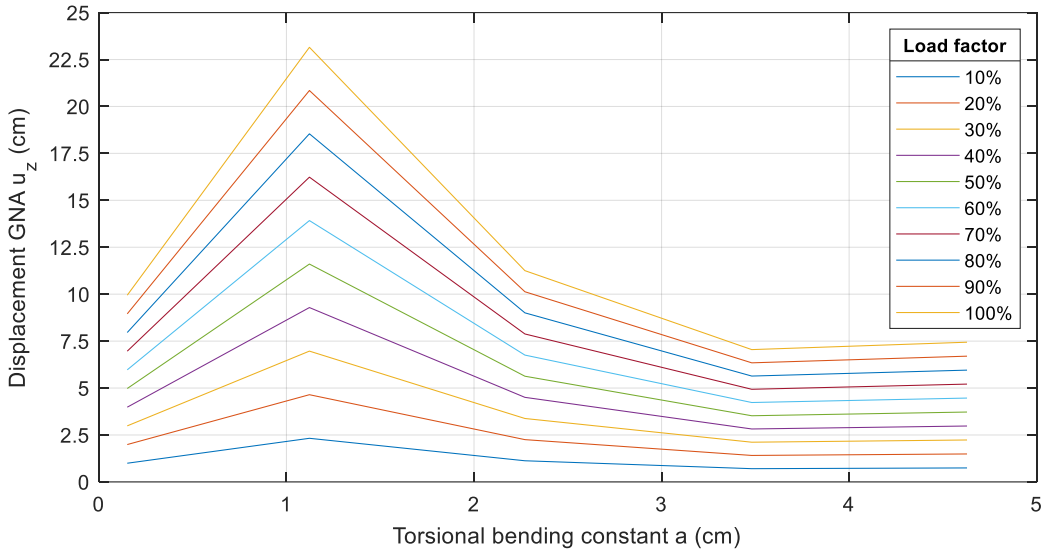

Figure A II.29Displacement u_z: fixed-free system, V_z load, closed profiles, and 1D elements

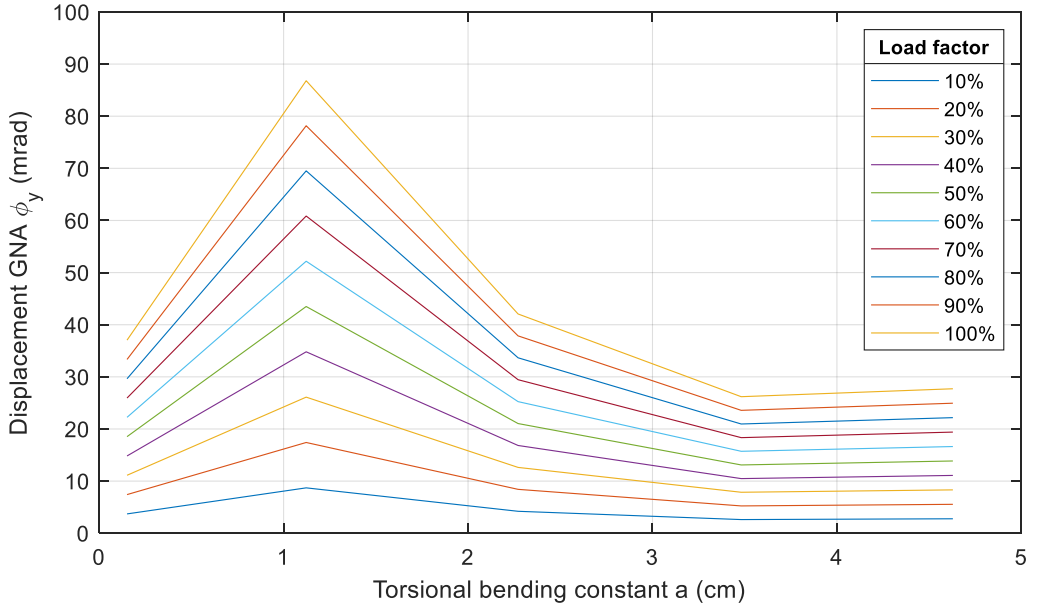

Figure A II.30Displacement φ_y: fixed-free system, V_z load, closed profiles, and 1D elements

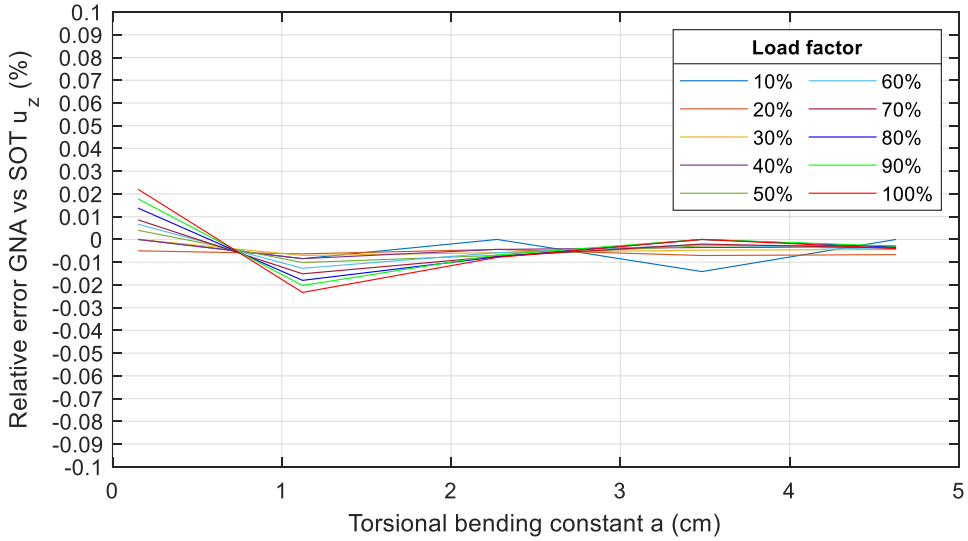

Figure A II.31Relative error u_z: fixed-free system, V_z load, closed profiles, and 2D elements

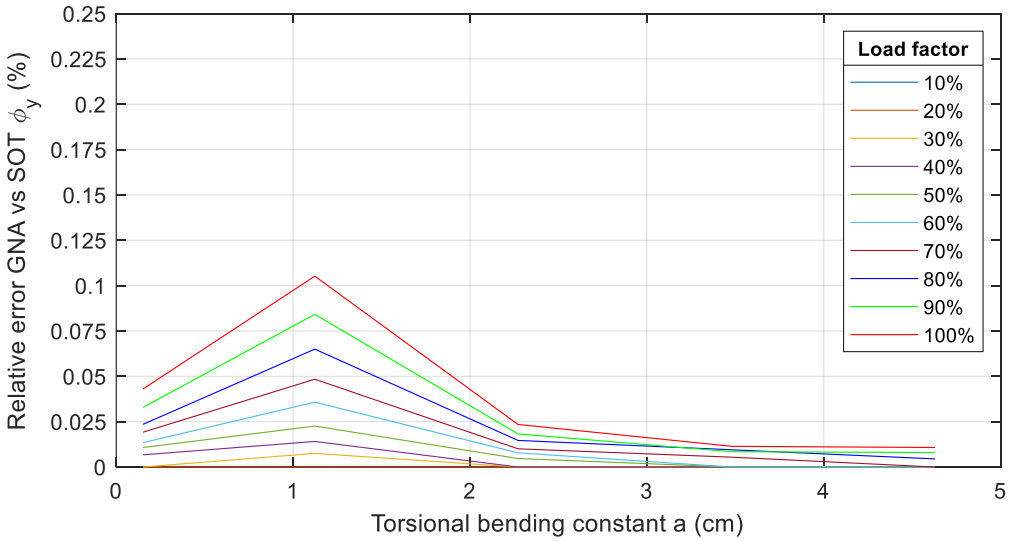

Figure A II.32Relative error φ_y: fixed-free system, V_z load, closed profiles, and 2D elements

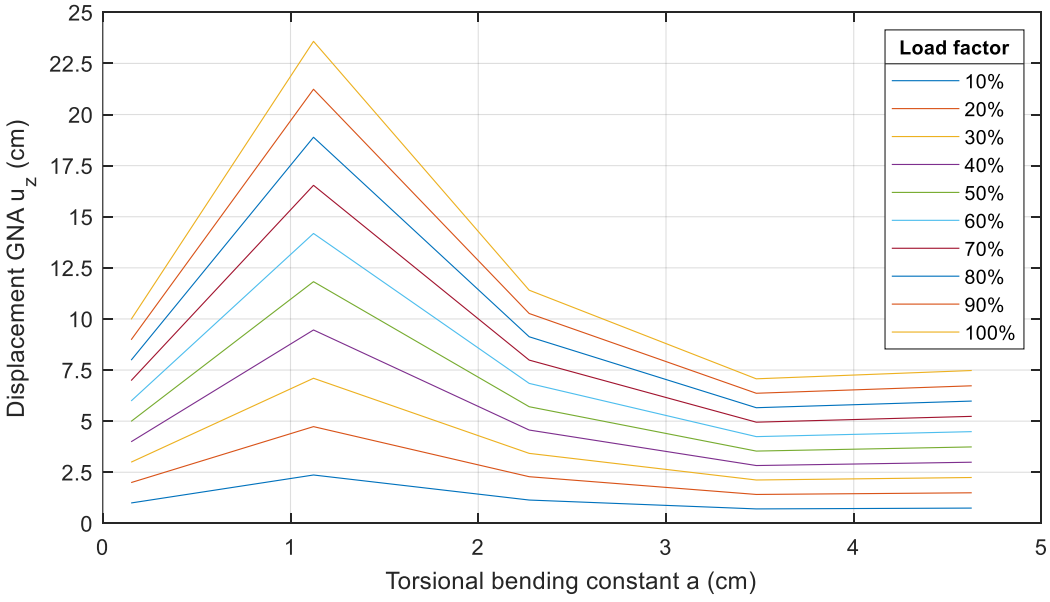

Figure A II.33Displacement u_z: fixed-free system, V_z load, closed profiles, and 2D elements

M_y

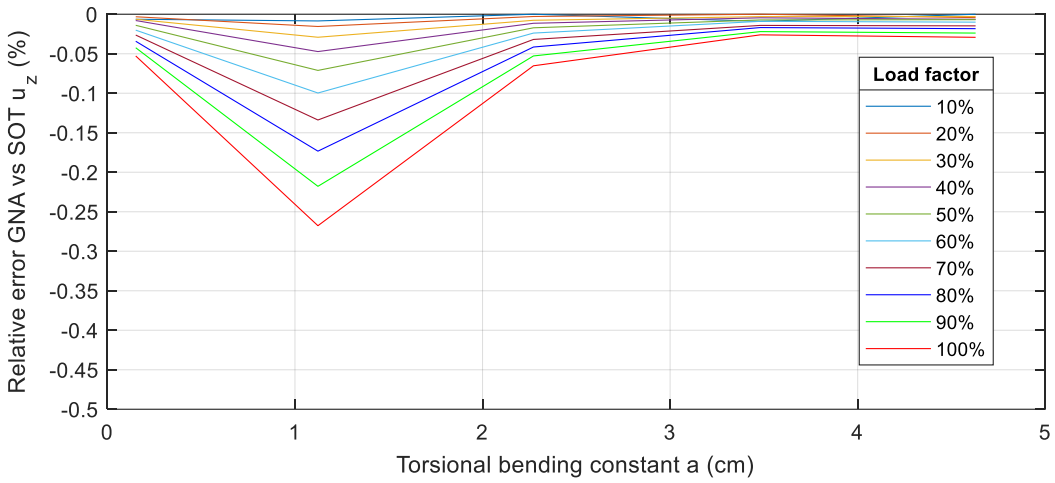

Figure A II.34Relative error u_z: fixed-free system, M_y load, closed profiles, and 1D elements

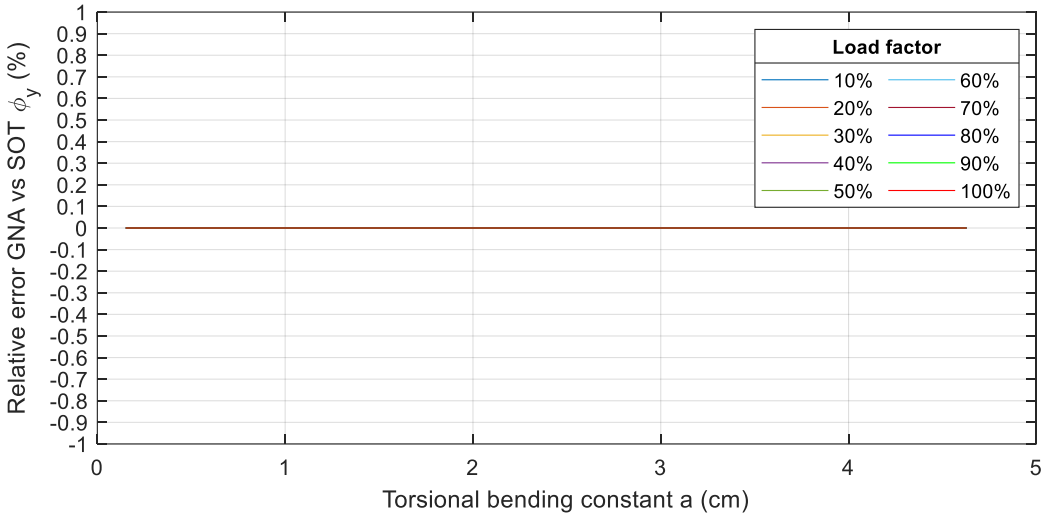

Figure A II.35Relative error φ_y: fixed-free system, M_y load, closed profiles, and 1D elements

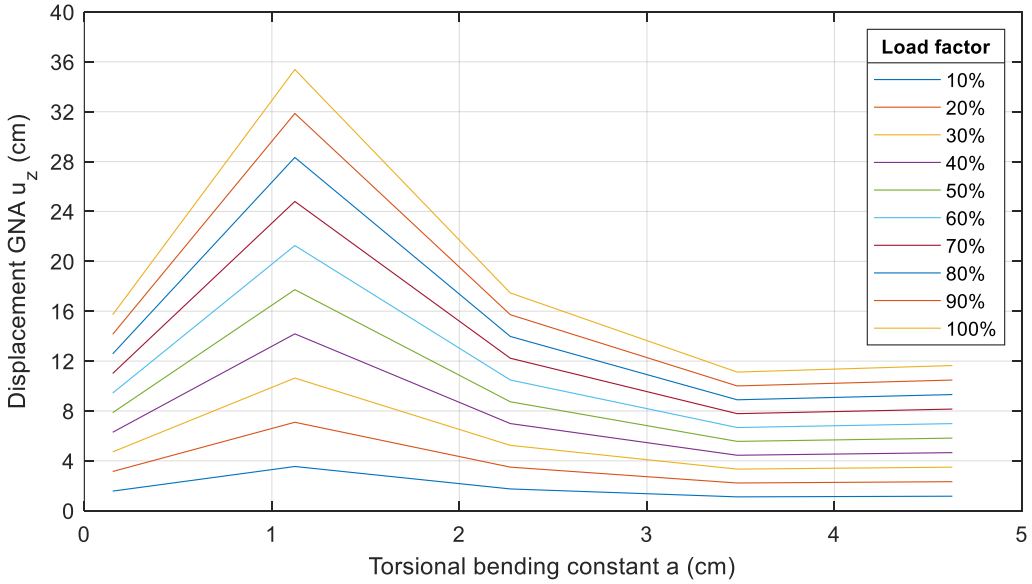

Figure A II.36Displacement u_z: fixed-free system, M_y load, closed profiles, and 1D elements

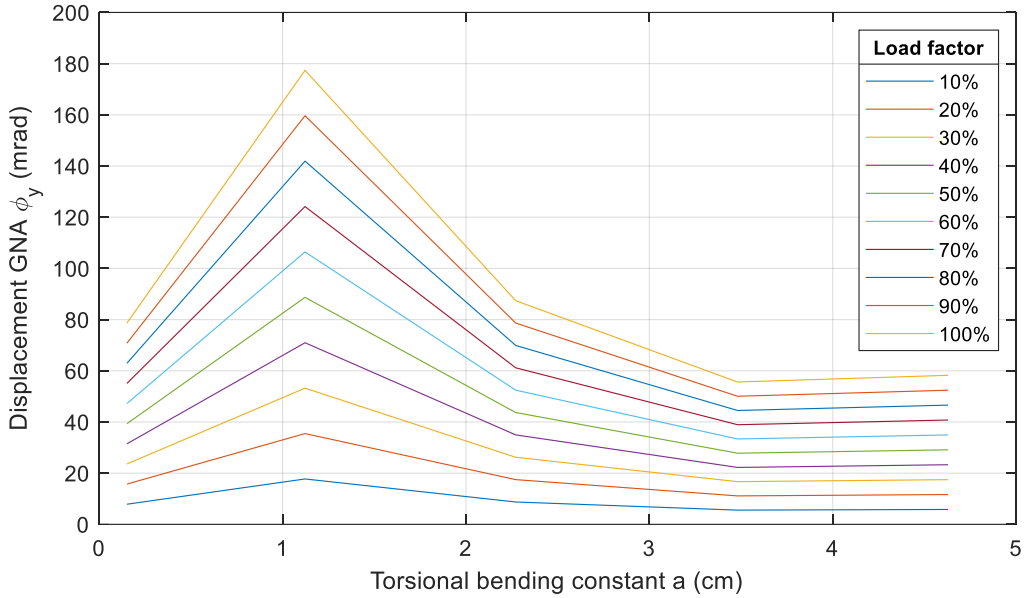

Figure A II.37Displacement φ_y: fixed-free system, M_y load, closed profiles, and 1D elements

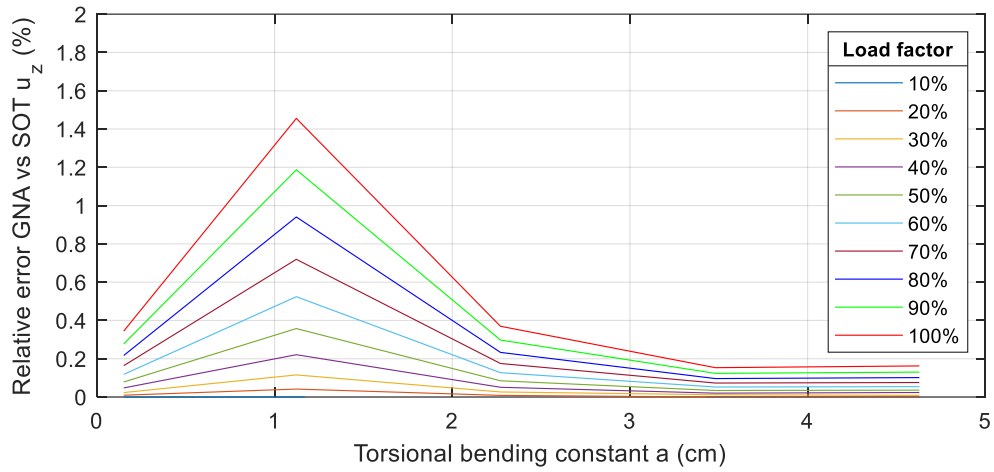

Figure A II.38Relative error u_z: fixed-free system, M_y load, closed profiles, and 2D elements

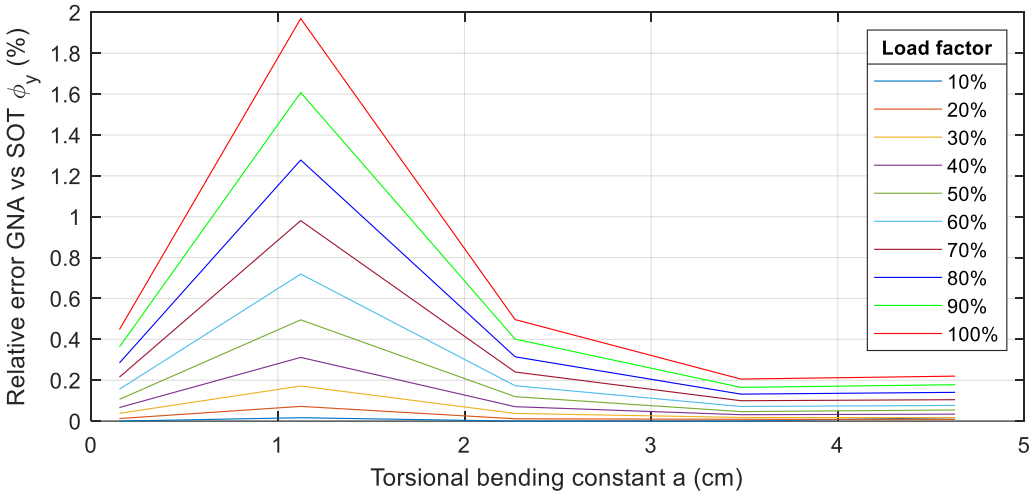

Figure A II.39Relative error φ_y: fixed-free system, M_y load, closed profiles, and 2D elements

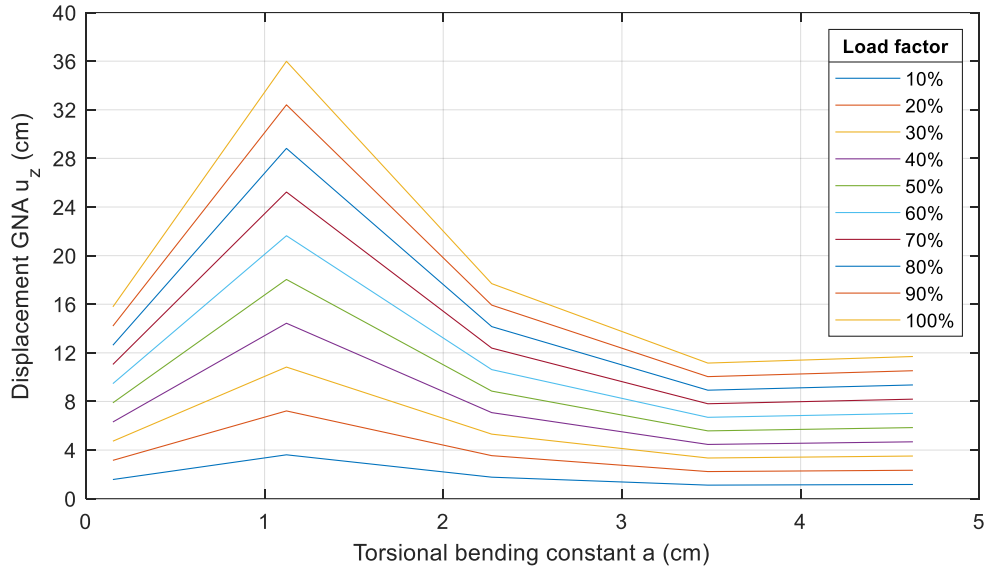

Figure A II.40Displacement u_z: fixed-free system, M_y load, closed profiles, and 2D elements

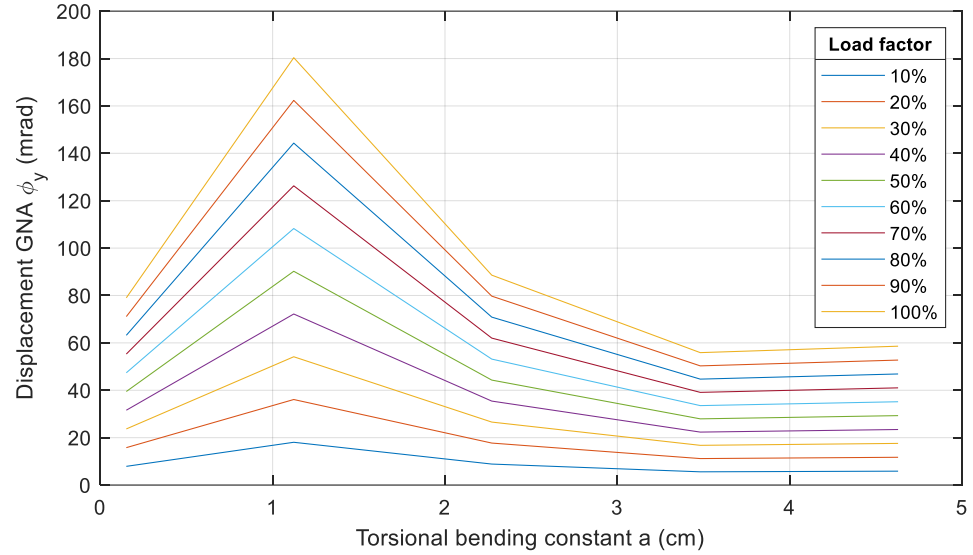

Figure A II.41Displacement φ_y: fixed-free system, M_y load, closed profiles, and 2D elements

M_T

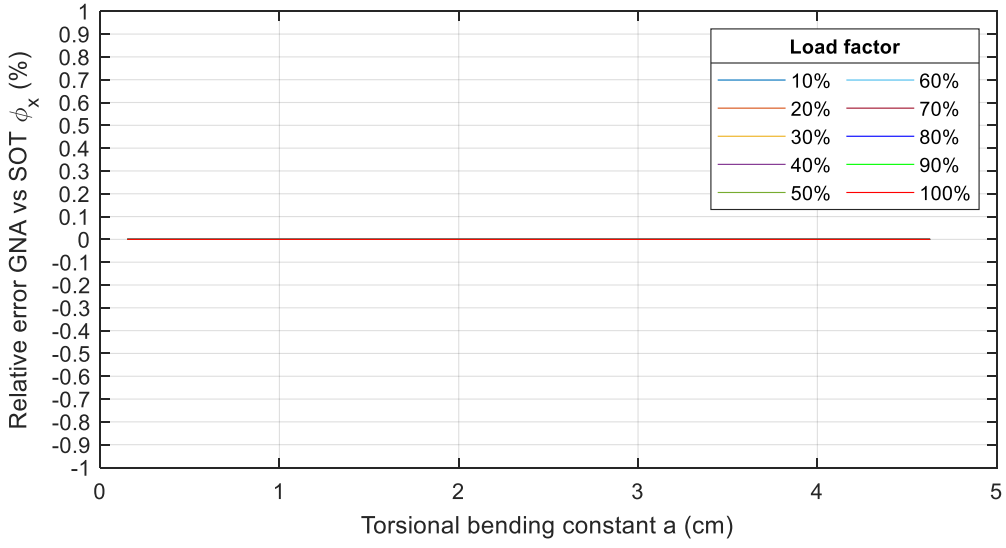

Figure A II.42Relative error φ_x: fixed-free system, M_T load, closed profiles, and 1D elements

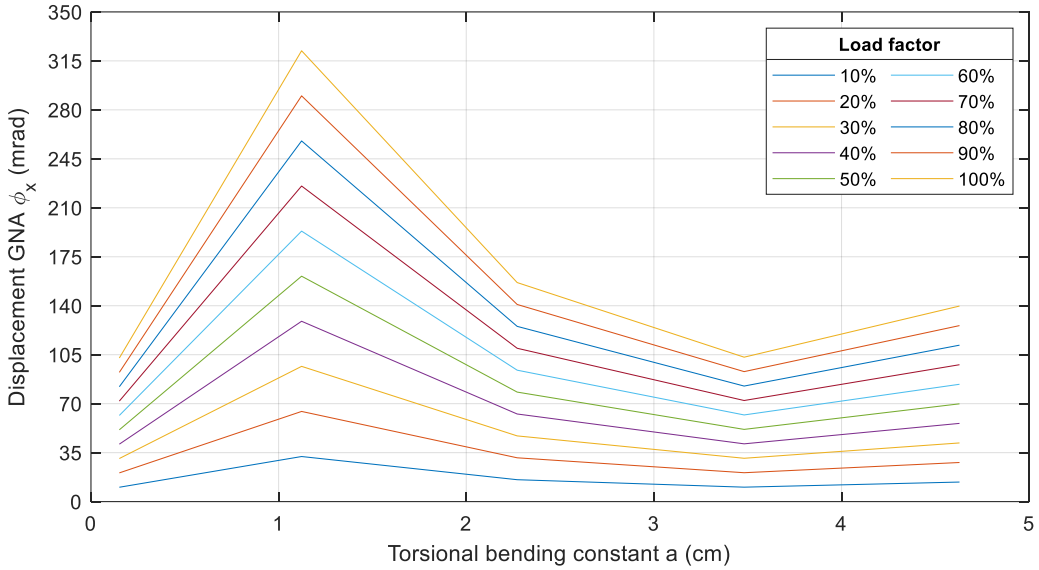

Figure A II.43Displacement φ_x: fixed-free system, M_T load, closed profiles, and 1D elements

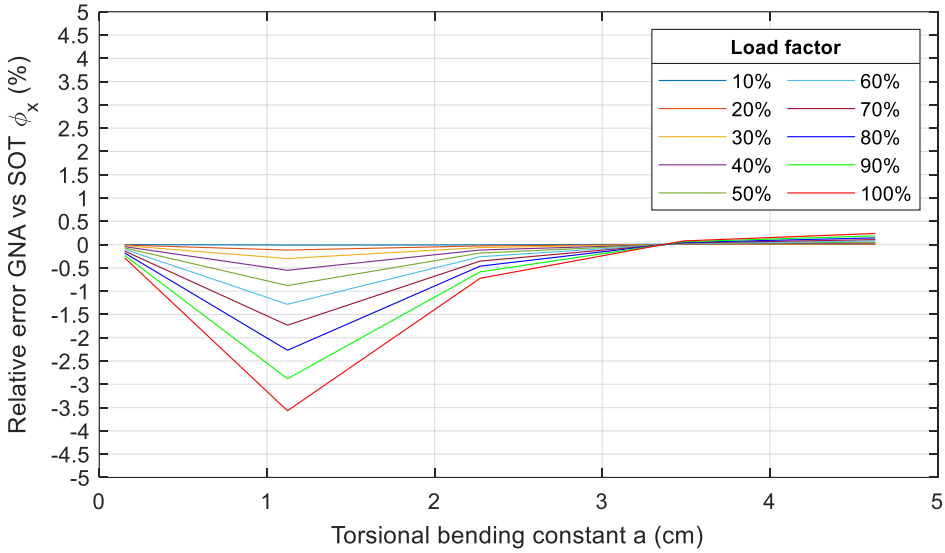

Figure A II.44Relative error φ_x: fixed-free system, M_T load, closed profiles, and 2D elements

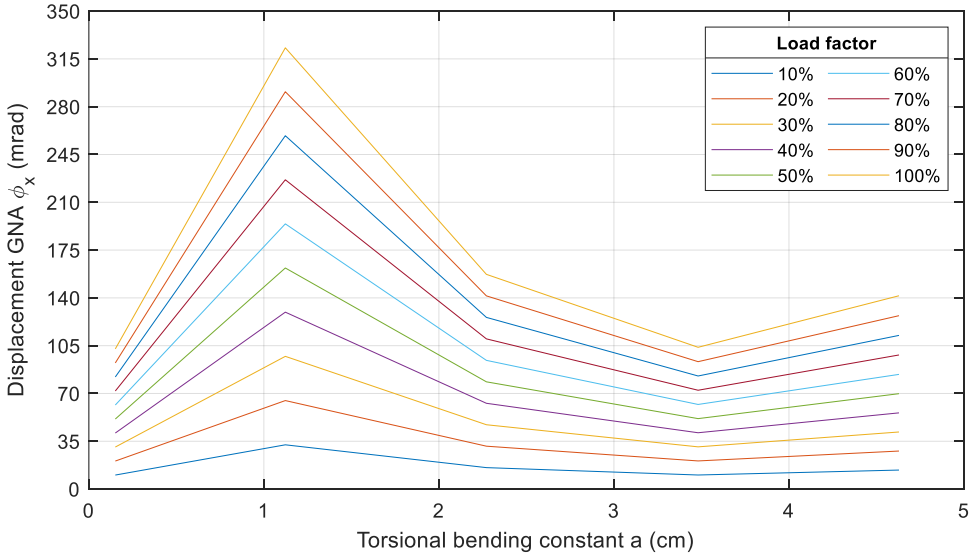

Figure A II.45Displacement φ_x: fixed-free system, M_T load, closed profiles, and 2D elements

Appendix II-2 Fork-fork system

Appendix II-2.1 Open cross-sections

V_z

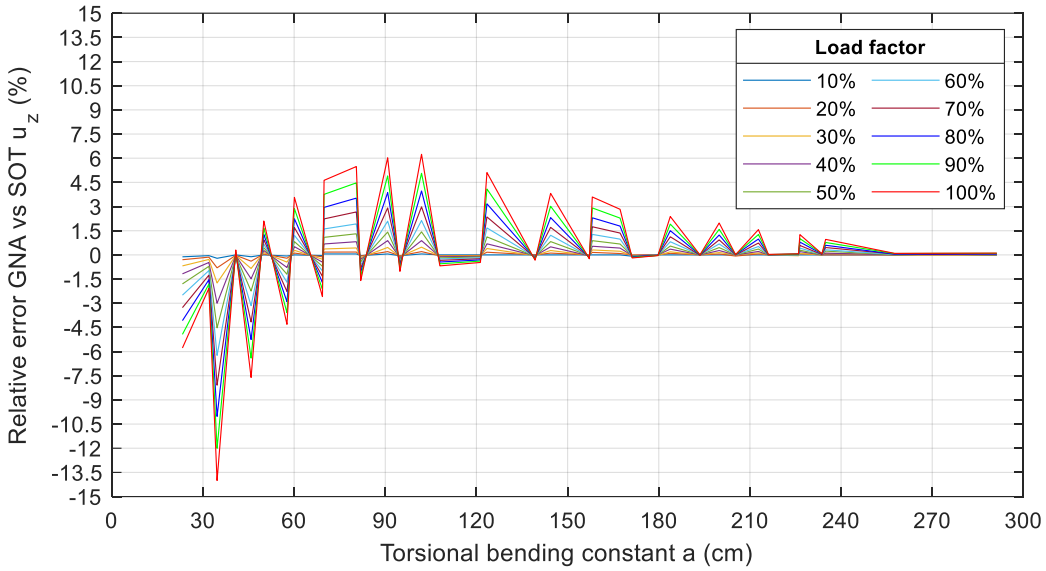

Figure A II.46Relative error u_z: fork-fork system, V_z load, open profiles, and 1D elements

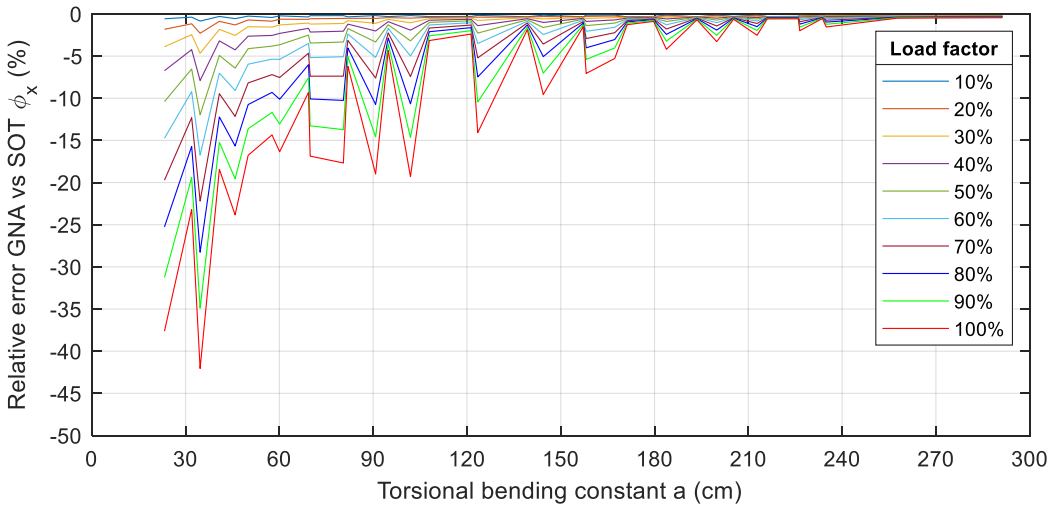

Figure A II.47Relative error φ_x: fork-fork system, V_z load, open profiles, and 1D elements

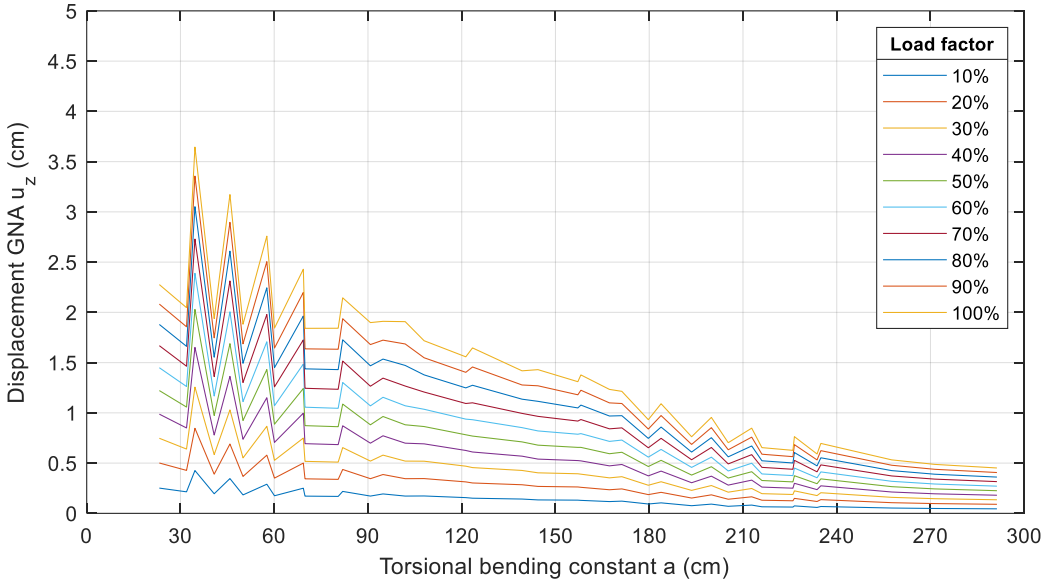

Figure A II.48Displacement u_z: fork-fork system, V_z load, open profiles, and 1D elements

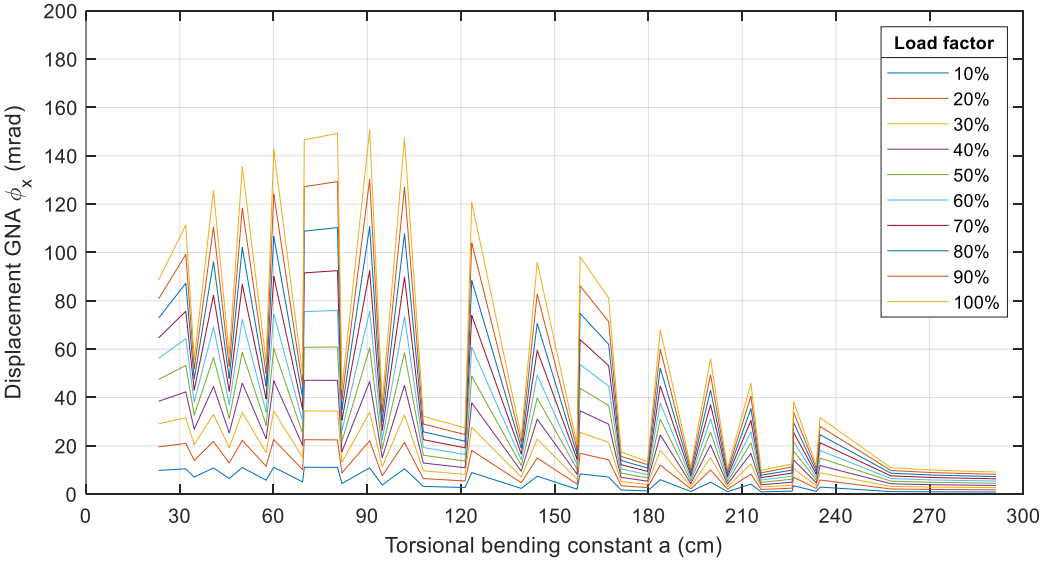

Figure A II.49Displacement φ_x: fork-fork system, V_z load, open profiles, and 1D elements

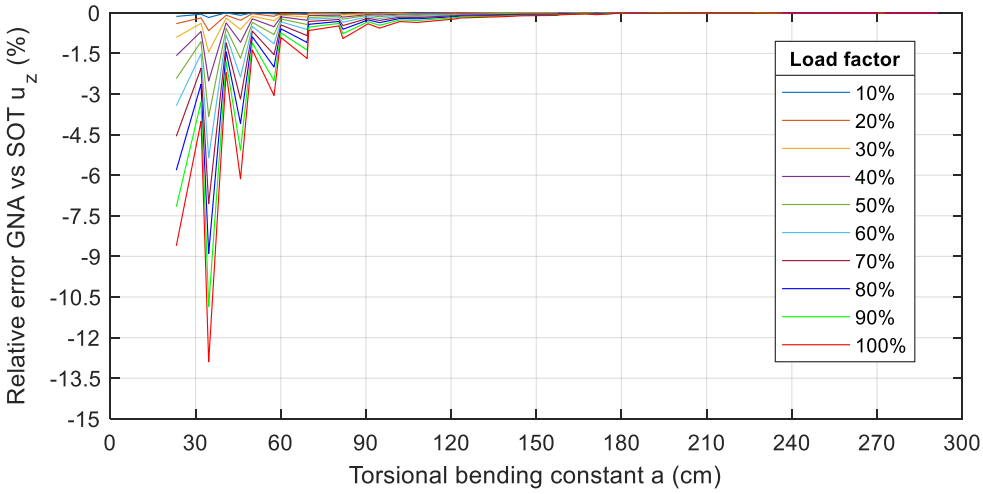

Figure A II.50Relative error u_z: fork-fork system, V_z load, open profiles, and 2D elements

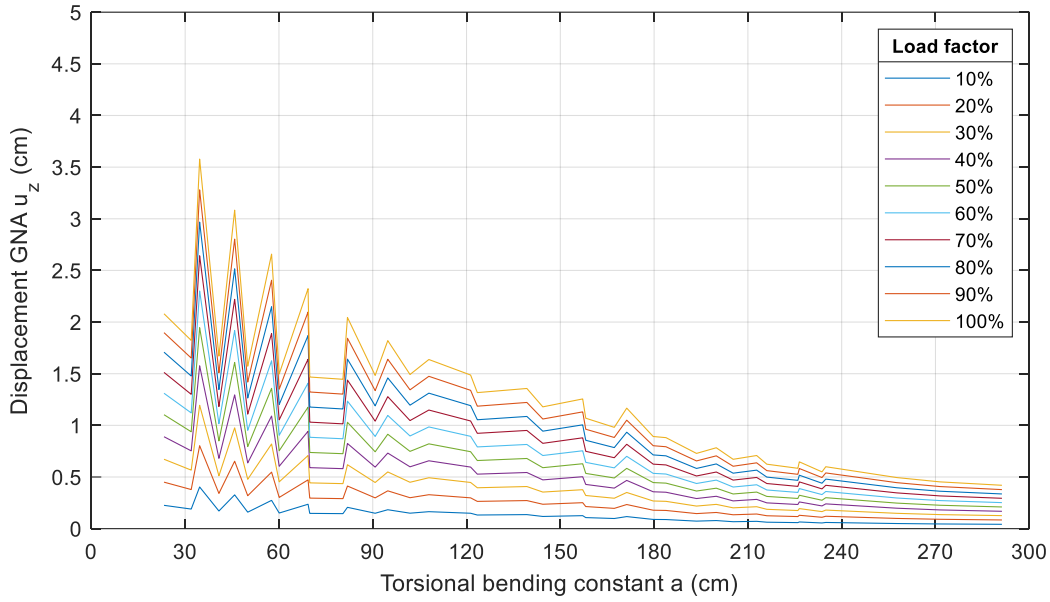

Figure A II.51Displacement u_z: fork-fork system, V_z load, open profiles, and 2D elements

M_y

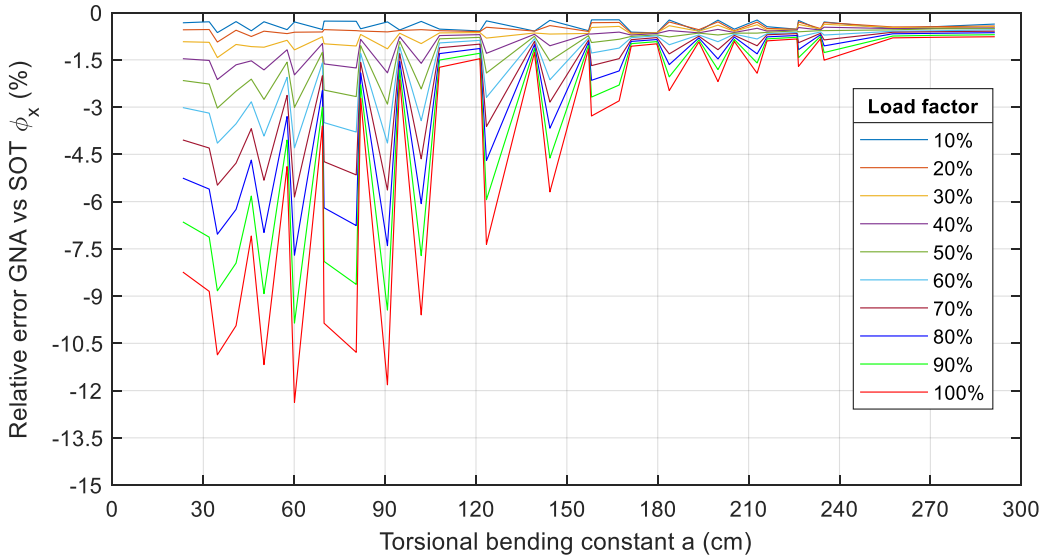

Figure A II.52Relative error φ_x: fork-fork system, M_y load, open profiles, and 1D elements

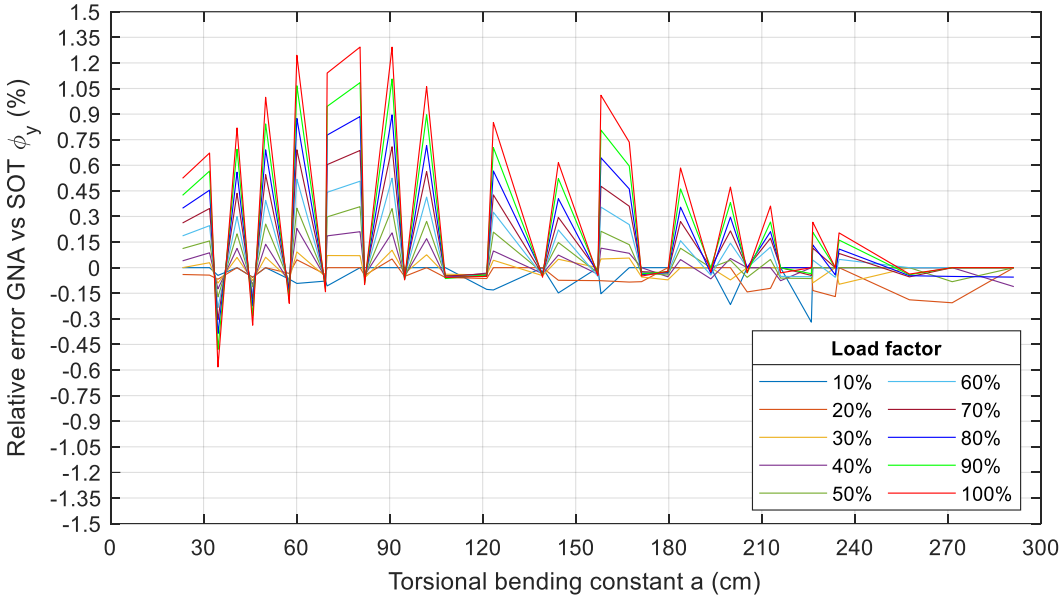

Figure A II.53Relative error φ_y: fork-fork system, M_y load, open profiles, and 1D elements

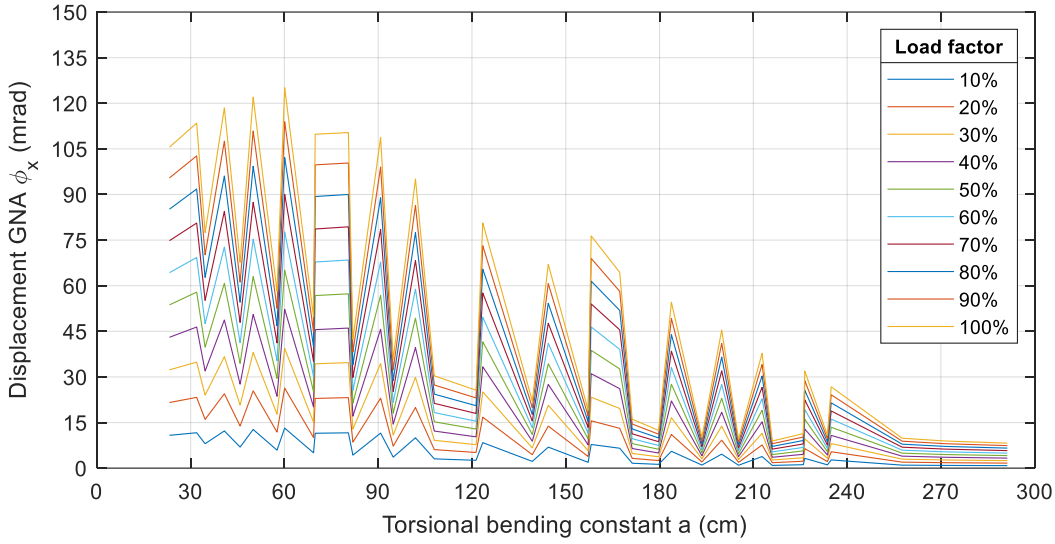

Figure A II.54Displacement φ_x: fork-fork system, M_y load, open profiles, and 1D elements

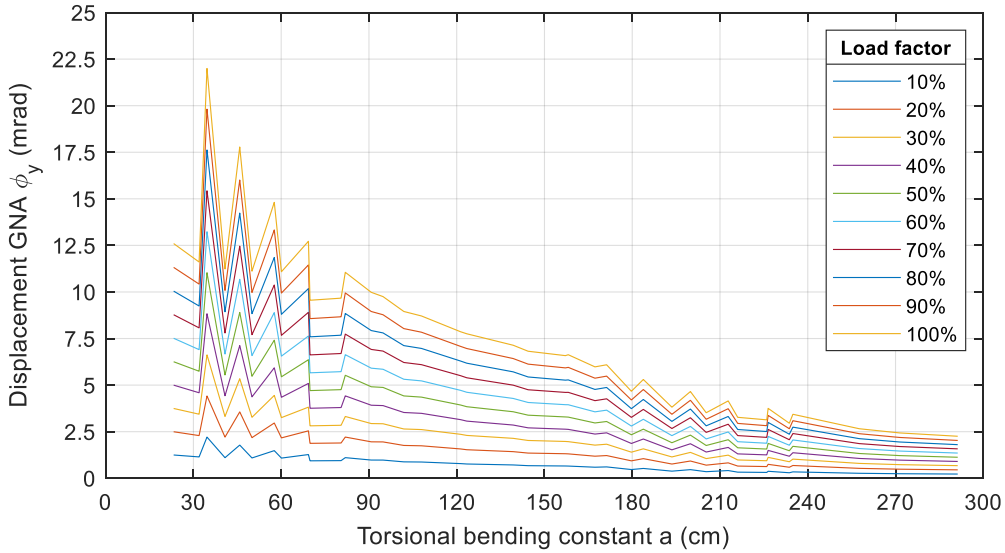

Figure A II.55Displacement φ_y: fork-fork system, M_y load, open profiles, and 1D elements

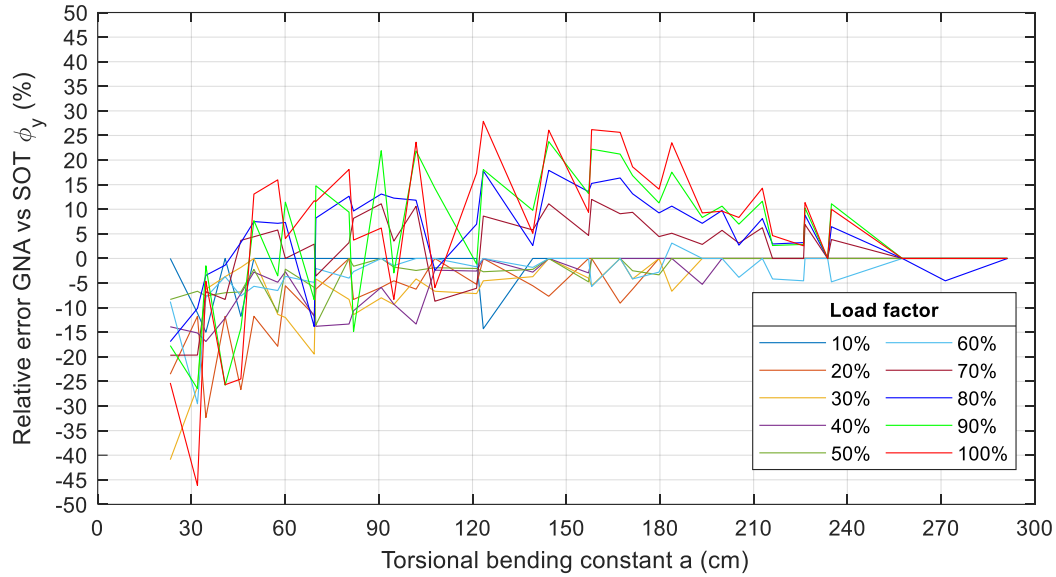

Figure A II.56Relative error φ_y: fork-fork system, M_y load, open profiles, and 2D elements

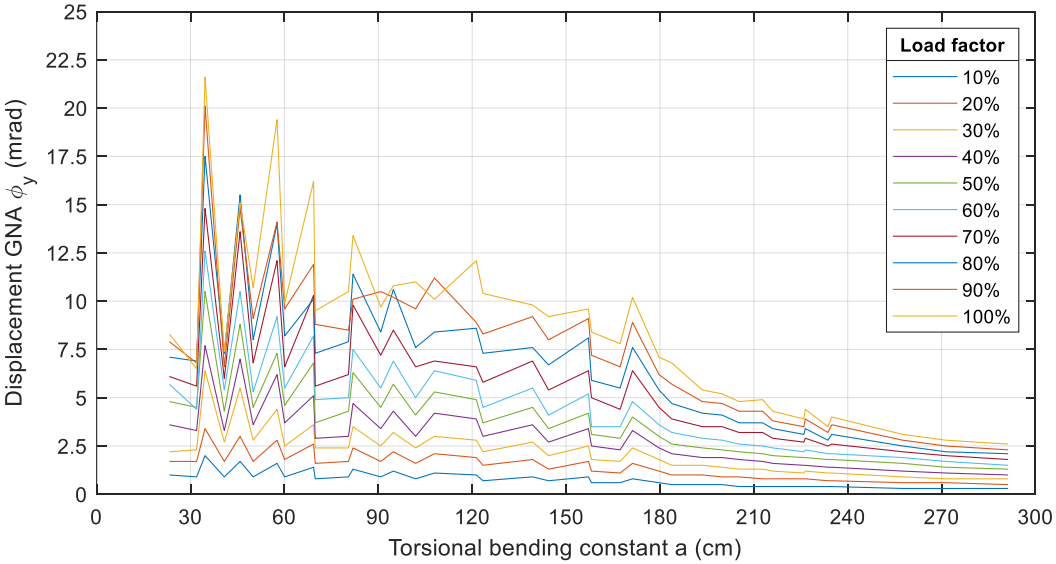

Figure A II.57Displacement φ_y: fork-fork system, M_y load, open profiles, and 2D elements

M_T

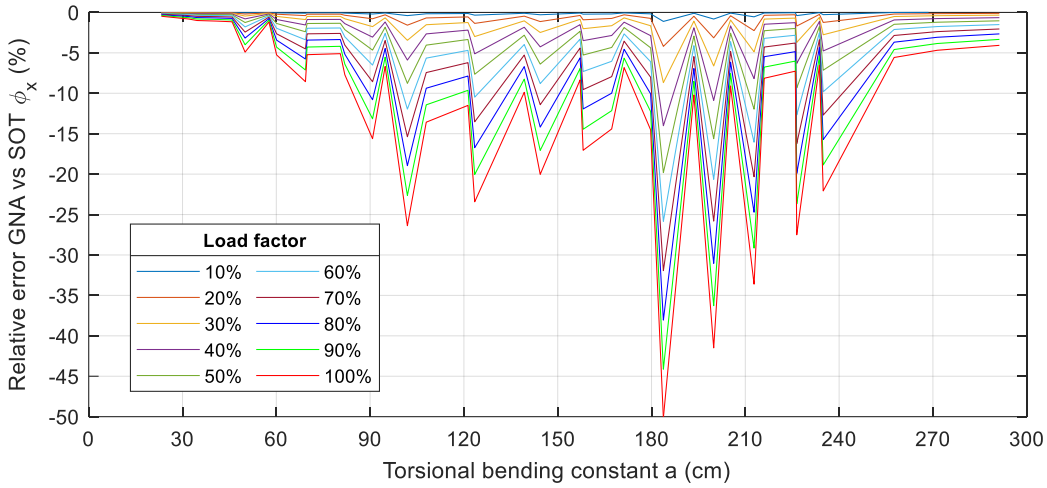

Figure A II.58Relative error φ_x: fork-fork system, M_T load, open profiles, and 1D elements

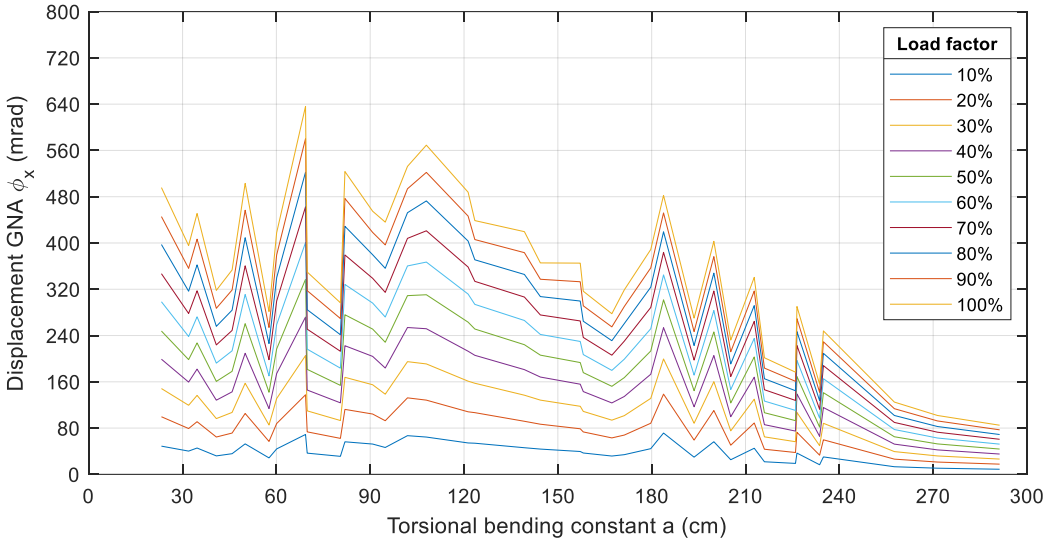

Figure A II.59Displacement φ_x: fork-fork system, M_T load, open profiles, and 1D elements

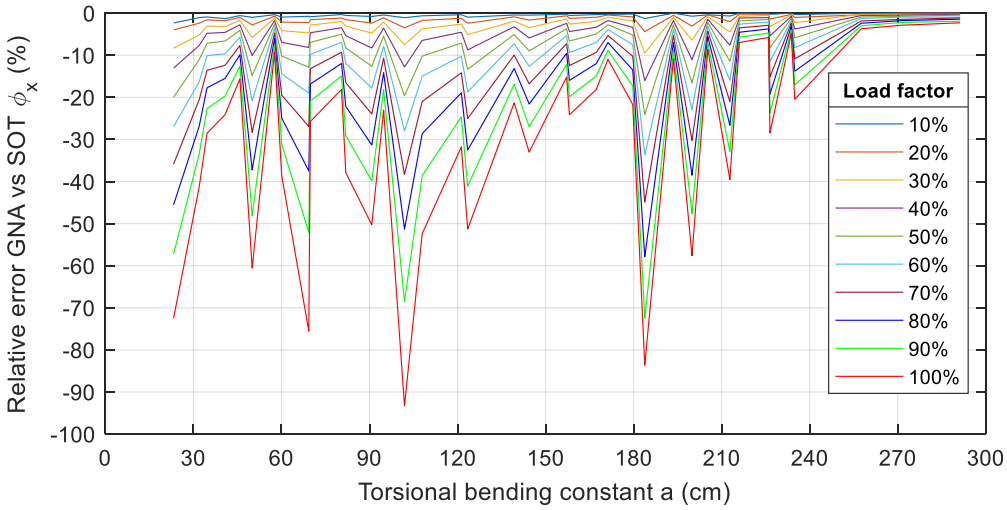

Figure A II.60Relative error φ_x: fork-fork system, M_T load, open profiles, and 2D elements

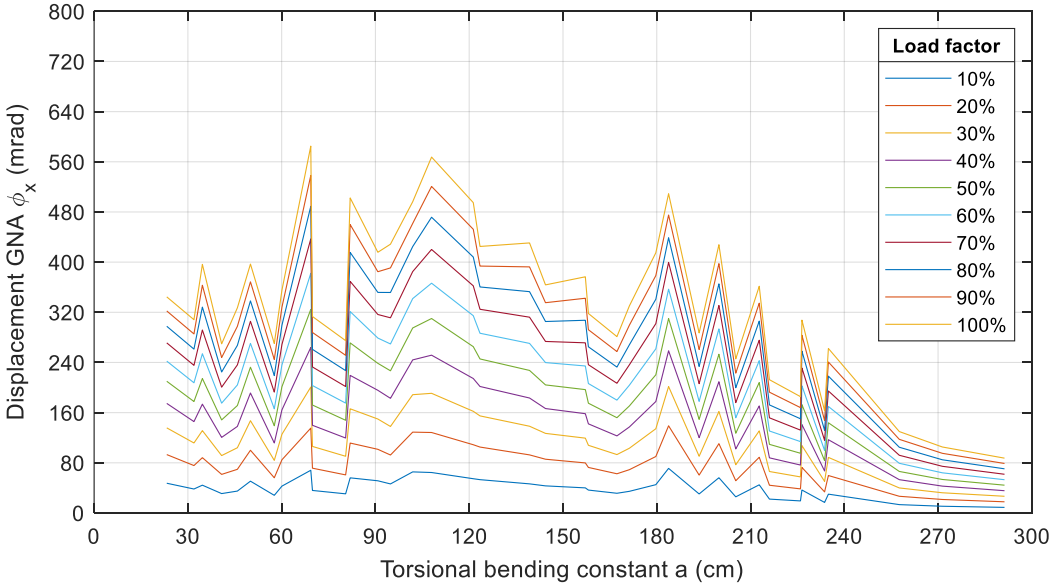

Figure A II.61Displacement φ_x: fork-fork system, M_T load, open profiles, and 2D elements

Appendix II-2.2 Closed cross-sections

V_z

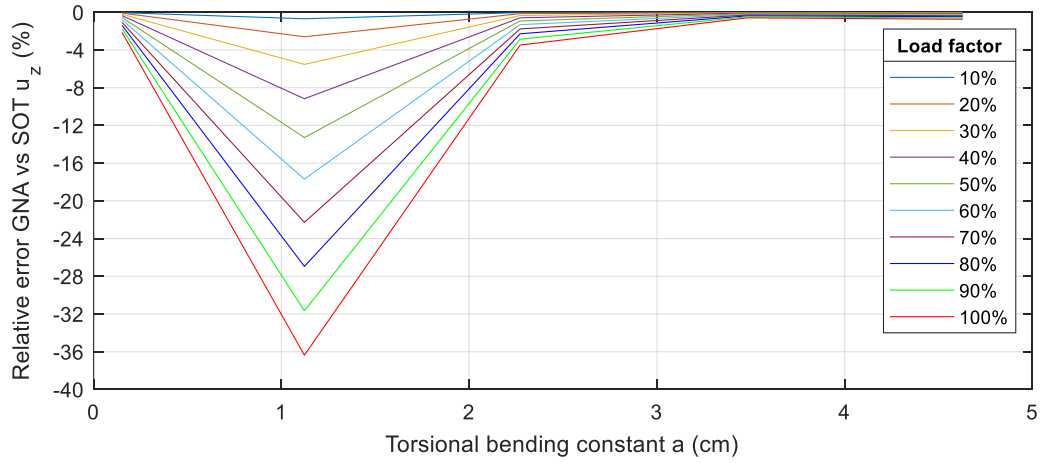

Figure A II.62Relative error u_z: fork-fork system, V_z load, closed profiles, and 1D elements

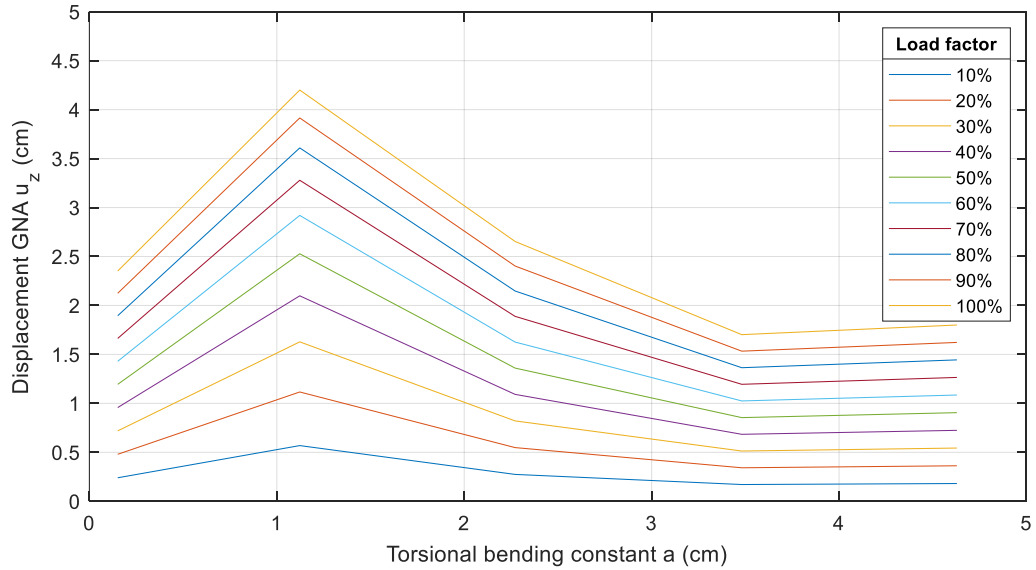

Figure A II.63Displacement u_z: fork-fork system, V_z load, closed profiles, and 1D elements

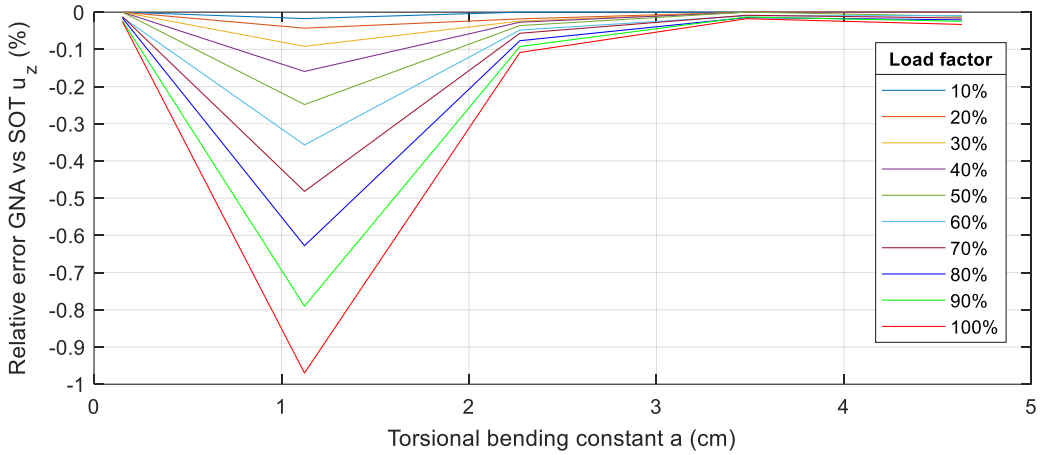

Figure A II.64Relative error u_z: fork-fork system, V_z load, closed profiles, and 2D elements

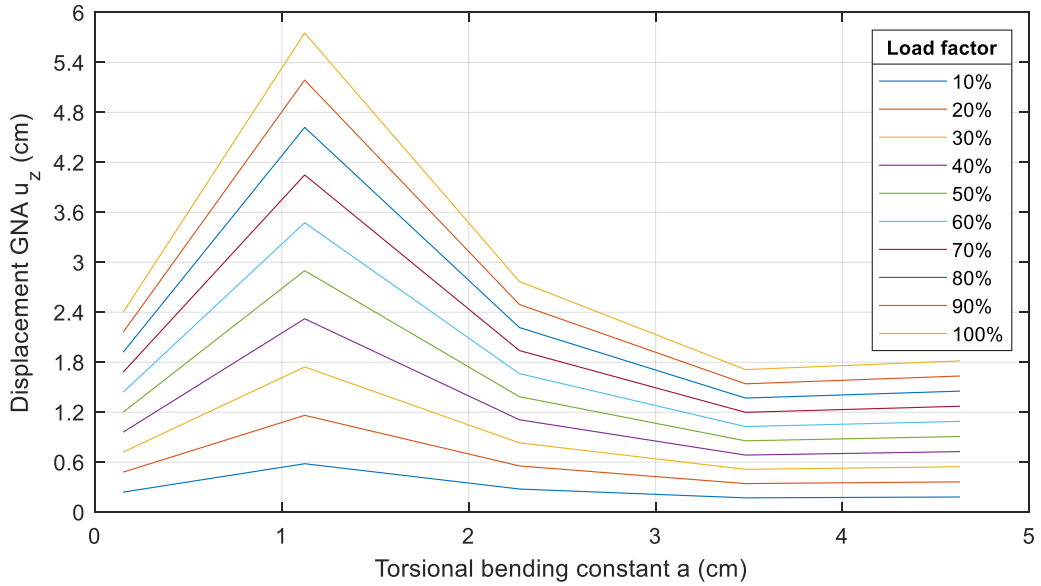

Figure A II.65Displacement u_z: fork-fork system, V_z load, closed profiles, and 2D elements

M_y

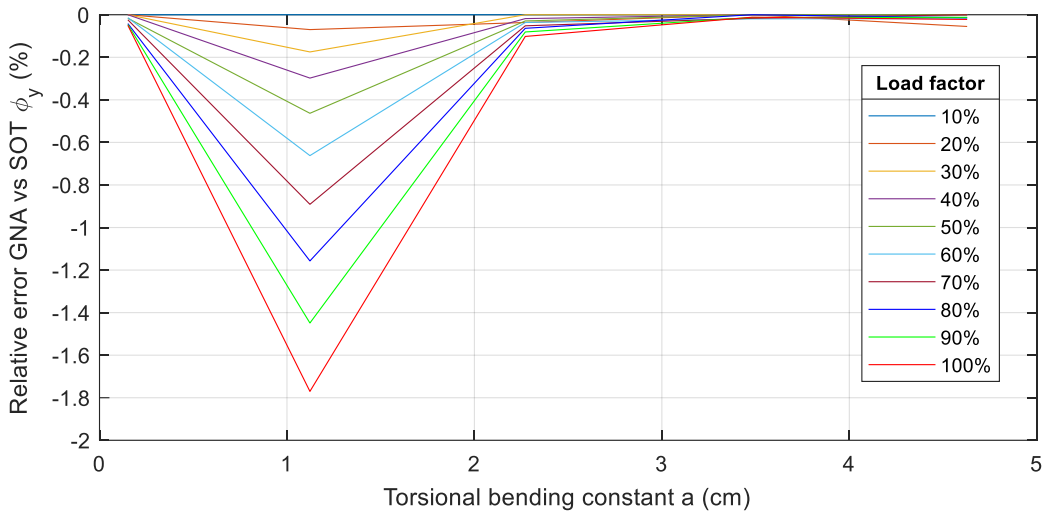

Figure A II.66Relative error φ_y: fork-fork system, M_y load, closed profiles, and 1D elements

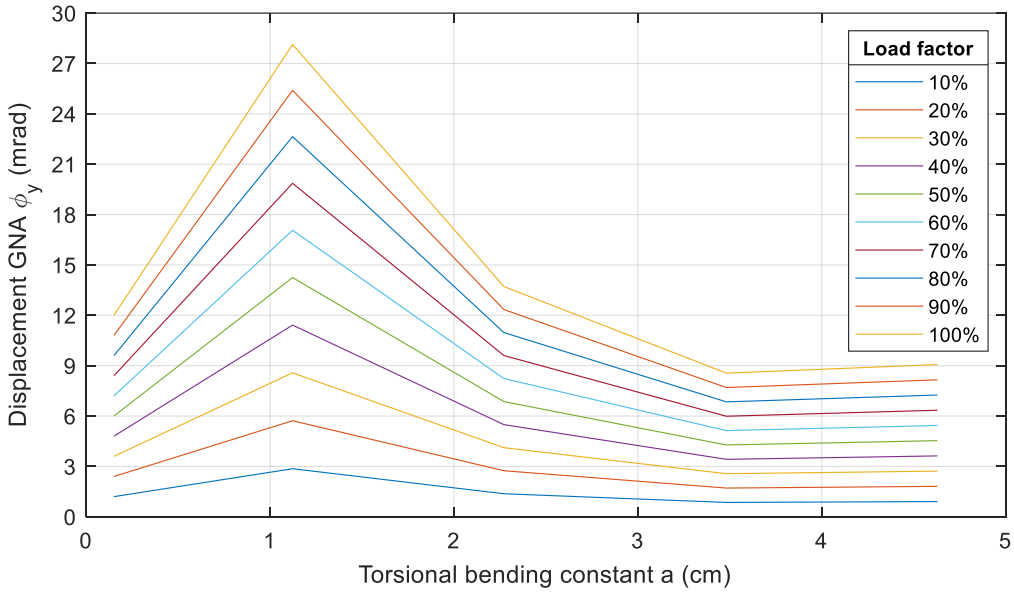

Figure A II.67Displacement φ_y: fork-fork system, M_y load, closed profiles, and 1D elements

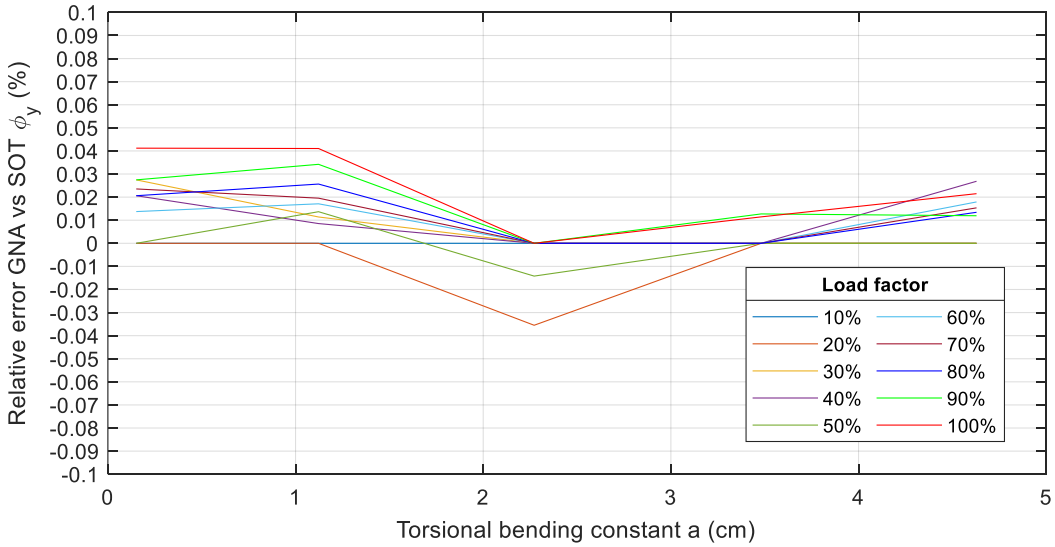

Figure A II.68Relative error φ_y: fork-fork system, M_y load, closed profiles, and 2D elements

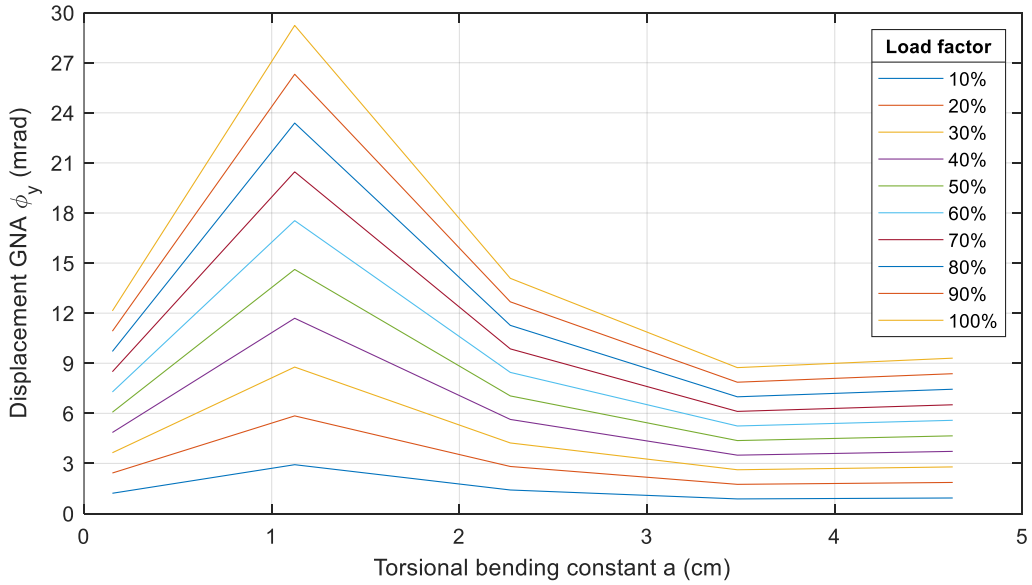

Figure A II.69Displacement φ_y: fork-fork system, M_y load, closed profiles, and 2D elements

M_T

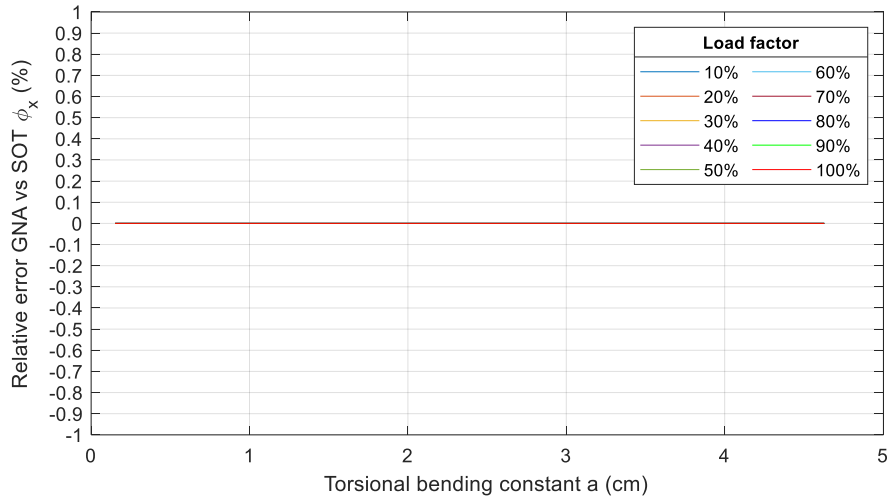

Figure A II.70Relative error φ_x: fork-fork system, M_T load, closed profiles, and 1D elements

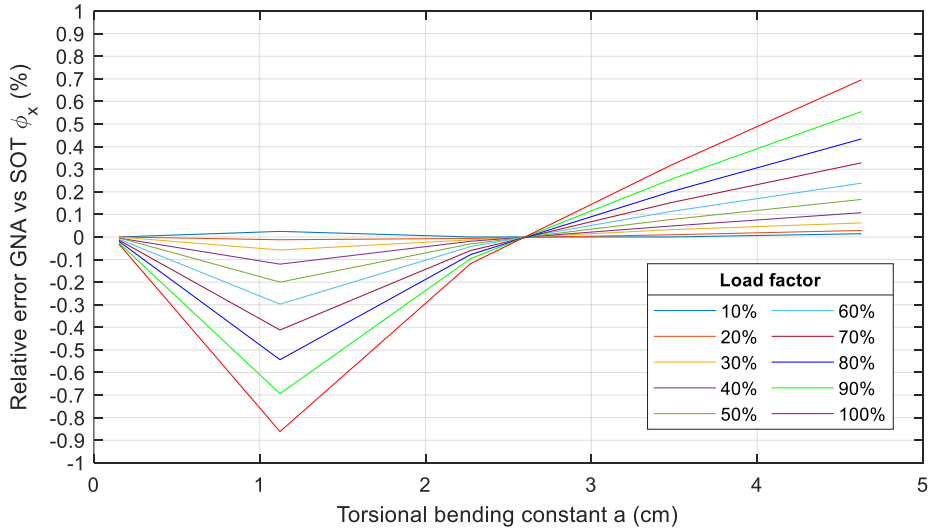

Figure A II.71Displacement φ_x: fork-fork system, M_T load, closed profiles, and 1D elements

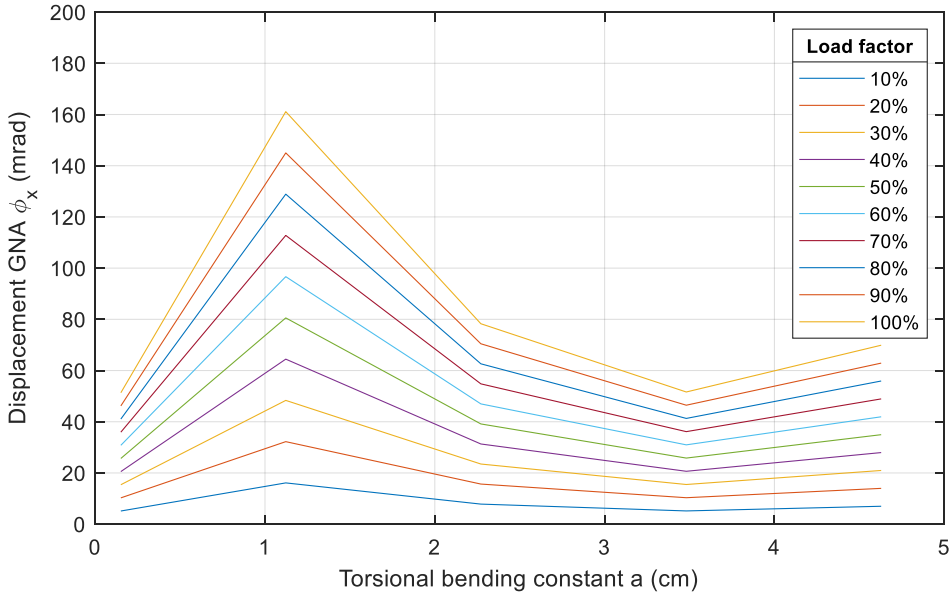

Figure A II.72Relative error φ_x: fork-fork system, M_T load, closed profiles, and 2D elements

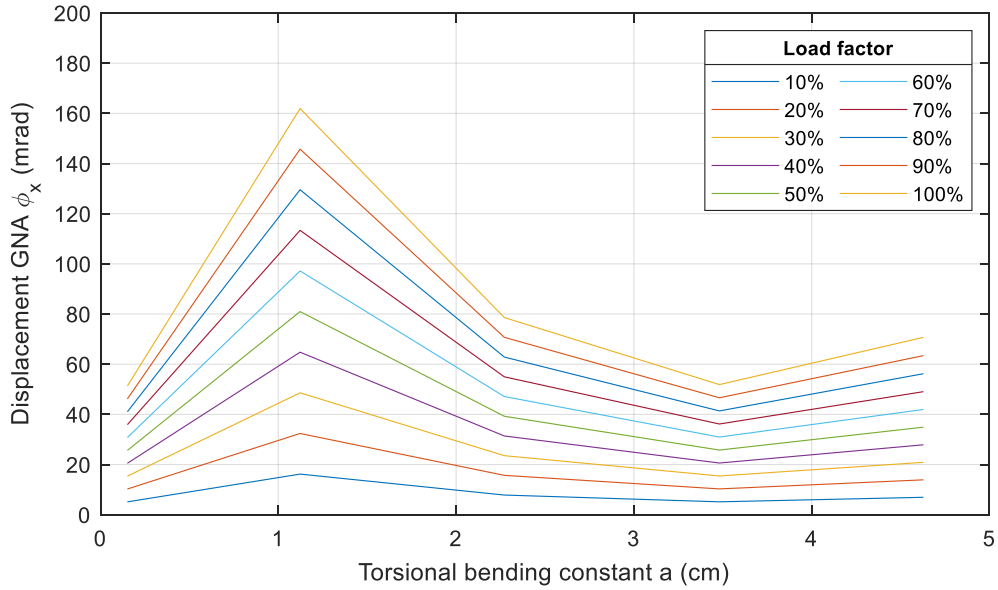

Figure A II.73Displacement φ_x: fork-fork system, M_T load, closed profiles, and 2D elements

Appendix II-3 Fixed-fixed system

Appendix II-3.1 Open cross-sections

V_z

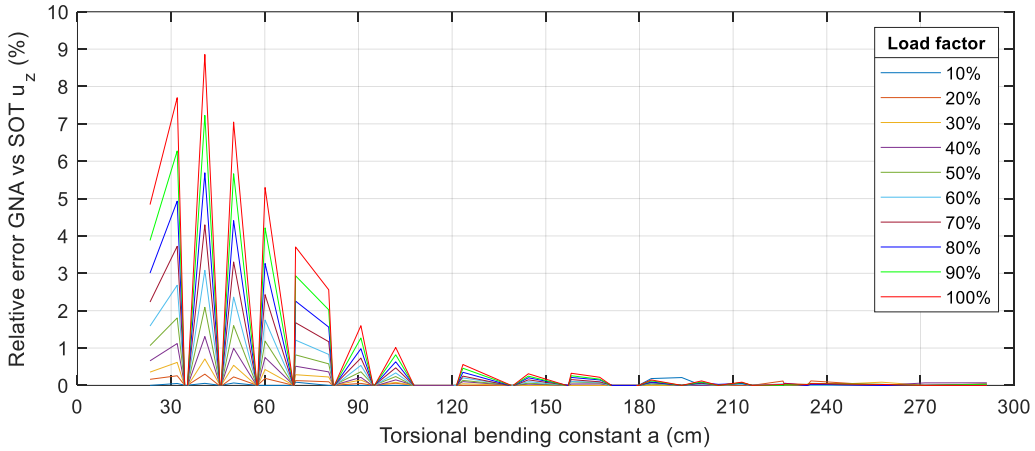

Figure A II.74Relative error u_z: fixed-fixed system, V_z load, open profiles, and 1D elements

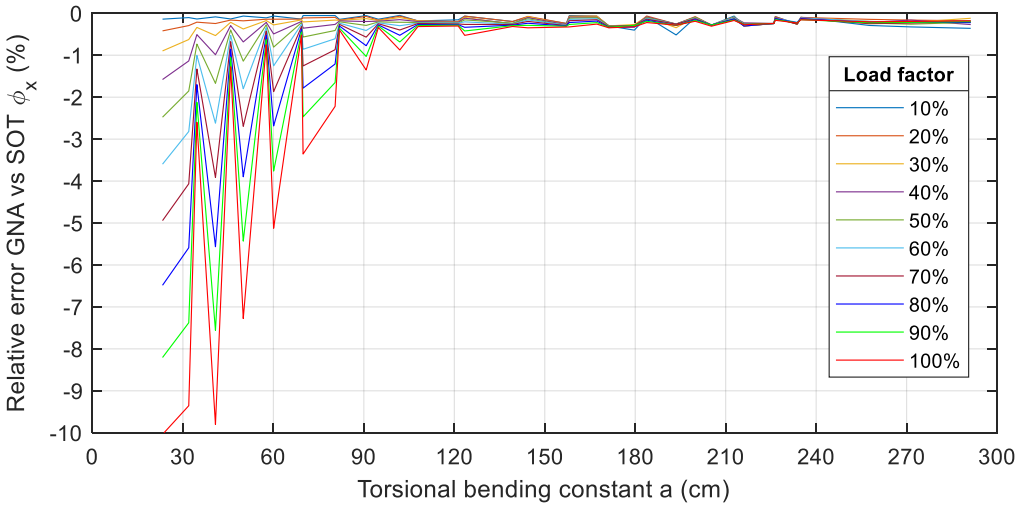

Figure A II.75Relative error φ_x: fixed-fixed system, V_z load, open profiles, and 1D elements

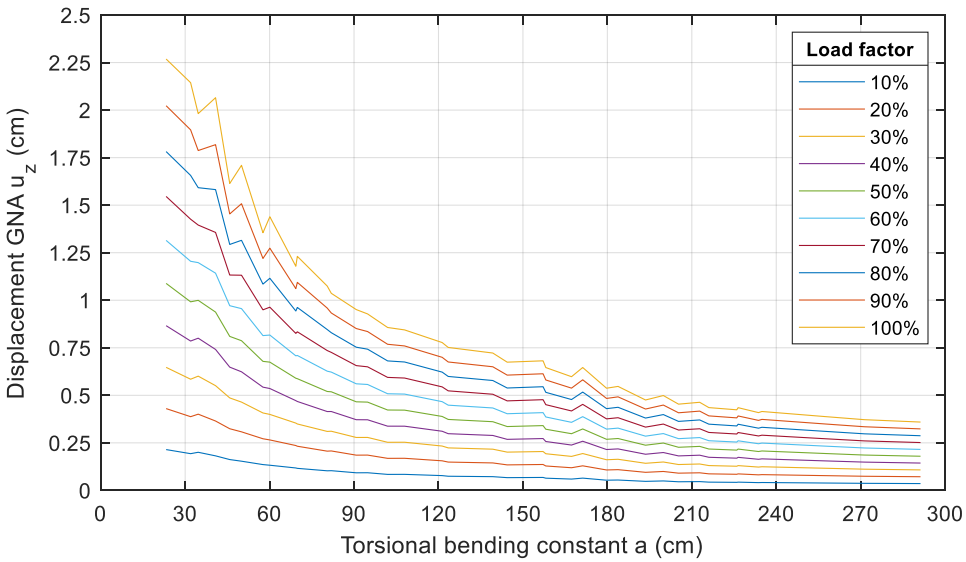

Figure A II.76Displacement u_z: fixed-fixed system, V_z load, open profiles, and 1D elements

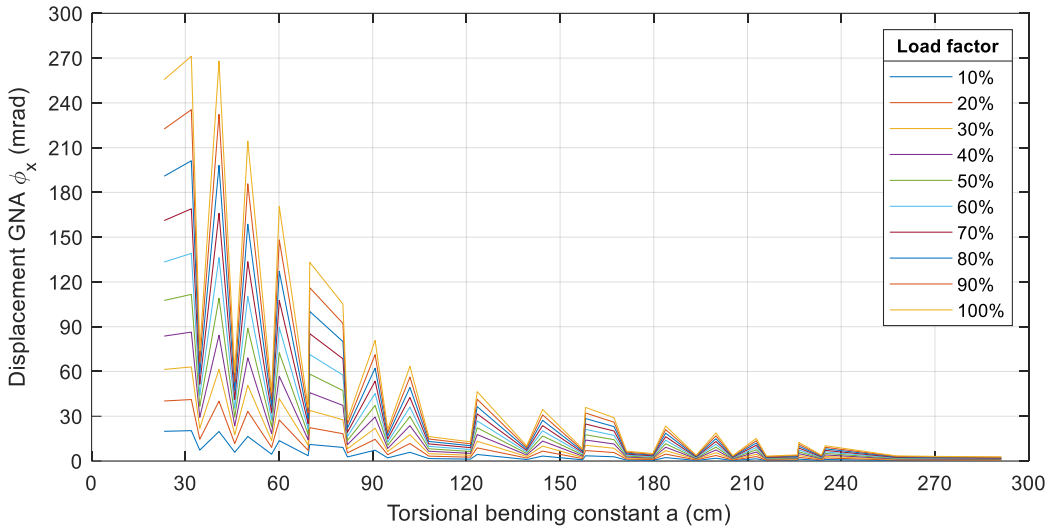

Figure A II.77Displacement φ_x: fixed-fixed system, V_z load, open profiles, and 1D elements

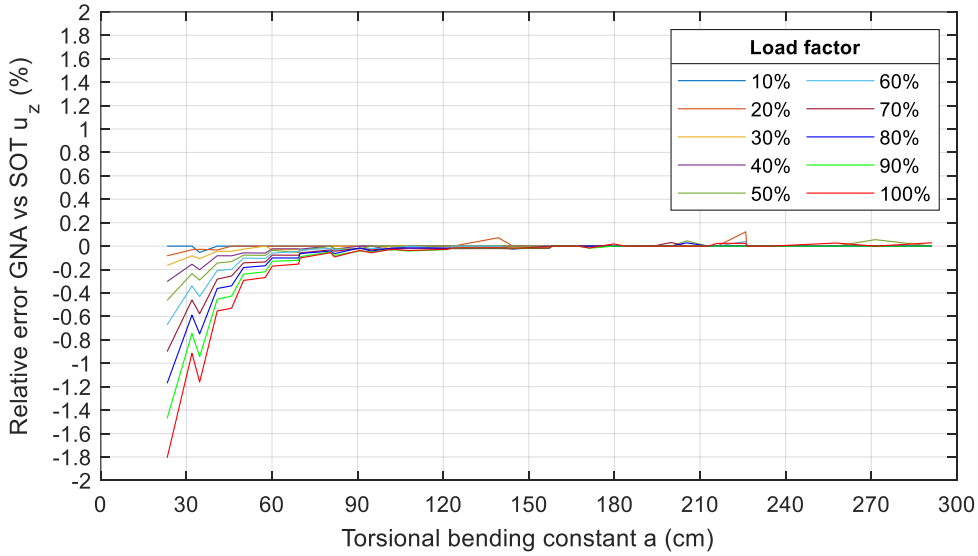

Figure A II.78Relative error u_z: fixed-fixed system, V_z load, open profiles, and 2D elements

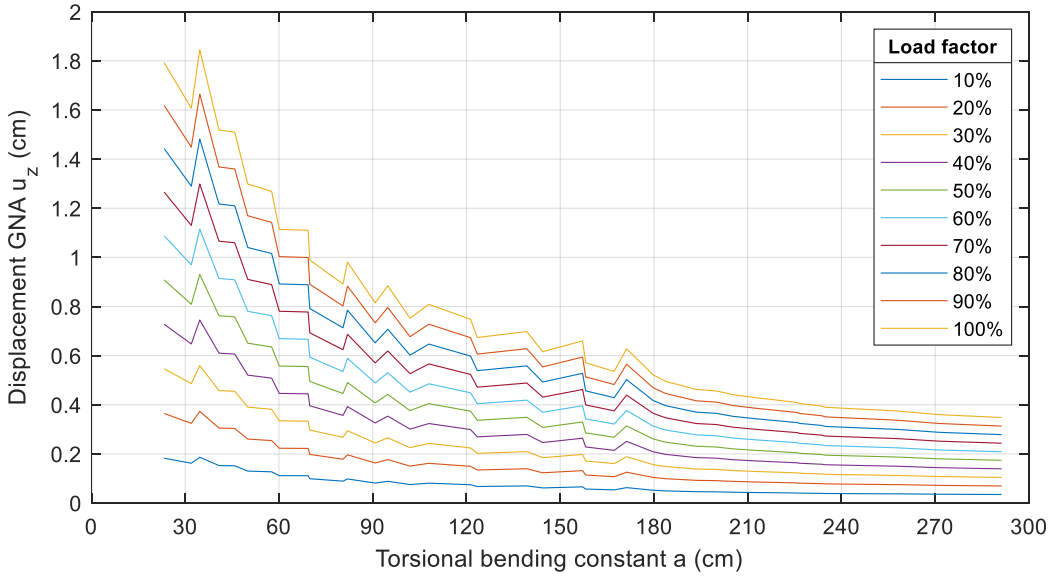

Figure A II.79Displacement φ_x: fixed-fixed system, V_z load, open profiles, and 2D elements

M_y

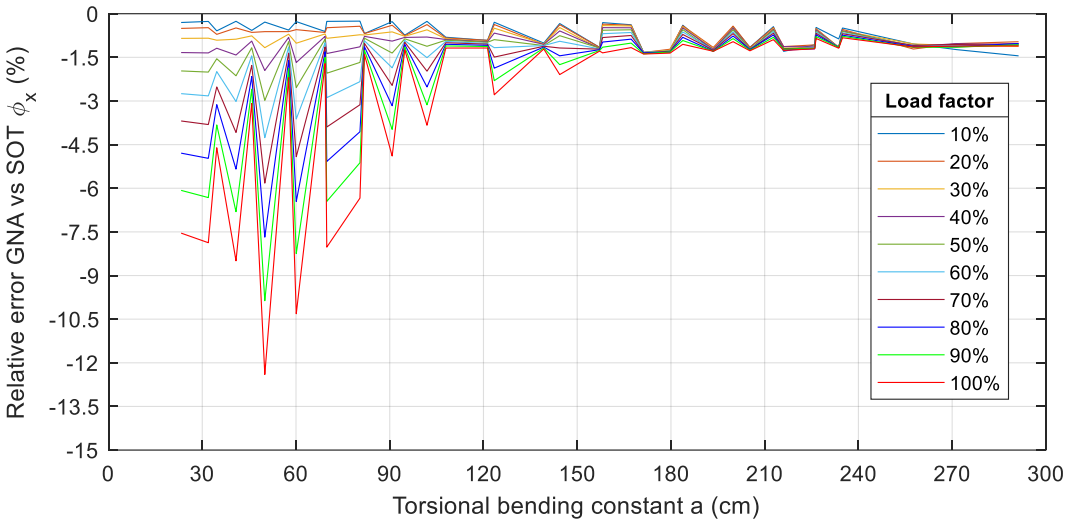

Figure A II.80Relative error φ_x: fixed-fixed system, M_y load, open profiles, and 1D elements

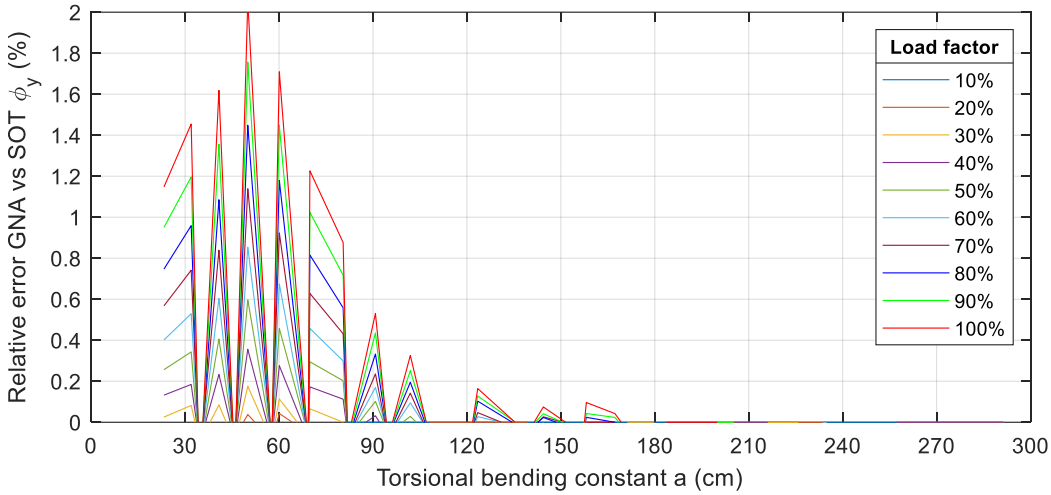

Figure A II.81Relative error φ_y: fixed-fixed system, M_y load, open profiles, and 1D elements

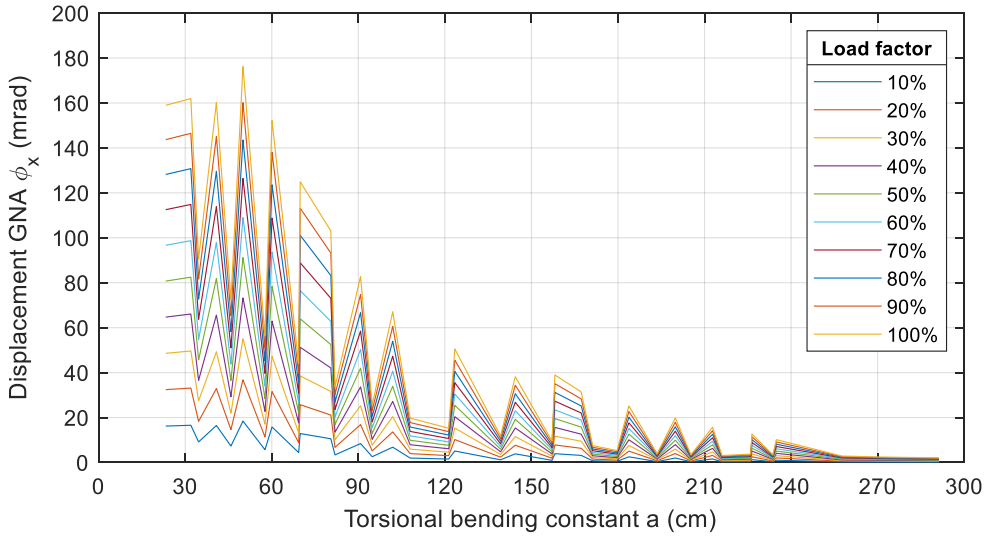

Figure A II.82Displacement φ_x: fixed-fixed system, M_y load, open profiles, and 1D elements

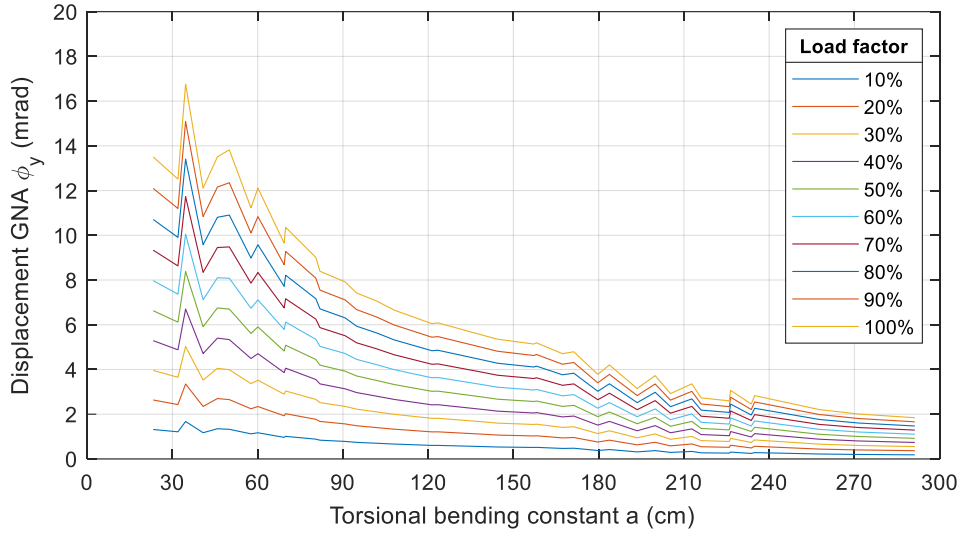

Figure A II.83Displacement φ_y: fixed-fixed system, M_y load, open profiles, and 1D elements

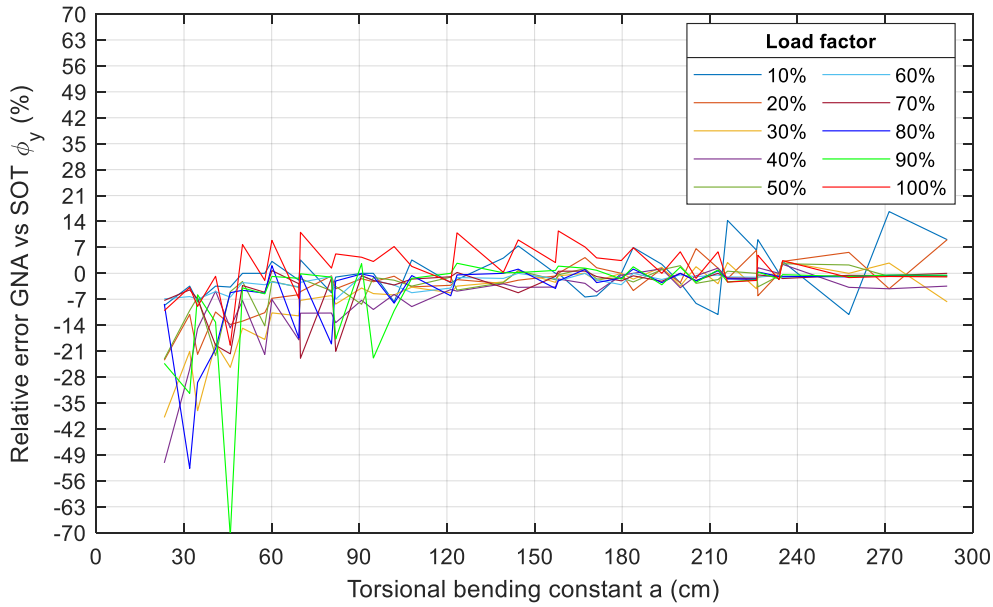

Figure A II.84Relative error φ_x: fixed-fixed system, M_y load, open profiles, and 2D elements

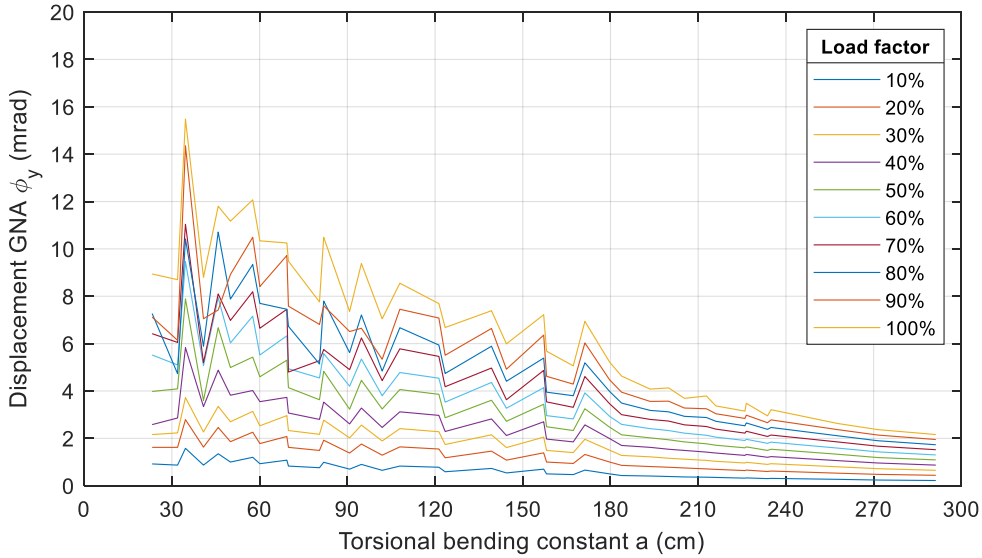

Figure A II.85Displacement φ_y: fixed-fixed system, M_y load, open profiles, and 2D elements

M_T

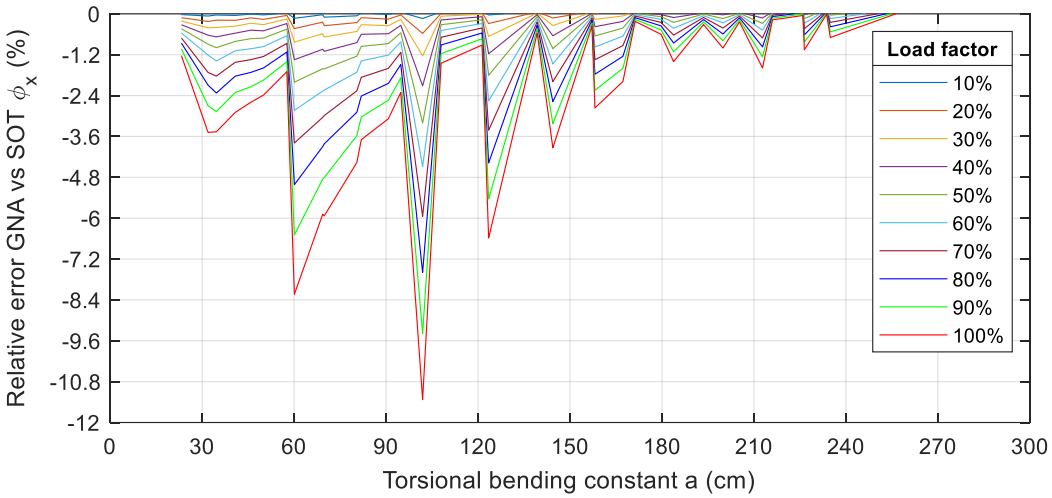

Figure A II.86Relative error φ_x: fixed-fixed system, M_T load, open profiles, and 1D elements

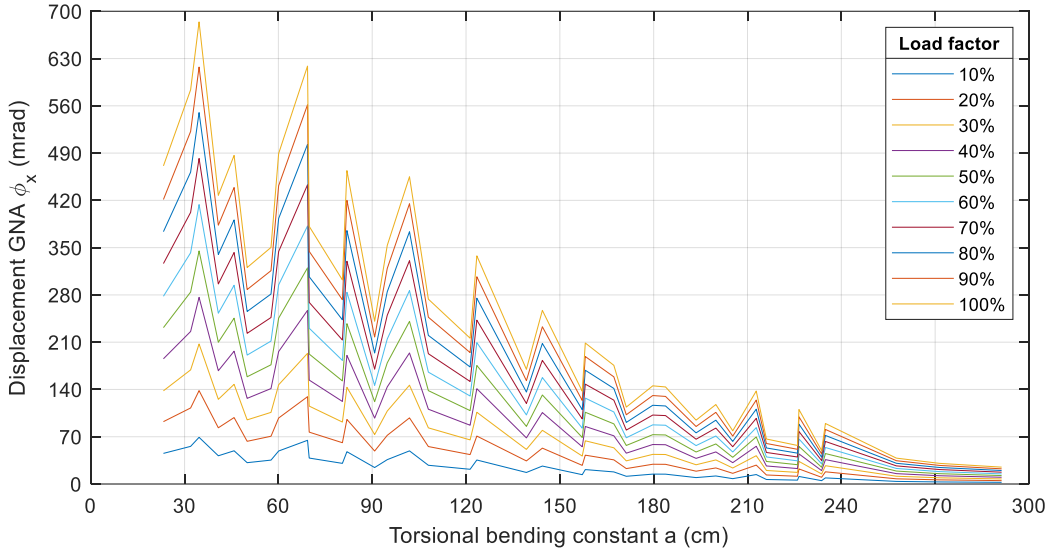

Figure A II.87Displacement φ_x: fixed-fixed system, M_T load, open profiles, and 1D elements

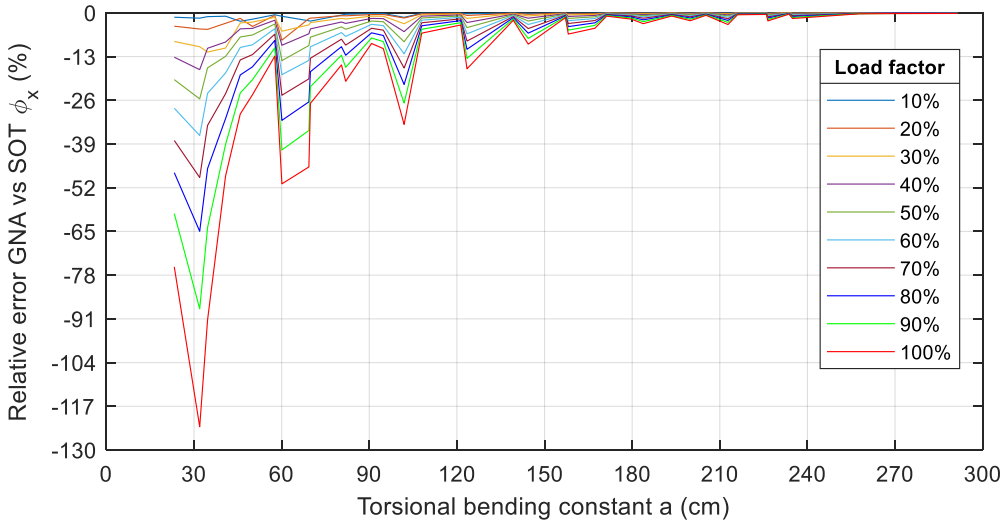

Figure A II.88Relative error φ_x: fixed-fixed system, M_T load, open profiles, and 2D elements

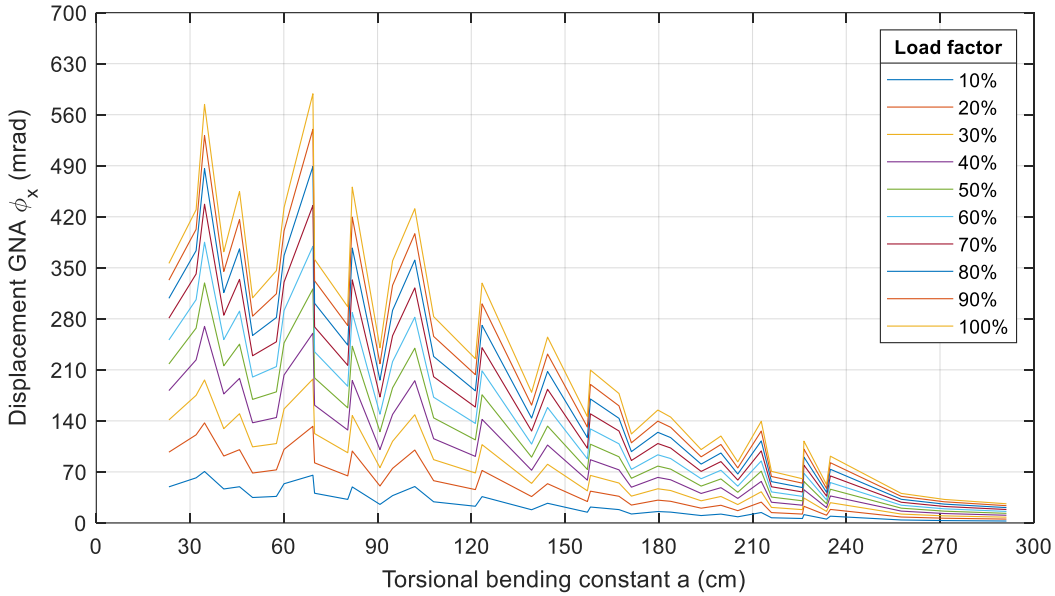

Figure A II.89Displacement φ_x: fixed-fixed system, M_T load, open profiles, and 2D elements

Appendix II-3.2 Closed cross-sections

V_z

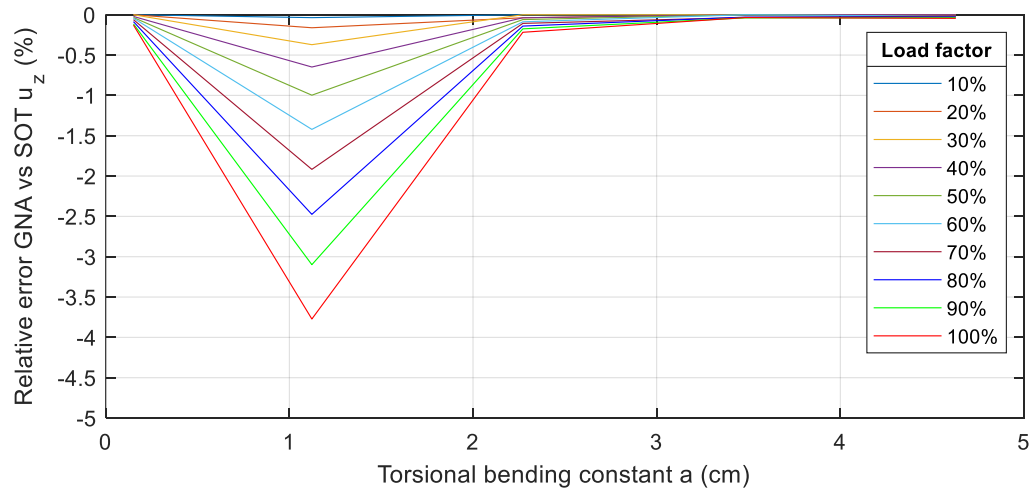

Figure A II.90Relative error u_z: fixed-fixed system, V_z load, closed profiles, and 1D elements

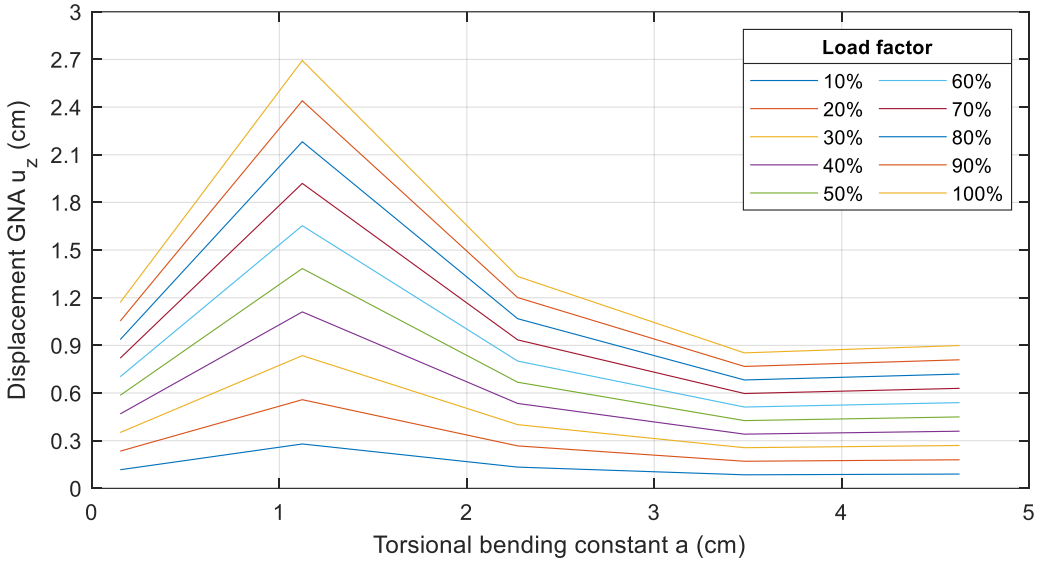

Figure A II.91Displacement u_z: fixed-fixed system, V_z load, closed profiles, and 1D elements

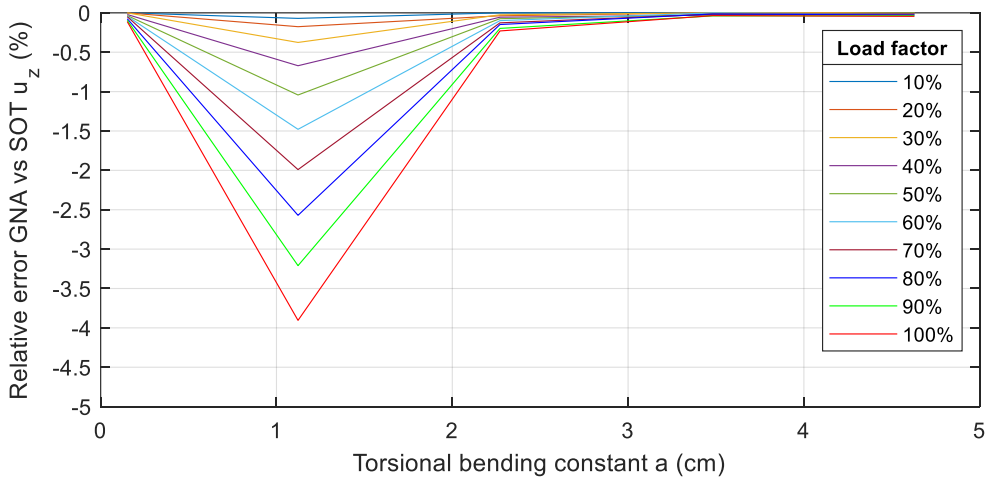

Figure A II.92Relative error u_z: fixed-fixed system, V_z load, closed profiles, and 2D elements

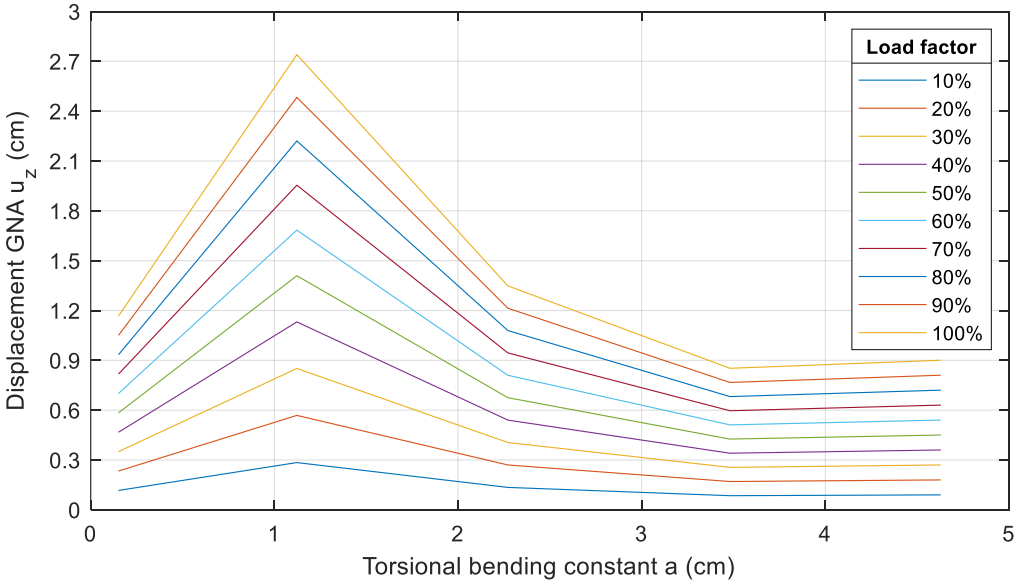

Figure A II.93Displacement u_z: fixed-fixed system, V_z load, closed profiles, and 2D elements

M_y

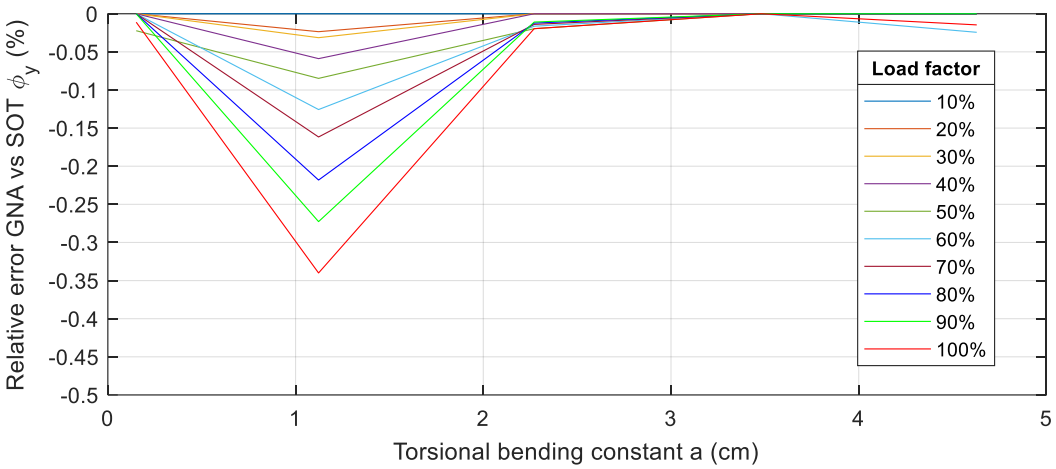

Figure A II.94Relative error φ_y: fixed-fixed system, M_y load, closed profiles, and 1D elements

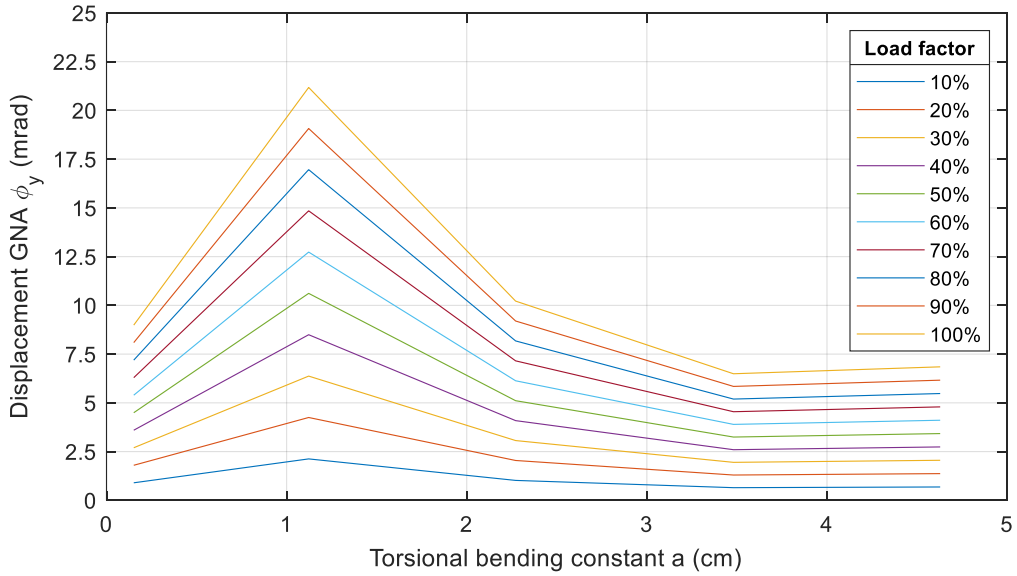

Figure A II.95Displacement φ_y: fixed-fixed system, M_y load, closed profiles, and 1D elements

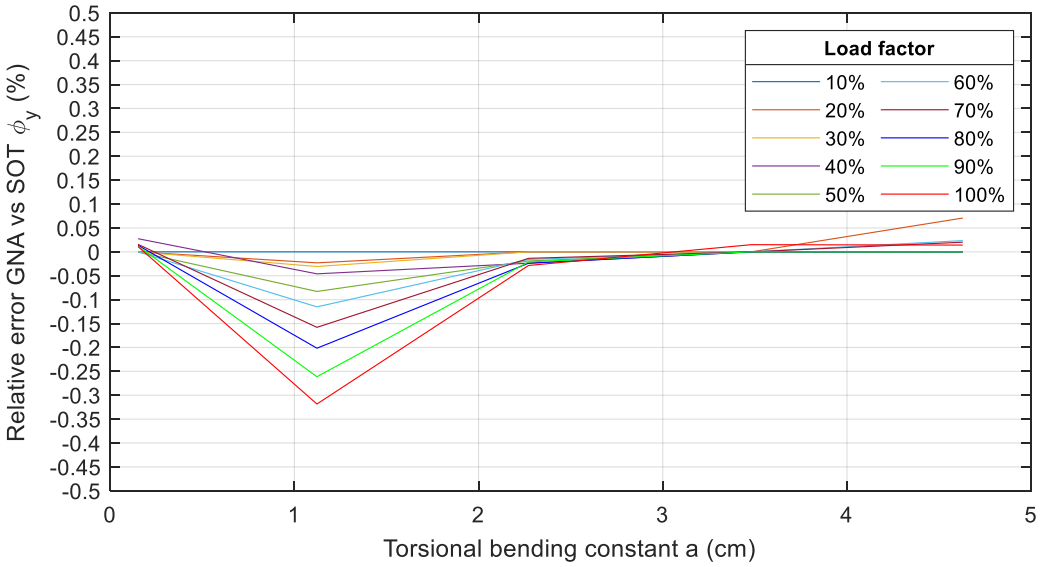

Figure A II.96Relative error φ_y: fixed-fixed system, M_y load, closed profiles, and 2D elements

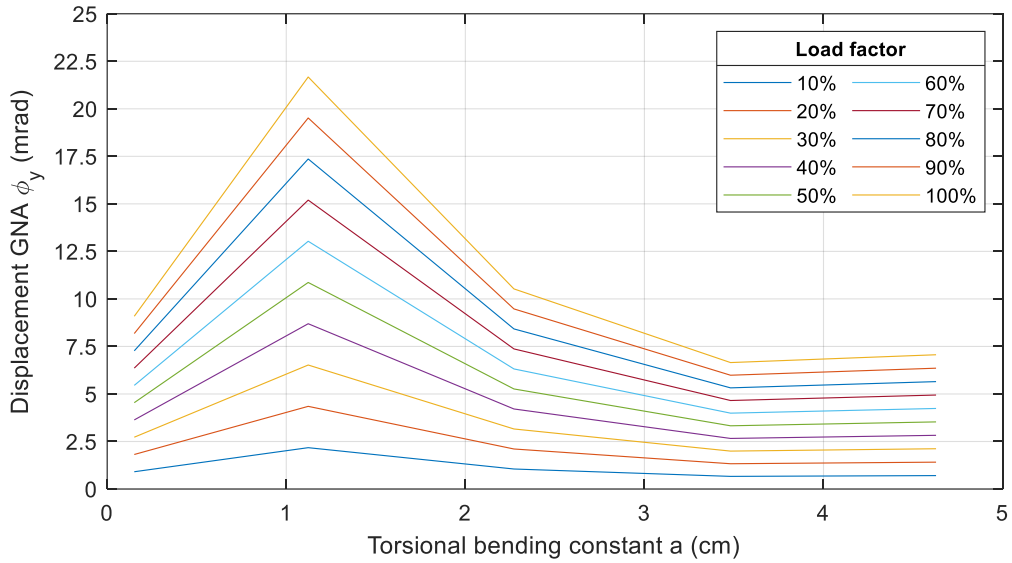

Figure A II.97Displacement φ_y: fixed-fixed system, M_y load, closed profiles, and 2D elements

M_T

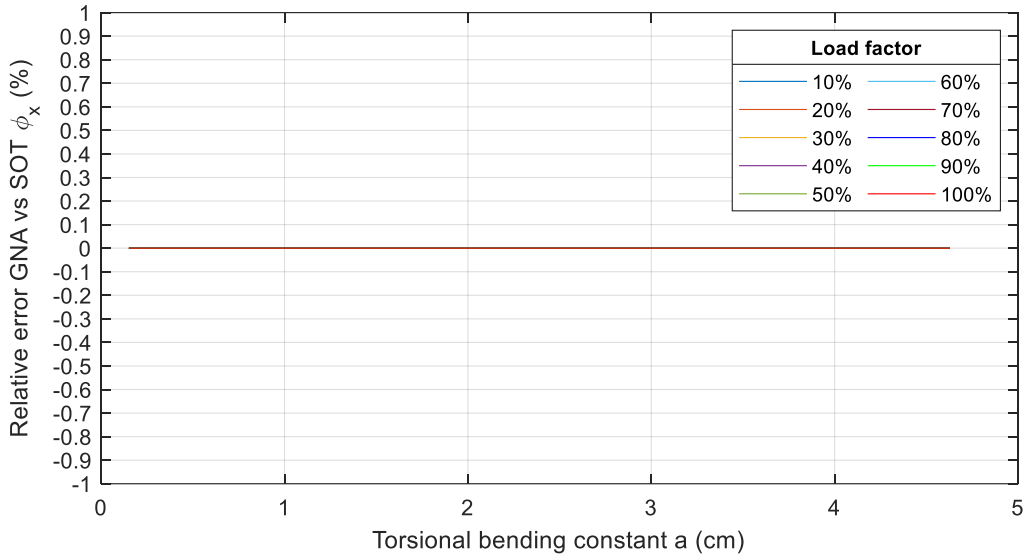

Figure A II.98Relative error φ_x: fixed-fixed system, M_T load, closed profiles, and 1D elements

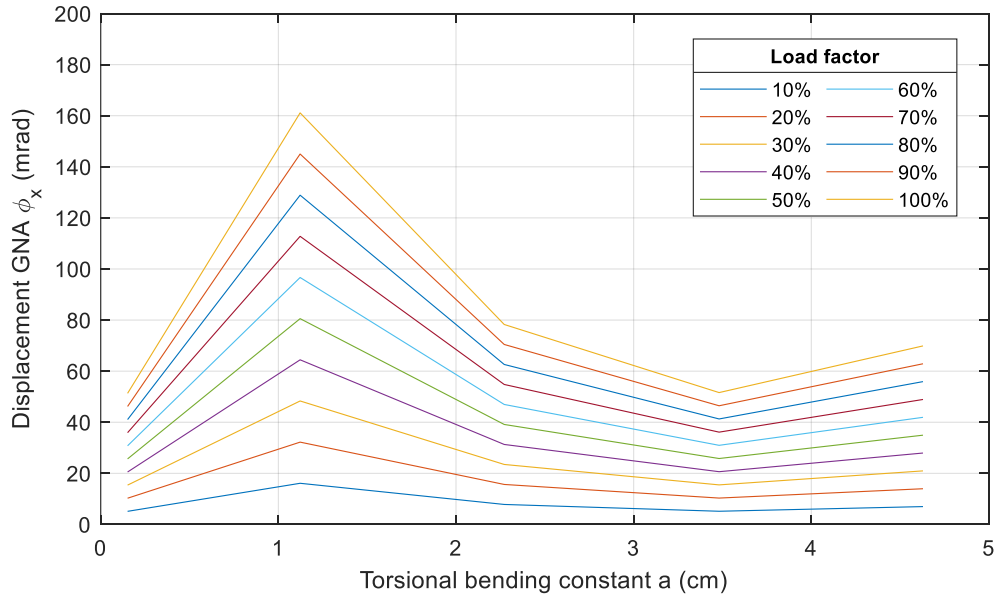

Figure A II.99Displacement φ_x: fixed-fixed system, M_T load, closed profiles, and 1D elements

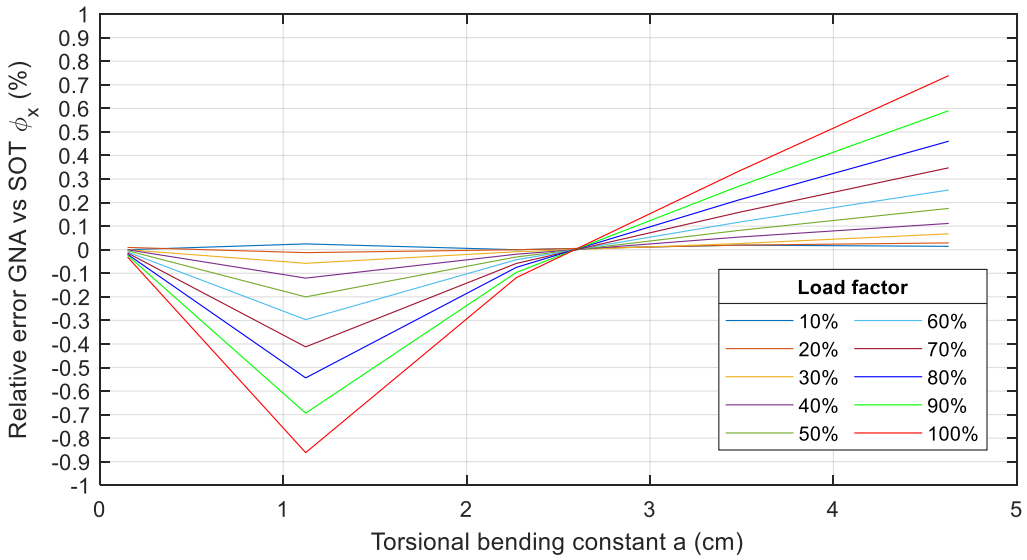

Figure A II.100 Relative error φ_x: fixed-fixed system, M_T load, closed profiles, and 2D elements

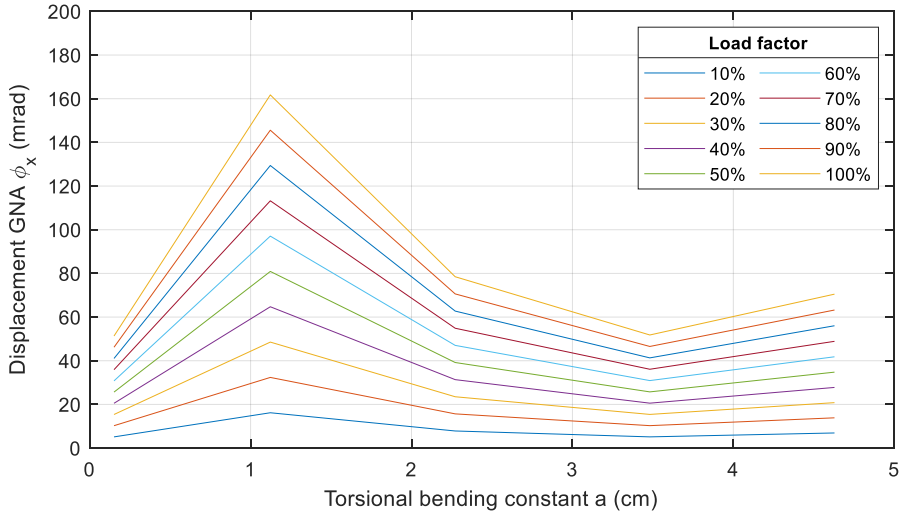

Figure A II.101 Displacement φ_x: fixed-fixed system, M_T load, closed profiles, and 2D elements

Appendix II-4 Fork-fixed system

Appendix II-4.1 Open cross-sections

V_z

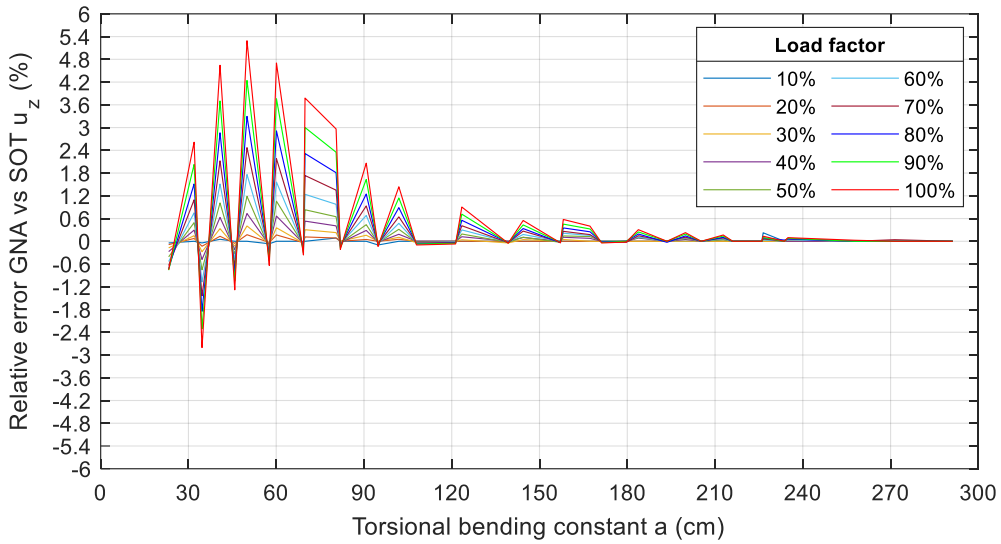

Figure A II.102 Relative error u_z: fork-fixed system, V_z load, open profiles, and 1D elements

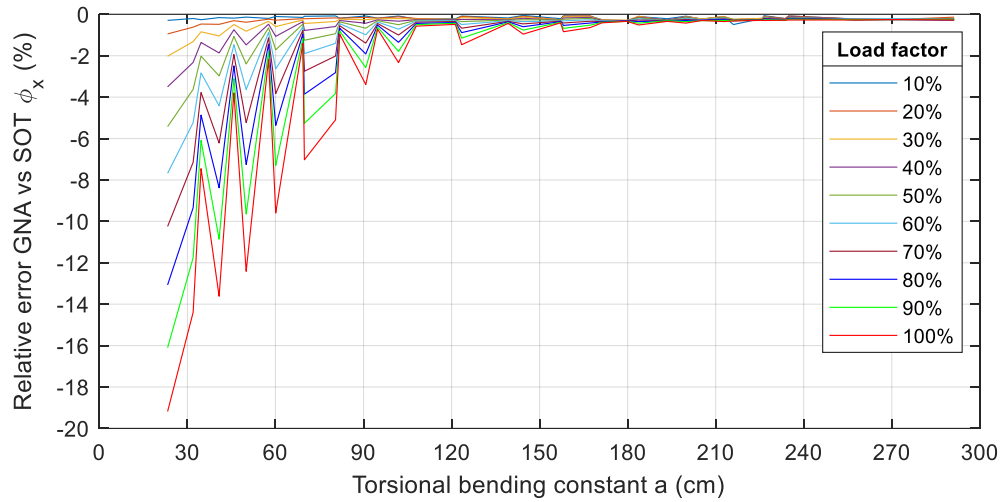

Figure A II.103 Relative error φ_x: fork-fixed system, V_z load, open profiles, and 1D elements

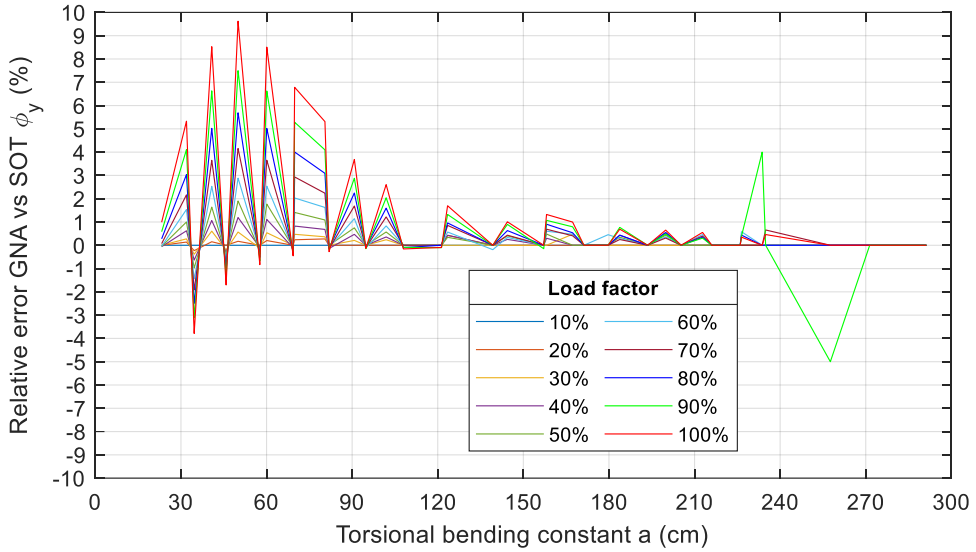

Figure A II.104 Relative error φ_y: fork-fixed system, V_z load, open profiles, and 1D elements

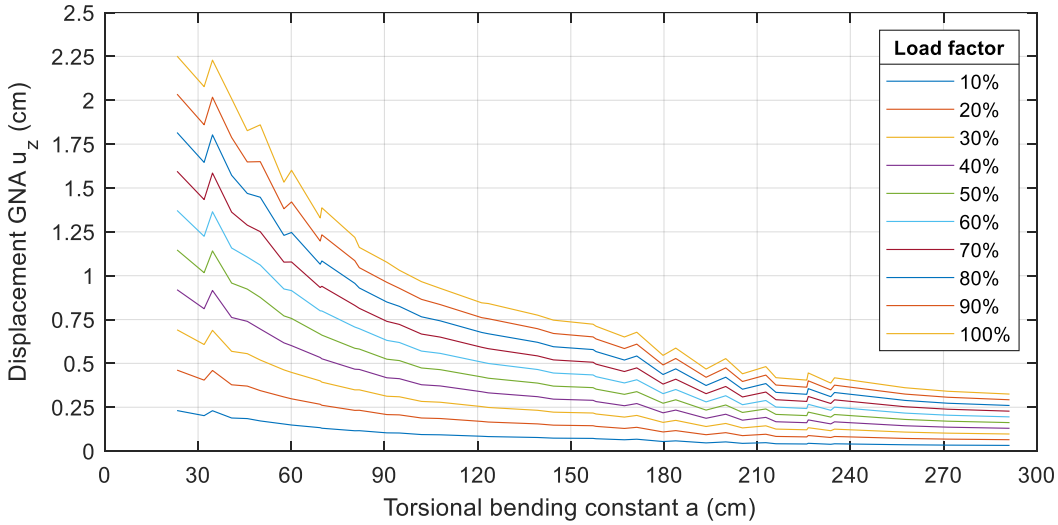

Figure A II.105 Displacement u_z: fork-fixed system, V_z load, open profiles, and 1D elements

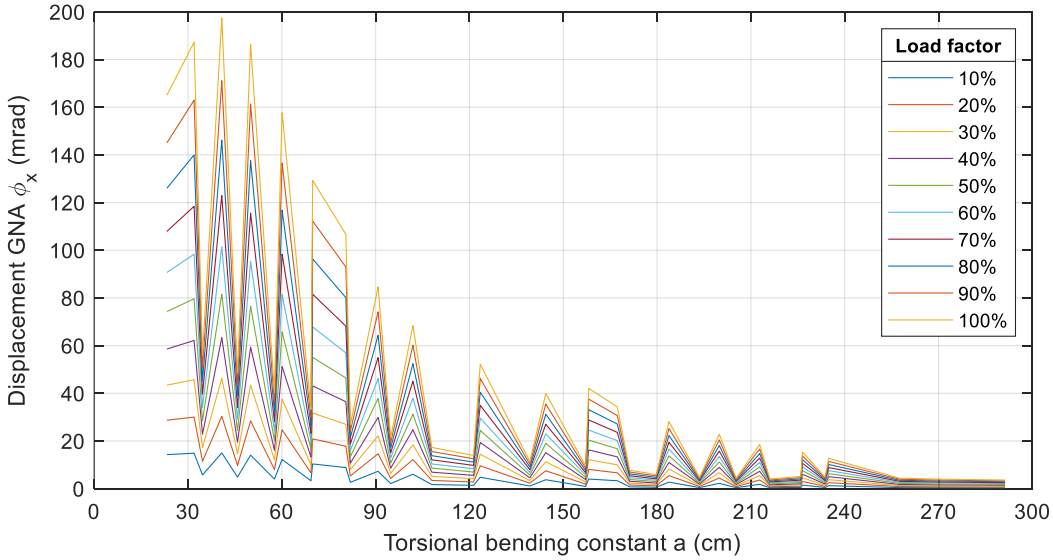

Figure A II.106 Displacement φ_x: fork-fixed system, V_z load, open profiles, and 1D elements

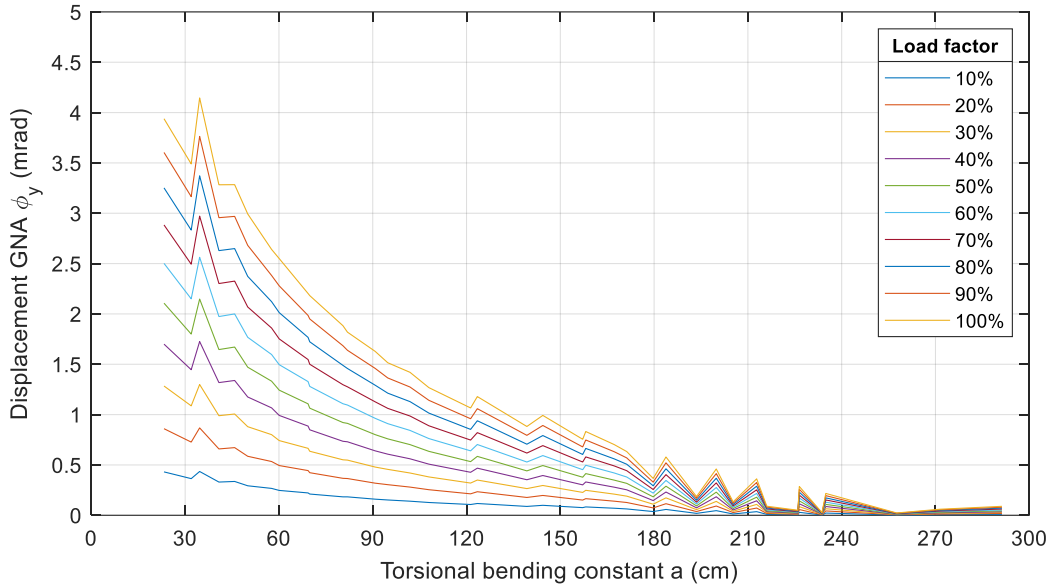

Figure A II.107 Displacement φ_y: fork-fixed system, V_z load, open profiles, and 1D elements

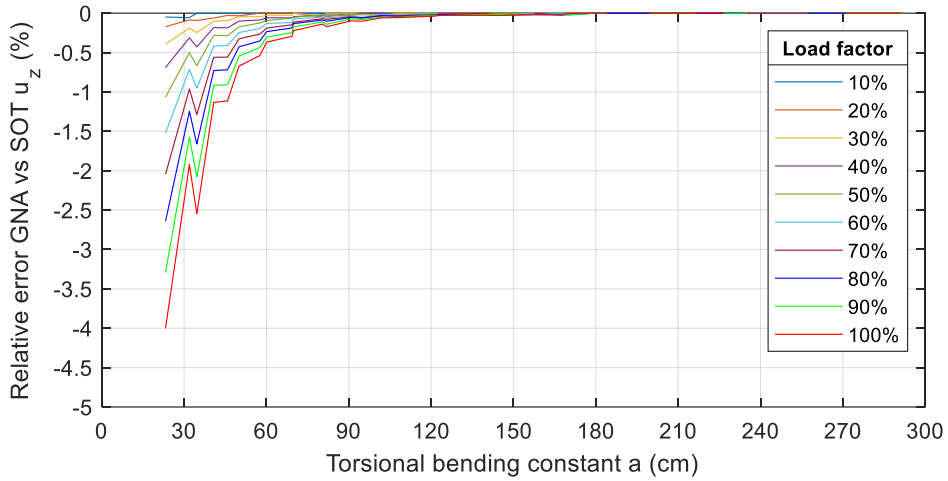

Figure A II.108 Relative error u_z: fork-fixed system, V_z load, open profiles, and 2D elements

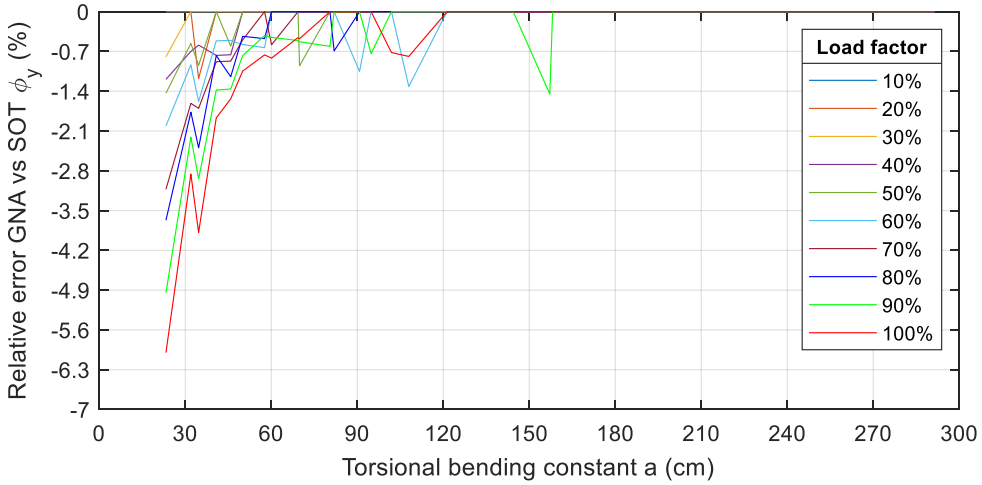

Figure A II.109 Relative error φ_y: fork-fixed system, V_z load, open profiles, and 2D elements

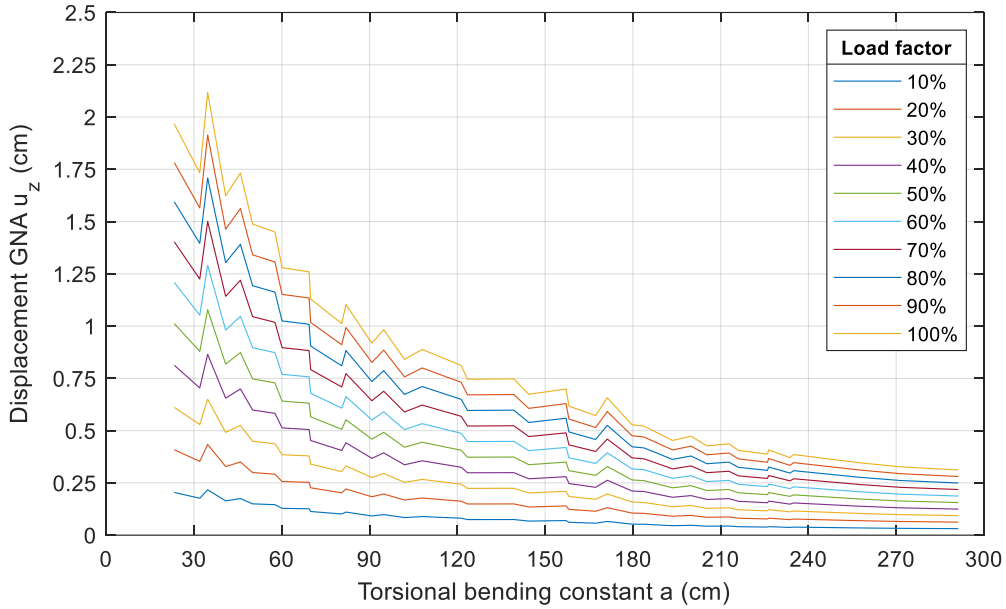

Figure A II.110 Displacement u_z: fork-fixed system, V_z load, open profiles, and 2D elements

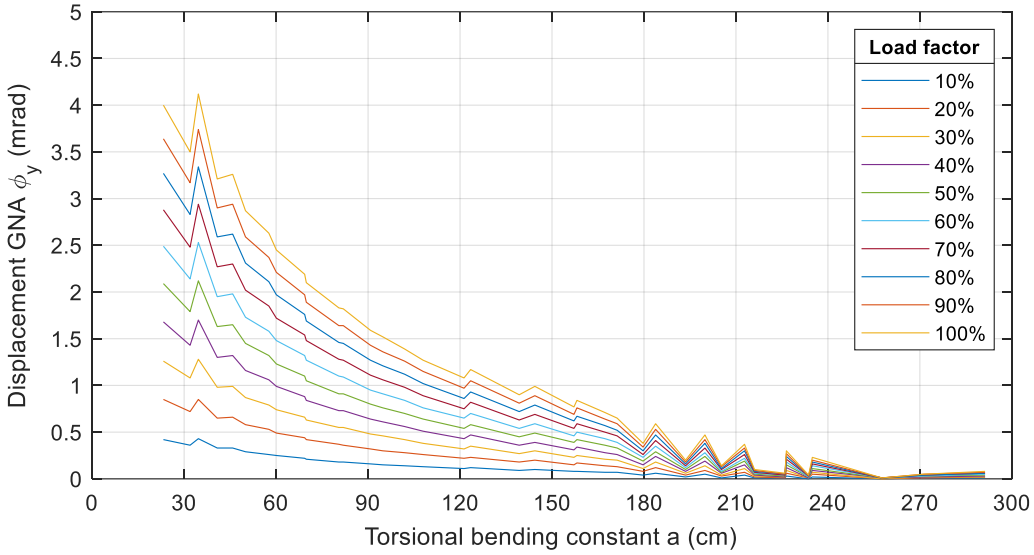

Figure A II.111 Displacement φ_y: fork-fixed system, V_z load, open profiles, and 2D elements

M_y

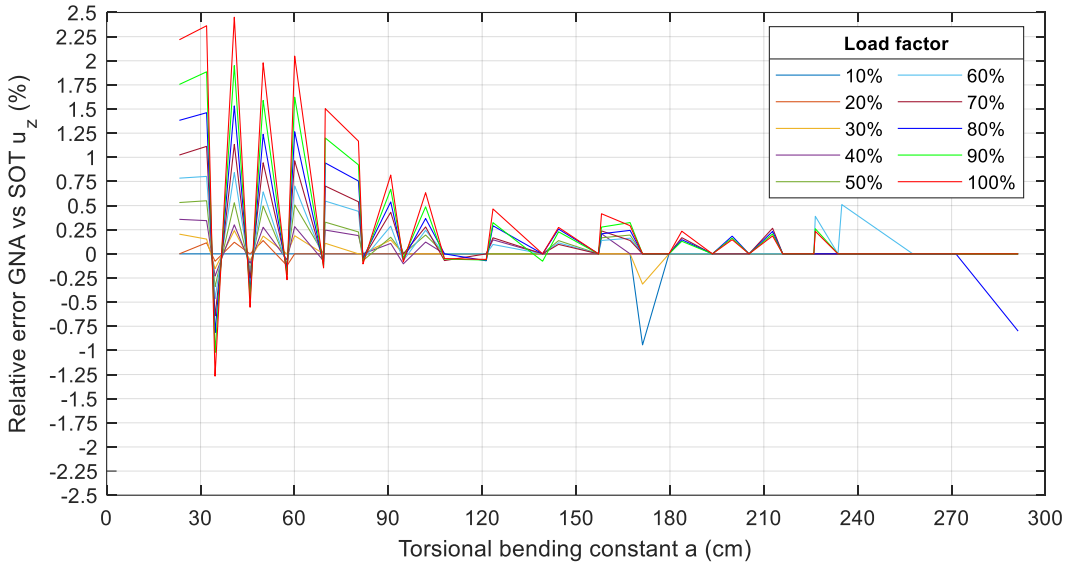

Figure A II.112 Relative error u_z: fork-fixed system, M_y load, open profiles, and 1D elements

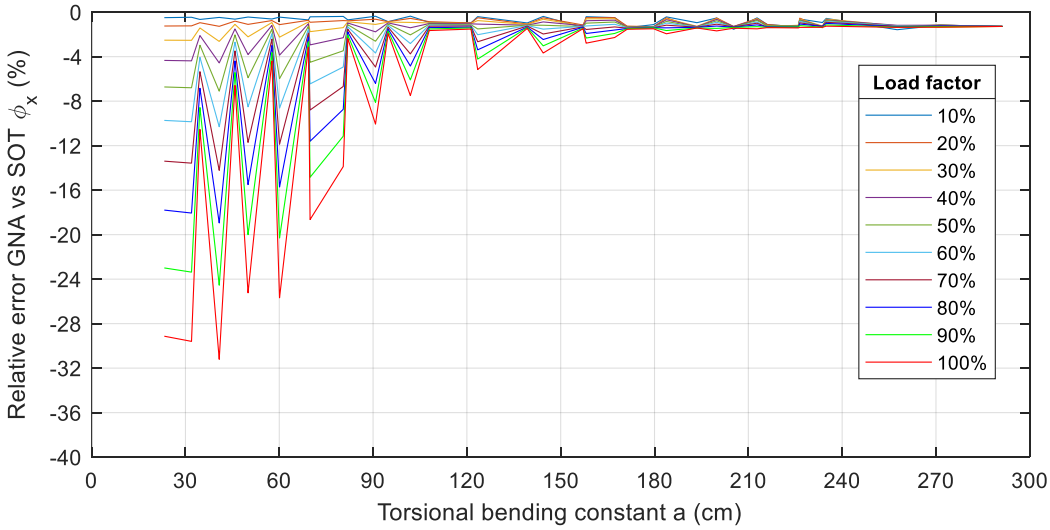

Figure A II.113 Relative error φ_x: fork-fixed system, M_y load, open profiles, and 1D elements

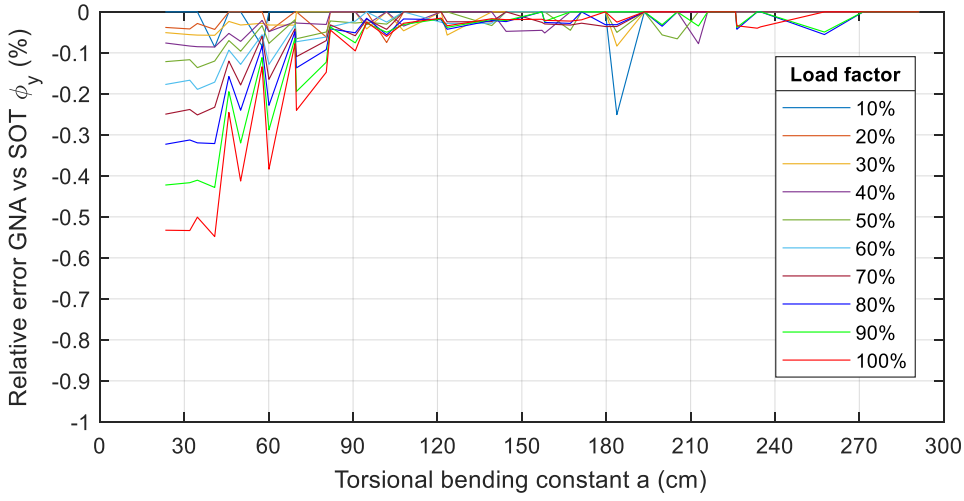

Figure A II.114 Relative error φ_y: fork-fixed system, M_y load, open profiles, and 1D elements

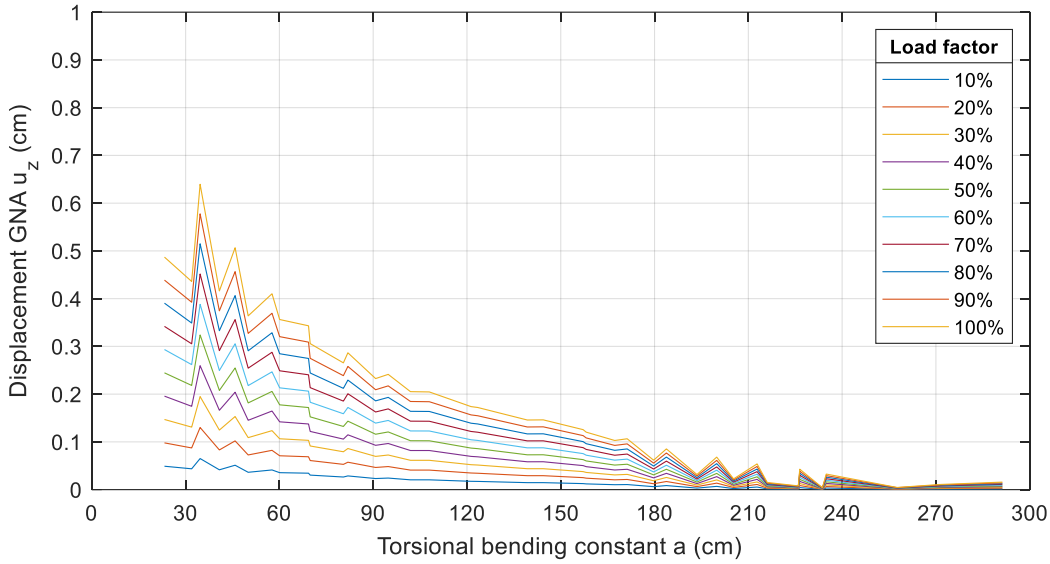

Figure A II.115 Displacement u_z: fork-fixed system, M_y load, open profiles, and 1D elements

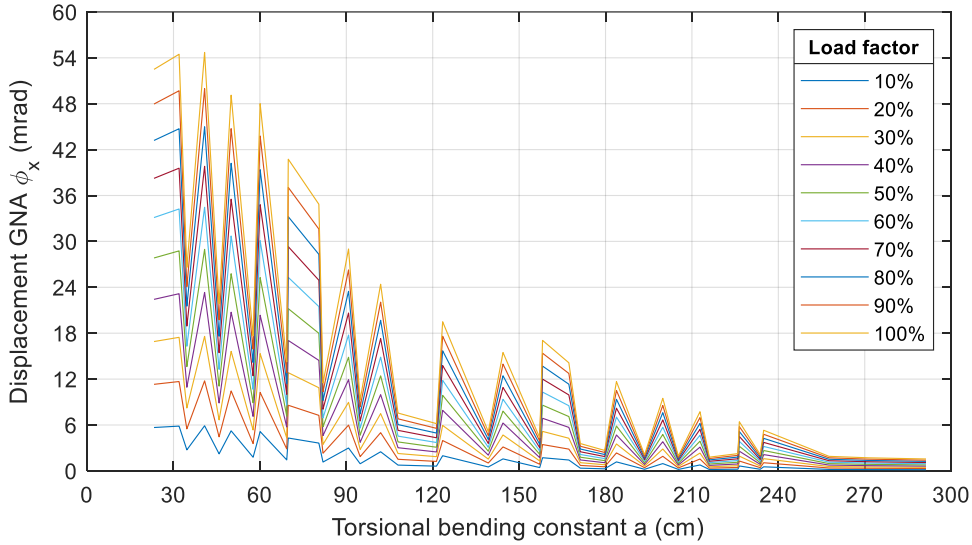

Figure A II.116 Displacement φ_x: fork-fixed system, M_y load, open profiles, and 1D elements

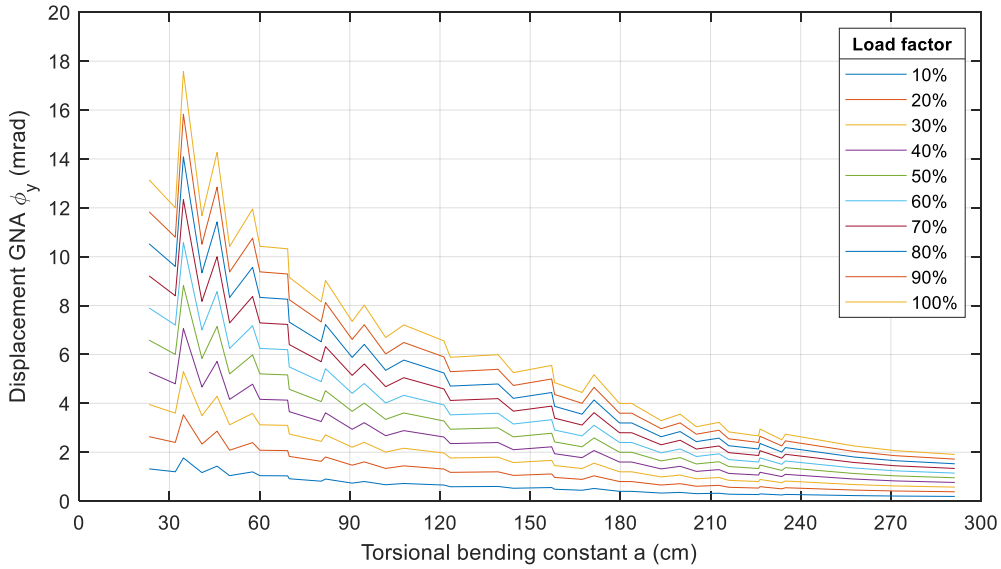

Figure A II.117 Displacement φ_y: fork-fixed system, M_y load, open profiles, and 1D elements

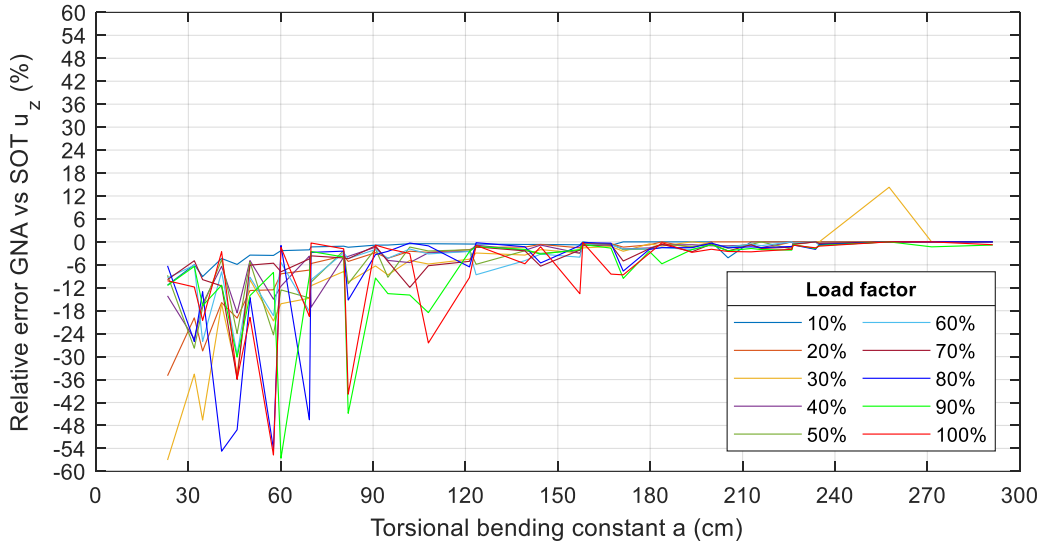

Figure A II.118 Relative error u_z: fork-fixed system, M_y load, open profiles, and 2D elements

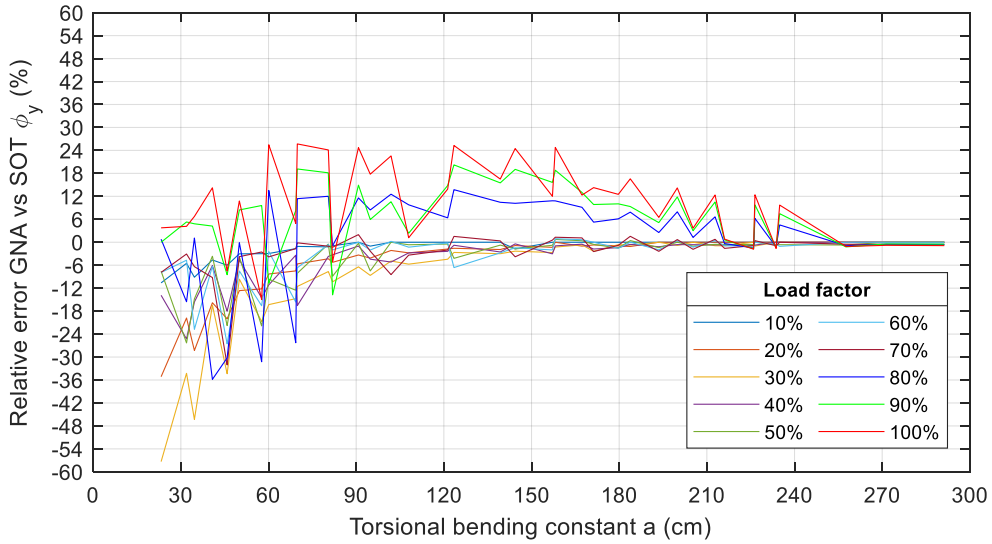

Figure A II.119 Relative error φ_y: fork-fixed system, M_y load, open profiles, and 2D elements

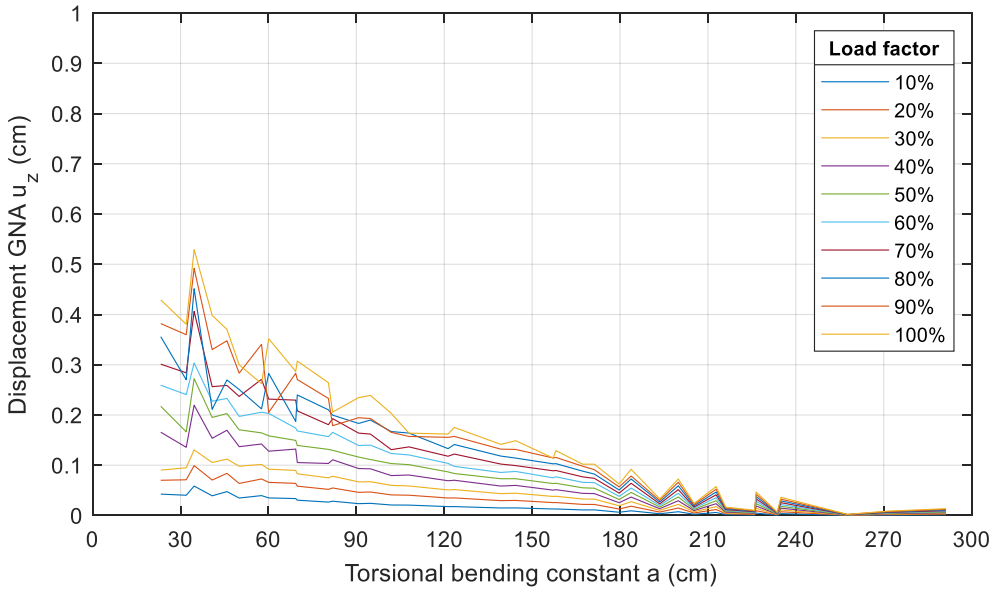

Figure A II.120 Displacement u_z: fork-fixed system, M_y load, open profiles, and 2D elements

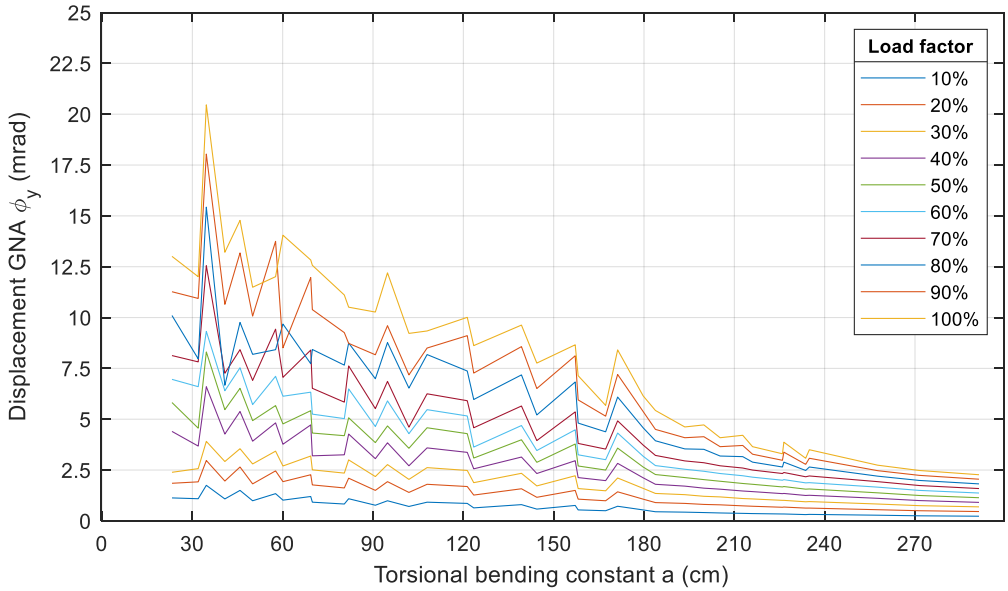

Figure A II.121 Displacement φ_y: fork-fixed system, M_y load, open profiles, and 2D elements

M_T

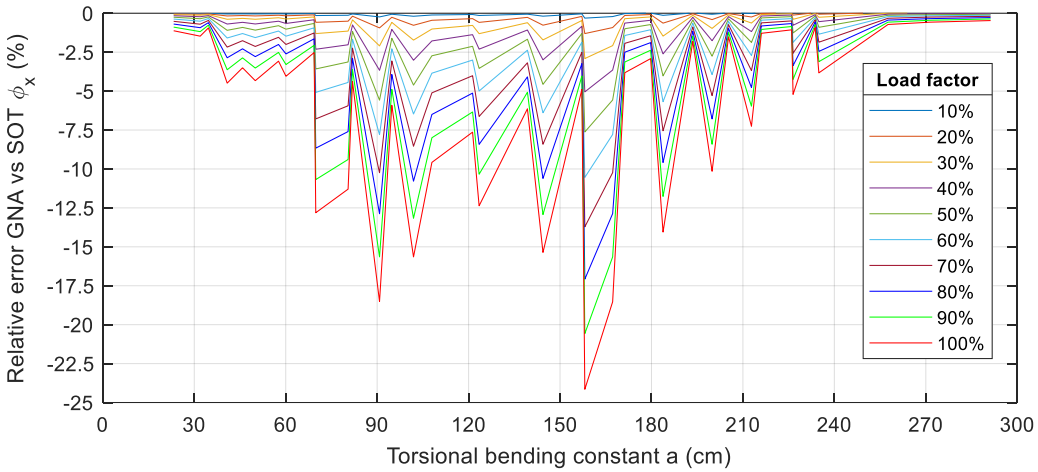

Figure A II.122 Relative error φ_x: fork-fixed system, M_T load, open profiles, and 1D elements

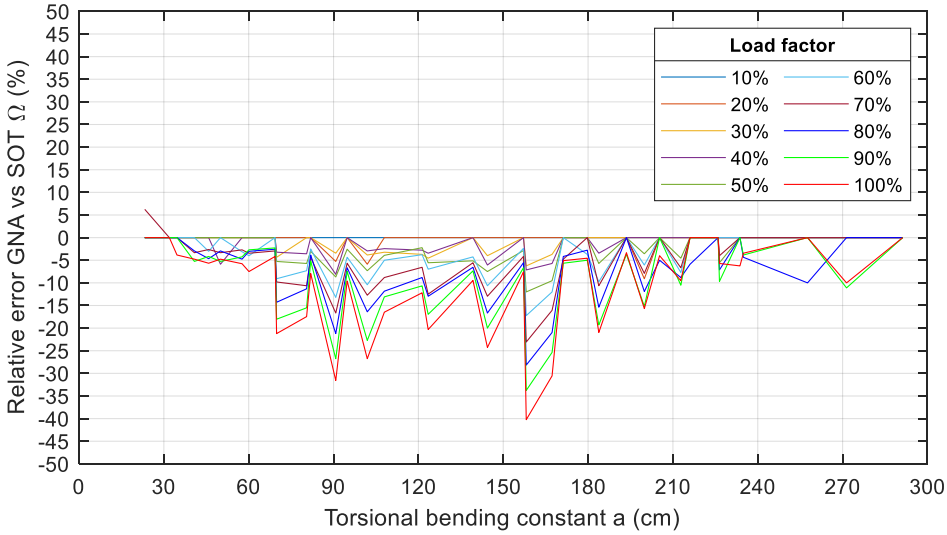

Figure A II.123 Relative error Ω: fork-fixed system, M_T load, open profiles, and 1D elements

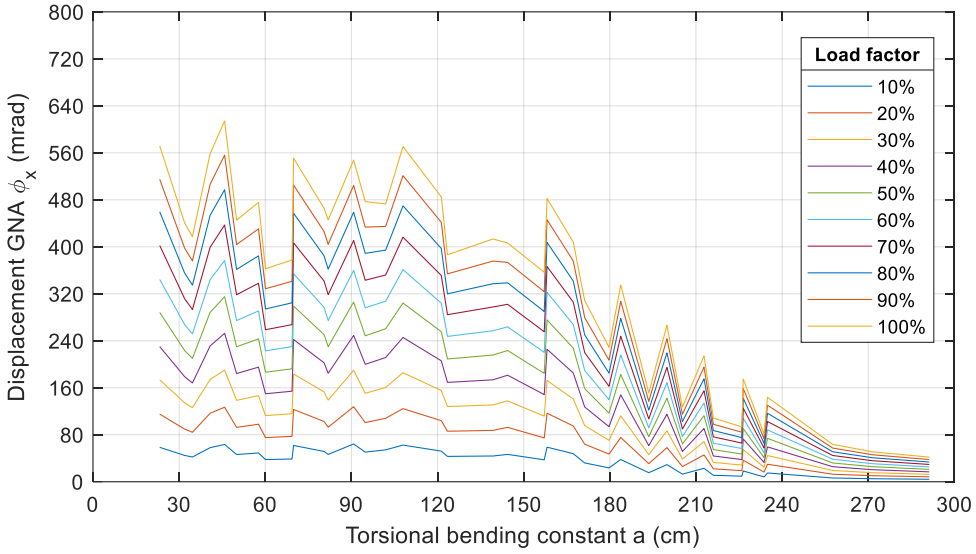

Figure A II.124 Displacement φ_x: fork-fixed system, M_T load, open profiles, and 1D elements

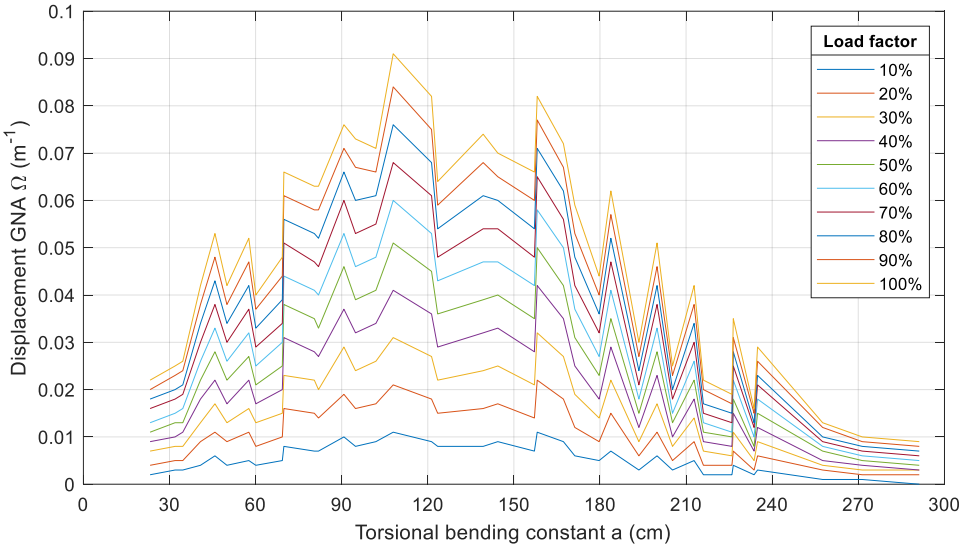

Figure A II.125 Displacement Ω: fork-fixed system, M_T load, open profiles, and 1D elements

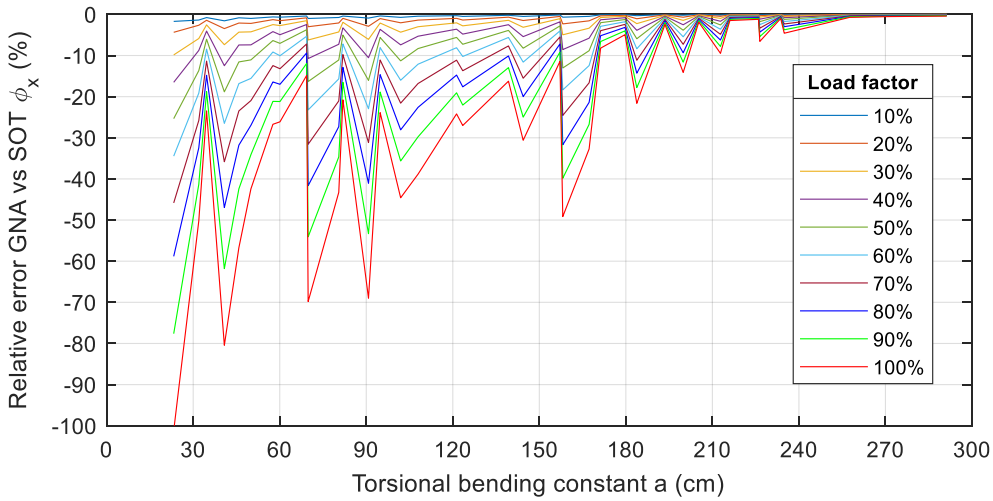

Figure A II.126 Relative error φ_x: fork-fixed system, M_T load, open profiles, and 2D elements

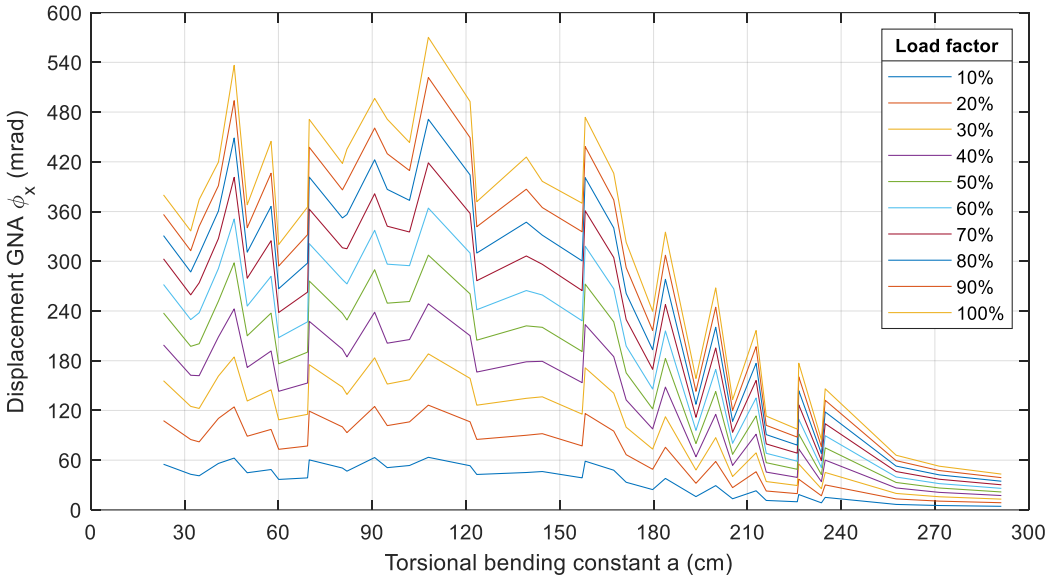

Figure A II.127 Displacement φ_x: fork-fixed system, M_T load, open profiles, and 2D elements

Appendix II-4.2 Closed cross-sections

V_z

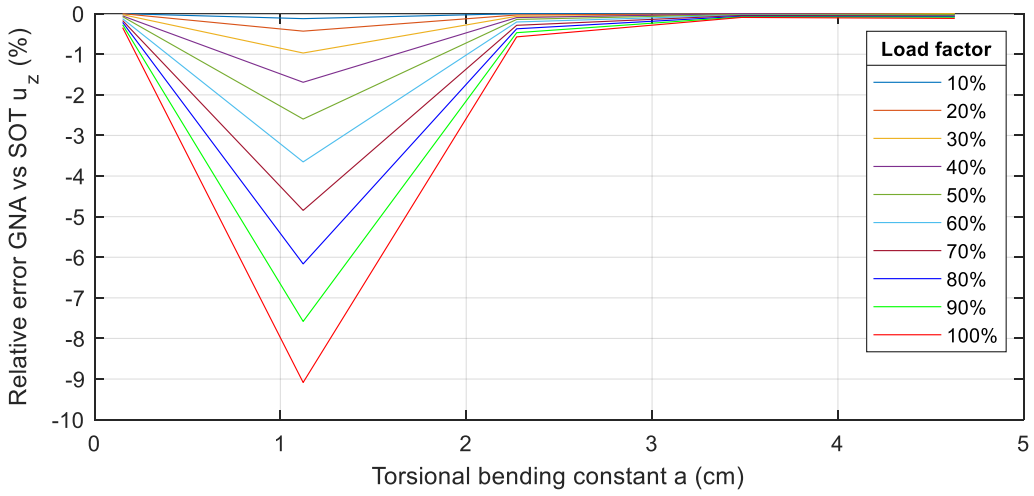

Figure A II.128 Relative error u_z: fork-fixed system, V_z load, closed profiles, and 1D elements

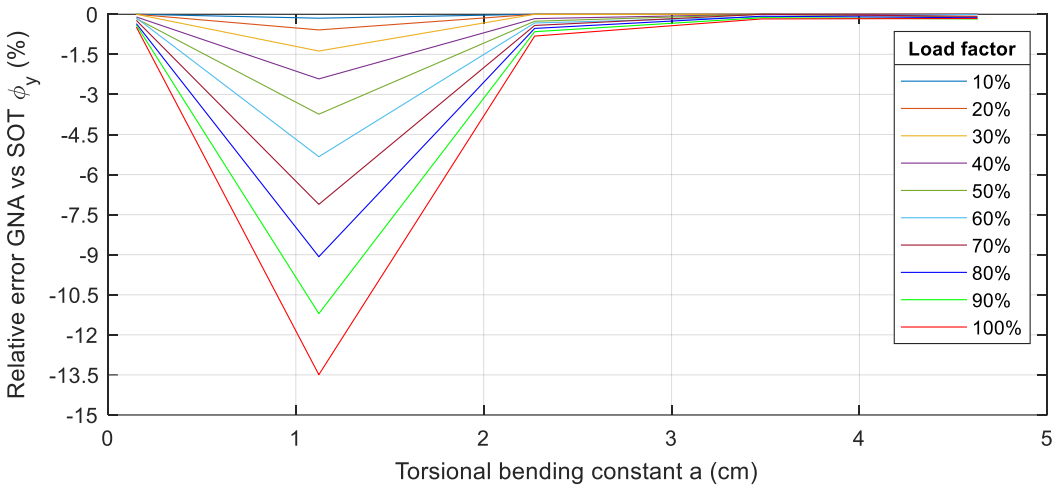

Figure A II.129 Relative error φ_y: fork-fixed system, V_z load, closed profiles, and 1D elements

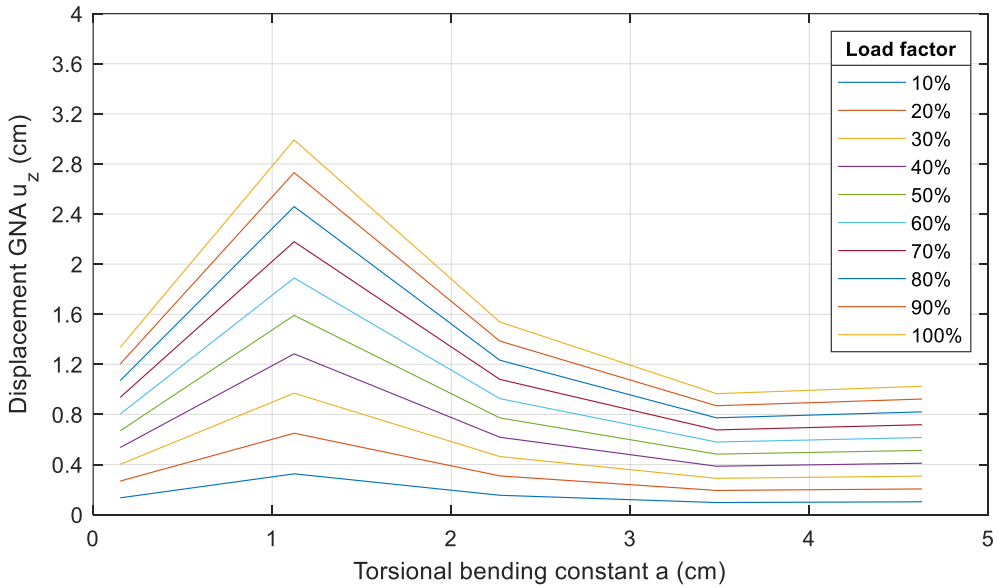

Figure A II.130 Displacement u_z: fork-fixed system, V_z load, closed profiles, and 1D elements

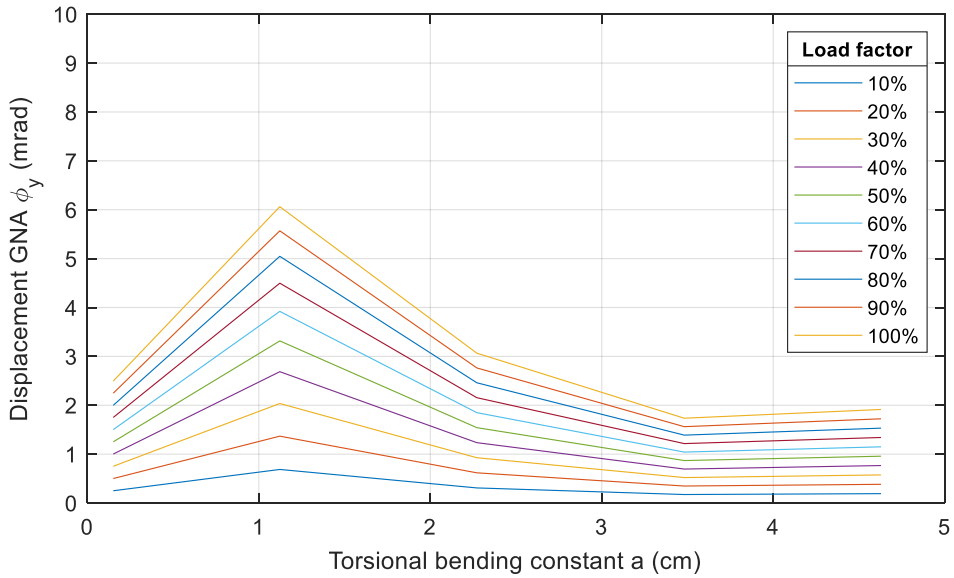

Figure A II.131 Displacement φ_y: fork-fixed system, V_z load, closed profiles, and 1D elements

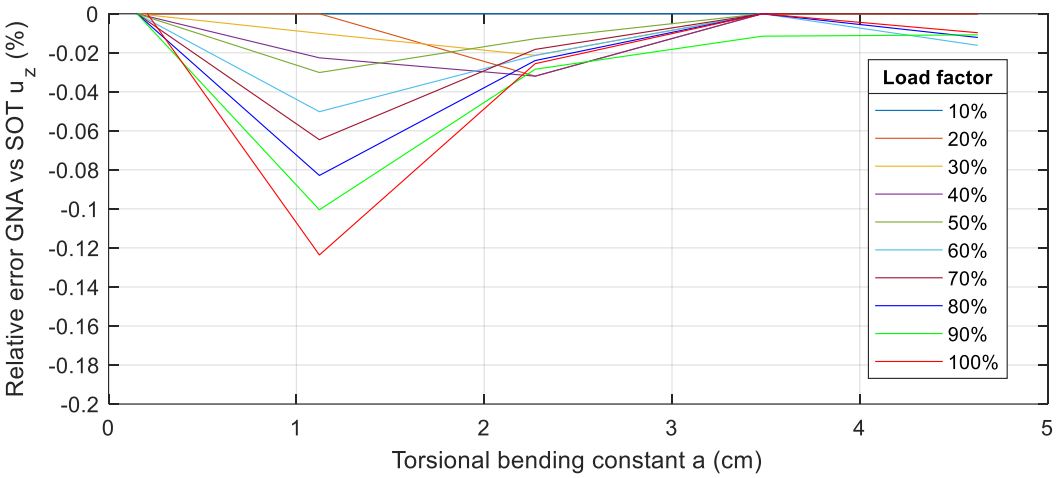

Figure A II.132 Relative error u_z: fork-fixed system, V_z load, closed profiles, and 2D elements

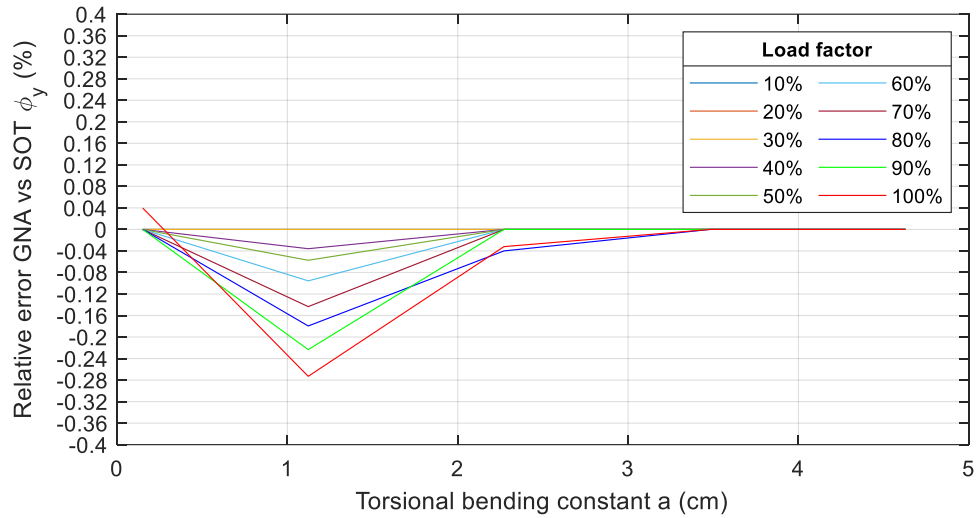

Figure A II.133 Relative error φ_y: fork-fixed system, V_z load, closed profiles, and 2D elements

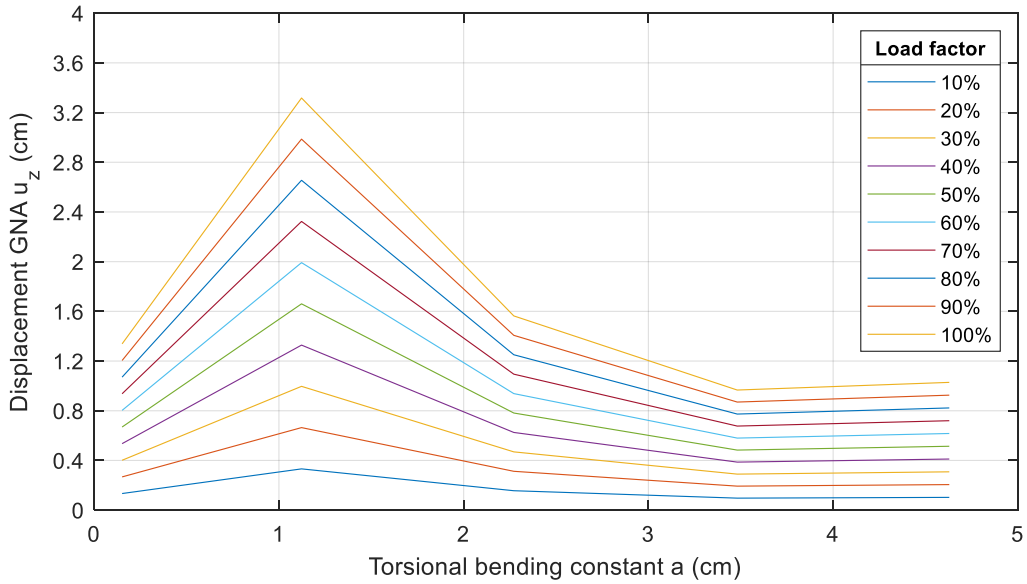

Figure A II.134 Displacement u_z: fork-fixed system, V_z load, closed profiles, and 2D elements

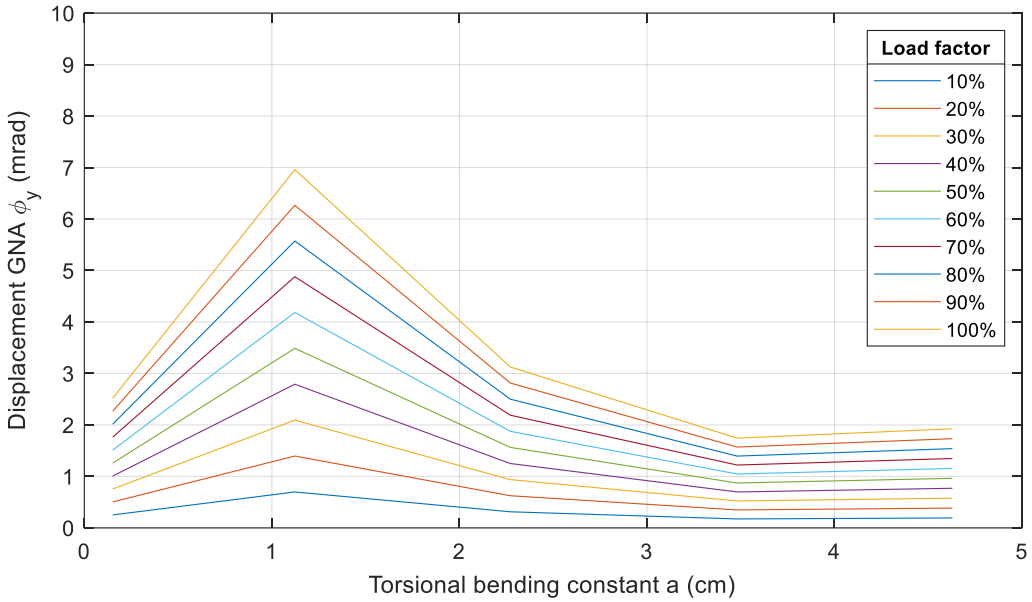

Figure A II.135 Displacement φ_y: fork-fixed system, V_z load, closed profiles, and 2D elements

M_y

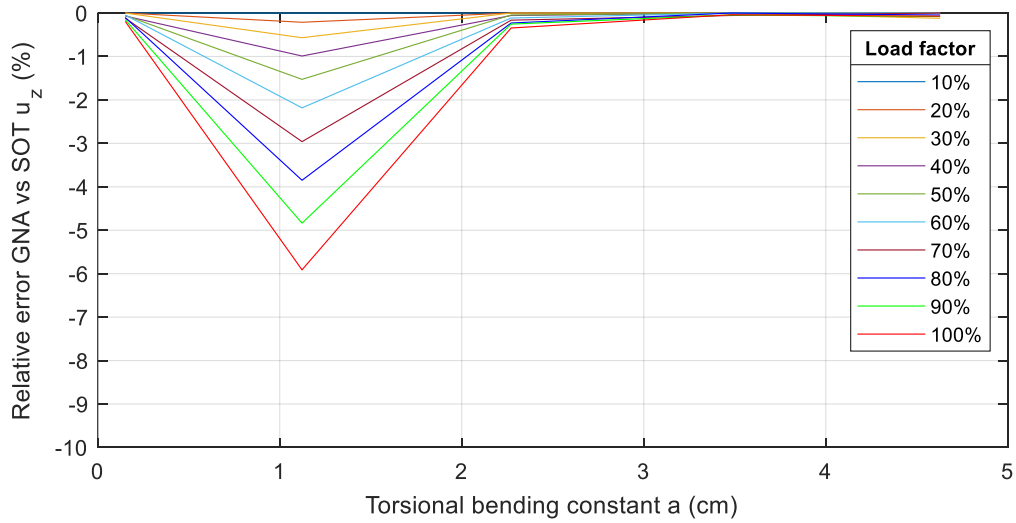

Figure A II.136 Relative error u_z: fork-fixed system, M_y load, closed profiles, and 1D elements

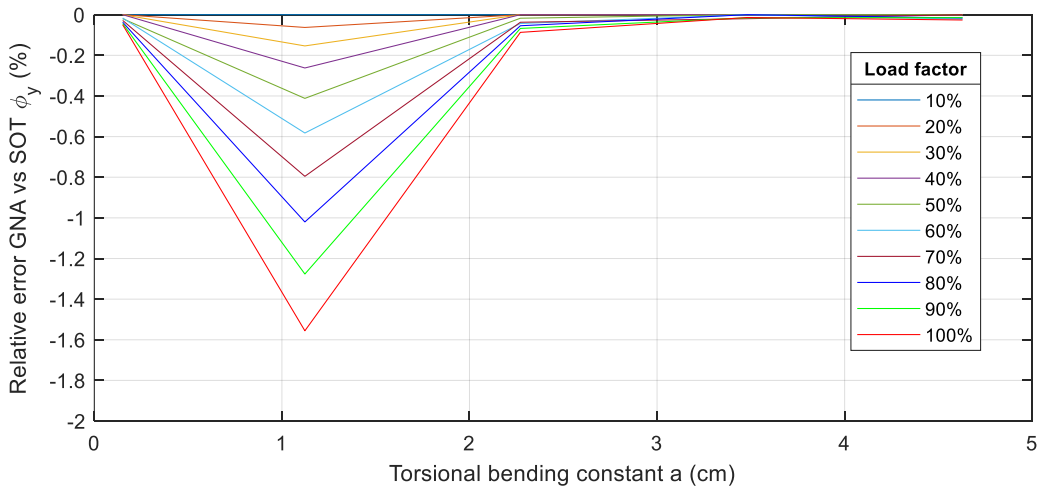

Figure A II.137 Relative error φ_y: fork-fixed system, M_y load, closed profiles, and 1D elements

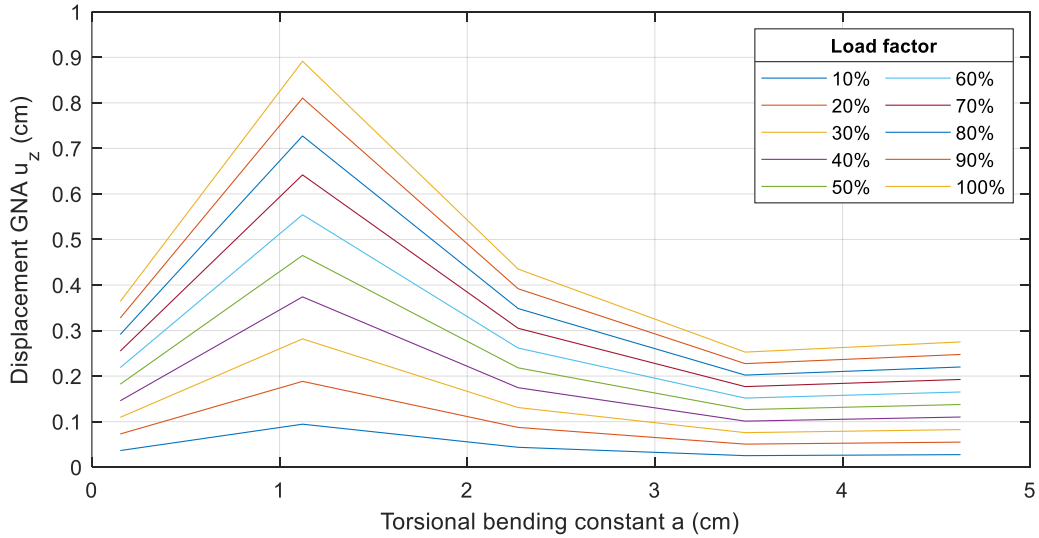

Figure A II.138 Displacement u_z: fork-fixed system, M_y load, closed profiles, and 1D elements

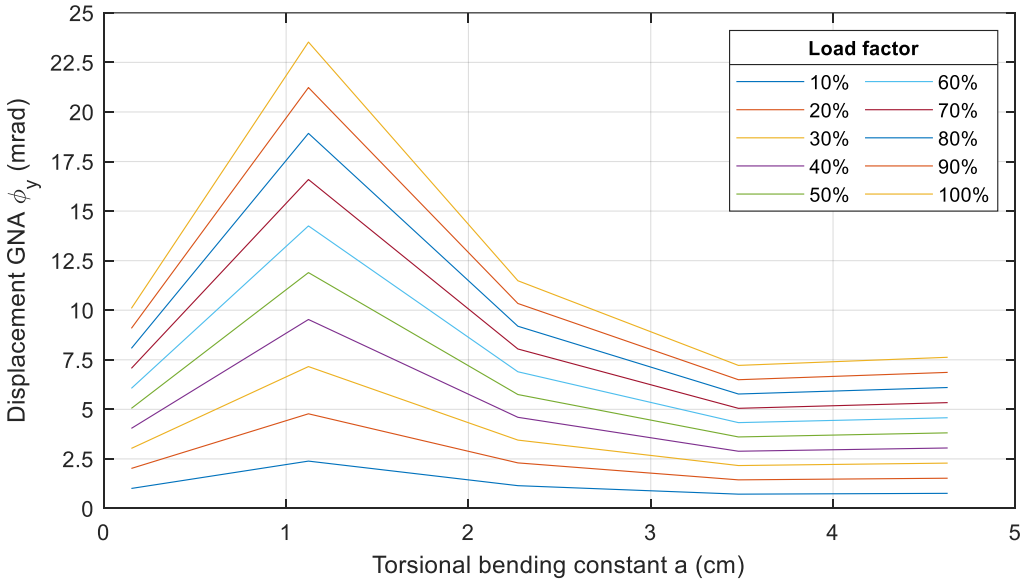

Figure A II.139 Displacement φ_y: fork-fixed system, M_y load, closed profiles, and 1D elements

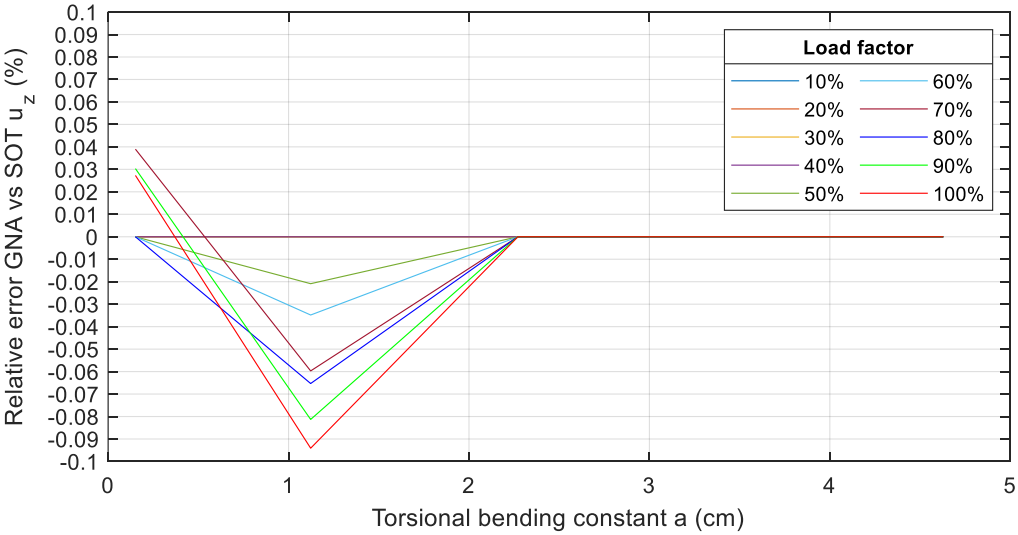

Figure A II.140 Relative error u_z: fork-fixed system, M_y load, closed profiles, and 2D elements

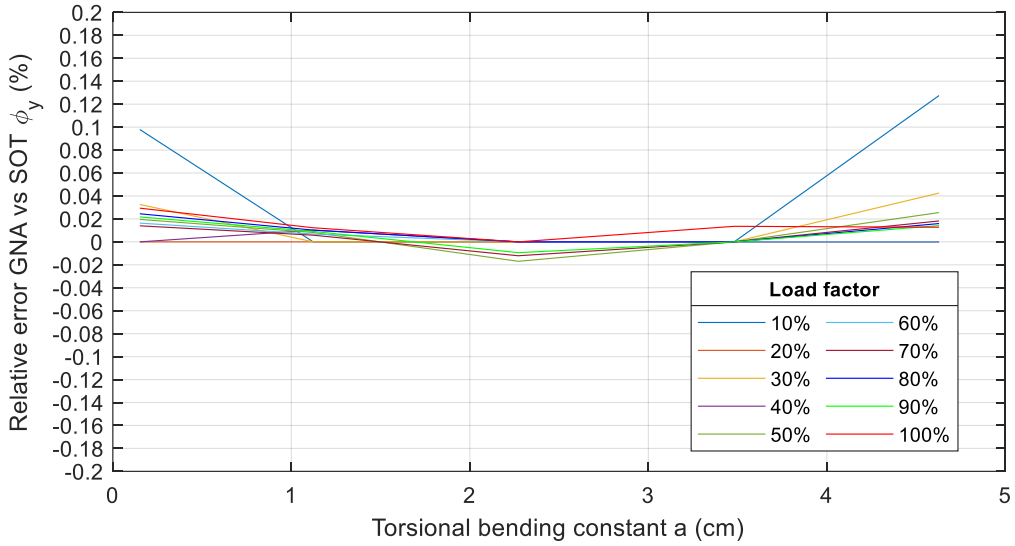

Figure A II.141 Relative error φ_y: fork-fixed system, M_y load, closed profiles, and 2D elements

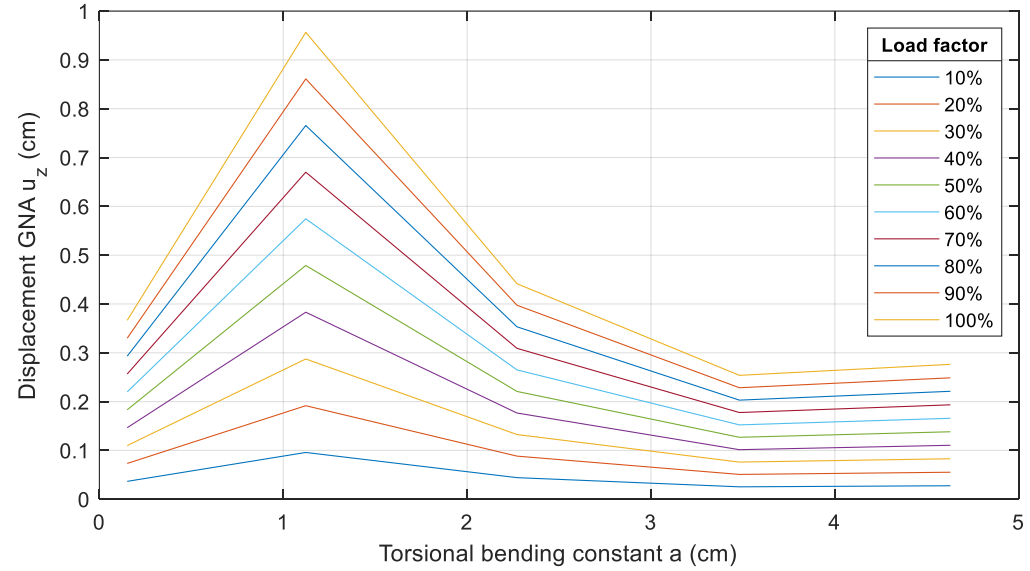

Figure A II.142 Displacement u_z: fork-fixed system, M_y load, closed profiles, and 2D elements

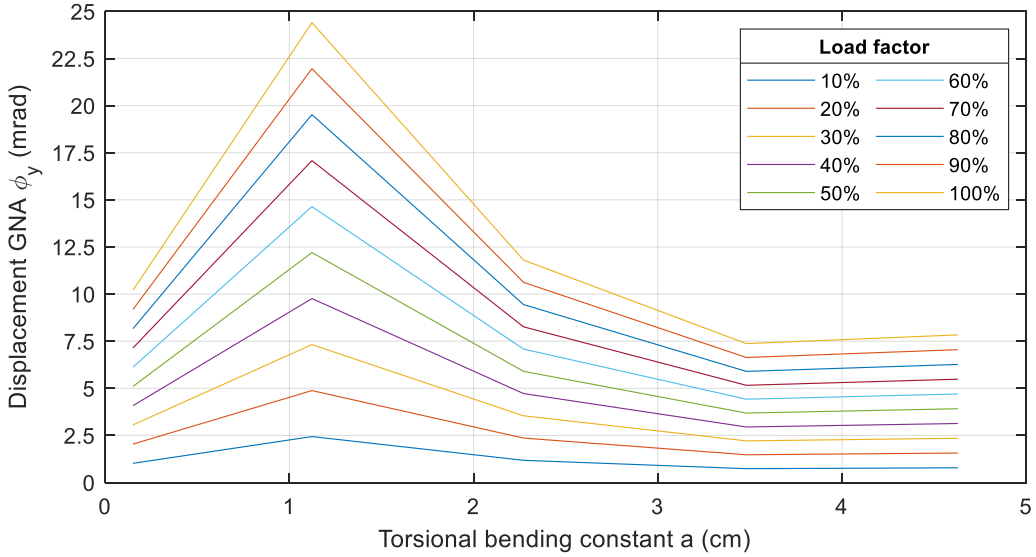

Figure A II.143 Displacement φ_y: fork-fixed system, M_y load, closed profiles, and 2D elements

M_T

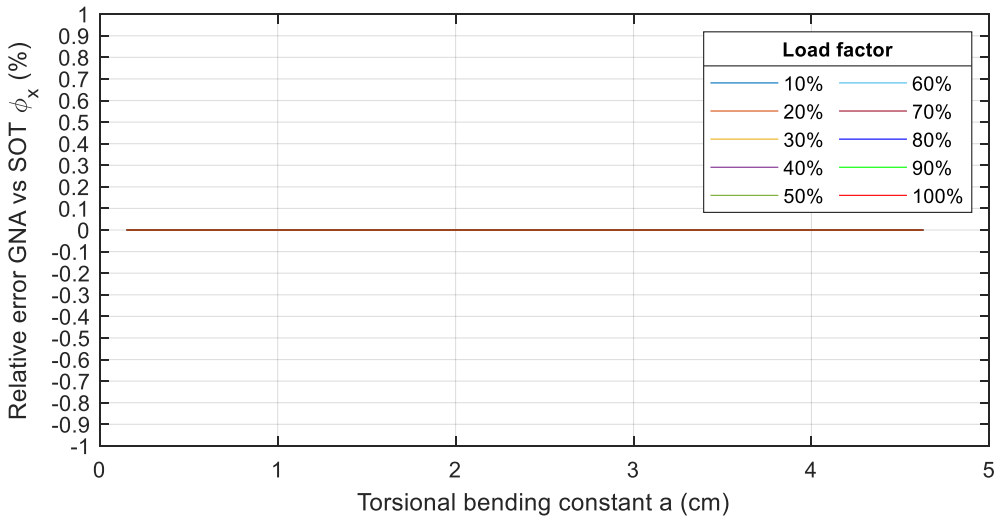

Figure A II.144 Relative error φ_x: fork-fixed system, M_T load, closed profiles, and 1D elements

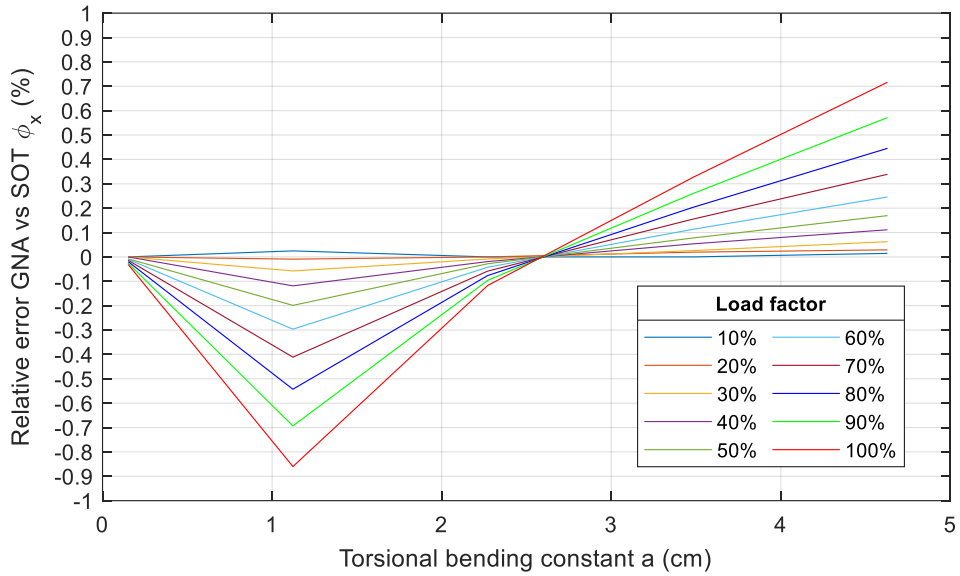

Figure A II.145 Displacement φ_x: fork-fixed system, M_T load, closed profiles, and 1D elements

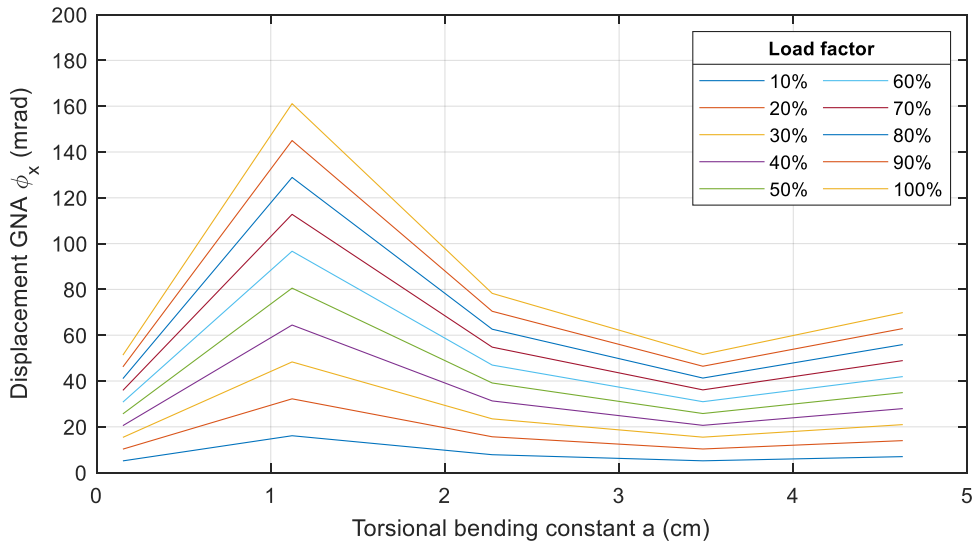

Figure A II.146 Relative error φ_x: fork-fixed system, M_T load, closed profiles, and 2D elements

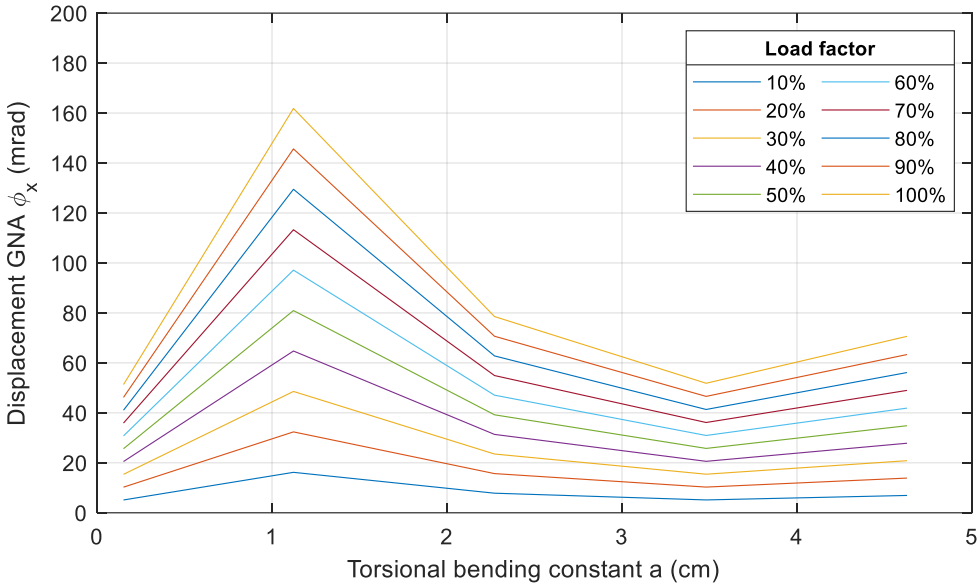

Figure A II.147 Displacement φ_x: fork-fixed system, M_T load, closed profiles, and 2D elements

Appendix III Internal forces results

In this appendix, all figures related to the main internal forces are presented. Both figures for relative errors and internal forces values for all structural systems, external loads, and profiles are shown.

Appendix III-1 Fixed-free system

Appendix III-1.1 Open cross-sections

V_z

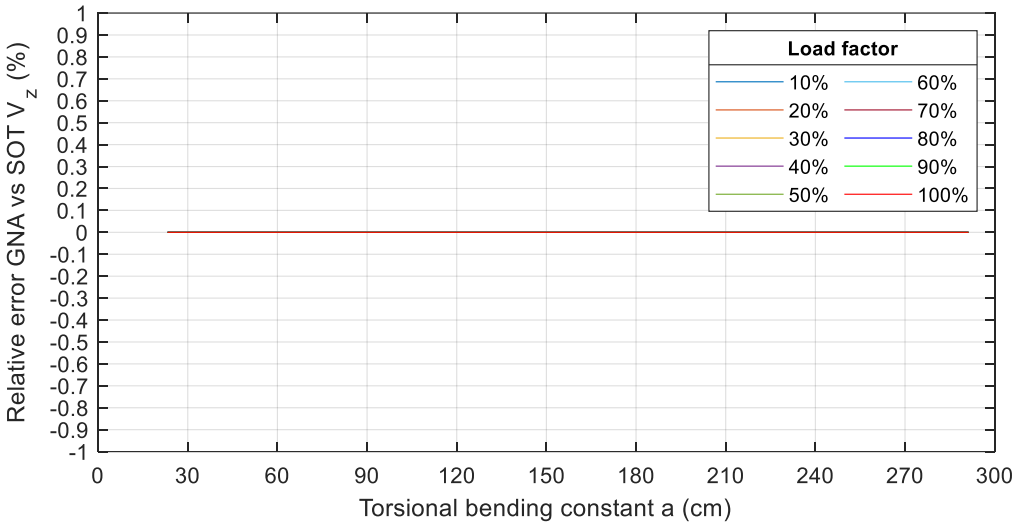

Figure A III.1 Relative error support V_z: fixed-free system, V_z load, open profiles

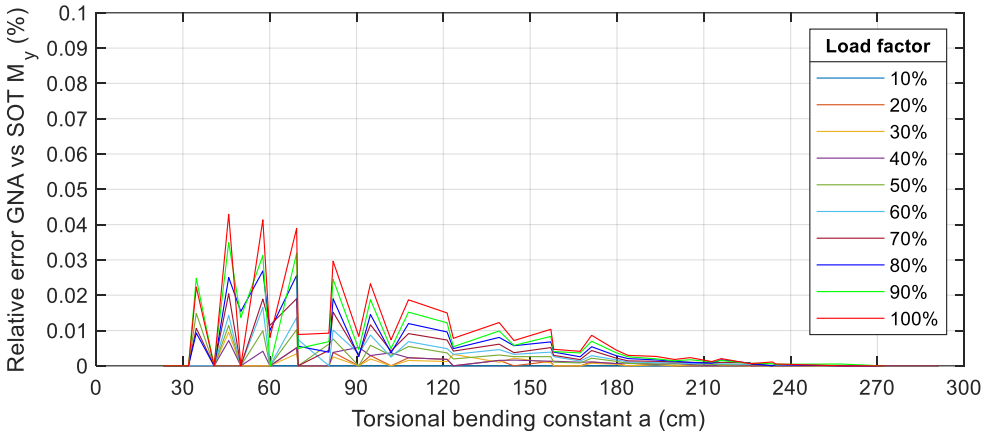

Figure A III.2 Relative error support M_y: fixed-free system, V_z load, open profiles

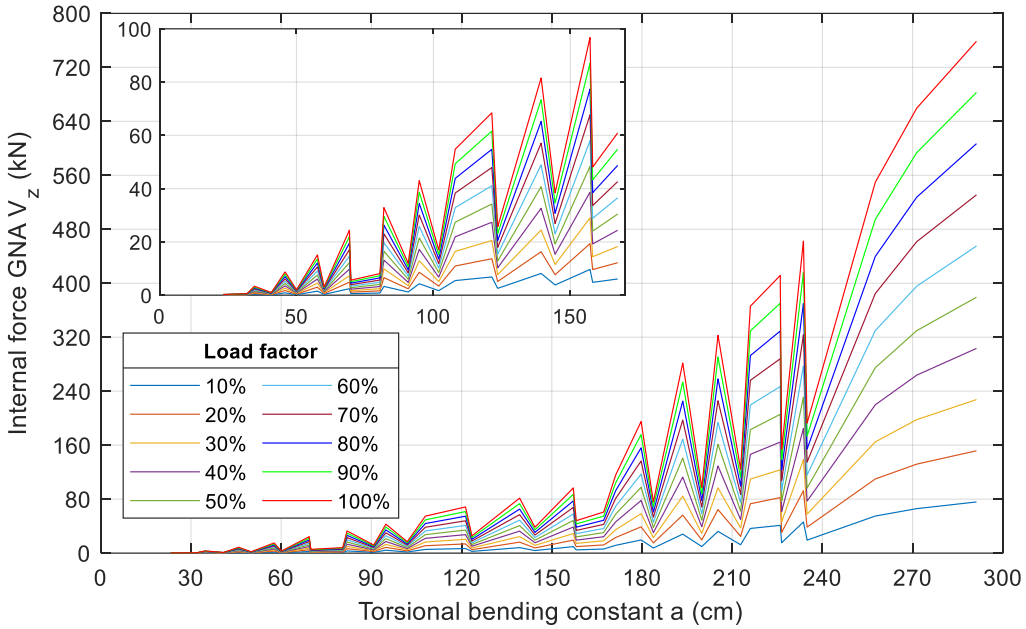

Figure A III.3 Internal force support V_z: fixed-free system, V_z load, open profiles / Inset of the graphic corresponds to values of a up to 170cm

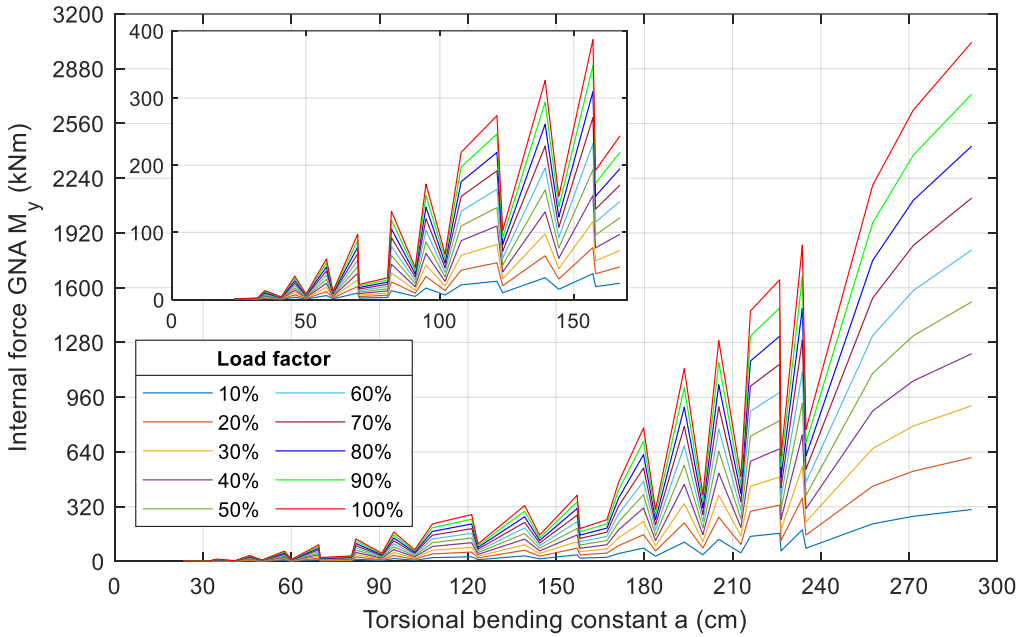

Figure A III.4 Internal force support M_y: fixed-free system, V_z load, open profiles / Inset of the graphic corresponds to values of a up to 170cm

M_y

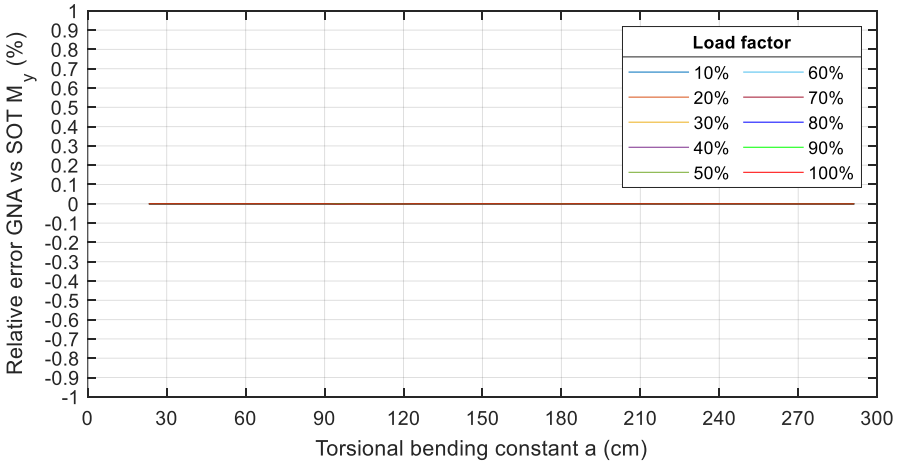

Figure A III.5 Relative error support M_y: fixed-free system, M_y load, open profiles

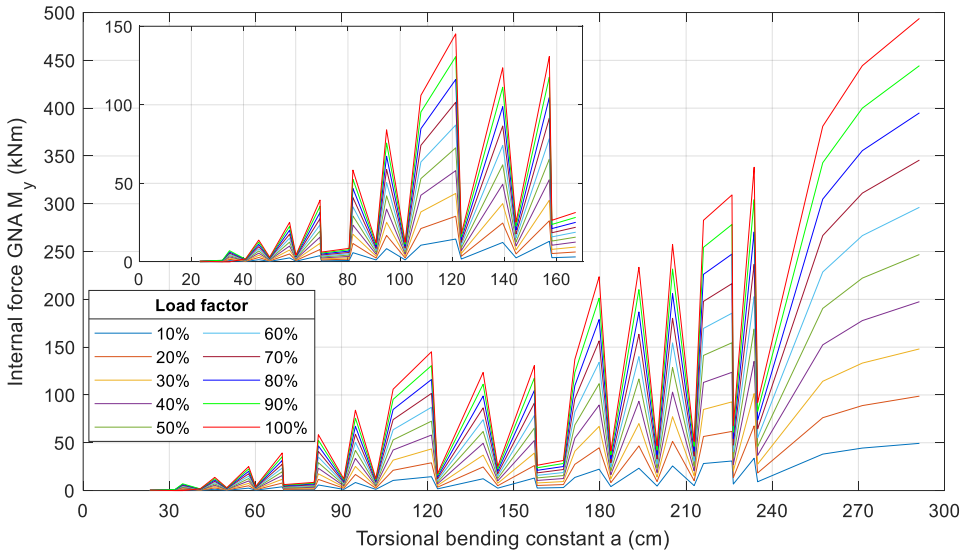

Figure A III.6 Internal force support M_y: fixed-free system, M_y load, open profiles / Inset of the graphic corresponds to values of a up to 170cm

M_T

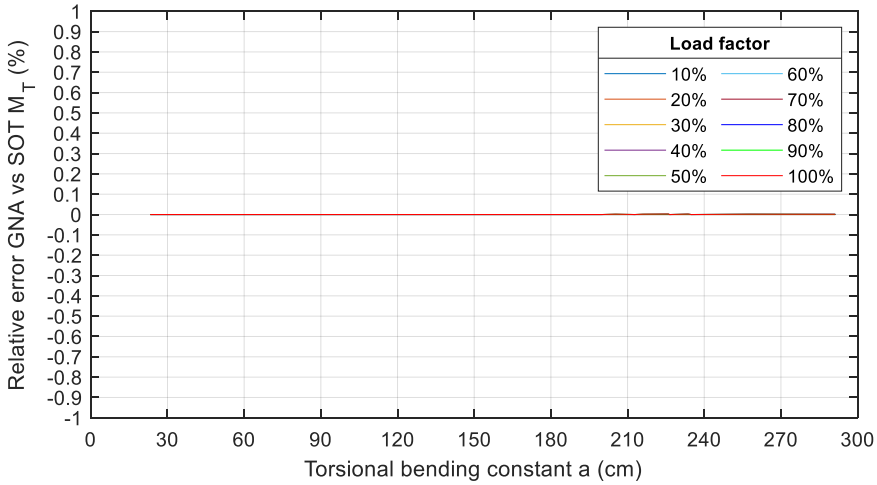

Figure A III.7 Relative error support M_T: fixed-free system, M_T load, open profiles

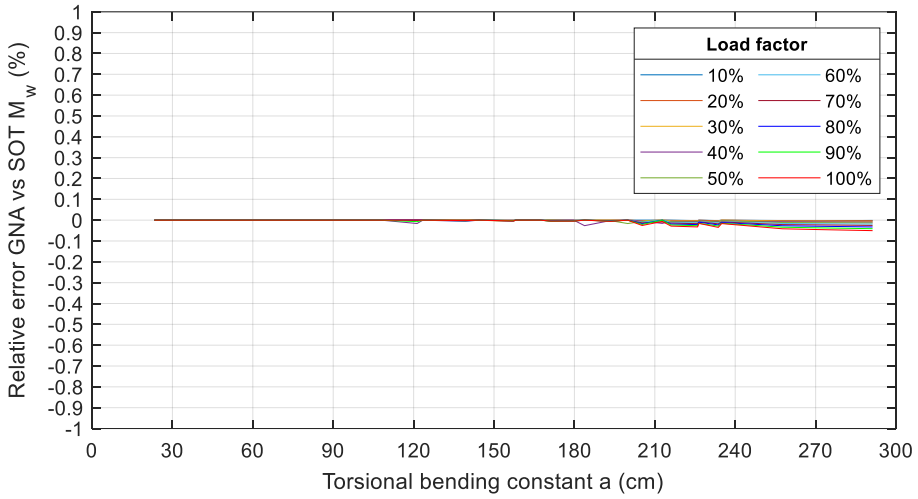

Figure A III.8 Relative error support M_w: fixed-free system, M_T load, open profiles

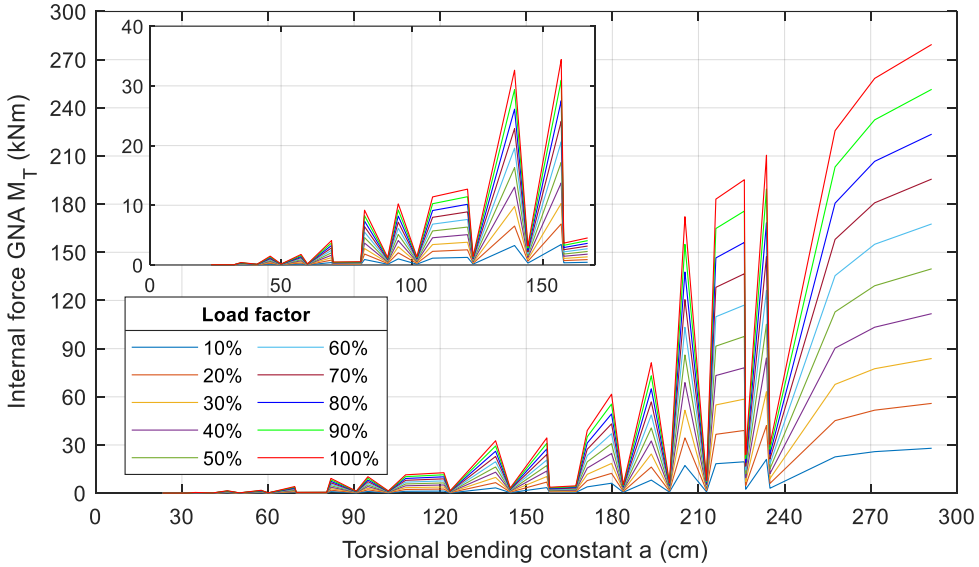

Figure A III.9 Internal force support M_T: fixed-free system, M_T load, open profiles / Inset of the graphic corresponds to values of a up to 170cm

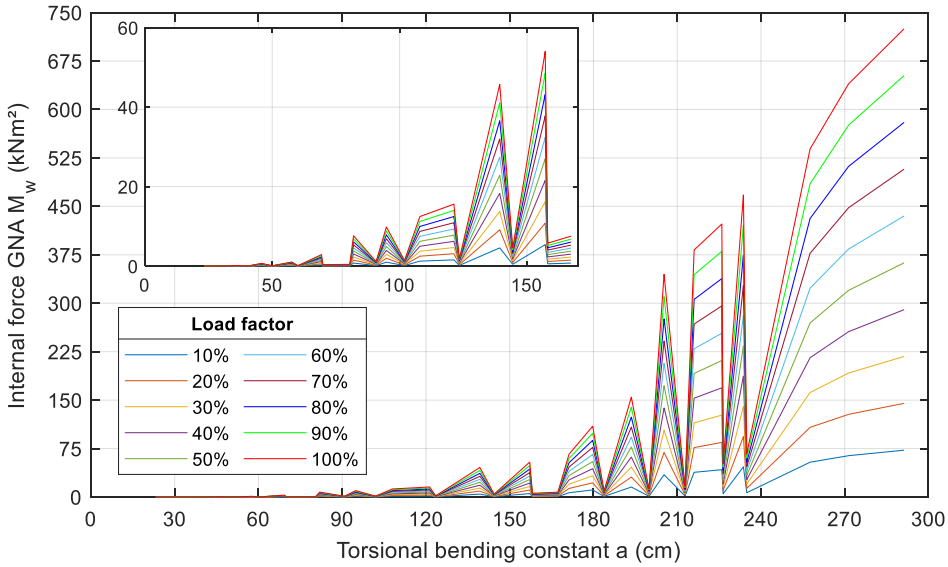

Figure A III.10 Internal force support M_w: fixed-free system, M_T load, open profiles / Inset of the graphic corresponds to values of a up to 170cm

Appendix III-1.2 Closed cross-sections

V_z

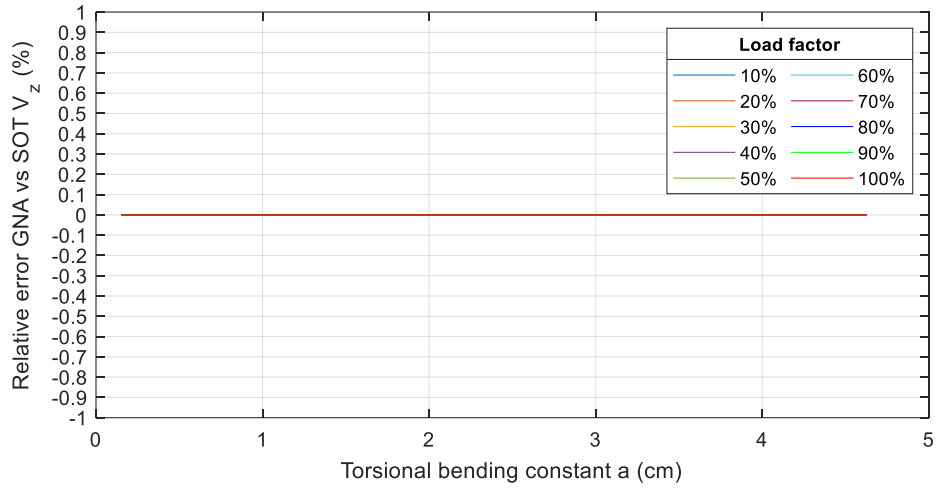

Figure A III.11 Relative error support V_z: fixed-free system, V_z load, closed profiles

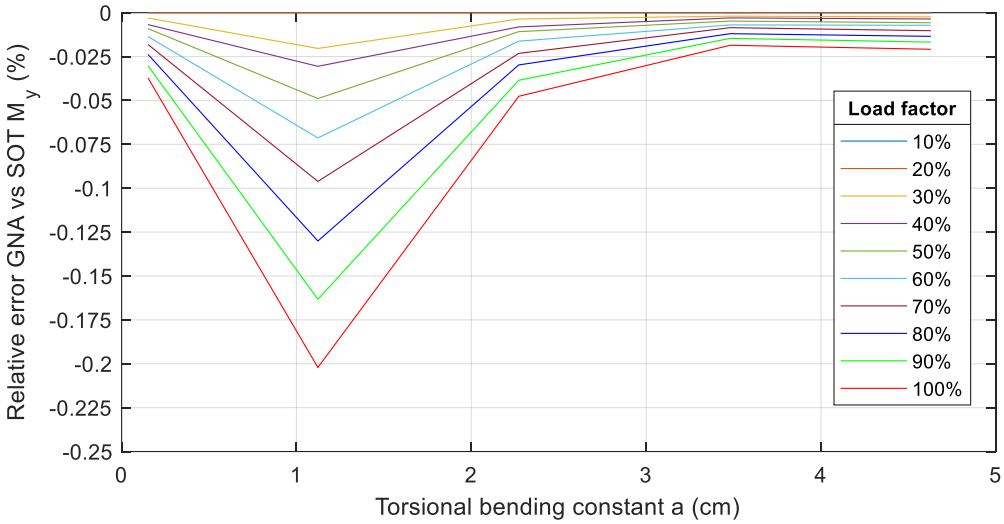

Figure A III.12 Relative error support M_y: fixed-free system, V_z load, closed profiles

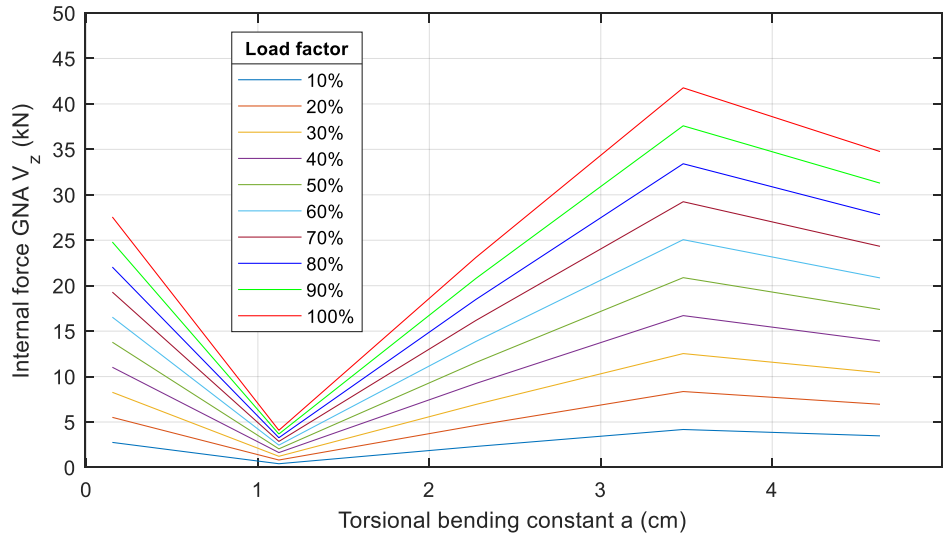

Figure A III.13 Internal force support V_z: fixed-free system, V_z load, closed profiles

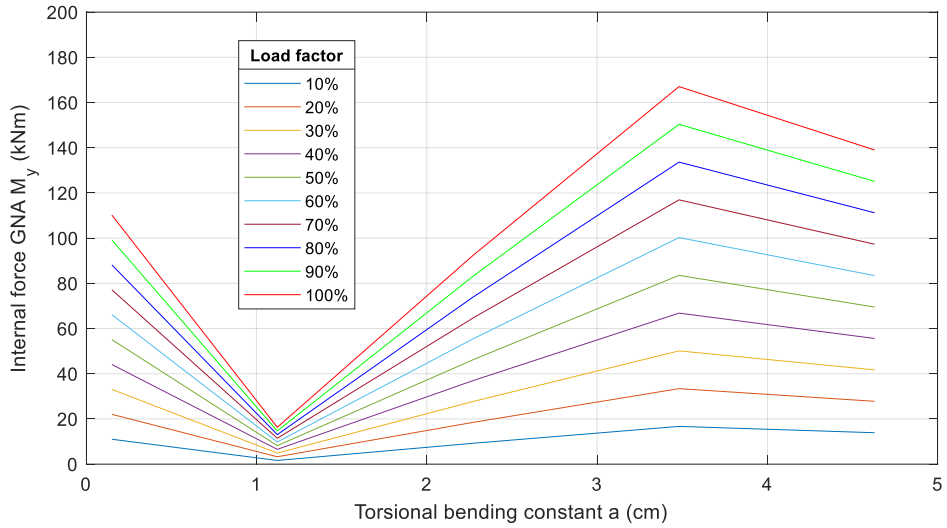

Figure A III.14 Internal force support M_y: fixed-free system, V_z load, closed profiles

M_y

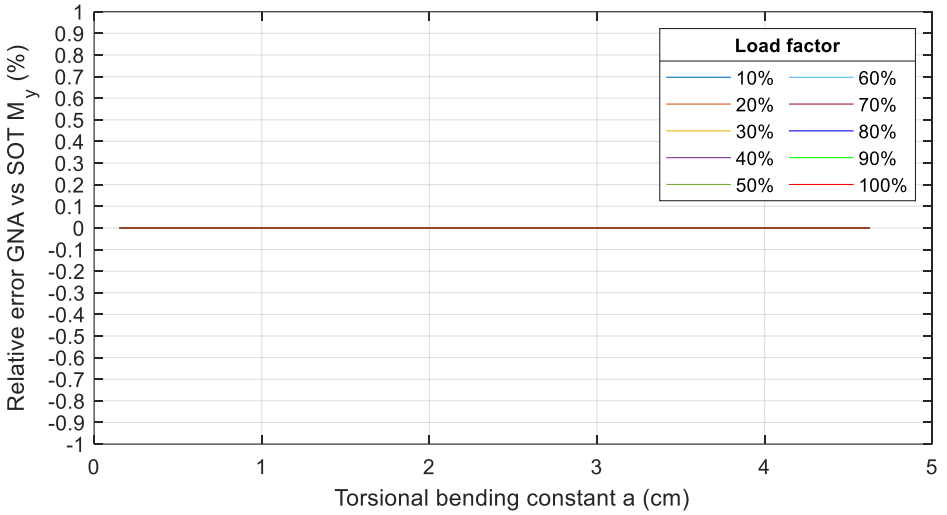

Figure A III.15 Relative error support M_y: fixed-free system, M_y load, closed profiles

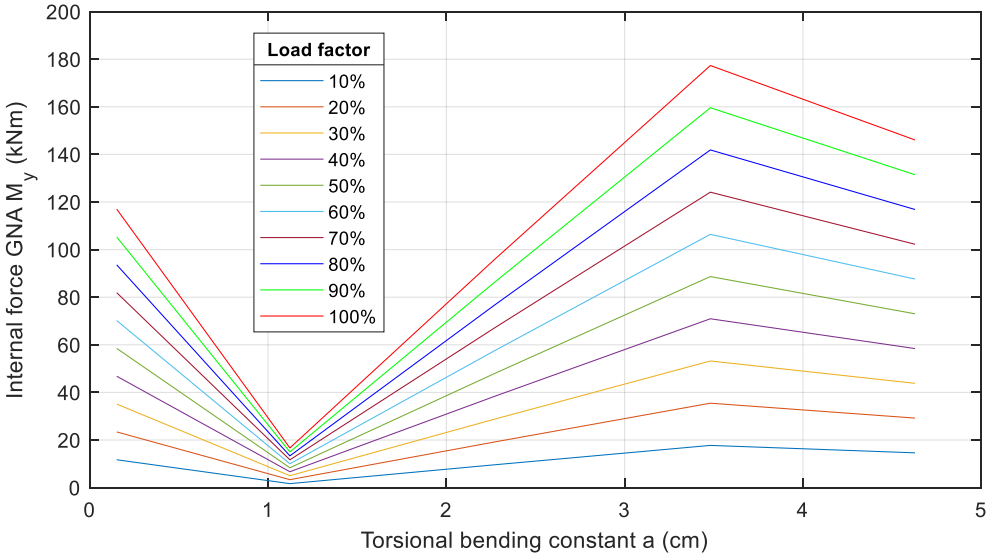

Figure A III.16 Internal force support M_y: fixed-free system, M_y load, closed profiles

M_T

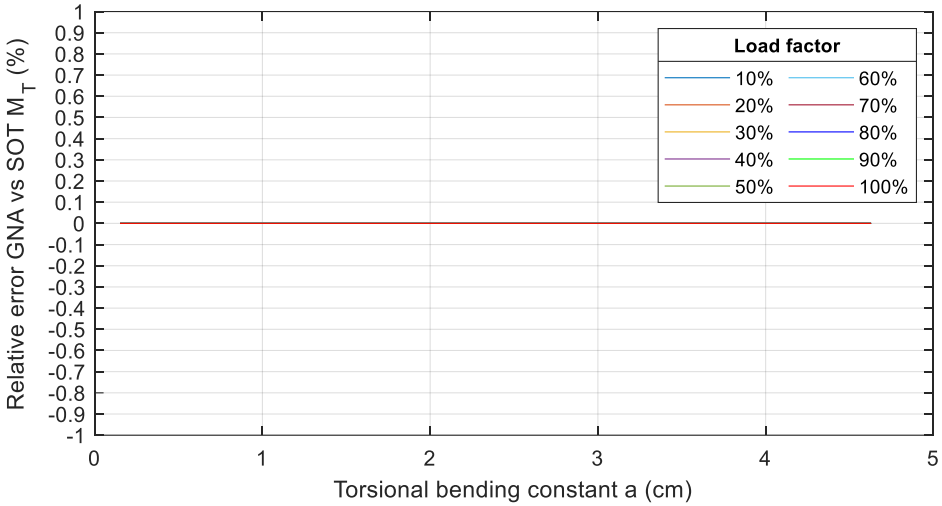

Figure A III.17 Relative error support M_T: fixed-free system, M_T load, closed profiles

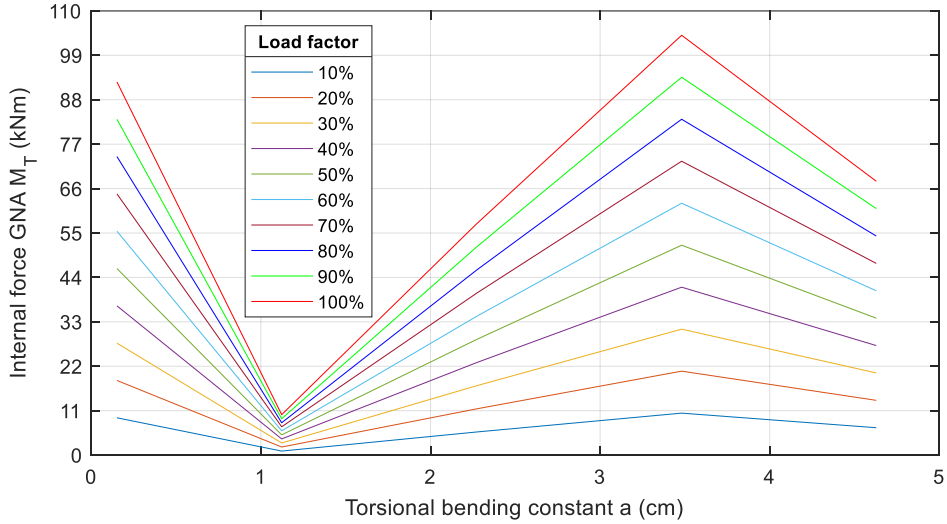

Figure A III.18 Internal force support M_T: fixed-free system, M_T load, closed profiles

Appendix III-2 Fork-fork system

Appendix III-2.1 Open cross-sections

V_z

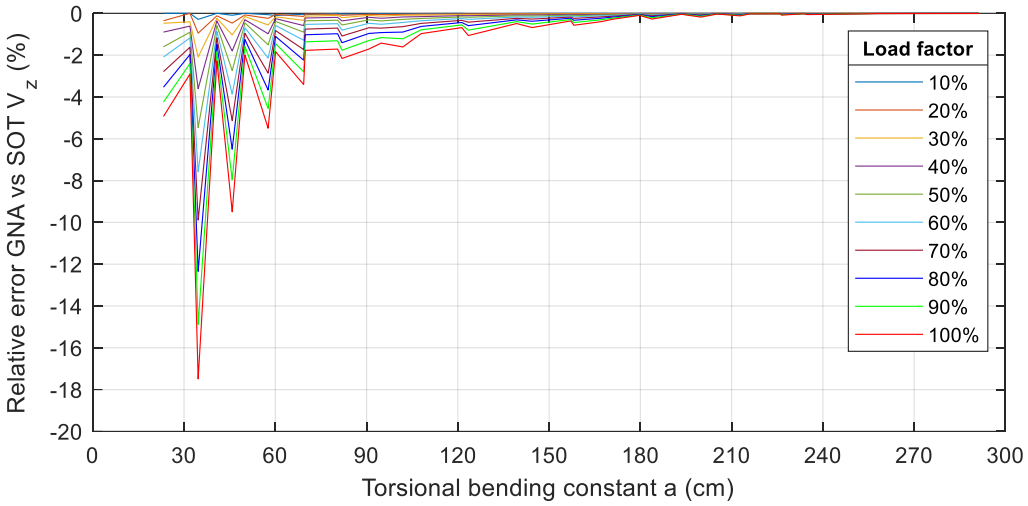

Figure A III.19 Relative error support V_z: fork-fork system, V_z load, open profiles

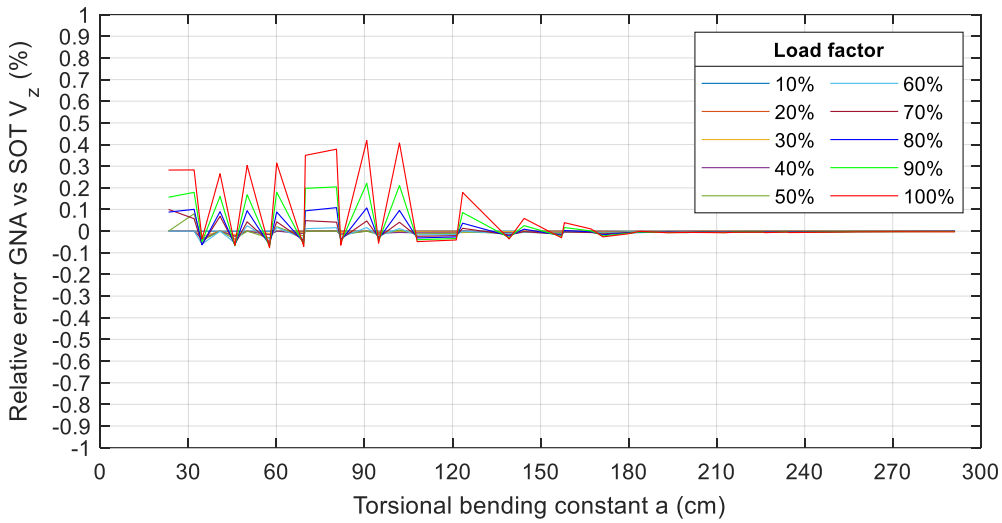

Figure A III.20 Relative error midspan V_z: fork-fork system, V_z load, open profiles

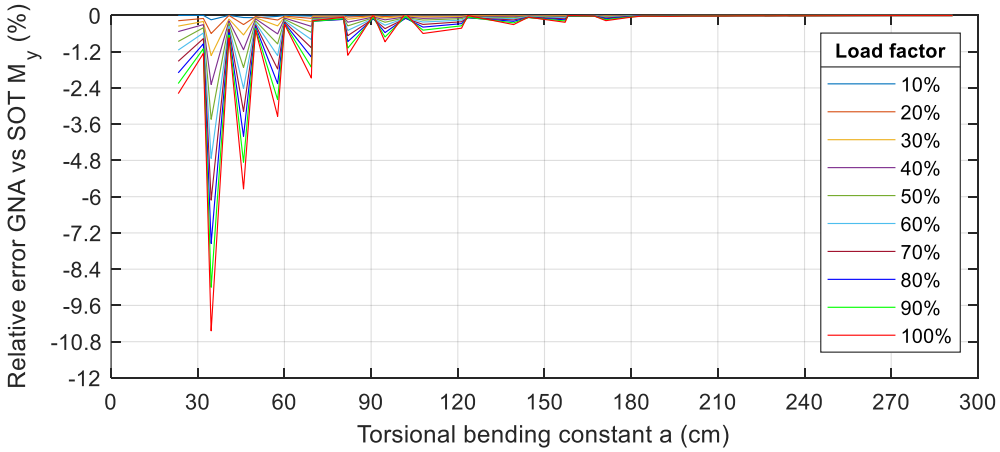

Figure A III.21 Relative error midspan M_y: fork-fork system, V_z load, open profiles

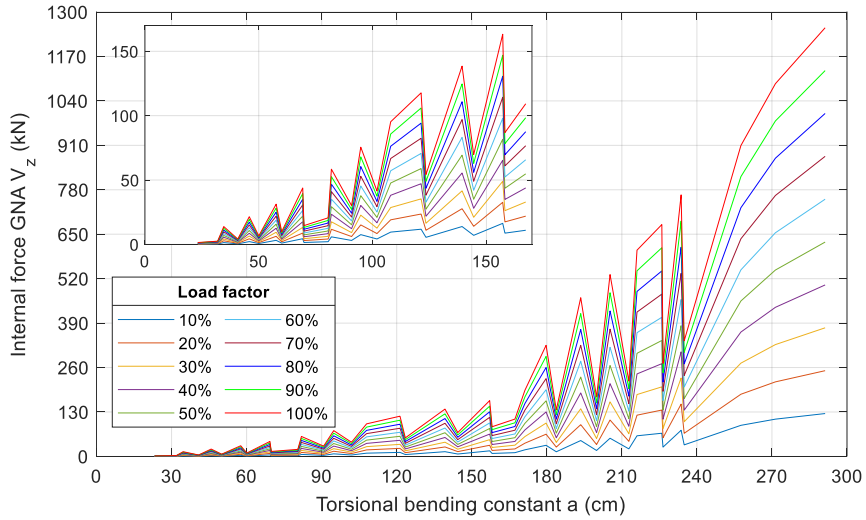

Figure A III.22 Internal force V_z: fork-fork system, V_z load, open profiles / Inset of the graphic corresponds to values of a up to 170cm

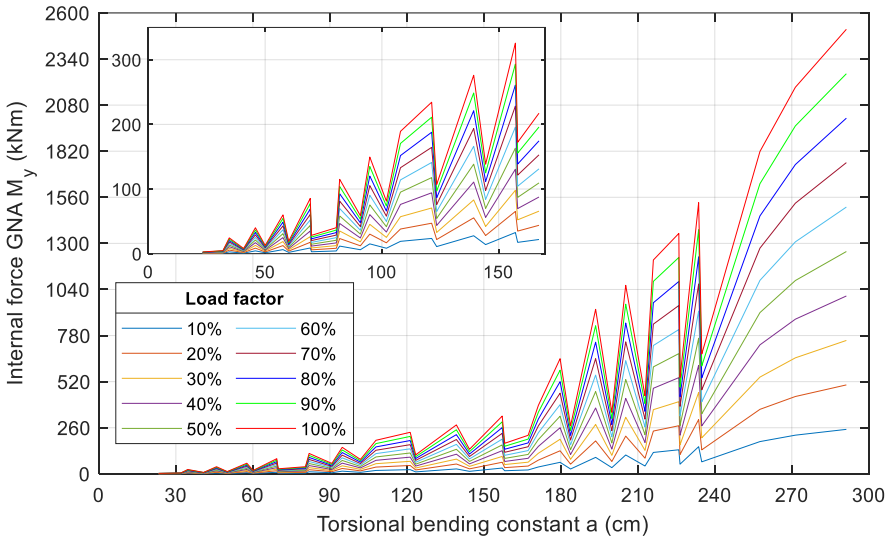

Figure A III.23 Internal force midspan M_y: fork-fork system, V_z load, open profiles / Inset of the graphic corresponds to values of a up to 170cm

M_y

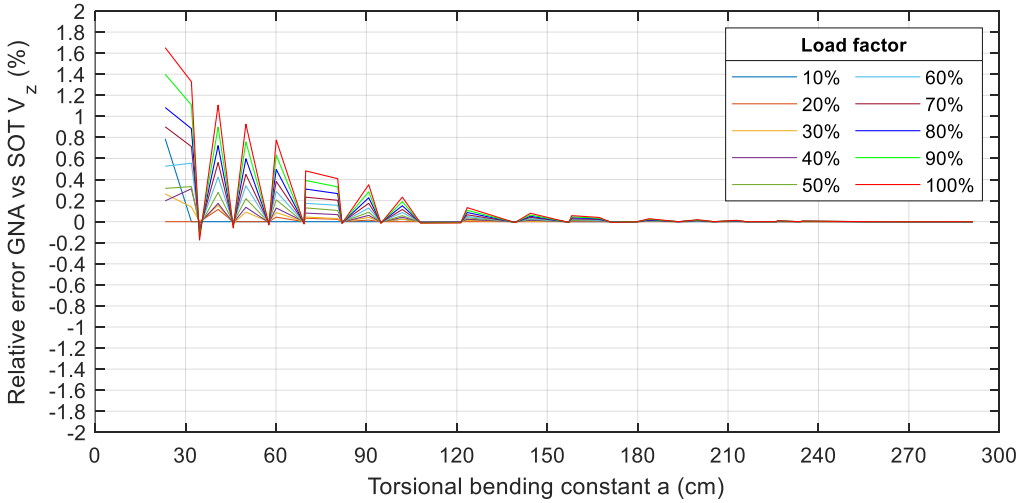

Figure A III.24 Relative error support V_z: fork-fork system, M_y load, open profiles

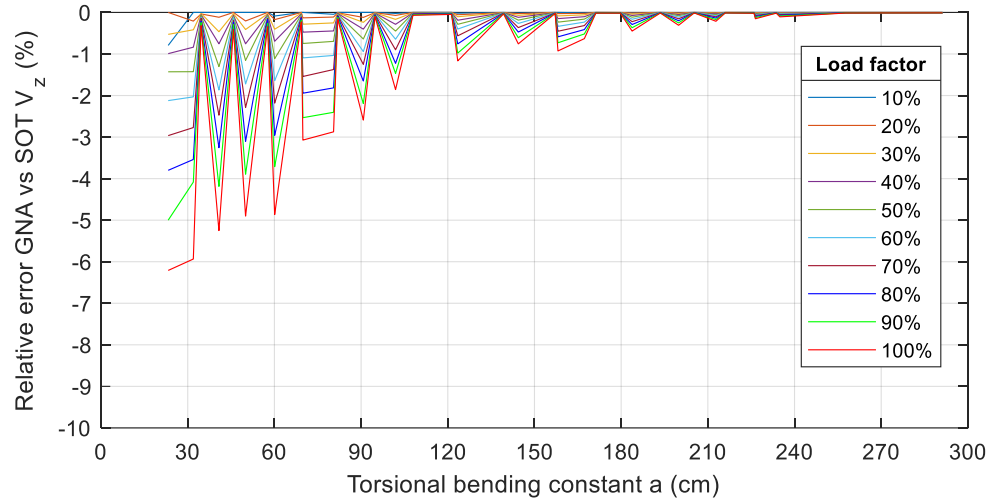

Figure A III.25 Relative error midspan V_z: fork-fork system, M_y load, open profiles

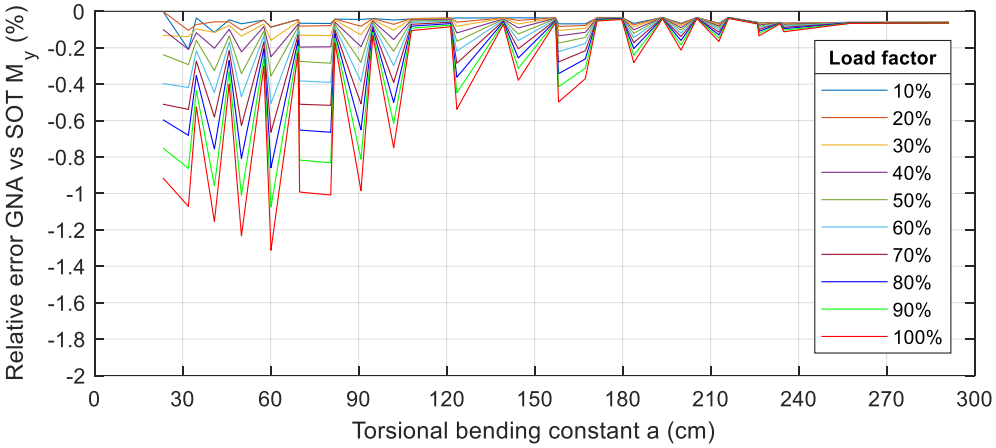

Figure A III.26 Relative error midspan M_y: fork-fork system, M_y load, open profiles

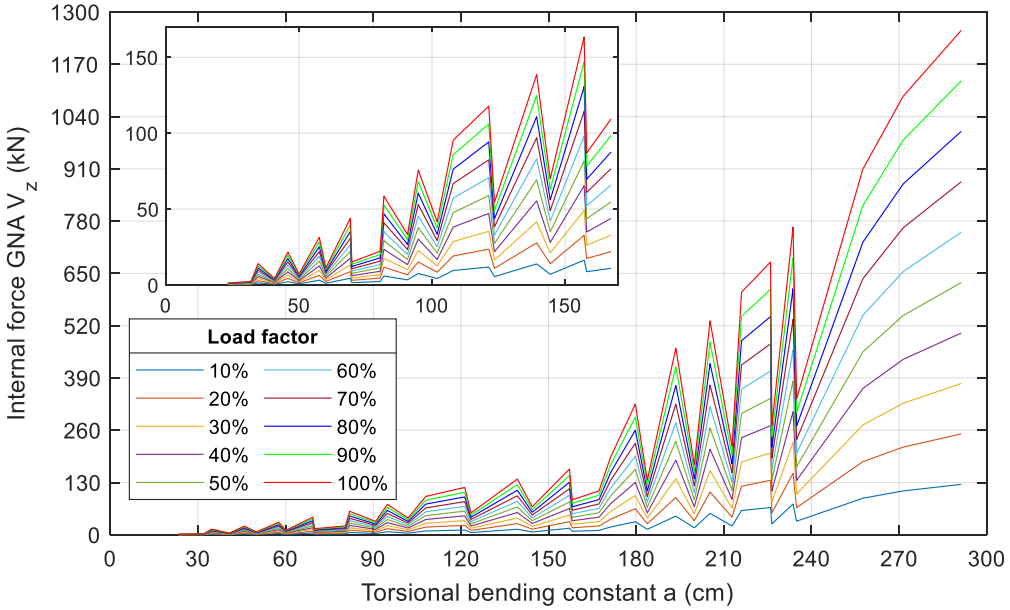

Figure A III.27 Internal force V_z: fork-fork system, M_y load, open profiles / Inset of the graphic corresponds to values of a up to 170cm

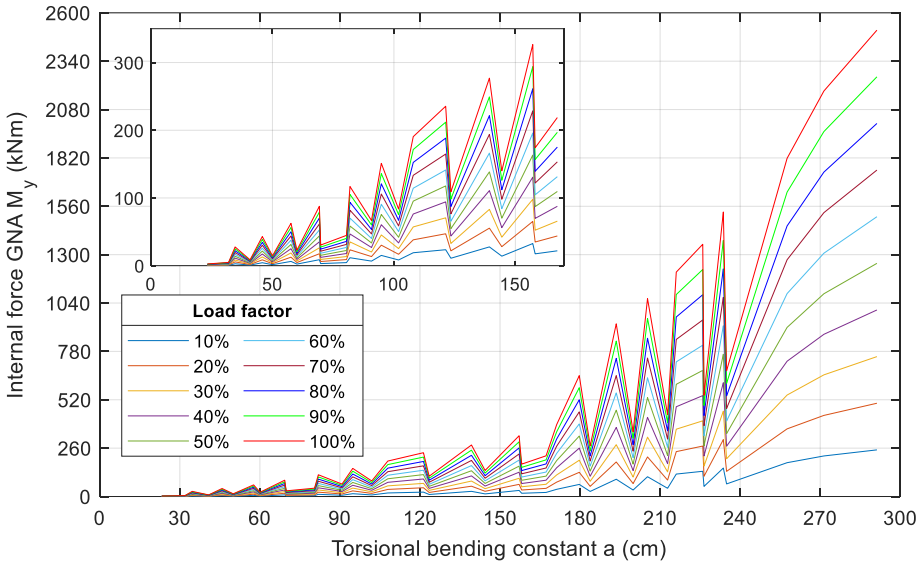

Figure A III.28 Internal force midspan M_y: fork-fork system, M_y load, open profiles / Inset of the graphic corresponds to values of a up to 170cm

M_T

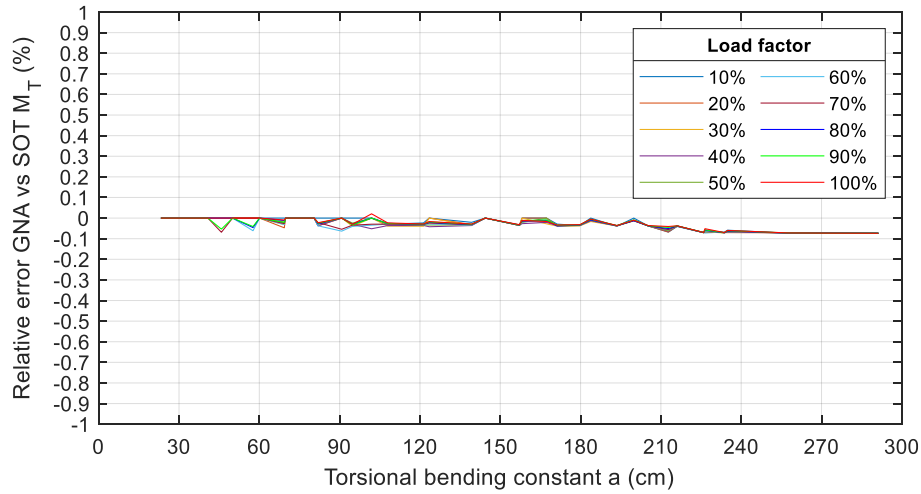

Figure A III.29 Relative error support M_T: fork-fork system, M_T load, open profiles

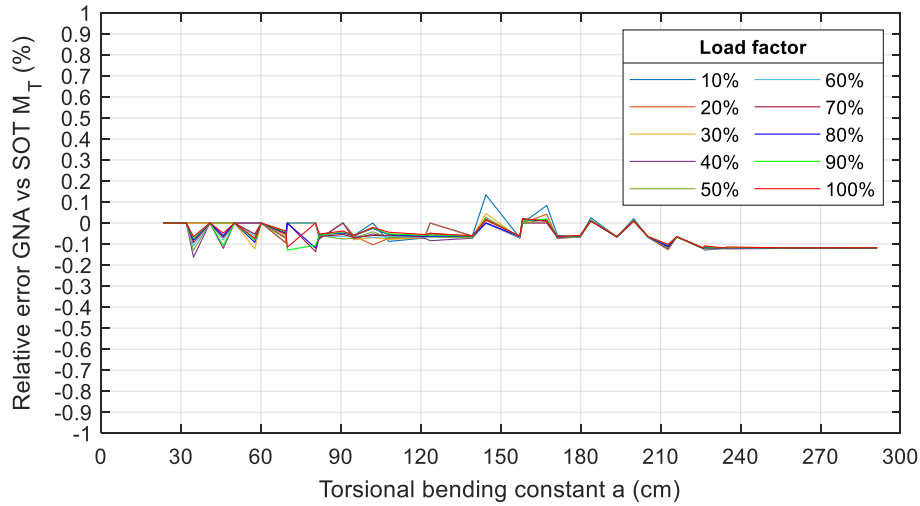

Figure A III.30 Relative error midspan M_T: fork-fork system, M_T load, open profiles

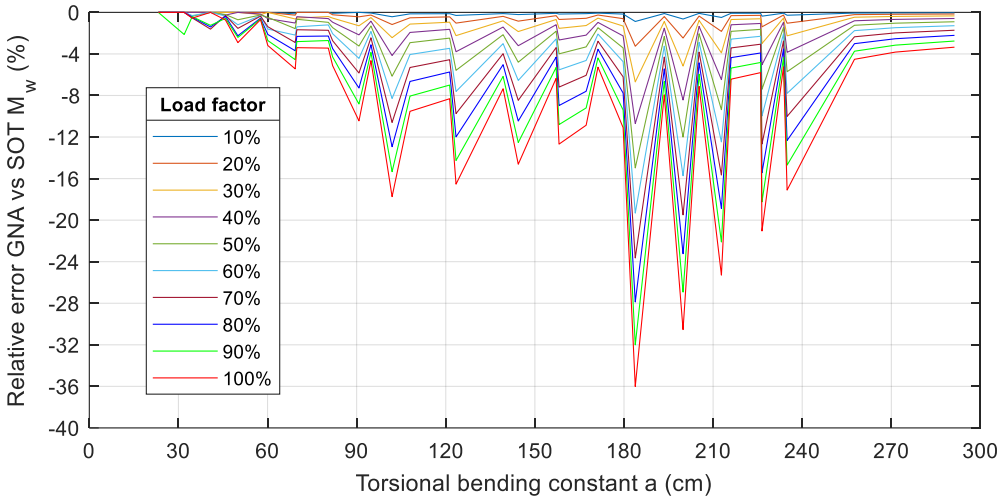

Figure A III.31 Relative error midspan M_w: fork-fork system, M_T load, open profiles

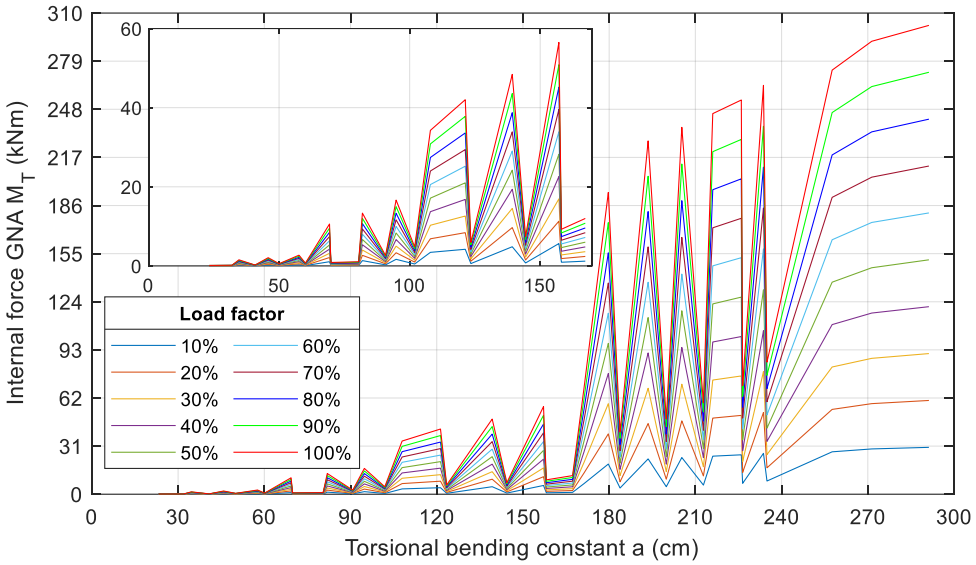

Figure A III.32 Internal force M_T: fork-fork system, M_T load, open profiles / Inset of the graphic corresponds to values of a up to 170cm

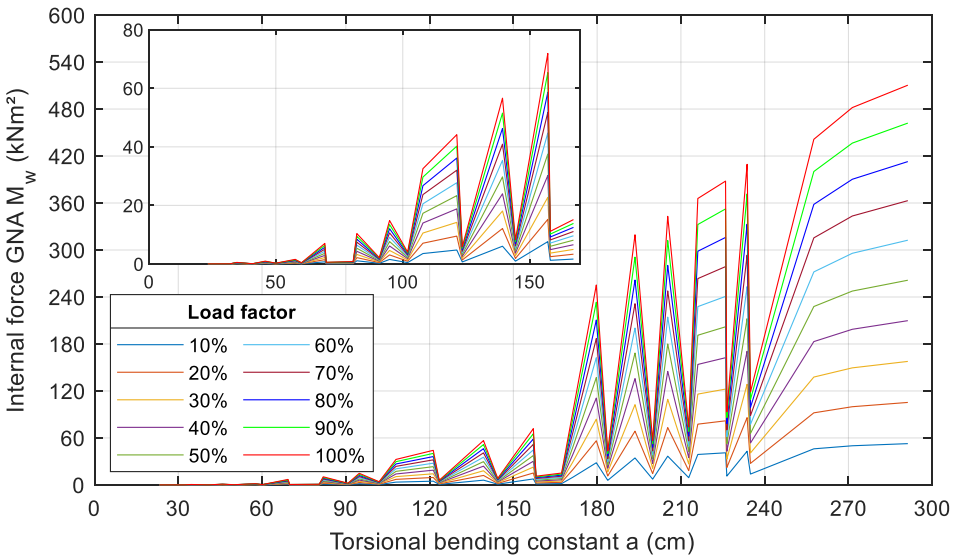

Figure A III.33 Internal force midspan M_w: fork-fork system, M_T load, open profiles / Inset of the graphic corresponds to values of a up to 170cm

Appendix III-2.2 Closed cross-sections

V_z

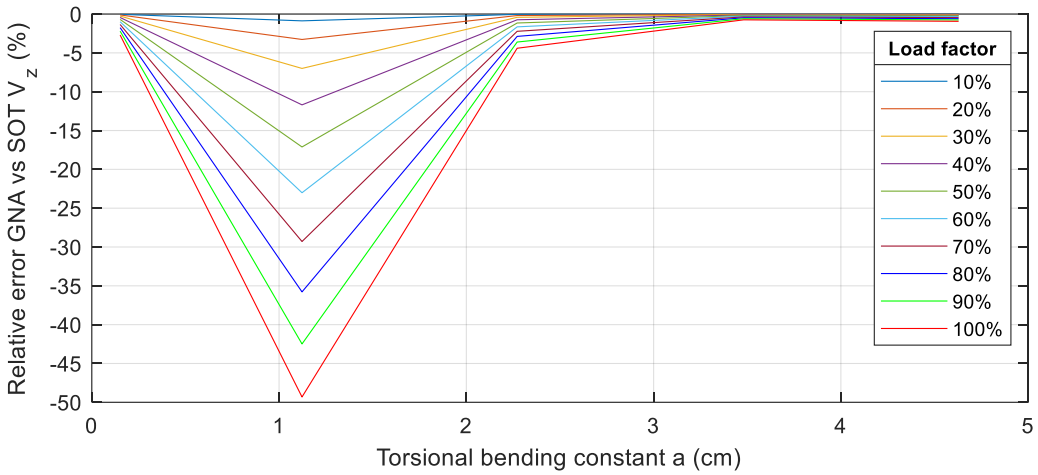

Figure A III.34 Relative error support V_z: fork-fork system, V_z load, closed profiles

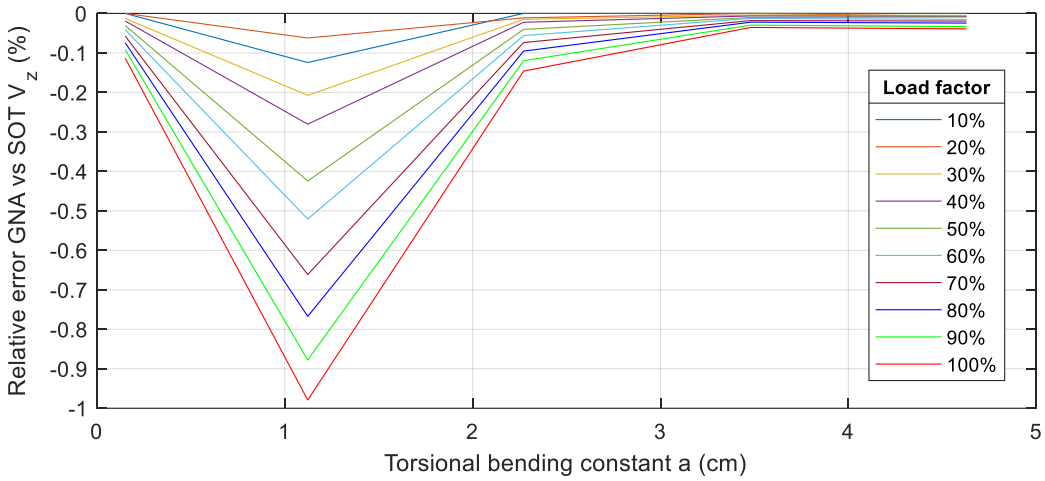

Figure A III.35 Relative error midspan V_z: fork-fork system, V_z load, closed profiles

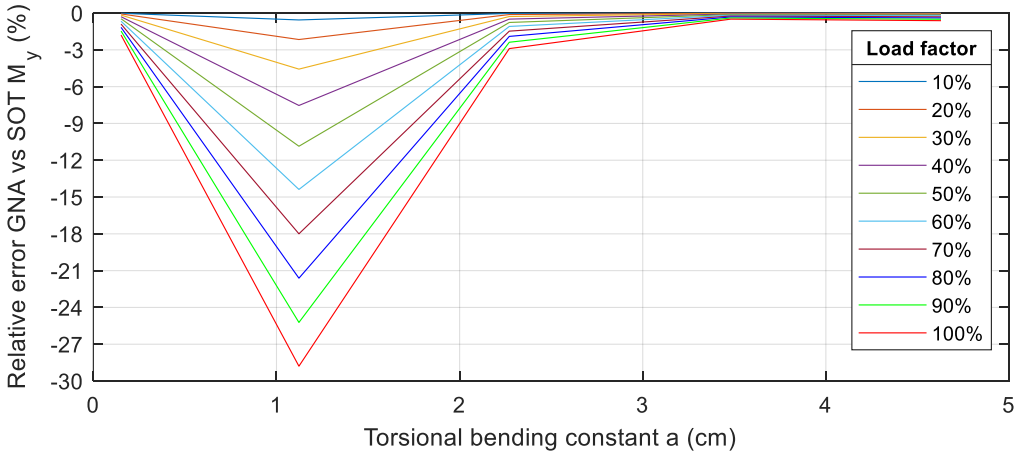

Figure A III.36 Relative error midspan M_y: fork-fork system, V_z load, closed profiles

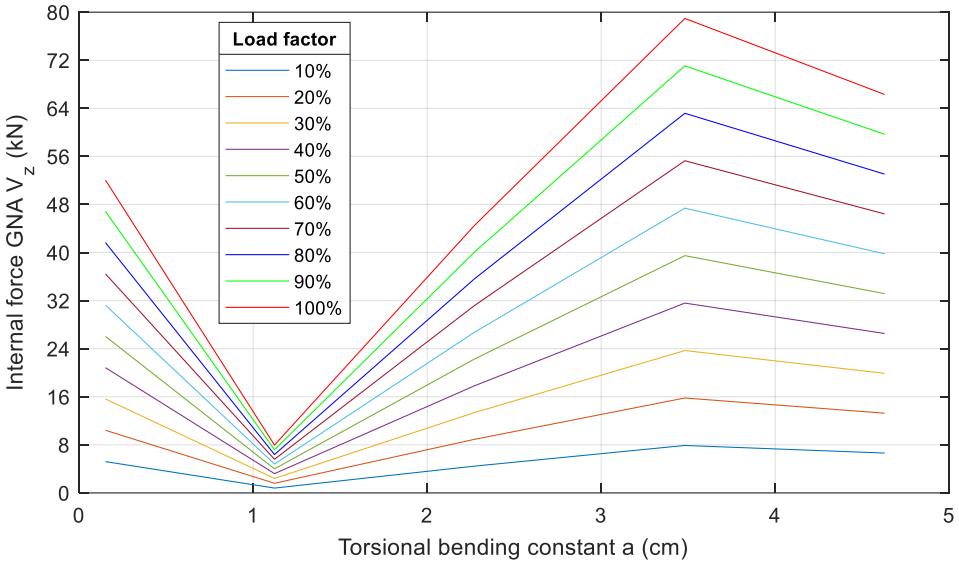

Figure A III.37 Internal force V_z: fork-fork system, V_z load, closed profiles

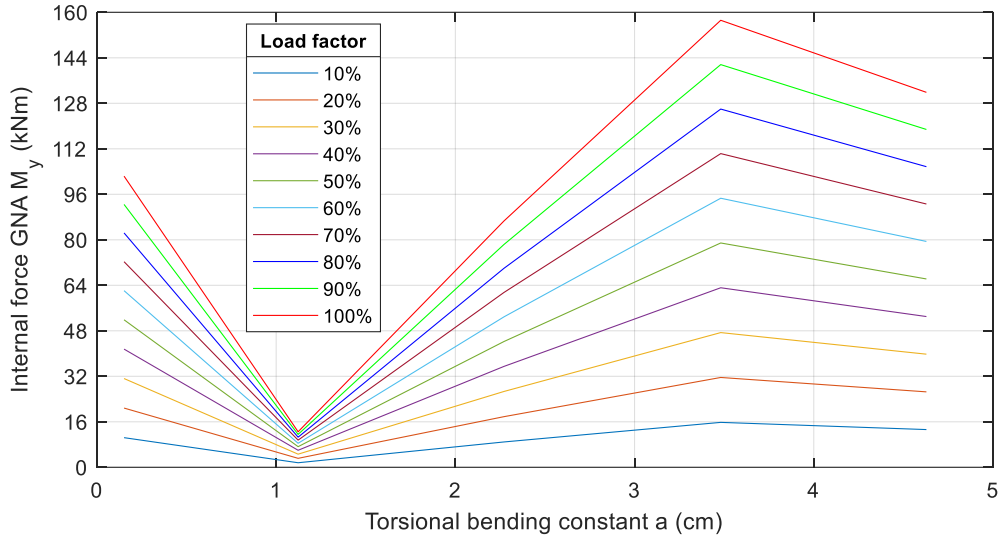

Figure A III.38 Internal force midspan M_y: fork-fork system, V_z load, closed profiles

M_y

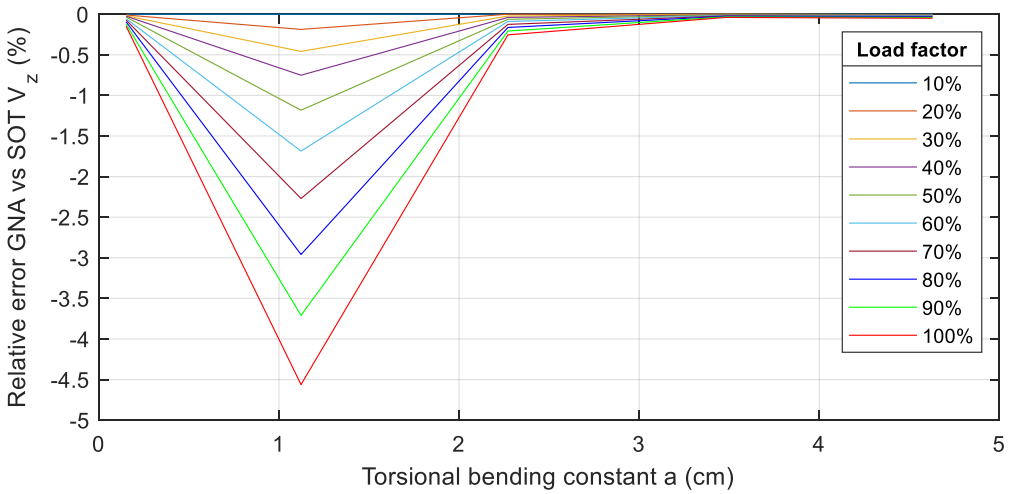

Figure A III.39 Relative error support V_z: fork-fork system, M_y load, closed profiles

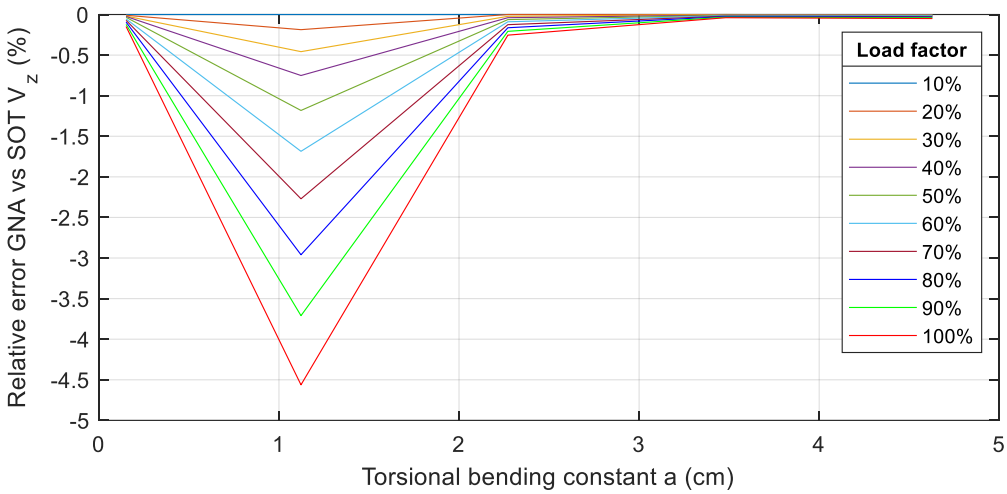

Figure A III.40 Relative error midspan V_z: fork-fork system, M_y load, closed profiles

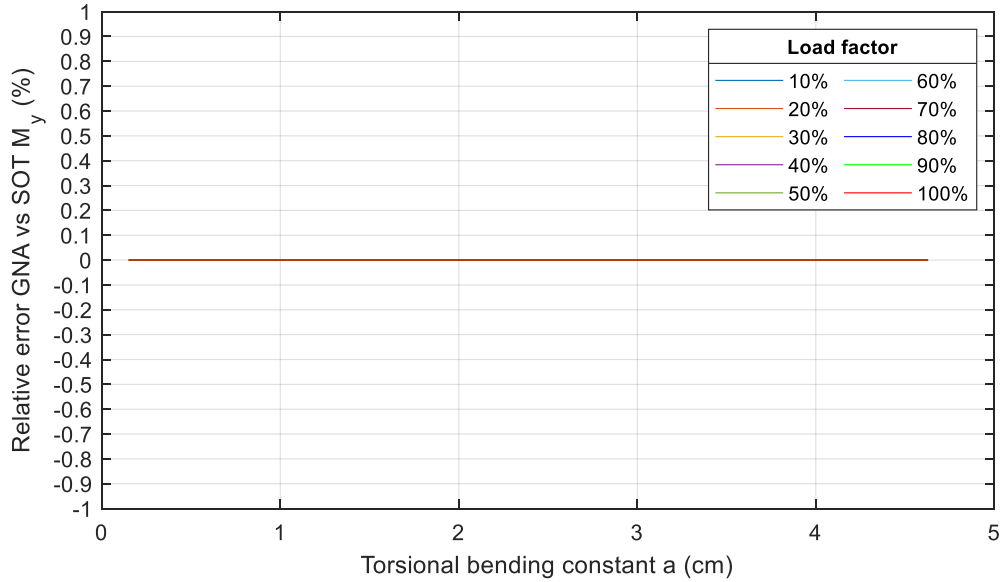

Figure A III.41 Relative error midspan M_y: fork-fork system, M_y load, closed profiles

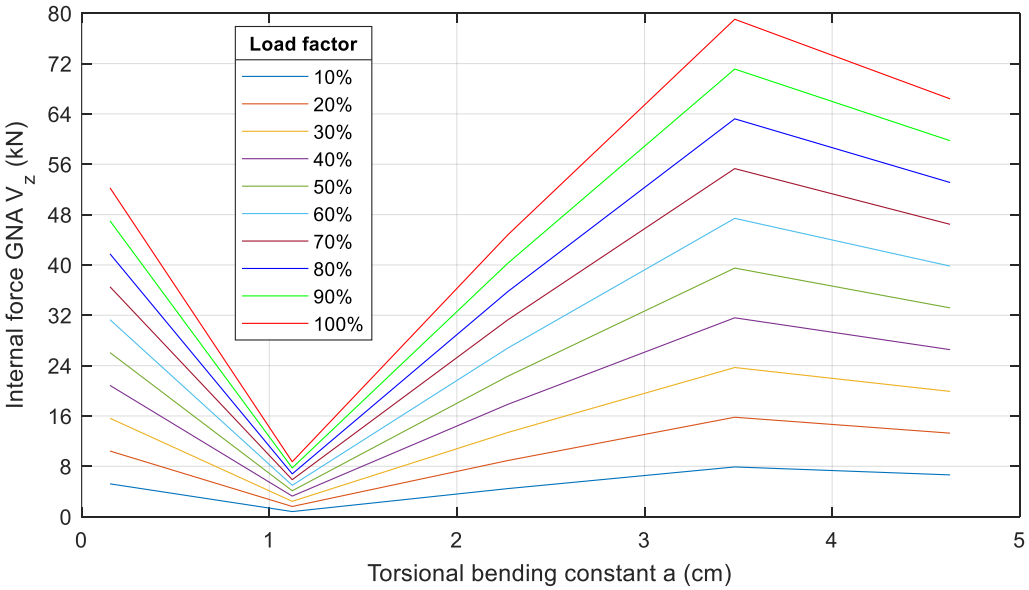

Figure A III.42 Internal force V_z: fork-fork system, M_y load, closed profiles

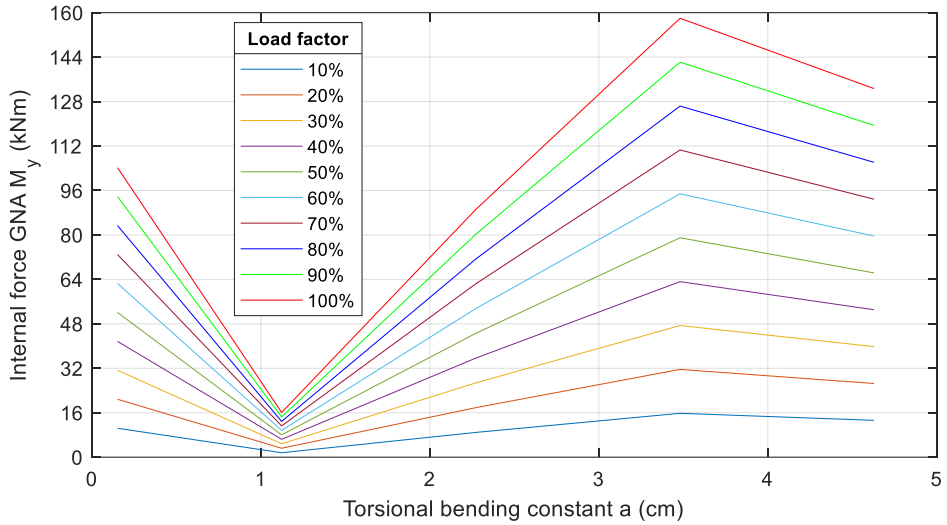

Figure A III.43 Internal force midspan M_y: fork-fork system, M_y load, closed profiles

M_T

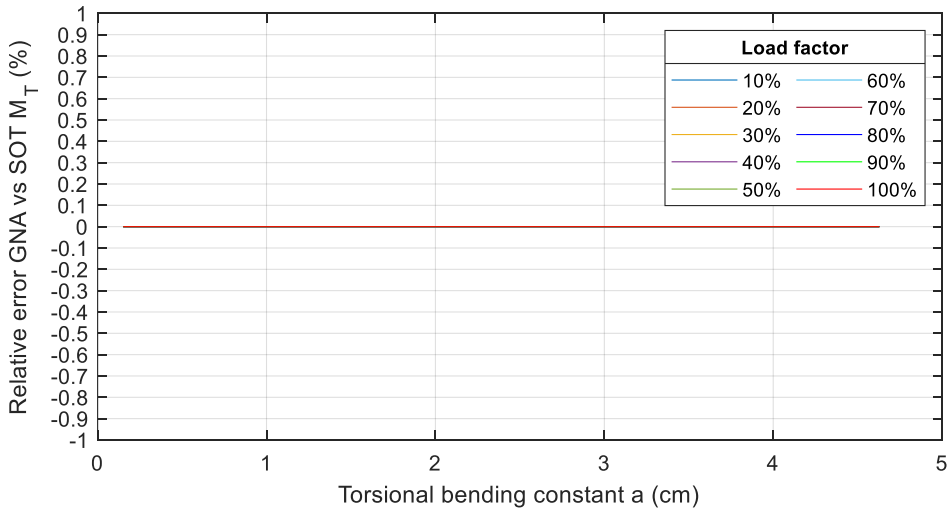

Figure A III.44 Relative error M_T: fork-fork system, M_T load, closed profiles

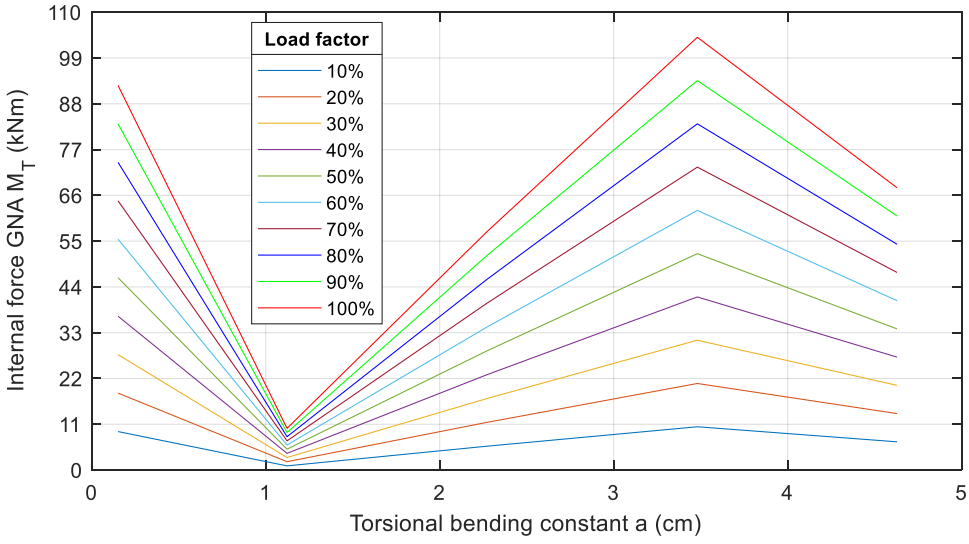

Figure A III.45 Internal force support M_T: fork-fork system, M_T load, closed profiles

Appendix III-3 Fixed-fixed system

Appendix III-3.1 Open cross-sections

V_z

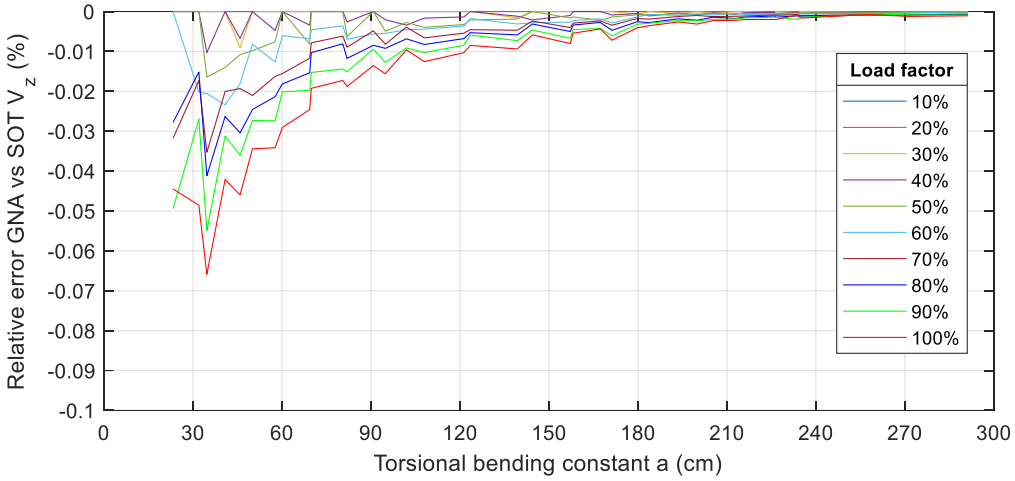

Figure A III.46 Relative error support V_z: fixed-fixed system, V_z load, open profiles

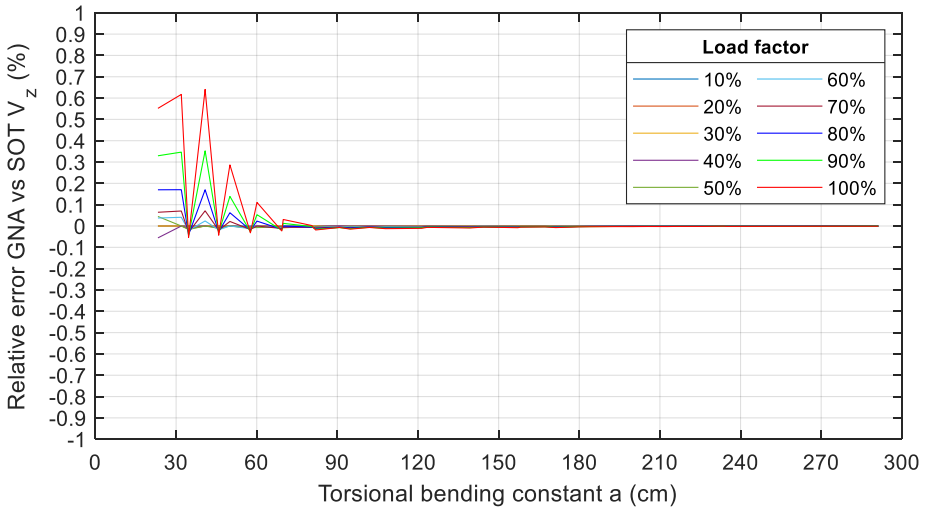

Figure A III.47 Relative error midspan V_z: fixed-fixed system, V_z load, open profiles

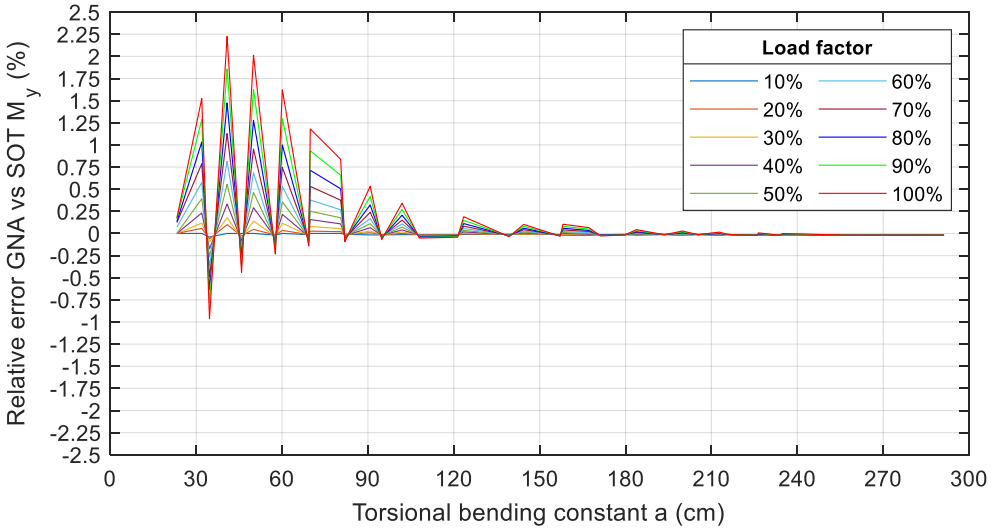

Figure A III.48 Relative error support M_y: fixed-fixed system, V_z load, open profiles

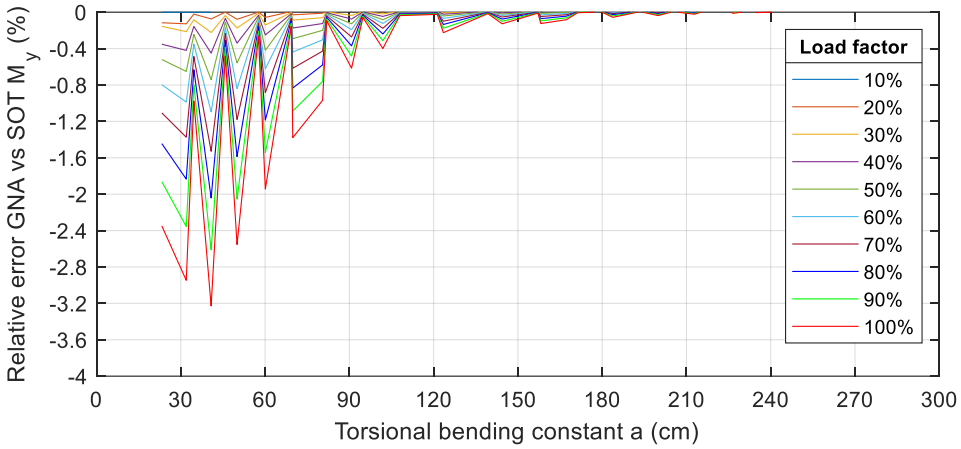

Figure A III.49 Relative error midspan M_y: fixed-fixed system, V_z load, open profiles

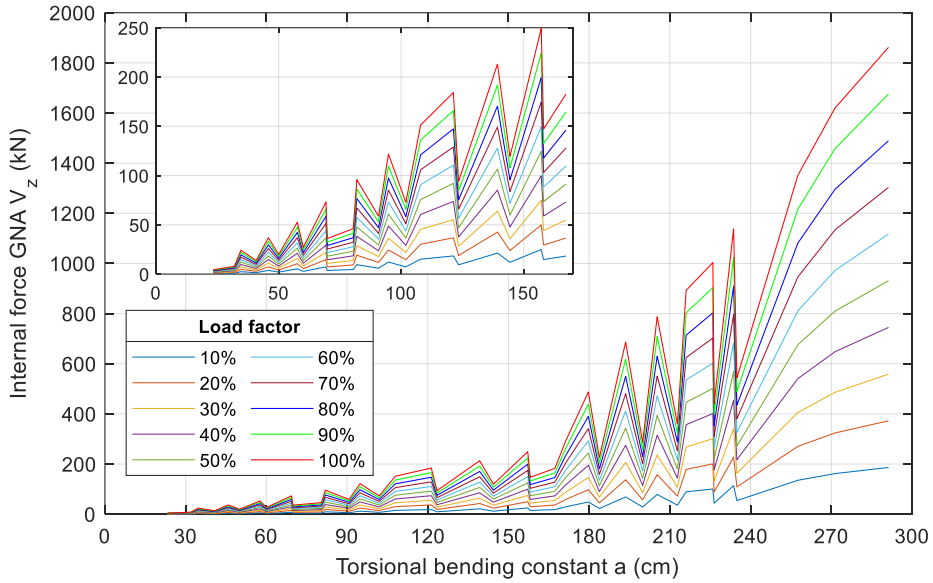

Figure A III.50 Internal force V_z: fixed-fixed system, V_z load, open profiles / Inset of the graphic corresponds to values of a up to 170cm

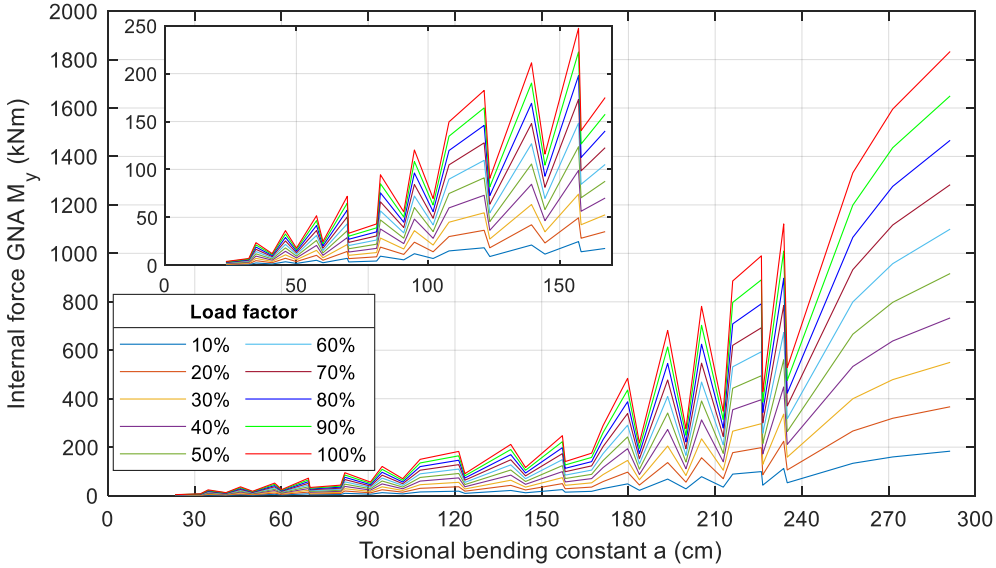

Figure A III.51 Internal force M_y: fixed-fixed system, V_z load, open profiles / Inset of the graphic corresponds to values of a up to 170cm

M_y

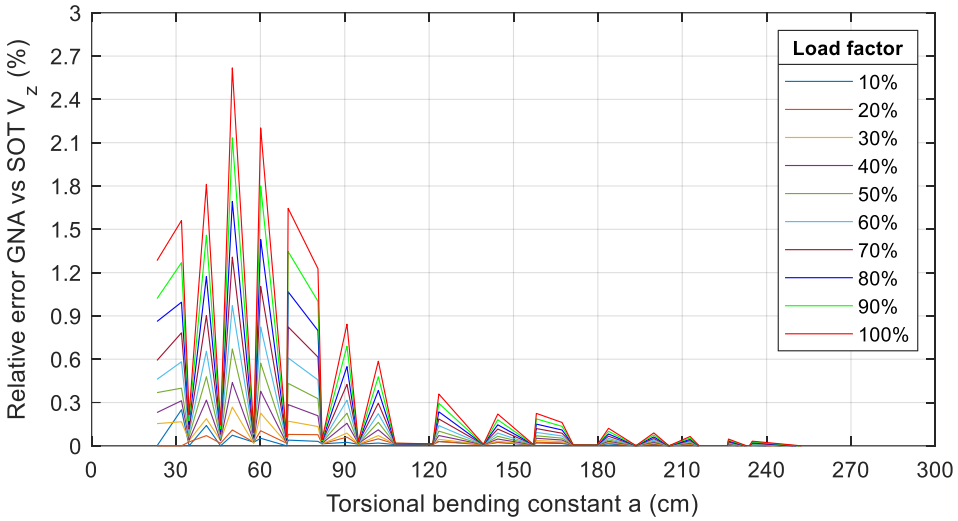

Figure A III.52 Relative error support V_z: fixed-fixed system, M_y load, open profiles

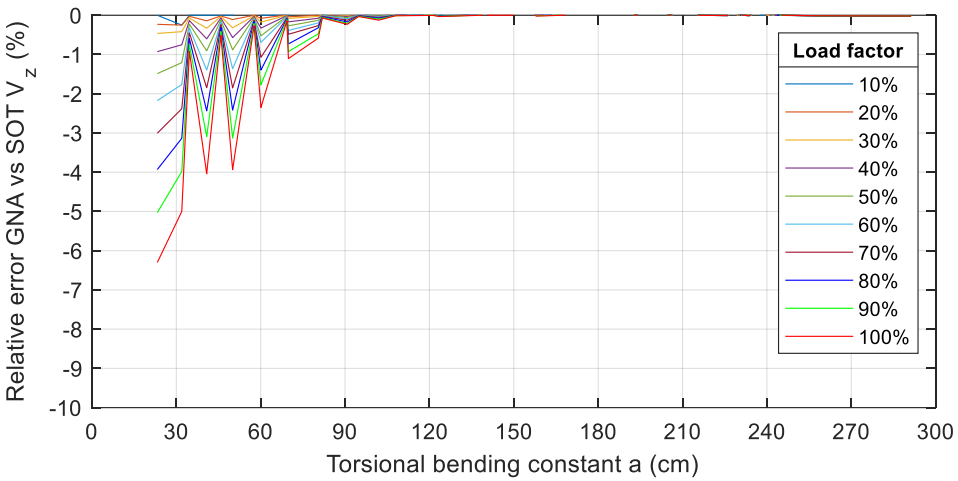

Figure A III.53 Relative error midspan V_z: fixed-fixed system, M_y load, open profiles

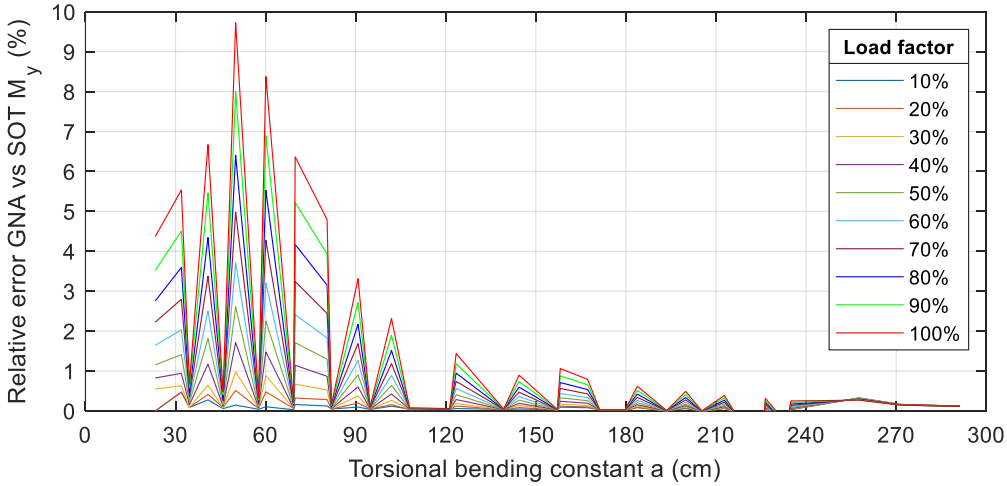

Figure A III.54 Relative error support M_y: fixed-fixed system, M_y load, open profiles

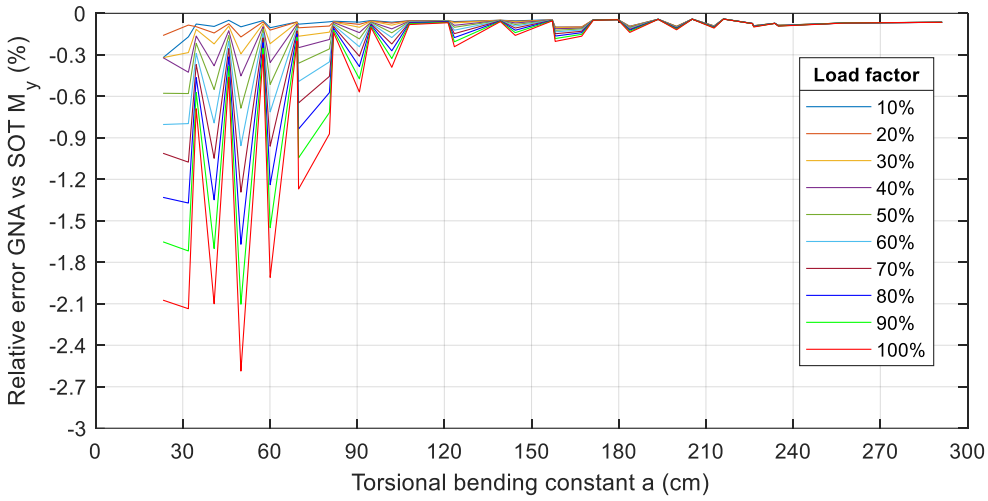

Figure A III.55 Relative error midspan M_y: fixed-fixed system, M_y load, open profiles

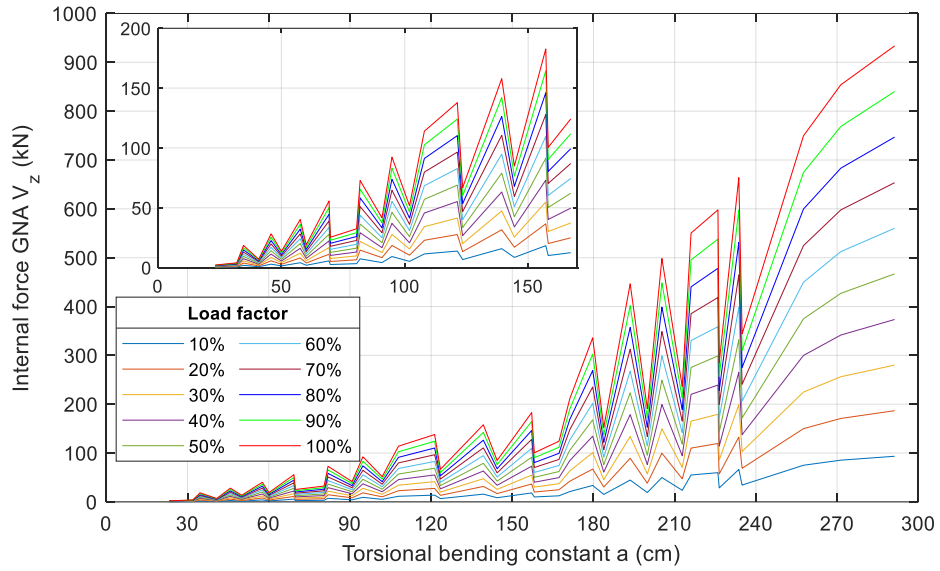

Figure A III.56 Internal force V_z: fixed-fixed system, M_y load, open profiles / Inset of the graphic corresponds to values of a up to 170cm

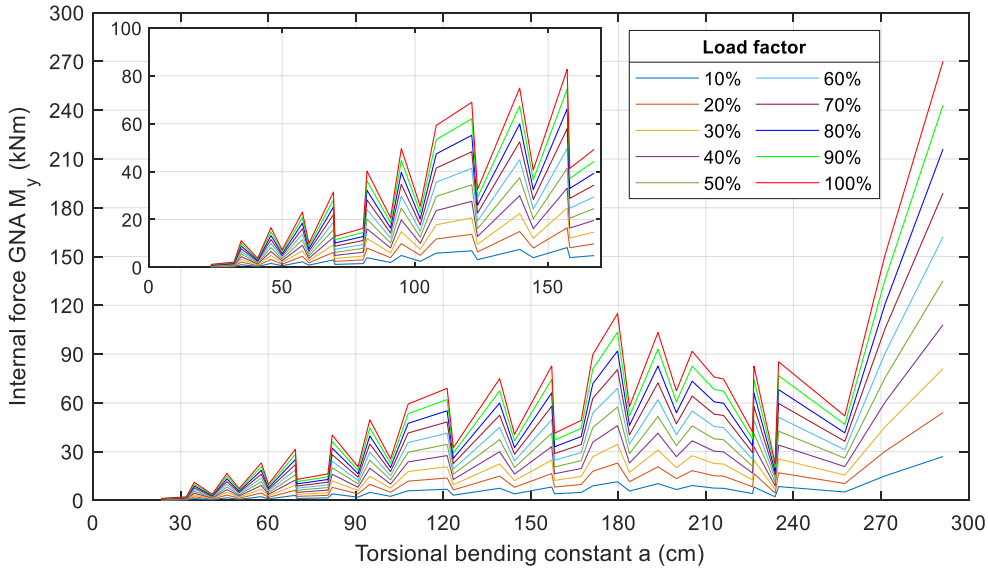

Figure A III.57 Internal force support M_y: fixed-fixed system, M_y load, open profiles / Inset of the graphic corresponds to values of a up to 170cm

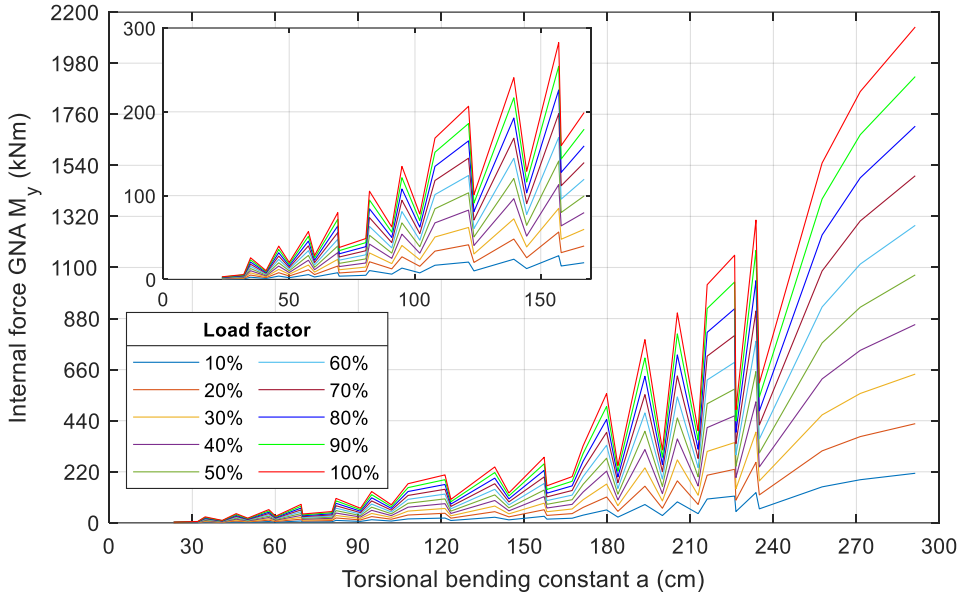

Figure A III.58 Internal force midspan M_y: fixed-fixed system, M_y load, open profiles / Inset of the graphic corresponds to values of a up to 170cm

M_T

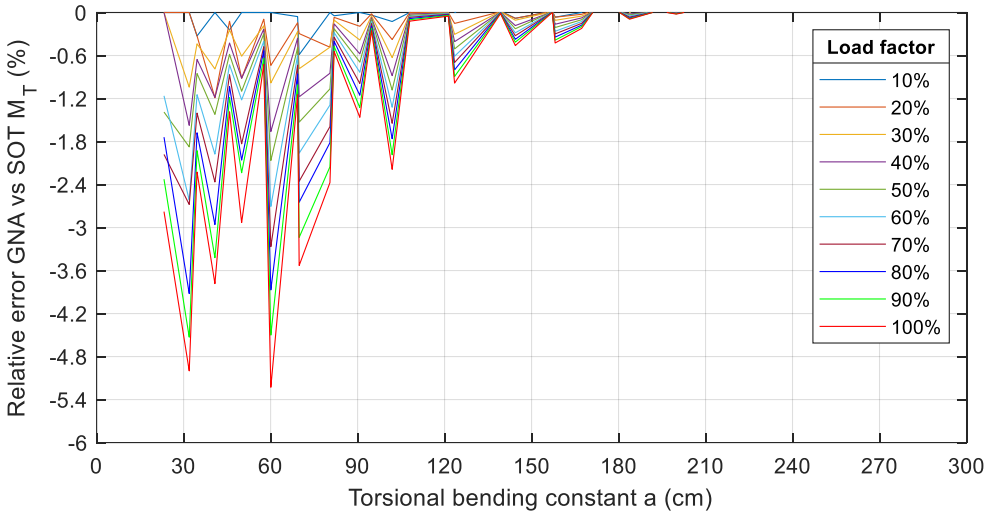

Figure A III.59 Relative error support M_T: fixed-fixed system, M_T load, open profiles

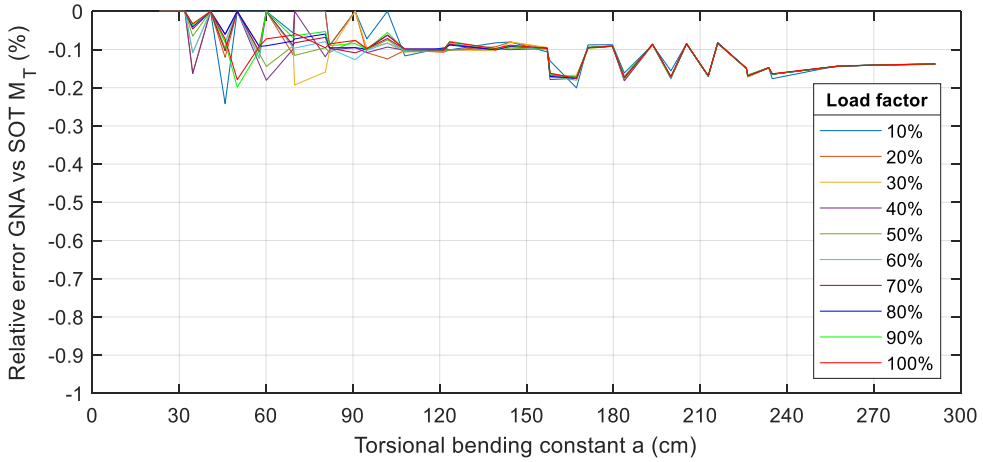

Figure A III.60 Relative error midspan M_T: fixed-fixed system, M_T load, open profiles

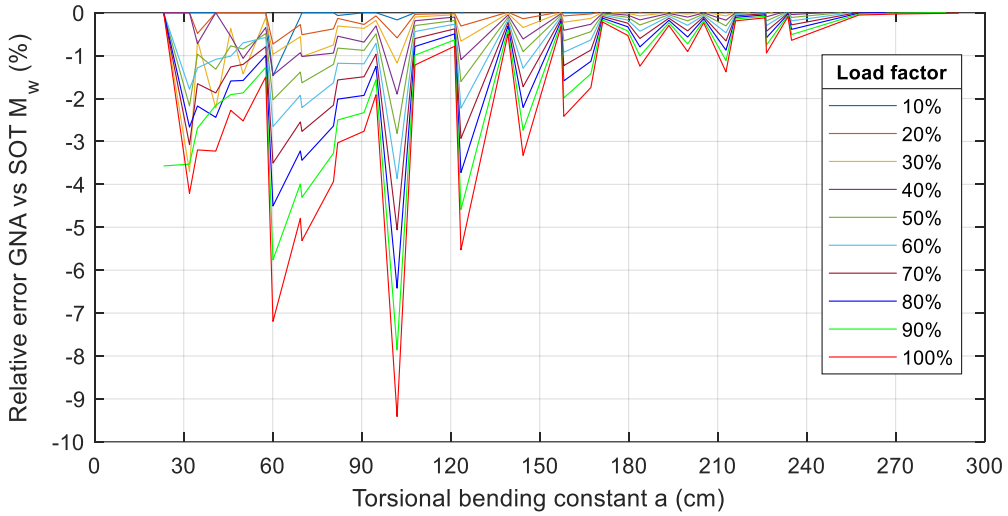

Figure A III.61 Relative error support M_w: fixed-fixed system, M_T load, open profiles

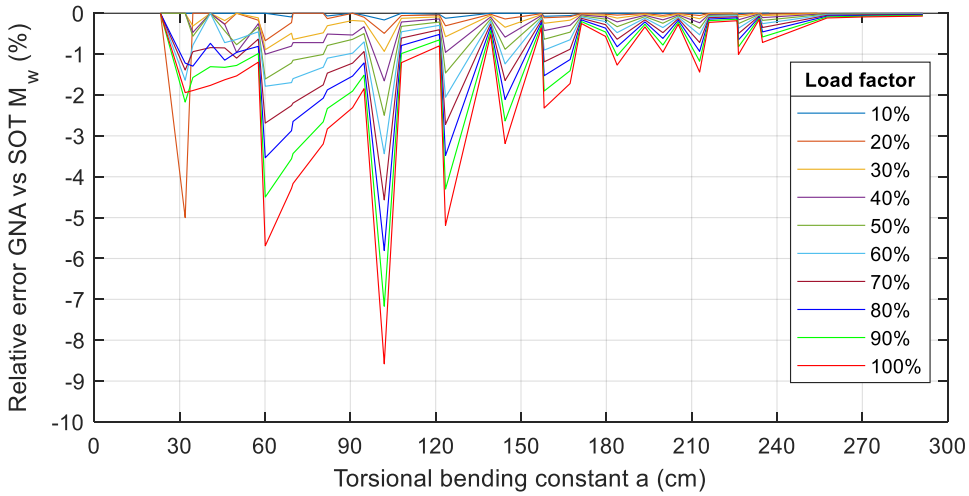

Figure A III.62 Relative error midspan M_w: fixed-fixed system, M_T load, open profiles

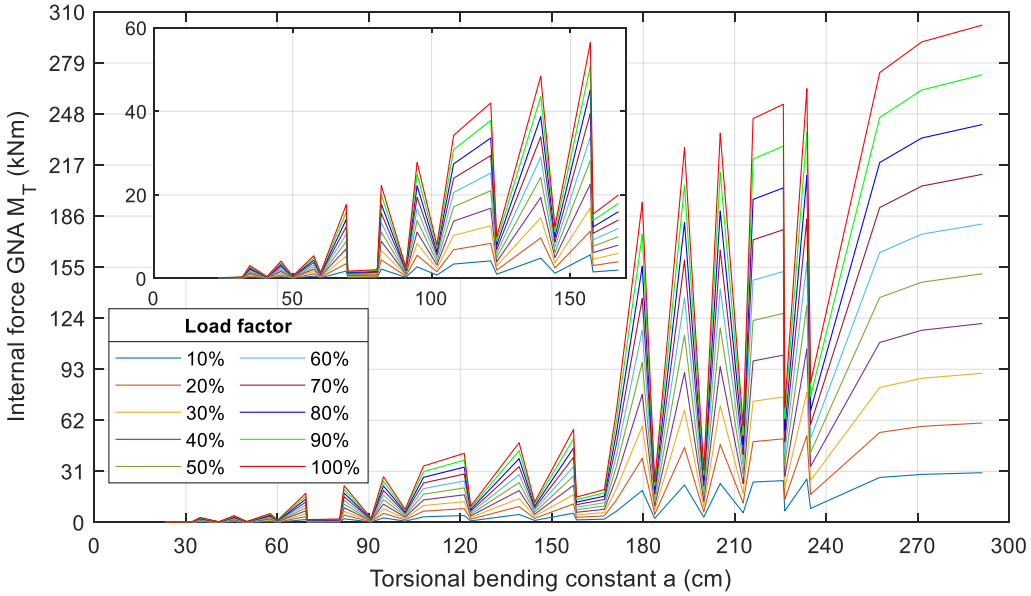

Figure A III.63 Internal force M_T: fixed-fixed system, M_T load, open profiles / Inset of the graphic corresponds to values of a up to 170cm

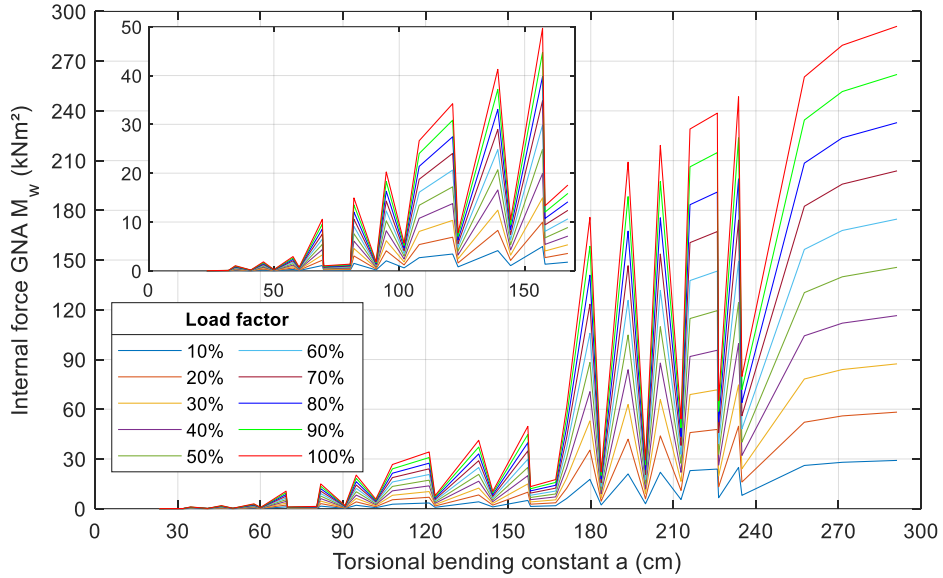

Figure A III.64 Internal force midspan M_w: fixed-fixed system, M_T load, open profiles / Inset of the graphic corresponds to values of a up to 170cm

Appendix III-3.2 Closed cross-sections

V_z

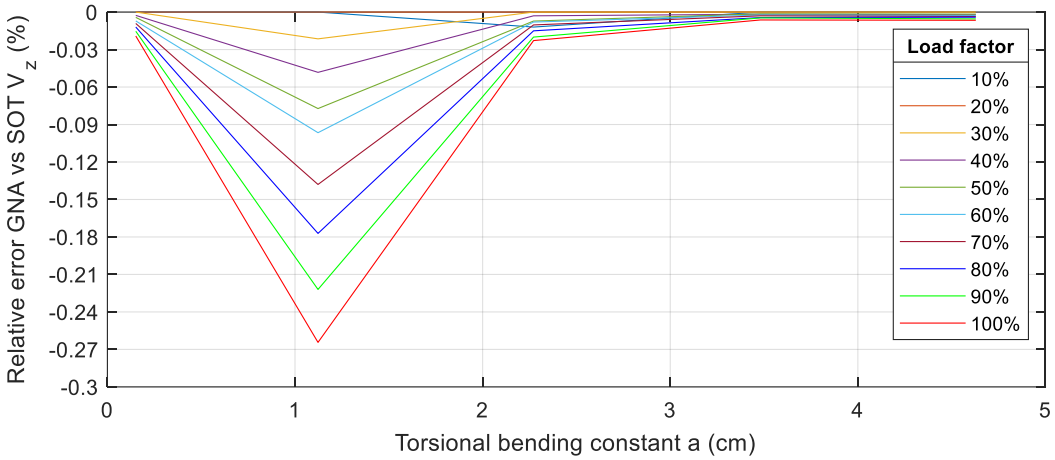

Figure A III.65 Relative error support V_z: fixed-fixed system, V_z load, closed profiles

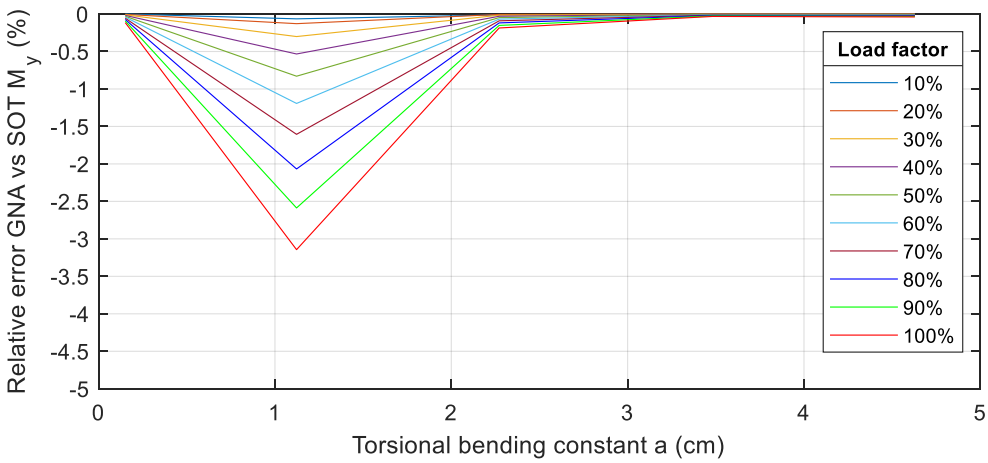

Figure A III.66 Relative error midspan M_y: fixed-fixed system, V_z load, closed profiles

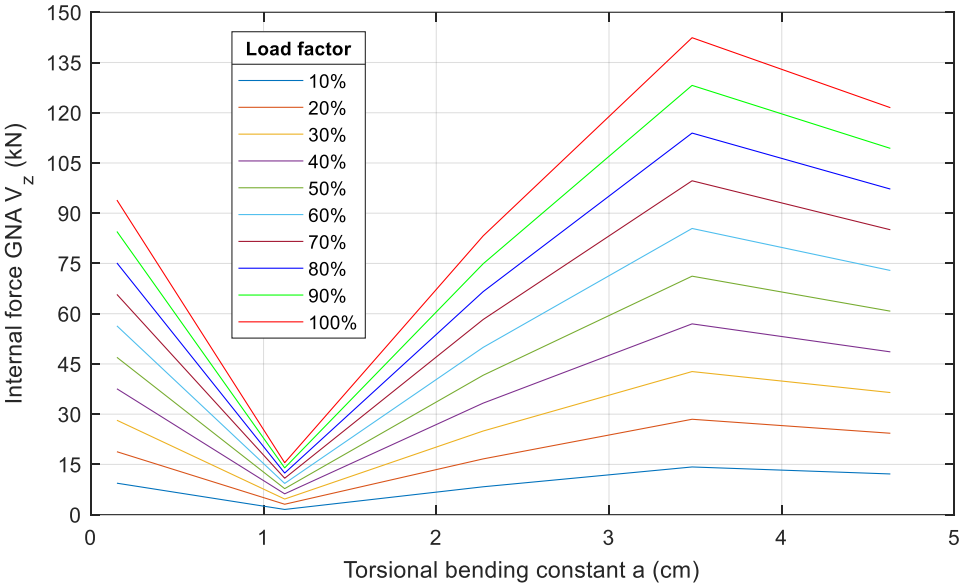

Figure A III.67 Internal force V_z: fixed-fixed system, V_z load, closed profiles

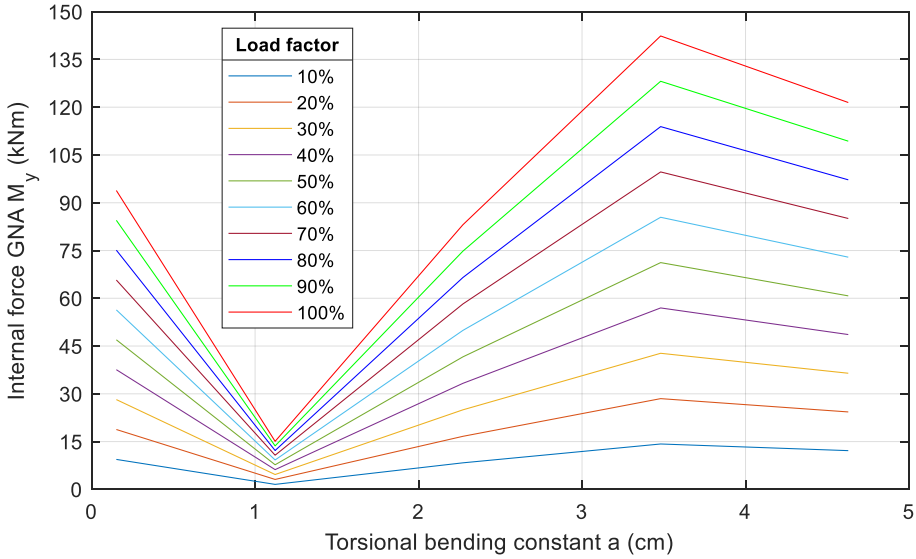

Figure A III.68 Internal force M_y: fixed-fixed system, V_z load, closed profiles

M_y

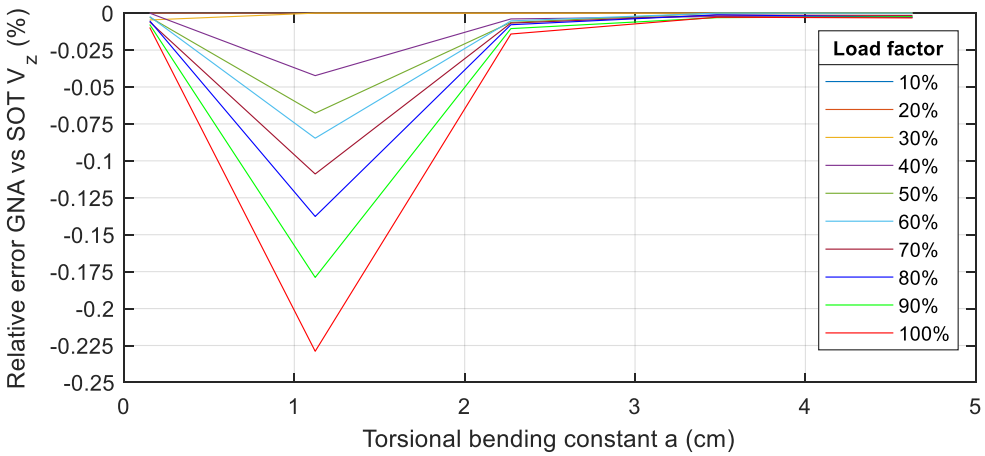

Figure A III.69 Relative error support V_z: fixed-fixed system, M_y load, closed profiles

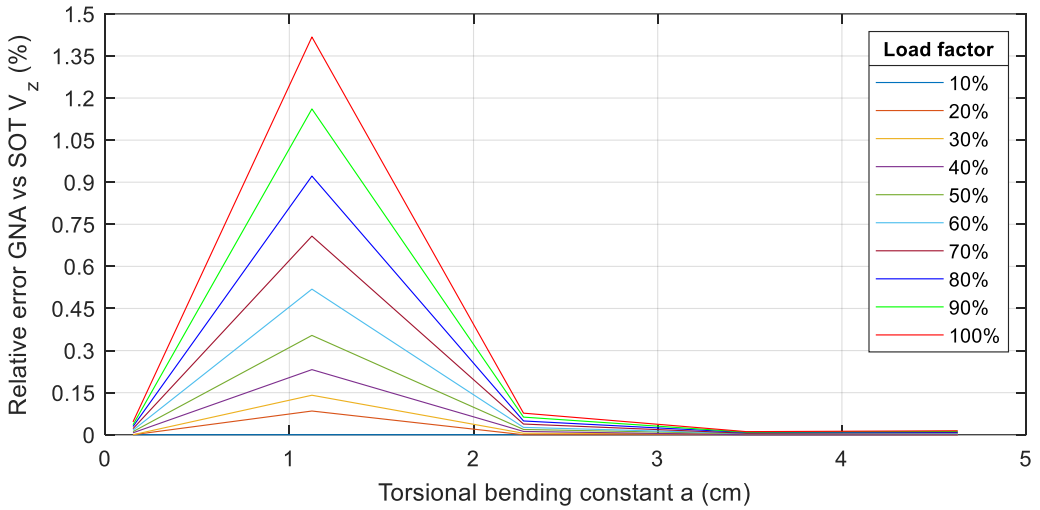

Figure A III.70 Relative error midspan V_z: fixed-fixed system, M_y load, closed profiles

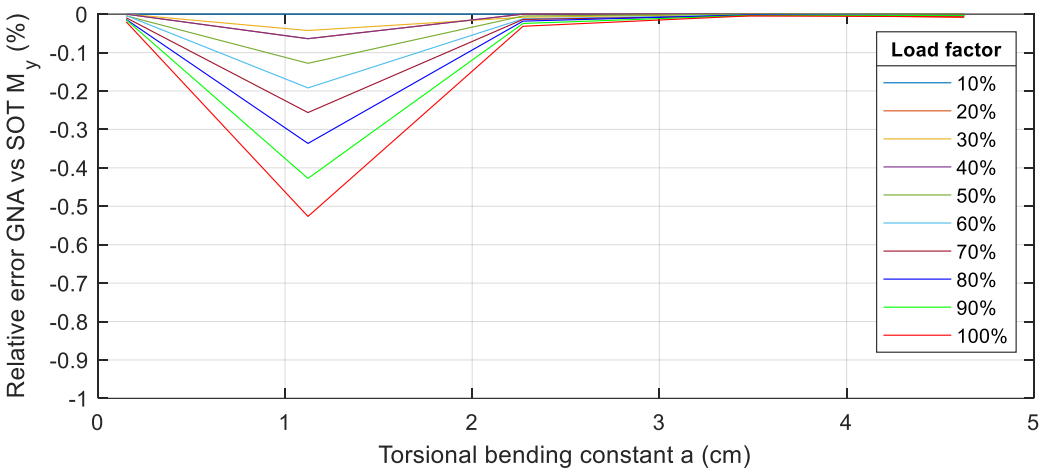

Figure A III.71 Relative error support M_y: fixed-fixed system, M_y load, closed profiles

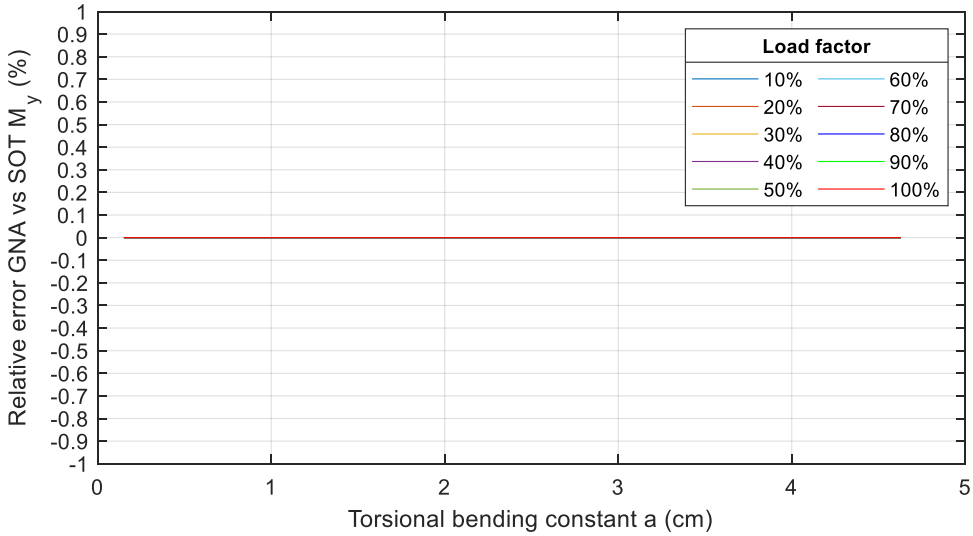

Figure A III.72 Relative error midspan M_y: fixed-fixed system, M_y load, closed profiles

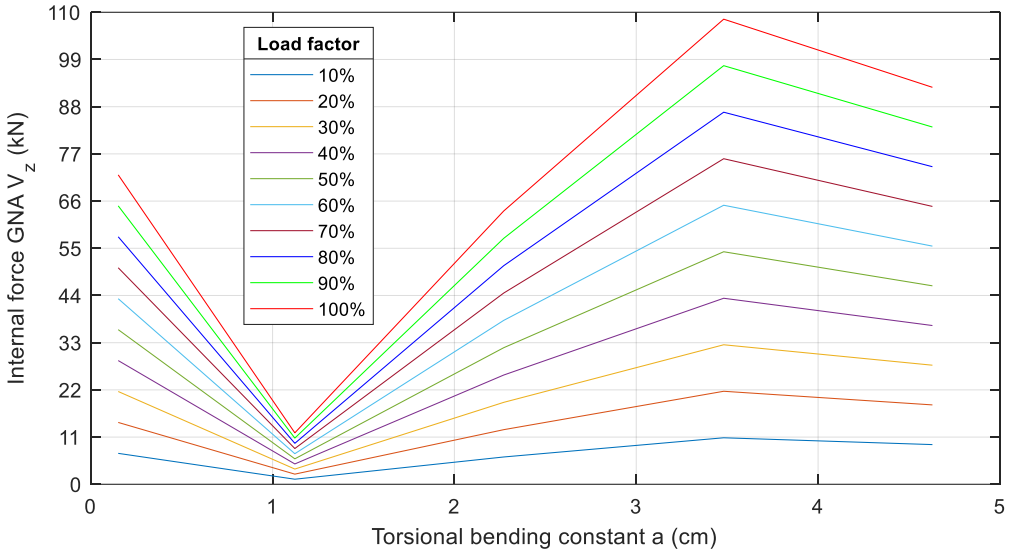

Figure A III.73 Internal force V_z: fixed-fixed system, M_y load, closed profiles

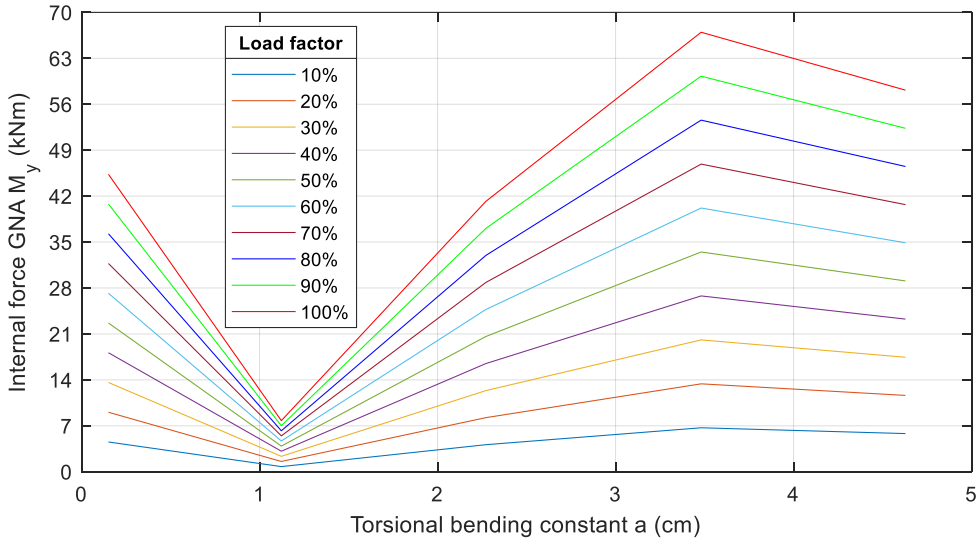

Figure A III.74 Internal force support M_y: fixed-fixed system, M_y load, closed profiles

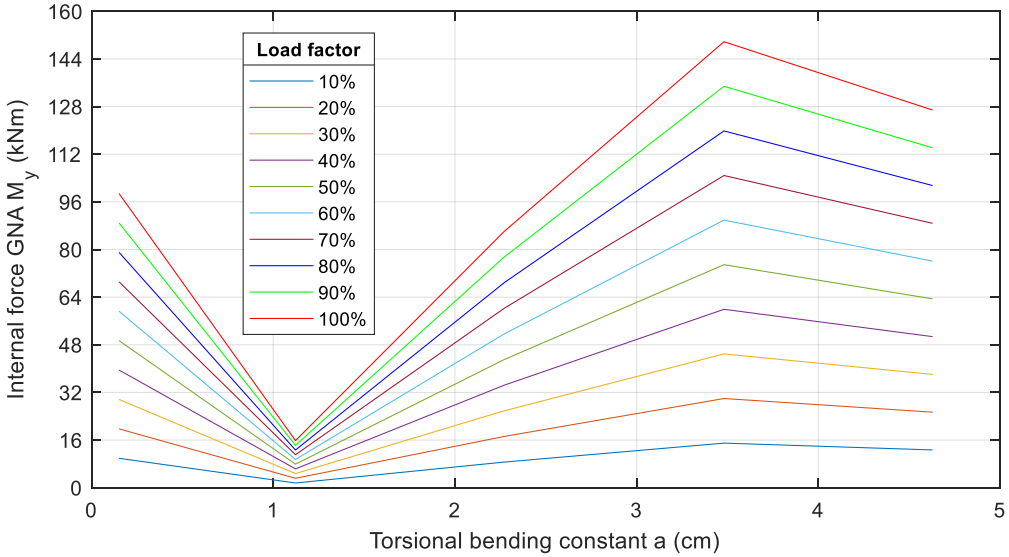

Figure A III.75 Internal force midspan M_y: fixed-fixed system, M_y load, closed profiles

M_T

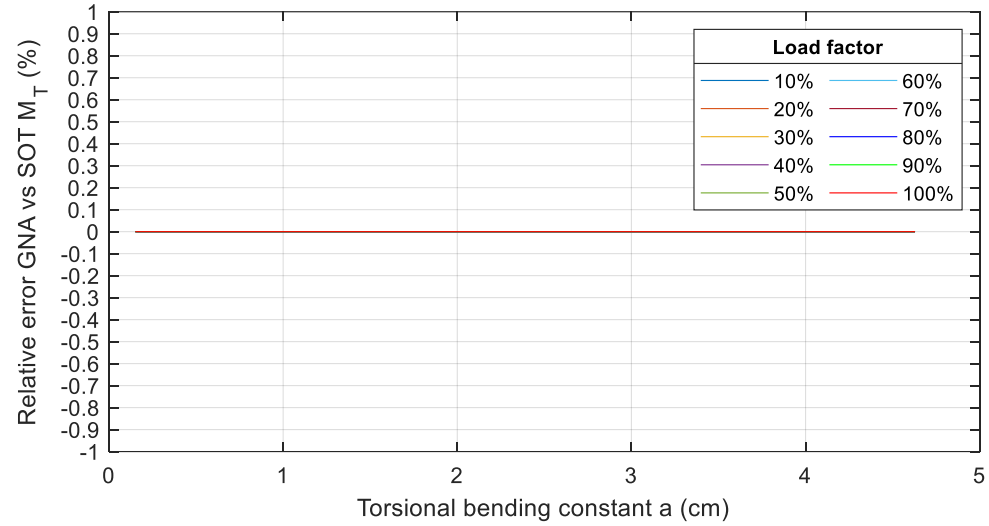

Figure A III.76 Relative error M_T: fixed-fixed system, M_T load, closed profiles

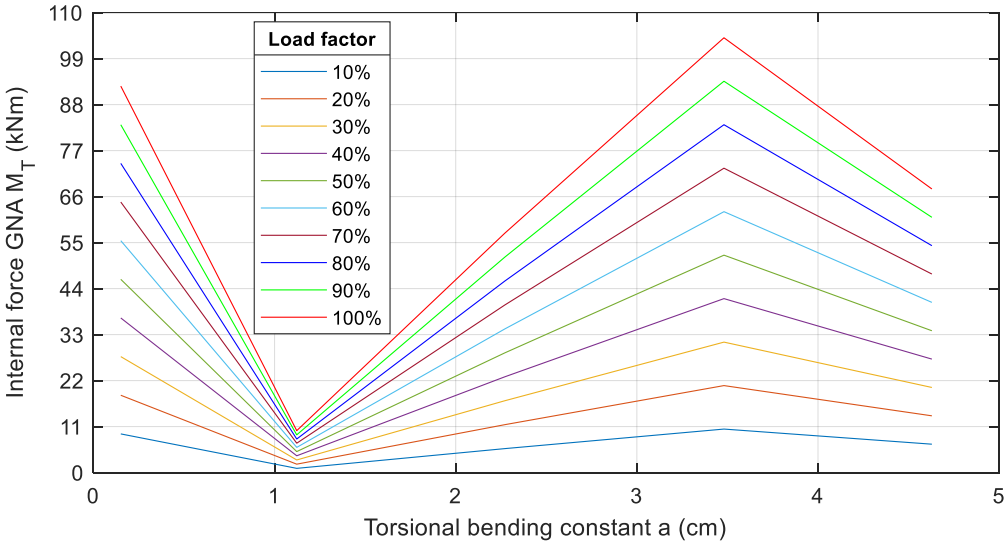

Figure A III.77 Internal force M_T: fixed-fixed system, M_T load, closed profiles

Appendix III-4 Fork-fixed system

Appendix III-4.1 Open cross-sections

V_z

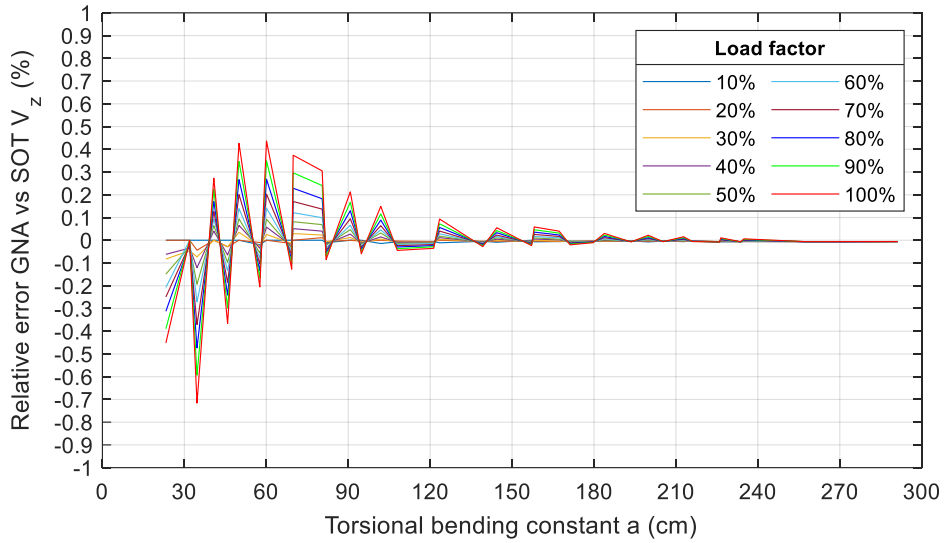

Figure A III.78 Relative error fixed support V_z: fork-fixed system, V_z load, open profiles

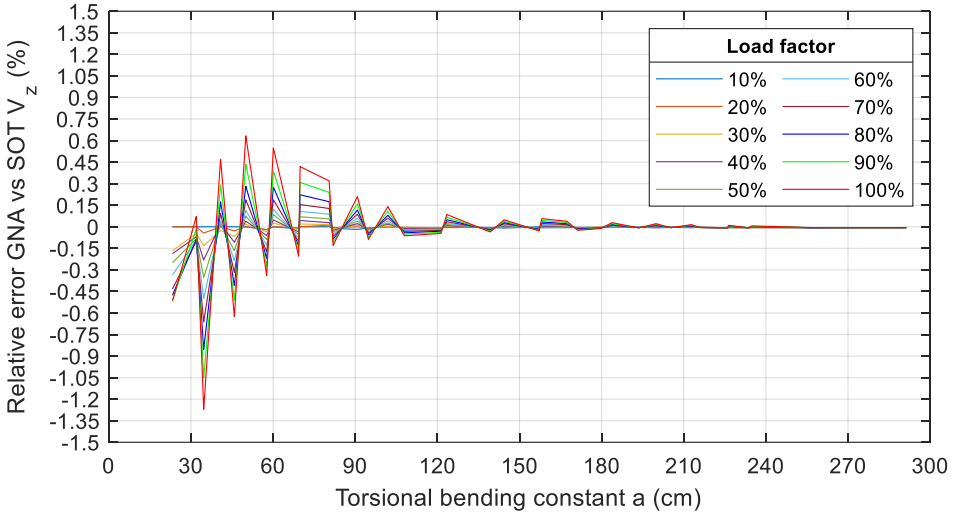

Figure A III.79 Relative error midspan V_z: fork-fixed system, V_z load, open profiles

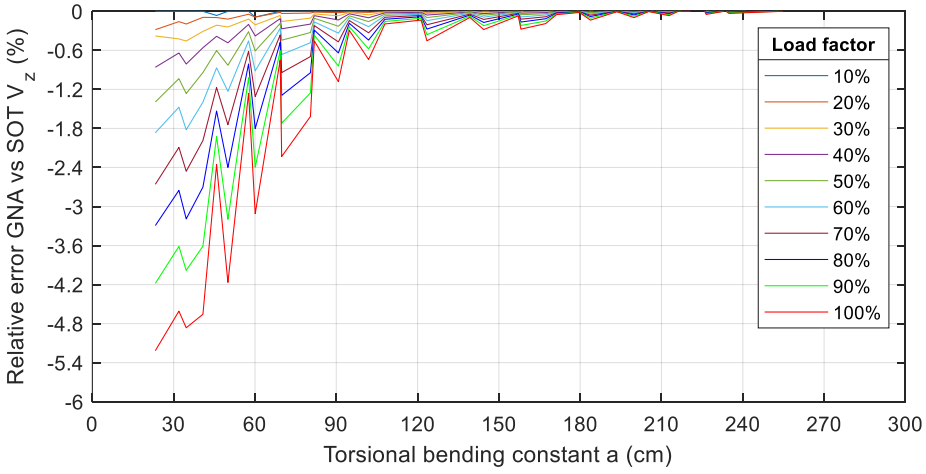

Figure A III.80 Relative error fork support V_z: fork-fixed system, V_z load, open profiles

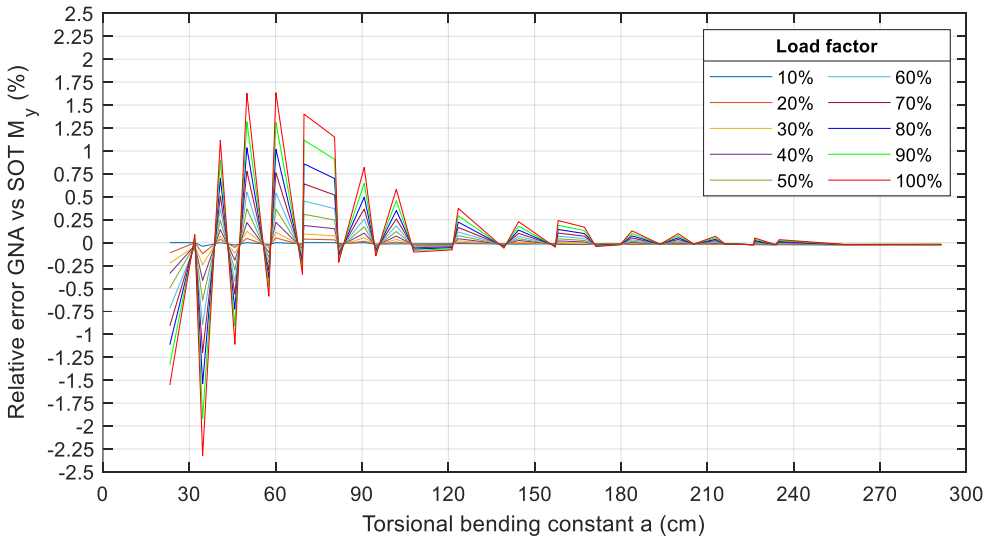

Figure A III.81 Relative error fixed support M_y: fork-fixed system, V_z load, open profiles

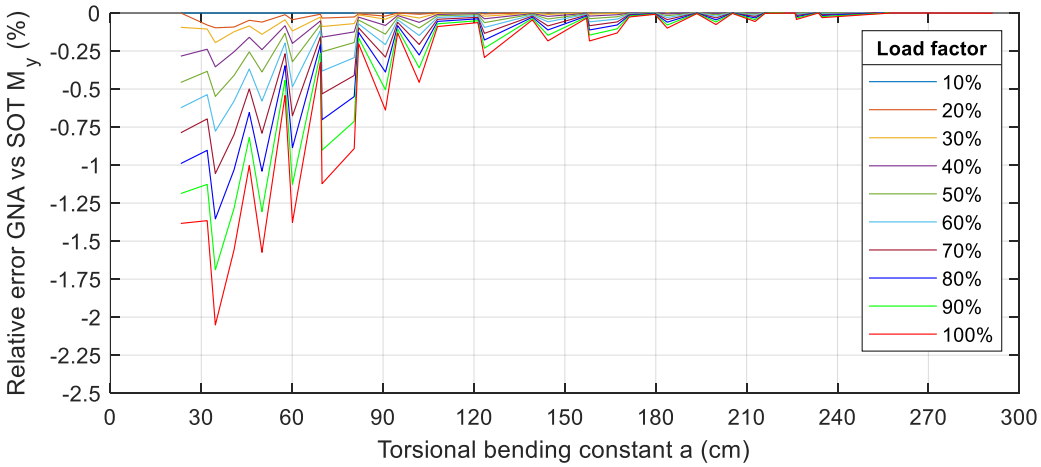

Figure A III.82 Relative error midspan M_y: fork-fixed system, V_z load, open profiles

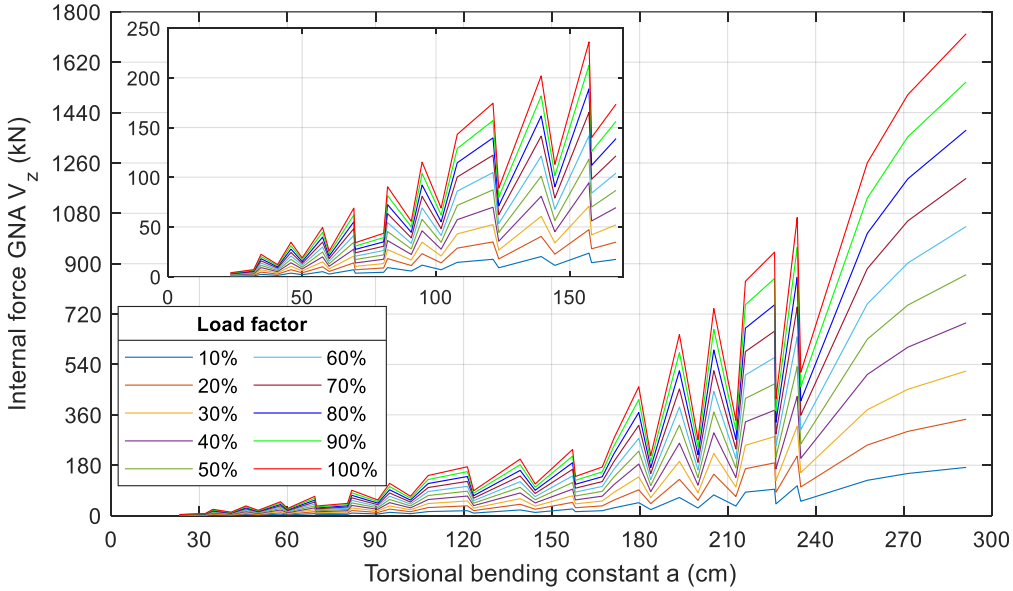

Figure A III.83 Internal force fixed support V_z: fork-fixed system, V_z load, open profiles / Inset of the graphic corresponds to values of a up to 170cm

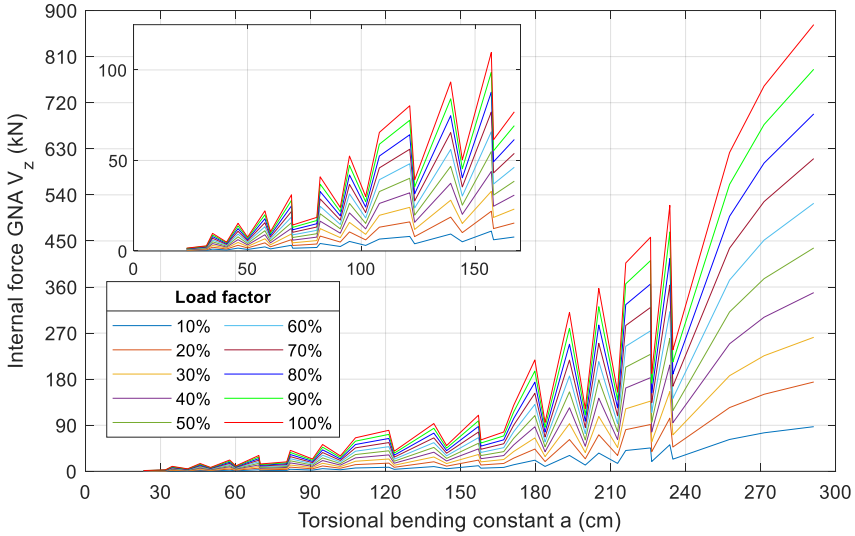

Figure A III.84 Internal force fork support V_z: fork-fixed system, V_z load, open profiles / Inset of the graphic corresponds to values of a up to 170cm

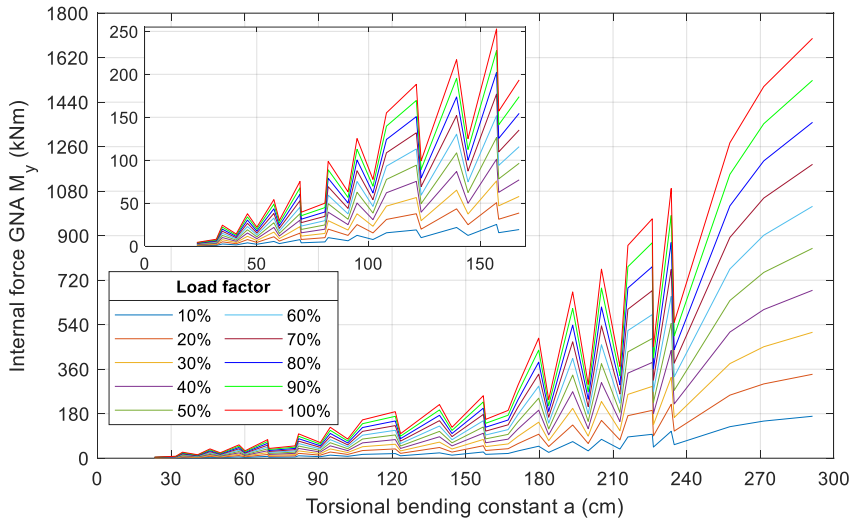

Figure A III.85 Internal force fixed support M_y: fork-fixed system, V_z load, open profiles / Inset of the graphic corresponds to values of a up to 170cm

M_y

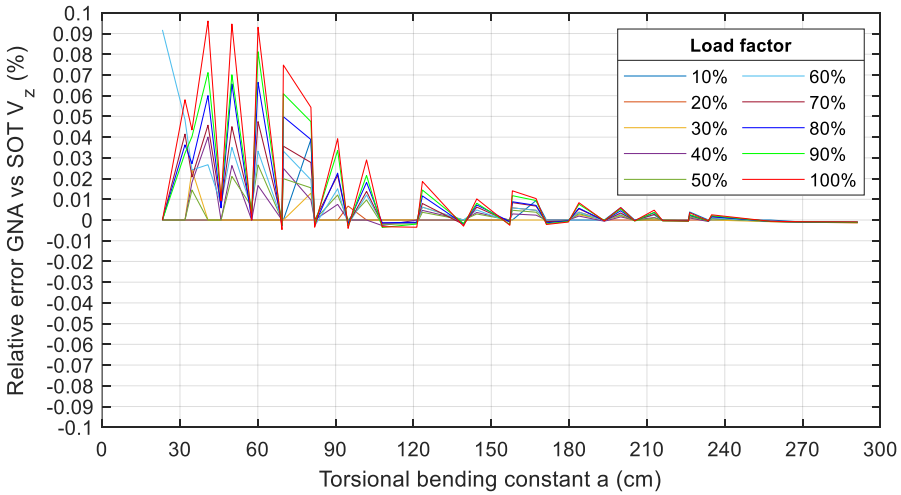

Figure A III.86 Relative error fixed support V_z: fork-fixed system, M_y load, open profiles

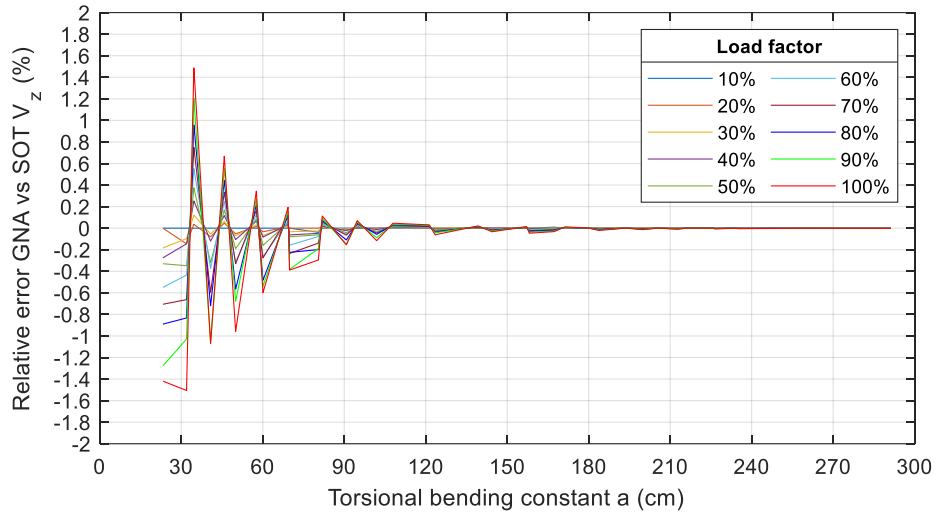

Figure A III.87 Relative error midspan V_z: fork-fixed system, M_y load, open profiles

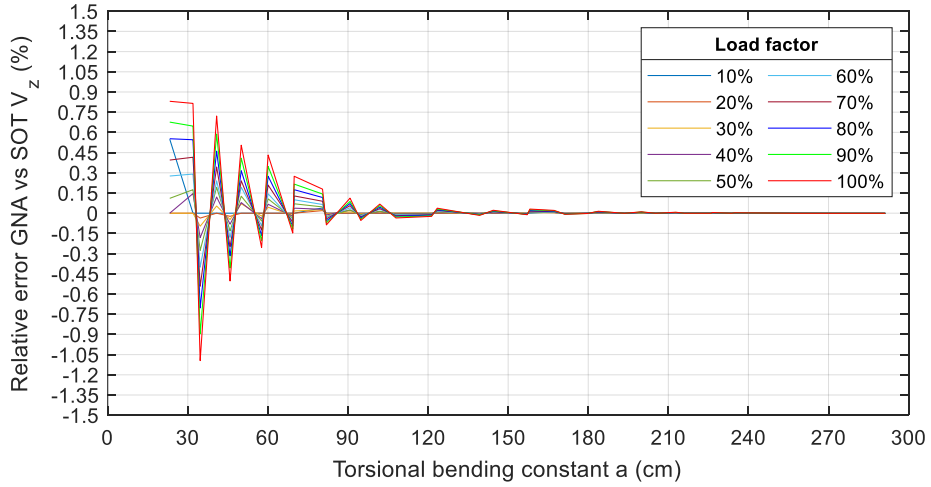

Figure A III.88 Relative error fork support V_z: fork-fixed system, M_y load, open profiles

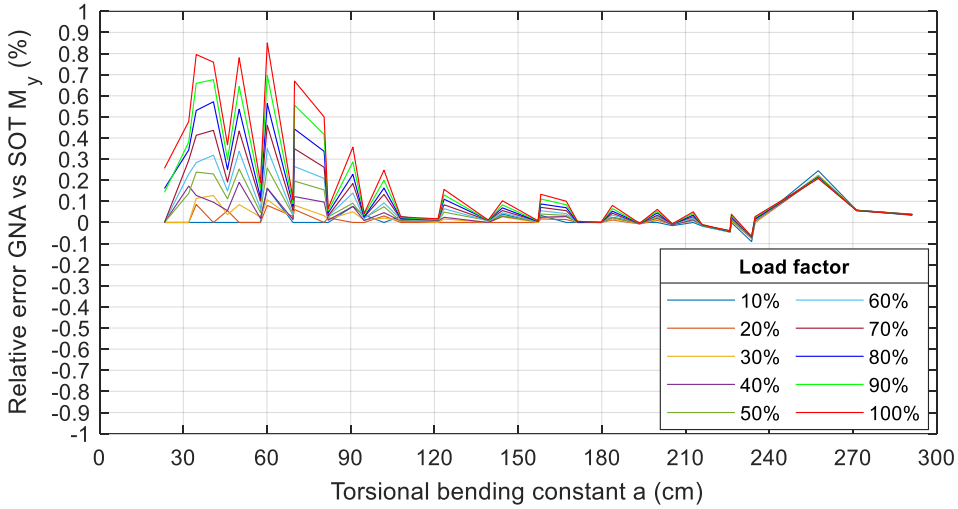

Figure A III.89 Relative error fixed support M_y: fork-fixed system, M_y load, open profiles

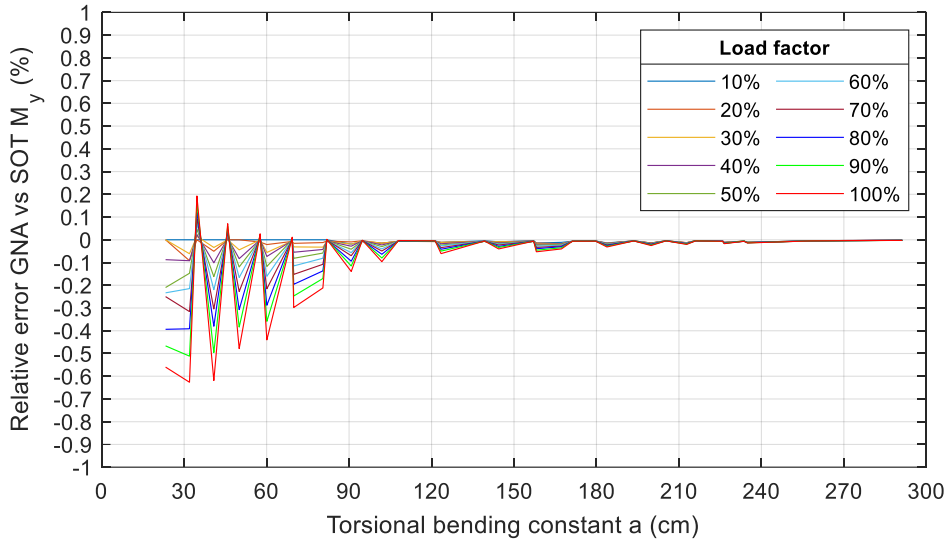

Figure A III.90 Relative error midspan M_y: fork-fixed system, M_y load, open profiles

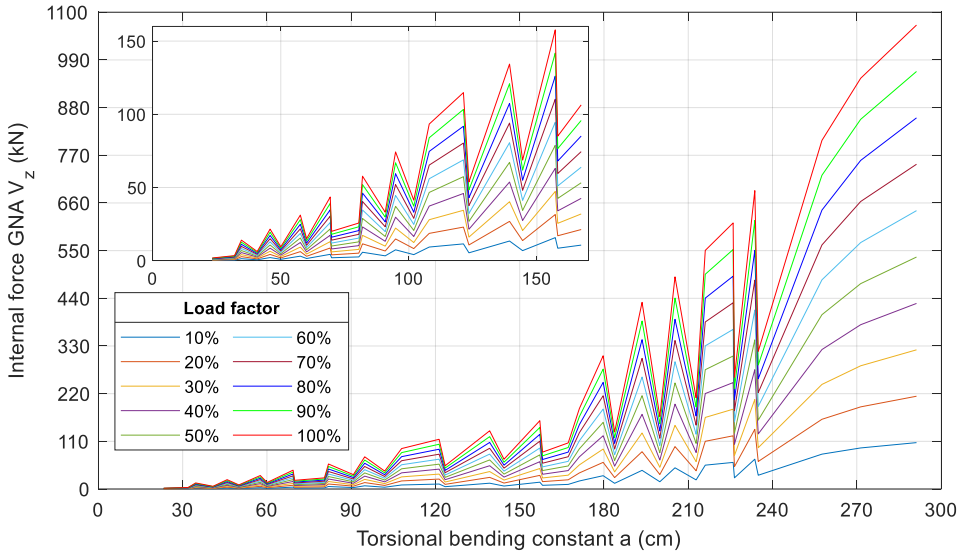

Figure A III.91 Internal force fork support V_z: fork-fixed system, M_y load, open profiles / Inset of the graphic corresponds to values of a up to 170cm

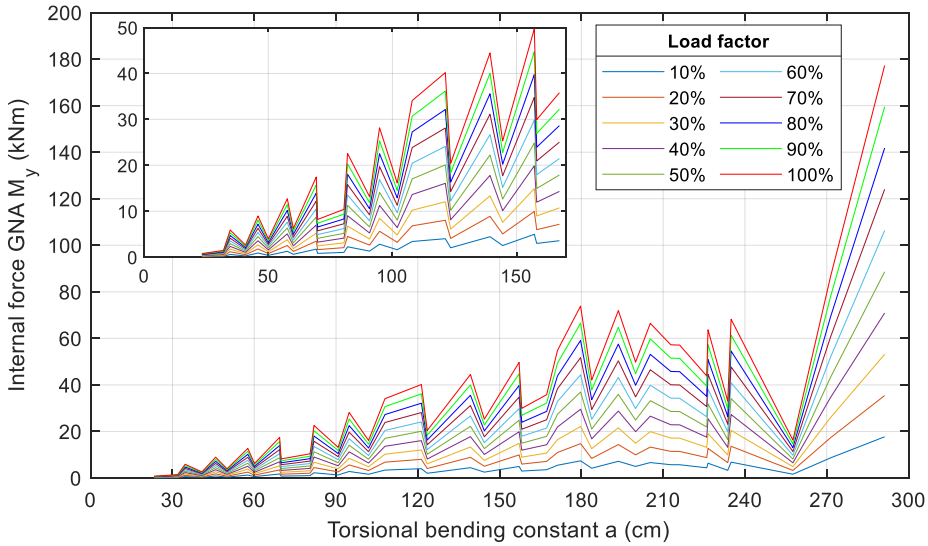

Figure A III.92 Internal force fixed support M_y: fork-fixed system, M_y load, open profiles / Inset of the graphic corresponds to values of a up to 170cm

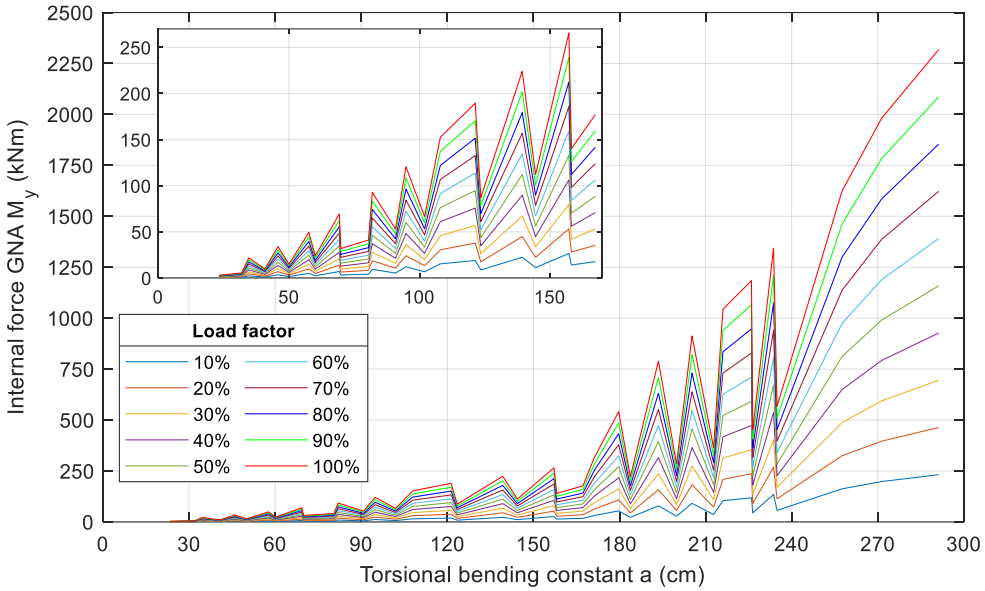

Figure A III.93 Internal force midspan M_y: fork-fixed system, M_y load, open profiles / Inset of the graphic corresponds to values of a up to 170cm

M_T

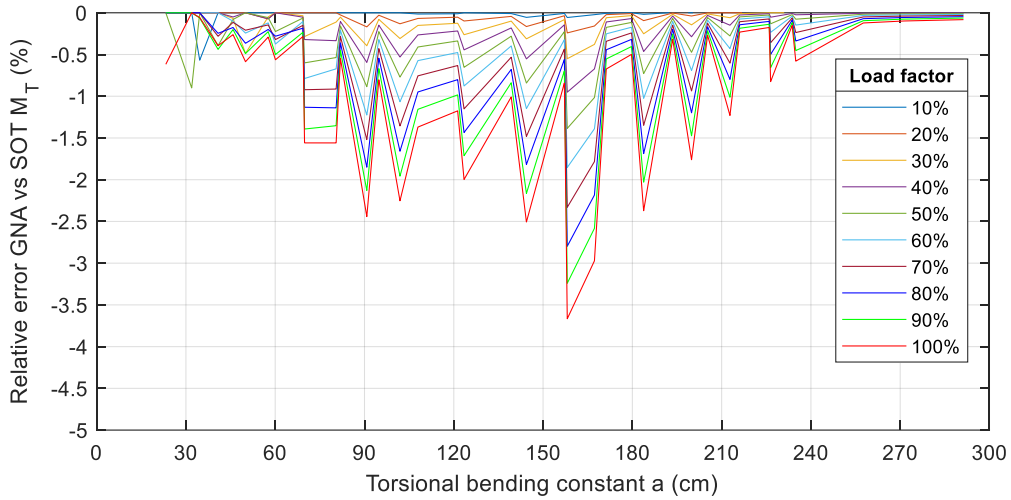

Figure A III.94 Relative error support M_T: fork-fixed system, M_T load, open profiles

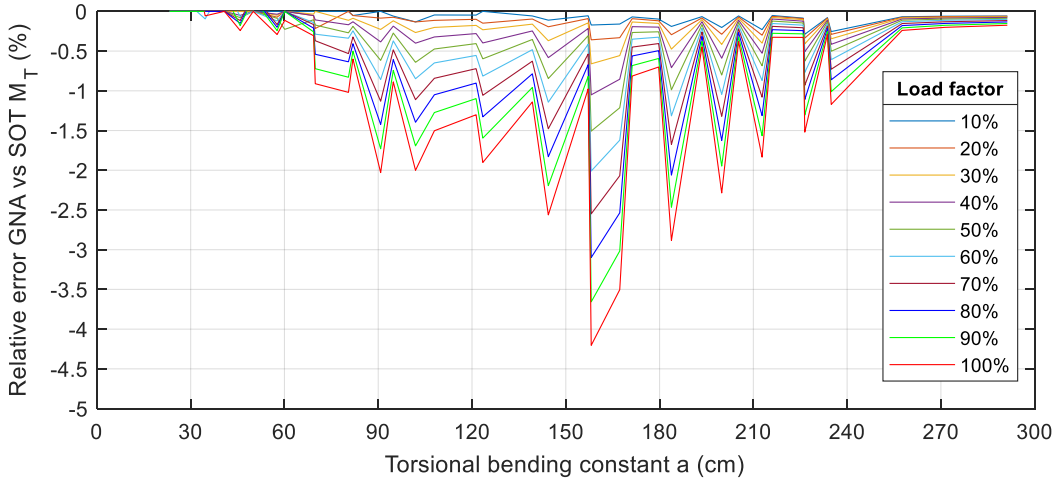

Figure A III.95 Relative error midspan M_T: fork-fixed system, M_T load, open profiles

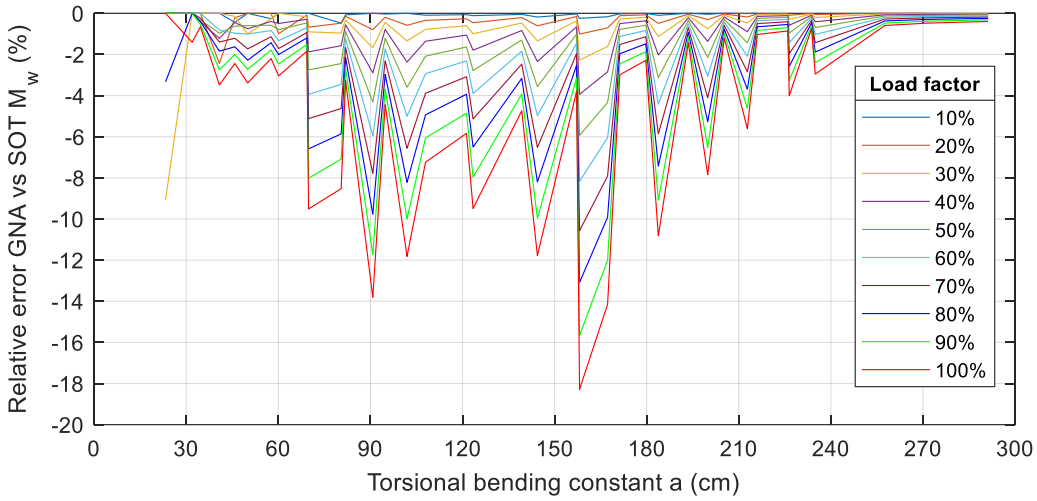

Figure A III.96 Relative error support M_w: fork-fixed system, M_T load, open profiles

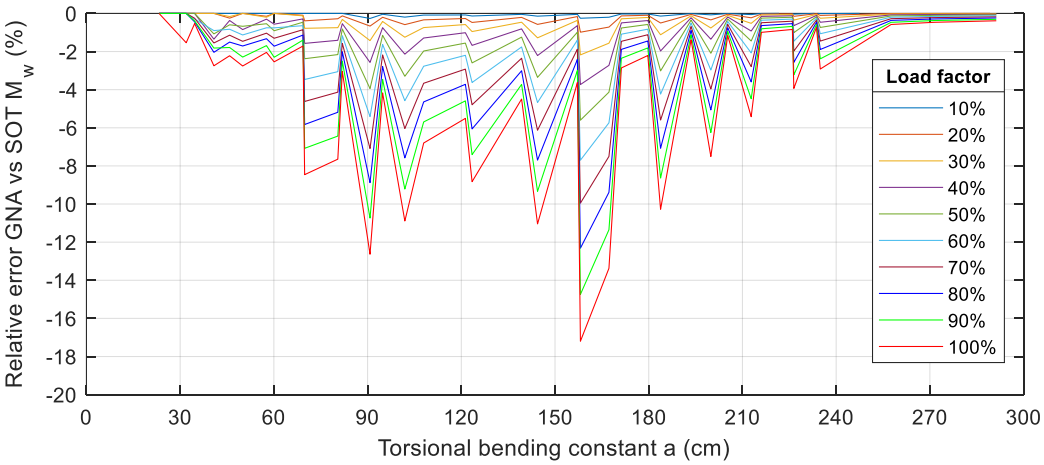

Figure A III.97 Relative error midspan M_w: fork-fixed system, M_T load, open profiles

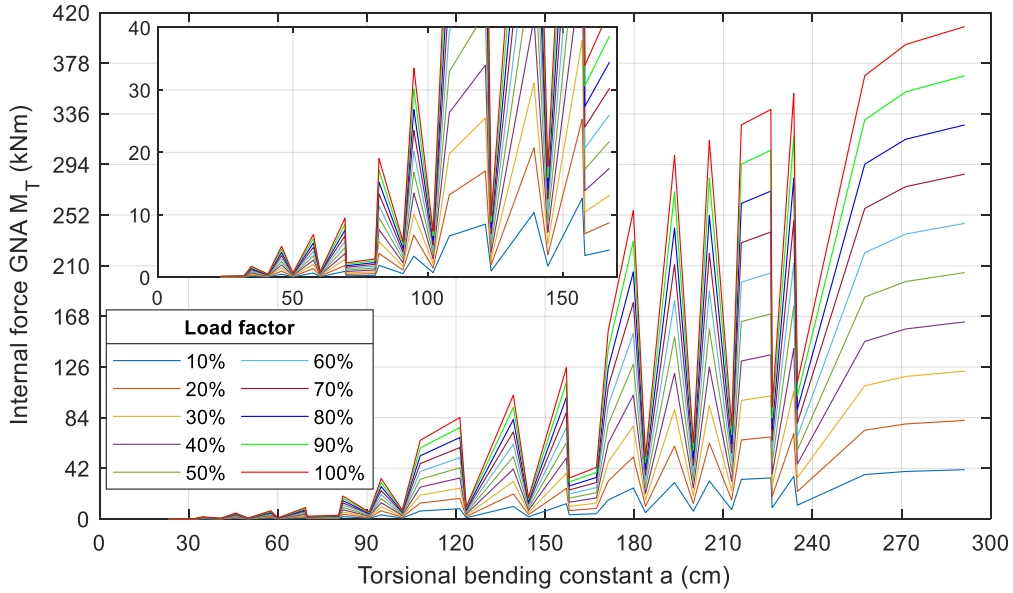

Figure A III.98 Internal force support M_T: fork-fixed system, M_T load, open profiles / Inset of the graphic corresponds to values of a up to 170cm

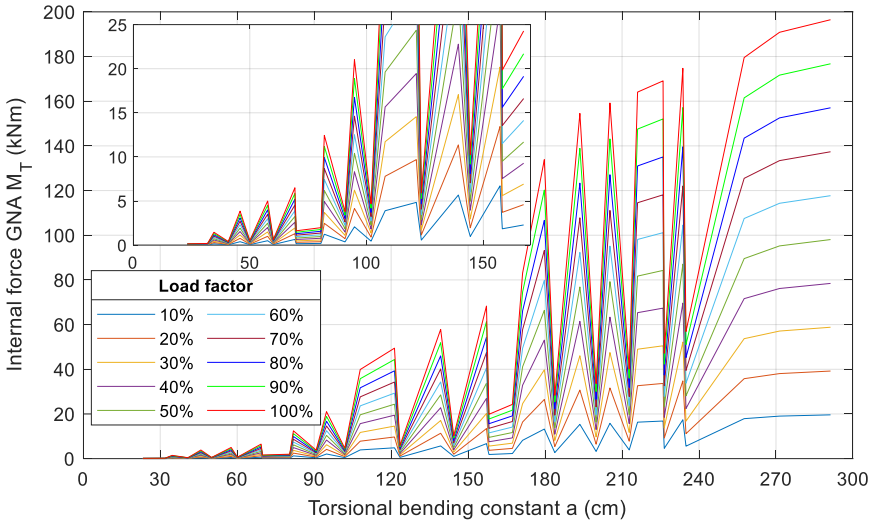

Figure A III.99 Internal force fork support M_T: fork-fixed system, M_T load, open profiles / Inset of the graphic corresponds to values of a up to 170cm

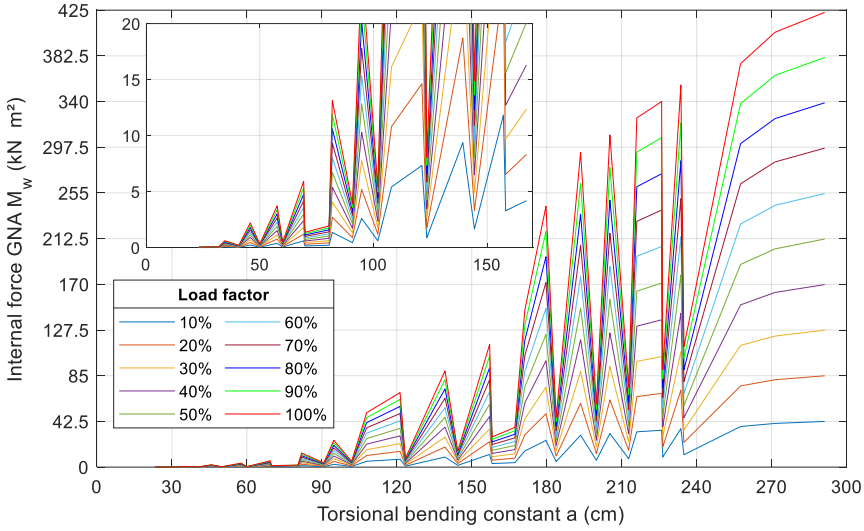

Figure A III.100 Internal force support M_w: fork-fixed system, M_T load, open profiles / Inset of the graphic corresponds to values of a up to 170cm

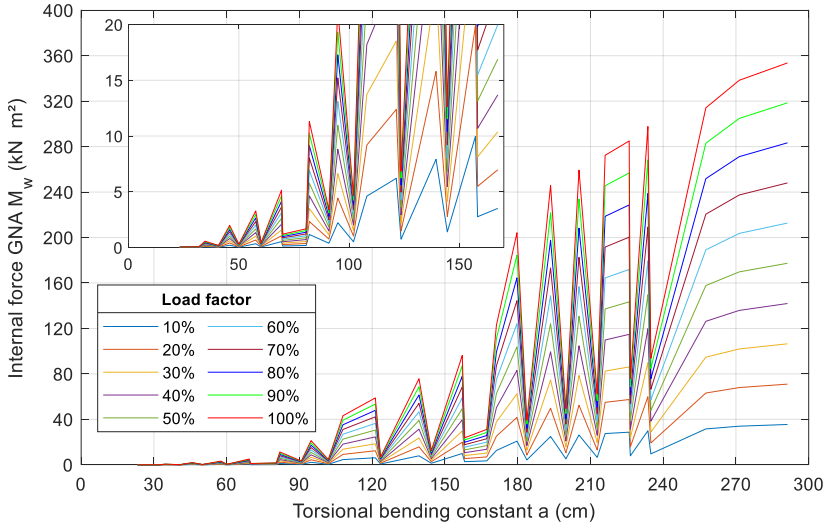

Figure A III.101 Internal force midspan M_w: fork-fixed system, M_T load, open profiles / Inset of the graphic corresponds to values of a up to 170cm

Appendix III-4.2 Closed cross-sections

V_z

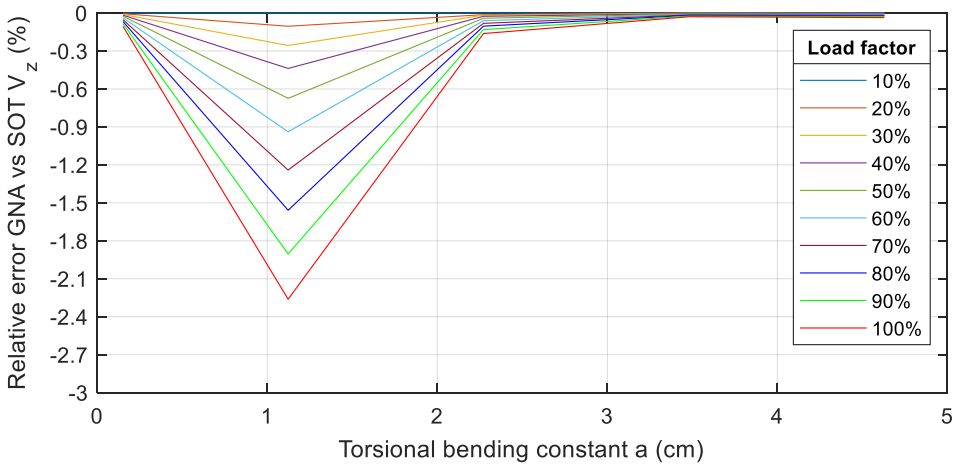

Figure A III.102 *Relative error fixed support V_z: fork-fixed system, V_z load, closed profiles*

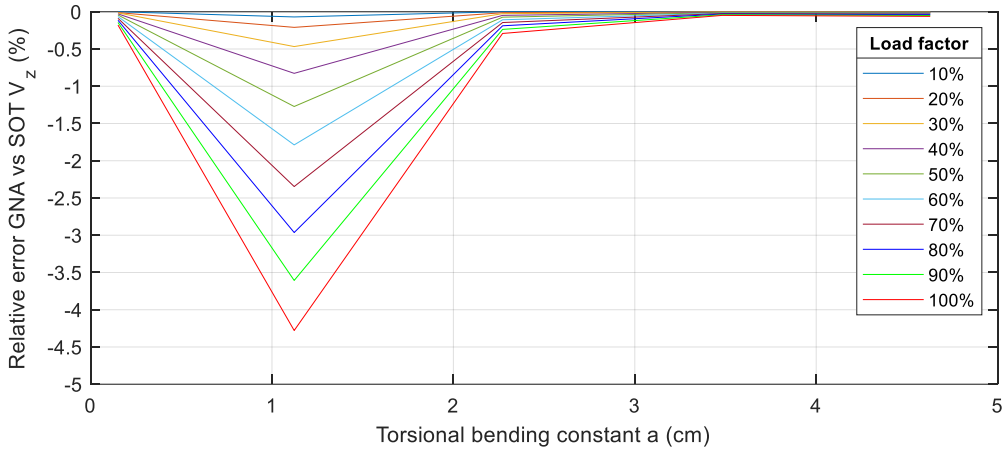

Figure A III.103 *Relative error midspan V_z: fork-fixed system, V_z load, closed profiles*

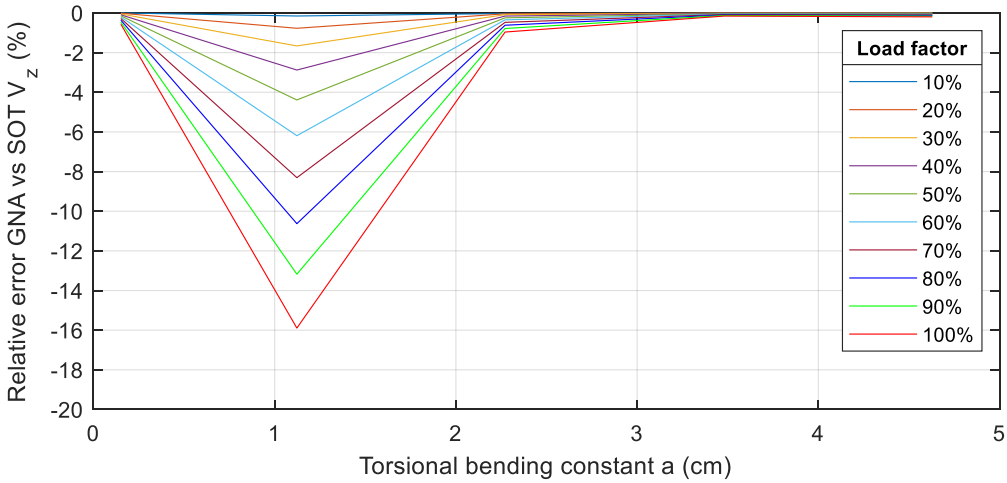

Figure A III.104 *Relative error fork support V_z: fork-fixed system, V_z load, closed profiles*

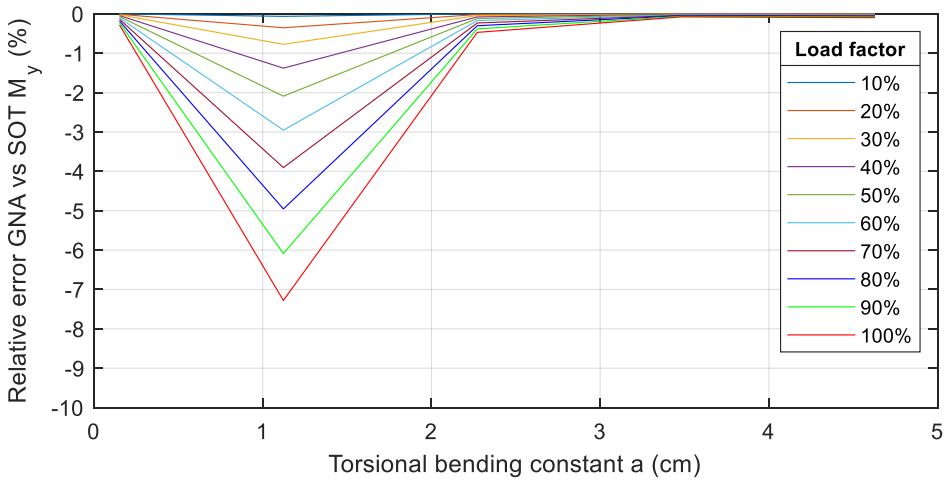

Figure A III.105 *Relative error fixed support M_y: fork-fixed system, V_z load, closed profiles*

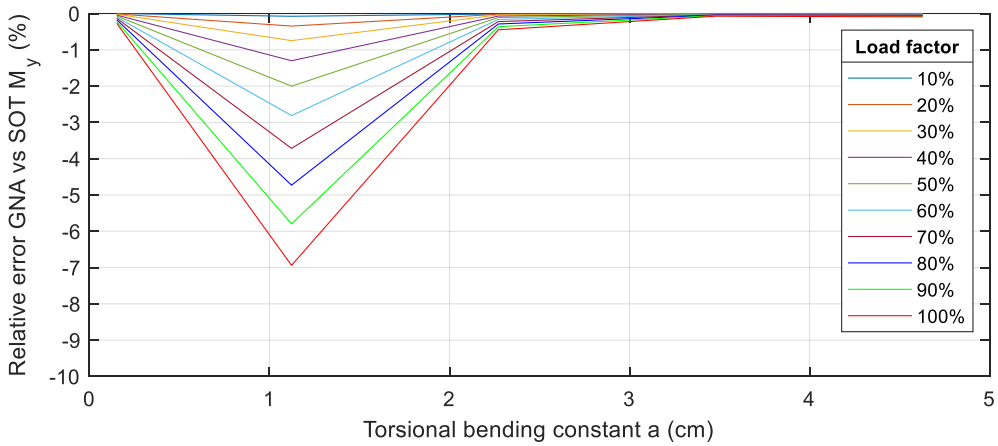

Figure A III.106 *Relative error midspan M_y: fork-fixed system, V_z load, closed profiles*

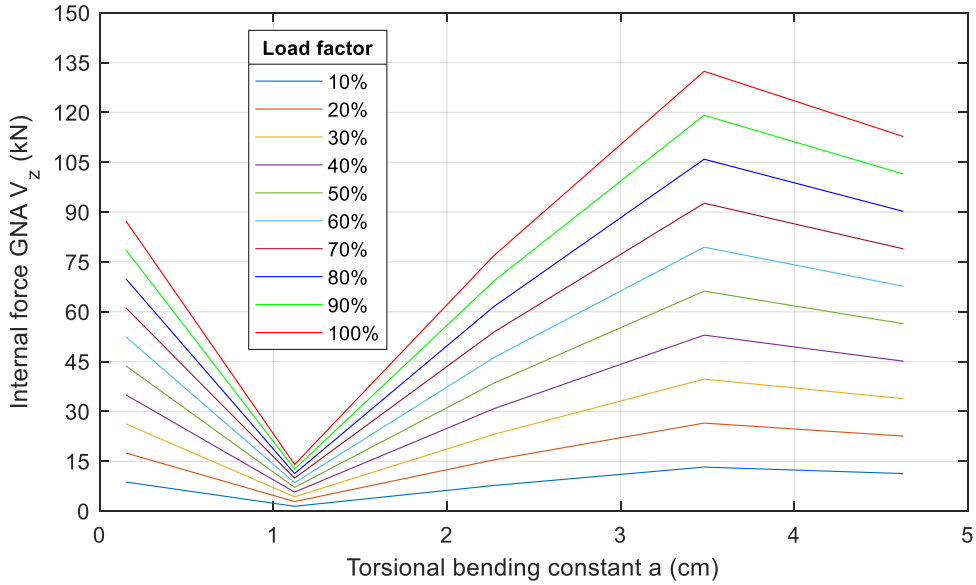

Figure A III.107 *Internal force fixed support V_z: fork-fixed system, V_z load, closed profiles*

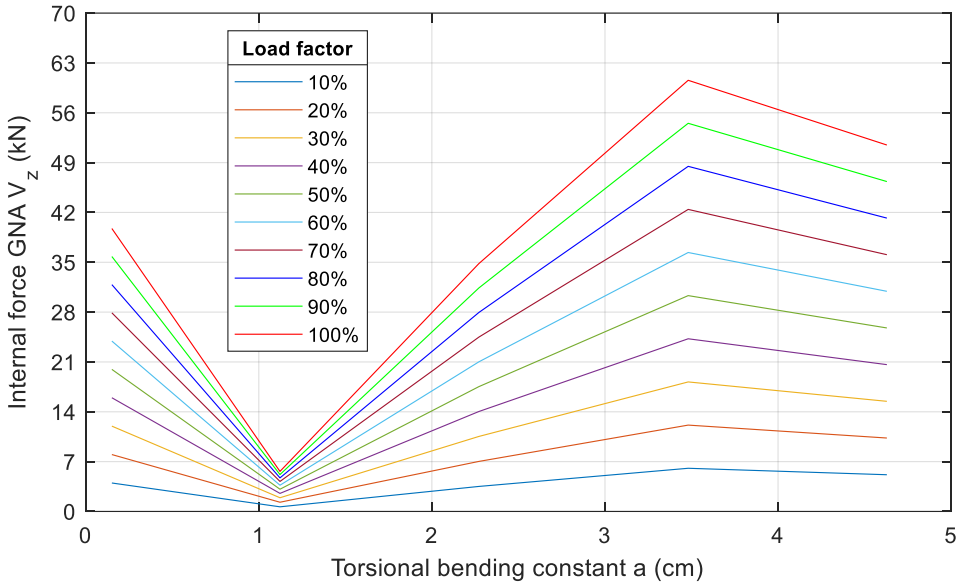

Figure A III.108 *Internal force fork support V_z: fork-fixed system, V_z load, closed profiles*

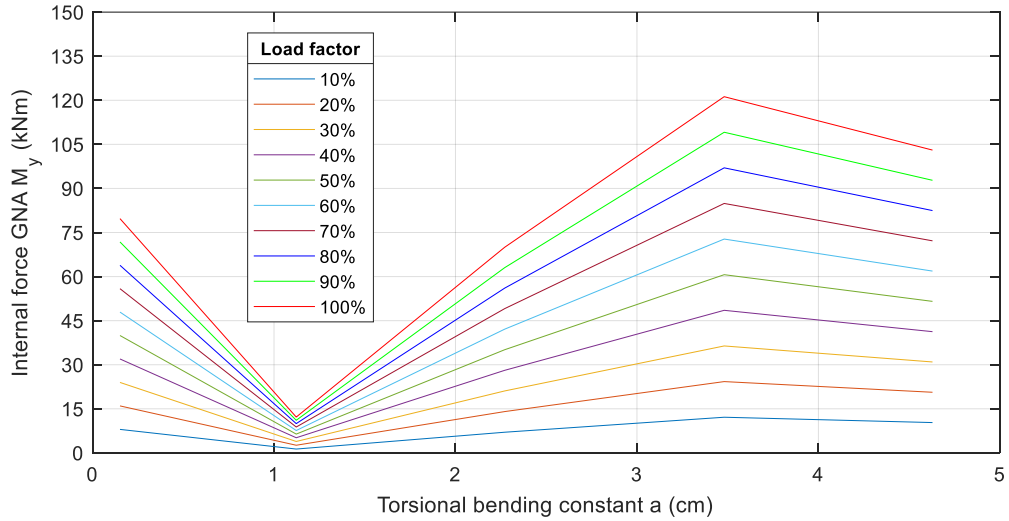

Figure A III.109 *Internal force fixed support M_y: fork-fixed system, V_z load, closed profiles*

M_y

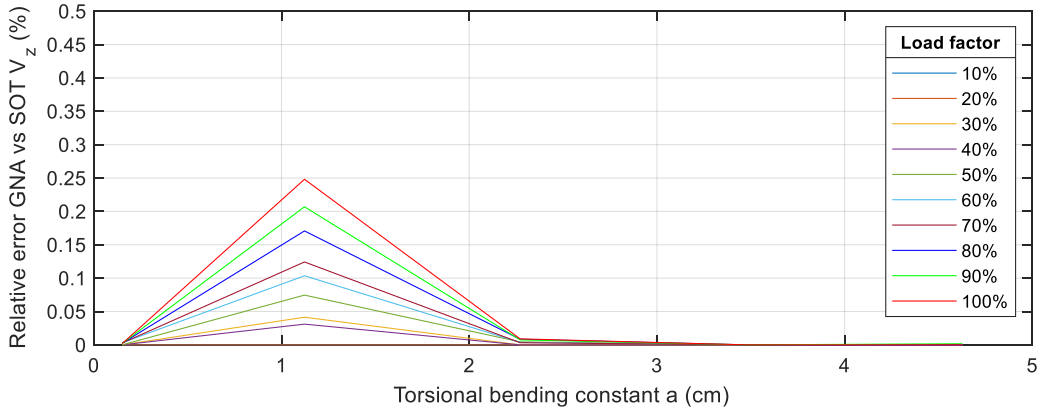

Figure A III.110 *Relative error fixed support V_z: fork-fixed system, M_y load, closed profiles*

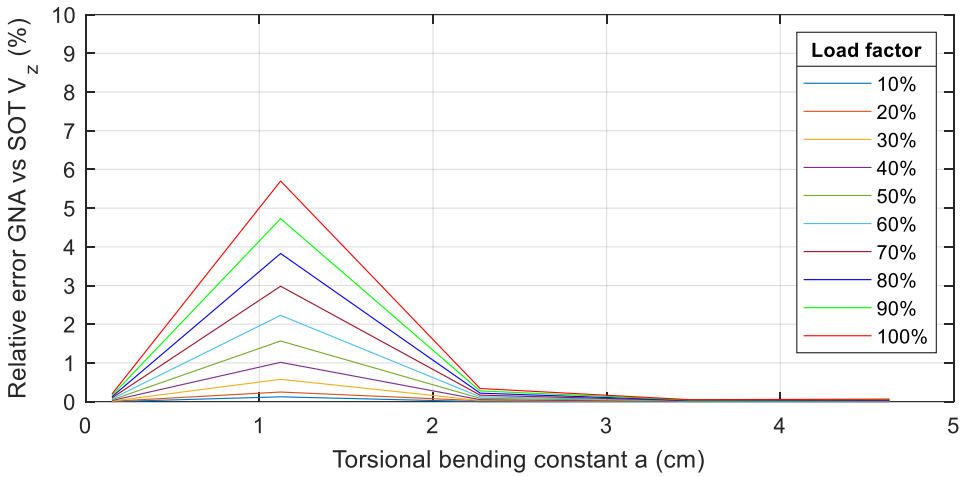

Figure A III.111 *Relative error midspan V_z: fork-fixed system, M_y load, closed profiles*

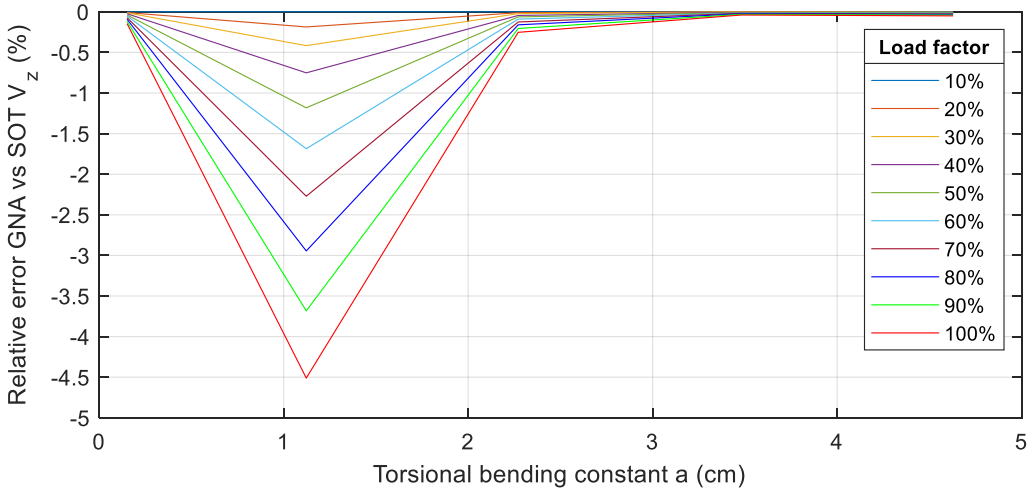

Figure A III.112 *Relative error fork support V_z: fork-fixed system, M_y load, closed profiles*

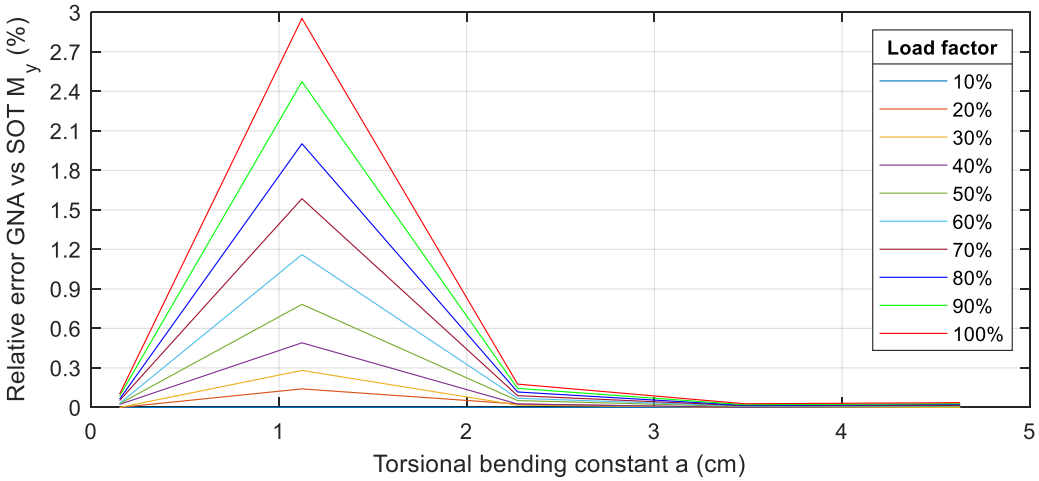

Figure A III.113 *Relative error fixed support M_y: fork-fixed system, M_y load, closed profiles*

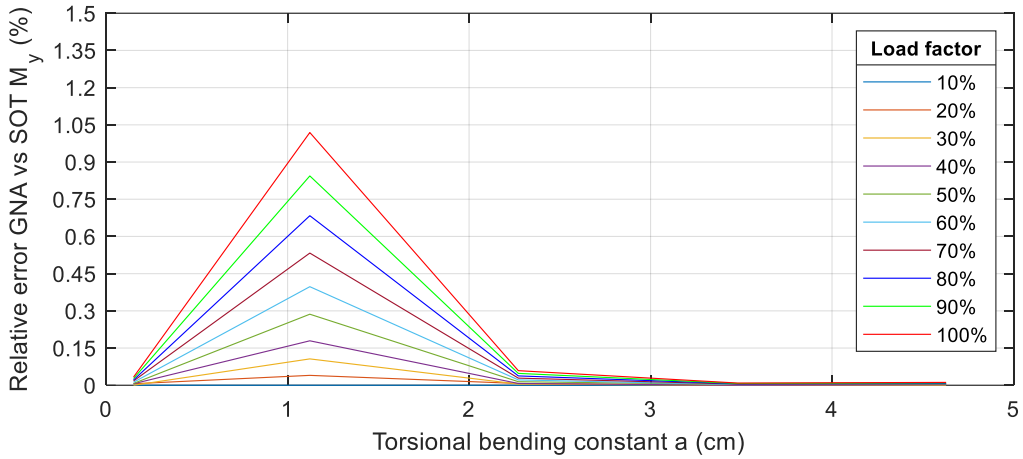

Figure A III.114 *Relative error midspan M_y: fork-fixed system, M_y load, closed profiles*

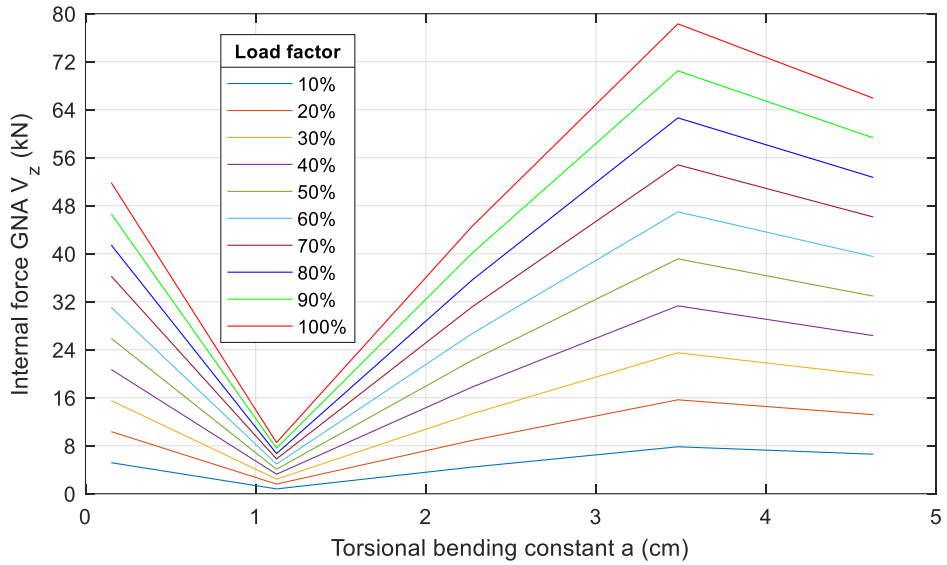

Figure A III.115 *Internal force fork support V_z: fork-fixed system, M_y load, closed profiles*

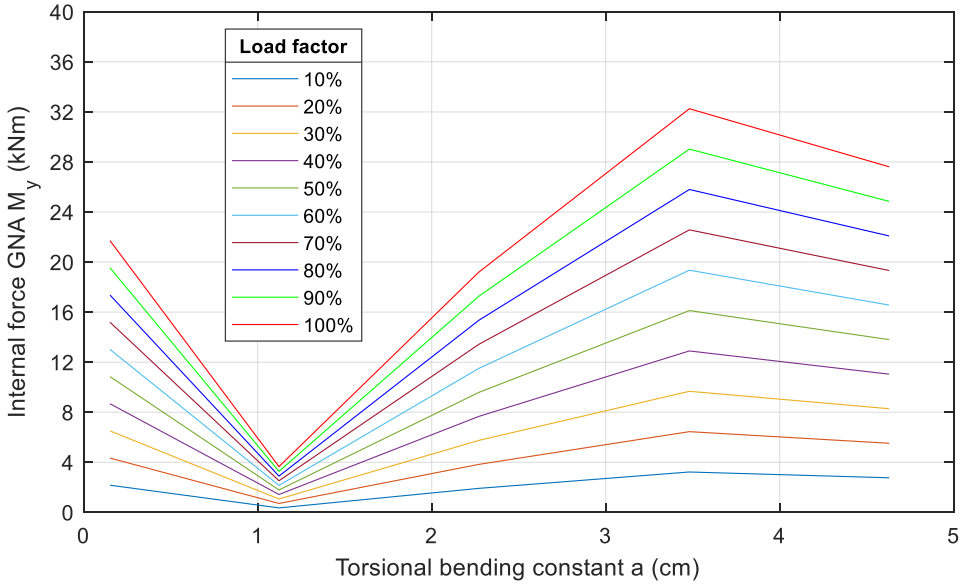

Figure A III.116 *Internal force fixed support M_y: fork-fixed system, M_y load, closed profiles*

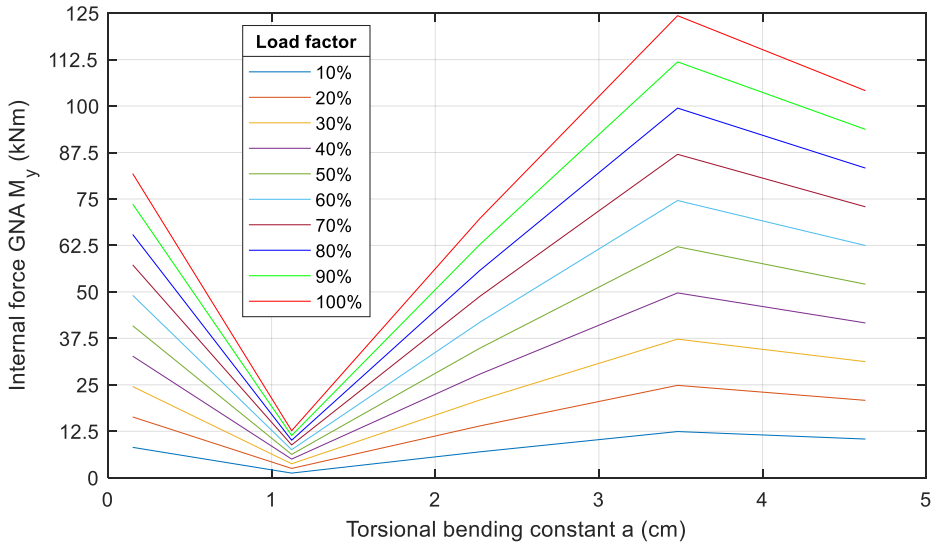

Figure A III.117 *Internal force midspan M_y: fork-fixed system, M_y load, closed profiles*

M_T

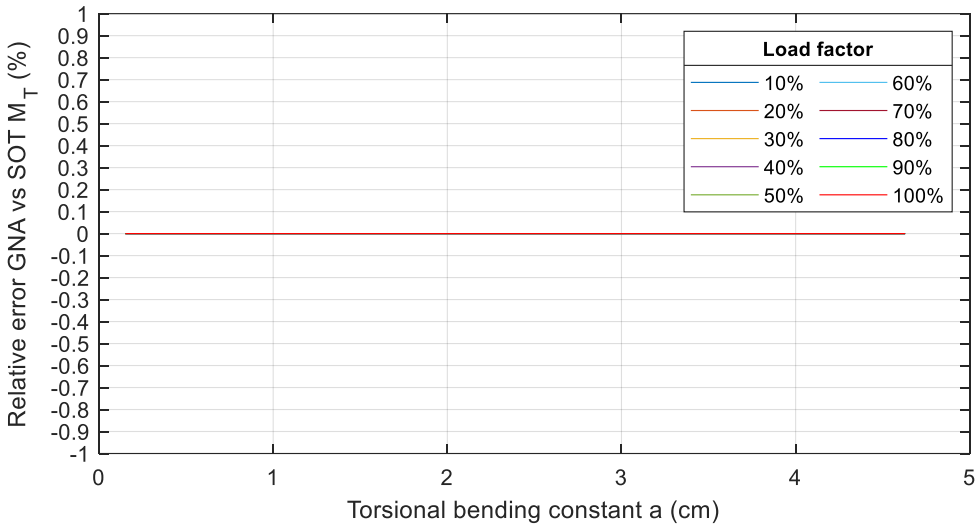

Figure A III.118 *Relative error M_T: fork-fixed system, M_T load, closed profiles*

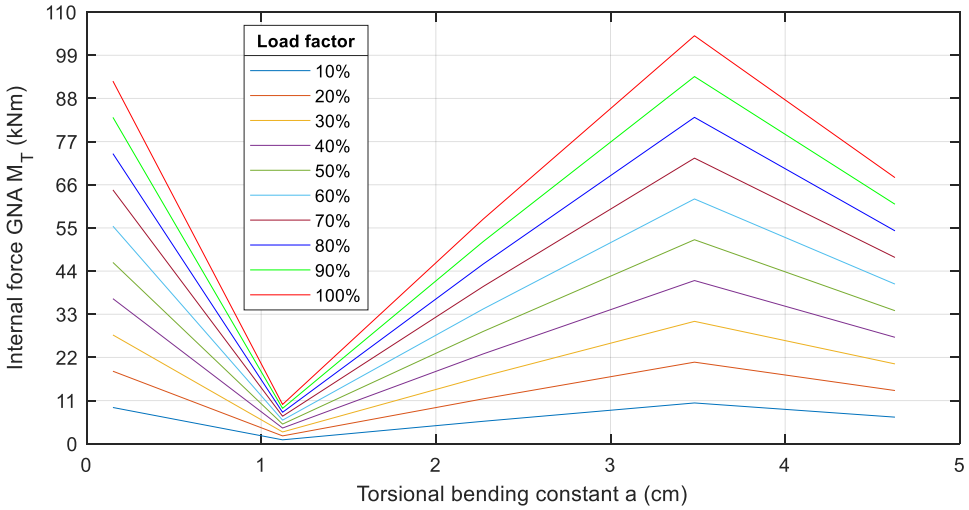

Figure A III.119 *Internal force M_T: fork-fixed system, M_T load, closed profiles*

Appendix IV Fitting curves validation

In this appendix, the fitting curves used for the validation in the six examples are presented (see section 4.3.3). In each figures, the red lines indicate the intersection location for the corresponding load factor (80%) and the torsional bending constant divided by the length *a*/L.

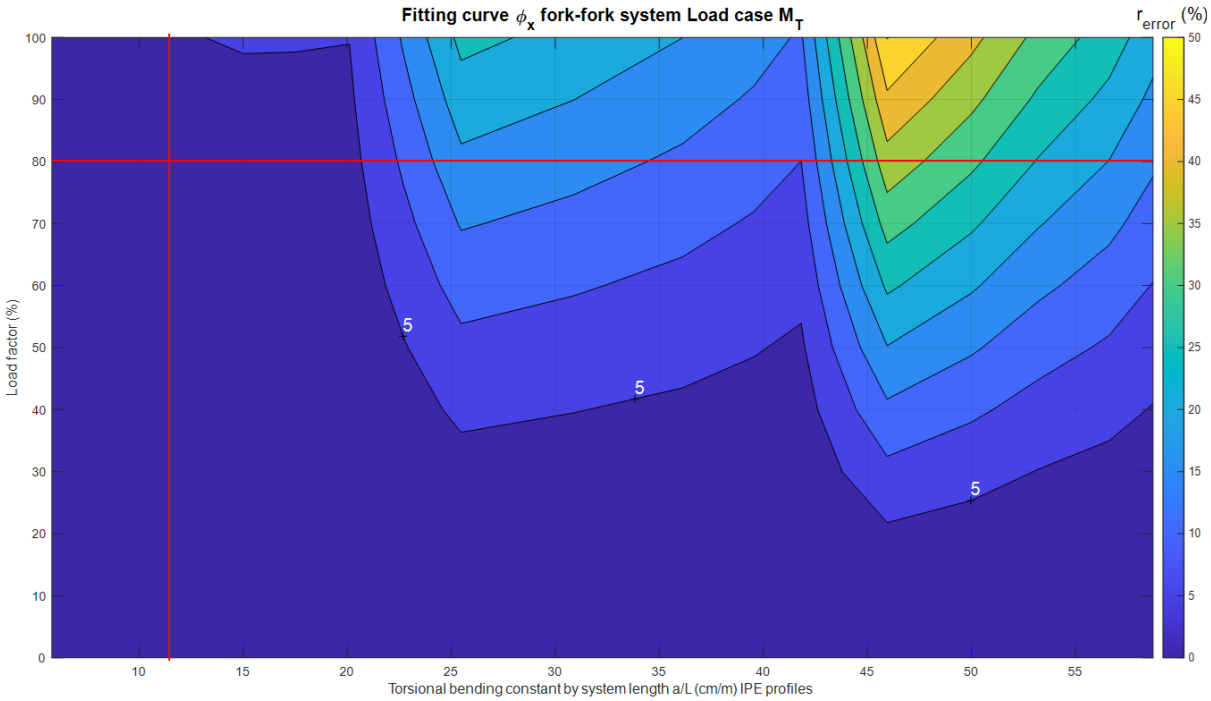

Figure A IV.1 Example 1 φ_x: IPE200, fork-fork system, and M_T load

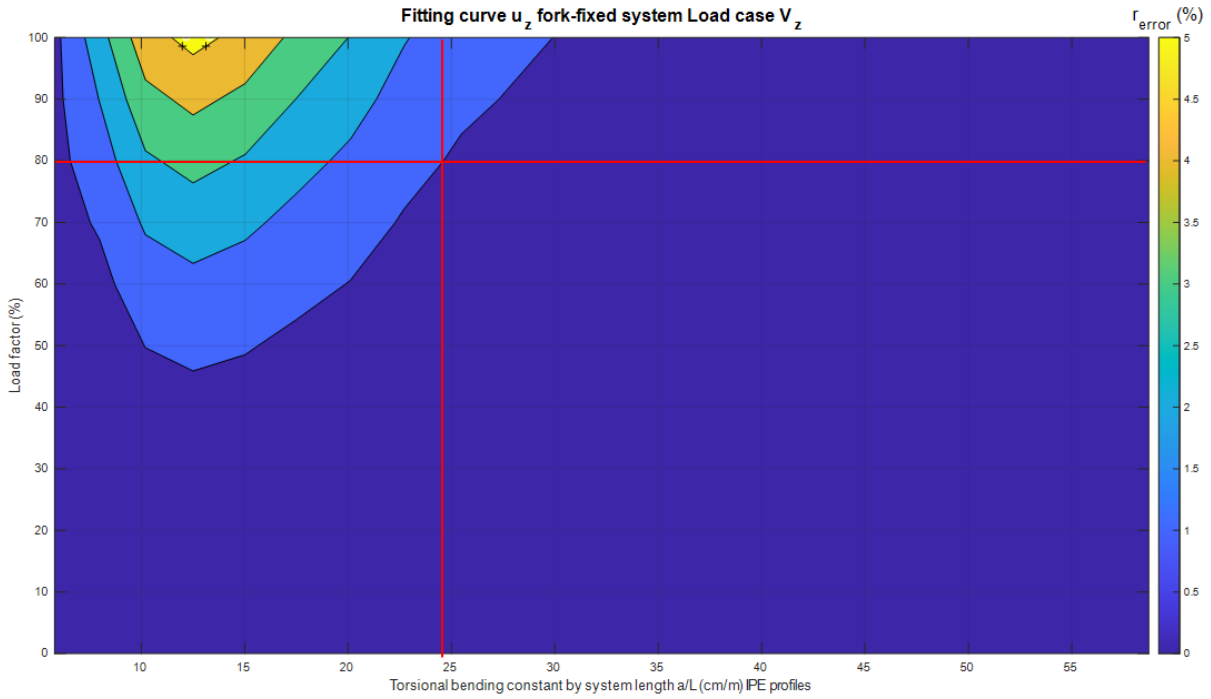

Figure A IV.2 Example 2 u_z: IPE360, fork-fixed system, and V_z load

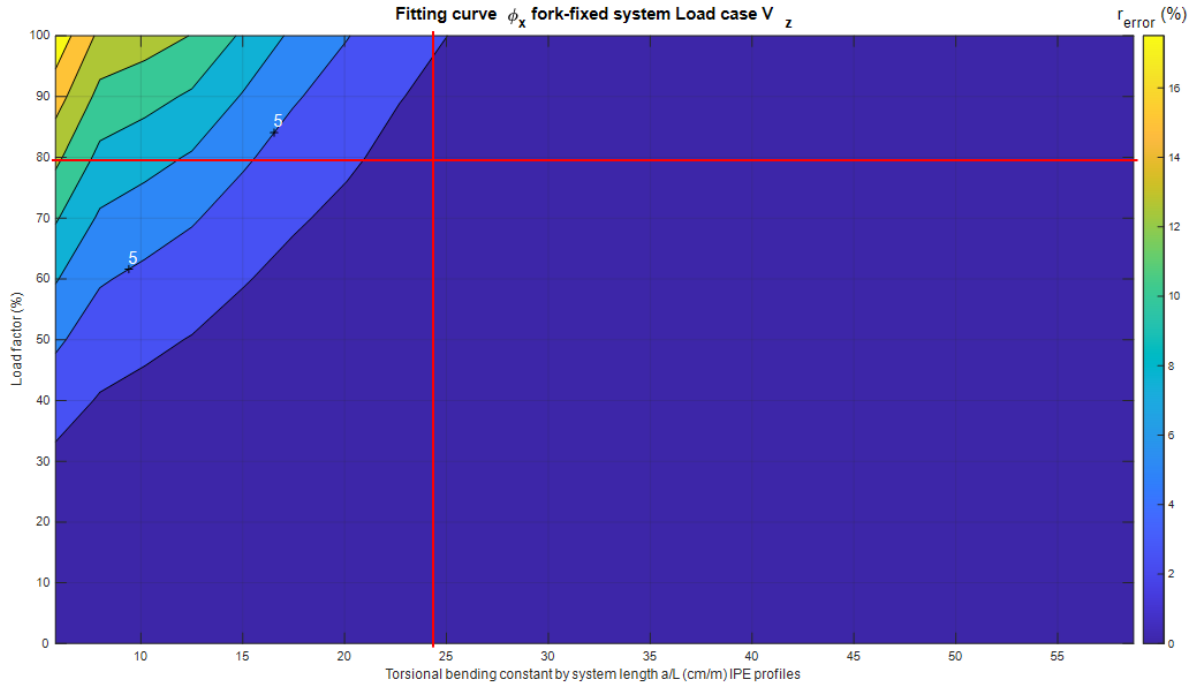

Figure A IV.3 Example 2 φ_x: IPE360, fork-fixed system, and V_z load

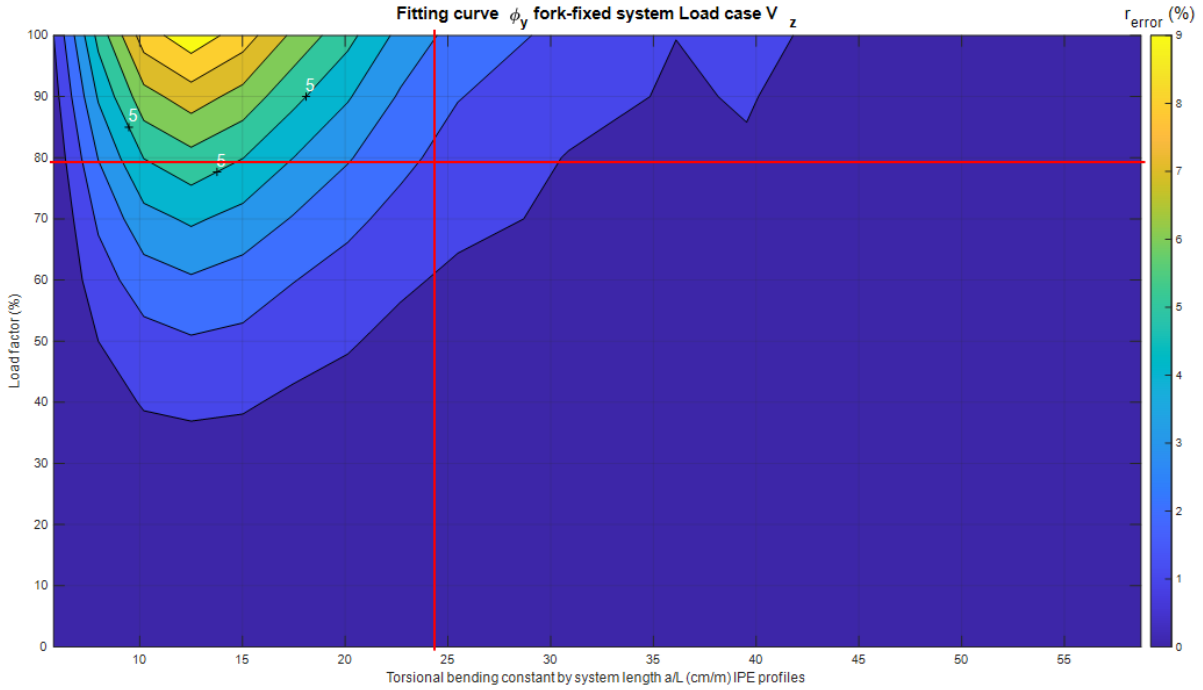

Figure A IV.4 Example 2 φ_y: IPE360, fork-fixed system, and V_z load

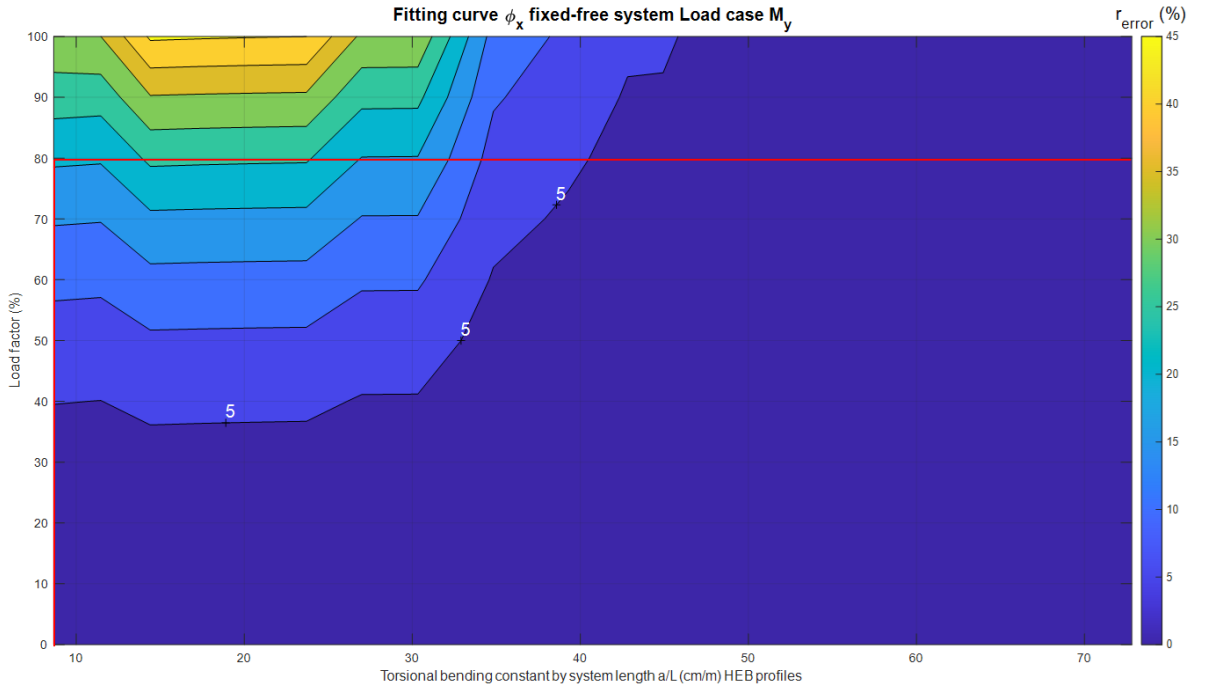

Figure A IV.5 Example 3 φ_x: HEB100, fixed-free system, and M_y load

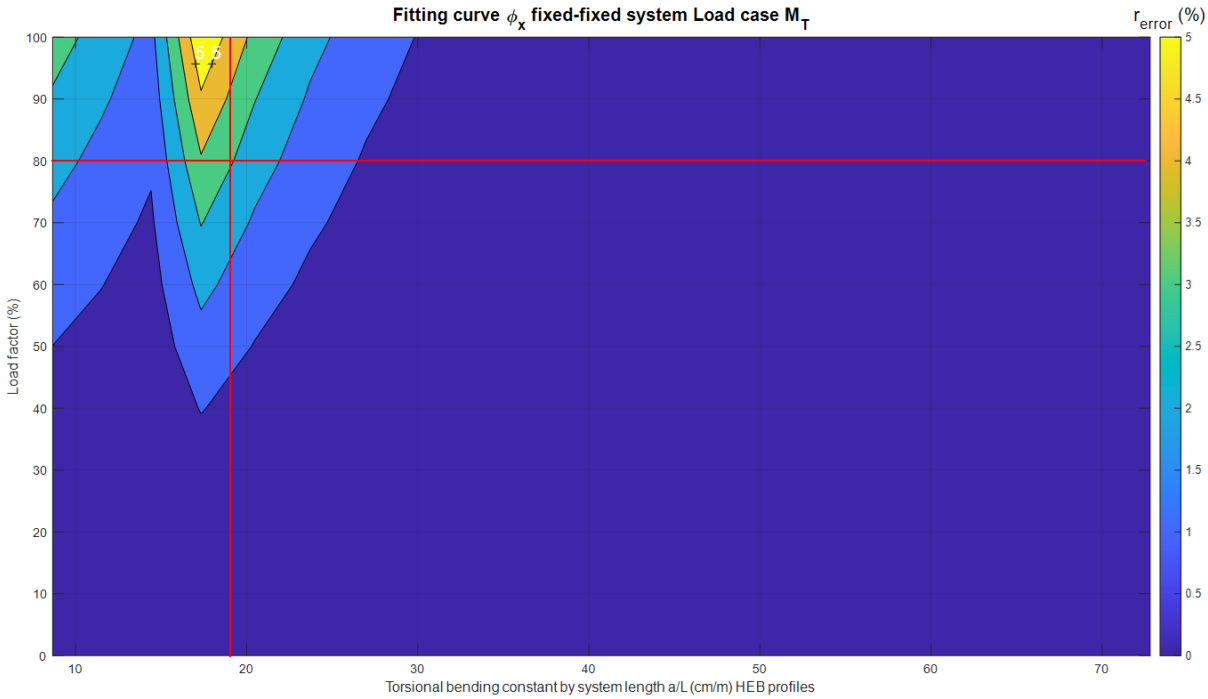

Figure A IV.6 Example 4 φ_x: HEB240, fixed-fixed system, and M_T load

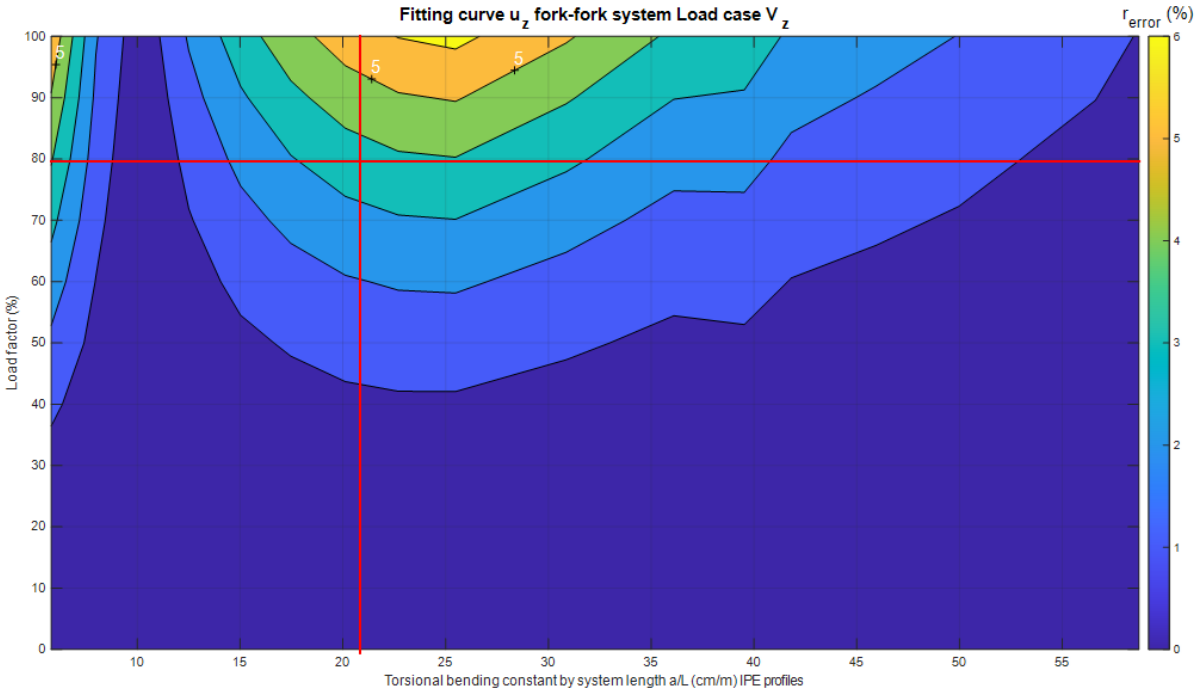

Figure A IV.7 Example 5 u_z: IPE300, fork-fork system, and q load

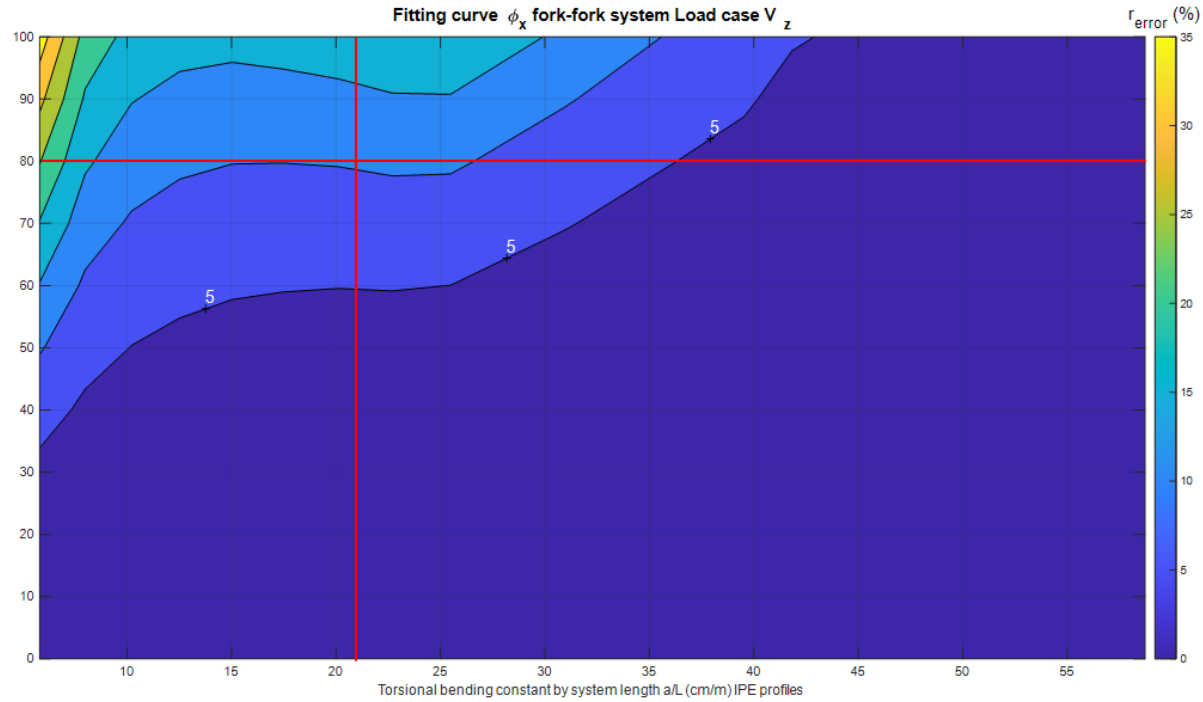

Figure A IV.8 Example 5 φ_x: IPE300, fork-fork system, and q load

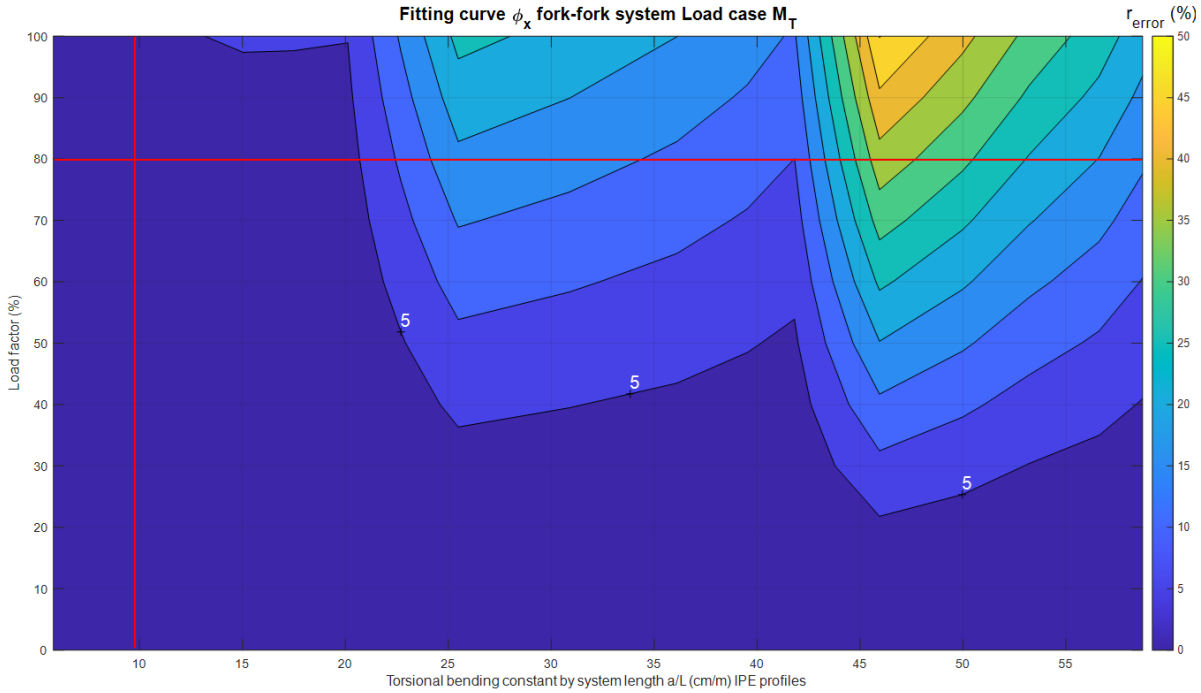

Figure A IV.9 Example 6 φ_x: UPE200, fork-fork system, and M_T load